ISSN 1738-1142

Volume 17(2) **2019**

KOREAN RADIOACTIVE WASTE SOCIETY

2019 추계학술논문요약집

| 일시 |

2019. 10. 30(수) ~ 11. 1(금)

| 장소 |

롯데호텔 제주

Abstracts of Proceedings of the
Korean Radioactive Waste Society
AUTUMN 2019

사단법인 한국방사성폐기물학회
Korean Radioactive Waste Society

2019 추계학술발표회

이 발표논문집은 2019년도 정부재원(과학기술진흥기금 및 복권기금)으로
한국과학기술단체총연합회의 지원을 받아 발간되었음

ISSN 1738-1142

Volume 17(2) **2019**

KOREAN RADIOACTIVE WASTE SOCIETY

2019
추계학술논문요약집

| 일시 |

2019. 10. 30(수) ~ 11. 1(금)

| 장소 |

롯데호텔 제주

Abstracts of Proceedings of the
Korean Radioactive Waste Society
AUTUMN 2019

사단법인 한국방사성폐기물학회
Korean Radioactive Waste Society

Contents

KOREAN
RADIOACTIVE WASTE
SOCIETY

1분과 핵주기정책·규제 및 비확산 (Oral)

09:00~09:20 Review of Measures to Ensure the Effectiveness of the Corrective Order ···· 25
Sang Cheol Hyung [KINAC]

09:20~09:40 Export Control for Small Quantity Nuclear Material in Equipment ····· 27
Sung Yoon Park [KINAC]

09:40~10:00 Analysis of Fuel Cycle Coupling SMR Using Partial TRU Recycling and SFR Burner ····· 29
Dae Hee Hwang, Ser Gi Hong [Kyung Hee Univ.]

10:00~10:20 A New Approach to Manage Nuclear Wastes in the ROK ····· 31
Yongsoo Hwang, Hong Chang, Hyo-On Nam [KAERI]

11:20~11:40 Overall Issues of the ACTR Programs ····· 33
Yongsoo Hwang [KAERI]

11:40~12:00 A Consideration on the IAEA Safeguards Policy Forwarded to A State-Level Approach ····· 35
Jae-Kwang Kim, Sung Yoon Park [KINAC]

12:00~12:20 Safeguards: Implementing the Updated State-Level Approach at KAERI ····· 37
IC Kim, SH Lee, BD Lee, HJ Kim, HS Kim, JA Jung, SM Han [KAERI]

12:20~12:40 Progress in the Development of REPF+ Safeguards Approach ····· 39
Se-Hwan Park, Bong Young Kim, Ho-Dong Kim, Chaehun Lee, Dae-Yong Song, Byung-Hee Won, Seong-Kyu Ahn [KAERI]

1분과 핵주기정책·규제 및 비확산 (Poster)

P0101 Review of Satellite Imagery Signatures From Open Source Analyses on Nonproliferation Monitoring Activities ····· 43
Jae-Jun Han, Minsoo Kim [KINAC]

P0102 Preliminary Investigation on Candidate Areas of Interest for H-program ····· 45
Nam Kyung Kim, Jung-Hyun Lee, Jae-Jun Han, Young Wook Lee [KINAC]

P0103 A Study on Approaches of the International Community to Strengthen Nuclear Security Since 2016 ····· 47
Jae San Kim [KINAC]

P0104 A Study on the Physical Protection Regulations for Nuclear Power Plants During Decommissioning ····· 49
Seung Rae Kim [KINAC]

P0105 Performance-based Vital Area Identification and Protection Measures Supporting IAEA NSS No. 16 Method ····· 51
Seung Rae Kim [KINAC]

P0106 Exemption and De-exemption in Safeguards ····· 53
Sung Ho Lee, I C Kim, B D Lee, H J Kim, H S Kim, J A Jung, S M Han [KAERI]

P0107 The Status of Nuclear Material Accountancy at KAERI ····· 55
Hyun-Jo Kim, In-Chul Kim, Byung-Doo Lee, Sung-Ho Lee, Hyun-Sook Kim, Juang Jung, Seong-Mi Han [KAERI]

P0108 Technical Review on R&D Trends in Unmanned System for Safeguards Inspection ····· 57
Ju Young Jeon, Sungmin Kim, Myungsoo Kim, Hyun Young Kim, Heejun Chung [KINAC]

P0109 Study of Soil Sampling Procedure for Safeguard Inspection ····· 59
Geon Yong Lee, Ju Young Jeon, Hyun Young Kim, Heejun Chung [KINAC]

P0110 Preliminary Measurements of Uranium Samples With Portable X-ray Fluorescence Equipment ····· 61
So Yeon Shin, Woojin Kim, Minsu Kim [KINAC]

P0111 LIBS Analysis of Simulated Electro Refining Salt Sampled Using the Dip Stick ····· 63
Seul-Ki Han, Se-Hwan Park, Seong-Kyu Ahn [KAERI]

P0112 Review of Domestic Applicability for NDA's Site End State Definition Process ····· 65
Hyejin Jung, Su-hee Lee [KHNP-CRI]

P0113 Status of Domestic Use and Regulations for Small Quantities of Nuclear Material ····· 67
Jihyun Ahn, Junsung Park, Hee Seo [Chonbuk Natl. Univ.] Seungmin Lee, Jae Woong Tae, Seung Ho Ahn [KINAC]

P0114 Status of KAERI's Activities on IAEA Collaboration for Safeguards Development for Pyroprocessing ····· 69
Seong Kyu Ahn, Ho-Dong Kim, Se-Hwan Park, Dae-Yong Song [KAERI]

P0115 Trend Analysis of Research on Proliferation Resistance ····· 71
Ji-song Jeong [UST], Ho-Dong Kim, Seong-Kyu Ahn [KAERI]

P0116 A Feasibility Study for Long-Life Molten Salt Reactor Core ····· 73
Sunghwan Yun, Sang Ji Kim [KAERI]

2분과 사용후핵연료 처분전관리 (Oral)

09:00~09:20 Comparison of Inert Hot Cell Atmospheric Systems ····· 77
Hyojik Lee, Byung Suk Park, Seung Nam Yu [KAERI]

09:20~09:40 Preliminary Criticality Analysis on the OASIS-37CAN Canister With 37 Spent Nuclear Fuel Assemblies of Kori-1 ····· 79
Joon Gi Ahn, Youngtae Han [KEPCO E&C]

09:40~10:00 Spent Fuel Burnup Measurement by CZT Gamma Detector ····· 81
Yongdeog Kim, Donghee Lee, Jinho Jeong [KHNP-CRI], Sehyun Oh [Users Co.,], Hee Seo [Chonbuk Natl. Univ.]

10:00~10:20 Forced Circulation Drying Test of Residual Water According to Pressure ··· 83
Kyoung-Sik Bang, Ju-Chan Lee, Seung-Hwan Yu, Woo-Seok Choi [KAERI], Kyung-wook Shin [Sae-an Eng.]

11:20~11:40 Analysis of Axial Burnup Profile Effects on the Shielding Calculation of the KORAD-21 Cask Using Monaco/MAVRIC ····· 85
Ye Seul Cho, Dong Jin Kim, Ser Gi Hong [Kyung Hee Univ.]

11:40~12:00 Development Status of AMORES Program for Automatic Source Term Evaluation of Spent Fuels ····· 87
Geon Hee Jung, Ye Seul Cho, Ser Gi Hong [Kyung Hee Univ.], Ara Go, Dae Sik Yook [KINS]

12:00~12:20 The Effects of Hydride Morphologies on the Responses of SNF Claddings to the Pinch-load ····· 89
Ho-a Kim, Yong-soo Kim, Won-young Lim [Hanyang Univ.], Jae-soo Noh [ACT]

12:20~12:40 Preliminary Studies on Residual Radioactivity Concentration of Spent Nuclear Fuel Dry Storage System After Design Lifetime ····· 91
Sae Geun Lee, Jae Hak Cheong [Kyung Hee Univ.]

2분과 사용후핵연료 처분전관리 (Poster)

P0201 Effect of Packing Density on Evaporation of Adhered Salt ····· 95
S.W. Kwon, J.H. Jung, S.J. Lee [KAERI]

P0202 Manufacture of Engineering-Scale Remote Injection Casting Device and Fuel Slug ····· 96
Hoon Song, Yoon-Myung Woo, Sang-Gyu Park, Jeong-Yong Park [KAERI]

P0203 Cladding Temperature Trend of a Spent Fuel Assembly in Boundary Condition With High Temperature ····· 98
Hyungjin Kim, Sang-Jin Lee [KORAD]

P0204 Status of Barrier Cladding Technology for Enhancing Performance of the Metal Fuel ····· 100
Jun Hwan Kim, Sunghwan Yeo, Sung Ho Eom, Sung Ho Kim, Jeong Yong Park [KAERI], Tai Hong Yim [KIT]

P0205 Integrity Verification of the CANDU Spent Fuel Using a Plastic Scintillator ·· 102
Yewon Kim, Myungsoo Kim, Heejun Chung, Seunghoon Park [KINAC]

P0206 Temperature Distribution of Innovative Metallic Fuel With Multi-hole Shapes ·· 104
Young-Ho Lee, Sung-Uk Lee, Sang-Gyu Park, ByoungOon Lee, KiHo Kim, Jeong-Yong Park [KAERI]

P0207 Criticality Evaluations of KN-12 Cask for Spent Nuclear Fuel Failure Scenarios ····· 106
Kyoonho Cha, Do-Yeon Kim [KHNP-CRI]

P0208 An Analytic Study on the Correlation Between Angularly Biased Emission of Prompt Neutrons and Sample Multiplication ····· 108
Seonkwang Yoon [UST], Hee Seo [Chonbuk Natl. Univ.], Young-su Kim [KIRAMS], Chaehun Lee, Ho-Dong Kim [KAERI]

P0209 Derivation of the Major Factors to Ensure the Operating Safety of the Spent Nuclear Fuel Storage Facility ····· 110
Jae Wook Kim, Han Young Joo, Joo Hyun Moon [Dankook Univ.]

P0210 Review of Periodic Verification on WOLSONG SNF Dry Storage Systems ·· 112
Sunghwan Chung, Donghee Lee, Taehyeon Kim, Kiyoung Kim, Yongdeog Kim [KHNP-CRI]

P0211 A Study on Applicability of NUREG-1520 for Pyroprocessing Facilities ····· 114
Gilsung You, Woojin Jo, Siwan Noh, Seungnam Yu, Hyojik Lee, Hohee Lee, Jeonghoe Ku, Seokjun Seo [KAERI]

P0212 Establishment of Data Acquisition System for Road and Sea Transportation Test of Surrogated Spent Nuclear Fuel Under Normal Conditions of Transport ··· 116
JaeHoon Lim, Sang Soon Cho, Yun-young Yang, Kiseog Seo, Woo-seok Choi [KAERI]

P0213 Multi-body Dynamics Analysis for Road Transportation Test of Surrogate Spent Nuclear Fuel Under Normal Conditions of Transport ····· 118
JaeHoon Lim, Sang Soon Cho, Gil-Eon Jeong, Yun-young Yang, Kiseog Seo, Woo-seok Choi [KAERI], Dae-Han Choi [ableMAX]

P0214 Autonomous Sensor Transport System for DCSS Inspection ····· 120
Daewon Kim, Kyoungwon Yoon, Kyoungyong Noh, Misuk Jang, Seoung Rae Kim [NESS]

P0215 Preliminary Test Plan of Vacuum and Forced Helium Drying for Canister ·· 122
Seung-hwan Yu, Ju-Chan Lee, Kyung-sik Bang, Woo Seok Choi [KAERI]

P0216 Scenario Evaluation for Damaged Spent Nuclear Fuel Transport ····· 124
Suk Woo Hong, Sangbok Ahn, Dosik Kim, Jeong-Nam Jang, Hyoung-Mun Kwon, Sung Geun Kim, In-Chan Kwon, Myung Chul Park, Jae Han Kim [KAERI]

P0217 Review of Container for Transporting Damaged Spent Nuclear Fuels ····· 126
Suk Woo Hong, Sangbok Ahn, Dosik Kim, Jeong-Nam Jang, Hyoung-Mun Kwon, Sung Geun Kim, In-Chan Kwon, Myung Chul Park, Jae Han Kim [KAERI]

P0218 Effect of Inlet Air Temperature on Adhesion Force of Vacuum Type Sensor Carrier ····· 128
Kyoungwon Yoon, Daewon Kim, Misuk Jang, Seoung Rae Kim [NESS]

P0219 Radiological Assessment Considering Irradiated Top Nozzle of Spent Fuel Assembly ····· 130
Kiyoung Kim, Donghee Lee, Sunghwan Chung, Yongdeog Kim [KHNP-CRI], Jaehun Ko [KONES]

P0220 Feasibility Analysis for Fire Test of CANDU Spent Fuel Transport Cask Using a Scaled-Down Model ····· 132
Ju-Chan Lee, Kyung-Sik Bang, Seung-Hwan Yu, Yun Young Yang, Woo-Seok Choi [KAERI]

P0221 Computational Analysis to Evaluate Similarities Between Full and Scaled-down Model in Drop Test of Radioactive Waste Transport Casks ····· 134
Jongmin Lim, Ki Seog Seo, Ju-Chan Lee, Jae-Han Lee, Woo-seok Choi [KAERI]

P0222 Mock-up for Remote Fuel Slug Fabrication ····· 136
Kiho Kim, Sanggyu Park, Jeongyong Park [KAERI]

P0223 Current Status of Application of Safeguards to Geological Repositories ····· 138
Ju Young Jeon [KINAC]

P0224 Development of Damaged Fuel Can for Wet and Dry Storage ····· 140
Seo Jeong Lee, Sung-Chang You, Kwang-Ho Lee, Eun-Ki Lee [KHNP-CRI]

P0225 Thermal Analysis of HI-STORM 100 Dry Storage Cask in Extreme Temperature Condition With Heterogeneous Fuel Assembly Using COMSOL MULTIPHYSICS Program ····· 142
Sun Woo Park, KwangHeon Park [Kyung Hee Univ.]

P0226 Development of Temperature Calculation Program for Spent Fuel Pools ····· 144
Taehyeon Kim, Donghee Lee [KHNP-CRI]

P0227 Separation Efficiency of Enhanced Melt-crystallization Method for Purification of LiCl Salt Waste ····· 146
Jung-Hoon Choi, Ki-Rak Lee, Hyun-Woo Kang, Hwan-Seo Park [KAERI]

P0228 Development of a Fuel Assembly Model for Spent Nuclear Fuel Transportation ····· 148
Joongjin Kim, Youngik Yoo, Jinseon Kim, Ohjoon Kwon, Kyounghong Kim, Kyoungbo Eom, Hyeongkoo Kim [KEPCO NF]

P0229 Neutron Activation Calculations for DFDF Hot Cell at KAERI ····· 150
Siwan Noh, Woo Jin Jo, Gil Sung You, Seungnam Yu [KAERI]

P0230 Influencing Factors for Assessing the Spent Nuclear Fuel Integrity During Handling and Transportation ····· 152
Wooyong Choi, Donghyo Lee, Janghwan Lim, Seongki Lee [KEPCO NF]

P0231 Uncertainty Quantification of Thermal Analysis for Dry Storage Cask ····· 154
Sung Yong Lee, Jae Hun Ko, Hyo Sub Kim, Dong Gyu Lee [KONES]

P0232 Response Spectrum Analysis for Selection of Representative Spent Fuel Under Normal Conditions of Transportation ····· 156
Donghyo Lee, Hyeongkoo Kim, Seongki Lee [KEPCO NF]

P0233 Application of the Computer Codes in the Nuclear Fuel Cycle Facility ····· 158
Woo Jin Jo, Siwan Noh, Hyo Jik Lee, Seung Nam Yu [KAERI]

P0234 Modification of Light System in Large Inert Gas Filled Facility PRIDE ····· 160
Ilje Cho, Youngkuk Jang, Seonho Noh, Heeseok Kang [KAERI]

P0235 Electrolytic Reduction of Nd_2O_3 With Ni Wire Electrode in Molten LiCl at 923 K ····· 162
Dokyu Kang, Sungyeol Choi [KAIST]

P0236 Estimation of On-site SF Storage Capacity With and Without Centralized Interim Storage by Using GoldSim Code ····· 164
Hong Jang, Hyo On Nam, Yong-Soo Hwang [KAERI]

P0237 Preliminary Performance Test of Drying Test System Using Inert Gas ····· 166
Kyung-Wook Shin, Gyung-Sun Chae, Geon-Hui Lee, Jae-Seok Park [SAE-AN Eng.], K.S.Bang, S.H.Yu [KAERI]

P0238 Analysis of Comparison Between Original and Quarter Scale Model of Transport Cask for Large Capacity SNF ····· 168
Yun-young Yang, Jongmin Lim, Woo-seok Choi [KAERI]

P0239 Effect of Surrogate Elements on the Electrochemical Behavior and Deposit Characteristics of U in LiCl-KCl-UCl_3 Molten Salts ····· 170
Chang Hwa Lee, Sung-Jai Lee [KAERI]

P0240 Experimental Studies for Two Operation Modes of Drying System of Pyroprocessing Automation Mockup ····· 172
Jonghui Han, Seungnam Yu [KAERI]

P0241 Preliminary Evaluation for Efficient Operation of Spent Fuel Pool Cooling System of Kori Unit 2 After Permanent Shutdown ····· 174
Ha-eun Jeong, Seokyoung Ahn [Pusan Natl. Univ.]

P0242 Model Development for Estimating Electrochemical Parameters in a Rotating Disk Electrode System ····· 176
Kwang-Rag Kim, Sung-Ki Kim, Hyo On Nam [KAERI]

P0243 Consideration on the Conversion Characteristic of Uranium Ions to Metal in the LiCl-KCl Salt With the Aid of Yttrium Metal ····· 178
Joon-Bo Shim, Dal-Sung Yoon, Sung-Jai Lee [KAERI]

P0244 Economics of a Nuclear Fuel Cycle Under Circumstances of the Energy Transition ····· 180
Hyo On Nam, Hong Jang [KAERI]

P0245 Surface Treatment of Zirconium Contamination Layer Using Laser Ablation ··· 182
Seong-Jun Ha, Young-Kook Lee [Yonsei Univ.], Ki-Hwan Kim, Jeong-Yong Park, Seoung-Woo Kuk [KAERI]

P0246 Radiation Shielding Evaluation for Large Capacity CANDU Spent Fuel Transportation Cask ····· 184
Jae-Hun Ko, Dong-Gyu Lee, In-Soo Jung [KONES]

P0247 Criticality Analysis for OASIS-24DFC Cask Capable of Loading Damaged Fuel Assemblies ····· 186
Tae Kyung Lee, Yong IL Kim, Joon Gi Ahn, Gyu Cheon Lee [KEPCO E&C]

P0248 Zr-based Cladding Fire During Loss-of-Coolant-Accident in a Spent Fuel Pool ····· 188
Sun Ki Kim, Dong Hak Kook [KAERI]

P0249 Development of a Spacer Grid Model for Spent Nuclear Fuel Assembly ····· 190
Youngik Yoo, Kyounghong Kim, Kyongbo Eom, Joonkyoo Park [KEPCO NF]

P0250 Modal Analysis of KORAD-21 Road and Sea Transport Test Model ····· 192
Gil-Eon Jeong, Yun-Young Yang, Jaehoon Lim, Sang Soon Cho, Ki-Seog Seo, Woo-Seok Choi [KAERI]

P0251 Canceled
Rotary Bending Fatigue Test of Section-wise Simulated Cladding for Spent Nuclear Fuel Transportation
Kang Hee Lee, Heung Seok Kang, Jae Yong Kim, Yong Sik Yang, Dong Hak Kook [KAERI]

P0252 Deformation Analysis on the Thermal Effect of Vol-oxidizer Reactor ····· 196
Younghwan Kim, JuHo Lee, Yungzun Cho [KAERI]

3분과 고준위폐기물처분 (Oral)

09:00~09:20 A Disposal Concept of Spent Nuclear Fuel in Deep Horizontal Drillholes ····· 201
Kyungsu Kim [KAERI]

09:20~09:40 Vitrification of the Spent Nuclear Fuel Using Iron Phosphate Glasses ····· 203
Cheong Won Lee, Jong Heo [POSTECH]

09:40~10:00 Sorption Characteristics of Strontium and Nickel on Container Corrosion Products Under the Disposal Conditions: Case Study for Mackinawite in Alkaline Conditions ····· 205
Chung-Kyun Park, Tae-Jin Park, Seung-Yup Lee, Jae-Kwang Lee [KAERI]

10:00~10:20 The Removal of Arsenic and Uranium From Aqueous Solution by Sorption Onto MgO-coated Waste Coal ····· 207
Bong-Ju Kim, Jang-Soon Kwon [KAERI], Soonjae Lee [Korea Univ.]

11:20~11:40 Numerically Investigating Effect of Dispersivity Ratio on Heat Transport in Fully Saturated Porous Medium ····· 209
Byeong-Hak Park [KAERI], Kang-Kun Lee [Seoul Natl. Univ.]

11:40~12:00 Spectroscopic Properties of Natural Organic Matters in KURT Groundwater ··· 211
Euo Chang Jung, Tae-Hyeong Kim, Jang-Soon Kwon, Wansik Cha, Min Hoon Baik [KAERI]

12:00~12:20 Saturated Hydraulic Conductivity Model for the Korean Compacted Bentonite Installed in In-DEBS ····· 213
Seunghun Park, Sangki Kwon [Inha Univ], Seok Yoon, Geonyoung Kim [KAERI]

12:20~12:40 Hydrogeochemical Investigation in the Geological Repository Site for LILW Disposal During Construction in Korea ····· 215
Jang-Soon Kwon, Yong-Kwon Koh [KAERI]

3분과 고준위폐기물처분 (Poster)

P0301 Hydrogeochemical Characteristics of the Deep Environment for Granitic and Gneissic Lithologies in South Korea ····· 219
Jang-Soon Kwon, Yong-Kwon Koh [KAERI], Soonyoung Yu [Korea Univ.]

P0302 Enhancement of Bayesian Belief in Flow Rates in the Repository for SNFs by Sequential Updating of the Hydraulic Conductivity Distribution ····· 221
Youn-Myoung Lee, Dong-Keun Cho [KAERI]

P0303 Effect of Geochemical Conditions on the Sorption of Radionuclides by Granite ····· 223
Jae-Kwang Lee, Min-Hoon Baik, Jongtae Jeong, Ji-Hun Ryu [KAERI]

P0304 Shearing Technology of Simulated Nuclear Fuel Rod Using Colling and Notching ····· 225
Younghwan Kim, Yungzun Cho, Jinmok Hur [KAERI]

P0305 Simulations of Dipole Flow Tracer Test for Estimating Locally Variable Hydraulic Property ····· 227
Nak-Youl Ko, Kyung-Woo Park, Sung-Hoon Ji [KAERI]

P0306 Investigation Plan for the Geological Environment for URL Site in Korea ····· 229
Jin-Wook Kim, Chang-Lak Kim [KINGS]

P0307 Physical and Mineralogical Changes of the Compact Bentonite in Underground Environment ····· 231
Minsoo Lee, Sung-Hoon Ji [KAERI]

P0308 Groundwater Chronology in Fractured Granitic Bedrock in South Korea ····· 233
Jihye Jeong, Jang-Soon Kwon, Yong-Kwon Koh, Jae-Kwang Lee [KAERI]

P0309 Investigation of Thermal Conductivity for the Bentonite Particles ····· 235
Seok Yoon, Geonyoung Kim [KAERI], Seunghun Park [Inha Univ.]

P0310 A Study on Concept Development of a Horizontal Disposal for CANDU Spent Fuels ····· 237
Jong-youl Lee, Hyun-a Kim, In-young Kim, Heui-joo Choi, Dong-keun Cho [KAERI]

P0311 Fracture Study Using Borehole Dara and Microstructural Analysis of Fracture Filling Minerals Around KURT Site ····· 239
Soolim Jung, Sung-Hoon Ji, Kyung-Su Kim [KAERI]

P0312 Analysis on Characteristics of Structural Materials in the PLUS7 PWR SNF ··· 241
In-Young Kim, Dong-Keun Cho [KAERI]

P0313 Development of an Input Database for the Post-closure Safety Assessment of a Radioactive Waste Repository ····· 243
Jongtae Jeong, Dong-Keun Cho [KAERI]

P0314 Thermal Behavior of Montmorillonite in Korean Bentonite Under the KURT Groundwater Saturated Conditions ····· 245
Tae-Jin Park [KAERI], Donghoon Seoung [Chonnam Natl. Univ.]

P0315 Development of Far-field Hydraulic Module of APro ····· 247
Jung-Woo Kim, Jaewon Lee, Kyung Woo Park, Dong-Keun Cho [KAERI], Minjeong Kim [UNIST]

P0316 Characteristic Sorption of Iodine by Heat-treated Samples of Cu_2S Under Anaerobic Conditions ····· 249
Hyo-Jin Seo, Seung Yeop Lee, Heejae Ju, Jae-Kwang Lee [KAERI]

P0317 Heat Transfer Modelling of A-KRS on the Contact Condition ····· 251
Seunghyun Kim, Sanghwan Lee, Sangjin Lee [KORAD]

P0318 Geochemical Model for the Oxidative Dissolution UO_2 in a Geological Repository ····· 253
Heejae Ju, Ji-Hun Ryu, Seung Yeop Lee, Jae-Kwang Lee [KAERI]

P0319 A Comparative Study of Using Single-component and Multi-components for a Geological Disposal System in APro ····· 255
Minjeong Kim [UNIST], Jung-Woo Kim, Jaewon Lee, Kyung Woo Park, Dong-Keun Cho [KAERI]

P0320 Development of Two-phase Transport Model of Radionuclides in Porous Media Using COMSOL Multiphysics ····· 257
Jaewon Lee, Jung-Woo Kim, Dong-Keun Cho [KAERI]

P0321 Geological Environments for Deep Disposal of Radioactive Wastes in Korea ··· 259
Won-Jun Choi [Pusan Natl. Univ.], Seongjin Ryu [Pukyong Natl. Univ.], Chang-Lak Kim [KINGS]

P0322 Assessment of Hydrogeological Characteristics in BDZ Boreholes in KURT ··· 261
Kyung-Woo Park, Sung-Hoon Ji, Nak-Youl Ko [KAERI]

P0323 Parameter Determination for the Mechanical Constitutive Model (BBM) of Bentonite Buffer: Saturated Material Constants ····· 263
Jae Owan Lee, Seok Yoon, Geon Young Kim [KAERI]

P0324 Hyrothermal Analysis of a Double-layered Bentonite in Two-layered Repository Using TOUGH2 Code: High Performance Buffer ····· 265
Jin-Seop Kim, Won-Jin Cho, Geon-Young Kim [KAERI]

4분과 중저준위폐기물관리 (Oral)

09:00~09:20 The Structural Stability Analysis of a 16-pack Disposal Container Disposed of in Gyeongju LILW Repository ····· 269
Hyeongjin Byeon, Gwan Yoon Jeong, Yeonghwan Jeon, Hyewon Shin, Jaeyeong Park [UNIST]

09:20~09:40 A Study on the Dose Assessment Methodology for Worker by Radioactive Waste Clearance Recycling Scenario ····· 271
Ji Young Song, Ki Baek Shin, Junhyuck Im [KAERI]

09:40~10:00 ISO/PWI 24389-1 Through 4, The Pre-disposal and Disposal for L&IL Radioactive Waste From Decommissioning ····· 273
Kwangyoung Sohn, Changhwan Cho, Sungjong Kim [MIRAE-EN], Namchan Cho [KEPCO NF]

10:00~10:20 Leaching Behaviors of Co_2, Cs, and I From Geopolymer and Cement Waste Forms Containing High-sulfate Sludge Waste ····· 275
Seongye Kwon, Jinmo Ahn, Wooyong Um [POSTECH]

11:20~11:40 Verification of Efficiency Calculation for an Overpack 320 L Drum Containing Compressed 200 L Radioactive Waste Drum ····· 277
Sang Mo Ham [Kyung Hee Univ.], Sung Yeop Jeong [Godo-Tech]

11:40~12:00 Dynamic Changes of Groundwater Chemistry in the LILW Disposal Facility Along the Coastal Area ····· 279
Eunhye Kwon, Jonghoon Park, Nam C. Woo [Yonsei Univ.]

12:00~12:20 Study on the Establishment of Grouping Analysis Range for KAERI's Radioactive Waste Using Concentration Averaging Method ····· 281
Dong-Ju Lee, Junhyuck Im, Dae-Seok Hong, Il-Sik Kang [KAERI]

12:20~12:40 A Proposal of "Innerpack" Design Concept for Efficient Transport and Disposal of Radioactive Waste ····· 283
Moonoh Kim, Wooyoung Kim, Nakhoon Sung [KONES]

4분과 중저준위폐기물관리 (Poster)

P0401 A Study on the Input Data for Radionuclides Behavior Assessment of Combustible Radioactive Waste in Decommissioning Nuclear Power Plants ··· 287
Sang Heon Lee, Jong Soon Song [Chosun Univ.], Jung Suk Park, Chang Hyun Ryu, Cheol Hyun Hwang [KEPCO NF]

P0402 Dissolution Characteristics of Silver Tellurite Glass Containing ^{129}I ····· 289
Cheong-won Lee, Bansuk Yu, Jong Heo [POSTECH]

P0403 Assessment of the Near Surface Disposal Facility According to Disposal Containers Usage Plan ····· 291
Hyungoo Kang, Changmin Shin, Sanghwan Lee, Hoseog Dho [KORAD]

P0404 Increased Homogeneity of Epoxy Solidifications by Ball-mill Treatment ····· 293
Seonggon Ryu, Misuk Jang, Seoung Rae Kim [NESS]

P0405 A Study on the Management of Radioactive Waste in Major Countries for Exporting Nuclear Power Plants ····· 295
Ji-woon Lee, Jin-kyu Choi, Eun-young Kim [KEPCO E&C]

P0406 Reviews of the Technologies to Carry Out the Development Project of NPP Decommissioning Radioactive Waste Certification Program (WCP) ····· 297
Tae-man Kim, Jae-chul Ha, Ji-seon Jang, Chun-hyung Cho [KORAD]

P0407 A Study on the Analytical Method for Clearance of Decommissioning Waste ···· 299
Younggook Kim, Jae Yong Oh [KHNP-CRI]

P0408 A Study on the Reduction Method of Radioactive Liquid Waste Using Outdoor Air Control Unit With Heat Pipe System ····· 301
Youngwoo Kwon, Heeseok Kang, Youngkuk Jang, Seonho Noh, Ilje Cho [KAERI]

P0409 Analysis of Disposal Container and Waste Acceptance Criteria for Landfill Disposal of Very Low Level Waste ····· 303
K.H. Park, K.H. Lee, U.J. Lee, S.W. Chung [ORIONENC]

P0410 The Implementation Scenario for Waste Certification Program (WCP) ····· 305
Sungjong Kim [MIRAE-EN], Jin-hang Lee, Jung-bo Yang, Seung-hoon Han [KEPCO NF]

P0411 The Economic Evaluation of Liquid Radioactive Waste Management System for SMART ····· 307
Jin-Kyu Choi, Han-Jeong Na, Jae-Hwa Yoon [KEPCO E&C]

P0412 A Study on Evaluation and Prediction of the Radionuclide Inventory for Efficient Operation of the Combined Disposal Facility ····· 309
Sun Il Kim, Ki Tae Yang, Jong Soon Song [Chosun Univ.]

P0413 A Study on Fractional Release Rates of Nuclides for Normal and Earthquake Scenarios From a Concrete Vault of Near-Surface Disposal Facility ····· 311
Hyosub Kim, Moonoh Kim, Beomho Park, Kihyun Kim, Jaewoo Park, Jae-Hun Ko, Dong-gyu Lee, Suk-Nam Lim, Nakhoon Sung, Young-Sun Jang [KONES]

P0414 Development of Equipment for Removing Free Water in Radioactive Waste Using Low-temperature Dry Air ····· 313
Hyung kwon Jeong, Dong kyu Jang, Cheol yeong Jeong, Jeong won Park [Actrmt]

P0415 Safety Comparison of Marine and Land Transport for Low and Intermediate Level Radioactive Waste ····· 315
JeongMi-Lee, ByeongMok-Park, AhRan-Cha, CheolWan-Park, SangJin-Lee [SAE-AN ENERTECH]

P0416 Development of Cement Waste Form for Decommissioning Wastes of Nuclear Power Plant ····· 317
Ju-hyeok Lee, Jaeeun Kang, Jaehyuk Kang, Wonseok Kim, Wooyong Um [POSTECH]

P0417 Application of ED-XRF Measurement on Uranium Contaminated Soil Waste for Regulatory Clearance ····· 319
Mal-Go-Bal-Gae-Bit-Na-La Yoo, Ji-Young Park, Jong-Myoung Lim, Won-Hyuk Jang, Dae-Seok Hong [KAERI]

P0418 Investigating the Necessity of a Waste Certification Program (WCP) to Manage Radioactive Waste From Decommissioned NPPs ····· 321
Hyeongmin Park, Sooyeun Park, Suri Park, Heekyung Kim, Eunsuk Choi, Sangkoo Han, Dongsik Jin, Heesoo Bae, Yongho Hong [ACT]

P0419 Experimental Study of the Cement Waste Forms With Concrete Waste ····· 323
Donghee An, Hyunkook Choi, Jaeyoung Kim [SungShin Cement]

P0420 Conceptual Design of Radioactive Waste Classification Using an Object Recognition Technologies ····· 325
Sung-Chan Jang, Dong-Ju Lee, Il-Sik Kang, Jeong-Guk Kim, Dae-Seok Hong, Hee-Seoung Park [KAERI]

P0421 Development of Glass for Vitrification of Fukushima Liquid Waste With Cold Crucible Induction Melter ····· 327
Sunghoon Hong, Young Hwan Hwang, Jung-Su Jung [KHNP-CRI], Toshiro Oniki [IHI Yokohama Eng. Center]

P0422 Preliminary Evaluation of the Surface Dose Rate for the Waste Package Type of Low and Intermediate Level Radioactive Waste ····· 329
Rin-Ah Kim, Ho-Seog Dho, Tae-Man Kim [KORAD]

P0423 Preliminary Radiation Shielding Evaluation of the Conceptual Disposal Container for the Decommissioning Waste ····· 331
Ho-Seog Dho, Taeman Kim, Chun-hyung Cho [KORAD]

P0424 Technology Development Status of High Integrity Container in Domestic and International ····· 333
Mi-Hyun Lee, Young Hawn Hwang, Ji-Hoon Lee [KHNP-CRI]

P0425 Leaching Behavior of Two Waste Glass Forms (Iodine-Tellurite and Rhenium-Tellurite) Under Radioactive Waste Repository Conditions ····· 335
Samiratu Atibun Isa, Jaeeun Kang, Jueun Kim, Sangsu Park, HyunJu Kim, Cheong Won Lee, Jae-Young Pyo, Jong Heo, Wooyong Um [POSTECH]

P0426 Stabilization of UF_6 in KAERI : Focused on D-UF_6 Sampling ····· 337
YuJeong Choi, Jongjin Kim, Jeong-Guk Kim, Dae-Seok Hong [KAERI]

P0427 Co^{60} & Eu^{152} Removal From Dissolved Concrete Liquor: Initial Precipitation Studies ····· 339
Richard I. Foster, Maengkyo Oh, Kwang-Wook Kim, Keunyoung Lee [KAERI]

P0428 Removal of Antimony From Effluents Generated During the Korean SENSEI Process: Iron Precipitation & Coagulation-Flocculation-Filtration Studies ····· 341
Richard I. Foster, Maengkyo Oh, Kwang-Wook Kim, Keunyoung Lee [KAERI]

P0429 Development of Hazardous Chemicals Treatment Technology in Radiation Management Area ····· 343
Jeongsu Jeong, Sunghoon Hong, Mi-Hyun Lee [KHNP-CRI]

P0430 An Analysis on Waste Treatment Research Trend for Designing a New Rad Waste Treatment Facility ····· 345
San Chae, Jongjin Kim, Jeong-Guk Kim, Dae-Seok Hong [KAERI]

P0431 Review on the Treatment and Disposal of Long-Term Decayed High-Dose Spent Filter in Nuclear Power Plant ····· 347
Hang-Rae Cho, Sung-Hoon Hong [KHNP-CRI]

P0432 Shielding Evaluation of 860L PC-HIC for Packaging of Concentrated Liquid Waste ····· 349
Jong-seon Jeon, Hong-goo Lee, Byung-Yoon Min [Kyelim], Jong-Min Park [KHNP], Ki-Ho Park [Soosan ENS]

P0433 Treatment System of Clearance Waste at KAERI ····· 351
Won Hyuk Jang, MalGoBalGaeBitNaLa Yoo, Tae Su Song, Joone Hee Lee, Jeong Guk Kim, Dae Seok Hong [KAERI]

P0434 Expansion of Deregulation System for Very Low-Level Waste (VLLW) ····· 353
Jeong-Guk Kim, Won Hyuk Jang, MalGoBalGaeBitNaLa Yoo, Dae-Seok Hong [KAERI]

P0435 A Preliminary Study on the Availability of Big Data for Isotopic Scaling Factor Effect on Radioactive Waste Storage Drum ····· 355
Seung Uk Yoo, Chang Je Park [Sejong Univ.]

P0436 Development of Candidate Porous Materials to Extract Alkanes From Liquid Radwastes ····· 357
Jongjin Kim, Junhyuck Im [KAERI], Hyungwoo Kim, Donghoon Seoung [Chonnam Natl. Univ.]

P0437 Radiological Dose Assessment for Regulatory Clearance of Soil Radioactive Waste at KAERI ····· 359
Ki-Baek Shin, Won-Hyuk Jang, Malgobalgaebitnala Yoo, Junhyuck Im, Dae-Seok Hong [KAERI]

5분과 제염해체 (Oral)

09:00~09:20 Development of the Pushing Type Cutting Device to Dismantle Biological Shield Concrete for Decommissioning of Nuclear Power Plant ····· 363
Bong-Jae Lee, Yong-Kyu Kwon, Chang-Dong Hong, Kyong-Nam Min [Sejong E&C]

09:20~09:40 Removal of Cobalt From the Radioactive Concrete Waste Using Sink-Float Separation ····· 365
Seok-ju Hong, Sangsoo Han, Seongsik Nam, Won-Seok Kim, Wooyong Um [POSTECH]

09:40~10:00 Underwater Cutting of Thick Stainless Steels With High-power Fiber Lasers Aimed at Dismantling Nuclear Facilities ····· 367
Jae Sung Shin, Seong Yong Oh, Hyunmin Park, Gwon Lim, Taek-Soo Kim, Lim Lee, Chin-Man Chung, Jonghwan Lee [KAERI]

10:00~10:20 Introduction a Case Study for Radio-cesium Fallout Pattern for Determination of Optimum Decontamination Depth in Forest Soil ····· 369
Seongjoo Kang, Seungil Kim, Dukwon Kang [Elim-Global], Minoru Yoneda [Kyoto Univ.]

11:20~11:40 Application of Gross Alpha Determination in Radioactive Waste Characterization ····· 371
Hyuncheol Kim, Mee Jang, Jong-Myoung Lim, Ji-Young Park, Ha-Jin Song, Young-Gun Ko, Sang-Bum Hong [KAERI]

11:40~12:00 Analytical Method for Determination of ^{41}Ca in Concrete ····· 373
Yong-Jin Lee, Ji-Young Park, Jong-Myoung Lim, Sang-Bum Hong, Hyuncheol Kim [KAERI], Jin-Hong Lee [Chungnam Natl. Univ.]

12:00~12:20 Chemical Decontamination Process for Primary Coolant System in Nuclear Facility ····· 375
Jungsoon Park, So-Jin Park [Chungnam Natl. Univ.], Hee-Chul Eun, Seonbyeong Kim, Changhyun Roh, Bumkyoung Seo [KAERI]

12:20~12:40 Synthesis of Chalcogenide Sorbent for Cs Removal ····· 377
Sangsu Park, Jaehyuk Kang, Wooyong Um [POSTECH]

5분과 제염해체 (Poster)

P0501 Magnetic Separation of ^{133}Cs–illite From Soil Using Surface Functionalized Fe_3O_4 Nanoparticles ····· 381
June–Hyun Kim [Kyungpook Natl. Univ.], Sung–Man Kim, In–Ho Yoon, Ilgook Kim [KAERI]

P0502 Review of Evaluation of Robotics and Automation for Decommissioning Task Applications ····· 383
Jihwan Yu, Jungwun Kim [KHNP–CRI]

P0503 An Approach to the Strategic Implementation for Stakeholder Involvement Management During Decommissioning of Nuclear Facilities ····· 385
KwanSeong Jeong, InHye Hahm, JaeHyun Ha, SangBum Hong, BumKyoung Seo [KAERI]

P0504 Methodology for Calculating the Internal Exposure Dose of Workers on Decommissioning Nuclear Power Plant ····· 387
Changyeon Yoon, Kirim Kim [KHNP–CRI]

P0505 Development of a Program to Calculate External Exposure Dose of Workers on Decommissioning Nuclear Power Plant ····· 389
Changyeon Yoon, Kirim Kim [KHNP–CRI]

P0506 Redistribution of WBS–based Korean NPP Decommissioning Cost by ISDC ·· 391
Jae Yong Oh, Jungwun Kim, Hyung–woo Seo [KHNP–CRI]

P0507 Development of 5D Program for Decommissioning Schedule, Waste Quantity and Cost ····· 393
Jae Yong Oh, Younggook Kim, Jihwan Yu, Taesik Yun, Jae–Gon Lee [KHNP–CRI], Kyeongmin Song, Ilsoo Park [WIBTEL], Nak–Hoon Sung, Seunghyuk Jung [KONES]

P0508 Preparation of Project Management in Final Decommissioning Plan ····· 395
Jae Yong Oh, Jin–Won Son, Jungwun Kim [KHNP–CRI]

P0509 Efficient Removal of Cesium Ions From Aqueous Solution Using Alginate/Prussian Blue Composite Hydrogel Bead ····· 397
Seung Han Woo [Hanbat Natl. Univ.], Ohemeng–Boahen, Godfred [Life Green Tech.]

P0510 Evaluation of Radionuclide Inventory in Concrete of Kori Unit 1 ····· 399
Mee Jang, Hyunchul Kim, Chang Jong Kim, Ji Young Park, Jong Myoung Lim [KAERI]

P0511 Logistical Simulation Prerequisites for a Soil Remediation Process Scheduling ····· 401
Eui–taek Lee, David Kessel, Chang–Lak Kim [KINGS]

P0512 Evaluation of Decommissioning Applicability of the Requirements for the Spread of Contamination and Minimization of Radioactive Wastes ····· 403
Hyo Jin An, Hyung Gon Jin [KAERI], Seung Kook Park, Jin Ho Park [NUDECOMM]

P0513 Permanganate Self-decomposition Behavior in the HyBRID Oxidative Decontamination Process by Using Cr_2O_3 Pellets ····· 405
Yoon-Ji Park, Hyun-Kyu Lee, Seungyeop Han, Wonzin Oh, Sang-June Choi [Kyungpook Natl. Univ.]

P0514 Case Study of Hanford Site-specific Hydrologic Parameter Establishing Procedure ····· 407
SangJune Park, Jihyang Byon, Seokyoung Ahn [Pusan Natl. Univ.]

P0515 Readiness Review of APR1400 Decommissioning Design for UK Export ····· 409
Hye-Young Shin, Dae-Jun Kim [KHNP-CRI]

P0516 Removal of Manganese Ion in the HyBRID Decontamination Process Using Electrochemical Method ····· 411
J.H. Sim, S.Y. Park, S.B. Kim [KAERI]

P0517 Production of Zr Metal by Decomposition of ZrCl at High Temperature ····· 413
Jungho Hur, Gwan Yoon Jeong, Younghwan Jeon, Hyeongjin Byeon, Hyewon Shin, Jaeyeong Park [UNIST]

P0518 Considerations of Hazardous Materials in Decommissioning of Nuclear Power Plant ····· 415
Su-Hee Lee, Hye-jin Jung [KHNP-CRI]

P0519 Prediction of Waste From Site Remediation for Kori 1 ····· 417
Kyung-Min Go, Chang-Lak Kim [KINGS]

P0520 Deep Soil Remediation and Regulatory Case in the U.S. ····· 419
Won-Jae Shin, Chang-Lak Kim [KINGS]

P0521 A Conceptual Study for the Separation of Clean Aggregate From Radioactive Concrete Waste ····· 421
Keunyoung Lee, Bum-Kyoung Seo [KAERI] Maengkyo Oh [Yonsei Univ.]

P0522 Process-Based Approach for Verification, Validation, and Testing (VVT) of Waste Stream in Comprehensive NPP Radioactive Waste Processing Facility ···· 423
Sun-Kee Lee, Chang-Lak Kim [KINGS]

P0523 Analysis of Uranium Contaminated Soil Characterization ····· 425
Seung Su Shin, Chang Heon Lee, Pu Reun Kim, Seung Min You [Nuclear Decommissioning Reasearch Institute]

P0524 Fenton-based Colorimetric Reaction for Sensitive Detection of Hydrazine Degradation ····· 427
Jungsoon Park, Hee-Chul Eun, Seonbyeong Kim, Bumkyoung Seo, Changhyun Roh [KAERI]

P0525 Solvent Extraction of Cobalt, Europium, and Calcium by Extractant D2EHPA in N-dodecane From the Hydrochloric Acid Solution ····· 429
Iksoo Kim, Maengkyo Oh, Keunyoung Lee [KAERI]

P0526 The Influence of Work Activities During the Transition of a Permanently Shut-Down NPP on Worker ····· 431
H.Y. Lee, S.I. Kim J.S. Song [Chosun Univ.]

P0527 Mock-up Test for the Decontamination Demonstration of a Contaminated RCP Shaft Using the Enhanced HyBRID Process Equipment ····· 433
Jung-Hyun Lee, Jung-Yeop Cha, Dong-Yeon Kim, Ju-Hyeon Park, Dae-Kyun Kang, Sung-Hyun Lee, Hye-Min Cho, Ki-Chul Kim [KEPCO KPS]

P0528 Preliminary Study on Improving Wastewater Treatment for HyBRID Decontamination Demonstration of a Contaminated RCP Shaft ····· 435
Jung-Hyun Lee, Dong-Yeon Kim, Sung-Hyun Lee, Hye-Min Cho, Ju-Hyeon Park, Sung-Sik Yoon, Seung-Ki Lee, Geun-Woo Kim, Ki-Chul Kim [KEPCO KPS]

P0529 Decontamination of Radionuclides in Wastewater After Soil-washing Process ····· 437
Jaeeun Kang, Juhyeok Lee, Seokju Hong, Won-Seok Kim [POSTECH]

P0530 Review of Groundwater Monitoring Program for the NPP Decommissioning ·· 439
Chan-Geun Park, Hyung-Woo Seo [KHNP-CRI]

P0531 A Feasibility Study on Soil/Groundwater Remediation for Decommissioning NPP ····· 441
Jong Sun Hwang, Hyung-Woo Seo, Jae Yong Oh [KHNP-CRI]

P0532 Study on Segmentation Process of the Bioshield Concrete ····· 443
Ju-Young Yoon, Young Hwan Hwang, Sunghoon Hong [KHNP-CRI]

P0533 A Study on Induction Melting of Radioactive Carbon Steel Waste for Decommissioning of NPPs ····· 445
Ji-Hoon Lee [KHNP-CRI]

P0534 Verification of Integrated Human Error Model Related to Decommissioning of Nuclear Power Plants ····· 447
Chang-Su Nam, Byung-Sik Lee, Sung-Mi Park [Dankook Univ.]

P0535 Data Scientific Approach for the Data of KAERI's Decommissioning Experiences ····· 449
Hyung Gon Jin [KAERI], Woori Kim [Virtual Rx]

P0536 Refinement of Performance Shaping Factors Through the Development of Integrated Human Error Model for Nuclear Power Plant Decommissioning Work ····· 451
Chang-Su Nam, Byung-Sik Lee, Sung-Mi Park [Dankook Univ.]

P0537 Analysis of Design Characteristics of Radioactive Waste Treatment Facility in Accordance With NRC Regulatory Guide 4.21 ····· 453
San Chae, Jongjin Kim, Jeong-Guk Kim, Dae-Seok Hong [KAERI],
Seungkook Park [NUDECOMM]

P0538 Analysis of Calculation Methodology on Gaseous Discharge During Decommissioning of NPPs ····· 455
Hyun Min Kim, Kwang Ho Jo [KHNP-CRI]

P0539 Study on Packaging Plan of Kori Unit 1 RV and RVI Segments ····· 457
Young Hwan Hwang, Ju-Young Yoon, Mi-Hyun Lee, Seong-Hoon Hong, Ji-Hoon Lee [KHNP-CRI], Kwang-Soo Park [Doosan HI&C]

P0540 Safety Assessment Approach for Deriving Potential Accident Scenarios During Decommissioning of Nuclear Power Plant ····· 459
Kwangho Jo, Hyun Min Kim [KHNP-CRI]

P0541 Pilot Scale Synthesis of the PB-Coated Carbonyl Iron Particles for Removal of Radioactive Cesium ····· 461
Hwa Min Kim, Hyo-Sun Bae, Chul Am Kim [Nspectra]

P0542 Contaminated Characteristic and Treatment Technology of Fine Particles (Silt/Clay) With Radionuclide ····· 463
In-Ho Yoon, Sung-Man Kim, Ilgook Kim, Chan-Woo Park, Hee-Man Yang, Bum-Kyoung Seo [KAERI]

P0543 High Resolution Measurement of Aerosols From Plasma Arc Torch Cuts on Various Metals for D&D Worker Internal Dose Calculation ····· 465
Wonseok Yang, Min-ho Lee, Nakkyu Chae, Sungyeol Choi [KAIST]

P0544 Simultaneous Removal of Both Cesium and Iodine Using Prussian Blue Functionalized Layered Double Hydroxides (PB-LDH) ····· 467
Jueun Kim, Jaehyuk Kang, Wooyong Um [POSTECH]

P0545 Utilization on Industry of NPP Decommissioning of Large-Area Compton Imaging System for Concrete Internal Activation ····· 469
Sanggeol Jeong, Sooyeun Park, Heekyung Kim, Hyeongmin Park, Taekyu Lee, Suri Park, Yong-Ho Hong [ACT], Chan Hyeong Kim, Jae Hyeon Kim, Junyoung Lee, Hyun Su Lee [Hanyang Univ.]

P0546 Plasma Assisted Cutting of Metals for Dismantling of Nuclear Reactor ····· 471
Min-Gyu Choi, Junseok Nam, Sang-Min Jeong, In-Mok Yang, Shi-Young Yang, Jun-Ho Seo [Chonbuk Natl. Univ.]

6분과 방사선환경 및 안전 (Oral)

09:00~09:20 A Development Strategy for Fully On-line Monitoring of ^{14}C From Releasing Stack in Nuclear Facility ····· 475
Sang-woo Noh, Joon-seok Lee, Seung-il Kim, Dam-hyang Kim, Duk-won Kang [Elim-Global]

09:20~09:40 Introduction to Boron Removal Technology for LRS of NPP ····· 477
Seungil Kim, Woohyeon Lee, Duckwon Kang, Sangwoo Noh, Seongjoo Kang, Damhyang Kim [Elim-Global]

09:40~10:00 The Determination of Trace U and Th Concentrations in Large Volume Groundwater Sample Using Actinide Resin and Alpha Spectrometry ····· 479
Yoo Gyum Kang, Ji-Young Park, Hyuncheol Kim, Jong-Myoung Lim, Won Young Kim [KAERI], Jin-Hong Lee [Chungnam Natl. Univ.]

10:00~10:20 Study on the Influence of ^{232}Th Daughter Nuclide in ^{222}Rn Measurement ···· 481
Giho Kwon, Seungjae Baek, Hoon Lee [KINS]

11:20~11:40 Development and Performance of Environmental Radiation Monitoring System Based on Diverse Survey Platforms ····· 483
Young-Yong Ji, Mee Jang, Kun Ho Chung, Mun Ja Kang [KAERI], Taehyung Lim [SI Detection]

11:40~12:00 Worker Dose Assessment of Continuous Radioactive Waste Treatment System ····· 485
Hyun Sik Kang, Kyoungyong Noh, Misuk Jang, Seoung Rae Kim [NESS]

6분과 방사선환경 및 안전 (Poster)

P0601 Measuring the Position of Gamma Emitting Radioactive Isotopes Using One-Dimensional Inorganic Scintillator Array Sensor ····· 489
Si Won Song, JinHong Kim, Hyun Young Shin, Bongsoo Lee [Chung-Ang Univ.]

P0602 Transfer Factors of ^{99}Tc Measured for Korean Staple Food Crops and Proposal on Their Usage ····· 491
Yong-Ho Choi, Kwang-Muk Lim, In-Jun, Dong-Kwon Keum, Hyo-Joon Jeong [KAERI]

P0603 Radiation Protection System in PRIDE Facility ····· 493
Seonho Noh, Youngwoo Kwon, Youngkuk Jang, Hee-seok Kang, Il Je Cho [KAERI]

P0604 Construction of Pretreatment and Detection System for Tritium and Gross Beta in Water Sample Around the Nuclear Facility ····· 495
UkJae Lee, Hee Reyoung Kim [UNIST]

P0605 3D Modeling of Hot Cell and Associated Utility Facility for Advanced Safety Analysis ····· 497
Seungnam Yu, Seokjun Seo [KAERI]

P0606 Application of Laser Marking Technology for Irradiated Material ····· 499
Y.M. Jung, S.J. Baik, G.S Kim, B.O. Yoo, Y.G Jin [KAERI]

P0607 The Evaluation of Absorbed Dose for Robot Transportation Device in Spent Fuel Storage Cask ····· 501
Kyoungyong Noh, Hyun Sik Kang, Misuk Jang, Seoung Rae Kim [NESS]

P0608 Effect of Exhaustion on the Indoor Thermal Environment ····· 503
Heeseok Kang, Youngwoo Kwon, Seonho Noh, Youngkuk Jang, Ilje Cho [KAERI]

P0609 Evaluation of Radiocesium Wash-off by Soil Erosion Using USLE Model ····· 505
Kyung-Suk Suh, Byung-Il Min, Jiyoon Kim, Kihyun Park [KAERI]

P0610 Optimum Sample to Detector Distance in Alpha Spectrometry ····· 507
JeongHyeon Ryu, JiYoung Park, Young Gun Ko, Jong-Myoung Lim, Wanno Lee [KAERI], Dong Jun Ahn [Korea Univ.]

P0611 Strengthen the Gas Safety Management in PRIDE ····· 509
Youngkuk Jang, Seonho Noh, Youngwoo Kwon, Hee-seok Kang, Ilje Cho [KAERI]

P0612 Radioactivity of Silicon and Silicon Carbide After Neutron Irradiation ····· 511
Ki-Man Lee, Byung-Gun Park [KAERI]

P0613 Development of a Dynamic Integrated Safety Analysis for Fuel Cycle Facilities ····· 513
Seok-Jun Seo, Seung Nam Yu [KAERI], Jong Yol Park [RIA Institute]

P0614 An Estimation of Carbon-14 Production Rate at KIJANG Research Reactor ···· 515
Ji Sung Park, Gyuhong Roh, Byungchul Lee [KAERI]

P0615 On-site Transport Risk Assessment in Hanul NPPs Using INTERTRAN Code ··· 517
Minchul Kim [KHNP-CRI]

P0616 Comparison of Atmospheric Dispersion Factors According to the Collection Period of Meteorological Data for Decommissioning of Nuclear Power Plants ····· 519
Seung-Hee Lee [KINGS], Won-Tae Hwang [KAERI], Chang-Lak Kim [KINGS]

P0617 Geochemical Factors Influencing the Radon Content in Groundwater ····· 521
Jaeeun Kang, Jinmo Ahn, Wooyong Um [POSTECH]

P0618 $DCGL_{EMC}$ According to the Variation of Baseline Area in Kori Unit 1 ····· 523
Jihyang Byon, Sangjune Park, Seokyoung Ahn [Pusan Natl. Univ.]

P0619 Study on Radiological Dose Assessment With Surface & Subsurface Layers Using RESRAD-ONSITE ····· 525
Kun-Su Lim, Sun-Kee Lee, Chang-Lak Kim [KINGS]

P0620 Radiation Measurement Uncertainty for Radiological Evaluation of Simulated Radwaste ····· 527
Ke Chon Choi, Chang Heon Lee, Se Chul Sohn, Seung Su Shin, Pu reun Kim, Seung Min You [Nuclear Decommissioning Research Institute]

7분과 방사화학 (Oral)

초청발표

09:00~09:30 Applicable Chemical/Biological Technologies to the Removal and Isolation of Radionuclides From the Nuclear Decommissioning Wastewaters and Soils ··· 531
Seung Yeop Lee, Hyo Jin Seo, Hee Jae Ju, Jae Kawng Lee [KAERI]

09:30~10:00 Chemisorption of Organic Iodides in a Metal–Organic Framework ····· 533
Jinhee Park, Byeongchan Lee [DGIST]

10:00~10:20 Treatment Technology for Contaminated Water Containing Iodine ····· 535
Jei–Won Yeon, TaeJun Kim, Minsik Kim [KAERI]

11:20~11:40 Review on Chemical Characterization of Spent Nuclear Fuel at KAERI ····· 537
Jong–Goo Kim, Jong–Yun Kim, Jeong mook Lee, Tae–Hyeong Kim, Junghwan Park, SangHo Lim [KAERI]

11:40~12:00 Study on the Interaction of Uranium(VI) With Aqueous Silicic Acid Using Time–resolved Laser Fluorescence Spectroscopy ····· 539
Tae–Hyeong Kim, Euo Chang Jung, Wansik Cha, Sang Ho Lim [KAERI], Yongheum Jo, Jong–Il Yun [KAIST]

12:00~12:20 Characterization of Colloidal U(IV) Particles Complexed With Organic Molecules Using Spectroscopic Techniques ····· 541
Hyejin Cho, Inhak Yoon, Wansik Cha [KAERI]

12:20~12:40 Boron Isotope Analysis Using Double–pulse Laser Ablation Molecular Isotopic Spectrometry ····· 543
Sung–Uk Choi, Sol–Chan Han, Jong–Il Yun [KAIST]

7분과 방사화학 (Poster)

P0701 PUREX Solvent Extraction Experiments Using ^{238}U, ^{152}Eu and ^{85}Sr Solution ··· 547
Il–Kwon Jung [KAIST], Jaeyeong Park [UNIST]

P0702 Performance of a Virtual Frisch–grid CdZnTe Detector for Prompt γ–ray Induced by 14–MeV Neutrons ····· 549
TaeWoong Lee, NakJeom Kim, SeongMin Jo [KEPCO KPS], YoungHak Kim, Ajin Jo, WonHo Lee [Korea Univ.]

P0703 Bias Correction of Density Data Obtained Using Dynamic Bubbler for High–Temperature Molten Salts ····· 551
Jong–Yun Kim, Sang–Eun Bae, Tae–Hong Park [KAERI]

P0704 In Situ High Temperature X–ray Diffraction Study of Dopant Doped Uranium Oxide ····· 553
Dong Woo Lee, Jeongmook Lee, Jong–Yun Kim, Sang Ho Lim [KAERI]

P0705 Algorithm for the Determination of Tafel Slope in the Electrochemical Analysis of Uranium Dioxide Oxidation ····· 555
Junghwan Park, Jong–Yun Kim, Tae–Hyeong Kim, Jeongmook Lee, Sang–Eun Bae, Sang Ho Lim [KAERI]

P0706 A Strategy for Desorption of Krypton Adsorbed on Porous Carbon Based on Vacuum Desorption for Krypton Enrichment ····· 557
Ju Ho Lee, Seok-Min Hong, Young-Soon Lee, Yung-Zun Cho [KAERI]

P0707 24-hour Report on the 5th Collaborative Materials Exercise (CMX-5) for Nuclear Forensic Analysis ····· 559
Na-Ri Lee, Jinkyu Park, Ranhee Park, Sun-Ho Han, Sang Ho Lim, Chi-Gyu Lee [KAERI]

P0708 2-Month Report on the 5th Collaborative Materials Exercise (CMX-5) for Nuclear Forensic Analysis : Uranium Age Dating ····· 561
Ranhee Park, Sun-Ho Han, Sang Ho Lim, Jinkyu Park, Na-Ri Lee, Chi-Gyu Lee [KAERI]

P0709 1-Week Report on the 5th Collaborative Materials Exercise for Nuclear Forensic Analysis ····· 563
Jinkyu Park, Ranhee Park, Sang Ho Lim, Sun Ho Han, Chi-Gyu Lee [KAERI]

P0710 Complementary Raman Spectroscopy and Simulation Approach to Verify the Structure of Metal-doped UO_2 ····· 565
Jeongmook Lee, Jandee Kim, Jong-Yun Kim [KAERI] Choah Kwon,
Byungchan Han [Yonsei Univ.], Young-Sang Youn [Yeungnam Univ.]

P0711 Determination of Chelating Agents by High Performance Liquid Chromatography-diode Array Detection (HPLC-DAD) ····· 567
Jihye Kim, Jai Il Park, Tae-Hong Park [KAERI], Kihwan Choi [KRISS]

P0712 Determination of O/U Ratio of UO_{2+x} by Chemical Method ····· 569
Jong-Goo Kim, Jong-Yun Kim, Jeong mook Lee, Tae-Hyeong Kim, Junghwan Park,
Hye-Ryun Cho, SangHo Lim [KAERI]

P0713 Study of 4-Nitrocatechol Adsorption on the Surface of U(IV) Nanoparticles Using Various Spectroscopic Methods ····· 571
I.H. Yoon, H.-R. Cho [UST], H. Cho, W. Cha [KAERI]

P0714 Trivalent Plutonium Hydrolysis Thermodynamics in Aqueous Solution ····· 573
S.K. Cho, H.-R Cho [UST], H.-K. Kim, W. Cha [KAERI]

P0715 Experimental Study on Electrolytic Reduction and Oxidative Extraction of Ce in LiCl-KCl/Bi System ····· 575
Jae Hong Yim, Beom Kyu Kim, Hwajeong Han, Byung Gi Park [Soonchunhyang Univ.]

1분과

핵주기정책·규제 및 비확산(Oral)

Review of Measures to Ensure the Effectiveness of the Corrective Order

Sang Cheol Hyung
Korea Institute of Nuclear Non-proliferation and Control, 1534, Yuseong-daero, Yuseong-gu, Daejeon, Republic of Korea
wakendragon@kinac.re.kr

1. Introduction

Under the Act on Physical Protection and Radiological Emergency (referred to as "Radiation Protection Act"), if a business operator has violated the protection requirements, the government orders a correction and imposes a penalty for violating the correction order.

It is necessary to examine whether the penalty clause can guarantee the effectiveness of the correction order when a nuclear licensee tries to continue to enforce it in violation of the government's order. This paper will look at the means to ensure the effectiveness of administration and see if any of these measures will be introduced in the nuclear sector.

2. Measures to secure the effectiveness of administration

2.1 Administrative punishment

A punishment as a sanction imposed by a state or local government against the other side of an administration in the event that the other party of the administration has violated its obligations under the administrative law. Penalties shall be imposed for direct violation of the purpose of public administration and fines for simple violations of duty.

2.2 Administrative forced enforcement

If an individual and specific obligation is not fulfilled, the administrative body exerts its ability directly to the body or property of the obligor to fulfill the obligation, or to realize the condition in which the obligation has been fulfilled. While administrative penalties are sanctions imposed against past violations of duties, forced enforcement is different in that it aims to realize the non-performing obligations toward the future.

- Execution by proxy: Where there is a default of duties that others may perform on their behalf, the administrative office concerned shall perform the duties on its own or a third party shall perform the duties and the expenses shall be collected from the obligator. This is the case if the owner of the building does not voluntarily withdraw the building within a certain period of time, even though the government ordered the building owner to voluntarily withdraw the building. There is no substitute for the professional and technical obligations that only the obligator can fulfil, and therefore execution by proxy cannot be applied.

- Compulsory collection: The act of realizing a condition in which the administrative office has forcibly fulfilled its obligation if obligator fails to perform its monetary obligation. For example, in the event of a failure to pay the national tax, a public sale is made.

- Charge for compelling the execution: In case of difficulties in execution by proxy, such as the demolition of an illegally constructed skyscraper, the enforcement penalty shall be imposed if the correction order is not fulfilled. It is a means to secure the fulfilment of an obligation by informing the obligatory in advance that a certain amount of money will be charged in the event of failure to perform duties.

- Direct compulsion: The act of applying force to the body and property of obligator to realize the same conditions as the obligator fulfilled his or her duty. For example, measures such as the installation of restricted access facilities are taken to close unregistered institutes.

2.3 Immediate Enforcement

It is to realize the necessary conditions directly required by the administrative agency in cases where there is no time, such as removing objects for the passage of fire trucks or protecting drunken people at police stations.

2.4 Administrative Survey

Activities such as on-site surveys, document views, or reporting requests to those subject to

investigation in order to collect information or data necessary to determine policies or perform duties (Article 2 of the Administrative Investigation Act)

2.5 Other means

(a) Penalty Surcharge- monetary sanctions imposed to deprive the entity of the economic benefits obtained by the offence or imposed on behalf of the cancellation or suspension of the business;

(b) sanctioning administrative measure – refuse, suspend, or revoke accreditation, authorization, etc. for a breach of duty.

3. Measures to secure the effectiveness of the nuclear energy field

3.1 Nuclear Safety Act

The Nuclear Safety Act can take two actions in the event of a violation of a corrective order as a result of an inspection, such as a penalty or cancellation of a permit

- Penalties of not more than 3 million won (Article 118)
- Cancellation of the permit or suspension of business/business, and penalty surcharge may be imposed instead of the suspension (Article 17, etc.)
- Penalties of 3 years and 30 million won (Article 116) for acts prescribed after the authorization is revoked or for violating a business suspension order
- Penalties and cancellations of permits can also be imposed

3.2 Radiation Protection Act

There are no licensing regulations in the Radiation Protection Act. So, there are no regulations for cancellation of the permit. Although a nuclear power operator is obliged to obtain approval for physical protection regulations, there is no requirement to cancel them, as the cancellation would create a larger gap in protection. There is just penalty clause of 1 year/10 million won is applied.

4. Complementing measures to ensure effectiveness

Under the current law, measures such as administrative punishment, administrative investigation, penalty surcharge and sanctioning administrative measure can be taken to ensure the effectiveness of the administration in the nuclear energy field. However, there is no such regulation as execution by proxy, Compulsory collection, direct compulsion, or immediate enforcement.

The corrective order issued in cases of violation of the operating permit criteria and physical protection requirements is technical, and the technical obligation is not replaceable, so the execution by proxy cannot be applied.
In addition, it is not an obligation to pay for money, so, Compulsory collection is not appropriate.

Immediate enforcement is difficult to introduce unless the occurrence of an accident is clearly foreseen because it can be invoked to eliminate existing obstacles or prevent imminent hazards in the near future[1].

In the case of non-alternative duties, the government can seek to secure the fulfilment of the obligations by imposing charge for compelling the execution. The charge for compelling the execution is stipulated in the Building Act, the Farmland Act, the Act on the Registration of Real Estate Real Estate Ownership, and the Parking Lot Act. In the nuclear sector, it is also necessary to introduce a enforcement penalty if the operator fails to fulfill the correction order by the set deadline.

5. Conclusion

If nuclear licensees do not abide by the government's order for correction, there will be a big gap in safety and protection. Financial sanctions are effective in securing the effectiveness of the correction order, but fines alone are not enough to secure it. Charge for compelling the execution has more meaning as a system suitable for the changing administrative environment. It is necessary to consider introducing a charge for compelling the execution in the nuclear field as well..

REFERENCES

[1] Jung Sun Hong, A Special Lecture on Administrative Law, p.451, The 8th Edition, Bakyoungsa, 2009.

Export Control for Small Quantity Nuclear Material in Equipment

Sung Yoon Park

Korea Institute of Nuclear Nonproliferation and Control, 1534, Yuseong-daero, Yuseong-gu, Daejeon, Republic of Korea

sypark12@kinac.re.kr

1. Introduction

The ROK conduct export control on its Nuclear materials in both the type and the amount. The large amount and high fissionable nuclear materials are regulated by the Foreign Trade Act as strategic item, and the small quantity nuclear materials are regulated by the Nuclear Safety Act. Because of the matter of detection, regulating small quantity nuclear materials , especially included in the equipment is difficult. Generally, these are found by HS code in custom clearance. It includes radiation shielding material, fission chamber, thorium ramp, hydrogen monitoring system, and dyeing material for electro-microscopes, etc.

Table 1. Strategic item criteria for nuclear material

Type	Amount
Special fissionable material	50 effective grams
Natural uranium	500 kilograms
Depleted uranium	1,000 kilograms
Thorium	1,000 kilograms

2. Current Problems

2.1 Custom Clearance

Because of the Office of Customs Administration checks custom clearance of the nuclear materials based on the HS code, it is hard to check materials included in the equipment, which are not on the list of items. Although the Korea Institute of Nuclear Safety uses radiation detector for safety regulation, it is hard to detect small quantity nuclear materials inside the equipment because of their weak radiation. Items that are not classified in public notification do not need to be approved by the Foreign Trade Act; therefore, the Office of Customs Administration can clear them without requisite confirmation. Furthermore, a penalty clause is missed from the requisite confirmation.

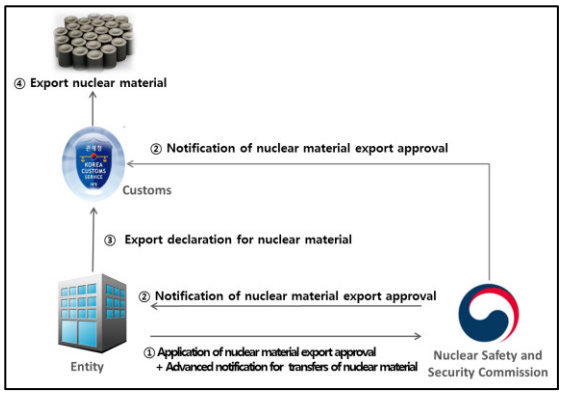

Fig. 1. Diagram for export of small quantity nuclear material.

2.2 Small Quantity Nuclear Material Control

Small quantity nuclear materials under a certain amount are the exception of Article 45 (Permit for Use, etc. of Nuclear Fuel Material) and Article 52 (Notification of Use of Nuclear Raw Material) of Nuclear Safety Act. Thus, importers/exporters of small quantity nuclear materials may not be aware of their export control system. This also leads to problems in accounting and control of nuclear materials,

because of difficulties on back-tracking the importers/exporters who did not get requisite confirmation.

2.3 Unclear definition for the non-nuclear purpose

When the Uranium and Thorium are in non-nuclear purpose in their final use, Article 24.2 of Regulation on Internationally controlled materials permits them not to be reported. Because of the exporters' misunderstanding on this clause, there are cases of missing the Nuclear Material Export Approval.

3. Suggestions for improvement

Suggestions for enhancing loop-hole for export control on small quantity nuclear materials included in the equipment are as follow.

3.1 Subdividing the HS codes

The HS codes can be subdivided. For example, containers include Depleted Uranium shielding materials, lamps include nuclear materials, 2844 (Compound of Uranium, Thorium, etc.), 2612 (Ore of Uranium, Thorium, etc.) may be set as a sub-HS code.

3.2 Outreach for suppliers

Enhanced management on suppliers list may strengthen export control on small quantity nuclear material. Expanding the target of regular outreach is needed not only for the export control but also for safeguarding domestic nuclear materials.

3.3 Association with the Safety Management Systems for Radiation in the Natural Environment

After the Radon issue, Nuclear Safety and Security Commission has improved database on the small quantity nuclear materials to strengthen the safety management system for radiation in the natural environment. Using a such database for export control may contribute to searching importers/exporters of small quantity nuclear materials.

4. Conclusion

Increasing volume of trade and individual's oversea purchase call upon the importance of export control. Export control of small quantity nuclear material is not only a problem for the ROK's export control system but a common problem of countries. The intense information exchange between stakeholders, including the Office of Customs Administration and Nuclear Safety and Security Commission is needed to establish a comprehensive export control system.

REFERENCES

[1] Nuclear Safety and Security Committee Notice 2017-85, "Nuclear material export/import approval".

[2] Nuclear Safety and Security Committee Notice 2017-84, "Advanced notification for transfers of nuclear material".

[3] Integrated Public Announcement of Ministry of Trade, Industry and Energy.

[4] J.S. Kim, "A Study on the Adequacy of legislation system on Ex-Import Control of the Internationally Controlled Goods under the Nuclear Safety Act", Law and Policy Research, 13(3), 1123-1153 (2013).

Analysis of Fuel Cycle Coupling SMR Using Partial TRU Recycling and SFR Burner

Dae Hee Hwang and Ser Gi Hong*
Kyung Hee University, 1732, Deogyeong-daero, Giheung-gu, Yongin-si, Gyeonggi-do, Republic of Korea
*sergihong@khu.ac.kr

1. Introduction

Nowadays, the disposal of spent nuclear fuel (SNF) is one of the most important issues in nuclear industry in our country. In this study, recycling of TRU (Transuranics) with MOX fuels and deep burning with FCM fuels without recycling in light water cooled SMR core were considered as a near-term option for reducing the inventory and radiotoxicity of nuclear spent fuel sent to repository. Eventually, the SMR core was coupled with SFR (Sodium cooled Fast Reactor) burner core having actinide recycling to further reduce TRUs going to the final depository.

2. Design of SMR and SFR Cores

In order to design and analyze the light water-cooled SMR core, DeCART2D/MASTER two-step procedure was used. The fuel assemblies (FA) which have 17×17 rod array are composed of MOX as well as FCM (Fully Ceramic Micro-encapsulated) fuel rods for deep burning of TRU. There are two types of FAs with different amount of burnable absorber. The SMR core has the power rate of 100 MWe (330 MWt). The 100MWe SMR core was designed up to 5^{th} cycle without TRU recycling in order to facilitate the search of the equilibrium cycle. In the next step, the SMR core was designed up to 20^{th} cycle with TRU recycling in MOX fuels (but TRUs in FCM fuels are not recycled). At the beginning of 20^{th} cycle, all of FAs contain five-times recycled TRUs.

In order to coupling with the SMR core described above, two kinds of SFR core having 400 MWe power were considered. The first SFR core was loaded with the TRU-U-10Zr metallic fuel throughout the core (i.e., U-containing core). The second SFR core was designed to have high TRU consumption rate without a considerable degradation of safety parameters by loading two kinds of metallic fuels composed of TRU-W-10Zr (i.e., U-free fuel) and TRU-U-10Zr (i.e., U-containing fuel).

3. Analysis of Fuel Cycle

In this chapter, a nuclear fuel cycle in conjunction with a commercial PWR, the SMR core, and the SFR cores was constructed, and the mass flow of U and TRU was analyzed. Figure 1 shows the PWR-SMR-SFR[a] fuel cycle and the mass flow of U and TRU. Table 1 shows the comparison of the characteristics of several fuel cycle options. The total energy of the reactor park was normalized to 1 TWhe. In case of PWR-SMR-SFR fuel cycle, TRUs from the commercial PWR core were recycled five times through only MOX fuels in SMR core and sent to the SFR core. As shown in Table 1, finally, the amount of TRU sent to repository was reduced by about 43% compared to once-through fuel cycle.

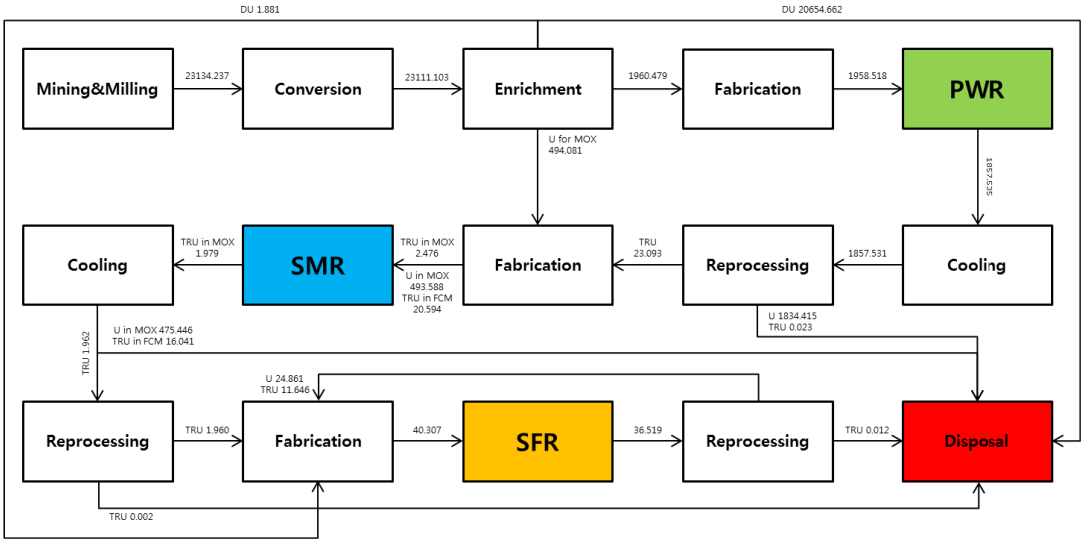

Fig. 1. Fuel cycle in conjunction with PWR-SMR-SFR[a] with mass flow of U and TRU in kg.

Table 1. Characteristics of several fuel cycle options

Option	Fraction in 1TWhe		TRU support ratio	Mass (kg)		
				Mining&Milling	Disposal	
Once-through	PWR	1.0000	-	22488.9	U	22309.7
					TRU	28.7
					Total	22338.5
PWR-SFR	PWR	0.6616	2.25	14879.5	U	14742.7
	SFR	0.3384			TRU	0.1
					Total	14742.9
PWR-SMR-SFR[a]	PWR	0.8045	26.55	23134.2	U	22964.5
	SMR	0.1606			TRU	16.1
	SFR	0.0349			Total	22980.6
PWR-SMR-SFR[b]	PWR	0.8122	36.52	23356.7	U	23186.4
	SMR	0.1622			TRU	16.2
	SFR	0.0256			Total	23202.6

SFR[a]: U-containing
SFR[b]: Hybrid

Although the amount of TRU sent to repository was still much higher than PWR-SFR fuel cycle, the energy fraction of SFR in the fuel cycle was able to be considerably reduced from 34% to 3.5% and 2.6%. As a result, the nuclear park can be constructed with a small number of SFR core requiring advanced technologies and it also has the advantage that the amount of fuel to be reprocessed is reduced in comparison with PWR-SFR strategy.

4. Conclusion

In this study, the fuel cycle in conjunction with commercial PWR, SMR, SFR was suggested and the mass flow of U and TRU in the fuel cycle was inter-compared with several options. It was found that the amount of TRU sent to repository was considerably reduced compared to once-through cycle with the significantly reduced fraction of SFR core in reactor park.

ACKNOWLEDGEMENTS

This work was supported by National Research Foundation of Korea (NRF) through project No. 2016M2B2A9911611.

REFERENCES

[1] D. H. Hwang, Y. S. Cho, and S. G. Hong, “TRU Multi-Recycling Analysis in SMR Core with MOX Rods and FCM Rods,” ANS Winter Meeting, Orlando, FL, November 11-15, 2018.

[2] W. S. You, S. G. Hong, “A Transition Cycle Analysis of an Advanced Sodium-cooled TRU Burner Reactor Core,” Transactions of the KNS Autumn Meeting, Gyeongju, Korea, October 26-27, 2017.

A New Approach to Manage Nuclear Wastes in the ROK

Yongsoo Hwang*, Hong Chang, and Hyo-On Nam
Korea Atomic Energy Research Institute, 111, Daedeok-daero 989beon-gil, Yuseong-gu, Daejeon, Republic of Korea
*yshwang@kaeri.re.kr

In the foreseeable near future, there will be major activities to manage nuclear wastes in the ROK. The first action is about the new round of the Public Engagement for managing Spent Nuclear Fuels in Korea. The second subject is the update of the Basic Plan to manage Spent Nuclear Fuels in Korea. The current 2016 plan which is significantly outdated shall be updated in 2021. Therefore, in 2020, there will be significant effort to develop the new plan with the final recommendations from the ongoing Public Engagement. The third action is the comprehensive planning of the R&D programs for the future Spent Nuclear Fuel managements. The new R&D plan shall be implemented from the beginning of the 2021. The new R&D program shall be authorized jointly by MOTIE and MSIT. In addition, the ongoing 10 year-long JFCS shall be closed in 2021. How to wrap up the program and to make a decision for the future cooperation will be an issue in 2020. The forth issue is to timely inauguration of the 2nd phase LLW repository in Gyongju. The last issue is the nuclear waste management in the DPRK if there is a solid comprehensive international agreement for the Korean Peninsular denuclearization. In this paper, the key subjects covering these five missions shall be discussed.

1. Proactive Measures

It is not clear what would be the national framework for the spent fuel management in the ROK yet. In the US system, there is the 1982 Nuclear Waste Policy Act and the 1987 amended act for the top level national policy. To support the acts, the so called 10CFR60 code, the generic regulation, was introduced well before the YMP was launched. In addition, the US NRC introduced the site specific regulation 10CFR63 for the YMP. In addition to this solid regulatory framework, the USNRC periodically announces and amends the proactive measure, Nuclear Waste Confidence, assuring whether the concerned nuclear waste can be safely managed for storage and final disposition. In Korea, the national basic policy was introduced in 2016 after the receiving recommendations from the PECOS. There have been significant changes for the fundamentals of that basic plan. This will alter the core context of the 2016 basic pan significantly. The new version will include the impact of the small cumulative arising of spent nuclear fuels. It will be much better to introduce the written regulations as early as possible and to wrap up the future vision in the form of the Nuclear Waste Confidence in the ROK to understand the legal responsibilities and the future prospects for the safe management of spent nuclear fuel.

2. Technical Approaches

Since 1997, KAERI has worked on the development of the final disposal of spent nuclear fuels and the HLW through the pyro-processing. The KRS is based on the traditional KBS concept developed in Sweden in 1983. The key concepts are the copper canister later upgraded as the composite waste container and the MX-80 type sodium bentonite. The total

weight of a waste canister is heavier than thirty tons and the traditional thermal constraint is still there in this traditional system. In practice, after developing the original KBS 3 type disposal concept, the implementation entity in Sweden, SKB developed the alternative options to replace its original disposal concept. After serious research SKB finally confirmed that the original concept KBS-3 is the final disposal option. Unfortunately, the new alternative options are not fully studied yet in the ROK even though there has been a limited scoping study to understand the Deep Borehole Project several years ago. In fact, the year 2053 stipulated as the official inauguration year for the final repository in the ROK via the 2016 basic plan shall be slightly delayed when there is significant reduction of the cumulative spent nuclear fuel arising after the adoption of the new Energy Transition Policy in this administration.

If there is a better idea to reduce the total weight of a canister, it will make it easy to handle the spent nuclear fuel transport and the final disposal in a repository tunnel. For example, the Canadian NWMO successfully demonstrated the validity of the cold copper spray technologies and the new concept for the integrated near field disposal system combining the bentonite barrier with a canister as one package.

There are many issues such as the optimum life time extension of a storage system especially for the high burn up spent nuclear fuels. Also, the validity of a dual purpose container for both storage and transportation is respected in many occasions. The revival of the TAD container will be also interesting subject specially for the ROK. When the TAD is commercialized then there will be no additional financial and the other investment for the disposal container later on. The real issue for the TAD will be the initial financial investment. The technical break-through as well as the comprehensive cost benefit analysis are recommended in this task.

3. Knowledge Management (KM)

The road from today to the final closing of a future spent nuclear fuel repository takes more than hundreds of years. Then, how to preserve all detailed information such as designing, datasets, and the engineering works will be a problematic matter in the real society. The comprehensive KM system should be urgently developed to secure all the information and its relevant QA procedures into a KM repository.

4. DPRK Issues

One of the critical issues will be the DPRK issues. When the denuclearization dialogue is successfully implemented, then there will be significant contribution opportunities for the ROK experts to assist the DPRK to develop the comprehensive plans and technologies for decommissioning, storage and transportation, and the final management of all radioactive wastes in the DPRK. Many fundamental new reaches shall be initiated to safely and securely manage liquid wastes from Yongbyon and the other wastes such as the mining by-products and the depleted uranium in the DPRK.

ACKNOLEDGEMENT

This study is supported by the Mid- and –Long-Term Nuclear R&D Program supported by MSI.

Overall Issues of the ACTR Programs

Yongsoo Hwang
Korea Atomic Energy Research Institute, 111, Daedeok-daero 989beon-gil, Yuseong-gu, Daejeon, Republic of Korea
yshwang@kaeri.re.kr

The DPRK is the unique country to claim to work on the denuclearization even though there is dispute over the exact meaning of the denuclearization. Since the political regime of the DPRK shall remain stable, the entire denuclearization processes are different from the case after the collapse of the Soviet Union. There are many issues at this moment for the potential denuclearization in Korean Peninsula. In this paper, these issues are summarized and for some issues, certain practical measures are proposed. In reality, there shall be a comprehensive grand package to integrate all efforts such as the denuclearization technical approached and the grand economic development. However, in this paper, only the issues directly engaged in the Korean Peninsula denuclearization shall be discussed.

1. Inspection, Verification and Final Management of SNM

There is a certain rule to manage the core materials and the sensitive technologies in association with core experts over the WMDs. There, the key issue is how to inspect, verify and finally manage the so called special nuclear materials and information. Traditionally, for the global nuclear non-proliferation and the security, the role of managing special nuclear materials are the responsibility of the P5 nations and IAEA. Throughout the implementation of the AF, all the official inspections are performed by IAEA with strong integrated support from the US. The same principle is expected to be implemented for the future case. However, how to initiate the so-called cooperative monitoring to manage some facilities and the environment and etc is a task for the concerned parties.

2. ACRT and Pre-CTR

One of the critical issues for the future denuclearization and the negotiation among the key stakeholder is the design and the implementation of the so-called Cooperative Threat Reduction programs tailor made for the DPRK, ACTR. As discussed in the precious AF occasion, how to properly manage the all different ranges of the scientists, engineers, and the administrative and the entry level workers who are now working on the WMD society is the fundamentally big issue. At least, more than twenty to thirty thousand staff members are believed to work in the WMD business in the DPRK. Among them, a couple of hundred core experts shall be carefully managed by the international society, practically the P5 states to prevent potential proliferation. How to manage the remaining staff members will be the time and money consuming issues. However, without implementing one generation long well

integrated human resource management program, it will be very challenging to discuss the key action planning of the actual denuclearization as well as the prevention of the sensitive technology proliferation. One of the bright spots is that the global society and the DPRK needs a comprehensive program to supply the electricity and the energy along with the micro- and the nation-wide electricity supply grid networks. Recently, the DPRK made a great effort to develop the series of the small and the medium scale power plants across the nation, especially the active construction of hydro-plants. Still, the DPRK will need very significant additional installations to support its economic development in the future. Many options can be studied for the energy supply. One of the feasible options for the energy supply is the introduction of the nuclear power stations. As fully agreed in the 2005 Six Party Agreement which is still fully recognized by all member states, the introduction of the nuclear installations will be the subject of interest considering the current and the future capacity of the grid networks in the DPRK and the NE Asia.

The other area is the new construction and the updating of the transportation systems. For that mission, the comprehensive management of the all transportation systems connecting Youngbyon with the combination of the railway systems, air transportation, roads, and seaports shall be required. For example, the DPRK operates the good highway systems between Kaesong and Pyongyang, Pyongyang and the Cheongchon-Gang area and Pyongyang and Wonsan. The railway system is connected with the nation-wide railway system so that the proper freight can be delivered. However, the current transportation system might have certain limitation to transport the heavy and radioactive nuclear materials. It will serve as a good job opportunity for many thousand DPRK staff members in the future.

3. Radioactive Waste Management

The proper decommissioning and the management of old facilities in the DPRK and the follow-up activities to manage all kinds of radioactive wastes will be a challenge but also cast a good opportunity for the additional job creation. One of the critical issues is how to safely manage all waste streams. The complicated liquid waste from the reprocessing will be a real hot issueAll these tasks shall be corner stones to develop more job transition opportunities for the DPRK staff members in the WMD industries.

ACKNOLEDGEMENT

This research study is financially supported by KAERI.

A Consideration on the IAEA Safeguards Policy Forwarded to A State-Level Approach

Jae-Kwang Kim* and Sung Yoon Park
Korea Institute of Nuclear Non-proliferation and Control, 1534, Yuseong-daero, Yuseong-gu, Daejeon, Republic of Korea
*jgwang@kinac.re.kr

1. Background

Since 1957's Establishment, the IAEA had developed a Partial Safeguards System of nuclear material which was outlined in IAEA official documents such as INFCIRC/26 and INFCIRC/ 66. Under a Partial Safeguards System, Member States voluntarily declared the nuclear material of which the IAEA verified peaceful use. On the success of nuclear bomb test by France and China, the IAEA officially published the Comprehen- sive Safeguards System which was formulated in INFCIRC/153 document in order to obstruct the proliferation of nuclear weapon [3].

As above, the Agency has changed the direction of the safeguards system according to international status. Of course, the Republic of Korea also has been under safeguards agreements with the Agency. There is a need to respond to the changing safeguards policy of the Agency. This paper analyses the Agency's historical changes in safeguards policy and recommends the measures corresponding national strategies.

2. The IAEA Safeguards Policy Changes

2.1 A Facility Level Safeguards Approach

A Facility Level Approach comprises Partial Safeguards Systems of INFCIRC/26, INFCIRC/ 66 and INFCIRC/153 under agreements between the Agency and Member States.

In 1961, the Agency had published the INFCIRC/26 officially to be applied to Member States firstly. The INFCIRC/26 system related only to research, test and power reactor under 100MWt as a first safeguards system. The INFCIRC/26 safeguards system was developed to the INFCIRC/66 system which extended to cover large power reactors, enrichment plants, reprocessing plants, conversion plants and fabrication plants[1][2]. The IAEA needed to strengthen the INFCIRC/66system consistent with the NPT treaty. The strengthened system is a Comprehensive Safeguards System which was published in INFCIRC153. Consistent with INFCIRC/153, the Agency applied Containment and Surveillance System to the strategic points in order to strengthen the INFCIRC/66 system [3].

2.2 A State Level Safeguards Approach

The timely detection, the goal of the INFCIRC/153 system, basically means that it could not prevent the intentionally undeclared nuclear program in advance [3].

A State Level Approach Concept was developed to strengthen only the effectiveness of safeguards under the INFCIRC153 system by evaluating a State as a whole. This approach is

additional to the INFCIRC/153 system which is stated in INFCIRC540 [3].

In this Approach, a State should submit all safeguards relevant activities that have been conducted in the State to the Agency first (i.e. Expanded Declaration) [4]. Secondly, the Agency can get extensive access to nuclear sites and locations where nuclear-related activities are conducted to ensure the absence of undeclared activities. Moreover, the Agency can approach elsewhere in the State if there is any question or inconsistency [4].

Otherwise, the Agency safeguards resources should be allocated in a largely uniform manner among States, but they are deficient and limited to cover all the expenses in safeguards planning, implementation and evaluation in this Approach Concept [5].

Consequently, The State Level Approach in integrated mode is developed to improve and strengthen both the effectiveness and the efficiency. In this Approach, the Agency would draw a broader conclusion that all nuclear material in the State remained in peaceful activities through evaluation of the State using this Approach. A broader conclusion means that there are no indications of diversion of declared nuclear material from peaceful nuclear activities in a State and there are no undeclared nuclear activities for the State as a whole [5].

3. Conclusion

Safeguards resource allocation and inspection burden seemingly appear to be determined by the size of each State's safeguarded nuclear activities in the State Level Approach in integrated mode. The Agency would like to increase the number of State with a broader conclusion and also improve the already optimized safeguards measures in a State with a broader conclusion like the ROK.

As a result, we have to keep an eye on the changing IAEA's Safeguards policy and prepare for its application such as Unannounced Inspections.

REFERENCES

[1] The Agency's Safeguards IAEA INFCIRC/26/Add.1, 9 Apr 1964.

[2] The Agency's Safeguards IAEA INFCIRC/66/Rev.2, 16 Sept 1968.

[3] The Structure and Content of Agreements Between The Agency and States Required in Connection with the Treaty on the Non-Proliferation of Nuclear Weapons, INFCIRC/153, Jun 1972.

[4] Model Protocol Addition to The Agreement(s) Between State(s) and The IAEA For the Application of Safeguards, INFCIRC/540/Corr.1, 12 Oct 1998.

[5] Analysis of the IAEA's Approach to Allocation of safeguards Resources, Managing the Atom Seminar, Kalman A. Robertson et al. 9 Dec 2015.

Safeguards: Implementing the Updated State-Level Approach at KAERI

IC Kim*, SH Lee, BD Lee, HJ Kim, HS Kim, JA Jung, and SM Han
Korea Atomic Energy Research Institute, 111, Daedeok-daero 989beon-gil, Yuseong-gu, Daejeon, Republic of Korea
*ickim@kaeri.re.kr

1. Introduction

Since the numbers of nuclear facilities subject to safeguards have been increased gradually and the technology of nuclear industry also has been sharply developed in the world, IAEA secretariat needs to introduce a new concept for an effective and efficient implementation of safeguards under limited budget. To solve this requirement, the IAEA secretariat determined to set the revised concept of SLC (State level Concept) in the plenary meeting of the IAEA on Sep, 2014. SLC means that the Agency implements safeguards under the consideration of the states' nuclear capabilities as a whole such as the nuclear facilities and related activities within the boundary of safeguards agreement between the Agency and the state. Implementation of safeguards at KAERI should follow the safeguards procedure determined by the IAEA and the government of the ROK. The Agency introduced and consulted the updated SLC and SLA (State Level Approach) in the ROK-IAEA JRM (Joint Review Meeting) on Apr. 2014 to the ROK. After both sides held the several deep discussions, the Agency sent the ROK a SC (Security Channel) letter to initiate an official application of the updated SLA on 1 Sep. 2015. The SLA means the Agency's internal document, which is approved by the board of governors.

2. The updated SLA in ROK

Fundamental conditions of credible safeguards in every state joined NPT (The Treaty of Non-Proliferation of nuclear weapons) are relatively varied. Therefore, the Agency basically leads to differentiated safeguards based on the state's conditions. This means that the Agency recognizes the state's conditions for safeguards and can't help differentiating the safeguards measures based on the defensible decisions supported by clear and transparent procedures not to be discriminated. To make an application for SLA to ROK, the Agency and ROK deeply discussed on the application methods of SLA. Based on advanced studies of the updated SLA initiated by the Agency, the ROK made a determination for the application of the updated SLA by means of considering the following factors.

- No problem to implement the updated SLA in ROK including UI
- The increase of the international confidence for the ROK's safeguards under the NPT
- The ROK's contribution of developing the implementation system of the NPT

Based on the State specific factors (SSF) that are particular to the state, the Agency reviews the fundamental information of the state and determines an SLA under the consideration of the states' nuclear capabilities. The followings are the Agency's reviews of SSF on the ROK.

Table 1. Reviews of SSF in ROK

SSF	Contents
Type of safeguards agreement	. CSA, Additional Protocol . Broad conclusion
Technical capabilities of nuclear fuel cycle	. Advanced open fuel cycle . Operating PWR,PHWR & additional construction . Pyro-processing
Technical capabilities of SSAC	. Domestic Inspection . ND Inspection equipment . Trusted accounting report
IAEA ability to implement safeguards	. Random interim inspection . Mail-box system . Unattended monitoring Sys.
Nature/ scope of cooperation	. Visa exemption with UNLP . Contribution for NPT
IAEA's experience	. Achievement of IAEA inspection target

3. The application of updated SLA at KAERI

IAEA suggested that sector approach should be based on the types and status of facilities and technical objectives reflecting the updates on the bases of the SSF that are introduced by the Agency. According to this kind of policy, the Agency notified the updated SLA for KAERI considering the followings.

- Pyro-processing related R&D facilities

grouped in one separated category under KAERI as Category III

- Safeguards equipment data from HANARO research reactor in RM mode
- Newly safeguards equipment (NGSS, EOSS)
- Newly constructing facilities like Kijang research reactor to be built
- Advanced open fuel cycle and versatile/ complicated relationships with the flow of nuclear materials as shown in the figure 1.

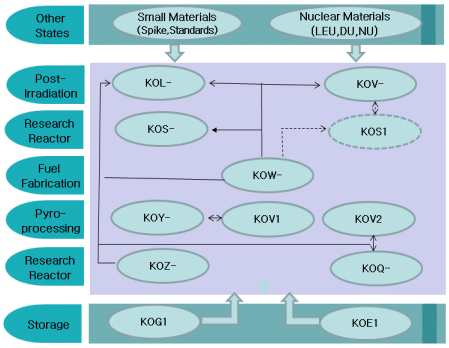

Fig. 1. The flow of NM between MBAs.

The Agency changed implementation procedure for inspection activities under the updated SLA to be applied to all facilities at KAERI. The most important changes are IAEA inspection activities for pyro related facilities and the categorization change of the facilities and LOF at KAERI as shown in table 2.

Table 2. Categorization of the Facilities at KAERI

Category	Content
Category I	. Self-contained capability that has at least 1 SQ of suitable NM . To support undeclared Pu production/ separation activities without any help
Category II	. Remaining facilities and LOF except Category I & III facilities.
Category III	. Pyro-processing related facilities which contain less than 1 SQ of NM but utilize technology/equipment related to recycling of spent fuel

Since updated the SLA, IAEA inspection activities have been increased and focused on the pyro-processing related facilities. Before the updated SLA, KAERI consisted of two categories (Category I and category II) of the facilities. According to the updated SLA, the Agency asks the changed advance facility information for RII as shown in table 3.

Table 3. Advance Facility Information

Category	Content
Category I	. Annual advance information . KOS-: FF receipt, SF cask closing, SF shipment. Etc. . Monthly/quarterly advance information
Category II	. Annual advance information
Category III	. Annual advance information . Monthly/quarterly advance information planned Campaigns, NM receipt/ shipment & any change of EE

Under CSA (Comprehensive Safeguards Agreement), KAERI still should provide the annual advance information and monthly reports for category I. Before the updated SLA launches, The Agency has adjusted the frequency of the RII with the relevant probability considering the facility characteristics. However, the concept of the probability of RII does not exist in the updated SLA.

4. Conclusion

The purpose of this study is to review the updated SLA implemented by the Agency and to find its influence to the KAERI. Since the updated SLA entered into forces on Sep. 2015, KAERI has faced the changed challenges from the Agency's enforced safeguards system. Even though, the most important change in the updated SLA for the ROK is to start the UI for the light water reactor, KAERI also has the important change for the Pyro-processing related facilities. In association with the updated SLA, the intensity of the Agency verification activities such as the frequency of the Agency inspection and the monthly/quarterly/annual reports for the Pyro-processing related facilities seems to be increased.

REFERENCE

[1] Jean-Philippe Morizot INMM Annual Meeting, "Developing a state-level safeguards approach: case study", 2016.

[2] Mark Pellechi Workshop Presentation, "Sector Approach: SG implementation a LWRs in the ROK", 2015.03.

[3] NSSC, "The implementation plan in terms of updated State-level Approach in the ROK", 2015.09.

[4] Neville Whiting INMM Annual Meeting, "Developing of a state-level integrated safeguards approach for Canada", 2012.

Progress in the Development of REPF+ Safeguards Approach

Se-Hwan Park*, Bong Young Kim, Ho-Dong Kim, Chaehun Lee, Dae-Yong Song, Byung-Hee Won, and Seong-Kyu Ahn

Korea Atomic Energy Research Institute, 111, Daedeok-daero 989beon-gil, Yuseong-gu, Daejeon, Republic of Korea

*ex-spark@kaeri.re.kr

1. Introduction

Korea Atomic Energy Research Institute (KAERI) is developing a safeguards approach of Reference Engineering-scale Pyroprocessing Facility plus (REPF+) through IAEA Member State Support Program (MSSP).

ROK is developing pyroprocessing with a goal of making it part of a strategy to manage spent fuel. Since the pyroprocessing is different from aqueous reprocessing, a safeguards approach suitable for it is required. Regarding this issue, IAEA contracted with ROK in 2008 for an MSSP. KAERI and Korea Institute of Nuclear Nonproliferation And Control (KINAC) developed a safeguards approach of Reference Engineering-scale Pyroprocessing Facility (REPF) [1, 2]. The REPF was a conceptually designed facility. The input material of the REPF was LWR spent fuel assembly, the output of the REPF were U/TRU ingot, U ingot and waste. The throughput of the REPF was 10 MTHM/yr. A campaign concept was introduced and a homogenation process, mixing a spent fuel assembly at once, was included to the head-end process of the REPF for the input material accountancy. Material Unaccounted For (MUF) uncertainty calculated in the REPF. A model Design Information Questionnaire (DIQ) of the REPF was developed, and an example Facility Attachment (FA) of the REPF was issued by IAEA.

IAEA proposed a following MSSP, and the MSSP was contracted with ROK in 2016, and the safeguards approach of the REPF+ has been developed. In this presentation, we provide the progress of the development of the safeguards approach of the REPF+.

2. Methods and Results

The conceptual pyroprocessing facility; REPF+ includes the pyroprocessing process and manufacturing process TRU fuel for SFR. The input material of the REPF+ is LWR spent fuel assembly, and output materials of the REPF+ are SFR fuel assembly, U ingot, and wastes. The annual throughput of the REPF+ is 30 tHM. All processes are zoned into cell areas and storages areas based on process characteristics and purpose. The transfer of process materials between the cells and storage areas is performed only through dedicated transfer ports.

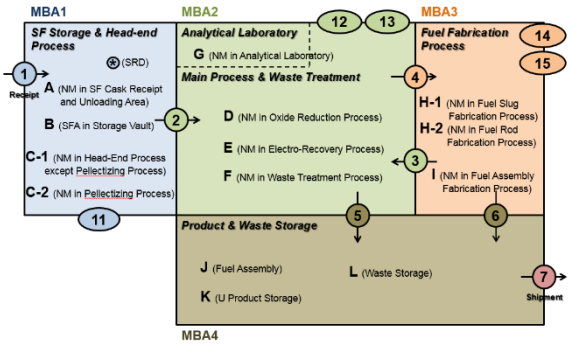

Fig. 1. MBA and KMP Structure of REPF+.

The Material Balance Area (MBA) and Key Measurement Point (KMP) structures of the REPF+ is shown in Figure 1. MBA-1 includes SF reception, SF storage, and head-end cell. MBA-2 includes oxide reduction cell, electro-refining process cell, waste treatment cell, and analytical laboratory. MBA-3 includes fuel fabrication cell, fuel assembly cell. MBA-4 includes fuel assembly storage, and U product & waste storage.

The operator's accounting methods for all the nuclear materials are identified. Diversion scenarios in the REPF+ are selected, and verification approaches in the REPF+ are identified; verification methods of PIV, verification methods of IIV, verification methods of inventory changes, and verification methods of nuclear material transfer within MBA. For each diversion scenario, the details of the diversion strategy and the corresponding safeguards measures are summarized. From these, the safeguards measures in the REPF+ safeguards approach are evaluated and the safeguards consideration to enhance the safeguardability in the REPF+ are deduced.

3. Summary

Safeguards-By-Design (SBD) is an approach to the design and construction of a nuclear facility whereby nuclear safeguards provision and features are designed into the facility from the very beginning of the design process. The present effort will be very helpful to the implementation of safeguards to the pyroprocessing facility more effectively and efficiently.

Acknowledgement

This work was supported by a National Research Foundation of Korea (NRF) grant funded by the Korean government's Ministry of Science and ICT (MSIT) (No. NRF-2017M2A8A5015084).

REFERENCES

[1] KAERI , "Final Report for the ROK MSSOP on Support for Development of a Safeguards Approach for a Pyroprocessing Plant", 2012.

[2] KINAC , "Final Report for the ROK MSSOP on Support for Development of a Safeguards Approach for a Pyroprocessing Plant", 2012.

1분과

핵주기정책·규제 및 비확산(Poster)

Review of Satellite Imagery Signatures From Open Source Analyses on Nonproliferation Monitoring Activities

Jae-Jun Han* and Minsoo Kim
Korea Institute of Nuclear Nonproliferation and Control, 1418, Yuseong-daero, Yuseong-gu, Daejeon, Republic of Korea
*jjhan@kinac.re.kr

1. Introduction and Background

With the spirits of 'Atoms for Peace and Development,' the international society has made a great effort to strengthen nuclear non-proliferation regime. Nonetheless, in rogue states, regretfully, atomic energy has been misused to develop nuclear weapons. The leading countries in the field of nuclear nonproliferation, including the Republic of Korea, have been trying to rectify the tragic phase with all means available. As part of that, the suspicious area where the nuclear fuel cycle-related facilities are located are being monitored.

Due to the development of remote sensing technology, high-quality satellite information has become easily achievable to the non-governmental (non-military) sector. From the early 2000s, by non-governmental organizations such as 38 North, ISIS and CSIS, the satellite imagery has been analysed to monitor nuclear activities in rogue states, and the results have been accumulated to date. North Korea, in particular, has always been at the forefront of controversy in the nuclear nonproliferation regime and therefore has been a main target for imagery analysts.

Interpreting satellite imagery requires expertise in target objects based on the (at least) fundamental knowledge of remote sensing (geospatial information). In order to infer nuclear activities from satellite images, analysts should have the fuel cycle expertise necessary for nuclear weapon development. As each of the two fields (remote sensing and nuclear fuel cycle) has extensively been developed, cultivating an expert in both is not an easy task. This can be proved that training materials and courses in the field of 'image interpretation' are available, while the image interpretation 'for nuclear activities' is very limited.

In this regard, this research reviews signatures on satellite imagery in use to identifying suspicious activities in North Korea. The articles released by the 38 North are chosen for quantitative analysis using text mining technique. After normalising the contents of articles, the word frequency is examined with implications for monitoring nuclear activities.

2. Text Data Processing

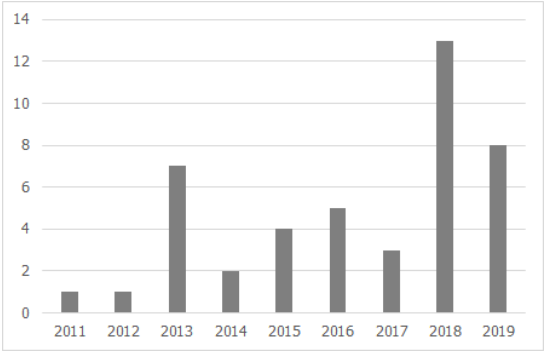

Fig. 1. Number of 38 North articles for satellite imagery analysis on the Yongbyon nuclear complex from November 2011 to August 2019.

Forty-four articles on the Yongbyon nuclear complex published online by 38 North from November 2011 to August 2019 [1] were chosen for review. Annual counts of articles are summarized in Fig. 1, showing an overall

increase with time. The text data processing was implemented via the Python language [2]. The raw data (40,040 unstructured words) was processed to meaningful words through cleaning, tokenisation, stopword removal, and stemming (lemmatisation). The familiar compound words such as the 5 MWe reactor, experimental light water reactor, fuel fabrication plant, etc., were dealt with in single words. In stemming process, the lemmatisation was applied through the comparative analyses of several stemming algorithms.

3. Results and Conclusions

The text data processing calculated the word frequency from the 44 articles. There were many abstract and proper nouns which are useless for image analysis. By eliminating them, Table 1 remains practical words that satellite imagery analysts frequently use when describing suspicious activities in the nuclear complex. Based on the word frequency, nine signature groups of satellite image analysis are derived in Table 2.

Table 1. The top 25 words of 38 North articles for satellite imagery analysis on the Yongbyon nuclear complex from November 2011 to August 2019

No.	Word	Count
1	experimental light water reactor	328
2	5 MWe reactor	213
3	river	94
4	radiochemical laboratory	94
5	thermal	78
6	vehicle	72
7	steam	69
8	pump house	67
9	dam	65
10	uranium enrichment plant	62
11	yard	60
12	equipment	56
13	cooling water	53
14	roof	45
15	crane	42
16	pipe	42
17	fuel rods	41
18	turbine	40
19	Kuryong river	39
20	truck	38
21	road	37
22	tank	34
23	plume	32
24	transformer	32
25	flow	31

Table 2. Satellite imagery signatures for identifying suspicious activities in the Yongbyon nuclear complex

Group	Word
vehicle	vehicle, truck, crane, car, railcar, flatcar, trailer
steam	steam, plume, vapor
personnel	personnel, people
cask	cask, tank
dam	dam, sand, dredging, Kuryong river, river, overflow
pump house	pump house, outfall, pipe, pipeline, cistern, piping
roof	roof, blue, bluish, snow, snow-free
waste	waste, excavation, Building 500
thermal pattern	thermal pattern

ACKNOWLEDGEMENT

This work was supported by the Nuclear Safety Research Program through the Korea Foundation Of Nuclear Safety (KoFONS) using the financial resource granted by the Nuclear Safety and Security Commission (NSSC) of the Republic of Korea (No. 1905009).

REFERENCES

[1] Articles - Satellite Imagery. Available at https://www.38north.org/

[2] Python Software Foundation. Python Language Reference, version 3.7. Available at http://www.python.org

Preliminary Investigation on Candidate Areas of Interest for H-program

Nam Kyung Kim*, Jung-Hyun Lee, Jae-Jun Han, and Young Wook Lee
Korea Institute of Nuclear Nonproliferation and Control, 1418, Yuseong-daero, Yuseong-gu, Daejeon, Republic of Korea
*namkkim@kinac.re.kr

1. Introduction

Shortly after the sixth nuclear test in September 2017, North Korea announced that it successfully tested a hydrogen bomb program (H-program), which can be mounted on ICBM due to its greater yield-to-weight ratio [1]. The large explosive yield to about 250 kilotons, which was derived from the magnitude estimates (6.1 to 6.3) by USGS and CTBTO, reaffirmed the reliability of North Korea's announcement for H--program [2].

To monitor suspicious activities related to North Korea's H-program, this paper suggests candidate areas of interest in Yongbyon nuclear scientific research center considering a priori knowledge. Further, the change detection regarding those areas of interest will be analyzed based on satellite imagery in future works.

2. Candidate facilities for H-bomb material

2.1 Key material for H-bombs: D, T, and ^6Li

H-bombs can be generally classified into the boosted fission weapons and the thermonuclear weapons, both of which were designed depending on the nuclear fusion reaction Eq. (1).

$$D + T \rightarrow \alpha + n \quad (1)$$

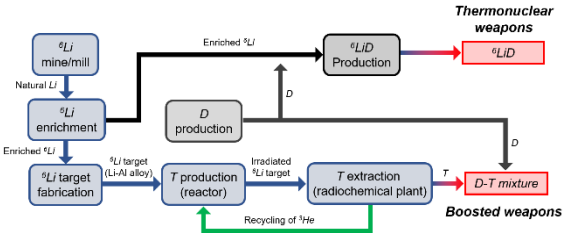

Fig. 1. H-bomb Development Process [1, 3].

Fig. 1 shows the H-bomb development process, which was modified from PNNL's model by J. Lee [1, 3]. The boosted weapons usually utilize deuterium-tritium (*D-T*) mixtures to trigger the nuclear fusion reaction; the thermonuclear weapons use lithium-deuteride (^6LiD) to produce tritium and set off the fusion reaction.

However, since what kind of H-bomb is in North Korea has been not known, it is necessary to identify facilities related to essential material for H-bombs, i.e. *D*, *T*, and ^6Li. Therefore, the next section investigated those facilities in Yongbyon.

2.2 Critical facilities related to D, T, and ^6Li

The critical facilities, i.e. deuterium production; lithium-6 target fabrication; and tritium production/extraction facilities, were investigated as shown in Fig. 2.

First, deuterium production facilities are known to be located in the Hungnam fertilizer complex near Hamhung [1, 4].

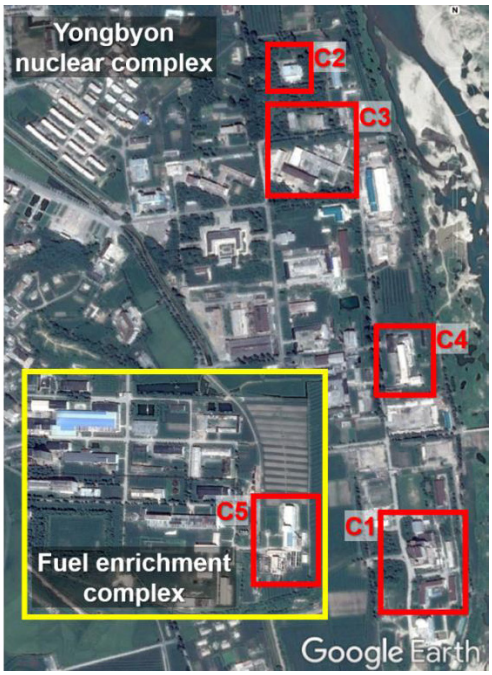

Fig. 2. T production/extraction and ^{6}Li target enrichment/ fabrication facilities in Yongbyon [1, 4].

Second, according to Eq. (2), the tritium production would take place at 5 MW(e) reactor (C1) where the lithium-6 target can be irradiated (IRT-2000 (C2) was not regarded as a tritium production facility due to no sign for operation since 2003.). In addition, tritium might be extracted from the irradiated target at the associated radiochemistry facilities (C3).

$$^{6}Li + n \rightarrow \alpha + T \quad (2)$$

Third, the lithium-6 might be enriched in an isotope separation facilities (C5) in Fig. 2. Then, the lithium-6 target (lithium-aluminum alloy) production facility might be the pilot fuel rod manufacturing facilities (C4) shown in Fig. 2.

3. Conclusion

In this paper, the candidate areas of interest related to key material for H-bombs, i.e. *D*, *T*, and ^{6}Li, were identified in satellite imagery of Yongbyon using a priori knowledge as followed.

- *D*: Hamhung (production)
- *T*: 5 MW(e) reactor (production), radiochemical facility (extraction)
- ^{6}Li: isotope separation facility (enrichment), pilot fuel rod manufacturing facility (target fabrication)

ACKNOWLEGEMENTS

This work was supported by the Nuclear Safety Research Program through the Korea Foundation Of Nuclear Safety (KoFONS) using the financial resource granted by the Nuclear Safety and Security Commission (NSSC) of the Republic of Korea (No. 1905009).

REFERENCES

[1] J. LEE et al., “Consideration on Technical Support to Denuclearization: Focused on H-program”, Trans. of the KNS Autumn Meeting, October 24-25, 2019, Jeju.

[2] F. V. Pabian et al., “North Korea’s Punggye-ri Nuclear Test Site: Satellite Imagery Shows Post-Test Effects and New Activity in Alternate Tunnel Portal Areas”, 38 north, September 12, 2017.

[3] Boyer and Brian D, “Nuclear Fuel Cycle & Vulnerabilities”, 2012 Nuclear Safeguards Technology & Policy Workshop, 2012.

[4] D. Albright et al., “North Korea’s Lithium 6 Production for Nuclear Weapons”, Institute for Science and International Security, 2017.

A Study on Approaches of the International Community to Strengthen Nuclear Security Since 2016

Jae San Kim

Korea Institute of Nuclear Nonproliferation and Control, 1534, Yuseong-daero, Yuseong-gu, Daejeon, Republic of Korea

jaesan@kinac.re.kr

1. Introduction

International community's efforts to promote global nuclear security have made considerable progress with the hosting of the Nuclear Security Summit (NSS) since 2010. Until the summit ended, participating countries had worked to strengthen practical capabilities in a wide variety of nuclear security fields, such as the build-up of legal capacity (ratification of amendment to the CPPNM/ICSANT), removing weapons-grade nuclear material, improving each countries' nuclear security regulations systems and preventing illicit activities on nuclear materials/radioactive sources, etc.

Despite the end of the final NSS, international community hoped that the momentum for strengthening the global nuclear security would continue to be maintained. This has led to the IAEA activities as a central role of strengthening nuclear security, maintaining the nuclear security contact group (NSCG) on the basis of gift basket in NSS outcomes and expert-level discussions through major NGO meetings. This paper analyzed the international community's efforts to strengthen nuclear security measures since 2016 and derived the implications from these efforts.

2. Progress Activities of IAEA

The central role of IAEA had emphasized on each NSS communique. With the end of summit process, the governmental and technical level attention has taken over IAEA practical format.

[Hold the International Conference continuously] The IAEA has held international conferences on nuclear security almost every year and has kept the expert-level practical discussions. During the 2016 International Conference on Nuclear Security, a ministerial-level discussion was also arranged and declaration was adopted. In this conference, IAEA decided to hold a ministerial-level meeting every three years, hoping to maintain political momentum.

Table 1. IAEA Nuclear Security Conferences since 2016

2016	International Conference on Nuclear Security: Commitments and Actions (CN-244)	2,100 participants from 139 states; 47 ministers; 29 organizations
2017	International Conference on Physical Protection of Nuclear Material and Nuclear Facilities (CN254)	Almost 800 participants from 112 states; 15 organizations
2018	International Conference on the Security of Radioactive Material: The Way Forward for Prevention and Detection (CN-269)	550 participants from over 100 countries and 15 organizations
2020	International Conference on Nuclear Security: Sustaining and Strengthening Efforts (ICONS2020)	Over 2000 participants from 139 states; 47 ministers; 29 organizations

[Continuous Publication of Nuclear Security Guidance] IAEA has continued to publish recommendations for strengthening member states' regulations implementation systems. Since 2016, IAEA additionally published Nuclear Security Series as one of the most

significant IAEA nuclear security documents. Those documents are like those.

Table 2. Guidance Documents of Nuclear Security since 2016

2017	Self-assessment of Nuclear Security Culture in Facilities and Activities
2018	Physical Protection of Nuclear Material and Nuclear Facilities (Implementation of INFCIRC/225/Rev5)
	Developing Regulations and Associated Administrative Measures for Nuclear Security
	Sustaining a Nuclear Security Regime
	Building Capacity for Nuclear Security
	Computer Security of Instrumentation and Control Systems at Nuclear Facilities
2019	Establishing a System for Control of Nuclear Material for Nuclear Security Purposes at a Facility during Use, Storage and Movement
	Planning and Organizing Nuclear Security Systems and Measures for Nuclear and Other Radioactive Material out of Regulatory Control
	Preventive Measures for Nuclear and Other Radioactive Material out of Regulatory Control
	Security during the Lifetime of a Nuclear Facility

In addition, the IAEA has conducted activities to enhance the nuclear security of member states through the International Physical Protection Advisory Services (IPPAS), Integrated Nuclear Security Support Plans (INSSPs) and etc.

3. NSCG Progress from 2016

The NSCG was established in 2016 NSS through the Joint Statement on Sustaining Action to Strengthen Global Nuclear Security. After 2016, NSCG has convened annually at the time of IAEA General Conference. This meeting has facilitated and evaluated the implementation of NSS outcomes like commitments, gift baskets, and any other kinds of pledges produced by NSS process. ROK is also participating in the NSCG meeting and has been discussing ways to strengthen the nation's implementation status and global nuclear security.

4. Other Activities from Relevant Organization like NTI

NTI's Materials Risk Management team has convened the unofficial dialogue meeting on global nuclear security since 2012. These meetings have continued to draw meaningful results among government officials, industry representatives, and nongovernment experts to help sustain attention and accelerate progress toward global nuclear security system. [1]

The main discussion topics were like those: 1) Follow-up activity on Review Conference of the Amended CPPNM, 2) Sustaining the high-level political attention on global nuclear security, 3) Strengthening the international communities including IAEA, UN, GICNT, etc.

5. Conclusion

Each country's efforts to strengthen international nuclear security have been consistently implemented. From now on, various measures that have been drawn up should be put into practice to each countries' nuclear facilities. In addition, as the Amendment to the Convention on the Physical Protection of Nuclear Material entered into force in 2016, the review conference should be used well so that it can serve as a venue for practical discussions at the governmental and non-governmental level on enhancing nuclear security measures.

REFERENCES

[1] NTI Website, NTI Hosts 9th meeting of the Global Dialogue on Nuclear Security, 2019.

A Study on the Physical Protection Regulations for Nuclear Power Plants During Decommissioning

Seung Rae Kim
Korea Institute of Nuclear Nonproliferation and Control, 1534, Yuseong-daero, Yuseong-gu, Daejeon, Republic of Korea
srkim@kinac.re.kr

1. Introduction

Starting with the permanent shutdown of Kori Unit 1, the decision to shut-down and decommissioning the nuclear power plants in Korea is slowly beginning. Accordingly, it is necessary to study the changes of physical protection requirements for nuclear power plants in the decommissioning phase and the corresponding regulatory measures.

In this study, we identified the changes related to physical protection during decommissioning, analyzed the need for mitigation and strengthening of physical protection requirements, and considered appropriate procedures for mitigation and strengthening.

Please note that this is a personal study and is not related to actual regulations.

2. Procedure for Power Plant Decommissioning

Decommissioning procedures for nuclear power plants in Korea have not been finalized. However, according to the draft procedure for decommissioning Kori Unit 1 of KHNP, the main procedures are as follows.

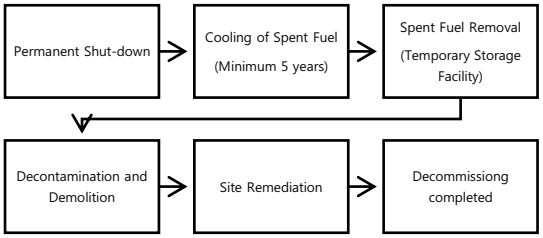

Fig. 1. Decommissioning Procedure.

3. Changes in physical protection requirements during decommissioning

3.1 Mitigation of Physical Protection Requirements

There are two periods of decommissioning procedures mentioned above that are likely to mitigate physical protection requirements.

First, it is the time after withdrawing fuel rods. After the fuel rods have been withdrawn from the reactor, cooling or safety-related systems may be unnecessary, allowing the lifting vital areas for some or most of the vital areas.

Second, it is the time after removal of spent fuel out of the site. If spent fuel is transferred to a temporary storage facility, nuclear material may not be present at the existing site. In such a case, the facility may only be required to comply with Article 7 in place of Article 1 through 6 of Annex 2, “Enforcement Decree of the Act on Physical Protection and Radiological Emergency”.

3.2 Strengthen Physical Protection Requirements

The main points of increasing vulnerability in terms of physical protection system(PPS) during decommissioning will be the below two points.

First is the period of transport of spent fuel to a temporary storage facility. At this time, a large amount of Class II nuclear material(spent fuel) should be transported on or off the site, so an appropriate physical protection plan should be established.

Second is the time to decommissioning. During the decommissioning, construction equipment and heavy tools should be brought in close proximity to the operating unit. Therefore licensees need to take protective measures against them.

4. Procedures for changing Physical Protection System

In order to change the physical protection system in response to the above-mentioned environmental changes, licensees should conduct the following two procedures.

4.1 Request for Change in Vital Areas

As mentioned above, in case it is deemed possible to change the vital areas if the withdrawal of nuclear material makes it impossible for sabotage to be caused by faults in the reactor and related systems, or for other reasons, the licensee may request a change review to a regulatory body.

4.2 Application for change of Physical Protection Regulations

The physical protection systems of plants are constructed in accordance with the physical protection regulations approved by the NSSC in accordance with Article 9 of the “Act on Physical Protection and Radiological Emergency”.

Therefore, if licensees wish to change a part of the physical protection system, including the change in vital areas, they shall apply for a change in physical protection regulations.

When applying for a change, objective evidence must be included to support the content. For example, if you want to change the physical protection regulations based on the release of nuclear material, you should have official data on nuclear material metering.

5. Conclusion

During the decommissioning, the environment related to physical protection will change. If the licensees want to relax the PPSs, they should apply for the change of physical protection regulations after the completion of the mitigation conditions have been completed, and if a strengthening is needed, they must apply for the change of the regulations before proceeding.

REFERENCES

[1] Korea Hydro & Nuclear Power Co., Ltd., Republic of Korea, accessed 4 September 2019, <http://www.khnp.co.kr>

Performance-based Vital Area Identification and Protection Measures Supporting IAEA NSS No. 16 Method

Seung Rae Kim
Korea Institute of Nuclear Nonproliferation and Control, 1534, Yuseong-daero, Yuseong-gu, Daejeon, Republic of Korea
srkim@kinac.re.kr

1. Introduction

The establishment and regulation of physical protection system for nuclear facilities is presented through IAEA recommend. However, most of the methods focus on nuclear facilities that newly constructed, which make it difficult to apply them directly to nuclear facilities during operation. In particular, vital area identification method is introduced in detail in IAEA NSS 16, but methodology is a very long time before technically deriving a protection set. In addition, the process of selecting vital area from protection set is briefly mentioned in NSS 16, but the procedure is one of the most important and difficult tasks for the operating nuclear facility. In this paper, the general approach follows the method of NSS 16. However, in the our method is applied to consider the nuclear facilities in operation and to reflect the changes in external threats and strengthening or weakening of physical protection system in the final vital area selecting.

2. IAEA NSS 16 method

2.1 Vital area identification (example)

In the virtual facility fault tree in Fig.1, there are two sabotage scenarios(SAB1 and SAB2). Safety system S1 is designed to mitigate SAB1, and S2 is designed to mitigate SAB2. System S1 has two train (T1, T2). If one of the two train works normally, S1 can successfully mitigate SAB1. L1~L6 can be expressed as a compartment where devices that guarantee the success of TRAIN are located. Analyzing Fig. 1 in the same way, the top event of fault tree can be expressed as follows.

$$\mathrm{HRC} = \mathrm{L8} * \mathrm{L2} + \mathrm{L9} * \mathrm{L3} * \mathrm{L5} + \mathrm{L9} * \mathrm{L3} * \mathrm{L6} \quad (1)$$

HRC (protection) can be derived as follows through the Boolean algebra complement operation of (1).

$$\mathrm{HRC(p)} = \overline{L8} * \overline{L9} + \overline{L8} * \overline{L3} + \overline{L2} * \overline{L9} + \overline{L2} * \overline{L3} + \overline{L8} * \overline{L5} * \overline{L6} + \overline{L2} * \overline{L5} * \overline{L6} \quad (2)$$

NSS 16 requires a variety of circumstances to be taken into account when deriving vital area from Eq. (2). Selects L2 and L9 combinations to designate vital area, the three possible combinations of events can be neutralized if the vital area protected.

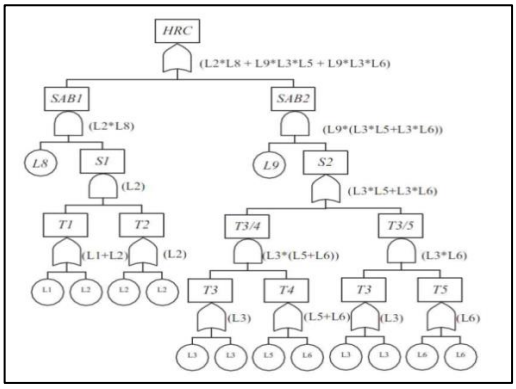

Fig. 1. Sample Figure.

3. Proposed methodology

The approach of proposed method is as follows. The performance-based approach limits the compartments listed in the Eq. (1). Performance factors include number of adversaries group and member, remain time after detection, internal force level, external force level. For example, a combination that destroys all of L9, L3, L5 of Eq. (1) can be excluded in advance through the above method. However, if a DBT is changed and a large number of adversaries group are added, it can be attackable combination, and in order to maintain the same vital area, other performance factors can be improved or solved through additional vital area designation. The following is how to derive and apply performance factors.

3.1 Number of adversaries group & member

The increase or decrease adversaries group directly affect the time required for malicious action. To simplify the problem, it is assumed that attack target for each group is set in advance, and that group first reaches the target goes to the remaining attack target. For example, if there are L9(3min), L3(2min), L6(1min)

compartments and two group intrude, the intrusion time will be less than 3min instead of 6min. Group A sets target L9, Group b sets L3, and Group b goes to L3 after completing its first mission. Since L6 (2nd) lead time goes to L3 to L6, it may take less time than 1min generally.

3.2 Remain time after detection

The time remaining after detection (TRAD) is a major factor. This is because the relationship between remain time and dispatch time of internal and external force is important factor.

If the TRAD is 10min and arrival time of response force is 5min, it can be classified as a protective compartment and removed from the attackable list. A 5 min margin was used here, but this can be set in consultation with the regulatory body. However, since the TRAD changes with time depending on the attack compartment, calculations are required for all compartments, and the arrival time of the response force will have special values unique to the facility.

Another problem is deciding when or where to be detected. It is difficult to establish where probability distribution is input to each detection sensor, the detection was made when the probability reached 95% through Monte Carlo method. The location where the probability of detection is 95% can change depending on intrusion path.

3.3 Application Example

Table 1 shows a result example of the proposed method. Additional measures are required for No 3. Attack method. At present, the facility is urgently required to deal with E3 and E4 compartment. It can be judged that it is generally economical to equip the E3 compartment with one minute of delay.

When IAEA NSS No 16 is applied, the HRC(p) of the facility may be E1, E3, E6. However, it is important to carry out the proposed method because the simple selection of vital area may not be achieved by securing delay time. In addition, the proposed method already secures sufficient delay time for E1 and E6 compartments. Also, if three team intrusion were made due to the change of DBT, HRC(p) could be E1, E3, E6. However, if the proposed method is applied, the attack of No. 4 is the most vulnerable because the TRAD becomes 7min, and the reinforcement of E6 is urgent, not the reinforcement of E3.

Table 1. Example

No	Target1	Target2	Target3	TRAD	RTMG
1	E1 (10min)			10min	10min
2	E2 (11min)	E3 (9min)		11min	10min
3	E3 (9min)	E4 (6min)		9min	10min
4	E4 (6min)	E5 (7min)	E6 (5min, from E4 or E5)	11min	10min
5	E6 (7min)	E7 (11min)		11min	10min

Table 2. Assumption lists

No	Assumption
1	Two teams invaded
2	Response time: 5min Margin: 5min (RTMG 10min)
3	Response force higher than invader. So probability of engagement is 100%
4	Detection 95% position was derived through Monte Carlo Simulation based on the weak path

4. Conclusion

IAEA NSS No 16 method has a proposition that all attack paths are blocked when all vital area are protected. However, the entire physical protection system, such as the delay time for each compartment, cannot be approached from a performance point of view, and the derived vital area is form of demorgan's law of attack set, which is not intuitive.

In this paper, we propose a performance-based attack set analysis that complements this and attach a simple example to apply it. In the future, the method of this paper will be further researched to develop a new procedure that performs performance evaluation (detection and response) more precisely and links with NSS No. 16 method.

REFERENCES

[1] IAEA Nuclear Security Series No. 16 "Identification of Vital Areas at Nuclear Facilities", 2012, VIENNA.

[2] Y.W Kang, "Tool for evaluation security system introduction and development status", IAEA CN-254 2017 Conference, 2017, VIENNA.

[3] Y.W Kang, "Simulation based PPS vulnerability assessment", The Korean Institute of Industrial ENG, 2019, GWANJU.

Exemption and De-exemption in Safeguards

Sung Ho Lee*, I C Kim, B D Lee, H J Kim, H S Kim, J A Jung, and S M Han
Korea Atomic Energy Research Institute, 111, Daedeok-daero 989beon-gil, Yuseong-gu, Daejeon, Republic of Korea
*shlee10@kaeri.re.kr

1. Introduction

KAERI operates 11 facilities(11 MBAs) for safeguards. Basically nuclear material for nuclear R&D as well as power generation should be under the application of the safeguards. But it seems that most researchers feel burdened to implement safeguards. Actually nuclear materials to be used for R&D are various in the aspect of the use, amount, concentration, enrichment, physical and chemical forms based on the research field. In some case, nuclear material can be used for not nuclear purpose such as medical, instrumentation, safety fields and others. There are many ways to treat nuclear material in safeguards. In this study, for the peaceful use of nuclear material, the system on exemption and de-exemption is studied based on long-term experience on safeguards.

2. Understanding of Exemption in Safeguards

2.1 Situation in the field

Basically, in the nuclear R&D field, activities on safeguards should be implemented before receiving nuclear material such as submission of DIQ (Design Information Questionnaire) including plan of treatment and safeguards of nuclear material. When the nuclear material is received to MBA, accounting the information should be reported by IAEA reports(normally ICR, PIL and MBR) regularly. Based on the DIQ and accounting reports, IAEA performs various kind of inspection to declared nuclear facility and nuclear material.

But some researchers carry out the R&D and treat nuclear material for non-nuclear purpose such as shielding material of radioisotope transportation container, instrumentation and calibration of nuclear equipment. This kind of nuclear materials above mentioned can be non-nuclear area as well as nuclear area in the safeguards view.

For this, IAEA permits the exemption and de-exemption system.

2.2 Exemption and de-exemption system

In safeguards, exemption system is used for the special cases in the field. Exemption system in safeguards is several characteristics as follows; first, exemption of safeguards is different from that of safety. Second, exemption in safeguards can be carried out under the approval of IAEA (Requirements are defined the Agreement between ROK and IAEA for the

application of safeguards in connection with the treaty on NPT). Third, exempted nuclear material is excluded from safeguards in temporary not permanent. Fourth, nuclear material exempted should be re-applied in safeguards, and then it can be used or terminated.

2.3 Consideration of exemption

KAERI has implemented for about 50 years. From the early time of safeguards, exemption was studied and carried out for the convenience of researchers. For example, nuclear materials exempted are not included in IAEA inspections But exemption activity should be carried out carefully in the field. The reason is why nuclear material exempted is apt to be left without management as time goes on. It can be difficult in the re-application of safeguards. Therefore, under the current exemption system, it is necessary to enhance as follows; increasing the safeguards capability of facility operators, maintaining long-term working career in safeguards, strict controlling the movement of material exempted, regular notice related to the facility operators.

3. Conclusion

Some of nuclear material can be included in the boundary of exemption requirements based on the purpose, amount, physical & chemical property. But those materials should be re-applied in safeguards at some future day. In the field nuclear material exempted is apt to be left without management as time goes on. To prevent this situation, 4 considerations are suggested as follows; increasing the safeguards capability of facility operators, maintaining long-term working career in safeguards, strict controlling the movement of material exempted, regular notice related to the facility operators.

REFERENCES

[1] Agreement between ROK and IAEA for the application of safeguards in connection with the treaty on NPT.

[2] IAEA Safeguards Glossary, 2001 Edition.

The Status of Nuclear Material Accountancy at KAERI

Hyun-Jo Kim*, In-Chul Kim, Byung-Doo Lee, Sung-Ho Lee, Hyun-Sook Kim, Juang Jung, and Seong-Mi Han
Korea Atomic Energy Research Institute, 111, Daedeok-daero 989beon-gil, Yuseong-gu, Daejeon, Republic of Korea
*keiki@kaeri.re.kr

1. Introduction

KAERI is a national nuclear research institute and conducts experiments using various types of nuclear materials. KAERI consists of 11 nuclear facilities subject to IAEA safeguards, which are divided into item facilities and bulk handling facilities according to the type of nuclear materials handled at a facility.

KAERI developed a KASIS (KAeri Safeguards Information treatment System) for near real-time nuclear material accounting to effectively cope with random interim inspection under Integrated Safeguards.

This paper describes the status of nuclear material accounting system in the nuclear facilities at KAERI and the problem at the bulk handling facilities.

2. Nuclear material accountancy at KAERI

2.1 Typical nuclear material accountancy

In terms of nuclear material accounting, nuclear facilities are divided into item facilities and bulk handling facilities. Item facility is a facility where all nuclear material is kept in item form and the integrity of the item remains unaltered during its residence at the facility. Examples of item facilities are most reactors and storage. Bulk handling facility is a facility where nuclear material is held, processed or used in bulk form. So physical and chemical form of nuclear material are changed during the process. Examples of bulk handling facilities are plants for conversion, enrichment and fuel fabrication.

The approach of the nuclear material accounting is applied differently depending on the whether the nuclear material is an item form or a bulk form. All inventory changes of nuclear material should be reported to IAEA in an item facility and the items should be maintained with the same batch name. On the other hand, in case of bulk handling facility, storage area is applied in the same way as the item facility, but in the process area, the physical and chemical form of nuclear materials are changed frequently. So, the inventory changes of nuclear material in process are not reported to IAEA and the total amount of nuclear material is managed.

2.2 Nuclear material accounting system at KAERI

KAERI developed a web-based nuclear material accounting system called KASIS to cope with short notice inspection under IS. Each facility operator inputs the accounting data into KASIS whenever the inventory changes of nuclear material are occurred.

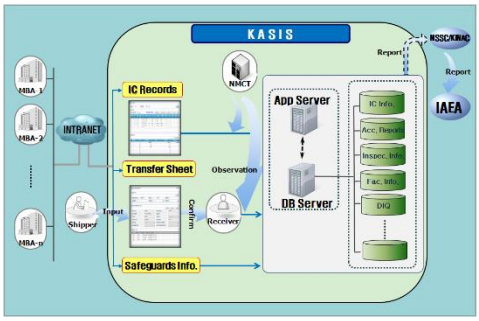

Fig. 1. Schematic Diagram of KASIS.

Since the KASIS is designed based on an item facility, it does not reflect the characteristics of in-process nuclear material in bulk handling facility. Therefore, it is recommended to rebatch after the process is completed in bulk handling facility. However, in case of R&D facility and LOF at KAERI, the amount of nuclear material is small and there are many uses of nuclear material, so the facility operators often do unnecessary rebatching on the in-process nuclear material for the management of the nuclear material inventory. On the other hand, HANARO fuel fabrication facility at KAERI has its own nuclear material inventory management system and it is connected with KASIS. Therefore, the in-process nuclear material is managed by its own system and only the inventory changes such as manufacturing of fuel rods/assembly and transfer from/into other MBAs are reported to IAEA.

In addition, the connection of KASIS to RFID system for radiation safety management also results in unnecessary rebatching. The facility operator has to input the RFID system when the nuclear material moves between buildings. Therefore, if there are several buildings in an MBA, unnecessary rebatching occurs for the transfer of nuclear material within the same MBA.

In order to solve the unnecessary rebatching problem in bulk handling facilities, it is necessary to establish its own inventory management system for each facility.

3. Conclusion

This paper reviewed the status of nuclear material accounting system at KAERI. KAERI has performed the nuclear material accounting using KASIS. Since KASIS is designed based on the item facility, some problems such as unnecessary rebatching may occur in bulk handling facility. Therefore, in case of bulk handling facilities that use small amount of nuclear material, it is necessary to establish their own inventory management system.

REFERENCES

[1] IAEA, “IAEA Safeguards Glossary”, 2001.

[2] IAEA, “Safeguards Implementation Practices Guide on Provision of Information to the IAEA”, 2016.

[3] B.D. Lee, “The Analysis of Nuclear Material Accounting System at KAERI site”, Proc. of the KRS 2016 Autumn Conference, 14(2), October 12-14, 2016, Jeju.

Technical Review on R&D Trends in Unmanned System for Safeguards Inspection

Ju Young Jeon, Sungmin Kim, Myungsoo Kim, Hyun Young Kim, and Heejun Chung*

Korea Institute of Nuclear Nonproliferation and Control, 1534, Yuseong-daero, Yuseong-gu, Daejeon, Republic of Korea

*hjchung2@kinac.re.kr

1. Introduction

The demand for new safeguards approaches and tools is on the rise due to a need to develop multi-disciplinary techniques such as application of an unmanned device in various fields and the emerging use of traditional techniques. The present authors, therefore, is trying to develop a novel safeguards approach to timely detect undeclared nuclear activities and find hidden nuclear materials by using unmanned vehicles and gamma-probes. As a first step, the technical review on international/domestic R&D trends for nuclear safeguards and security was conducted.

2. Design Concept

The initial design concept of the unmanned system is 1) to collect geological information at suspected area, 2) spread out gamma-probes to collect radiological information, and 3) transmit the information via wireless system [Fig. 1].

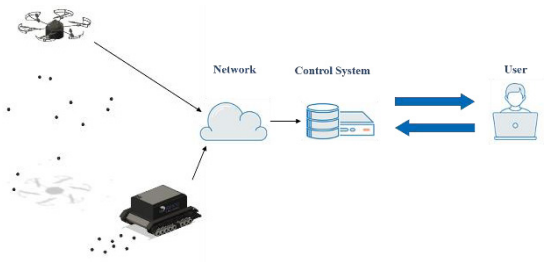

Fig. 1. The initial design concept of the unmanned system.

3. Technical Review

3.1 Unmanned Aerial Vehicles (UAVs)

After the nuclear accident of Fukushima Daiichi Nuclear Power Plants, many countries focus on unmanned system and discuss about technical issues through international meeting (Aerial Measuring System, AMS) hosted by the U.S. National Nuclear Security Administration [1]. More than 10 countries are participated AMS every year and the main topic of each year are listed in Table 1.

Table 1. AMS International technical exchanges

Year	Topic
2012	Constantly improve aerial measurement mission
2013	AMS consequence management operation
2014	AMS data analysis
2015	Radiological anomaly detection algorithms
2016	UAV/UAS for radiological emergencies
2018	Uncertainty in radiological aerial measurement
2019	Training and exercises for aerial measurement

From those meetings, several new techniques for radiological aerial monitoring system have been discussed. The most outstanding results from the meeting are to share 1) the technology and information of each participated country, 2) detailed radiation mapping technique, 3) uncertainty evaluation skill, and 4) wireless technique to transmit geological and

radiological information. These shared techniques and information are expected to be applied to the proposed concept of the unmanned system.

3.2 Unmanned Ground Vehicles (UGVs)

In fact, many robot technologies have been accelerated and emerged into nuclear engineering for radiation monitoring, damage investigation and inspection, and removal of radioactive debris after Fukushima disaster [2].

Recently, UGVs are equipped with a VR camera, radiation detector, and GPS system in order to provide the more detailed environmental information to an operator. Besides, it is possible to collect and transfer the target objects with a heavy manipulator arm [Fig. 2].

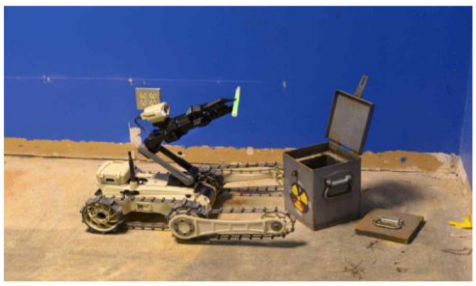

Fig. 2. Unmanned Ground Vehicle.
(Photo by Randy Montoya, Sandia National Lab)

Some technical issues are still remained such as heavy weight with various equipped devices, short battery lifetime, or radiation hardening for a sensor and circuit.

3.3 Gamma Probes

A gamma-probe is a mapping tool mainly employing a small size gamma detector and wireless transmitter [Fig. 3].

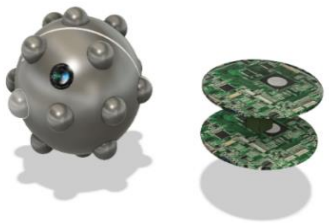

Fig. 3. The initial design concept of the gamma-probe.

The location of hidden nuclear materials can be easily identified by the difference of signal strength collected from each probe spread out at suspected area.

Only few studies have been conducted to develop a gamma-probe but some similar techniques have been developed in the field of nuclear medicine. Therefore, it is expected to perform the inter-disciplinary study for a gamma-probe between nuclear safeguards and medicine.

4. Conclusion

This study conducted an in-depth analysis of the advances of the unmanned technique and gamma-probe, and assessment of the initial design concepts suggested by the present authors. A further step will be to finalize the design, build prototype devices, and carry out the feasibility test.

REFERENCES

[1] Wasiolek, P, “Brief History of AMS Technical Exchanges”, RSL, DOE/NV/03624-0166 (2019).

[2] Hisashi OSUMI, “Application of Robot Technologies to the Disaster Sites”, The Japan Society of Mechanical Engineers (2014).

Study of Soil Sampling Procedure for Safeguard Inspection

Geon Yong Lee, Ju Young Jeon, Hyun Young Kim, and Heejun Chung*
Korea Institute of Nuclear Nonproliferation and Control, 1534, Yuseong-daero, Yuseong-gu, Daejeon, Republic of Korea
*hjchung2@kinac.re.kr

1. Introduction

The quality assurance of 'pre-analysis procedure' including sample collection, handling, transportation to laboratory is one of the most important factors for data quality. KINAC has to provide the national procedure in order to verify undeclared nuclear activities and find hidden materials. For that, Korea Industrial Standard (KS) and American Society Testing and Material (ASTM) technical standard for soil sampling have been reviewed, and technical requirements and approaches to set up the soil sampling procedure in denuclearization area were suggested in this study.

2. Methods and Results

2.1 Korea Industrial Standard (KS)

KS describes some methods for soil sampling in agriculture and horticulture. It suggests that samples are obtained via W or X method [Figure 1]. Those samples are then mixed and analyzed to acquire well-defined data represented site characterization.

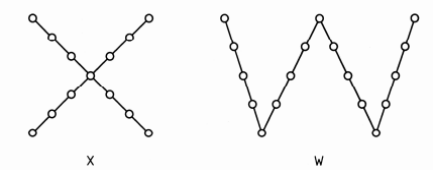

Fig. 1. X and W method of sampling [1].

KS also suggests the circular grid sampling method to assess the variation and distribution of contamination across a field. To apply this method, it is required to set the radius around the facility in order to determine sampling points [Figure 2]. This method is often used to detect residual contamination around a storage tank or facility.

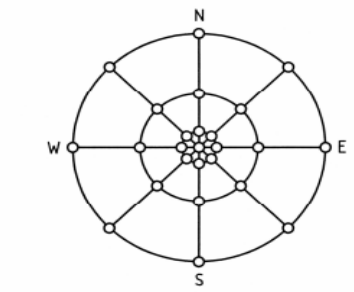

Fig. 2. Circular grid sampling method [1].

KS additionally provides some methods for sampling design regarding various site characterization.

2.2 American Society Testing and Material (ASTM)

Since the types of samples are taken at various sites, it is important to take the proper sampling equipment. ASTM provides the sampling equipment and materials in detail.

Auger boring is one of the simplest soil sampling equipment widely used. There are many kinds of auger so the proper type of an auger has to be selected according to the

purpose of soil sampling. To select the proper equipment, it is necessary to identify any obstructions on the surface.

Typically, a screw type auger is suitable for shallow depth soil sampling and a mud auger is suitable for wet and clay soil samples. In case of hard soil, the helica auger is widely employed.

Ensuring the quality of taken samples is also important so those samples has to be securely protected and the appropriate procedure for sample transportation should be established. The samples are supposed to be sealed in a suitable container with the sample information label.

2.3 Application of Sampling Procedure

An action or progress on the denuclearization of Korean peninsula is currently facilitated. Considering nuclear facilities in N. Korea, the technical requirements and approaches for soil sampling are summarized in Table 1 [3].

Table 1. Technical requirements and approaches for the soil sampling procedure

Site selection and collection interval
● 1m end of waste storage facility ● Circular method for sampling around a facility ● Adopting the X-type sampling method for sites without obstacles ● Requires at least 5 samples per point ● Collect samples at intervals of up to 35 m by point
Depth of sampling and equipment
● Top soil layer: U8 vessel, Scoop ● Other: Screw type Auger, Ship-type Auger, Thin-walled Tube ● Hard soil: Helica Auger, Power auger ● Clay: Dutch-type Auger, Barrel Auger (Use drill-type extraction equipment for deep sampling)
Expected sample composition
● Nuclear fuel materials: U, UO_2, PuO_2 ● Uranium enrichment: UF_6 ● Fuel fabrication: UF_4, Ca, Mg(powder), $MgFe_2$ ● Reprocessing process: TBP, HNO_3, H_2SO_4, NaOH ● Etc : HF, F_2, H_2SO_4
Sample storage container
● Acid samples: Plastic containers, glass bottles (HNO_3, H_2SO_4) ● Basic samples: Plastic containers (NaOH) ● Organic Compounds: PTFE containers (dodecans)
Sampling report details
● Sample name, date of sampling, time of sampling, type of sampling ● Name, address, phone number of the user ● Weight, quantity, density, GPS location of sample ● Description of type, depth, section, and particulars of sampling soil ● Equipment and sampling process

3. Conclusions

This study aims at developing the well-suited tools and procedures for a sample collection, handling, and transportation in order to verify a declaration of nuclear activities or identify concealed nuclear materials. As a first step, technical requirements and approaches for soil sampling were summarized by reviewing the international and domestic standards. As a final goal, the national procedures for various types of environmental samples such as air, water, and soil will be established through this work.

REFERENCES

[1] KS, Soil Sampling Part1: Guidance on the design of sampling programs, KS I ISO 10381-1.

[2] ASTM, Standard Practice for Soil Exploration and Sampling by Auger Borings, ASTM D1452/D1452M-16.

[3] KAERI, Preparation of D&D Strategy opposed to the denuclearization of North Korea, KAERI/RR-3091/2009.

Preliminary Measurements of Uranium Samples With Portable X-ray Fluorescence Equipment

So Yeon Shin, Woojin Kim*, and Minsu Kim
Korea Institute of Nuclear Nonproliferation and Control, 1534, Yuseong-daero, Yuseong-gu, Daejeon, Republic of Korea
*kimwj@kinac.re.kr

1. Introduction

Nuclear forensics plays an important role in the makeup of national nuclear security systems [1], and is recognized as a key factor supporting the management of radiological related crime scene and the investigation of nuclear security events [2]. In this study, we conducted preliminary experiments and results analysis of measurement spectra for the possible application of portable x-ray fluorescence (XRF) equipment in nuclear forensics, where such equipment may be used for elemental or chemical characterization in the event of discovery of unknown nuclear material.

2. Instrument

The specifications of the XRF spectrometer used in this experiment are as follows. The Bruker Tracer III-SD has an X-ray tube with a rhodium target and a silicon drift detector (Si PIN diode). It contains no radioactive material. The Tracer III-SD operates with a resolution of 147 eV FWHM for 5.9 keV, at 200,000 counts per second. The X-ray beam is collimated with dimensions of 4 mm x 3 mm. The spot size of analysis is approximately 10 mm in diameter. The maximum voltage is 40 keV, which is in the soft X-ray range.

3. Results and Discussion

A low-enriched uranium (LEU) pellet of 4.1% $^{235}U/^{238}U$ and a depleted uranium (DU) disk held in KINAC were employed in a measurement performance test of nuclear material with portable XRF. The spectrometer measured at right angles to the plane of the specimen at 15 kV, 30 kV, and 50 kV for 3 min.

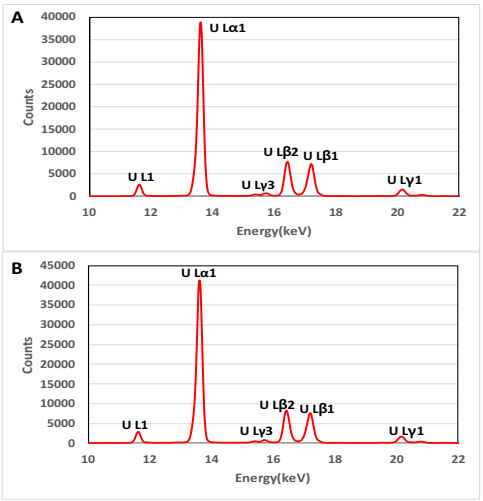

Fig. 1. L-lines XRF spectra of (a) DU and (b) LEU.

The spectrum at 30 kV was the clearest, and was therefore chosen to be the subject of analysis in this study. Both samples showed a dominant U L_α peak at 13.61keV and then a smaller U L_β peaks at 16.43keV and 17.22keV. This is similar to an XRF analysis of the previously known pure uranium.

Table 1. Measurement results for uranium

Element	K_α/L_α (keV)	K_β/L_β (keV)	A: Conc (%)	B: Conc (%)
Al_2O_3	1.49	1.56	2.193	1.219
K_2O	3.31	3.59	5.824	5.127
Rb	13.40	14.96	3.426	3.279
Nb	16.62	18.62	2.247	2.370
Mo	17.48	19.61	1.911	2.052
Ce	4.84	5.26	1.093	1.051
U	13.61	17.22	40.278	44.263

A: depleted uranium, B: low-enriched uranium (LEU)

In the analyzed spectra, trace amounts of impurities were detected for elements K, Al, Rb, Nb, Mo, and Ce, although most peaks found were for uranium.

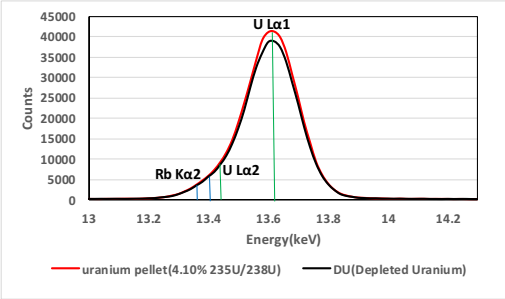

Fig. 2. Magnified U Lα peaks from the XRF spectrum for LEU (red) and DU (black).

These impurities were difficult to identify from the spectrum, as seen in Figure 2, because for example the rubidium Kα peak overlaps with the uranium Lα peak, and further, different amounts of rubidium can be determined depending on deconvolution. Thus it is difficult to determine the existence of other impurities, including rubidium, making it necessary to identify the exact trace elements through other analytical devices such as ICP-MS.

In addition, a difference between the LEU pellet and DU Lα peak counts was observed. Because there are various complicating effects, such as differences between uranium and oxygen bonds, matrix effects, surface effects, and so on., the exact cause of the difference could not be determined. In this regard, further experiments are needed in a limited environment.

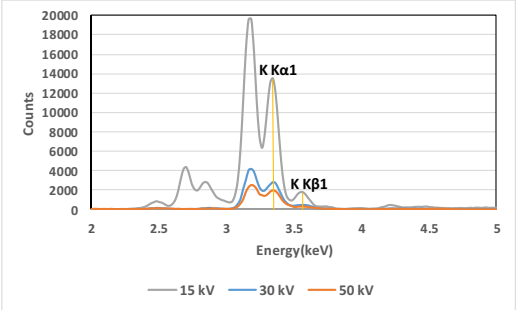

Fig. 3. XRF spectrum of magnified potassium.

Other elements did not show much variation in terms of voltage, but in the case of potassium, the difference in the peaks was particularly large. As discussed in a related report, this is due to the fact that the energy range of the x-rays increases as the voltage increases [3].

4. Conclusion

For the application of portable XRF to the characterization of uranium specimens, we will preliminarily use uranium standard substances to draw calibration curves and compare XRF data for various materials, including uranium. With this data, experimental procedures for portable XRF in field type nuclear forensic analysis and related data analysis methods will be systematized.

REFERENCES

[1] IAEA NSS No.15, Nuclear Security Recommendations on Nuclear and Other Radioactive Material out of Regulatory Control.

[2] IAEA NSS No.22-G, Radiological Crime Scene Management.

[3] Environmental pollution measurement and analysis technology development of portable ED-XRF.

LIBS Analysis of Simulated Electro Refining Salt Sampled Using the Dip Stick

Seul-Ki Han, Se-Hwan Park*, and Seong-Kyu Ahn

Korea Atomic Energy Research Institute, 111, Daedeok-daero 989beon-gil, Yuseong-gu, Daejeon, Republic of Korea

*ex-spark@kaeri.re.kr

1. Introduction

The Korea Atomic Energy Research Institue (KAERI) has explored Laser Induced Breakdown Spectroscopy (LIBS) as a promising technique for pyroprocessing safeguards measures because a remote, in-situ analysis of a material is possible.[1] LIBS is based on the optical analysis of the plasma generated by concentrating a strong laser beam on the surface of the sample. LIBS has characteristic such as real-time analysis, multi elements analysis and no sample preparation before the analysis.[2-5] The dip stick is a measuring device which can quantitatively analyze the concentration of elements in a molten salt by using the salt when it is immersed in the molten salt and then pulled out. It is very useful in that no sample preparation process is required. In this study, U and lanthanide element in LiCl - KCl salt are measured as electrorefining process material of pyroprocessing via LIBS, using a dip stick for real-time analysis without making samples.

Fig. 1. Dip stick.

2. Methods and Results

In this experiment, simulated electro-refining salt samples were made by adding $LaCl_3$, $CeCl_3$, $BaCl_2$, $PrCl_3$, $NdCl_3$, YCl_3 , $SmCl_3$ and UCl_3 to LiCl-KCl salt. The concentration of U in the samples were from 1.0wt% to 8.0wt%. Composition materials of the samples were placed in the Al_2O_3 crucible, and they were heated up to 650°C to melt. It was maintained for 7 hours, and Sampling was performed using a dipstick. Experiments were conducted in a glove box with an atmosphere of Ar gas with moisture and oxygen content of 100 ppm or less for samples with high deliquescence. A laser beam was injected through the port of the glove box and the plasma emission light was collected through optical fiber. The sample surface was somewhat irregular and the distance between the sample and the focusing lens was corrected each time the sample surface was changed by interlocking the XYZ moving sample table with a high precision distance meter to match the same focal length. A beam of Q-switched Nd: YAG pulse laser (Brilliant B, Quantel) with a wavelength of 532 nm is focused on the sample surface to generate plasma and Echelle spectroscopy with 20,000($\lambda/\Delta\lambda$) resolution to detect plasma emission line and ICCD camera was used. The emission lines of U and other emission line were selected in the wavelength region of 200 to 410 nm where spectroscopy is permitted. The number of laser pulses in the measurement was 30. After collecting of LIBS spectrum at 9 different position, the sample was moved to obtain the scan data of the sample surface. The measured U spectrum in the wavelength 304.413nm was analyzed. The U peak intensity is normalized with peak intensity of the Nd 363.430 nm line.

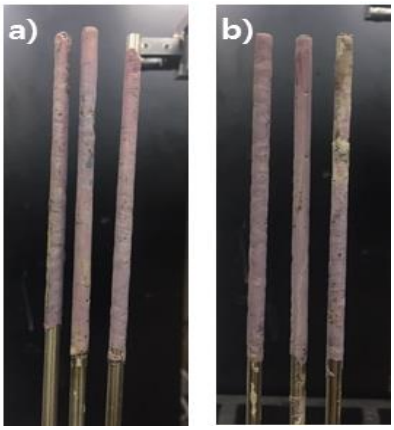

Fig. 2. Salt sampled using the dip stick
a) no stirring, b) stirring.

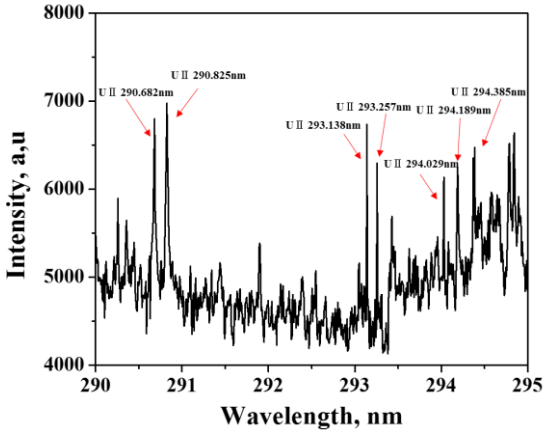

Fig. 3. U spectrum in a Salt sampled using the dip stick.

3. Summary

LIBS is a promising technology as the process monitoring technology applicable to the pyroprocessing safeguards. The uranium concentration in LiCl-KCl salt were measured using LIBS system, and the quantitative analysis performance of LIBS such as repeatability and Limit of Detection (LOD) are analyzed. Our result is promising for application of the LIBS to the safeguards.

ACKNOWLEDGEMENT

This work was supported by a National Research Foundation of Korea (NRF) grant funded by the Korean government's Ministry of Science and ICT (MSIT) (No. NRF-2017M2A8A5015084). And, this work was partly supported by the Nuclear Safety Research Program through the Korea Foundation Of Nuclear Safety (KoFONS) using the financial resource granted by the Nuclear Safety and Security Commission (NSSC) of the Republic of Korea (No. 1903014)

REFERENCES

[1] B.Y. Han et al., Analysis of the applicability of LIBS to address safeguards needs with respect to pyroprocessing, KAERI/TR-6607/2016, 2016.

[2] Ammon N. Williams at el., Elemental Detection of Cerium and Gadolinium in Aqueous Aerosol via LIBS, Appl. spectrosc, Vol 70, pp.1700-1708, 2016.

[3] Cremers. D.A at el., Remote elemental analysis by laser-induced breakdown spectroscopy using a fiber optic cable", Appl. Spectrosc, Vol 49, pp. 857-860, 1995.

[4] Davies. C.M at el.t, Quantitative analysis using remote laser-induced breakdown spectroscopy, Spectrochim. Acta Part B, Vol 50, pp. 1059-1075, 1995.

[5] Andrew I. Whitehouse, Laser-induced breakdown spectroscopy and its application to the remote characterisation of hazardous materials, Spectroscopy Asia, Vol 2, No. 2, pp. 13-18, 2006.

Review of Domestic Applicability for NDA's Site End State Definition Process

Hyejin Jung* and Su-hee Lee
KHNP Central Research Institute, 70, Yuseong-daero 1312beon-gil, Yuseong-gu, Daejeon, Republic of Korea
*junghj8113@khnp.co.kr

1. Introduction

The decommissioning of Kori Unit 1 is the first decommissioning for commercial Nuclear Power Plant (NPP) in Korea, and the pending issue not only to nuclear power officials but also to the public. The decommissioning of NPP also implies that the current generation will pay its debts to future generation for the benefits of using nuclear facilities. Therefore, it is necessary to lead the decommissioning of NPP with thorough preparation and clarification of the final goal including the site end state. To this end, this paper reviews the UK Nuclear Decommissioning Authority (NDA)'s site end state definition process and suggests domestic applicability.

2. NDA's Process Overview

2.1 Objective

The objective of the process is to come up with a solution that satisfies the desires of the community (the stakeholders), is technically and commercially feasible and is aligned with the national perspective. The process set out in this paper incorporates a series of stages aimed at defining End States solutions that fall within this range of acceptability and desirability – the outcome of which will be reconciled by the NDA incorporated into the NDA Decommissioning Strategy.

2.2 End state definition

The 'End State' of a site is the physical condition of the site at the point at which the NDA has finished its business.

A key point to note with this definition is that it does not necessarily require that all radiological material be removed from the site, since it is possible for the site to remain under long-term institutional control even after the NDA has finished its work.

It is possible that a site End State may be mixed – it may consist of a number of areas remediated to standards appropriate for differing potential re-uses.

2.3 Responsibilities

2.3.1 NDA.

- Lead the End State definition process by agreeing the process to be used by the SLCs and ensuring SLCs provide support to SSGs.
- Undertake reconciliation of suggested End States with issues of national strategy.
- Incorporate output of process into NDA Strategy.

2.3.2 Site License Company (SLC).

- Facilitate the process for consultation with the stakeholders.
- Provide technical expertise to define a range of feasible End State solutions.
- Engage stakeholders on End State solutions

2.3.3 Site Stakeholder Groups (SSG).

- Agree a process for consultation that includes consideration of how to engage with the wider local stakeholder community (i.e. those not already represented within the SSG).
- Review consultation responses and arrive at a hierarchy of Site End Uses that represents the desires of the broad range of local stakeholders.
- Provide NDA with representative feedback on End States presented by the SLCs.

3. NDA's Site End State Definition Process

The process for achieving End State definition is represented by the flow diagram in Figure 1.

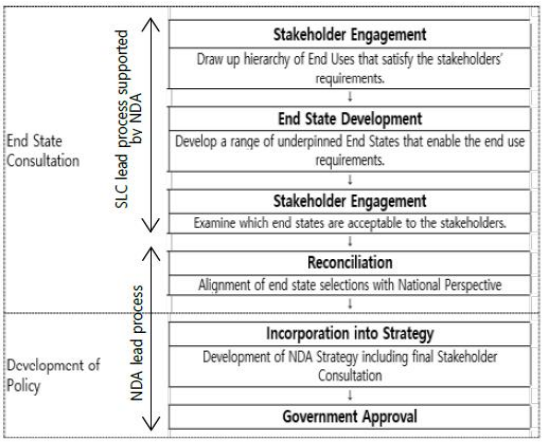

Fig. 1. Site End State Definition Process.

3.1 Stakeholder consultation on end uses

The process will begin by understanding the

stakeholders' preferences for the End Use of site through the first phase of stakeholder consultation. As part of this process, stakeholders will be encouraged to define a hierarchy of End Uses, comprising a range of End Uses of varying degrees of preference.

Table 1. Use of Site

Site End Use	Example
Industrial and commercial	Power generation, Business park, Manufacturing/processing Facility, Port (air/sea), Hospital
Waste management	Radioactive or non radioactive waste conditioning/processing, Radioactive or non radioactive waste repository
Research	Science park, Environmental restoration centre
Recreational (non licensed only) and nature conservation	Theme park, Nature reserve, Industrial history museum, Holiday park, Leisure centre, Zoo / Safari park, Outward bound centre
Accommodation (non licensed only)	Housing estate, Residential care home
Agriculture (non licensed only)	Pastoral/Arable farming

3.2 End State development

The SLC will then use the hierarchy of End Uses to develop a set of End States that meet the stakeholders' requirements for End Use. As part of this work, the SLC will also be responsible for underpinning the commercial and technical feasibility of achieving particular End Uses and identifying the long and short-term consequences associated with achieving the End States. Contaminated land may be an important issue in determining the feasibility of specific End States as it is a major determinant of the amount of remediation required to achieve certain End States.

3.3 Stakeholder consultation on end states

During the second phase of stakeholder consultation, the SLC will engage with stakeholders on the list of defined End States and the consequences of achieving them. The aim of this process is to understand which End States would be acceptable to the stakeholders, noting that this may consist of mixed End States.

3.4 Reconciliation

The output of this process of stakeholder engagement will then be passed to the NDA, who will collate the output for site and reconcile the End State solutions with other strategic issues such that they take account of the national perspective. The outcome of this process will involve developing proposed End States to be incorporated into the NDA's next draft Strategy, which will be published for national public consultation before being submitted to the Government for approval.

A key point to note here is that the stakeholders have multiple opportunities to input into the strategy during the development of the initial end states, and then during the public consultation on the NDA Strategy. Additionally, the Strategy must be reviewed at least every five years, so there will be further opportunities for stakeholder engagement, and for changes in understanding or national policy to be considered.

4. Conclusion

The level of remediation of Kori Unit 1 site is planned to be 'restricted reuse', but the site utilization plan (i.e. end state) is not yet defined. It aims to be established by 2032 after receiving local opinions and expert advices. The site end state should take into account domestic and international social impacts and technical issues, and reflect the merits through benchmarking best practices for decommissioning nuclear power plants abroad. In addition, a decision-making process is needed to define end state of the site.

This paper reviewed the decision-making process of the UK NDA as follows: 1) Determining a hierarchy of End Uses for the site through a result of a dialogue between the Site Owner and Stakeholders, 2) Defining a range of End States that match the hierarchy of End Uses identified by the stakeholders, 3) Discussion between the stakeholders and the Site Owner on the range of End State definitions to understand the acceptability of particular End States to the stakeholders, 4) Drawing together the output from the End State consultation process and reconciling this with the outcomes of other strategic initiatives to ensure that they reflect national as well as local requirements. This process will be applicable to the process of determining the end state of Kori Unit 1.

REFERENCES

[1] NDA, "Site End State Definition Process", NDA REPORT Engineering Directorate, EGR015 (2006).

[2] KHNP, "Final Report for Establishment of a Decommissioning Strategy Considering the Domestic Situation", Technical Draft(2019).

Status of Domestic Use and Regulations for Small Quantities of Nuclear Material

Jihyun Ahn[1], Junsung Park[1], Hee Seo[1,*], Seungmin Lee[2], Jae Woong Tae[2], and Seung Ho Ahn[2]

[1]Chonbuk National University, 567 Baekje-daero, Deokjin-gu, Jeonju, Jeollabuk-do, Republic of Korea

[2]Korea Institute of Nuclear Nonproliferation and Control, 1534, Yuseong-daero, Yuseong-gu, Daejeon, Republic of Korea

[*]hseo@jbnu.ac.kr

1. Introduction

The use of small quantities of nuclear material (SQNM) exempted from licensing and reporting obligations under the Nuclear Safety Act has recently increased in Korea; however, domestic systems and measures to systematically manage the SQNM exempted are insufficient in terms of effective and efficient IAEA safeguards implementation. Needless to say, the government needs to comply with international obligations under the Korea-IAEA Safeguards Agreement and establish a systematic control system of the SQNM. In this study, the domestic use and characteristics of the SQNM were surveyed. Then, the domestic regulations and the foreign legislations for nuclear material control were reviewed to draft an improved way for controlling the SQNM in Korea.

2. Small Quantities of Nuclear Material

2.1 Domestic use of SQNM

Korea Institute of Nuclear Nonproliferation and Control (KINAC), as a technical expert organization for the nuclear security and safeguards in Korea, manages the SQNM through the web-based management system [1]. The organizations that use the SQNM are classified as locations outside facilities (LOFs). The national LOFs consist of a single material balance area (MBA) with three key measurement points (KMPs) in Korea according to the characteristics of each organization.

In KMP A, there are 70 organizations that mostly uses depleted uranium (DU) as a shielding material for a commercial gamma-ray irradiator in non-destructive testing applications (transmission imaging or thickness gauge). In KMP B, there are 50 organizations, mostly universities and research institutes, which use the SQNM for research purpose or standards materials. In KMP C, there are 3 industrial companies that use the SQNM mainly for manufacturing the filaments or measuring the temperature of liquid glass.

2.2 Characteristics of SQNM

Among the various uses of the SQNM, following three uses were identified as the major uses of the SQNM in Korea: shielding material with DU, standard materials, and thorium added electrodes.

DU used for shielding material is denser than lead by 67%. It has a high melting point

(~1130°C) and a tensile strength comparable with that of most steels. DU metal and DU-metal alloys are commonly used for shielding and collimator material in industrial radiographic imaging and gauging devices.

The standard materials are used for analyzing isotopic/elemental compositions of a sample in destructive and nondestructive assay.

Small amount of thorium oxide, usually 1-2% by weight, is used for the tungsten electrode in a tungsten inert gas arc welding (TIG welding), which improves the high temperature strength of the tungsten and arc stability. Due to good electron emission characteristics, tungsten added with thorium oxide is also used as an electrode for hot cathode, photoelectric and discharge tubes. Additionally, tungsten filament coated with thorium oxide is used for incandescent light.

3. Control Systems of SQNM

3.1 Domestic regulations

The users who want to use nuclear materials need to be licensed from or report to the regulatory body. However, depending on the quantity or the intended use, it may be exempted from the license or report obligations according to Article 71 of Enforcement Decree of the Nuclear Safety Act, Article 56 of Enforcement Regulations for the Nuclear Safety Act, and Article 1 of NSSC Notice 2017-43 [2].

Even if the license or reporting obligations are excluded under the Nuclear Safety Act, there is an obligation to submit reports regarding the nuclear material inventories according to Article 98 of the Nuclear Safety Act. However, there is the reporting exemption clause (Article 5 of NSSC Notice 2017-84) resulting in insufficient voluntary reporting by the users.

3.2 Foreign legislations

In Japan, even if a small amount of nuclear material is excluded from the permission for use of nuclear materials, the user shall be licensed for the use of internationally controlled materials and regulation on nuclear material control and accountancy should be enacted [3]. In Canada, all activities shall be licensed except for the handling of nuclear materials as in nature, and the exemption from license is limited to activities using below the specified quantity by law [4].

4. Conclusion

The effective and efficient control system for the SQNM is essential in terms of nuclear security and safeguards. In this study, the status of domestic use and regulations for the SQNM were reviewed. The next step should be drafting an improved way for controlling the SQNM with the consideration of domestic and foreign regulations.

REFERENCES

[1] https://smtl.kinac.re.kr/
[2] http://law.go.kr/
[3] KINAC, KINAC/RR-28/2008 (2008).
[4] KAERI, KAERI/RR-2835/2007 (2007).

Status of KAERI's Activities on IAEA Collaboration for Safeguards Development for Pyroprocessing

Seong Kyu Ahn*, Ho-Dong Kim, Se-Hwan Park, and Dae-Yong Song

Korea Atomic Energy Research Institute, 111, Daedeok-daero 989beon-gil, Yuseong-gu, Daejeon, Republic of Korea

*skahn76@kaeri.re.kr

1. Introduction

The IAEA establishes and implements a specific and appropriate safeguards approach for applying safeguards, based on the planning and design information provided by the member countries. Without an official plan for the construction and operation, the IAEA does not need to apply (or even develop) safeguards approach. Regarding the pyroprocessing safeguards, there is neither of previously applied safeguards experiences or planed facility which makes the IAEA to prepare to apply. The strategy that can be chosen to ensure that the IAEA will continue to support research and development in areas where the IAEA is expected to need it in the future when the obligation to apply safeguards to actual spent fuel processing facilities arises. These areas include the development of safeguards (techniques) that make up the safeguard approach, the technical documentation required for the analysis of diversion scenario, and technical training for inspectorates on new processing technologies.

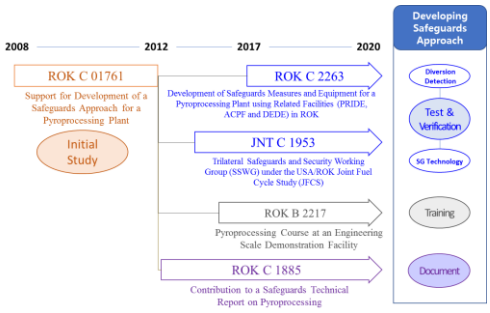

Fig. 1. Efforts and worth of MSSP for developing safeguards for pyroprocessing.

The pyroprocessing safeguards Support Program currently undertaken in Korea covers the development of safeguards, technical documentation and training for inspectors. Figure 1. shows the titles and the correlation between them.

2. Main

2.1 First Pyro Safeguards MSSP

Prior to the four programs, the MSSP for the development of the first pyro-related safeguards approach was implemented from 2008 to 2011. The development of a safeguards approach for the Reference Engineering-scale Pyroprocessing Facility (REPF) was carried out. The model design information questionnaire (DIQ) was developed, and the concept of safeguards system and draft independent verification scheme was drawn. Based on this, the IAEA developed an example Facility Attachment, which is a guideline for implementing a safeguards approach.

2.2 Pyroprocess Training Course MSSP

In September 2014, ROK and the IAEA discussed the possibility of training for IAEA inspectors using the Pyroprocessing Integrated Inactive DEmonstration (PRIDE) facilities. Since PRIDE is a globally unique facility, we have mutually recognized that it can contribute to IAEA safeguards and the reliability and transparency of Pyro technology in Korea, and we have consulted over two years on the training schedule and related matters.

In the first course, from 14 to 17 November

2017, 8 IAEA trainees and 4 domestic trainees participated, and 4 IAEA instructors and 6 researchers from KAERI were supported as instructors. In the second course, October 16-19, 2018, seven IAEA trainees, four domestic trainees, three IAEA instructors, and six KAERI instructors participated. The curriculum was originally scheduled to be held every two years, but the first and second courses were conducted continuously at the request of the IAEA, and the next schedule will be discussed later.

2.3 Pyro Safeguards Measures MSSP

Since the end of the first pyro-related MSSP from 2008 to 2011, we have continued to discuss MSSPs on the development of safeguards measures and technologies using Pyro-related facilities in Korea. In this process, while continuously discussing the scope of MSSP harmonizing the scope of joint study undertaken by the Korea-US-IAEA. In December 2016, the meeting with the IAEA finally agreed to form a detailed study of the title and proposal of the new MSSP, and in January 2017, the IAEA sent its final proposal to Korea, which was undertaken when Korea accepted it. The new MSSP agreed on is titled "Development of Safeguards and Equipment for Pyroprocessing Facilities Using Related Facilities in Korea."

2.4 Other Programs

Near Real Time Accountancy (NRTA) may be used to achieve timely detection and political inspection objectives for IAEA safeguards. Since the NRTA system has been developed worldwide, it has been a long time since it was built with interfaces and calculation programs in different environments. Based on the need to maintain and maintain existing NRTA systems and to improve them with the latest techniques or methodologies, the IAEA plans to document and establish common requirements for existing systems and methodologies for integration with future facilities' NRTA systems. In response, the IAEA started the new MSSP program entitled “NRTA system documentation and requirements gathering” and requested support from Member States

Proposed to the United States, the United Kingdom, Germany, France, Japan, and Korea with the goal of performing for about two years. The reason why the IAEA proposed to Korea is that we are developing an NRTA analysis tool as a study of safeguards measures for pyroprocessing technology. Experience in developing NRTA analysis programs using statistical techniques can contribute to the derivation of requirements for future nuclear facilities' NRTA systems and data.

3. Conclusion

There are common safeguards approaches for the same or similar facilities for facilities with a lot of existing operating experience. However, no safeguards approach is available for inexperienced facilities, such as pyroprocessing facilities. Recently, the IAEA is pursuing preparation for the future nuclear energy system and pyroprocessing is one them. In this respect, KAERI's development and support of technical information, training, and safeguards measures for pyro facilities are very meaningful activities for the realization of actual spent fuel treatment technology.

REFERENCES

[1] Hee-Sung Shin, et. Al., “Development of a safeguards approach for a pyroprocessing plant by IAEA Member State Support Program”, KAERI/RR-3342 (2011).

Trend Analysis of Research on Proliferation Resistance

Ji-song Jeong[a,b], Ho-Dong Kim[b,*], and Seung-kyu Ahn[b]
[a] University of Science & Technology, 217 Gajeong-ro, Yuseong-gu, Daejeon, Republic of Korea
[b] Korea Atomic Energy Research Institute, 111, Daedeok-daero 989beon-gil, Yuseong-gu, Daejeon, Republic of Korea
[*] khd@kaeri.re.kr

1. Introduction

Studies about Proliferation Resistance(PR) have been carried out for decades. Proliferation resistance is a feature that must be taken into account when considering safeguards in Nuclear Energy System. For this reason, as nuclear energy systems technology developed, research on PR has been steadily advanced. In order to understand and see the trends in the field of PR, the following research has been conducted. In this paper, the research trend of PR from 2000 to 2019 were investigated by using keyword analysis method. We collected papers related to the keyword "proliferation resistance" and analyzed the research trends in time series. Papers were collected via Scopus and visualized via VosViewer.

2. Research Methods

We searched papers that related to “Proliferation Resistance” in the nuclear field on Scopus. As a result of the search, it was judged that the number of papers before 2000 was small and not suitable for analysis. Therefore, 20 years from 2000 to the present are divided into 5 years, and 4 times analysis are totally performed. As a result, a total of 499 papers were collected through Scopus and Vosviewer which is a map algorithm to know the relationship between keywords was used. Before using Vosviewer, data preprocessing like matching keywords with synonyms and abbreviation is required to increase the certainty of result. Table.1 shows some examples of it.

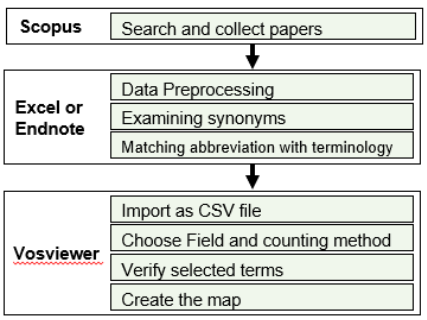

Fig. 1. Basic Framework of analysis.

Table 1. Matching keywords and synonyms

Keywords	Synonyms
Generation iv nuclear energy system	GEN4, Future generation reactor, GEN iv, Generation iv system, Generation iv nuclear power system, Generation iv, GEN 4 system, Generation 4, Next generation nuclear, Next generation nuclear reactor, Next generation system, Next generation nuclear energy system
Proliferation resistance	Nuclear Proliferation resistance, PR, Proliferation resistance assessment, PR assessment, PR assessment methodology, PR methodology, Proliferation resistance evaluation, PR evaluation, nonproliferation assessment
INPRO	IAEA INPRO Methodology, Inpro methodology, Inpro assessment methodology, The international project on innovative nuclear reactors and fuel cycles, INPRO international project, INPRO assessment study, INPRO activity, INPRO study, INPRO user manual

3. Results

On the graph, the closer to the keyword “PR” and the larger the size of the circle, the more actively that study was conducted.

3.1 From 2000 to 2005

There were a total 116 papers in this period. As a result of analysis, according to Fig.2, bottom side of the keyword ‘PR’, ‘fuzzy logic’ which was developed by NCSU in the early 2000s is located. This methodology is combined with "fuzzy logic" and PR characteristics evaluated based on the TOPS barrier factor. Fig.2 also shows that there were the ‘International Project on Innovative Nuclear Reactors and Fuel Cycles(INPRO)’ in 2000. As the International Project progresses, research on next-generation nuclear reactors like SFR, KAMILAR-600 and gas reactors became active.

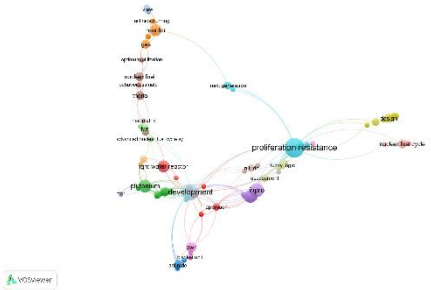

Fig. 2. PR Research trends from 2000 to 2005.

3.2 From 2006 to 2010

There were a total 181 papers in this period. According to Fig.3, it is possible to know that the research on the PR evaluation of the next generation reactor was mainly focused on. In addition, it can be seen that research on the recycling of minor Actinide, which can be the main feature of the next generation nuclear reactor, has been conducted.

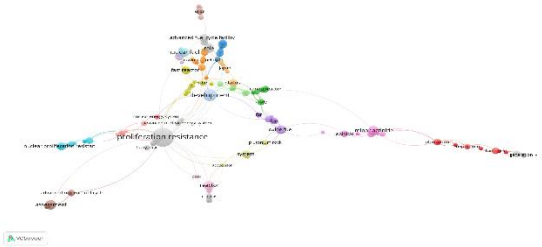

Fig. 3. PR Research trends from 2006 to 2010.

3.3 From 2011 to 2015

There were a total 151 papers in this period. Fig.4 shows that PR evaluation methodology has progressed well. While international projects such as GIF, INPRO were conducted, many papers such as Physical Protection, implementation of safeguards, and breakout scenarios were written.

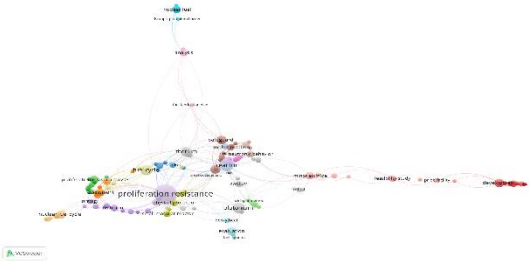

Fig. 4. PR Research trends from 2011 to 2015.

3.4 From 2016 to 2019

There were a total 51 papers from 2016 to 2019. Fig.5 shows that PR evaluation by composition of fuel in Canada Deuterium Uranium (CANDU) was studied actively. Also, according to Fig.5, researchers keep studying thorium blanket related to Advanced Burner Reactor.

Fig. 5. PR Research trends from 2016 to 2019.

4. Conclusion

In this study, the trend analysis of research on PR was performed. Firstly, it was confirmed that PR study about specific facility such as Dupic, SFR was mainly conducted. And then, as international collaborative projects like INPRO, GIF have progressed, results shows that various factors such as PR and Physical Protection(PP) were taken into account when evaluating Safeguards. As a part of that, KAERI also keep studying nonproliferation research such as development of safeguard systems and PR for the nuclear fuel cycles which can contribute to enhancing nuclear nonproliferation security.

REFERENCES

[1] H.D. Kim, S.K. Ahn, and J.S. Jeong, “Evaluation Methodology for Proliferation Resistance and Protection of Generation Ⅳ Nuclear Energy Systems”, KAERI/TS-333/2018 (2018).

[2] S.K. Ahn, H.S. Shin, B.Y. Han, H.D. Kim, T.H. Lee, S.H. Park, D.Y. Song, J.M. Oh, and Y. Choi, “A Review of Proliferation Assessment Methodologies and Definition of the Related Terms”, KAERI/AR-902/2011 (2011).

A Feasibility Study for Long-Life Molten Salt Reactor Core

Sunghwan Yun* and Sang Ji Kim
Korea Atomic Energy Research Institute, 111, Daedeok-daero 989beon-gil, Yuseong-gu, Daejeon, Republic of Korea
*syun@kaeri.re.kr

1. Introduction

In the recent years, there has been a growing interest in the Molten Salt Reactor (MSR), which is originally suggested by the Oak Ridge National Laboratory (ORNL) for a military aircraft nuclear propulsion project, owing to its unique characteristic in liquid fuel cycle management [1-2].

In 1965, representative Molten Salt Reactor Experiment (MSRE), adopting graphite assemblies and liquid molten salt fuel, was built and became critical by ORNL [3]. On the basis of this, continuous design studies were carried out using graphite moderator for thermal MSR concept [4].

In this study, based on the denatured molten salt reactor (DMSR) concept suggest by the Ref. [4], preliminary MSR core concept for long-life operation was suggested with modern neutronics and depletion calculation codes and libraries, the MCNP6, FISPACT-II, and ENDF/B-VII.1 library [5, 6].

2. Basic DMSR Parameter

Since this study was started based on the DMSR core, we adopted identical material compositions, i.e., liquid LiF-BeF_2-$(HM)F_4$ fuel and graphite moderator, which were used in the DMSR. The detailed fuel compositions are shown in Table 1. For density of liquid LiF-BeF_2-$(HM)F_4$ fuel, 2.945 g/cc was used considering thermal expansion based on the Ref. [7]. Since the operating temperature of the DMSR are between 566°C and 704°C, cross-sections used in the core analysis were approximated as those at 600°C.

Table 1. LiF-BeF_2-$(HM)F_4$ fuel composition

	Weight fraction
TH-232	33.88%
U-235	1.06%
U-238	4.31%
LI-7	9.22%
BE-9	2.64%
F-19	48.89%

3. Determination of the MSR Core Configuration

At the beginning of the conceptual core design study for Long-Life Molten Salt Reactor (LL-MSR) core, we performed optimization of core configuration for 100 MWth power condition. In the liquid fuel loaded core, core configuration will be determined by the neutron economy rather than thermal heat conduction or convection unlike conventional solid fuel loaded core.

Figures 1 and 2 show basic core configuration of LL-MSR core. The log type graphite moderator concept had been used for the DMSR while the hexagonal lattice type graphite moderator is suggested by this study. In the basic configuration, 5 m height and diameter were approximated for core region while 0.2 m thickness plenum, 0.65 m thickness axial reflector, and 0.8 m thickness radial reflector were approximated. Identical to the DMSR, homogenized fuel and reflector materials were used for reflectors and plenum with 1 % and 50 % fuel volume fraction, respectively.

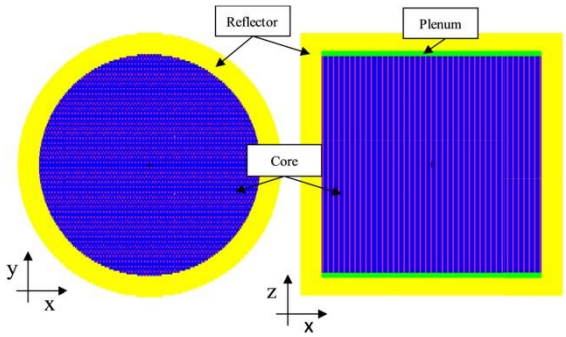

Fig. 1. Basic Configurations for the LL-MSR Design Study.

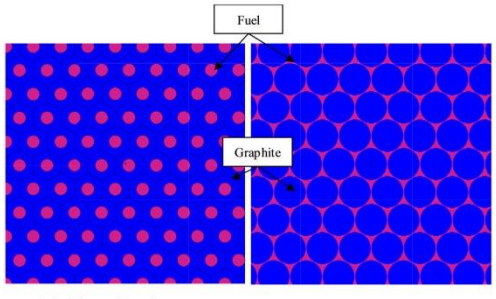

(a) Hex. Lattice type (b) Log type

Fig. 2. Detailed configuration of fuel and moderator.

Figures 3 and 4 show neutronics analysis results of criticality for various geometry dimensions. The hexagonal lattice type moderator design shows better results than the log type moderator design because of optimized fuel volume fraction, 6.9 %.

Consequently, hexagonal lattice with 21 cm pitch and 2.8 cm radius were selected for the core inner configurations.

pitch

< Hex. Lattice type >

Rad.

	3	6	9	12	15	18	21	24	27	30
0.2	1.06619	0.83685	0.81965	0.81262	0.81077	0.80861				
0.4	1.15191	1.07129	0.8822	0.83854	0.82505	0.81901	0.81552	0.81156	0.81112	0.81044
0.6	1.02611	1.1811	1.07195	0.92782	0.85739	0.83843	0.8279	0.82294	0.81881	0.81561
0.8	0.86344	1.18614	1.16844	1.07146	0.95894	0.87806	0.85006	0.83691	0.82795	0.82402
1	0.72971	1.14455	1.20079	1.15421	1.06852	0.97692	0.89781	0.86107	0.84401	0.83636
1.2	0.64761	1.08087	1.20145	1.1932	1.1395	1.06641	0.98703	0.91453	0.87106	0.8547
1.4	0.66463	1.00483	1.18435	1.21075	1.18045	1.12744	1.06166	0.99224	0.92766	0.88087
1.6	0.69504	0.92279	1.1527	1.21254	1.20528	1.16814	1.11627	1.05617	0.99245	0.93412
1.8	0.73308	0.84053	1.11239	1.20211	1.21656	1.19491	1.15481	1.10536	1.04957	0.99204
2	0.77308	0.76736	1.06382	1.18397	1.2179	1.21007	1.18135	1.14074	1.09364	1.04159
2.2	0.81308	0.70957	1.0121	1.16091	1.21286	1.21772	1.19896	1.16828	1.12725	1.08247
2.4	0.85308	0.66308	0.95889	1.13001	1.19985	1.21896	1.21174	1.18746	1.15299	1.11414
2.6	0.89308	0.63146	0.9029	1.09967	1.18508	1.21499	1.21817	1.20101	1.17442	1.141
2.8	0.93308	0.60931	0.84482	1.0617	1.1662	1.21032	1.21991	1.21172	1.19038	1.15953
3		0.59635	0.79601	1.02426	1.14493	1.19989	1.21884	1.21741	1.20094	1.17545
3.2		0.59114	0.74893	0.98443	1.12029	1.1855	1.21513	1.21875	1.20879	1.18806
3.4		0.59229	0.70946	0.94117	1.09347	1.17064	1.20617	1.21928	1.21637	1.19845
3.6		0.59868	0.67642	0.89888	1.06492	1.15245	1.19994	1.21586	1.21703	1.20632
3.8		0.60968	0.64891	0.8578	1.03297	1.13462	1.18679	1.21048	1.21946	1.20941
4		0.62498	0.62856	0.81753	1.00122	1.113	1.17461	1.20521	1.21461	1.21252
4.2		0.64308	0.61308	0.7787	0.96748	1.0918	1.16211	1.19671	1.21275	1.21261
4.4		0.66308	0.60125	0.74304	0.93603	1.06729	1.14607	1.18734	1.20845	1.21194
4.6		0.68308	0.59383	0.7127	0.89937	1.0428	1.12794	1.17763	1.2015	1.21198
4.8		0.70308	0.59126	0.68725	0.86517	1.01577	1.11064	1.16648	1.19441	1.20743
5		0.72308	0.59308	0.66221	0.8314	0.98771	1.0916	1.15216	1.18697	1.204
5.2		0.74308	0.59894	0.64318	0.80238	0.96235	1.07222	1.13856	1.17853	1.19875

Fig. 3. Criticalities for hexagonal lattice type MSR core.

pitch

< Log type >

Dia. - pitch

	3	6	9	12	15	18	21	24	27	30
0	1.07524	1.10953	1.13391	1.15066	1.16298	1.1711	1.18031	1.18446	1.18918	1.19236
-0.1	0.8794	1.00502	1.06665	1.10385	1.12782	1.14327	1.15577	1.16528	1.1718	1.1773
-0.2	0.76835	0.9274	1.01225	1.06299	1.09694	1.11906	1.1356	1.1477	1.15826	1.16536
-0.3	0.70566	0.86291	0.96271	1.02487	1.06679	1.09556	1.11714	1.1331	1.14418	1.15367
-0.4	0.66593	0.81079	0.92038	0.99078	1.03971	1.07311	1.09797	1.11587	1.1296	1.14112
-0.5	0.64177	0.77003	0.88198	0.9581	1.01403	1.05113	1.07897	1.10016	1.11677	1.12873
-0.6	0.62523	0.73811	0.846	0.92827	0.98606	1.02986	1.05965	1.08472	1.10463	1.11734
-0.7	0.61597	0.71217	0.81533	0.90112	0.96244	1.00849	1.04461	1.07037	1.09135	1.10519
-0.8	0.61086	0.69093	0.78798	0.87377	0.93925	0.98944	1.02415	1.05451	1.0769	1.09409

Fig. 4. Criticalities for log type MSR core.

Since the LL-MSR core will be operated with critical condition, the required minimum size of core was also studied and, as a result, 2 m size in diameter and height was selected for the LL-MSR core. Hence required fuel mass for core is estimated as 1,231.1 kg.

4. Fuel Cycle Analysis

In the LL-MSR, reactivity loss by depletion of fuel is supplemented by continuous insertion of fissile fuel, Low-Enriched Uranium (LEU; 20 wt.% uranium) in this study, while the identical mass of fertile fuel, Th-232 in this study, is extracted continuously to maintain total heavy metal mass. Figure 5 show required 20 wt.% uranium feed during 2,400 EFPD operation which is resulted by the iterative MCNP6 and FISPACT-II calculation. For 2,400 EFPD operation, total 308.0 kg uranium is additionally required to maintain criticality of the LL-MSR core.

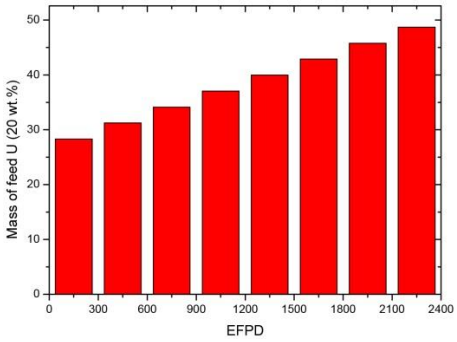

Fig. 5. Required mass of feed fuel in the LL-MSR core.

5. Conclusion

In this paper, preliminary core design study was performed for the 100 MWth long-life MSR based on the DMSR design. As a result, we can conclude that the long-life MSR core can be feasible up to 2,400 EFPD with additional about 300 kg fuel feed.

ACKNOWLEDGMENTS

This work was supported by the National Research Foundation of KOREA (NRF) funded by the Ministry of Science and ICT (No. NRF-2018M2A8A4081307), South Korea.

REFERENCES

[1] Antonio Cammi, Carlo Fiorina, Claudia Guerrieri, Lelio Luzzi, Dimensional Effects in The Modelling of MSR Dynamics: Moving on From Simplified Schemes of Analysis to A Multi-Physics Modelling Approach, Nuclear Engineering and Design, Vol. 246, pp. 12– 26, 2012.

[2] E. S. Bettis et al., The Aircraft Reactor Experiment-Design and Construction, Nuclear Science and Engineering, Vol. 2, p.804, 1957.

[3] R. H. Guymon, MSRE Systems and Components Performance. Technical Report, ORNL-TM-3039, 1973.

[4] J. R. Engel et al., Conceptual Design Characteristics of a Denatured Molten-Slat Reactor with Once-Through Fueling, ORNL/TM-7207, 1980.

[5] D. B. Pelowitz, et al., MCNP6™ USER'S MANUAL, LA-CP-13-00634, LANL, 2013.

[6] M. Fleming, et al., The FISPACT-II User Manual, UKAEA-R(18)001, UKAEA, 2018.

[7] S. Cantor, Density and Viscosity of Several Molten Fluoride Mixtures, ORNL-TM-4308, 1973.

2분과

사용후핵연료 처분전관리 (Oral)

Comparison of Inert Hot Cell Atmospheric Systems

Hyojik Lee*, Byung Suk Park, and Seung Nam Yu
Korea Atomic Energy Research Institute, 111, Daedeok-daero 989beon-gil, Yuseong-gu, Daejeon, Republic of Korea
*hyojik@kaeri.re.kr

1. Introduction

A system to maintain inert atmosphere in hot cells is important engineered safety feature because that belongs to the confinement boundary with hot cell structures and shielded windows to prevent or mitigate radioactive material release through the boundary. This paper investigated various inert atmosphere systems. Two argon cells in Idaho National Laboratory (INL) such as Fuel Conditioning Facility (FCF) and Hot Fuel Examination Facility (HFEF) are investigated to compare those safety features with ones of the Advanced spent fuel Conditioning Process Facility (ACPF).

2. Inert Cell Atmosphere Systems

2.1 FCF

The FCF argon has a fixed volume of 66,000 ft^3 filled with pure argon gas to maintain an inert atmosphere. The FCF argon cell atmosphere control systems maintain the in-cell pressure at -3 inch water gage (iwg) with reference to the FCF basement atmospheric pressure. They also maintain the in-cell temperature at 90˚F(32°C).

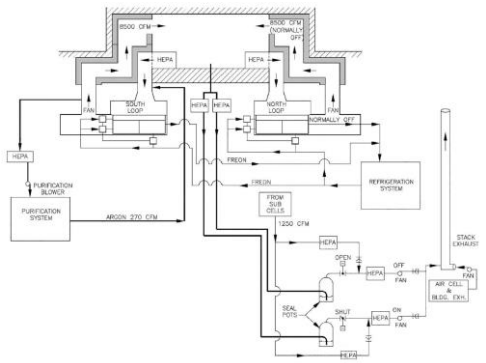

Fig. 1. Argon Cell Atmosphere System of FCF [1].

Some of the material in the cell is pyrophoric in an atmosphere containing at least 4 % oxygen (40,000 ppm) and the cell is normally maintained between 55 and 85 ppm oxygen and between 40 and 100 ppm moisture. Pressure temperature control system (PTCS) senses argon cell pressure and temperature, and send control signals to the argon cell refrigeration and Feed/Bleed systems for position control of Freon expansion valves for refrigeration and on-off control of vacuum pumps for the Feed/Bleed system. The argon cell safety exhaust system (SES) automatically activates and exhausts the argon cell whenever the argon cell pressure rises to -1 iwg.

2.2 HFEF

The main cell contains high-purity argon atmosphere of 65,000 ft^3. The gas is recirculated through a high-volume cooling system (about 13,000 cfm) and HEPA filters. A small portion of the gas flow passes through a purification system to remove oxygen and water vapor to nominal levels of 25 and 50 ppm, respectively. The nitrogen concentration is controlled by exhausting the cell gas and replenishing it with fresh argon. The main cell atmosphere is maintained at a nominal reduced pressure of -1 to -4 iwg. The main cell is designed to maintain a minimum of -22 iwg and maximum of 3 iwg for structural integrity. The temperature in the main cell normally ranges from 70 to 100°F (21~32°C) but it can be controlled within a minimum of 65°F (18°C) and a maximum of 105°F (40°C)

There are two safety exhaust systems at HFEF to relieve over and under pressure of cells. One is a normal vent system to relieve a bit over pressurized cell atmosphere to the cell exhaust system when the cell pressure rises to the set -1 in WG. This exhaust cell gas through seal pot-1 in Fig. 2.

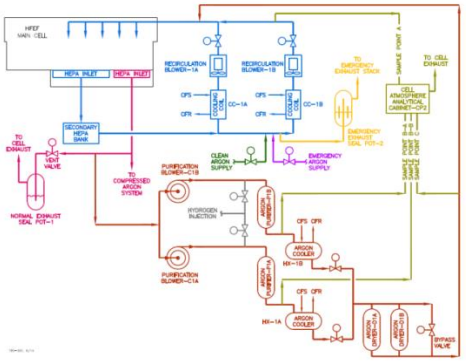

Fig. 2. HFEF argon circulation system piping diagram [2].

The other one is called emergency over- and under- pressure relief system. It vents gas from the cell or allows air to be drawn into it to prevent excessive pressure differentials that could cause

structural damage to walls, windows and other components providing confinement of the cell atmosphere. The venting of gas through the pressure relief system will start when the mail cell is over pressurized and reaches 2.25 iwg (0.75 iwg relief valve cracking pressure plus 1.5 iwg oil seal). On the other hand, air will start to flow back into the cell through the pressure relief system when the pressure at the seal pot falls to about 22 iwg below atmospheric pressure (11 iwg relief valve cracking pressure plus 11 iwg oil seal).

2.3 ACPF

KAERI refurbished ACPF in 2014 to divide one large air cell into a small argon atmospheric compartment of 330 ft^3 and air atmospheric one. Since the previous ACPF cell was air atmosphere there was no need for argon circulation system to keep the cell atmosphere inert with low concentrated oxygen and moisture. The new argon system at ACPF has two purification systems to remove moisture and oxygen but they are operated separately. When a purification system runs, the other one is regenerated or stationary.

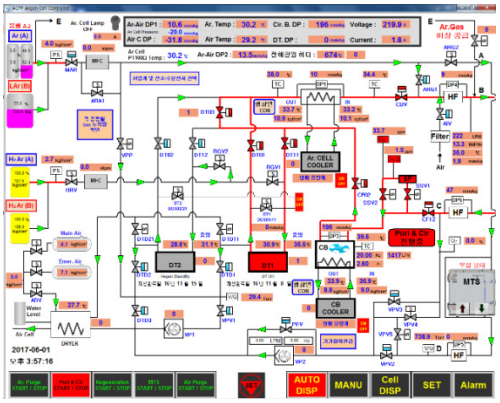

Fig. 3. ACPF argon circulation system piping diagram [3].

It has only one safety exhaust system. It has one seal pot even though it is a safety significant component according to Department of Energy (DOE) standards. It also has one argon cell cooler provided. The seal pot activates whenever the pressure difference of argon cell in reference to air cell rises to 0.8 iwg. The gas out of argon compartment through the seal pot goes to the air cell. The air cell also has its own ventilation system so the exhausted gas is filtered again through the air-handling unit and released to the stack of facility. The ACPF argon system was not designed with defense in depth (DID) concept and in case of failures, a very long maintenance period is expected.

3. Functional Comparison

Table 1. Comparison of Key Functions

Component/ function		FCF	HFEF	ACPF
Seal pot		2 (redundant)	2 (different type)	1
Pass-through pressure(iwg)		<-22 or >-1[†]	>-1[†] <-22 or >2.25[††]	>0.8[‡]
Cell pressure (iwg)		-3~-1	-4~-1	-1.5~-1[‡‡]
Cell gas (ppm)	Oxygen	55~85	25~100	<50
	Nitrogen	<4700	n/a	n/a
	Hydrogen	<100	n/a	n/a
	Moisture	40~100	20~100	<50
Cell temperature ($^oC(^oF)$)		32(90)	21(70)~ 37(100)	25(77)~ 35(95)[‡‡]
Cell volume (ft^3)		66,000	52,500	330
Leak rate (cfm)		<5	<5	<0.002
# of Blowers & coolers (ea)		2	2	1

[†] Ar cell pressure with reference to their basement atmospheric pressure

[††] Air will start to flow back into the cell through the seal pot if the pressure falls to about -22 iwg below atmospheric pressure and venting of gas will start if the cell pressure exceeds 2.25 iwg above atmospheric pressure

[‡] Ar cell pressure with reference to the air cell pressure

[‡‡] Pressure and temperature ranges of the air cell in ACPF are the same as the ones in argon cell

4. Conclusion

Three different argon atmosphere systems are compared and those safety features are analyzed. The FCF and HFEF have solid safety exhaust systems and redundant designs. However, the ACPF has a redundant system only for purifier so it needs to be upgraded to have conservative safety measures and management for the failures of critical components.

REFERENCES

[1] C. L. Pope et al., Fuel conditioning facility inert gas filled reprocessing hot cell leak rate measurement, ANE, 111, 676-682 (2018).

[2] R. Johansen, Hot Cell Design and Maintenance, INL/EXT-17-41766-Rev.0 (2017).

[3] B. S. Park, Construction of ACPF Argon Cell System, KAERI/TR-6242 (2015).

Preliminary Criticality Analysis on the OASIS-37CAN Canister With 37 Spent Nuclear Fuel Assemblies of Kori-1

Joon Gi Ahn* and Youngtae Han

KEPCO Engineering & Construction Company, 111, Daedeok-daero 989beon-gil, Yuseong-gu, Daejeon, Republic of Korea

*jgahn@kepco-enc.com

1. Introduction

KEPCO E&C has been developing the OASIS-37CAN dry storage canister for 37 PWR spent nuclear fuel (SNF) assemblies of Kori-1 WEC-type 14×14 fuel assembly (FA). This canister has same external shape and dimensions of the canister in OASIS-32D cask [1] which is a dual purpose (for both transport and storage) metal cask developed by KEPCO E&C. Thus, the OASIS-37CAN canister can be transported and/or stored using the OASIS-32D cask body.

The amount of uranium loaded in a WEC-type 14×14 FA is less than that in the ACE7 17×17 FA. Therefore, the total amount of uranium loaded in OASIS-37CAN canister (37 Kori-1 FA) is almost same with that in OASIS-32CAN canister (32 ACE7 FA). If both FAs have the same burnup and cooling period, the decay heat and radiation sources of these canisters are also almost the same. This means that the results of structural analysis, thermal analysis, and shielding analysis on the OASIS-32D cask model could be applied to the OASIS-37CAN canister as a preliminary design data.

However, the criticality safety is influenced by the number of loaded FAs, array configuration, separation distance between FAs, and the parameters of the loaded FA. Therefore, the preliminary criticality calculation is performed based on the basket cell arrangement, geometry, dimensions, materials of the OASIS-37CAN canister and the parameters of Kori-1 WEC-type 14×14 FA. The burnup credit (BUC) assumption is applied on the criticality safety evaluation of the OASIS-37CAN canister.

2. OASIS-37CAN Criticality Analysis Model

2.1 Kori-1 WEC-type 14×14 FA

The design parameters of the Kori-1 WEC-type 14×14 FA and ACE7 17×17 FA are compared in Table 1.

Table 1. Design Parameters of Kor-1 FA

Parameters	Kori-1 FA	ACE7 FA
Array of fuel rods	14×14	17×17
No. of fuel rods (/FA)	179	264
Fuel pellet dia. (mm)	9.294	8.192
Fuel rod pitch (mm)	14.12	12.6
Fuel length (active) (mm)	3658	3658
FA width (mm)	197.7	214.2
U loading (/FA) (Kg)	402.7	461.3
U loading (/Canister) (Kg)	14,899.9 (37 FA)	14,761.6 (32 FA)

2.2 OASIS-37CAN Fuel Basket

The fuel basket in canister has a 7×7 array in which 37 FAs can be loaded. The design

parameters of the fuel basket and the canister of OASIS-37CAN are presented in Table 2.

Table 2. Design Parameters of OASIS-37CAN Canister

Parameters	Value
Basket cell array	7×7
No. of basket cells	37
Basket cell pitch (mm)	218.4
Basket plate thickness (mm)	8.0
Neutron absorber plate	
- Material	MAXUS
- Thickness (mm)	3.5
- Width (mm)	175.0
- Areal boron density (g B^{10}/cm^2)	0.04
Canister inner dia. (mm)	1735.0

2.3 Criticality Calculation on OASIS-37CAN

The loaded FA's enrichment and burnup are assumed to be 1.8 wt% (U-235) and no burned fresh fuel. To consider the limiting conditions of the dry storage, transportation, and handling process, it is assumed that the inner space of the canister is filled with unborated full density water.

The criticality calculation for the OASIS-37CAN canister was performed using the CSAS module of SCALE6.1 code. Figure 1 shows the horizontal view of the geometry model of the calculation.

3. Results and Conclusions

The calculated k-eff of the OASIS-37CAN canister with 37 FAs of Kori-1 was 0.89450 (+/- 0.00016). The calculational bias and associated uncertainties (typically ~0.02 Δk/k for fresh fuel) should be included to the calculated k-eff to generate the final evaluated k-eff. However, a sufficient margin is available between the calculated k-eff (0.89450) and the criticality safety limit (k-eff of 0.95). Thus, it is believed that the OASIS-37CAN canister meets the criticality safety requirement.

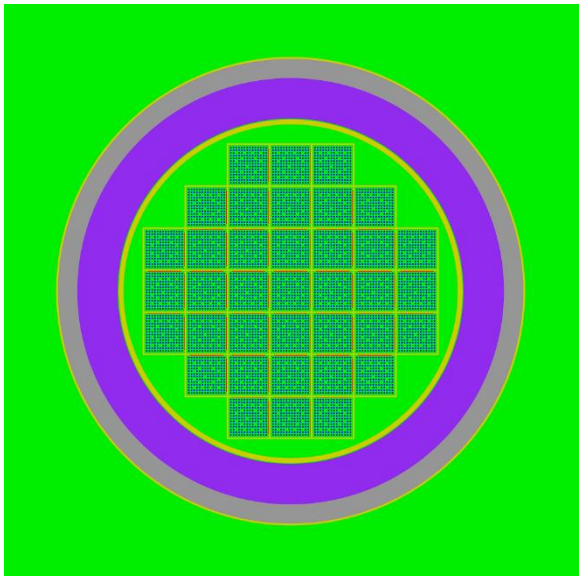

Fig. 1. Geometry Configuration of OASIS-37CAN Calculation Model (Mid-plane Horizontal View).

In summary, the OASIS-32D cask, which was developed for loading of 32 ACE7 FAs or PLUS7 FAs, can be used for loading of 37 Kori-1 FAs using the OASIS-37CAN canister.

REFERENCES

[1] K.J. Ko, et al, "Design Features of an OASIS-32D Metal Cask for both Transport and Storage of SNF," Transactions of the Korean Nuclear Society Spring Meeting, Jeju, Korea, May 18 -19, 2017.

Spent Fuel Burnup Measurement by CZT Gamma Detector

Yongdeog Kim[1,*], Donghee Lee[1], Jinho Jeong[1], Sehyun Oh[2], and Hee Seo[3]
[1]Central Research Institute, Korea Hydro & Nuclear Power Co., Ltd., 70, Yuseong-daero 1312beon-gil, Yuseong-gu, Daejeon, Republic of Korea
[2]Users Co., Ltd., 65, Techno 3-ro, Yuseong-gu, Daejeon, Republic of Korea
[3] Chonbuk National University, 567 Baekje-daero, Deokjin-gu, Jeonju, Jeollabuk-do, Republic of Korea
[*]yongdkim@khnp.co.kr

1. Introduction

The nuclear properties of spent fuel are determined by the initial fuel composition, burnup experienced in a nuclear reactor, cooling time, and etc. The reactivity assessment of the spent fuel assembly can be performed from initial enrichment, burnup, and cooling time of the fuel assembly. The average burnup value of each spent fuel assembly is especially determined at the time of discharge from the reactor history and the distribution of in-core neutron flux measurement during operation. IAEA has specified data requirements of records for spent fuel management and the average burnup of the spent fuel is one of the key data to be managed [1]. A burnup verification measurement has been contributed to get a burnup credit by providing nuclear criticality safety in US[2] and European countries. The application of burnup credit can result in more efficient way to arrange spent fuel assemblies in a storage or transportation cask, therefore, it can significantly reduce cost and risk.

This study has been performed to investigate an applicable burnup verification measurement by comparing the measurement data with the reactor record data of the spent fuel assemblies. The well-known cadmium-zinc-tellurium (CZT) semiconductor gamma-ray detector that can measure gamma-ray counts at room temperature has been used in this study (Fig. 1) [3].

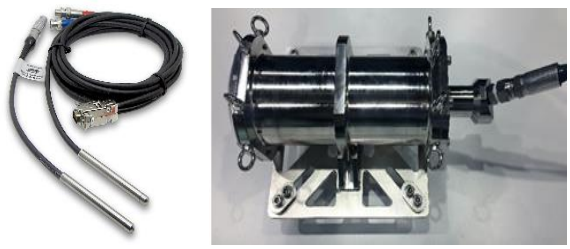

Fig. 1. CZT gamma-ray detector.

2. Verification Measurements

2.1 Spent Fuel Selection

Fourteen spent fuel assemblies were selected for the burnup verification measurement study. The initial enrichment of the assemblies ranged from 2.01 to 4.51 wt.% U-235. The range in average assembly burnup was from 16.5 to 55.1 GWd/MTU and the cooling times ranged from 4.3 to 23.4 years. The various kinds of fuel types were selected such as KSFA, PLUS7, GUARDIAN that have 16×16 array and KOFA has 17×17 array in a fuel assembly.

2.2 Burnup Measurement Test

The burnup measurement test was performed at the spent fuel pool storage side in nuclear power plant. During the burnup measurement test, both the gamma-ray detector and test fuel assembly were placed on the empty cell position among the region 1 of spent fuel pool to minimize background radiation from neighboring spent fuel. The gamma-ray counts were measured at a central axial position of four faces of each spent fuel assembly for 10 minutes. The burnup measurement test has also been performed along the vertical axial direction of the fuel assembly to investigate the axial burnup distribution of the assebly.

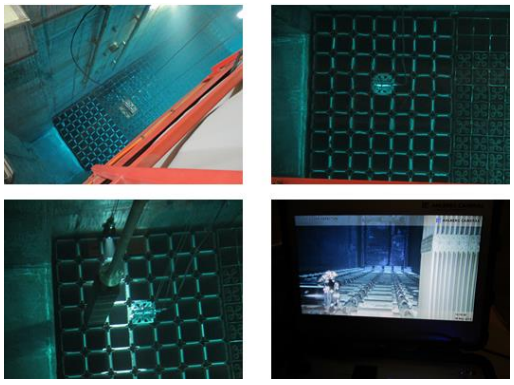

Fig. 2. Burnup measurement in the spent fuel pool storage side.

3. Results and Discussion

Measured burnup value was determined associated with the Cs-134/Cs-137 activity ratio with efficiency correction by Geant4 or MCNP Monte Carlo simulations. The activity ratio, i.e. count rate ratio, as a function of burnup was obtained by ORIGEN calculations. Fig. 3 shows typical Cs-134 and Cs-137 gamma-ray spectrums from the four faces of a spent fuel. The Cs-137 peak was found at 662 keV and the Cs-134 peaks were found at 796 and 802 keV respectively. It didn't show significant difference in gamma-ray counts value between the faces of the spent fuel assembly. The average Cs-137 count rate as a function of the fuel assembly axial height was shown in Fig. 4.

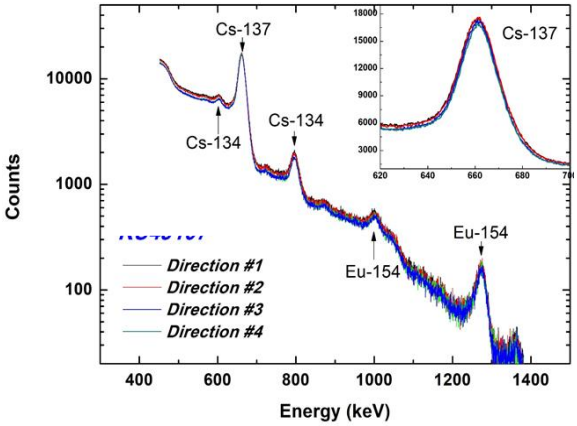

Fig. 3. Typical Cs-134 and Cs-137 gamma-ray spectrums from four faces of a spent fuel.

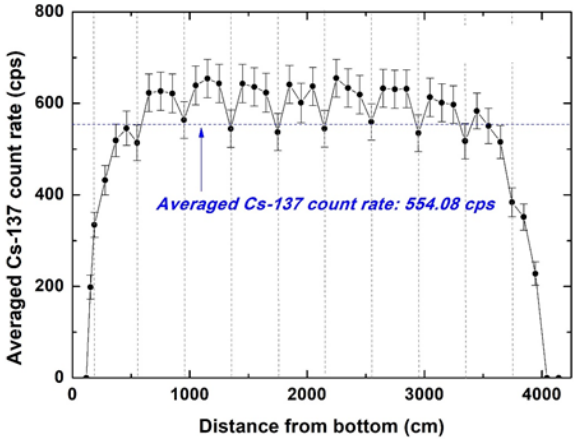

Fig. 4. Measured Cs-137 gamma-ray spectrums distribution as a function of fuel assembly height.

The overall measured burnup error was approximately 4.6%, which showed a good agreement with the reactor record data based on in-core neutron flux measurement. It is expected that the burnup measurement system by the CZT semiconductor gamma-ray detector could fulfill an important role as a means of burnup verification method.

4. Conclusions

The burnup measurement study on the spent fuel has been performed to investigate an applicable burnup verification measurement by comparing the measurement data with the reactor record data of the spent fuel assemblies based on in-core neutron flux measurement. The overall measured burnup error was approximately 4.6%, which showed a good agreement with the reactor record. It is expected that the CZT burnup measurement system can be utilizes as a means of burnup verification method in the future.

REFERENCES

[1] IAEA TECDOC-1519, "Data Requirements and Maintenance of Records for Spent Fuel Management", 2006.

[2] EPRI TR-113169, "The Fork+ Developmental Measurement Campaign at Maine Yankee", 1999.

[3] Hee Seo et al., "Burnup Measurement of Spent Fuel Assembly by CZT-based Gamma-Ray Spectroscopy for Input Nuclear Material Accountability of Pyroprocessing", IEEE Transactions on Nuclear Science, 2014.

Forced Circulation Drying Test of Residual Water According to Pressure

Kyoung-Sik Bang[a,*], Ju-Chan Lee[a], Seung-Hwan Yu[a], Woo-Seok Choi[a], and Kyung-wook Shin[b]
[a]Korea Atomic Energy Research Institute, 111, Daedeok-daero 989beon-gil, Yuseong-gu, Daejeon, Republic of Korea
[b]Sae-an Engineering Corporation, 184, Gasan digital 2-ro, Geumcheon-gu, Seoul, Republic of Korea
[*]nksbang@kaeri.re.kr

1. Introduction

To maintain the integrity of spent nuclear fuel when storing spent nuclear fuel by dry type, canister water is drained to the outside, and the remaining water is physically bound to the canister, and spent fuel must then be dried and stored in an inert gas atmosphere.

Methods for removing residual water from dry storage system canisters include vacuum drying and forced circulation drying. The degree of drying that can be approved in the case of forced circulation drying involves as follows: The dew point temperature at the canister outlet should be maintained below -5 °C for more than 30 min, or the temperature at the dehumidifier should be maintained below -6 °C for more than 30 min [1].

The aim of the present paper is to evaluate the characteristics of forced circulation drying according to the pressure inside the canister. To do so, a forced circulation drying system and small-sized canister were designed and fabricated. Forced circulation drying tests were conducted using our forced circulation drying system and canister.

2. Forced Circulation Drying Test

2.1 Description of the Forced Circulation Drying Test Equipment

A forced circulation drying system comprises a small-sized canister, a helium circulation pump, a heater, a condenser, and a flow controller. Three small-sized canisters of 50 cm (65 ℓ) and 100 cm (130 ℓ) lengths were used for a drying test. The bodies of the small-sized canisters were made of stainless steel and each had a diameter of 40.6 cm and a thickness of 1.27 cm. The canister lid had a water inlet and drain port, and there was a port for installing a pressure gauge to measure pressure.

2.2 Test Results and Discussion

The forced circulation drying test was performed thirty two times in total.

Fig. 1. Forced Circulation Drying Test Equipment.

2.2.1 Test using a 65 liter canister.

- Water temperature: 25 °C

In the case of 0.5 atm, 125 g of 130 g of water in the canister had dried, and 5 g of water remained. The dew point temperature was measured at - 5 °C after 31 min of drying test time.

In the case of 1.0 to 2.0 atm, the dew point temperature was measured at - 5 °C after 56 min, 56 min, and 32 min of drying test time. All of the water in the canister had dried.

- Water temperature: 30 °C

In the case of 0.5 atm, 129 g of 130 g of water in the canister had dried, and 1 g of water remained. The dew point temperature was measured at - 5 °C after 59 min of drying test time.

In the case of 1.0 to 2.0 atm, the dew point temperature was measured at - 5 °C after 48 min, 51 min, and 49 min of drying test time. All of the water in the canister had dried.

- Water temperature: 35 °C

In the case of 0.5 atm, 128 g of 130 g of water in the canister had dried, and 2 g of water remained. The dew point temperature was measured at - 5 °C after 52 min of drying test time.

In the case of 1.0 to 2.0 atm, the dew point temperature was measured at - 5 °C after 46 min, 49 min, and 43 min of drying test time. All of the water in the canister had dried.

- Water temperature: 40 °C

In the case of 0.5 atm, 129 g of 130 g of water

in the canister had dried, and 1 g of water remained. The dew point temperature was measured at - 5 °C after 49 min of drying test time.

In the case of 1.0 to 2.0 atm, the dew point temperature was measured at - 5 °C after 40 min of drying test time. All of the water in the canister had dried.

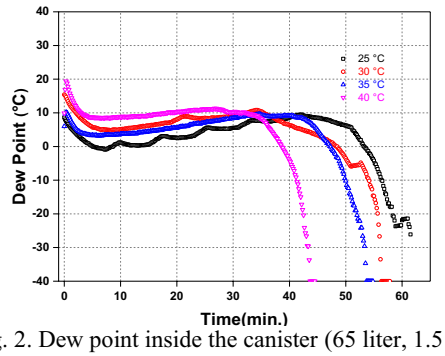

Fig. 2. Dew point inside the canister (65 liter, 1.5 atm).

2.2.2 Test using a 130 liter canister.

- Water temperature: 25 °C

In the case of 0.5 atm, 129 g of 130 g of water in the canister had dried, and 1 g of water remained. The dew point temperature was measured at - 5 °C after 86 min of drying test time. In the case of 1.0 atm, 128 g of 130 g of water in the canister had dried, and 2 g of water remained. The dew point temperature was measured at - 5 °C after 70 min of drying test time.

In the case of 1.5 to 2.0 atm, the dew point temperature was measured at - 5 °C after 71 min, and 67 min of drying test time. All of the water in the canister had dried.

- Water temperature: 30 °C

In the case of 0.5 atm, 129 g of 130 g of water in the canister had dried, and 1 g of water remained. The dew point temperature was measured at - 5 °C after 64 min of drying test time.

In the case of 1.0 to 2.0 atm, the dew point temperature was measured at - 5 °C after 71 min, 62 min, and 62 min of drying test time. All of the water in the canister had dried.

- Water temperature: 35 °C

In the case of 0.5 atm, 129 g of 130 g of water in the canister had dried, and 1 g of water remained. The dew point temperature was measured at - 5 °C after 59 min of drying test time.

In the case of 1.0 to 2.0 atm, the dew point temperature was measured at - 5 °C after 65 min, 53 min, and 50 min of drying test time. All of the water in the canister had dried.

- Water temperature: 40 °C

In the case of 0.5 to 2.0 atm, the dew point temperature was measured at - 5 °C after 53 min, 61 min, 56 min, and 49 min of drying test time. All of the water in the canister had dried.

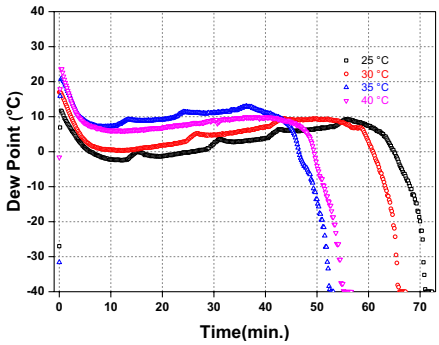

Fig. 3. Dew point inside the canister (130 liter, 2.0 atm).

3. Conclusion

A forced circulation drying system and small-sized canister were used to conduct forced circulation drying tests to evaluate the characteristics of forced circulation drying according to the pressure inside the canister. The main results of our study are as follows:

- When the canister volume was small, drying time was short.
- When the water temperature was high, the drying of the water was faster, and the temperature rise of the water (ΔT_2: Water temp. at start – Water temp. at stop) was less.
- When the canister pressure was high, the temperature rise of the water (ΔT_2) was high, and drying time was short.
- The overall ΔT_1(Cavity temp. – Water temp) or initial ΔT_1 was large, and the drying time was short.

ACKNOWLEDGMENTS

This work was supported by the Korea Institute of Energy Technology Evaluation and Planning (KETEP) and the Ministry of Trade, Industry & Energy (MOTIE) of the Republic of Korea (No. 20181720201020).

REFERENCES

[1] Dry Storage Handbook, 2015 Edition. Fuel Performance in Dry Storage. ANT International, Mölnlycke, Sweden.

Analysis of Axial Burnup Profile Effects on the Shielding Calculation of the KORAD-21 Cask Using Monaco/MAVRIC

Ye Seul Cho, Dong Jin Kim, and Ser Gi Hong*
Kyung Hee University, 1732, Deogyeong-daero, Giheung-gu, Yongin-si, Gyeonggi-do, Republic of Korea
*sergihong@khu.ac.kr

1. Introduction

The KORAD-21 cask was designed and manufactured to transport 21 PWR WH and CE type spent fuels. The shielding analysis for KORAD-21 under the transport conditions was performed by KORAD [1] at which the realistic axial burnup distribution data were not considered. In addition, assumption is applied for each node of the burnup distribution.

The objective of this work is to perform a shielding calculation considering realistic axial burnup distributions for the spent fuels discharged from Hanbit Unit 3. In particular, we assessed whether the axial burnup distribution obtained with the previous method is conservative from aspect of shielding.

2. Methods and Results

2.1 Previous Axial Burnup Distribution

The axial burnup distribution applied in the previous shielding evaluation was produced from 42,000 ~ 46,000MWD/MTU burnup group among the 3,169 axial burnup distribution data of 20 nuclear power plants in the United States (YAEC-1937) [2]. The axial burnup distributions were evaluated with 18 axial nodes and the final axial burnup distribution used for shielding analysis was determined by taking the largest normalized burnup value for each axial node among several axial distributions. Then, the axial burnup distribution was finally renormalized. In addition, it was assumed that the axial release rates of the gamma are proportional to the axial burnup distribution and that the axial release rates of the neutron are proportional to the fourth-order of the axial burnup distribution. The previous axial burnup distribution is compared in Figure 1 with the selected ones of the Hanbit 3 spent fuels.

2.2 Selection of Axial Burnup Distribution of Hanbit 3

In order to use the axial burnup distribution of Hanbit 3, core following calculations from 1 cycle to 13 cycles were performed [3] using the STREAM/RAST-K code system [4]. From these core follow calculations, 192 axial burnup distributions were generated with 24 axial nodes in the 42,000 ~ 46,000MWD / MTU burnup range. To evaluate the effects of axial burnup distributions on shielding analysis, we considered five different axial burnup distributions. The first one (Distribution 1) was obtained with the previous method given in Sec. 2.1. The second one (Distribution 2) is the bounding profile from view point of criticality safety analysis among the 192 distributions and the third one (distribution 3) is a typical axial burnup distribution. The fourth one (Distribution 4) has a high burnup at bottom which was selected to show the effects of bottom-skewed burnup profile on the dose rate in the lower region of the cask. The final one (Distribution 5) has a high burnup at top of spent fuel assembly.

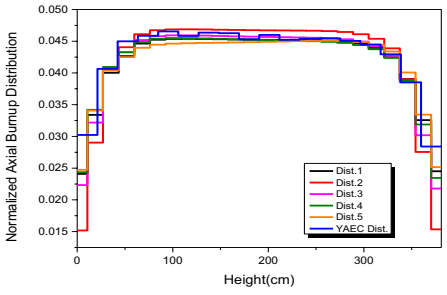

Fig. 1. Normalized Axial Burnup Distributions.

2.3 Results of Shielding Analysis

The shielding analysis for KORAD 21 cask was conducted using Monaco/MAVRIC [5] sequences of SCALE6.1 which is a code system dedicated for shielding analysis with automatic variance reduction. The dose rates are tallied on the cask surface with 72 divisions on azimuthal

direction ranging 0 to 180 degree and 50 meshes on axial direction. Fig. 2 shows the cask modeling and the distribution of tallied neutron dose rate which is more dominant than gamma dose rate. As shown in Fig. 2, the high dose rates are observed both in low and upper regions where neutron shields are absent. Fig. 3 shows the total dose rates on the side surface tally regions along the axial direction at 0 azimuthal angle for the considered axial burnup distributions. The considered different burnup distributions gives considerable differences in the dose rates less than 10%.

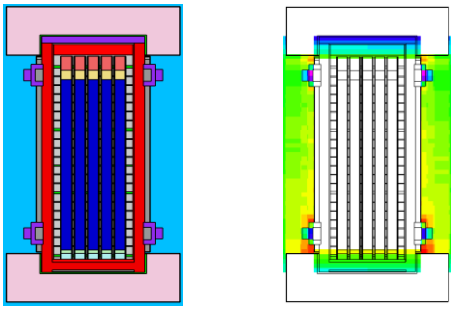

(a) modeling (b) tallies

Fig. 2. KORAD-21 modeling and tallies (neutron dose rate).

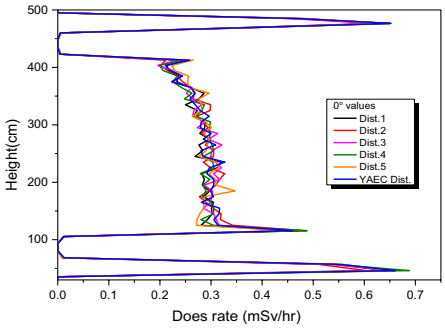

Fig. 3. Side dose rate (mSv/hr) at 0 degree.

Table 1 shows the maximum side dose rates at 0 and 45 degree azimuthal angles for each distributions. Maximum dose rate values were evaluated primarily in the top and bottom regions of the cask due to the absence of neutron shields above and below the cask. From Table 1, it can be seen that the 6% higher dose values were evaluated at Distribution 4 having bottom-skewed distribution than Distribution 1 using the previous method. The Distribution 4 also gives higher maximum dose rate even than the one determined with YEAC distributions. In the case of Distribution 2 with the blanket, the bottom has very low burnup, which gives the lowest result which is 11% lower than value of Distribution 4.

Table 1. Comparison of maximum side dose rates (mSv/hr) at 0 and 45 degree azimuthal angles

Dist. #	Dist.1	Dist.2	Dist.3	Dist.4	Dist.5	YAEC
0°	0.6494	0.6196	0.6583	0.6880	0.6477	0.6604
45°	0.8521	0.7920	0.8377	0.8783	0.8553	0.8650

3. Summary and Conclusions

In this work, we performed a shielding calculation considering realistic axial burnup distributions of the spent fuels from Hanbit Unit 3. From the analysis, it was shown that the hig dose rates were evaluated at the low and high axial regions due to the absence of neutron shields and that the axial burnup profiles obtained with the previous method do not give the conservative dose rates in comparison with those obtained with the bottom-skewed burnup profile of Hanbit Unit 3 spent fuels. Finally, it is concluded that the shielding analysis should be conducted with the bounding axial burnup profile obtained with considering the shield arrangement.

REFERENCE

[1] Woo-seok Choi et al, “A Study on Puncture Simulation of Transportation Cask”. Transactions of the Korean Nuclear Society Spring Meeting, Jeju, Korea, May 17-18, 2018.

[2] "Axial Burnup Profile Database Pressurized Water Reactors", YAEC-1937, Yankee Atomic Electric Company, Bolton, Massachusetts, May 1997.

[3] Dong Jin Kim et al, “Production of Axial Production of Axial Burnup Profiles of Spent Nuclear Fuels Discharged from OPR-1000 using STREAM/RAST-K Core Follow Calculations”, Transactions of the Korean Nuclear Society Spring Meeting, Jeju, Korea, May 23-24, 2019.

[4] Jiwon Choi, Verification and validation of STREAM/RAST-K for PWR analysis, Volume 51, April 2019 Pages 356-368.

[5] Oak Ridge National Laboratory, Scale: A Comprehensive Modeling and Simulation Suite for Nuclear Safety Analysis and Design, ORNL/TM-2005/39, Version 6.1, June 2011.

Development Status of AMORES Program for Automatic Source Term Evaluation of Spent Fuels

Geon Hee Jung[a], Ye Seul Cho[a], Ser Gi Hong[a,*], Ara Go[b], and Dae Sik Yook[b]
[a]Kyung Hee University, 1732, Deogyeong-daero, Giheung-gu, Yongin-si, Gyeonggi-do, Republic of Korea
[b]Korea Institute of Nuclear Safety, 62 Gwahak-ro, Yuseong-gu, Daejon 305-338, Korea
[*]sergihong@khu.ac.kr

1. Introduction

Besides the public acceptance, the preparation of new spent fuel storage facilities such as interim dry storage requires resolving several technical issues. In particular, it is required to secure the safety of the transportation and storage facilities considering various aspects such as radiation shielding, heat generation, and criticality. The safety analysis of the transportation and storage facilities requires accurate estimation of the source terms. We have developed and updated the AMORES program for automatic evaluation of source terms for a huge number of spent fuels under a support from KINS [1]. The purpose of this paper is to report the development status of the AMORES program.

2. Methods and Results

2.1 Overview of AMORES Program and Development Status

Originally, AMORES was started to be developed to reduce the burden in preparing ORIGEN input files, in executing them and in analyzing the results for a large number of spent fuels for giving source terms for various analyses. Then, the AMORES program has extended to incorporate various calculational functions. Figure 1 explains the overview of AMORES.

The main functions of the AMORES program can be summarized as follows: 1) Validation of SNF DB information data, 2) Source term evaluation of the selected number of spent nuclear fuel (SNF)s using automatic ORIGEN-S calculation and extraction of needed data, 3) Projection of future SNF inventories based on the input scenario and evaluation of source terms in an observation time point, 4) Providing user-friendliness GUIs for simulation.

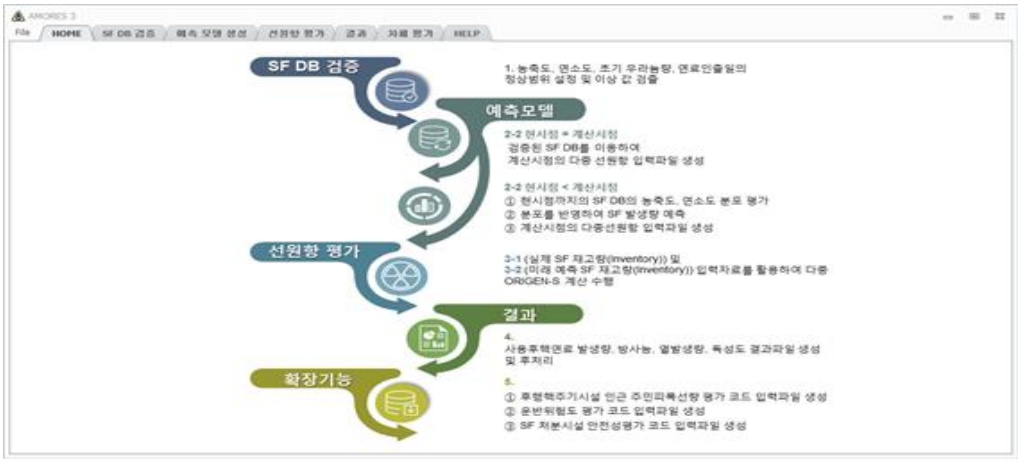

Fig. 1. Overview of AMORES Program.

2.2 Calculation Flow

AMORES starts by importing and processing a SNF BD file. Recently, AMORES incorporated new SNF DB file which does not only include SNF-wise depletion and cooling histories but also the cycle-wise plant operation history data such as effective full power days, fuel loading date, initial criticality approach date, shutdown date, fuel withdrawal date, and so on. Then, AMORES checks if there are wrong data in SF DB data and prints out the information on the wrong data. Then, the ORIGEN-S input files for the SNFs selected by user and a batch file for their executions are automatically prepared with the new or old SNF DB file. When the old SNF DB is used, a single cycle independent specific power (e.g., 40 MWD/kg for PWR SNF) is considered in ORIGEN-S depletion calculation. Then, the batch file is activated to execute ORIGEN-S calculations and various SNF characteristic parameters can be automatically extracted from ORIGEN-S outputs and displayed through GUI. The projection of SNFs with a scenario model is also possible to estimate the source term in a future observation time point. In this case, two different type ORIGEN-S input files are automatically prepared : 1) Input files for the existing SNFs, and 2) input files for the newly generated SNFs by projection with a scenario. The total source terms are generated by adding these two different ORIGEN-S calculations.

2.3 Effects of Detailed SNF Depletion and Cooling Histories

In this section, new version AMORES was applied to show the effects of new SNF DB considering detailed SNF-wise depletion and cooling histories on SNF characteristics. We used only SNFs from Hanbit Unit 3. The SNF characteristics are evaluated using the new and old SNF DB files at 2035. Fig. 2 compares the discrepancies of SNF-wise radioactivity and thermal power between the old and new SNF DB files. From these figures, it was shown that AMORES with new SNF DB gives considerable discrepancies in radioactivity and thermal power in comparison with the results obtained with the old SNF DB.

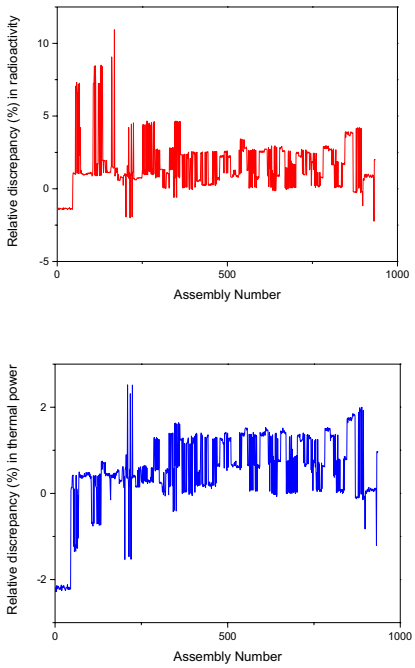

Fig. 2. Discrepancies of radioactivity (above) and thermal power (below) between old and new SNF DB.

3. Summary and Conclusions

This paper described new version of AMORES program and calculation flow. The new version of AMORES has been successfully extended to incorporate new detailed SNF DB. The numerical tests showed that the consideration of new SNF DB gives considerable differences in the SNF characteristics from those obtained the old SNF DB.

REFERENCE

[1] G. Kim et al,, “A Scenario Study on PWR Spent Fuel Characteristics using Updated AMORES Program”, Transactions of the Korean Nuclear Society Spring Meeting, Jeju, Korea, May 17-19, 2017.

The Effects of Hydride Morphologies on the Responses of SNF Claddings to the Pinch-load

Ho-a Kim[a,b,*], Yong-soo Kim[a], Won-young Lim[a], and Jae-soo Noh[b]
[a]Hanyang University, 222, Wangsimni-ro, Seongdong-gu, Seoul, Republic of Korea
[b]Atomic Creative Technology Co., Ltd., 1434, Yuseong-daero, Yuseong-gu, Daejeon, Republic of Korea
[*]pissan@hanyang.ac.kr

1. Introduction

As the burnup of spent nuclear fuel (SNF) increases, Zircaloy-4 cladding increases the risk of brittle failure under normal and hypothetical accident conditions that may occur in handling, storage and transportation. As shock and vibration are expected to occur during the transportation of SNF, it is especially important to understand a pinch-load effect in accident condition.

Ductility and pinch-load resistance of SNF claddings can be reduced due to precipitated hydride. Especially, hydride precipitation issues are highlighted in high burnup fuel. High burnup Zircaloy-4 cladding can contain hydrogen up to 600-800 wppm, and this hydrogen is precipitated circumferentially under its terminal solid solubility. However, hydrogen can be precipitated radially during vacuum drying process of dry storage and these radial hydrides can act as a crack propagation path and degrade cladding ductility and pinch-load resistance.

In this study, ring compression tests were conducted to evaluate the effects of hydride morphologies on the responses of SNF claddings to the pinch-load using Zirclaoy-4 cladding tube with circumferential and radial hydrides.

2. Experimental

2.1 Specimen preparation

Stress-relieved (SR) Zircaloy-4 cladding tube was used in this study. Two specimen types were used: one is circumferential hydride (CH) specimen and the other is radial hydride (RH) specimen. Hydrogen was charged in CH and RH specimens using a Sievert type apparatus aimed at 200-700 wppm, and RH specimens were pressurized with Ar gas under 90 and 150 MPa hoop stresses. Hydrogen element analysis on CH and RH specimens was partially conducted and additional analysis will be conducted. CH and RH specimens were classified in Table 1.

Table 1. Classification of the CH and RH specimen

Specimen	Hoop stress (MPa)	Hydrogen concentration (wppm)		
		1	2	3
CH	150	200	400	700
RH	150	200	400	700

2.2 Ring compression test (RCT)

Ring compression test is a test method that can simulate pinch-load during the normal transportation of RCT. RCT was used to evaluate the relative effect of the circumferential and radial hydride. Compression tests were conducted with 10 mm rings of the CH and RH specimen using a universal testing machine. Load-displacement curves for the specimen were obtained from the test results and offset strain [1] and fracture energy per unit area [2] were calculated from the load-displacement curves. Before and after the tests, images on hydride morphology of the specimens were observed by optical microscope and crack path and length will be evaluated by analyzing the hydride morphology images.

3. Results and discussions

3.1 Specimen hydride morphology

Fig. 1 shows hydride morphologies of the CH and RH specimens before the RCTs and hydride morphologies. After the RCTs, microstructure analysis will be added to analyze the crack path and length. As hydrogen concentration increases, precipitated hydride also increases in both CH and RH specimens. In RH specimen, the fraction of radial hydride decreases as hydrogen concentration increases. To evaluate radial hydride, additional image analysis will be conducted.

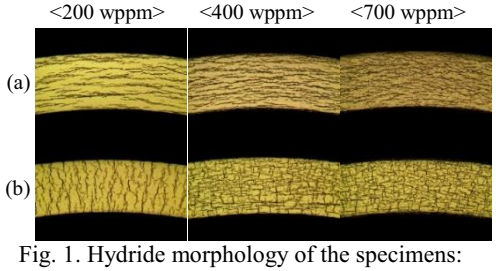

Fig. 1. Hydride morphology of the specimens: (a) CH specimen; (b) RH specimen.

3.2 Offset strain

To classify ductile and brittle failure, Billone suggests “offset strain” concept. Based on offset strain, cladding with ≥1% permanent strain and ≥2% offset strain prior to the first crack extending through >50% of the wall is classified as ductile. Cladding that cracks through >50% of the wall prior to achieving 2% offset strain is classified as brittle [1]. Fig. 2 shows offset strain vs. temperature of the CH and RH specimens. Offset strain of the CH specimen decreases as the test temperature increases and the hydrogen concentration decreases. The offset strain values are convergent at high temperature (>150 °C). Offset strain of the RH specimens shows <2% at the temperature below 100 °C. Offset strain of 200 wppm are lower than 400 and 700 wppm at 150-200 °C. It means the fraction and formation of radial hydride is critical than hydrogen concentration at certain temperature ranges.

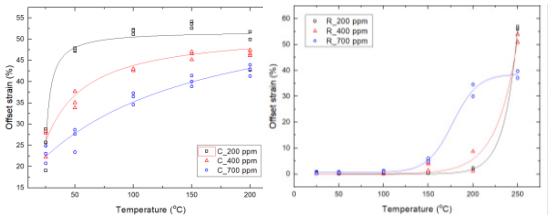

(a) (b)

Fig. 2. Offset strain vs. temperature of the specimens: (a) CH specimen; (b) RH specimen.

3.3 Fracture energy per unit area

Kim et al. [2] suggest “fracture energy” which is an accumulated energy until a specimen is failed. Fracture energy is divided into cross-sectional area of the specimen to revise an error of specimen length (10 mm). Fig. 3. shows fracture energy per unit area vs. temperature of the CH and RH specimens. The results show a similar tendency to offset strain results. This means fracture energy can be considered as a method to measure pinch-load resistance along with offset strain.

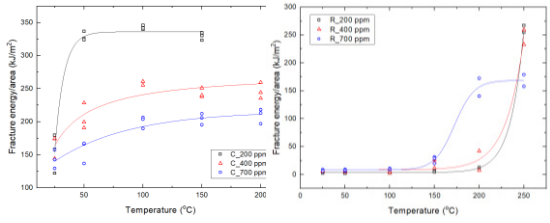

(a) (b)

Fig. 3. Fracture energy per unit area vs. temperature of the specimens: (a) CH specimen; (b) RH specimen.

4. Conclusions

Ring compression tests were conducted to evaluate the effects of hydride morphologies on the responses of SNF claddings to the pinch-load and hydride morphology, offset train, fracture energy per unit area were analyzed. The test results are as follows:

1. The offset strains decrease by increasing the hydrogen concentration. However, in case of RH specimen, slightly opposite results occurred at certain temperature ranges due to the fraction and formation of radial hydride.
2. Based on the offset strain results of RH specimen, the radial hydrides highly reduce the pinch-load resistance under 100 °C.
3. In RH test results, a specimen with high hydrogen concentration which has mixed circumferential and radial hydrides can be resistant to crack propagation than a specimen with low hydrogen concentration which has mainly radial hydrides. It is assumed that circumferential hydrides disturb the radial crack growth and divert the crack path, which shall be confirmed by future works to link the relationship between the hydride morphology and the fracture.

ACKNOWLEDGEMENT

This work was supported by the Korea Institute of Energy Technology Evaluation and Planning(KETEP) and the Ministry of Trade, Industry & Energy(MOTIE) of the Republic of Korea (No. 20181710201770).

REFERENCES

[1] M. C. Billone et al., FCRD-USED-2012-000039, ANL-13/05 (2011).
[2] J. S. Kim et al., J. Nucl. Mater. 456 (2015) 235-245.
[3] M. C. Billone, NUREG/CR-7139, ANL-11/52 (2012).

Preliminary Studies on Residual Radioactivity Concentration of Spent Nuclear Fuel Dry Storage System After Design Lifetime

Sae Geun Lee and Jae Hak Cheong*
Kyung Hee University, 1732, Deogyeong-daero, Giheung-gu, Yongin-si, Gyeonggi-do, Republic of Korea
*jhcheong@khu.ac.kr

1. Introduction

According to Korea Hydro & Nuclear Power Co., Ltd. (KHNP), the temporary storage capacity of spent nuclear fuel (SNF) for domestic Pressurized Water Reactors (PWRs) reached about 71% as of the end of October 2018. However, Korea does not have any experiences in operation of interim storage of SNF from PWR. In 2016, The Ministry of Trade, Industry and Energy (MOTIE) only announced plans to promote the construction and operation of SNF interim storage facilities on the site where permanent disposal facilities would be located [1]. Following the plan, dry storage cask system will be adopted due to its variety, ease of capacity expansion and operation.

Therefore, a large number of dry storage casks would be used in interim storage facilities. By the way, components of dry storage system are to be irradiated and activated by neutrons released from stored SNF through their design lifetime. As a result, components dismantled after design lifetime would be able to classified as radioactive wastes. International Atomic Energy Agency (IAEA) says during decommissioning of SNF storage facility, even when the bulk of the residual process material has been removed, a significant amount of contaminated material may remain [2]. And also U.S. Nuclear Regulatory Commission (U.S. NRC) says after the casks have been decontaminated, the major sources may be those resulting from activation of the system components, such as the reinforcing steel [3]. In Korea, however, it is lacked that in-depth evaluations about becoming radioactive waste and generation of secondary waste of the SNF dry storage system that would be used in interim storage facilities [4].

Therefore, after selecting the concrete storage system widely used abroad, it was evaluated that radioactivity concentration after design lifetime by neutron activation, according to the spent fuel burnup, enrichment, cooling time, and impurity in the structural material of the dry storage system components.

Through this, it was quantitatively assessed that a large number of used dry casks, which are expected to occur in the future, will be classified as non-radioactive waste below the clearance level or higher level radioactive waste exceeding the clearance level after the design lifetime. At the same time, this study aims at minimizing the secondary waste from SNF dry storage system through sensitivity analysis and suggesting factors to be considered by operators.

2. Materials and Methods

In this study, HI-STORM 100 of HOLTEC International was selected as the dry storage system to be evaluated. HI-STORM 100 was selected in various prior studies and widely used in actual dry storage facilities abroad as its design feature to accommodate various types of spent fuel.

CE type 16 × 16, a PLUS-7 fuel used in OPR-1000 and APR-1400 which occupy most of the PWRs except the nine units of PWR types and System 80 types. And the specifications of the loaded spent fuel used in the initial calculation of the dry storage container to be evaluated are shown in Table 1.

Table 1. A specifications of HI-STORM 100 and loaded spent fuel assumed in this study

Item	Description
Concrete overpack	O.D 3,366mm × 5,874mm
Inner cavity	O.D 1,867mm × 4,839mm
MPC	O.D 1,737mm × 4,839mm
Capacity	24 PWR SNF Assemblies
Burnup	55,000 MWD/MTU
Enrichment	4.2 wt%
Cooling time	10 Years
Type of SNF loaded	CE 16 × 16 type
Design lifetime	40 Years

For calculating radioactivity concentration, in this study, three computer codes were used: ORIGEN-ARP, MCNPX, and ORIGEN-2. In this study, the ORIGEN-ARP module of SCALE 6.1 computer code is used to calculate the neutron source term for the SNF. Based on the total neutron flux for 24 bundles of fuel calculated using ORIGEN-ARP, the neutron flux and reaction rate for the target component were

calculated by using MCNPX computer code. The MCNP computer code can model various complex geometries in detail and is widely used in various fields such as radiation shielding, dose calculation, etc. And neutron activation of each component was calculated using ORIGEN-2. However, the ORIGEN-2 cross-section library is based on reactor core region and cannot reflect actual reality, so in this study, a new cross-section library is calculated using MCNP result such as the neutron flux and reaction rate of the target component and interpolated into the existing library of ORIGEN-2.

Figure 1 is the schematic diagram of radioactivity concentration assessment model adopted in this study.

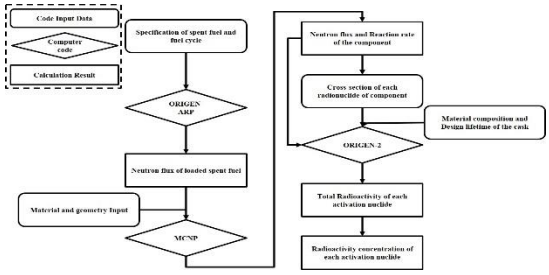

Fig. 1. Schematic diagram of the assessment model for radioactivity concentration by neutron activation.

3. Results and Discussions

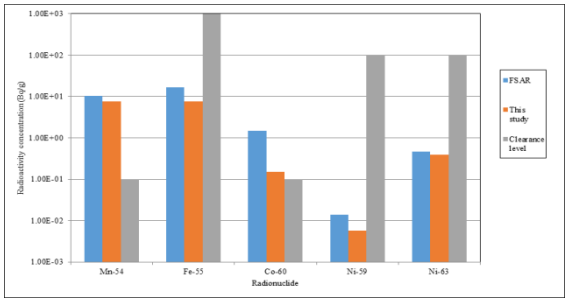

Fig. 2. Radioactivity comparison between HI-STORM 100 FSAR and this study.

Figure 2 shows the comparison between HI-STORM 100 Final Safety Analysis Report (FSAR) and this study about MPC's radioactivity concentration of major radionuclide immediately after the design lifetime for validation [5]. It shows there is little differences between FSAR and this study, the reason seems that differences of source term, activation calculation code, material isotope composition, etc.

Figure 3 shows that the MPC basket's radioactivity concentration of major radionuclide immediately after the design lifetime along with varying burnup. Radioactivity concentration of Co-60 is very high, it means impurity of system material composition is very important to activation analysis and it should be managed for reducing volumetric contamination.

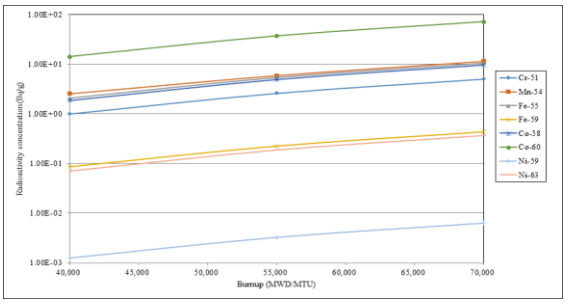

Fig. 3. MPC basket radioactivity according to each burnup.

4. Conclusion

This study assessed the radioactivity concentration of spent nuclear fuel dry storage cask after its design lifetime. Considering the Korean regulation on radioactive waste classification and clearance standards, it seems necessary that both operator and regulatory body should evaluate this quantitatively before cask decommissioning.

ACKNOWLEDGEMENT

This work was supported by "Human Resources Program in Energy Technology" of the Korea Institute of Energy Technology Evaluation and Planning (KETEP), Granted financial resource from the Ministry of Trade, Industry & Energy, Republic of Korea. (No. 20184030202170)

REFERENCES

[1] The Ministry of Trade, Industry and Energy, Republic of Korea, Basic Plan for High Level Radioactive Waste Management (2016).
[2] IAEA, Storage of Spent Nuclear Fuel, IAEA Safety Standard Guide No. SSG-15, IAEA, Vienna (2012).
[3] U.S. NRC, Standard Review Plan for Spent Fuel Dry Storage Systems at a General License Facility, NUREG-1536 (2010).
[4] Tae-Man Kim et al., Activation Analysis of Dual-purpose Metal Cask After the End of Design Lifetime for Decommission, JNFCWT Vol. 14 No.4 (2016).
[5] HOLTEC INTERNATIONAL, HI-STORM 100 Final Safety Analysis Report, HI-2002444, Revision 13 (2016).

2분과

사용후핵연료 처분전관리 (Poster)

Effect of Packing Density on Evaporation of Adhered Salt

S.W. Kwon*, J.H. Jung, and S.J. Lee

Korea Atomic Energy Research Institute, 111, Daedeok-daero 989beon-gil, Yuseong-gu, Daejeon, Republic of Korea

*swkwon@kaeri.re.kr

Abstract

The electrorefining process is generally composed of two recovery steps – the deposit of uranium onto a solid cathode and the recovery of the remaining uranium and TRU elements simultaneously by a liquid cadmium cathode. The salt distillation is needed to separate salt from the uranium dendrites in the pyroprocessing. It is very important to increase the throughput of the salt evaporation in solid cathode processing. Several methods have been proposed to increase the capacity of the salt separation system. In this study, the effect of deposit packing density on the evaporation of the adhered salt was investigated for the effective separation of the salt. The salt evaporation behaviors were investigated for a salt in steel balls, a salt in steel chips, and a salt in uranium deposits. 100 grams of salt was mixed with 100 grams of steel balls with a diameter of about 10 mm. 100 grams of salt was mixed with 100 grams of steel chips with length of 5-15 mm and width of 1-2mm. 150 - 200 grams of uranium deposits was used for the comparison. The apparent evaporation rate of a salt with steel ball was similar to that of a salt without deposits. This was caused by the morphology of the deposits. During the distillation of the salt, the balls separated from the balls and settled down to the bottom of the crucible. The salt vapor evaporated from the liquid salt surface can emigrate freely to the atmosphere owing to the sedimentation of the balls. The salt evaporation behaviors were compared between the conventional nonporous crucible and the porous crucible. Two step weight reductions took place in the porous crucible, whereas the salt weight reduced only at high temperature by distillation in a nonporous crucible. The first weight reduction in the porous crucible was caused by the liquid salt penetrated out through the perforated crucible during the temperature elevation until the distillation temperature. It was found that the salt evaporation rate depends on the morphology and packing density of the deposits in the crucible.

ACKNOWLEDGEMENT

This work was supported by a National Research Foundation of Korea (NRF) grant funded by the Korean Government (MSIP) (No. 2017M2A8A5015079).

Manufacture of Engineering-Scale Remote Injection Casting Device and Fuel Slug

Hoon Song*, Yoon-Myung Woo, Sang-Gyu Park, and Jeong-Yong Park
Korea Atomic Energy Research Institute, 111, Daedeok-daero 989beon-gil, Yuseong-gu, Daejeon, Republic of Korea
*hsong@kaeri.re.kr

1. Introduction

Metallic fuels, such as the U-Pu-Zr alloys, have considered as a nuclear fuel for a sodium-cooled fast reactor (SFR) related to the closed fuel cycle for managing minor actinides and reducing the amount of highly radioactive spent nuclear fuels since the 1980s. Metallic fuels fit well with such a concept owing to their high thermal conductivity, high thermal expansion [1,2]. Because all the manufacturing process performed in hot cell facility due to high radiation material of recycled nuclear fuel, it is important to develop the remote fabrication technology. In this study, we had developed the engineering-scale remote injection equipment following the laboratory scale and engineering-scale remote injection casting tests conducted.

2. Methods and Results

2.1 Experiment Procedure

KAERI (Korea Atomic Energy Research Institute) had developed the engineering-scale remote injection casting equipment (Fig. 1). The engineering-scale injection casting tests with Cu and Cu-Ni repeated many times before uranium casting test to find the proper casting process parameters such as melting batch, melt casting temperature, mold preheating time, and melt deposition time selected to produce the sound fuel slug. After that, engineering scale 78 U-Zr fuel slugs casting test performed. After fabricating a considerable amount of fuel slugs in the casting furnace, the diameter of the fuel slugs was measured at 3 axial points: top, middle, bottom, measured in two perpendicular directions at each axial position. The density of the slug measured using an Archimedean immersion method.

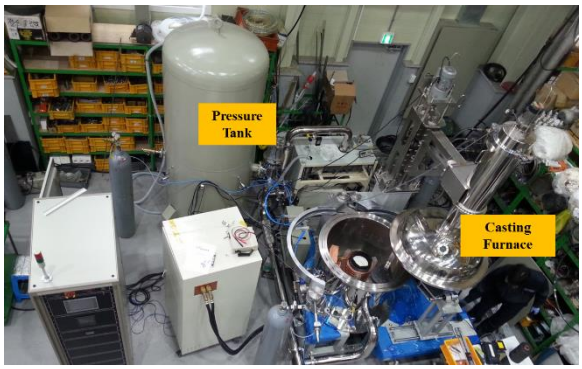

Fig. 1. Engineering-scale injection casting equipment.

2.2 Results

The fuel slug specification consistent with the practical reactor core design was previously set as the average diameter precision ±0.05mm, total impurities (O, C, N, Si) less than 2,000 ppm. The specification was satisfied in a series

of engineering-scale tests. Figure 2 shows U-Zr fuel slugs obtained in the tests. The total amount of impurities (O, C, N, Si) was still lower than the provisional limit: 2,000 ppm.

Table 1. Process variable conditions of the test

No	Session
Initial charge (kg)	16.4
Number of molds	78
Length of molds (mm)	450
Pressure before injection (Torr)	400
Molten metal temp. at injection (°C)	1,550
Pressurization rate(bar/sec)	2.81

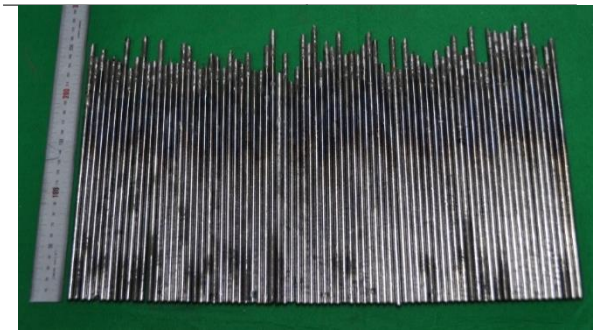

Fig. 2. U-Zr fuel slug after mold removal.

3. Conclusion

U-Zr metal fuel slugs fabricated by performing remotely casting test to verify the feaibility of manufacturing a fuel slug after construction of remote engineering-scale metal fuel fabrication equipment for manufacturing a recycled metal fuel slug in a hot cell.

REFERENCES

[1] C.L. Trybus, J.E. Sanecki, and S.P. Henslee, “Casting of Metallic Fuel Containing Minor Actinide Additions”, Journal of Nuclear Materials, 204, 50-55 (1993).

[2] H.F. Jelinek, G.M. Iverson, “Equipment for Remote Injection Casting of EBR-II Fuel”, Nuclear Science and Engineering, 12(3), 405-411 (1962).

Cladding Temperature Trend of a Spent Fuel Assembly in Boundary Condition With High Temperature

Hyungjin Kim* and Sang-jin Lee
Korea Radioactive Waste Agency, 174, Gajeong-ro, Yuseong-gu, Daejeon, Republic of Korea
*hjkim@korad.or.kr

1. Introduction

Thermal evaluation of the spent fuel cask using three-dimensional models is especially difficult if the spent fuel assemblies are modeled explicitly and included in the analysis. Therefore, these assembly elements are modeled as solids with homogenous "smeared". This solid method can predict the peak cladding temperatures of casks with reasonable accuracy [1, 2]. One of the solid methods is CFD simulation on transverse cross-section of a spent fuel assembly [3]. The 2D CFD simulation has used the conduction and radiation for heat transfer.

In this work, the temperatures of a spent fuel assembly were calculated by using the conduction, convection and radiation in heat transfer. The CFD simulation is performed by using the FLUENT 2019 R1 and SpaceClaim.

2. Modeling and method

2.1 Spent fuel Modeling

16×16 PWR spent fuel type is selected for 3D CFD simulation. The assembly heat load is 796.2W. Fig. 1 shows the modeling and meshing results of the assembly which has the gap between fuel rods and cladding. The elements are over 64 million elements.

Thermal properties of materials are used with a temperature-dependent value [4]. The emissivity is 0.8, 0.36 for zircaloy and stainless steel respectively.

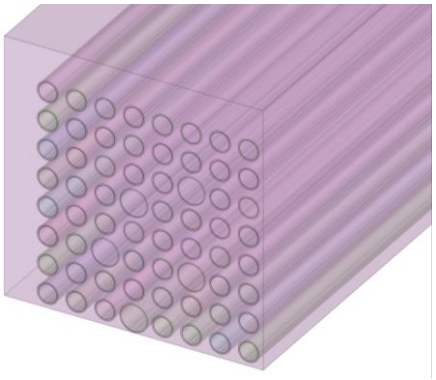

(a) 3D modeling of 16×16 PWR spent fuel

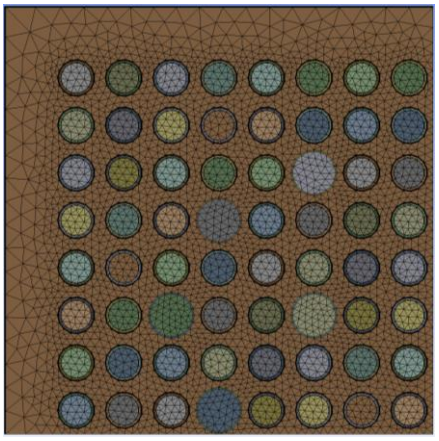

(b) Top view of meshing result

Fig. 1. Modeling and meshing for 3D CFD simulation.

2.2 Physics model and solution method

The discrete ordinates (DO) radiation model was selected to solve the radiation of spent fuel assembly. The value of angular discretization and pixelation available in the discrete ordinates radiation model significantly affects the behavior of temperature. The constants were determined to solve this work: 3×3 for pixelation, 5×5 for discretization recommended by ANSYS.

The pseudo-time progression method has been used to obtain a converged solution. This method works by using a steady calculation and introducing a pseudo-time term to relax the equation. The first layer thickness near the wall is calculated from y+ (<10).

UDF(User define function) of FLUENT is used for axial power distribution according to the height of fuel, and the profile of axial power is in Fig. 2.

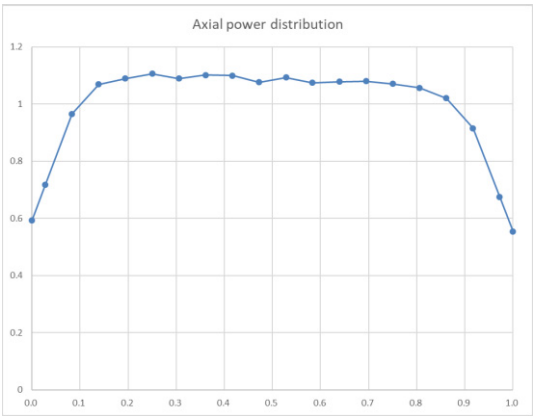

Fig. 2. Axial power distribution of fuel assembly.

3. Results and discussion

In Fig. 3, temperature distribution of a 16x16 assembly is shown for 700K of basket wall temperature. The maximum temperature is about 710K. There is nearly no maximum temperature difference between 2D and 3D simulation [3]. The lower temperature in 3D simulation would result from convection heat transfer.

Fig. 3. Temperature distribution of 16×16 fuel assembly.

In the thermal analysis of a cask, one could know that effective thermal conductivity (ETC) would depend on the spent fuel height.

4. Conclusions

3D CFD simulation was performed to predict the cladding temperature of the spent fuel assembly. There is temperature difference between 3D and 2D simulation. This would come from the difference of heat transfer modes used for simulation.

From this work, one knows that the use of ETC for the cask analysis needs the change. This work will be expanded with various basket wall temperatures.

ACKNOWLEDGEMENTS

This work was supported by the National Institute of Supercomputing and Network/Korea Institute of Science and Technology Information with supercomputing resources including technical support (KSC-2016-S1-0028).

REFERENCES

[1] EnergySolutions, FuelSolutions™ storage system final safety analysis report, WSNF-220 (2007).

[2] Babcock & Wilcox Fuel Company, BR-100 100-ton rail/barge spent fuel shipping cask, No. 51-1203400-01 (1991).

[3] H. Kim, O. J. Kwon, G. U. Kang and D. G. Lee, “Comparisons of prediction methods for peak cladding temperature and effective thermal conductivity in spent fuel assemblies of transportation/storage casks,” Annals of Nuclear Energy, Vol. 71 (2014).

[4] Korea Radioactive Waste Agency (KORAD), Safety analysis report of KORAD21 spent fuel transportation cask (2016).

Status of Barrier Cladding Technology for Enhancing Performance of the Metal Fuel

Jun Hwan Kim[1,*], Sunghwan Yeo[1], Sung Ho Eom[1], Sung Ho Kim[1], Jeong Yong Park[1], and Tai Hong Yim[2]

[1] Korea Atomic Energy Research Institute, 111, Daedeok-daero 989beon-gil, Yuseong-gu, Daejeon, Republic of Korea

[2]Korea Institute of Industrial Technology, 156, Gaetbeol-ro, Yeonsu-gu, Incheon, Republic of Korea

[*]junhkim@kaeri.re.kr

1. Introduction

To reduce the amount of spent fuel from LWR, metal fuel has been selected as a fuel for Sodium-cooled Fast Reactor (SFR) in Korea in connection with pyroprocessing. However, stainless steel used as cladding in SFR react with the elements in the metal fuel so that its use is limited under high temperature. To suppress such phenomenon as Fuel-Cladding Chemical Interaction (FCCI), a concept of barrier cladding by applying FCCI-resistant functional material between cladding and metal fuel has been suggested. Electroplating and metal liner fabrication have been chosen as important candidates for barrier technique based on parametric analysis regarding materials and manufacturing processes [1]. This study summarized the technical status of barrier cladding development in Korea for enhancing performance of metal fuel.

2. Development of Barrier Cladding Technology

2.1 Electroplating

Electroplating process contains various parameters (temperature, current density, current shape, etc.) that affect layer property. It is known that Cr layer composes of nodular structure, where develops into a crack during the operating temperature so that it acts as a path for fuel constituent. Suppressing crack inside the Cr plating is needed to enhance layer performance. Solution temperature, current density and current shape (pulse current) and post-plating treatment has been scoped to enhance the microstructure. Conversion of nitride by post-treatment has been performed, which coalesces the crack so that it enhances the property of Cr layer.

Coated tube sample has been manufactured to demonstrate the coating technology into the tube inner surface. Electroplating was carried out by applying current at the electrolyte which flows inside the cladding tube. The results showed that 20μm of Cr layer has uniformly coated at the 300mm length HT9 cladding (7.4mm outer diameter and 0.5mm thickness).

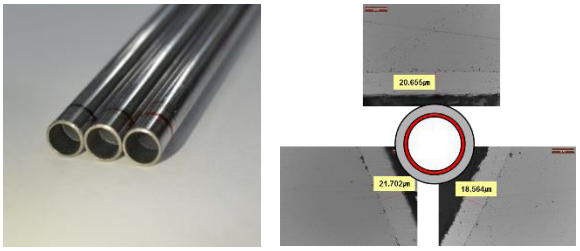

Fig. 1. Manufacture of Cr-electroplated HT9 cladding (20μm).

Performance tests have been done over the manufactured barrier cladding. Out-of pile FCCI test by diffusion couple test (Surrogate materials like rare-earth alloys and U-Zr) has been performed. In-pile FCCI test was being done at HANARO (1st at 2010, 2nd is in preparation), where it shows that Cr layer can hinder interdiffusion between fuel and cladding component. Mechanical tests by uniaxial tension and biaxial burst test showed that Cr layer can sustain sufficient strain (5% plastic strain) prior to rupture [2].

2.2 Metal Liner

Metal liner technology has been selected as one of the barrier candidates because it can assure stable barrier property once its manufacturing technology has been established. Parametric studies of liner tube by the material selection, the effect of cold working, the heat treatment and the joining between tubes have been carried out. After several feedbacks, manufacturing process has been drawn by preparing separate tube (Cold pilgering over liner tube and cold drawing over cladding tube) then joining together by cold pilgering to adjust the required dimension. Based on the procedure, 50μm of Zr has been successfully lined at the inner surface of HT9 cladding. Further studies by applying various liner materials (Ti) and extending longer length is being progressed.

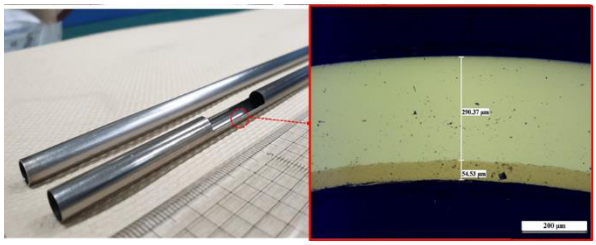

Fig. 2. Production of Zr-lined HT9 cladding (50μm).

3. Conclusions

Studies were conducted to develop the barrier cladding by applying functional material at the inner side, where 20μm of Cr by electroplating and 50μm of Zr by lining has been applied at the HT9 cladding. Further studies like enhancing cladding length as well as optimizing manufacturing parameters will be performed.

ACKNOWLEDGMENTS

This project has been carried out under the Nuclear R&D program by Ministry of Science and ICT.

REFERENCES

[1] J. H. Kim, “Development of Barrier Technology for preventing Fuel-Cladding Chemical Interaction”, GLOBAL 2011, Dec. 11-16, 2011, Chiba, Japan.

[2] J. H. Kim, “Evaluation of Material Properties on the Inner Surface of Cr plated Cladding Tube for preventing Fuel-Cladding Chemical Interaction”, Korean Journal of Metals and Materials, 54(11), 855-861 (2016).

Integrity Verification of the CANDU Spent Fuel Using a Plastic Scintillator

Yewon Kim, Myungsoo Kim, Heejun Chung, and Seunghoon Park*
Korea Institute of Nuclear Nonproliferation and Control, 1534, Yuseong-daero, Yuseong-gu, Daejeon, Republic of Korea
*yewonkim@kinac.re.kr

1. Introduction

Optical Fiber Probe System, OFPS is safeguards inspection instrument. It was developed by KINAC for the spent fuels integrity verification at the CANDU spent fuel pool. KINAC developed the system for the IAEA national inspection. This system had been certified by IAEA and has been performing well in real safeguards inspections [1]. The system uses a depleted in ^{6}Li glass scintillator which is not only difficult to be supplied but also is not cost effective. Thus, KINAC tried to find an alternative proper material for many years.

2. Materials and Methods

2.1 Glass scintillators

For the gamma signal detection of the spent fuel, ^{6}Li depleted glass scintillator is imbedded in OFPS in order to decrease the neutron sensitivity.

Glass scintillators are divided into three types based on the lithium content. In each type, the lithium is present in its natural isotopic ratio, enriched in ^{6}Li to 95 %, or depleted in ^{6}Li (99.99 % ^{7}Li). The properties of the different glasses within each type are similar except for neutron sensitivity. All of the glasses are formulated to have extremely low backgrounds (less than 20 dpm/100 g of alpha activity) making it no longer necessary to order special types having this property. Neutron sensitivity is higher for ^{6}Li enriched glass, while ^{6}Li depleted glass is almost insensitive to neutrons [2][3]. A GS30 (99.99 % ^{7}Li) glass scintillator with 1 mm diameter and 5 mm long was used in this experiment. The light output relative to anthracene of the GS30 is 20~30 % and the decay time is 105 ns.

2.2 Plastic scintillators

Plastic scintillator has been considered improper materials for the radiation spectroscopy since no photo-peaks are observed on the energy spectrum. However, it has advantages such as easy fabrication for large area and the cost effective material. For example, radiation portal monitors (RPM) which should cover large size samples and use gross counting method use a plastic scintillator. Thus, we were considered that a plastic scintillator with better light output is proper material for the OFPS. Because spectroscopic method finding the energy of the photo peaks is not necessary. A BC-400 polyvinyl toluene (PVT) based plastic scintillator with 1 mm diameter and 5 mm long was used in this experiment. The light output

relative to anthracene of the BC-400 is 65% and the decay time is 2.4 ns.

3. Result

3.1 Comparison of the gross count

The rod of the OFPS coupled with a scintillator and optical fibers rewound from the bottom of the pool to measure the radiation signal. Fig. 1 indicates the gross count measured the OFPS with a PVT and a ^{6}Li depleted glass scintillator. The measured gross count with the PVT is about ten times larger than that of the glass scintillator.

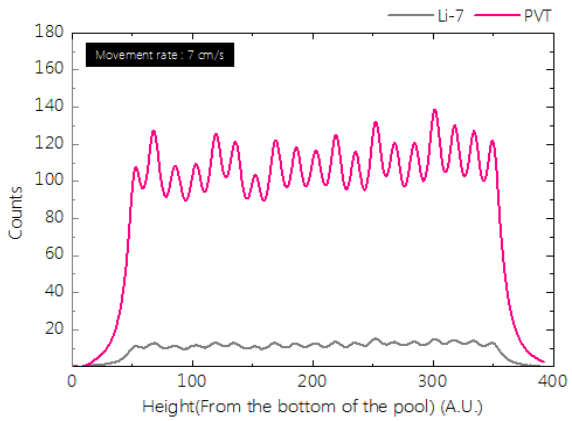

Fig. 1. Comparison of the gross count measured by a PVT and a glass scintillator.

3.2 Comparison of the peak shape

Fig. 2 shows the peak shape measured the OFPS with a PVT and a ^{6}Li depleted glass scintillator. Measured signal from PVT scintillator is more distinguishable than that of the glass scintillator. Because the amplitude of the signal measured by a PVT scintillator is larger than that of the glass scintillator.

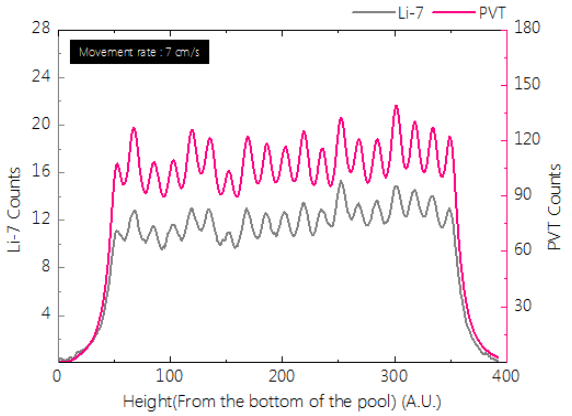

Fig. 2. Comparison of the peak shape measured by a PVT and a glass scintillator.

4. Conclusion

The instrument performance has been increased after the application of the PVT scintillator to the OFPS. As a result, it is expected that the replacement of the OFPS scintillator would greatly help the international safeguards inspection.

REFERENCES

[1] S. Park, “Application of national safeguards instruments for spent fuel verification to the IAEA inspections”, Transaction of the Korean Nuclear Society Spring Meeting (2018).

[2] TYRRELL, Glenn C. Phosphors and scintillators in radiation imaging detectors. Nuclear Instruments and Methods in Physics Research Section A: Accelerators, Spectrometers, Detectors and Associated Equipment, 2005, 546.1-2: 180-187.

[3] A. Paul, R. W. Douglas, Phys. Chem. Glasses 6(1965) 212.

Temperature Distribution of Innovative Metallic Fuel With Multi-hole Shapes

Young-Ho Lee*, Sung-Uk Lee, Sang-Gyu Park, ByoungOon Lee, KiHo Kim, and Jeong-Yong Park
Korea Atomic Energy Research Institute, 111, Daedeok-daero 989beon-gil, Yuseong-gu, Daejeon, Republic of Korea
*leeyh@kaeri.re.kr

1. Introduction

The advantage of annular fuel is to maintain outstanding heat transfer performance and lower fuel temperature, which could improve economy and safety of sodium-cooled fast reactor with high power density and low pressure drop [1]. Recently, additive manufacturing technique enables us to design complicated fuel shape without any significant consideration of applied manufacturing methods. Thorium dioxide with a specific cubic shape was fabricated by stereolithography-based 3D printing method and photopolymer resin, which shows a potential application for advanced nuclear fuel concepts despite of its significant shrinkage ratio [2]. In previous study [3], however, we proposed various innovative fuel shapes for increasing the power density by 20% in low conversion ratio cores with metallic fuels. In this study, the temperature distributions of one of the proposed shapes with different hollow sizes and distributions were investigated for designing an innovative fuel shape with optimized fuel performance.

2. Proposed Fuel Shape

In this study, a multi-hole shape with 3 holes dispersed at 120° intervals was selected as temperature distribution model and a schematic view of its cross-section is shown in Fig. 1. In this model, a hollow size is designed to have 0.18, 0.27 and 0.36 with ratio of hole to fuel pin diameter (i.e., diameter ratio) and this area is assumed to fill with sodium or helium gas for comparing heat conductivity effects.

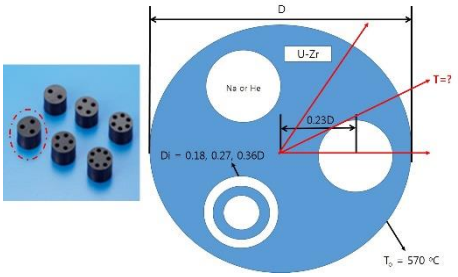

Fig. 1. Schematic views of temperature analysis model used in this study.

3. Findings and Summary

In order to verify the temperature analysis procedure, metallic fuel without porosity (i.e., solid fuel) was analyzed to validate the temperature distribution of applied model used in this study. After then, temperature analysis of the multi-hole model has been performed by applying different hole sizes and internal gases. Fig. 2 shows typical results of temperature profiles at solid region of both reference and multi-hole fuel, which has a diameter ratio of 0.27 with the different internal gases. In case of solid metallic fuel, maximum temperature at the

center region is about 612 °C and this result is comparable with the previous study.

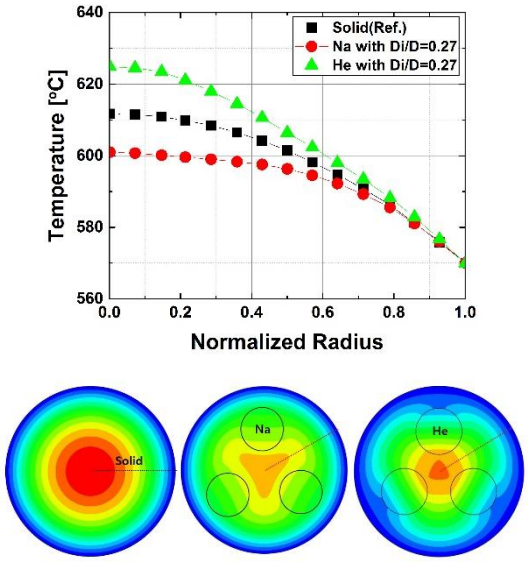

Fig. 2. Typical results of temperature distribution at solid region in each fuel pin.

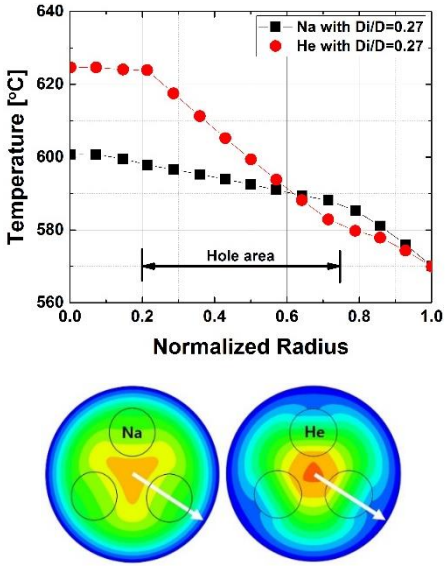

Fig. 3. Temperature distribution of both sodium and helium gas region with diameter ratio of 0.27.

However, center temperature of multi-hole model with He gas-filled porosity shows higher temperature compared with Na-filled model because of different thermal conductivities. Fig. 3 shows temperature distribution at hole region with the same diameter ratio at both sodium and helium conditions. It was interesting that there is no significant temperature difference between solid and hole region in multi-hole model. Based on this result, optimized fuel shape could be evaluated and a surrogate metallic fuel could be manufactured by an additive manufacturing.

ACKNOWLEDGEMENT

This work was supported by a National Research Foundation of Korea (NRF) grant funded by the Korean government (MSIP) (2017M2A8A5014888).

REFERENCES

[1] M. Memmott, J. Buongiorno, and P. Hejzlar, “An Evaluation of the Annular Fuel and Bottle-shaped Fuel Concepts for Sodium Fast Reactors”, Nuclear Technology, 173(2), 162-175 (2011).

[2] A. Bergeron, J.B. Crigger, “Early progress on additive manufacturing of nuclear fuel materials”, Journal of Nuclear Materials, 508 344-347 (2018).

[3] Y.-H. Lee, et al., “A Study on Innovative Metallic Fuel Shapes and Their Manufacturing Requirements”, Proc. of the KRS 2018 Fall Conference, 16(2), October 31-November 2, 2018, Jeju.

Criticality Evaluations of KN-12 Cask for Spent Nuclear Fuel Failure Scenarios

Kyoonho Cha* and Do-Yeon Kim
Central Research Institute, Korea Hydro & Nuclear Power Co., Ltd., 70, Yuseong-daero 1312beon-gil, Yuseong-gu, Daejeon, Republic of Korea
*khcha.cri@khnp.co.kr

1. Introduction

A transport cask for spent nuclear fuel (SNF) should be demonstrated by performing critical, shielding, thermal and structural analyses to ensure safe transportations of SNF. However, it was reported that high burnup SNFs typically increased the fuel failure potential due to the degradation of fuel and cladding materials [1, 2]. It is necessary that criticality analysis under hypothetical accident conditions by the high burnup SNFs should be conducted to verify the k-eff to meet the design basis of transport casks.

The purpose of this study is to investigate the results of potential fuel failures on the criticality for a transport cask. Criticality evaluations for fuel failure scenarios which the geometric structure or conditions of SNF assemblies and fuel rods are changed due to beyond design basis accidents are performed for KN-12 transport cask. KENO-VI Monte Carlo code was used to evaluate the criticality for those conditions of the cask.

2. Criticality Evaluations

KN-12 is a transport cask for WEC type SNFs. In this study, WEC 17×17 fuel assembly with 5wt% concentration was selected. KN-12 cask body, neutron absorber and fuel baskets were also used as described in its safety analysis report. The acceptance criteria of criticality are described in the section 6-4 of NUREG-1617 [3].

2.1 Evaluations for normal condition

The k-effs of KENO-VI and MCNP6 calculation for normal condition are shown in Table 1. The k-eff values are so close to each other that the KENO-VI modeling is validated for being utilized as the criticality evaluation tool in this study for KN-12 transport cask of SNFs.

Table 1. Calculated k-effs of Normal Condition

Code	k-eff	Std. dev.
KENO-VI	0.87057	0.00018
MCNP6	0.87113	0.00018

2.2 Evaluations for fuel failure scenarios

For the purpose of assessing the criticality under hypothetical accident conditions with high burnup SNFs, several assumptions were made as internal and external structures within the cask, the basket structures with neutron absorbers, especially fuel assemblies, are maintained as their original states.

In addition, fuel failure scenarios are assumed to be within the scope of severe accidents. Three cases which are unlikely to occur are chosen as the accident scenarios.

Firstly, criticalities of 39 scenarios were calculated for the number which means loss of designated fuel rod as shown in Fig. 1 and the results are depicted in Fig. 2 respectively.

IT			GT			GT		
1	2							
3	4	5						
GT	6	7	GT			GT		
8	9	10	11	12				
13	14	15	16	17	GT			
GT	18	19	GT	20	21	22		
23	24	25	26	27	28	29	30	
31	32	33	34	35	36	37	38	39

Fig. 1. Scenarios for loss of single fuel rod.

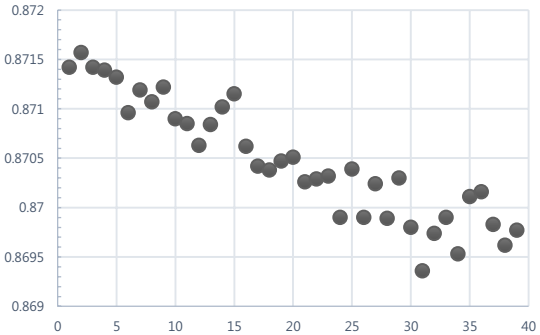

Fig. 2. K-effs for loss of single fuel rod.

As shown in Fig. 2, the calculated k-eff values from 1st to 16th fuel rod loss are slightly increased compared with the k-eff of normal condition. This has an important meaning that fuel assemblies are designed to be under-moderated;

however, when single fuel rod is occurred to be lost from an assembly, the area being lost a rod is to become higher-moderated then makes the k-eff value being increased.

These are because the removal of a rod near the water hole in the middle of the fuel assembly promotes k-eff value to be increased due to the moderation growth. On the other hand, the removal of a rod from the edge of the fuel assembly decreases the k-eff slightly because of the increased moderation near the neutron absorber panels.

And secondly, various criticality calculations were performed for the loss of multiple fuel rods. The removals of fuel rods adjacent to the water holes of the assembly were simulated sequentially as shown in Fig. 3; the removals are carried out concentrically for the 1st case and dispersedly for the 2nd case respectively. And the results are shown in Fig. 4.

The k-eff values are increased up to a certain value than the normal condition and are seemed to be saturated to the point of the number of around 40 and then are sharply decreased for the 2nd case. This phenomena are very curious but it is assumed that the bulk of water around the water holes works as a neutron absorber.

On the other hand, the k-eff values are increased gradually by removing the rods up to around 45 (about 17% of the entire fuel rods), and after that the k-eff values are seemed to be saturated by removing additional rods from the fuel assembly for the 2nd case.

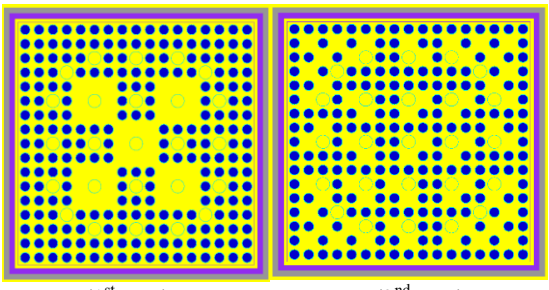

(1st case) (2nd case)

Fig. 3. Scenarios for loss of multiple fuel rods.

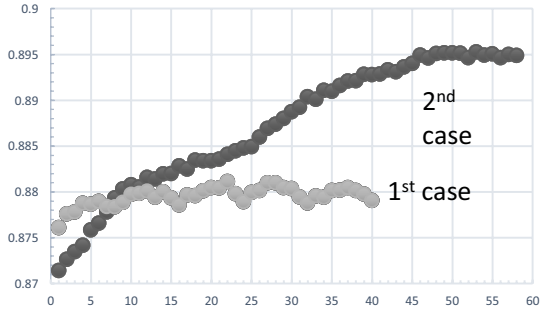

Fig. 4. k-effs for loss of multiple fuel rods.

Finally, the fuel failures of loss of rod claddings were also analyzed by simply removing the cladding from all rods within the fuel assemblies. A total of twelve k-eff values are calculated cumulatively for the fuel assemblies without cladding.

The material formerly filled with rod cladding was replaced with water. This provides extra moderating conditions to the under-moderated fuel system then increases the k-eff values by a substantial amount as shown in Fig. 5.

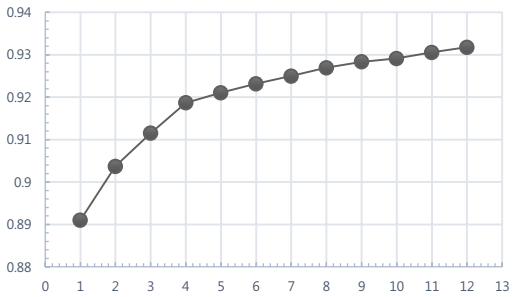

Fig. 5. k-effs for loss of rod claddings.

3. Conclusions

Critical evaluations of the KN-12 transport cask were performed using the KENO-VI code. In case of normal condition, we compared MCNP6 code with the result for modeling verification and confirmed that the criticality was within the statistical error range.

Criticality evaluations were performed for three types of fuel failure scenarios; loss of a single fuel rod, loss of multiple fuel rods, and loss of rod cladding. And the results show that the criticality of loss of cladding material accidents was much higher than other scenarios. Fortunately, this is also within the acceptance criteria of NUREG-1617.

REFERENCES

[1] K.R. Elam, J.C. Wagner, C.V. Parks, "Effects of Fuel Failure on Criticality Safety and Radiation Dose for Spent Fuel Casks," NUREG/CR-6835, ORNL, Sept. 2003.

[2] J.M. Scaglione, G. Radulescu, W.J. Marshall, K.R. Robb, "A Quantitative Impact Assessment of Hypothetical Spent Fuel Reconfiguration in Spent Fuel Storage Casks and Transportation Packages," NUREG/CR-7203, ORNL, Sept. 2015.

[3] "Standard Review Plan for Transportation Packages for Spent Nuclear Fuel," NUREG-1617, March 2000, U.S. Nuclear Regulatory Commission.

An Analytic Study on the Correlation Between Angularly Biased Emission of Prompt Neutrons and Sample Multiplication

Seonkwang Yoon [a,b], Hee Seo [c], Young-su Kim [d], Chaehun Lee [b], and Ho-Dong Kim [b,*]
[a] University of Science & Technology, 217 Gajeong-Ro, Yuseong-gu, Daejeon, Republic of Korea
[b] Korea Atomic Energy Research Institute, 111, Daedeok-daero 989beon-gil, Yuseong-gu, Daejeon, Republic of Korea
[c] Chonbuk National University, 567 Baekje-daero, Deokjin-gu, Jeonju, Jeollabuk-do, Republic of Korea
[d] Korea Institute of Radiological & Medical Science, 75 Nowon-ro, Gongneung i-dong, Nowon-Gu, Seoul, Republic of Korea
[*] khd@kaeri.re.kr

1. Introduction

Neutron detection based nuclear material accounting (NMA) system has been used to verify and quantify special nuclear materials in unknown samples. The development of a thermalized neutron multiplicity counter was a brilliant achievement. However thermal system has faced economical challenge relevant to ^{3}He gas as the demand to nuclear security has risen. Therefore alternative techniques and methodologies have been globally explored. KAERI has been trying to develop a plastic scintillators based fast neutron detector system via to utilize nuclear fission information; e.g. emission angle, energy. In this paper, the correlation between angularly biased emissions and sample multiplication were investigated for ^{240}Pu and ^{252}Cf using Monte Carlo codes.

2. Theoretical Basis

In neutron multiplicity counting it is possible to determine ^{240}Pu effective mass via measuring singles, doubles and triples rates which can be described as functions of three unknown factors; e.g. α, M_L and $^{240}Pu_{eff}$ [1]. However detecting triplets is hardly probable so triples rate is used not to show statistical significance even for thermal system of high detection efficiency. Therefore at least one parameter must be deduced through other means.

2.1 Sample Multiplication

Fission neutrons can induce consecutive fissions in a sample, and this mechanism is called fission chain reaction. The ratio between the total number of neutrons for all series of generations and the primary number of neutrons in the sample is the total multiplication (M_T) [2].

$$M_T = \frac{1}{1-k_{eff}} = \frac{1}{1-pv_i} \quad (1)$$

2.2 Angular Emission of Prompt Neutrons

Once fission occurs, an atomic nucleus splits into fission fragments and several neutrons are immediately emitted from them. Such kinetics e.g. energy and direction of prompt neutrons are directly affected by momentum of fission fragments. Fission fragments tend to move forward at an angle of 0 or 180 because their positive charge makes repulsive force each other. Consequently prompt neutrons also follow the kinematic tendency.

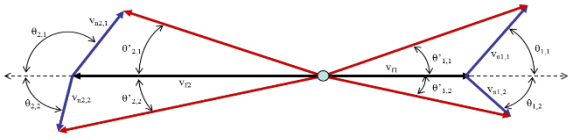

Fig. 1. Description of kinetics of prompt neutrons from fission fragments [x].

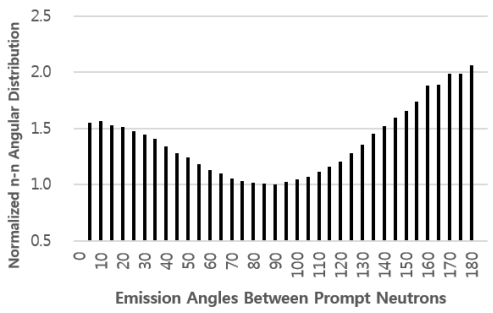

Fig. 2. Simulated angular distribution of ^{252}Cf using Geant4.

2.3 Research Theory

To derive multiplication through neutron coincidence detection, it must be done ahead to find correlationship between angular characteristic and either multiplication or doubles respectively. Then it might be possible to mathematically describe multiplication as a function of doubles rates. Inhere we analyzed correlation between an asymmetric parameter regarded to the angular distribution and multiplication.

3. Methods and Results

Two Monte Carlo codes, MCNP6 and Geant4 were integrated with FREYA, and used for acquisition of sample multiplication and angular distribution according to the sample mass of ^{240}Pu and ^{252}Cf. We considered several parameters to analysis the asymmetry of angular distribution and selected one, 'gradient' that had showed largest normalized variance. Finally that gradient decreases according to multiplication increases was confirmed. This is because neutrons from induced fissions contributed to angular distribu-tion as random correlation.

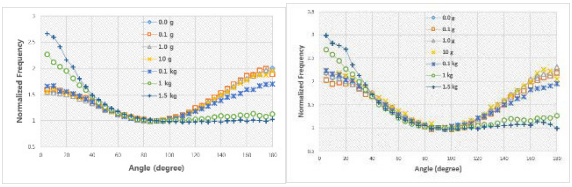

Fig. 3. Simulated angular distributions of ^{252}Cf (left) and ^{240}Pu (right) using Geant4.

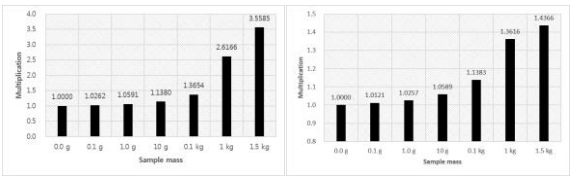

Fig. 4. Sample multiplications according to sample mass for ^{252}Cf (left) and ^{240}Pu (right) using MCNP6.2.

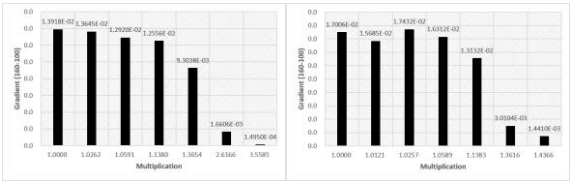

Fig. 5. Gradient according to sample multiplication for ^{252}Cf (left) and ^{240}Pu (right).

4. Conclusion

KAERI has been developing an advanced NMA system based on fast neutron coincidence counting with utilization of fission informative approaches. In this study prompt neutrons angular distribution was analyzed using Monte Carlo codes. It was confirmed the asymmetry of the angular distribution is inversely proportional to sample mass or multiplication. In further research, the correlationship between multiplication and asymmetry defined as a function of coincidence detection probability will be mathematically investigated.

ACKNOWLEDGE

This work was partly supported by Basic Science Research Program through the National Research Foundation of Korea (NRF), and grant funded by the Ministry of Education, Korean government (MSIP) [NRF-2017M2A8A5015084, NRF-2018R1D1A1B0-7043515]

REFERENCES

[1] N. Ensllin, W. C. Harker, M. S. Krick et al., "Application Guide to Neutron Multiplicity Counting", LA-13422-M, pp. 63-64 (1998).

[2] Matthew C. Tweardy et al., "A Point Kinetics Model for Estimating Neutron Multiplication of Bare Uranium Metal in Tagged Neutron Measurements", IEEE Transactions on Nuclear Science, 64(7), July 2017.

[3] L. Holewa, "Angular anisotropy of correlated neutrons in lab frame of reference and application to detection and verification", Texas A&M University, p. 5 (2012).

Derivation of the Major Factors to Ensure the Operating Safety of the Spent Nuclear Fuel Storage Facility

Jae Wook Kim, Han Young Joo, and Joo Hyun Moon*
Dankook University, 119, Dandae-ro, Dongnam-gu, Cheonan-si, Chungcheongnam-do, Republic of Korea
*jhmoon86@dankook.ac.kr

1. Introduction

Spent nuclear fuel (SNF) is stored in the temporal storage pools at nuclear power plant, but the storage pools are expected to be filled from 2021. Due to this fact, a site for interim storage of SNF has to be sought in the near future.

SNF has a variety of radionuclides and emits high-level radiation, so it has to be thoroughly managed. There are two types of SNF storage: wet and dry. Recently, dry storage facility is widely used for interim storage of SNF [1].

This paper, through scrutiny of multiple sources, identified major factors to have influence on safety of the interim dry storage facility of SNF, which should be considered in operating the facility.

2. Literature Survey

2.1 IAEA Safety Standards (SSG-15) [2]

The IAEA safety standards (Specific Safe Guide No.15, SSG-15) set up the basic safety goals for safe SNF storage as follows.

- Provide confinement of radioactive material;
- Ensure radiation protection of workers, members of the public and the environment;
- Maintain sub-criticality;
- Ensure removal of decay heat; and
- Ensure retrievability of SNF.

This guide also presented safety standards in areas of structure, heat, shielding, and criticality for the SNF storage facility and the site.

2.2 U. S. NRC (NUREG-1536/1567) [3], [4]

U.S. NRC report (NUREG-1536/1567) presented the design criteria of the SNF dry storage facility. These reports included standard review plans for the storage facilities. These reports also included the detailed evaluation criteria to be considered for construction and operation of the storage facilities. The criteria were for areas of structure/system/equipment, heat, shielding, confinement and criticality.

2.3 Nuclear Safety Act of ROK

The technical guidance on structure and equipment of SNF interim storage facility is specified in the Nuclear Safety and Security Commission (NSSC) Notice 2015-19. This notice includes safety requirements of basic design, radiation shielding and protection, handling equipment, removal of decay heat, nuclear criticality and confinement come up as considerations.

3. Results

3.1 Derivation of Major Factors

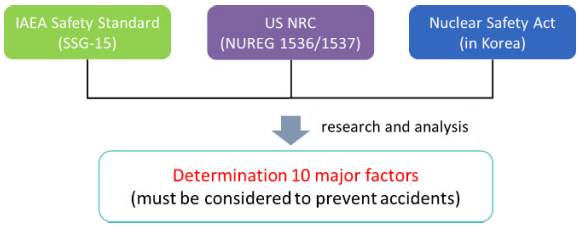

Fig. 1. Performance process.

Figure 1 shows the whole process to derive the 10 major factors important to ensure safety of the SNF interim storage facility. By scrutinizing foreign and domestic regulations, we found that all the documents suggested the same factors that should be considered to ensure safety of the SNF interim storage facility. From this, we derived the 10 major factors, and summarized in Table 1.

Table 1. Major factors for the SNF interim storage facility

Major Factors
1. Alarm device
2. Design
3. Confinement
4. Emergency power source
5. Equipment
6. Fire protection
7. Lighting
8. Nuclear criticality safety
9. Radiation shielding and protection
10. Removal of decay heat

We also proposed the sub-items of each major factor to satisfy the safety standards for the major factors. Table 2 shows example of the sub-items. There are 3 to 10 sub-items for every factor.

Table 2. Example of the sub-items

Factor : Containment	
	Sub-items
1	Is the containment sealed to prevent leakage of radioactive materials?
2	Are there monitoring systems to check the containment performance?
3	Are there facilities for safe handling of damaged SNF?

4. Conclusion

This paper scrutinized foreign and domestic regulations and derived the 10 major factors to have influence on safety of the interim dry storage facility of SNF. Based on the result, we proposed the sub-items of each major to satisfy the safety standards for the major factors. We hope that our study contributes to enhance the safety of the SNF interim storage facility.

REFERENCES

[1] Yong Soo Hwang, “Analysis on Storage of Spent Nuclear Fuel”, KAERI/TR-3784/2009, 2009.

[2] IAEA Safety Standard No. SSG-15, “Storage of Spent Nuclear Fuel”, International Atomic Energy Agency, Vienna, 2012.

[3] U. S. NRC, NUREG-1536, “Standard Review Plan for Spent Fuel Dry Storage Systems at a General License Facility”, 2010.

[4] U. S. NRC, NUREG-1567, “Standard Review Plan for Spent Fuel Dry Storage Facilities”, 2000.

Review of Periodic Verification on WOLSONG SNF Dry Storage Systems

Sunghwan Chung*, Donghee Lee, Taehyeon Kim, Kiyoung Kim, and Yongdeog Kim
Central Research Institute, Korea Hydro & Nuclear Power Co., Ltd., 70, Yuseong-daero 1312beon-gil, Yuseong-gu, Daejeon, Republic of Korea
*sunghchung@khnp.co.kr

1. Introduction

Since the 1980s, NPPs around the world have operated SNF dry storage facilities. However, as storage facilities are subject to time constraints for a limited lifetime, countries operating SNF dry storage facilities are working to ensure the safe performance of long-term operations of storage facilities, and IAEA recommends that SNF storage facilities be regularly assessed for long-term storage. Korea also has been operating SNF dry storage facility using two types of dry storage systems in WOLSONG NPP since 1992 (Fig.1). As the concern about the integrity of storage facility is increasing, it is necessary to secure safety and increase acceptability of local residents for long-term storage management. Korea's regulatory body added WOLSONG dry storage facility in NPP's PSR, so it is necessary to prepare countermeasures. Since NPP's PSR is based on NPP facilities, it is advisable to review a verification plan for SNF dry storage systems. USNRC's regulations and guidelines were analyzed for concrete dry storage systems and a periodic verification plan suitable for WOLSONG dry storage systems was reviewed.

Fig. 1. WOLSONG SNF dry storage systems.

2. Verification Guidelines

License renewal for continuous and safe operation of SNF dry storage systems must include time-limited aging analyses (TLAAs) to demonstrate that the dry storage systems continue to perform their intended function and aging management programs (AMPs) for aging issues that could adversely affect the dry storage systems in accordance with USNRC's NUREG-1927 (Fig. 2).

Scoping evaluation identifies structures, systems and components (SSCs) important to safety (ITS) of dry storage systems to be reviewed for aging effects (Fig. 3). SCCs are grouped into three safety categories of A (critical to safe operation), B (major impact on safety) and C (minor impact on safety) referring to USNRC's NUREG/CR-6407. And six ITS functions of SCCs are defined as CB (confinement boundary), CC (criticality control), HT (heat transfer), RS (radiation shielding), SS (structural support) and FR (fuel retrievability).

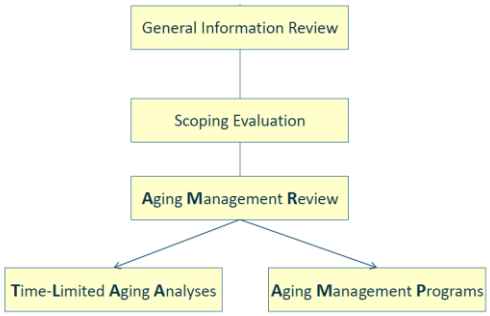

Fig. 2. License renewal process.

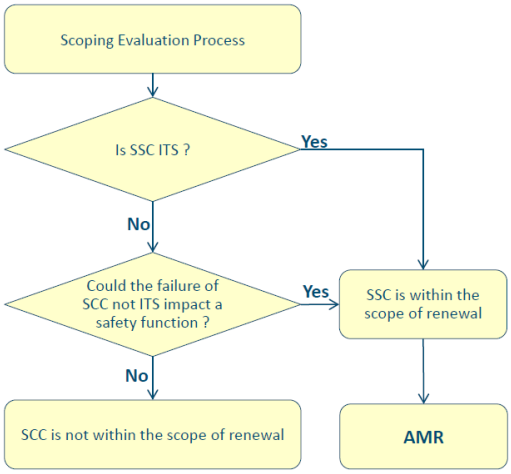

Fig. 3. Scoping evaluation process.

Aging management review (AMR) is to assess aging management activities (AMAs) for SSCs and addresses aging effects. Figure 4 shows the process for SSCs that are determined to be within the scope. AMR defines two methods for addressing of TLAAs and AMPs for potential aging effects. TLAAs are calculations or analyses to demonstrate that SCCs will maintain their intended function during the extended operation.

TLAAs account for environmental effects and are used to assess fatigue or time-limited life. AMPs monitor and control the degradation of SCCs so that aging effects will not result in a loss of functions. AMP includes all activities that are credited for managing aging effects for SSCs. Effective AMPs prevent, mitigate or detect aging effects and provide for the prediction of aging effects and timely corrective actions. Generic TLAAs for SNF dry storage systems presented by US ANL are fatigue of concrete and metal structures, corrosion analysis of metallic components, time-dependent degradation of neutron-absorbing and/or radiation-shielding material, environmental qualification of equipment, and other specific TLAAs for SCC of stainless steel canister welds and reduction in strength of concrete structures exposed to radiation and elevated temperatures. AMPs for SNF dry storage systems presented by US ANL are concrete structures monitoring (S1), steel structures monitoring (S2), mechanical components monitoring (M1), ventilation system surveillance (M2), welded canister leakage monitoring (M3), bolted cask leakage monitoring (M4), internal structural and functional integrity monitoring (M5).

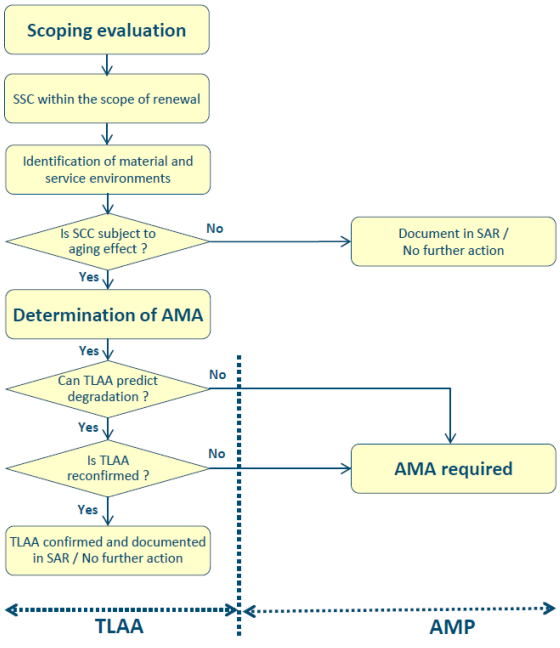

Fig. 4. Aging management review process.

3. Conclusion

AMR items of concrete structures, plugs, closures, internal structures, air inlets/outlets, baskets, fuel and pads for dry storage systems were selected by scoping evaluation (Table 1). Based on AMAs determined according to US guidelines for concrete dry storage systems, TLAAs and AMPs for WOLSONG SNF dry storage systems were identified (Table 2). And inspection items and period for each AMP were reviewed for periodic verification (Table 3).

Table 1. Scoping evaluation

SSCs		Safety	Function
Structures	Reinforced concrete structures	A	SS,RS,HT
	Carbon steel top closures	B	CB,SS
	Concrete shielding plugs	A	CB,SS,RS,HT
	Internal carbon steel cylinders	B, C	CB,SS,RS,HT
Components	Stainless steel baskets	A	CB,SS,HT,FR
	Zirconium alloys fuel	A	CB,FR
Pads	Reinforced concrete structures	B	SS

Table 2. TLAAs and AMPs

TLAAs		
Generic	Concrete structures Internal cylinders Baskets	Concrete strength evaluation Irradiation effect assessment Chloride effect assessment Shielding evaluation Fuel life-time evaluation Aging-related analyses
AMPs		
S1	Concrete structures	Structure inspection
S2	Internal cylinders	Carbon steel conditions
M1	Internal cylinders Baskets	Corrosion, crack
M2	Air inlets/outlets	Air temperature
M3	Basket weld-parts	SCC, corrosion, crack
M5	Internal cylinders	Temp. effect assessment Radiation effect assessment
Retrievability	Fuel Baskets Containment system	Fuel integrity Containment condition

Table 3. Periodic verification

Inspection items	Period	AMPs
Dose rates	Daily	S1,M3,M5
Contamination	Weekly	S1,M3,M5
Air temperature	Weekly	S1,S2,M2
Plug/closure welds	Twice a year	S1,S2,M1
Leakage	1st year : quarterly 2nd year : twice a year After 3rd year : yearly	S1,S2,M1,M3
Surface water	Weekly	S1,S2,M1,M3,M5
Underground water	Quarterly	S1,S2,M1,M2,M3
Cumulative dose	Quarterly	S1,M3,M5
Concrete structure	Every 5 years	S1

REFERENCES

[1] IAEA TRS No.443, Understanding and Managing Ageing of Material in SF Storage Facilities, 2006.

[2] USNRC NUREG-1927, Rev.1, SRP for Renewal of SLs and CoCs for Dry Storage of SNF, 2011.

[3] US DOE FCRD-UFD-2013-000294 (ANL-13/15), Rev.1, Managing Aging Effects on Dry Cask Storage Systems for Extended Long-Term Storage and Transportation of UF, 2013.

[4] USNRC NUREG-1801, Rev.2, Generic Aging Lessons Learned (GALL) Report, 2010.

A Study on Applicability of NUREG-1520 for Pyroprocessing Facilities

Gilsung You*, Woojin Jo, Siwan Noh, Seungnam Yu, Hyojik Lee, Hohee Lee, Jeonghoe Ku, and Seokjun Seo
Korea Atomic Energy Research Institute, 111, Daedeok-daero 989beon-gil, Yuseong-gu, Daejeon, Republic of Korea
*yougil@kaeri.re.kr

1. Introduction

KAERI has been developing pyroprocessing technology for an effective disposal or reusability of spent fuel from nuclear power plants. For this technology development and application, a special facility with hot cells and auxiliary systems will be needed [1]. In this paper, the NUREG-1520 guidance for fuel cycle facilities (not applicable to reprocessing facilities) in the United States is introduced, and its applicability for pyroprocessing facilities is studied.

2. Pyroprocessing of Spent Fuels

Pyroprocessing has been used for purification of spent fuels. It uses anodization of metal spent fuels into a molten salt electrolyte and reduction at a cathode to make a more purified metal.

ANL and KAERI have been developed the pyroprocessing technology for treatment of LWR oxide spent fuels. This technology includes several processes, such as voloxidation, electrolytic reduction, electro-refining, cathode processing, waste treatment, and etc.

For LWR fuel pyroprocessing, spent fuel rods are cut into small segments and voloxidized. The fuel metal from oxide reduction becomes the anode in an electro-refiner. The anode contains stable metal elements and one cathode contains most of the uranium as metal. The other cathode contains some of the uranium and rare earth fission products plus essentially all of the TRU elements as metal. The molten salt contains most of the fission products. The cathodes are separately inserted into a cathode processor in which the entrained electrolyte salt and cadmium are recovered for recycle by vacuum distillation. The uranium metal is converted to an appropriate form, either hexafluoride for reenrichment or oxide for direct reuse or disposal. The TRU metal goes to an injection casting furnace where it is refabricated into new fuel for a fast transmutation reactor [2].

3. NUREG-1520 and its Improvement for Spent Fuel Treatment Facilities

NUREG-1520 is a guidance of US NRC for reviewing and evaluating the health, safety, and environmental protection aspects of applications for fuel cycle facility licenses. This guidance addresses the longstanding health, safety, and environmental-protection requirements of 10 CFR Part 20 and 10 CFR Part 70, as well as the accident safety requirements reflected in Subpart H, “Additional requirements for certain licensees authorized to possess a critical mass of special nuclear material,” of 10 CFR Part 70. Subpart H of 10 CFR Part 70 identifies risk-informed performance requirements and requires applicants and existing licensees to conduct an Integrated Safety Analysis (ISA) [3].

The ISA is a systematic, risk-informed and performance-based analysis

However, the presence and processing of large quantities of fission products and TRU isotopes at spent fuel processing facilities have the potential to greatly increase consequences far above the 10 CFR Part 70 high-consequence thresholds for some accident sequences, therefore, 10 CFR Part 70 is not appropriate for spent fuel processing facilities**.** For this spent fuel processing facilities, the NRC has been studied an enforced risk criteria as described in the SECY-0136. [4-9].

4. Korean Rules and Applicability of NUREG-1520 for Pyroprocessing Facilities

The Korean Nuclear Safety Act requires applicants to conduct a standard safety analysis methodology similar to that of nuclear power reactor, such as deterministic and defense-in-depth safety methodologies. The Paragraph (3) of Korean Nuclear Safety Act article 35 requires that a person, who intends to carry on the spent fuel processing business, shall submit to the competent minister an application for the permit or the designation together with radiation environmental report, safety control regulations, explanatory statement of design and work

methods, quality assurance program for the operation of the business and other documents as prescribed by the Ordinance of the Prime Minister [10].

In Korea the pyroprocessing facilities are regulated as one of fuel cycle facilities under the Korean Nuclear Safety Act. The act describes the safety requirements for the license and operation of fuel cycle facilities.

Pyroprocessing is inherently a batch process which means that materials must be moved as solid physical objects among most of the various steps. The size of the batches is limited by criticality considerations. Therefore, the large number of movements of highly radioactive objects containing fissile materials is needed, and it also requires high equipment reliability, low accident likelihood, and a greater need for nuclear material accountability [2].

NUREG-1520 contains all the safety measures for nuclear fuel cycle facilities. [3]

These all measures except the chapter 3 can be applied to pyroprocessing facilities. The Integrated Safety Analysis (ISA) in the chapter 3 is a systematic, risk-informed and performance-based safety analysis methodology. The ISA provides the framework and establishes the needed safety basis to assure that the handling of nuclear material is within the programmatic requirements, that the safety program is appropriate for the risk, and that the measures for carrying out the safety program are appropriately monitored.

However, the presence and processing of large quantities of fission products and TRU isotopes at pyroprocessing facilities have the potential to greatly increase consequences far above the 10 CFR Part 70 high-consequence thresholds for some accident sequences. Recently US NRC has been developed an enforced ISA methodology for regulating of spent fuel recycling facilities [4-6]. For development of safer pyroprocessing facilities safety analysis is needed through a better safety analysis methodology that can reflect the properties of pyroprocessing.

Applying the NUREG-1520 improved with an enforced ISA to pyroprocessing facilities would very useful for developing a safer and more reliable facility.

5. Conclusions

For development of safer pyroprocessing facilities it is necessary to evaluate the safety through a better analysis methodology that can reflect the properties of pyroprocessing. The enforced ISA developed by US NRC is a systematic, risk-informed and performance-based analysis methodology for spent fuel treatment facilities including pyroprocessing facilities. Applying the NUREG-1520 improved with an enforced ISA to pyroprocessing facilities would very useful for developing a safer and more reliable facility.

REFERENCES

[1] Gil-Sung You, et al., “Concept and Safety Studies of an Integrated Pyroprocess Facility, Nuclear Engineering Design”, No. 241, pp. 415～424 (2011).

[2] US NRC, NUREG-1909, “Background, Status, and Issues Related to the Regulation of Advanced Spent Nuclear Fuel Recycle Facilities”, ACNW&M White Paper (2008).

[3] US NRC, NUREG-1520 rev.2, “Standard Review Plan for Fuel Cycle Facilities License Applications” (2015).

[4] US NRC, SECY-0136, “Draft Regulatory Basis for Licensing and Regulating Reprocessing Facilities” (2011).

[5] Gilsung You, et al., “Adaptability Study of Hybrid ISA-PSA Method on Safety of Pyroprocess Facilities”, Proc. of the KRS 2017 Spring Conference, 15(1), May 24-26, 2017, BuSan.

[6] Gilsung You, et al., “Enforced Risk Criteria for SF Recycling Facilities in US and Its Availability in Korea”, Proc. of the KRS 2017 Fall Conference, 15(2), Oct 18-20, 2017, ChangWon.

[7] Gilsung You, et al., “Applicability of the ANSI/ANS-58.16 on Pyroprocessing Facilities”, Proc. of the KRS 2018 Spring Conference, 16(1), May 30-June 1, 2018, BuSan.

[8] Gilsung You, et al., “Methodologies and Properties of Safety Analyses for Pyroprocessing Facilities”, Proc. of the KRS 2018 Fall Conference, 16(2), Oct 31-Nov. 2, 2018, JeJu.

[9] Gilsung You, et al., “Benefits of the ISA Application to Pyroprocessing Facilities”, Proc. of the KRS 2019 Spring Conference, 17(1), May 8-10, 2019, BuSan.

[10] Korean Nuclear Safety Act (2018).

Establishment of Data Acquisition System for Road and Sea Transportation Test of Surrogated Spent Nuclear Fuel Under Normal Conditions of Transport

JaeHoon Lim*, Sang Soon Cho, Yun-young Yang, Kiseog Seo, and Woo-seok Choi
Korea Atomic Energy Research Institute, 111, Daedeok-daero 989beon-gil, Yuseong-gu, Daejeon, Republic of Korea
*jhlim85@kaeri.re.kr

1. Introduction

Currently, the development of evaluation technology for vibration and shock load characteristics and spent nuclear fuel structural integrity under normal conditions of transport is being conducted in the Republic of Korea.

Acceleration and strain data will be measured during road and sea transportation test. The road test is going to be conducted in 2020 and the sea test will be conducted in 2021. However, it is expected that the test environment is not favorable to data acquisition system. Fig. 1 shows the previous transportation test named MMTT (Multi-modal Transportation Test) which is performed by the international research team composed of USA, Spain and Republic of Korea [1]. As shown in the figure, the data acquisition system is loaded on the transportation platform, and thus the system should be strong and robust to withstand the vibration and shock loads occurred during the transportation tests. Moreover, the system should be able to measure the data with dust and humid environment.

Therefore, in this study, the requirement of the data acquisition system is established and appropriate model was selected.

Fig. 1. Data Acquisition System for Multi-modal transportation test (2017).

2. Requirement of Data Acquisition System

The requirements of the present data acquisition system are summarized in Table 1.

Table 1. Requirements of the data acquisition system

No. of channels for strain gages	32
No. of channels for IEPE type accelerometer	48
No. of channels for piezo resistive type accelerometer	16
GPS sensor	connectable
Protection class (dust, humidity/water)	> IP65
Sample rate	> 10,000
Internal data storage	3 days for 96 channels
Mechanical test-vibration	10 g
Mechanical test-shock	75 g

The strain gages and piezo resistive type accelerometers will be attached on the surrogated fuel rods and the IEPE type accelerometer will be used for measuring accelerations on trailer platform, cradle, cask, canister, basket and assembly nozzle as shown in Fig. 2. GPS sensor will also be used for recording the route of the test. To perform the handling test, the data acquisition system should have high sample rate which is over 10,000 Hz. Moreover, sufficient storage should also be provided for sea test.

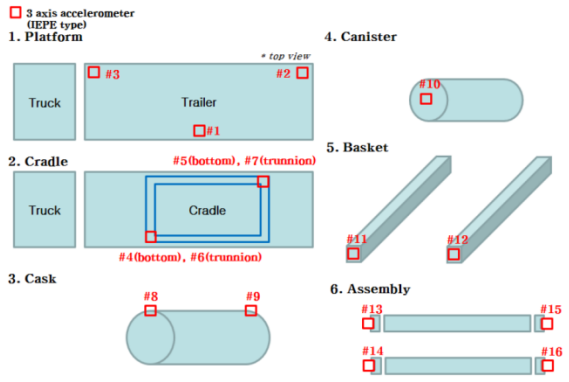

Fig. 2. IEPE type accelerometer location.

Furthermore, considering the harsh environment, IP65 protection class are required and 10 g vibration load resistance and 75 g shock loads resistance should be secured.

3. Selection of Data Acquisition System

Among the various data acquisition systems, modular data acquisition system for harsh environment named SomatXR was selected. SomatXR products meet the requirements listed in Table 1. Moreover, they have modular architecture as shown in Fig. 3, and thus the established data acquisition system will be used for other tests such as drop test, vibration and fatigue test.

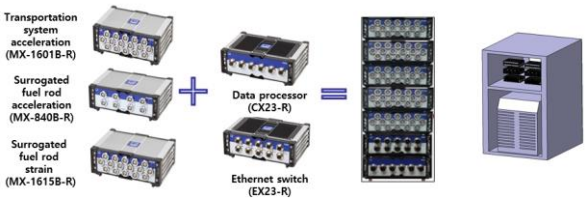

Fig. 3. Modular data acquisition system.

4. Conclusion

Requirements of data acquisition system for road and sea transportation test of surrogated spent nuclear fuel under normal conditions of transport were obtained and appropriate existing data acquisition system was determined considering the obtained requirements.

ACKNOWLEDGEMENTS

This work was supported by the Korea Institute of Energy Technology Evaluation and Planning(KETEP) and the Ministry of Trade, Industry & Energy(MOTIE) of the Republic of Korea (No. 2018170201770).

REFERENCES

[1] P. McConnell, S. Saltzstein, and K. Sorenson, “Fuel Assembly Tests under Normal Conditions of Transport,” The 18th International Symposium on the Package and Transportation of Radioactive Materials, Kobe, Japan, September 18-23, 2016.

Multi-body Dynamics Analysis for Road Transportation Test of Surrogate Spent Nuclear Fuel Under Normal Conditions of Transport

JaeHoon Lim[1,*], Dae-Han Choi[2], Sang Soon Cho[1], Gil-Eon Jeong[1], Yun-young Yang[1], Kiseog Seo[1], and Woo-seok Choi[1]

[1]Korea Atomic Energy Research Institute, 111, Daedeok-daero 989beon-gil, Yuseong-gu, Daejeon, Republic of Korea

[2]ableMAX, 234, Teheran-ro, Gangnam-gu, Seoul, Republic of Korea

[*]jhlim85@kaeri.re.kr

1. Introduction

In 2017, MMTT (Multi-Modal Transportation Tests) including road, sea, and rail transport were performed by research institutes from the US, Spain and the Republic of Korea as shown in Fig. 1 [1]. Currently, the development of evaluation technology for vibration and shock load characteristics and spent nuclear fuel structural integrity under normal conditions of transport is being conducted in the Republic of Korea by the present authors.

A test model of KORAD-21 transportation cask is being designed as shown in Fig. 2 and will be manufactured for the transportation tests. The road transportation test at Doosan Heavy Industry yard is planned in 2020 and the coastal ship test is planned in 2021. Prior to perform the road test, road transportation simulation by using multi-body dynamics package is being conducted with various operating conditions. Based on the resulted data by the simulation, shock response spectrums on the cask will be obtained and compared with those of the MMTT. The result will be a useful data to determine the sensor attachment location for road test.

Fig. 1. MMTT Road test.

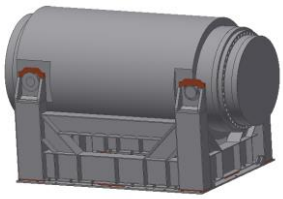

Fig. 2. Present KORAD-21 Cask-Cradle 3-D Model.

2. Modeling Strategy

A comparison study was conducted by NRCA (National Road Transportation Commission) in Australia to investigate if there is acceptable agreement between simulation from computer-based models of heavy vehicles created with different computer-based modeling packages including ADAMS, AUTOSIM, UMTRI code [2]. And additional validation study for UM (Universal Mechanism) by using the data of Ref. 2 was also performed [3].

Based on the modeling strategies and spring and damper coefficients described in Ref. 1 and 2, the multi-body dynamics modeling for road transportation is being conducted by using UM package by the present authors. Generally, all components are modeled by a rigid component for multi-body dynamics analysis. However, in order to consider the flexibility of the trailer deck and cask-cradle system, those are going to be modeled by FEM. A separate modal analysis will be conducted using the developed FEM mesh by using ANSYS APDL and then, the results will be transferred to the UM. As a result, the acceleration data from the desired locations will be obtained.

3. Analysis Cases

It is expected that vertical and horizontal acceleration will be applied to the transportation cask during normal conditions of transport. To simulate the vertical loads, a few speed bump will be modeled and simulated with the velocity of 10, 20, and 30 km/h. To simulate the horizontal acceleration, pulse steer and step steer maneuver analysis will be conducted.

Originally, the pulse steer simulation is for estimating yaw damping. From an initial straight path, the vehicle is subjected to a short duration input of steering at a speed of 60 km/h as shown in Fig. 2.

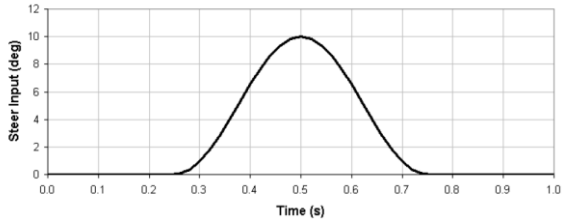

Fig. 3. Pulse steer input based on the haversine function [2].

The step steer simulation is very similar in form to the pulse steer except that the steer angle instead of returning to zero, is held at its maximum value for the duration of the simulation as shown in Fig. 3.

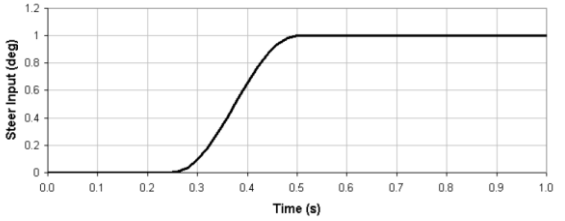

Fig. 4. Step steer input based on the haversine function [2].

4. Conclusion

The multi-body dynamics modeling for road transportation simulation is being conducted by using UM package. Based on the resulted data by this simulation, shock response spectrums on the cask will be obtained and compared with those of the MMTT. It is expected that the simulation result will be a useful data to determine the sensor attachment location for road test.

ACKNOWLEDGEMENTS

This work was supported by the Korea Institute of Energy Technology Evaluation and Planning(KETEP) and the Ministry of Trade, Industry & Energy(MOTIE) of the Republic of Korea (No. 2018170201770).

REFERENCES

[1] P. McConnell, S. Saltzstein, and K. Sorenson, “Fuel Assembly Tests under Normal Conditions of Transport,” The 18th International Symposium on the Package and Transportation of Radioactive Materials, Kobe, Japan, September 18-23, 2016.

[2] Prem, H., et all, Comparison of Modelling Systems for Performance-Based Assessments of Heavy Vehicles. National Road Transport Commission, Melbourne, Australia. http://www.ntc.gov.au/filemedia/Reports/ComparisonModellingSystemsPerfor.doc

[3] Pogorelov, D., et all, Comparision of Universal Mechanism Software and Other Modeling Packages for Performance-Based Assessments of Heavy Vehicles.

Autonomous Sensor Transport System for DCSS Inspection

Daewon kim, Kyoungwon Yoon, Kyoungyong Noh, Misuk Jang, and Seoung Rae Kim
Nuclear Engineering Services & Solutions, 756-27, Daedeok-daero, Yuseong-gu, Daejeon, Republic of Korea
*nessrnd@ness.re.kr

1. Introduction

The issue of disposal of spent nuclear fuel is under discussion worldwide. Until the mid-1980s, wet storage with abundant experience was mainly adopted, but after the 1990s, Dry Cask Storage System (DCSS), which is advantageous in terms of capacity expansion and long-term management, has been adopted. Most dry casks are made of concrete for economic aspects, and the issues and ideas have been open to the public how to maintain this dry cask.

The dry cask is composed of environments that cannot be directly inspected by humans due to high radiation fields, high temperatures, and narrow passages. Therefore, research is underway on nondestructive inspection sensor transport systems for dry cask maintenance[1,2]. For non-destructive testing in dry casks, the transport system must first be made of radiation-resistant, heat-resistant material, and designed to be able to move in the vertical and horizontal directions.

2. Methods and Results

2.1 Design SETS Models

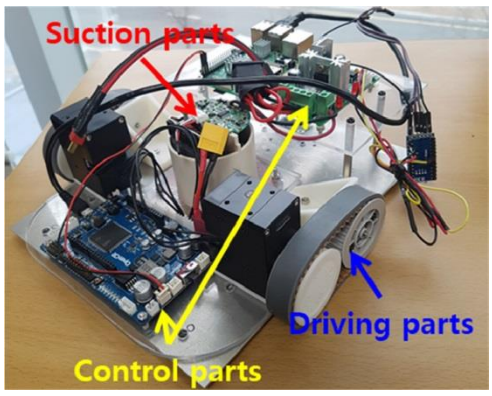

Fig. 1. Actual SETS model for DCSS inspection.

The NESS designed a vacuum suction method SEnsor Transfer System (SETS) using impeller for vertical and horizontal transportation as shown in Fig. 1. First of all, the NESS made the body composed of aluminum material radiation and temperature resistance. Second, the control parts were constructed by using the control boards which can install the Robot Operating System (ROS) for using autonomous driving packets. Finally, SETS consists of suction parts for vertical attachment and driving parts for navigation.

2.2 Configuration of SETS

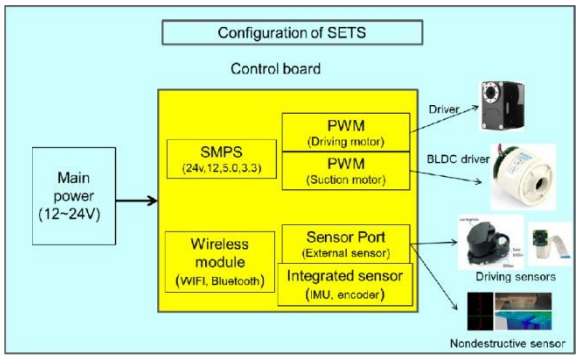

Fig. 2. Configuration of SETS.

The body of SETS can be conveyed using internal or external power shown in Fig. 2. When powered, the SMPS converts the power so that it can be supplied to each sensors and drivers. Based on the results detected by the driving sensor, the motor and the adsorption motor are PWM controlled through the driving algorithm, respectively.

2.3 Control logic of SETS

It is very effective to drive horizontally using the autonomous driving package developed in the ROS operating system from the robot

interface. Therefore, the NESS utilized ROS's Autonomous packages in Ubuntu 16.04, kinetic environment. SETS takes the shortest route to the destination with a global planner to take advantage of route planning and map algorithms and a local planner to avoid obstacles ahead. We use A * algorithm for global planner and Dynamic Window Approach algorithm for local planner.

However, in order to utilize autonomous driving packets for vertical driving, a modification of the driving algorithm is required below. The modified algorithms moving from (x, y, 0) -> (x', y', z) can be abbreviated in three steps

Modified Driving algorithms

Step 1. (x, y, 0) -> (x', y',0)
Step 2. Horizontal-Vertical transition
Step 3. (x', y', 0) -> (x', y', z)

The first step is to move the shortest distance from the x, y coordinates to the x ', y' coordinates. This can be implemented through the aforementioned driving algorithm. The second step is the process of transferring the SETS from a horizontal plane to a vertical plane when the SETS moves in a path down or up. This can be done by recognizing the wall through the drive sensor and attaching SETS to the wall via the suction motor. Finally, the movement in the vertical wall is (x ', y', 0)-> (x ', y', z). The third step can be performed by converting autonomous driving in the x-y planes to autonomous driving in the x-z planes and using a driving algorithm.

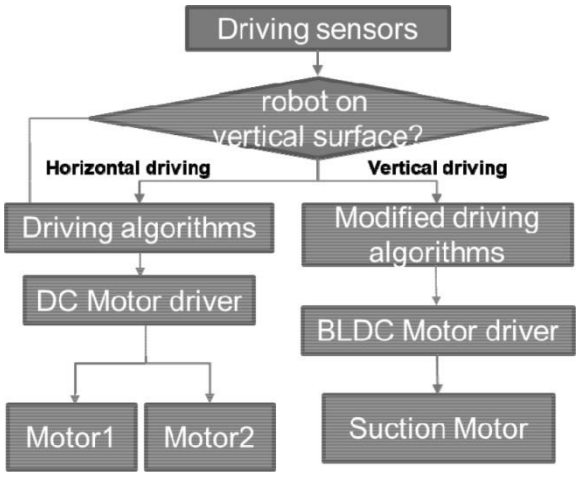

Fig. 3. Overall Control logic of SETS.

3. Conclusions

In this paper, the NESS propose Vacuum Suction Transfer system using an impeller for DCSS inspection. In order to automate nondestructive inspection, autonomous driving packages used in the ROS were used. In addition, the NESS developed and integrated the autonomous driving algorithm of SETS for the movement of STEP-shaped path of DCSS structure. By using this control logic, SETS can go through the step-shaped path through autonomous driving.

ACKNOWLEDGEMENTS

This work was supported by the Korea Institute of Energy Technology Evaluation and Planning(KETEP) and the Ministry of Trade, Industry & Energy(MOTIE) of the Republic of Korea(No.20171520101780).

REFERENCES

[1] S.Chu, "Dry Canister Storage System Inspection and Robotic Delivery System Development, EPRI, Palo Alto, 2016.
[2] IgMo Koo, "Design and Control of Wall Climbing Robot using Impeller", KRS journal, pp.177-185, 2010.

Preliminary Test Plan of Vacuum and Forced Helium Drying for Canister

Seung-hwan Yu*, Ju-chan Lee, Kyung-sik Bang, and Woo Seok Choi
Korea Atomic Energy Research Institute, 111, Daedeok-daero 989beon-gil, Yuseong-gu, Daejeon, Republic of Korea
*shyu80@kaeri.re.kr

1. Introduction

The drying process of the spent nuclear fuel is the first step of the dry storage. There are two kinds of drying process method. One is the vacuum drying. The vacuum drying is widely used. The vacuum drying uses vacuum pump to lower the pressure inside the canister. As the pressure decreases, the water evaporates more quickly. In the vacuum drying process, the dryness criteria is that the internal pressure is less than 3 torr for 30 min without the vacuum pump operation. The other drying process is the forced helium drying. The forced helium drying process removes residual moisture in a fuel storage container by an inert gas blowdown.

There are some advantages and disadvantages of both drying processes. The purpose of this study is to practically examine the drying process of vacuum and forced helium drying. The first step of this study is to design and set up the test system.

2. Design of Drying Test System

2.1 Basic concept and design

In other to compare both drying process, the vacuum and forced helium drying system are combined in one system. Fig 1 is the simple diagram of vacuum drying test. It is consisted of a vacuum pump and a cold trap.

Fig 2 is the diagram of the forced helium drying test system. This system is more complicated than the vacuum drying test system. This system is consisted of a pre-cooler, an air cooler, a circulation pump and a heater. The combined drying test system is illustrated in Fig 3. The vacuum drying test system is simply added to the forced helium drying test system. 2 stages (pre-cooler and air cooler) of water removal module in the forced helium drying are simplified to one module (adjustable cooler).

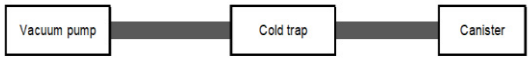

Fig. 1. Diagram of vacuum drying test system.

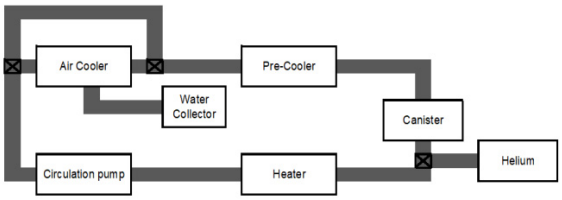

Fig. 2. Diagram of forced helium drying test system.

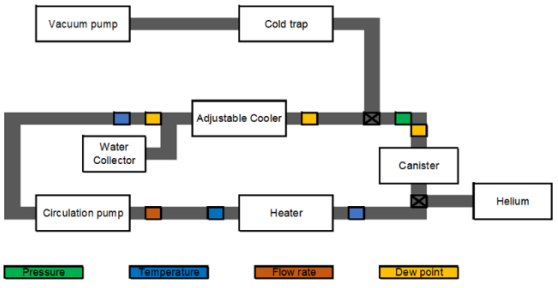

Fig. 3. Diagram of combined drying test system.

2.2 Data acquisition system and sensors

The data acquisition system is Keysight 34970A with 34901A module. Our sensors require dc volts input and thermocouple input. The Keysight 34970A is suitable to acquire test data from selected sensors.

Four kinds of sensors are selected for test data (flow, pressure, temperature, dew point). The flow sensor is MFC KOREA TSM-D230 model. The flow rate of 30~100 L/min can be measured. The K-type thermocouple are used with 1/4 NPT compression fitting due to leak problem. The pressure sensor is FNS KP370 NT Pirani gauge. It consists of Pirani and Piezo pressure sensors. It can measure the pressure range of 10^{-3}~1,000 torr. The dew point sensor is OMEGA HX80A.

The PC program of DAQ was developed based on Labview. The prototype Labview VI is Fig. 4.

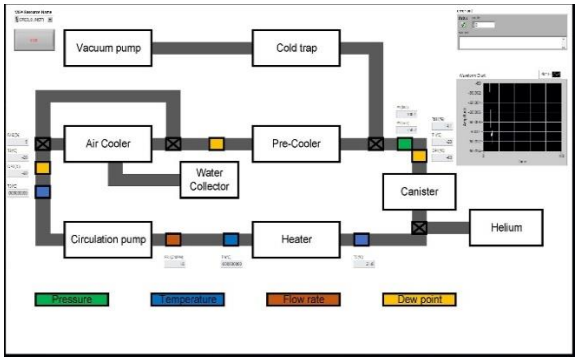

Fig. 4. Diagram of combined drying test system.

3. Module of Drying Test System

3.1 Circulation pump

In the forced helium drying system, the helium should be circulated in a closed drying loop. The helium particle is so small that the helium leak from the loop easily happens. The priority of considering option for selection of the circulation pump is the leakage. The KNF diaphragm gas pump was selected. The gas tightness of this pump is less than $6\times10^{-6}\,\mathrm{std\,cm^3/s}$.

3.2 Adjustable cooler

The main purpose of the adjustable cooler is to dehydrate the wet helium from the outlet of canister. The way of dehydration is to cool down the hot helium. If the temperature of the helium decreases, the saturate vapor pressure also decreases. In other words, the lower temperature helium could hold less amount of water vapor. The vapor whose pressure over the saturate vapor pressure is condensed and the condensation water is trapped in cooler module.

3.3 Heater

The temperature of helium form the adjustable cooler is below -5°C. If the cool helium from the cooler enters directly into the canister with the spent nuclear fuel, the temperature inside the canister could suddenly drop. It could be the thermal shock to the fuel cladding. To prevent the sudden temperature drop in the canister, the cool helium must be heated before entering the canister.

4. Conclusion

The combined drying test system was developed. Each modules are ready for performance test. The target canister should be required for the drying test. We are now designing the scale-down canister. When the canister is ready, our combined drying test will start.

ACKNOWLEDGEMENT

This work was supported by the Korean Ministry of Trade, Industry, and Energy (MOTIE) as a part of the Radioactive Waste Management Technology Development Project (20181720201020).

REFERENCES

[1] ASTM, Standard Guide for Drying Behavior of Spent Nuclear Fuel, ASTM C1553-16, 2016.

Scenario Evaluation for Damaged Spent Nuclear Fuel Transport

Suk Woo Hong*, Sangbok Ahn, Dosik Kim, Jeong-Nam Jang, Hyoung-Mun Kwon, Sung Geun Kim,
In-Chan Kwon, Myung Chul Park, and Jae Han Kim
Korea Atomic Energy Research Institute, 111, Daedeok-daero 989beon-gil, Yuseong-gu, Daejeon, Republic of Korea
*hongsw@kaeri.re.kr

1. Introduction

The Post Irradiation Examination Facility (PIEF) of Korea Atomic Energy Research Institute (KAERI) is a facility operated for the purpose of supporting fuel R&D, identifying the cause of fuel damage and etc. To date, 1699 rods have been transported from the Nuclear Power Plant(NPP) to PIEF. Various post irradiation tests have been performed with the transported fuels, and are safely stored in various forms, such as intact/damaged rods and fragments/specimens after tests. However, the congress and citizen are concerned about the dangers of Spent Nuclear Fuel(SNF) stored in the PIEF, because the PIEF is located in the big city. In December 2016, the KAERI announced a comprehensive safety measure for nuclear research. One of the main points is to transport SNF to NPP. The first step to do this is to establish a damaged fuel transport technology that has not yet been secured. Therefore, in this paper, the technology that can guarantee the safety of all stages of damaged fuel transportation was reviewed. The present state of SNF in storage is described, and various performance requirements and technical standards for transporting rods, fragments and specimens are reviewed.

2. Status of Spent Fuel Storage in PIEF

As described above, SNF rods stored in PIEF are existed in various forms through post irradiation tests. The SNF in the PIEF is stored in the following forms. First, when brought into the Fuel Assembly(FA) form, the top nozzle is dismantled or separated to pull out the fuel rods. At this case, since the handleability of the assembly is lost, thus it is placed in the assembly container and stored in the pool. Second, in case of SNF brought in rod, it is stored independently in Fuel Rod Storage Basket(FRSB) or Fuel Rod Storage Rack(FRSR). Third, when the fracture tests of SNF is performed, the shape and specification are changed to fragments and specimens. These are placed in a Rod Cut Container(RCC) and stored wet condition, or stored dry condition in hotcell.

3. Return Scenario

For safe transportation and management of SNF, it is necessary to conduct a review of suitable technologies to ensure safety at all stages of transportation and this should lead to detailed scenarios.[1, 2] For these, what functions should be maintained in the whole transportation process, and the performance

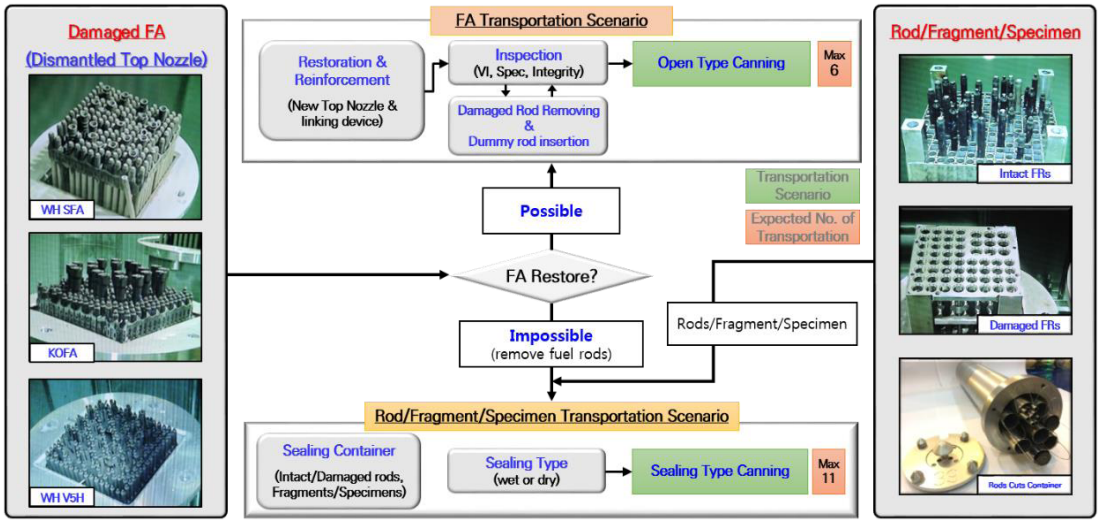

Fig. 1. Established SNF transport scenario.

requirements and technical standards to satisfy these functions are reviewed. The main evaluation criteria are not only the availability and completeness of the technology, the effectiveness of the core function implementation, the applicability of regulatory requirements, budget, and the burden of work, but also, the preference, applicability and compatibility of the recipient. In particular, the social acceptance of the scenario was reflected. The transport scenarios were evaluated according to the SNF storage type and status. The selected scenarios are shown in Fig. 1.

4. Conclusion

In this paper, to transport the SNF stored in KAERI-PIEF to the NPP, various scenarios were reviewed and evaluated considering the requirements, technical standards and etc. As a result, the transport scenario is established as follows. For the top nozzle dismantled FA, it will be restored and reinforced, and for the fuel rods, fragments and specimens, the sealing type canning technology will be introduced.

REFERENCES

[1] “Packaging and Transportation of Radio Active Material”, 10CFR Part71, USNRC.

[2] “Licensing Requirements for the Independent Storage of SNF”, 10CFR Part72, USNRC.

Review of Container for Transporting Damaged Spent Nuclear Fuels

Suk Woo Hong*, Sangbok Ahn, Dosik Kim, Jeong-Nam Jang, Hyoung-Mun Kwon, Sung Geun Kim,
In-Chan Kwon, Myung Chul Park, and Jae Han Kim
Korea Atomic Energy Research Institute, 111, Daedeok-daero 989beon-gil, Yuseong-gu, Daejeon, Republic of Korea
*hongsw@kaeri.re.kr

1. Introduction

The Post Irradiation Examination Facility(PIEF) of Korea Atomic Energy Research Institute(KAERI) stores 1699 spent fuel rods including fragments and specimens that changed shape after the post irradiation tests. For this reason, the congress and citizen are concerned about storing many nuclear fuels in large city. Accordingly, KAERI announced the 'comprehensive measures for safety of nuclear research', and decided to prepare a foundation for transporting nuclear fuels to Nuclear Power Plant(NPP) by 2021. Currently, the containers for handling and transporting nuclear fuels in the form of rod, fragment and specimen are already commercialized overseas, but even in Korea, no attempts has been made to develop the container. In order to minimize uncertainties and risks, PIEF tried to introduce a licensed and commercialized container, and after internal evaluation, it was decided to introduce the container of Westinghouse Electric Sweden AB(WSE). In this paper, the container of WSE is introduced which is designed to suit the domestic situation.

2. WSE Container for SNF

The container of WSE is named Quiver and it can handle, store and transport the leaking fuel rods, broken fuel rods, rod fragments and specimens. In other words, the Quiver can handle various types of fuel rods and is designed to be vacuum, dry and transport.[1] In addition, the shape and specifications of the Quiver can be designed and manufactured in the same way as the general fuel assembly. The Quiver has recently been approved by NAGRA(National Cooperative for the Disposal of Radioactive Waste) in Switzerland as an applicable alternative for disposal of damaged fuel. Also, SKB, which is in charge of interim storage and final disposal in Sweden, will use the Quiver for the Ringhals, Oskarshamn and Forsmark NPPs. The Quiver's core design strategy is based on the premise that it must have at least equivalent safety to fuel assemblies in handling, storage, transport and disposal environments.

3. Quiver's Technical Advantages

The first advantage of the Quiver is that it can manage nuclear fuel more safely. To solve the

problem of irradiation assisted stress corrosion cracking, the Quiver uses low-carbon austenitic stainless steel, which is less sensitive in the irradiated environment. In addition, it is structurally superior to the fuel assembly, and thus has high safety during storage and transportation. Also, it has a much higher containment safety than the cladding tube responsible for primary containment of nuclear fuel, because the Quiver uses high strength stainless steel to encapsulate nuclear fuel. Second, the Quiver has a competitive price in terms of fuel capacity. The PWR Quiver can hold up to 80 fuel rods, depending on the design. Therefore, the number of transports can be minimized, so the acceptability of residents is high, and the burden of KAERI, which is responsible for the transport, can also be minimized. Third, when considering intermediate storage of damaged fuel, the drying process is essential. The Quiver can be dried by connecting the hoses with a separate drying equipment outside the pool. On the other hand, in the case of other companies, a complicated configuration is required, such as a portable hotcell to be installed outside the pool for drying the container. Therefore, both PIEF and NPP minimize the burden on drying. Fourth, the Quiver can be used for both wet and dry storage using two types of lids. Thus, there is flexibility to choose according to user's storage environment. Fifth, if there is a need to inspect fuel or to respond to IAEA nuclear material safety measures, the Quiver lid's unique design features make it easy to open for inspection, and recoverability of fuel rod is also easy. Sixth, since it has the same handling as a general fuel assembly, it does not require any special handling skills or complicated tools. Therefore, the ease of operation is high. As such, Quiver has many advantages, therefore, it can be handled without problems in PIEF, NPP and dry storage facility.

4. Conclusion

In this paper, information on the container that will be used to transport SNF stored in KAERI-PIEF to NPP is described. WSE's Quiver meets various requirements and is considered to be a container that can be satisfied in various environments such as handling, storage and transportation.

Fig. 1. The Basic model of PWR Quiver with handling lid (left) and long-term storage lid (right) [1].

REFERENCES

[1] Westinghouse Electric Company, internet: http://www.westinghousenuclear.com

Effect of Inlet Air Temperature on Adhesion Force of Vacuum Type Sensor Carrier

Kyoungwon Yoon*, Daewon Kim, Misuk Jang, and Seoung Rae Kim
Nuclear Engineering Services & Solutions, 756-27, Daedeok-daero, Yuseong-gu, Daejeon, Republic of Korea
*nessrnd@ness.re.kr

1. Introduction

Sensor carrier, sensor transport system(SeTS) is under development for defects inspection of dry cask storage system(DCSS) for spent fuels. The SeTS is classified into a magnetic wheel type carrier and a vacuum wheel type carrier according to the climbing wall material or the wall climbing method.

This sensor carrier should be possible to move cask and inside of canister to 90° and other different angles under the environments such as high temperature, high radiation and so on.

This paper focuses on the operating temperature among the factors. The changes of suction pressure affecting the adhesion were investigated by changing the temperature from 25°C, which is the room temperature, to 120°C, which is the maximum temperature inside the dry storage cask [1].

2. Analysis Method

2.1 Governing equations

We use ANASYS CFX 17.0, which is commercial CFD program based on FVM(Finite Volume Method) in order to get the solution of RANS governing equations.

Continuity equation, momentum equation and energy equation about 3-dimensional incompressible and normal turbulence flow are as below. [2]

- Continuity equation

$$\frac{\partial U_i}{\partial x_i} = 0 \tag{1}$$

- Momentum equation

$$U_j\frac{\partial U_i}{\partial x_j} + \frac{\partial(\overline{u_i' u_j'})}{\partial x_j} + \frac{\partial p}{\partial x_i} - \frac{1}{Re}\nabla^2 U_i = 0 \tag{2}$$

- Energy equation

$$\rho C_p\left(u\frac{\partial T}{\partial x} + v\frac{\partial T}{\partial y} + w\frac{\partial T}{\partial z}\right) = k\left(u\frac{\partial^2 T}{\partial x^2} + v\frac{\partial^2 T}{\partial y^2} + w\frac{\partial^2 T}{\partial z^2}\right) \tag{3}$$

In this analysis, it was used model among generally 2-equation turbulence models and set the convergence condition of the solution to the residual.

2.2 Analysis area

According to Yoo's Results [3] show that the pressure generated gradually decreases with increasing temperature when the same fluid is at the same flow rate.

The purpose of this analysis is to confirm how the pressure changes as the temperature of the fluid drawn into the lower chamber rises in the analysis region shown in Fig. 1.

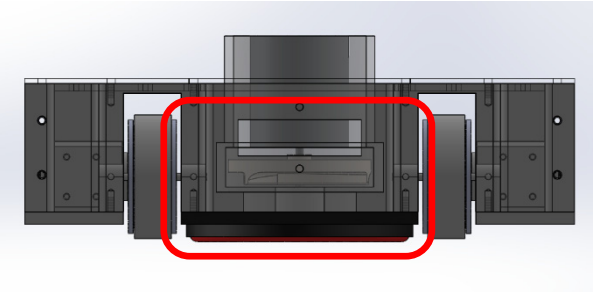

Fig. 1. Interpretation Area of SeTS.

2.3 Analysis and Boundary Conditions

The analysis conditions were selected in consideration of the fiducial discharge of centrifugal impeller with the highest lift compared to the discharge. The shape of the lower chamber of impeller was assumed that a fluid enters through the lower intake of 0.1mm and exits through the outlet of impeller. The temperature of the fluid passing through the centrifuge impeller was individually. interpreted into 3 cases : 25°C, 80°C and 120°C.

Details of analysis and boundary conditions are given in Table 1 and Table 2, respectively.

3. Results of Analysis

Figures 2 to 4 show the pressures at 25 °C to 120 °C with the same flow rate conditions.

As a result of the analysis, it can be seen that as the temperature increases, the pressure of the inlet decreases.

Table 1. Boundary conditions

Working fluid	Air
Inle	Total pressure
Outlet	Mass flow rate
Turbulent closure	$k-\epsilon$model
Interface area	Frozen-rotor
Wall	No-slip

Table 2. Temperature conditions

Case	Temperature
1	25°C
2	80°C
3	120°C

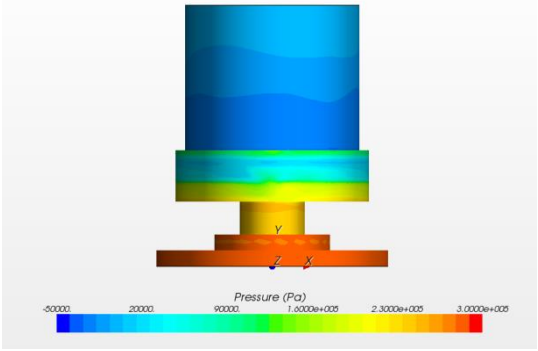

Fig. 2. Pressure of 25°C.

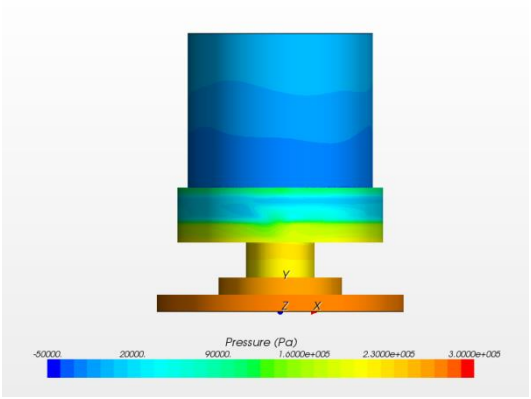

Fig. 3. Pressure of 80°C.

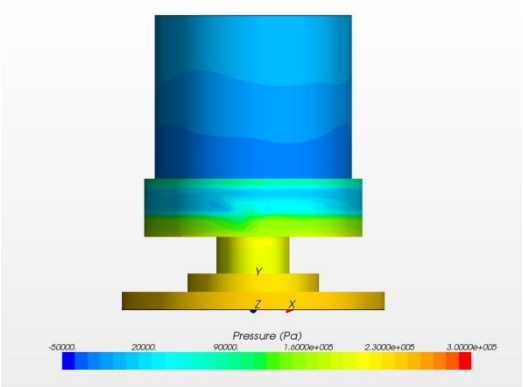

Fig. 4. Pressure of 120°C.

4. Conclusion and Discussion

The results from previous studies [3,4] show that the lower generated pressure trend to be at the higher temperatures. the higher the temperature, the lower the generated pressure. Therefore, it can be expected that the adhesion of SeTs increases as the temperature inside the dry storage container increases.

Analysis is currently being carried out under the various temperature conditions to confirm the expected results.

ACKNOWLEDGEMENTS

This work was supported by the Korea Institute of Energy Technology Evaluation and Planning (KETEP) and the Ministry of Trade, Industry & Energy (MOTIE) of the Republic of Korea (No.201715201017800).

REFERENCES

[1] Jeremy Renshaw, Inspection and Delivery Systems for Dry Canister Storage System Inspection, March 6, 2015, EPRI.

[2] Kyeong Ho, Jeong, A study on temperature reduction method through analysis of thermal flow in turbine building of steam power plants, 2016, Keimyung University.

[3] Jae gu, You, Experimental study of pressure fluctuation in the Polyethylene pipe system with temperature variation, June, 2007, Yonsei University.

[4] Performance Evaluation of Wall Climbing Sensor Carrier for Dry Concrete Cask Storage System, September, 2018, PBNC.

Radiological Assessment Considering Irradiated Top Nozzle of Spent Fuel Assembly

Kiyoung Kim[a,*], Donghee Lee[a], Sunghwan Chung[a], Yongdeog Kim[a], and Jaehun Ko[b]
[a]KHNP Central Research Institute, 70, Yuseong-daero 1312beon-gil, Yuseong-gu, Daejeon, Republic of Korea
[b]Korea Nuclear Engineering & Service corp., 798-1, Yuseong-daero, Yuseong-gu, Daejeon, Republic of Korea
[*]kiyoungkim@khnp.co.kr

1. Introduction

Radiological assessment is performed to show that dose rate on the water surface of spent fuel pool (SFP) is less than 25 uSv/h[1-2]. Radiation sources in SFP are contaminants in the SFP water, a spent fuel assembly in transit and loaded spent fuel assemblies but a spent fuel assembly in transit is the most dominant factor in radiological assessment. In this analysis, dose rate is computed considering the gamma source from a spent fuel assembly in transit and especially, the irradiated top nozzle was considered in a spent fuel assembly modeling.

2. Evaluation Methodology

2.1 Assumption

Gamma dose rate on the water surface of SFP is evaluated for a spent fuel assembly only in transit. Neutron dose rates from spent fuel neutron source are neglected since this is effectively shielded by pool water. A water level is considered as 3.05 m (10 ft) over the top of an active fuel of a single spent fuel assembly in transit according to the regulatory guide. WH17X17 is considered for source term calculation and the cooling time is 100hr after plant shutdown. The specifications of a spent fuel assembly is in Table 1.

Table 1. Specification of Spent Fuel Assembly

Fuel Type	Enrichment [wt%]	Burnup [MWD/MTU]
WH17X17	5.0	60,000

2.2 Evaluation Methodology

Normally, licensing in radiological assessment is considered an active fuel only of a spent fuel assembly in transit. In this paper, three cases of spent fuel assembly modeling were evaluated in this paper: a) The case of modeling an active fuel only. b-1) The case of modeling an active fuel with non-irradiated top nozzle. b-2) The case modeling an active fuel with irradiated top nozzle. The activation of top nozzle is simulated by Co-60 that is converted from Co-59 in top nozzle.

MCNP6.1 version is used for radiological assessment. MCNP is a Monte Carlo code that can be used for neutron, photon, or neutron /photon transport and developed by Los Alamos National Laboratory. The code treats an arbitrary three-dimensional configuration of materials in geometric cells bounded by first and second-degree surfaces and some special fourth-degree surfaces [3]. Figure 1 shows the MCNP modeling of a spent fuel assembly in transit in SFP.

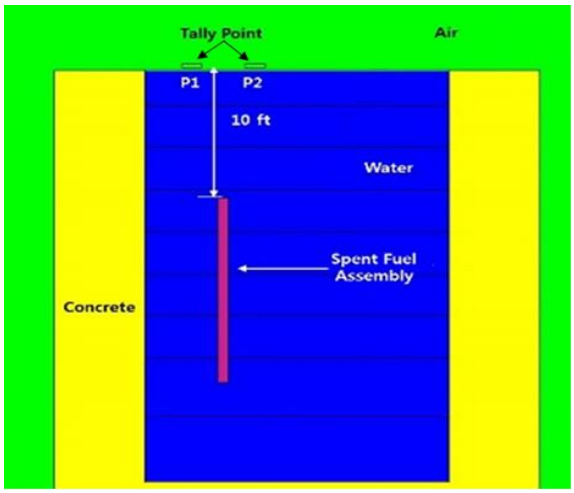

(a) Without Top Nozzle

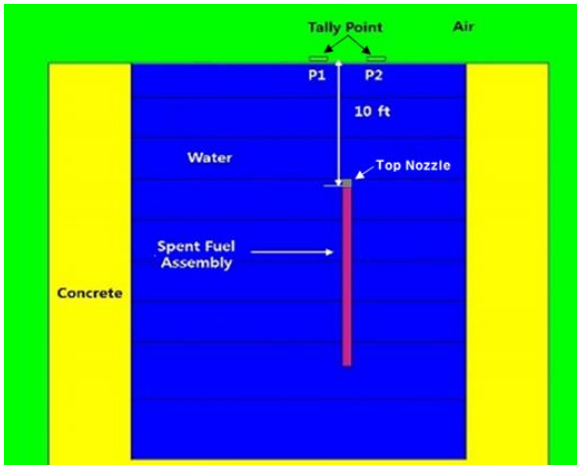

(b) With Top Nozzle

Fig. 1. MCNP modeling of a spent fuel assembly in transit in SFP.

3. Result

Table 2 shows the dose rate on the water surface in radiological assessment according to the cases: (a) The case of modeling an active fuel only. (b-1) The case of modeling an active fuel with non-irradiated top nozzle. (b-2) The case modeling an active fuel with irradiated top nozzle. As the result, (a) case and (b-2) case show the similar dose rate on the water surface. This means that the effect of the irradiated top nozzle is negligible and therefore it does not need to be considered in radiological assessment. For reference, (b-1) case shows is slightly lower than the others. That is why the top nozzle will block the gamma rays from an active fuel.

Table 2. Dose rate on the water surface considering irradiated top nozzle

Cases	Dose Rate (uSv/hr)
(a) Without top nozzle	20.36
(b-1) With non-irradiated top nozzle	20.09
(b-2) With irradiated top nozzle	20.37

4. Conclusion

The dose rate on the water surface of SFP was evaluated considering three cases of spent fuel assembly modeling. As the result, we confirmed that the effect of the irradiated top nozzle is negligible. That is why the gamma source from the irradiated top nozzle is relatively small compared to the gamma source from the active fuel. Therefore, it does not need to be considered in radiological assessment of SFP.

REFERENCES

[1] ANSI/ANS-57.1, “Design Requirements for Light Water Reactor Fuel Handling Systems.

[2] ANSI/ANS-57.1, “Design Requirements for Light Water Reactor Fuel Handling Systems.

[3] Los Alamos National Laboratory, “A General Monte Carlo N Particle Transport Code, Version 6.0”, MCNP6, Rev.0, 2013.

Feasibility Analysis for Fire Test of CANDU Spent Fuel Transport Cask Using a Scaled-Down Model

Ju-Chan Lee*, Kyung-Sik Bang, Seung-Hwan Yu, Yun Young Yang, and Woo-Seok Choi
Korea Atomic Energy Research Institute, 111, Daedeok-daero 989beon-gil, Yuseong-gu, Daejeon, Republic of Korea
*sjclee@kaeri.re.kr

1. Introduction

Large capacity transport cask for CANDU spent fuel is being developed from 2017. The weight of the cask is more than 70 tons. Thermal testing using a full-scale model is expensive and time consuming. Slice models are mostly used for the thermal testing of the PWR spent fuel casks with large length-to-diameter ratio. The CANDU spent fuel transport cask has a cuboid shape. In this study, thermal testing using a scaled-down model was proposed to efficiently perform the thermal testing.

2. Thermal Analysis Modeling

2.1 Determination of fire duration for scaled-down model

Type B packages should be designed to withstand the thermal test at the flame temperature of 800 °C for 30 minutes. Fire duration of the half-scale model is calculated by the following equations [1].

$$Q_P = A_{SP}\sigma F \frac{{T_F}^4}{M_P}\, t_R \quad (1)$$

$$t_H = \frac{Q_P\, M_H}{A_{SH}\, \sigma\, F\, {T_F}^4} \quad (2)$$

Where,

Q_P: Heat input for prototype cask [J/kg]

A_{SP}: Surface area of prototype cask [㎡]

A_{SH}: Surface area of half-scale model [㎡]

σ : Stefan-Boltzmann constant
$[5.67\text{x}10^{-8}\, W/m^2\, K^4]$

F : View factor for a fully engulfing fire

T_F : Fire temperature [K]

M_P: Mass of the prototype cask [kg]

t_R : Regulatory fire duration [s]

t_H : Fire duration of half-scale model [s]

The heat input into the prototype package is calculated as 202,400 J/kg from the Eq. (1). The fire duration of the half-scale model is calculated as 900 seconds (15 minutes) from the Eq. (2).

2.2 Thermal analysis model

Three-dimensional quarter section model was used for ANSYS Fluent solver as shown in Fig. 1. The analysis model consists of about 20 million meshes.

The decay heat from the half scale model is reduced by 1/4 to conserve the cask surface temperature. The total decay heats of the prototype cask and the half-scale model are 2,268 W and 567 W, respectively.

Thermal analyses were conducted for normal and accident conditions. The ambient temperature is considered as 38 °C with solar insolation and decay heat from the spent fuel for normal condition. The flame temperature is considered as 800 °C for 30 minutes for the

prototype cask. Fire duration is considered as 15 minutes for the half-scale model.

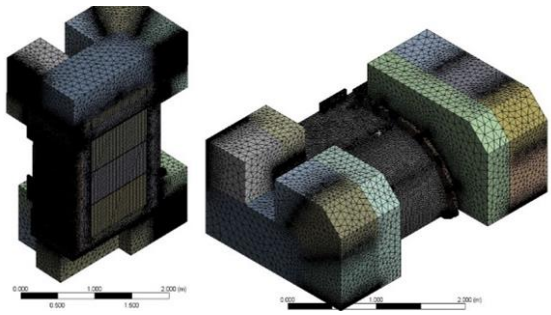

Fig. 1. Thermal analysis model.

3. Results and discussion

Fig. 2 shows the temperature contours of the prototype cask. Tables 1 and 2 show the maximum temperatures of the main parts under normal and fire conditions for the prototype cask and half-scale model. The temperature at the cask surface is conserved between the prototype cask and the half-scale model in the normal condition. The temperature difference between the inner and outer walls is reduced to about 1/2 in the half-scale model.

The temperature difference of the cask between the normal and fire conditions is similar for the prototype cask and half-scale model. Therefore, the overall temperature distributions of the prototype cask could be predicted using the half-scale model.

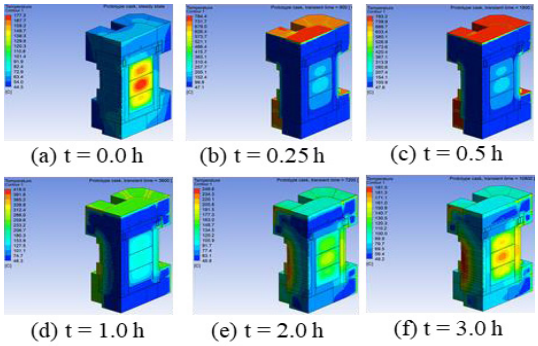

Fig. 2. Temperature contours for prototype cask.

Table 1. Thermal analysis results for prototype cask

Location	Maximum temperatures (°C)							△T
	Normal	Fire phase		Post fire (t > 0.5 h)				
		0.25	0.5	0.6	0.75	1.0	1.5	
Fuel bundle	177	177	177	177	177	177	177	0
Fuel basket	151	151	151	151	151	151	151	0
Cask lid(o-ring)	65	80	129	147	157	155	147	92
Lid carrier	66	278	427	391	351	293	216	361
Carrier housing	65	476	576	479	399	317	226	511
Inner shell	71	118	195	212	210	198	183	141
Outer shell	67	634	734	539	478	330	276	667

Table 2. Thermal analysis results for half-scale model

Location	Maximum temperatures (°C)							△T
	Normal	Fire phase		Post fire (t>15Min.)				
		7.5	15.0	17.5	22.5	30	45	
Fuel bundle	128	128	128	128	128	128	128	0
Fuel basket	113	113	113	113	113	114	119	6
Cask lid(o-ring)	65	99	151	163	164	160	157	99
Lid carrier	65	270	394	368	308	251	201	329
Carrier housing	65	134	523	442	346	273	209	458
Inner shell	67	135	213	234	212	199	185	167
Outer shell	66	564	671	503	368	321	265	605

4. Conclusion

The thermal analyses were carried out for the prototype and half-scale model. It was possible to predict the overall temperature distributions of the prototype cask by using the half-scale model. Therefore, the feasibility of the fire test using a scaled-model was confirmed. The results of this study can be used for the thermal testing of the cask using a scaled-down model.

REFERENCES

[1] W.S. Choi et al., “Safety analysis report for hot cell transport cask”, KAERI/TR-4287/2011, KAERI (2011).

Computational Analysis to Evaluate Similarities Between Full and Scaled-down Model in Drop Test of Radioactive Waste Transport Casks

Jongmin Lim*, Ki Seog Seo, Ju-Chan Lee, Jae-Han Lee, and Woo-seok Choi
Korea Atomic Energy Research Institute, 111, Daedeok-daero 989beon-gil, Yuseong-gu, Daejeon, Republic of Korea
*jmlim86@kaeri.re.kr

1. Introduction

In this paper, computational results for estimation of similarities between a full and scaled-down model in a drop test of radioactive waste transport casks is described. A rectangular metal cask is considered for the analysis, and concrete fills the inside of cask as an internal content of the cask.

2. Scale factor and test model

2.1 Scale factor in an impact test

The geometric scale factor considered in this paper is 1/2 and 1/4, and the scale factors corresponding to the geometric scale factor in an impact test are shown in Table 1.

Table 1. Scale factors in the impact test

Quantity	Similarity	1/2 model	1/4 model
Linear Dimension	S_L	1/2	1/4
Mass	S_L^3	$1/2^3$	$1/4^3$
Time	S_L	1/2	1/4
Strain/Stress	1	1	1
Force	S_L^2	$1/2^2$	$1/4^2$
Energy	S_L^3	$1/2^3$	$1/4^3$

Due to lack of an impact limiter of the considered metal cask, a significant damage at impact end of the cask can be caused. It can induce the large amplitude stress wave and high vibration, which makes more complex impact response [1].

2.2 The test model for the drop analysis

For the similarity analysis, the rectangular metal cask is considered as shown in Fig. 1, and it is assumed that an internal content of the cask is filled by the Type-I Portland cement. The mass of full-scale model is about 16 tons, and the drop height corresponding to the regulation of an A-type transport cask is 0.3 m. The drop direction is a short side drop. LS-Dyna is utilized for the computational drop analysis. A carbon steel SS275 is used for metallic parts, and the concrete is simulated by CSCM concrete material model in LS-Dyna.

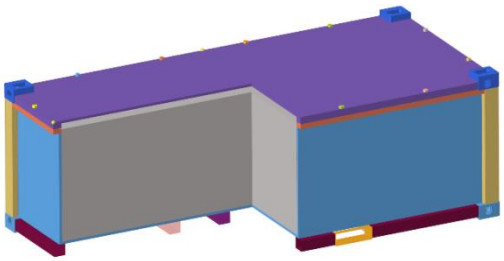

Fig. 1. The rectangular metal transportation cask for a radioactive waste material.

3. Comparison of computational results with respect to similarity law

All results except the internal energy are low-pass filtered with a cut-off frequency, and the cut-off frequency is also determined by the similarity law. The results of scaled model are multiplied by the reciprocal of the its scale factor.

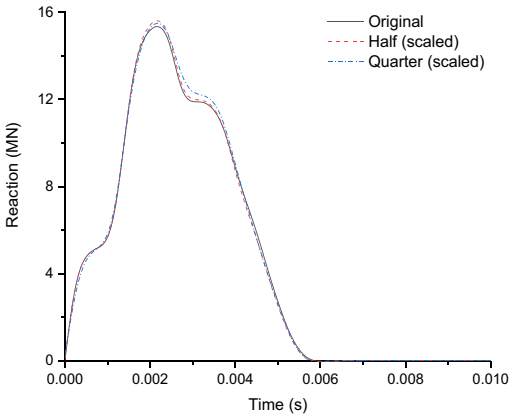

Fig. 2. Reaction Force.

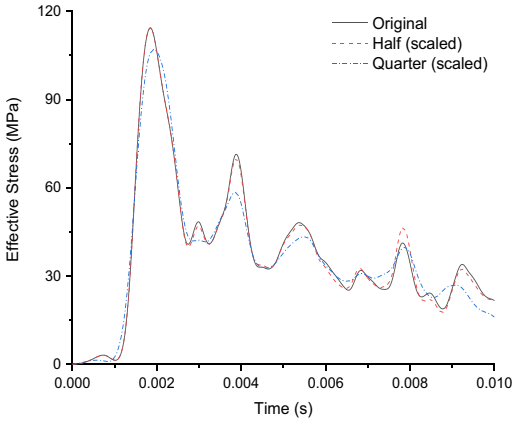

Fig. 3. Effective stress.

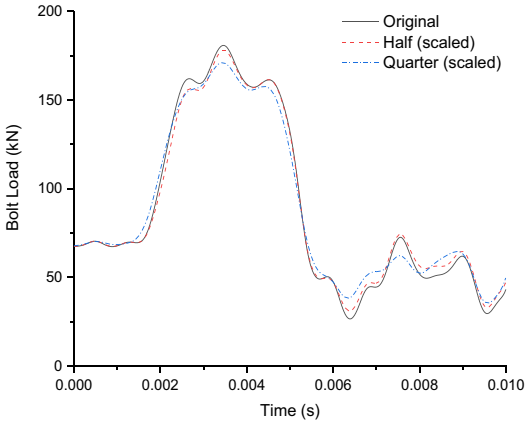

Fig. 4. Bolt load.

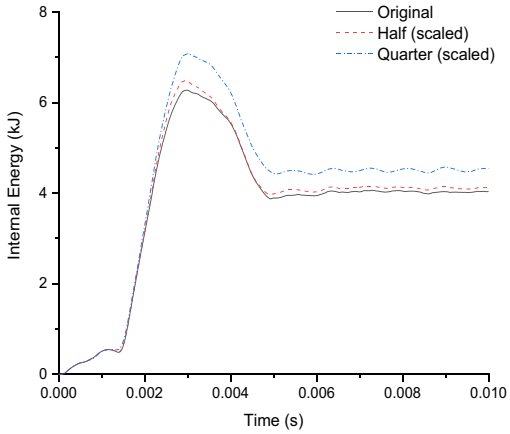

Fig. 5. Internal energy absorbed by the internal content.

Most results of the scaled model show good match with the original model. In the effective stress and bolt load, the quantities tend to be slightly underestimated as the geometric scale factor is low. The result of the internal energy absorbed by the internal content shows a significant difference between the quarter and original model. This kind of the internal impact is one of the major factors violating the similarity law in the impact test. For this reason, the behavior of the internal content is carefully evaluated when using the scaled model. Therefore, a proper correction technique to conservatively compensate this difference could be required or the largest scaled-down model that can be handled in the drop test should be selected.

4. Conclusion

In order to evaluate the similarity law in the drop test of the rectangular metal transportation cask for the radioactive waste material, the computational analysis is utilized. Using the drop analysis of the metal rectangular cask, the similarities with respect to the geometric scale factor can be compared. Based on the computational results, a real test including the scaled-down model will be performed in the future work.

REFERENCES

[1] UCRL-ID-121673, “Guidelines for Conducting Impact Tests on Shipping Packages for Radioactive Material”.

Mock-up for Remote Fuel Slug Fabrication

Kiho Kim*, Sanggyu Park, and Jeongyong Park
Korea Atomic Energy Research Institute, 111, Daedeok-daero 989beon-gil, Yuseong-gu, Daejeon, Republic of Korea
*khkim5@kaeri.re.kr

1. Introduction

The Korea Atomic Energy Research Institute is developing a metallic nuclear fuel technology. This technology helps fabricate metallic fuel slugs using transuranium (TRU) ingots produced through pyroprocessing. The fabricated TRU metallic fuel slugs are to be used as a fuel materials in sodium fast reactors (SFRs).

Regarding the metallic fuel technology development, it is necessary to fabricate TRU metallic fuel slugs in a shielded cell owing to the high radioactivity of TRU ingots. In addition, all operations and maintenance activities of the in-cell equipment for TRU metallic fuel slug fabrication should be conducted remotely because once the cell is active, direct access for workers to the in-cell equipment is not possible. In this paper, we describe the development status of the mock-up for the above-mentioned metallic fuel slug fabrication at KAERI.

2. Mock-up Development

We designed and constructed a remote testbed for metallic fuel slug fabrication using surrogates or depleted uranium. The testbed, named "remote fuel fabrication mock-up (RFFM)," was constructed at the Fuel and Material Facility of KAERI in 2018 and is specifically designed to incorporate remote operation and maintenance.

The RFFM is a testbed demonstrating the full spectrum of the remotely operated metallic fuel slug fabrication processes. Figure 1 shows the full-scale graphical model of the RFFM and the constructed RFFM. The RFFM mainly comprises two subsystems: a system for metallic fuel slug fabrication, which is located inside the cell, and a system for remote handling, which is located both inside and outside the cell. The former uses injection casting to fabricate metallic fuel slugs. It comprises several components: an injection-casting furnace (1), a high-frequency generator (2), a vacuum pump (3), an argon pressure tank (4), a filter device (5), a chiller (6), and a mold assembly (7); the component numbers within the parentheses are indicated in Figure 1. The injection-casting furnace (1), the main component of the system, was designed and constructed in modules to facilitate remote operation and maintenance when necessary. All equipment pertaining to the system for metallic fuel slug fabrication is located inside the cell and requires remote handling for operation, replacement, maintenance, and transportation.

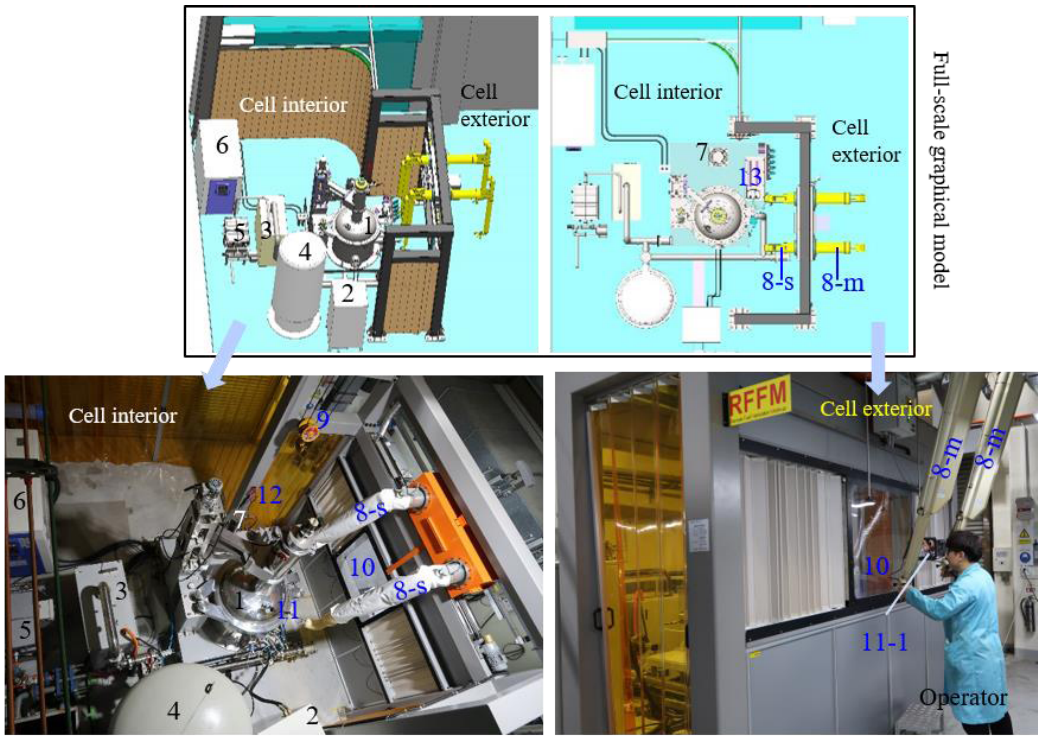

Fig. 1. Full-scale graphical model of the RFFM and the constructed RFFM.

The latter enables operators to fabricate metallic fuel slugs remotely inside the cell of the RFFM. It comprises two pairs of master (8-m)-slave (8-s) manipulators (MSMs), one overhead crane (9), one movable viewing window (10), and other auxiliary tools such as a camera (11) and a display panel (11-1), a hanger (12), and an impactor (13); the component parentheses are indicated in Figure 1. All of these remote handling devices are operated remotely by an operator.

3. Summary

Tests for metallic fuel fabrication using copper ingots were conducted satisfactorily at the constructed RFFM. From the perspective of remote operation, the metallic slug fabrication processes were performed satisfactorily through remote handling of the various components of the metallic fuel slug fabrication system at the RFFM.

ACKNOWLEDGMENTS

This work was supported by Nuclear Research & Development Program of the National Research Foundation of Korea funded by Ministry of Science and ICT (NRF-2017M2A8A5014888).

REFERENCES

[1] K. Kim, S. Park, H. Song, and J. Park, “Remote Fuel Fabrication Mock-up”, To be published in Proc. of Int’l Fuel Cycle Conference, September 22-27, 2019, Seattle.

Current Status of Application of Safeguards to Geological Repositories

Ju Young Jeon
Korea Institute of Nuclear Nonproliferation and Control, 1534, Yuseong-daero, Yuseong-gu, Daejeon, Republic of Korea
Jeonjy@kinac.re.kr

1. Introduction

The Application of Safeguards to Geological Repositories (ASTOR) group was established in order to continue the advisory function on safeguards for final disposal of spent nuclear fuel in geological repositories and to promote sharing information between Member State and IAEA.

The main objective of the ASTOR group is to support the maintaining a assurance that technologies related to geological disposal activities are compatible with peaceful use only.

In this study, we have described the historical background of the ASTOR Meeting and identified the activities for the preparation of geological disposal safeguards.

2. Background

2.1 History of ASTOR

The IAEA began to consider safeguards issues about spent fuel and measured discards in the mid-1980s. The Advisory Group Meeting was hosted to develop policy recommendations regarding termination of IAEA safeguards on spent fuel in 1988. The 16 states participants recommended against terminating safeguards on spent fuel before or after emplacement in a geological repository. In 1991 and 1995, a consultant meetings were held to develop the recommendations on the requirements, methods and policies for implementing safeguards on the disposal of spent fuel. After that, the IAEA held a second Advisory Group Meeting to review a conceptual safeguards approach and IAEA's policy reports in 1997.

2.2 A Support through the MSSP

The IAEA organized the Member State Support Program(MSSP) task " Programme for the Development of Safeguards for the Final Disposal of Spent Fuel in Geological Repositories (SAGOR)" in 1994 and recommendations including encapsulation plant, operating repositories and closed repositories were documented at STR-312(1998). Following SAGOR, the SAGOR-II programme was implemented, which evaluated the safeguards measures to implement the concept of safeguards and to make recommendations on integrated safeguards in geological repository facilities.

In 2006, the programme was renamed ASTOR that changed focus from the geological safeguards development to IAEA safeguards technical approaches for the specific facility in Finland and Sweden and the ASTOR meeting is being held in line with the MSSP.

3. Necessity of ASTOR meeting

3.1 Role of ASTOR

Initially, the main objective of the ASTOR group is to support the preparation of model-integrated safeguards approaches and Design Information Questionnaires(DIQ) for encapsulation plant and operating geological repositories. After the documents have been approved, ASTOR is monitoring the status of geological repositories activities and reviewing the safeguards measures. In addition, the meeting discuss the technical needs for efficient safeguards on a range of spent fuel measurements, identification of disposal canisters and various technologies.

3.2 The 11th ASTOR meeting in Korea

Since 2006, experts from the IAEA MSSP member countries have gathered a total of 13 times to share the current status of studies on waste disposal and national policies information.

Especially, Republic of Korea hosted the 11th ASTOR Conference in Gyeongju from April 20-22, 2015. In this meeting, all presenters provided information about the technical development carried out in their states related to geological repositories safeguards. In addition, the topic of technical procedures for applying safeguards to ground disposal facilities was actively discussed.

4. Conclusion

The IAEA began its study on the application of safeguards to Geological Repositories facilities in the 1980s. The status of each country and information gathered through the sharing of experts' information will be published as an official document. The main contents of documents are expected to be based on design information verification technology, containment & surveillance measures and canister ID, geophysical techniques, NDA verification and long-term data management. It will be used as an important document for IAEA inspections, as the IAEA apply safeguards measure to the disposal facilities in Finland and Sweden.

REFERENCES

[1] Donghyuk LIM, et al, “Discussion on Application of Safeguards to Geological Repositories(ASTOR) according to ROK Support Program”, INMM 2015.

Development of Damaged Fuel Can for Wet and Dry Storage

Seo Jeong Lee*, Sung-Chang You, Kwang-Ho Lee, and Eun-Ki Lee
Korea Hydro & Nuclear Power Co. Ltd., 70, Yuseong-daero 1312beon-gil, Yuseong-gu, Daejeon, Republic of Korea
*s.jeong2@khnp.co.kr

1. Introduction

For dry storage of damaged fuel, there is need for a way to enable the handling of damaged fuel as intact fuel. If a fuel cladding is damaged, it is removed from the assembly and stored in the Quiver system, or the entire assembly is put into a damaged fuel can(DFC). Currently, there are DFC in the domestic spent fuel pools(SFP), but those are not available in dry storage because those were provided for wet storage only. Therefore, a new DFC has been developed for dry storage.

2. Performance and Design Requirements

2.1 Performance Requirements

The DFC including one damaged fuel should be capable of being stored in SFP and dry storage cask. In particular, the spent fuels in the Kori unit 1 SFP, which is scheduled to be decommissioned, will be stored in the other plant's SFP until the interim dry storage facility is operated.

A fuel rod with hairline cracks of less than 1mm is considered to be intact fuel in United States, so the DFC apply confinement concept to prevent the leakage of particles of 1mm or more.

And it is designed to handle with the existing spent fuel handling machine for ease of handling.

2.2 Design Requirements

DFC should meet the criticality, shielding, thermal and structural requirements as required by NUREG-1536 and NUREG-2215[1,2]. In addition, the integrity should be maintained not only under normal conditions but also under artificial or natural accident conditions. It should be also designed to be retrieve if necessary.

3. Safety Evaluation

3.1 Criticality

The criticality evaluation was performed on the SFP of all domestic nuclear power plants. By comparing the criticality before and after the installation of the DFC, it is determined that there is no effect of criticality if it is decrease. In some cases, the criticality was reduced by a minimum of 28pcm and a maximum of 516pcm. This is due to the effect of reducing the amount of water by the volume occupied by the DFC and thermal neutrons are reduced.

3.2 Cooling Performance

The thermal safety evaluation is performed to ensure that the cladding temperature meet the

criterion. In the SFP, if the heat transfer is degraded by disturbing natural convection due to increased local flow resistance by DFC, the temperature of the cladding may increase. Through this evaluation, the mesh size of the upper and lower mesh screen was determined.

As a results, in case of 10% of mesh opening area, the maximum local temperature of the SFP is 91.55 °C that is satisfied with the criterion (<115 °C). Therefore, the minimum opening area of mesh screen was designed to be 10% or more.

3.3 Structural Integrity

The Structural integrity evaluation is divided into buckling, dropping and lifting evaluation. Buckling evaluation is to determine plastic deformation occurs due to the collision of damaged fuel with DFC by the rotation or eccentricity of the fuel when the fuel is loaded into a DFC. Drop accident evaluation is to determine the integrity of spent fuel storage rack when the DFC is dropped to the upper region or bottom of the rack. Lifting evaluation is to assess the integrity of the load position during the lifting of the DFC containing the damaged fuel under the load equivalent to 4g. In all evaluations, integrity of DFC was satisfied.

3.4 Vacuum Drying

During the vacuum drying process, if water remaining in the fuel cladding suddenly becomes vaporized, the internal pressure of the DFC may increase, causing rupture of the mesh screen.

If two mesh sheets are overlapped under the DFC's internal pressure 3MPa condition, the stress of the mesh is 415.8MPa that is less than the material's ultimate strength of 679MPa, and integrity of the mesh is maintained.

4. Conclusion

The DFC prototype was manufactured and conducted factory test and working test using WH 14×14 type dummy fuel, and some supplements is being applied. The development will be completed by the end of this year. The DFC design will be applied for the dry storage of damaged fuels at all domestic nuclear power plants, starting with Kori unit 1.

REFERENCES

[1] U.S.NRC, "Standard Review Plan for Spent Fuel Dry Storage Systems at a General License Facility, NUREG-1536 (2010).

[2] U.S.NRC, "Standard Review Plan for Spent Fuel Dry Storage Systems Facilities, NUREG-2215 (2017).

Thermal Analysis of HI-STORM 100 Dry Storage Cask in Extreme Temperature Condition With Heterogeneous Fuel Assembly Using COMSOL MULTIPHYSICS Program

SunWoo Park and KwangHeon Park*

Kyung Hee University, 1732, Deogyeong-daero, Giheung-gu, Yongin-si, Gyeonggi-do, Republic of Korea

*kpark@khu.ac.kr

1. Introduction

Due to the dismantling of nuclear power plants and the saturation of wet storage pool, the concept of dry storage has become an essential option. In a typical dry storage cask thermal analysis, homogeneous fuel assembly condition is applied. Uncertainty increases due to the artificial properties used in homogeneous fuel assembly condition analysis. Therefore, in this study, analysis with heterogeneous fuel assembly condition was performed. In addition, summer conditions have the effect of reducing the cooling effect of the dry storage cask. In order to confirm the effect, analysis was performed with the conditions of summer ambient temperature and insolation.

2. Procedure and Result

In this study, the extreme temperature condition considered thermal analysis of a HI-STORM 100 dry storage cask with WH14×14 heterogeneous fuel was performed using COMSOL MULTIPHYSICS 5.4 program.

2.1 Geometry and mesh setting

The specifications of HI-STORM 100 CASK, MPC-24, and WH14×14 fuel assembly refer to HOLTEC INTERNATIONAL's FSAR. Geometry is composed of 4,021,868 meshes in total. The average quality of the mesh is 0.3707. Geometry and mesh are shown in Fig. 1 below.

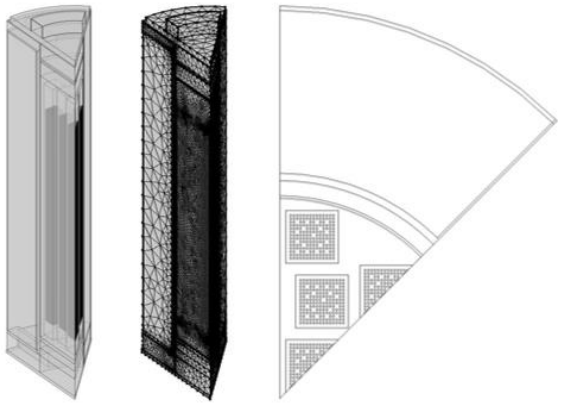

Fig. 1. Geometry and mesh of HISTORM-100 cask with WH14×14 heterogeneous fuel assembly.

2.2 Conditions of extreme temperature

In the normal condition analysis, the ambient temperature was set to 25°C and the insolation values of the cask top and side were set to 775W/m^2 and 388W/m^2. In the extreme temperature condition analysis, the ambient temperature was set to 40°C and the insolation

values of the cask top and side were set to 1,200W/m^2 and 600W/m^2. Insolation data is based on the figure below.

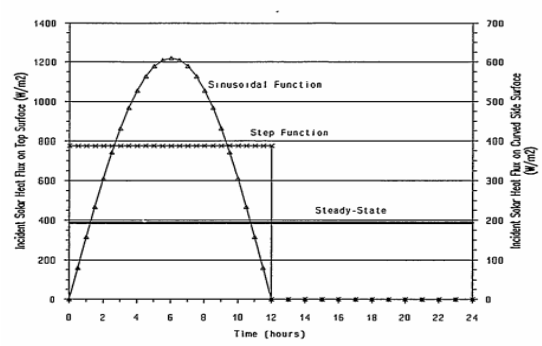

Fig. 2. Insolation data of 10CFR71.

2.3 Computing result

The difference between the FSAR result and the COMSOL MULTIPHYSICS program result is about 10°C. Based on the above normal condition model, calculation considering the extreme temperature condition was performed. The PCT difference between the normal and extreme temperature condition is about 7°C. Overpack outer shell temperature difference between the normal and extreme temperature condition is about 36°C. The calculation results are shown in Fig. 3 and 4.

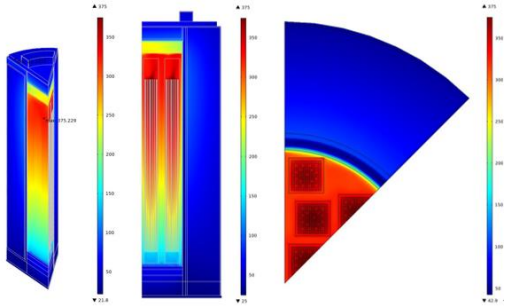

Fig. 3. 3D temperature profile, 2D temperature profile of 45° cutting plane, and 2D temperature profile of PCT height region.

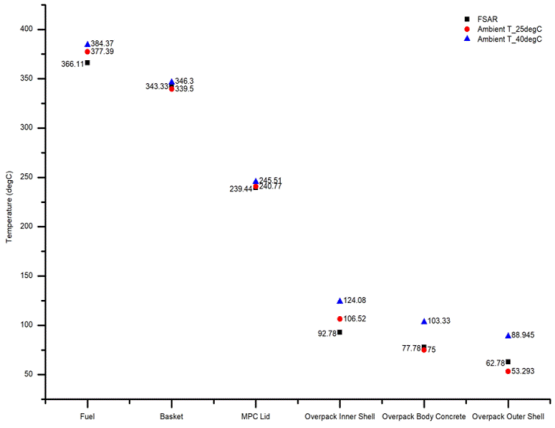

Fig. 4. Comparison of FSAR and COMSOL MULTIPHYSICS results.

3. Conclusion

The temperature of the overpack concrete increased by 28°C compared to the normal condition. The average temperature in the thickness direction of onverpack concrete was 103°C. However, the maximum temperature of the overpack concrete was 126°C. This was close to the concrete limit design temperature of 148°C. Based on the above results, additional thermal analysis reflecting domestic summer weather condition will be conducted.

REFERENCES

[1] Wu Yongjia, Klein Jackson, Zhou Hanchen, Zuo Lei, “Thermal and fluid analysis of dry cask storage containers over multiple years of service”, Annals of Nuclear energy, Vol.112, 132-142 (2018).

Development of Temperature Calculation Program for Spent Fuel Pools

Taehyeon Kim* and Donghee Lee
Central Research Institute, Korea Hydro & Nuclear Power Co., Ltd., 70, Yuseong-daero 1312beon-gil, Yuseong-gu, Daejeon, Republic of Korea
*taehyeon.kim@khnp.co.kr

1. Introduction

According to Nureg-0800 and the FSAR of the Korea Nuclear Power Plants (NPP), the spent nuclear fuel pool (SFP) must have sufficient cooling capacity for both all previous and new discharged spent fuels (SF). The average temperature of SFPs should be maintained below the acceptable limits for several offloads and cooling system alignment scenarios. In addition, the average temperature of the SFP should be calculated by transient analysis in consideration of decay heat load and cooling performance against time. In order to calculate the maximum temperature of SFPs over time, a program is needed to simultaneously calculate the heat of decay of spent fuel and the temperature of the SFPs. In this study, I developed a program to calculate the temperature of SFP together with the heat of decay of spent fuel.

2. Decay Heat Load Calculations

The decay heat of the SFP is generated in the spent fuel assembly stored therein. Due to the exponential nature of radioactive decay, heat generation in spent fuel assemblies will always decrease over time. Thus, the heat of decay of the fuel assembly in the SFP will continue to decrease over time. In order to conservatively simplify the decay heat calculation, the total decay heat is considered to come from two different groups of assemblies.

The first group of fuel assemblies is referred to as previously offloaded fuel. During the relatively short overestimated period of this study, the heat release rate of these assemblies decreases very slowly over time due to the exponential nature of the radioactive decay and the relatively long decay period. Thus, the decay heat contribution of these assemblies can be treated conservatively and uniformly ignoring the decrease in decay heat contribution during the evaluation period.

The second group of fuel assemblies is called recently offloaded fuel. The heat release rate of these assemblies decreases rapidly over time, so the decay heat contribution of these assemblies changes over time.

The following equation defines the generation of total decay heat in the SFP.

$$\mathrm{Q_{total}} = Q_{prev} + TR_{SF} \times Q_{recent} \qquad (1)$$

The total generation heat ($\mathrm{Q_{total}}$) is calculated by previously offload fuel's decay heat (Q_{prev}) and recently offload fuel's decay heat (Q_{recent}) with considering fuel transfer rate (TR_{SF}). Where, the contribution of the decay heat of both previously loaded fuels and recently loaded fuels is determined using the methodology of Branch Technical Position (BTP) ASB9-2[1] or ANSI / ANS-5.1[2]. The decay heat contributions of both the previously offloaded and recently offloaded fuel are determined for offloads from the plant reactor to the SFP for the following scenarios.

Scenario 1 – Normal Power Operation – A refueling batch is discharged into the SFP with the SFP already containing the maximum possible number of previously discharged assemblies, completely filling all possible fuel storage locations. The discharge takes place at the end of a normal-length operating cycle.

Scenario 2 – Refueling Operation – The full core is discharged into the SFP with the SFP already containing the maximum possible number of previously discharged assemblies,

completely filling all possible fuel storage locations. The discharge takes place at the end of a normal-length operating cycle.

Scenario 3 – Abnormal Operation – The full core is discharged into the SFP with the SFP already containing the maximum possible number of previously discharged assemblies, completely filling all possible fuel storage locations. The discharge takes place 480 hours after the shutdown for a previous scheduled refueling.

Figure 1 shows the transient heat load of each scenarios that calculated by new developing program using above equation. In this figure, the blue line represents scenario 1 and overlaps the yellow line (scenario 3) by 580 hours. This is because scenario 3 is the same as scenario 1, but the whole core is discharged again after 580 hours. The red line represents scenario 2 in which the full core is discharged, and the fuel transfer rate is assumed to be 6 assemblies per hour in all scenarios.

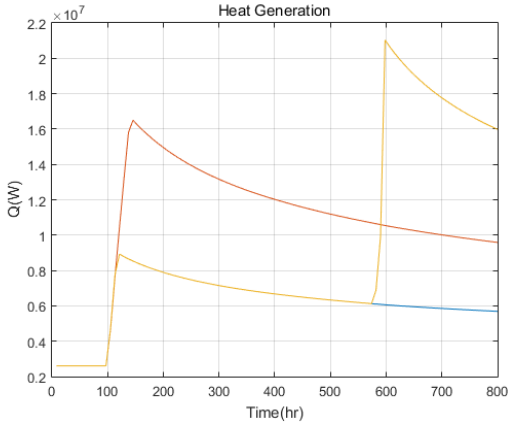

Fig. 1. Transient heat load of each scenarios.

3. Bulk Temperature Calculations

The transient temperature is calculated by using follow heat balance equation considering the SFP and the SFP cooling systems.

$$C_p \Delta T = Q_{prev} + TR_{SF} \times Q_{recent} - Q_{CS} - Q_{surf} \quad (2)$$

where, Q_{CS} and Q_{surf} is heat rejection by SFP cooling system and passive heat loss from water surface at that temperature, respectively. Passive heat loss from water surface is calculated using a turbulent natural convection heat transfer outside of the fuel handling building neglecting effects of wind. Figure 2 shows the transient temperature of each scenarios that calculated by new developing program using above temperature calculation equation. In this figure, the blue line represents scenario 1, the red line represents scenario 2, and the yellow line represents scenario 3.

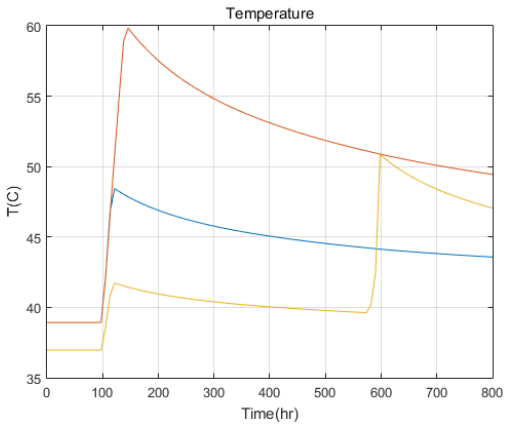

Fig. 2. Transient temperature of each scenarios.

4. Conclusion

The temperature calculation program was developed to predict bulk water temperature of the SFPs. The developed program provides good performance in the calculation of heat load and temperature for each scenario. The calculation resulted that the temperature of the pool was below the allowable limits required for each scenario. This program is expected to replace the temperature calculation part of the Carepool program.

REFERENCES

[1] USNRC Branch Technical Position ASB 9-2, “Residual decay energy for light reactor for long term cooling”, Rev. 2, 1981.

[2] ANSI/ANS-5.1-2014, “Decay Heat Power in Light Water Reactors,” American Nuclear Society, 2014.

Separation Efficiency of Enhanced Melt-crystallization Method for Purification of LiCl Salt Waste

Jung-Hoon Choi*, Ki-Rak Lee, Hyun-Woo Kang, and Hwan-Seo Park
Korea Atomic Energy Research Institute, 111, Daedeok-daero 989beon-gil, Yuseong-gu, Daejeon, Republic of Korea
*mrchoijh@kaeri.re.kr

1. Introduction

Korea Atomic Energy Research Institute (KAERI) is developing pyrochemical process for the recycling of PWR spent nuclear fuels using electrochemical method to achieve the volume reduction of radioactive waste [1-3]. During the process, LiCl salt wastes are planned to be recycled using melt-crystallization process. In this study, elimination method of corrosion products from reaction vessel has been investigated. Also, separation efficiencies for LiCl salt waste has been analyzed under the enhanced melt-crystallization process.

2. Experimental

Melt-crystallization tests were conducted using lab-scale melt-crystallization system capable of 3kg/batch treatment. In this study, the tests were conducted using 3 kg of surrogate LiCl salt waste having Cs, Sr, Ba, RE nuclides with (or without) Li_2CO_3 precipitation agent. Surrogate LiCl salt wastes were melted at 700 ^oC in the crystallization furnace. Then, crystallizer having 2 crystallization plates were immersed in the molten LiCl salt waste and the LiCl crystals were recovered on the 2 crystallization plates by cooling the plates using Ar coolant gas. Separation efficiencies (%) were calculated by the relationship of $(C_{before}-C_{after})/C_{before}\ x\ 100$, where C_{before} and C_{after} are nuclides concentration in the LiCl salt waste before and after crystallization process.

3. Results and Discussion

Fig. 1 shows recovered LiCl salt crystal after melt-crystallization without and with precipitation agent. In general, the crystal on the crystallizer shows some colors owing to the corrosion product generated from reaction vessel. To eliminate the corrosion product from crystal, the precipitation method has been applied and clear LiCl crystal has been obtained after crystallization test. Separation efficiencies were analysed to be over 90% even under the precipitation agent.

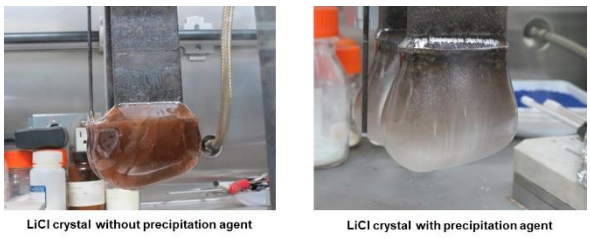

(a) (b)

Fig. 1. Recovered LiCl crystal (a) without precipitation agent and (b) with precipitation agent.

4. Conclusion

In the present study, clear LiCl crystal has been obtained using precipitation method eliminating the corrosion products. Also, it was found that the separation efficiencies were not affected by the precipitation agent.

REFERENCES

[1] H.S. Lee, J.M. Hur, J.G. Kim, D.H. Ahn, Y.Z. Cho, and S.W. Paek, “Korean Pyrochemical Process R&D activities”, Energy Procedia, 7, 391-395 (2011).

[2] H.S. Lee, G.I. Park, K.H. Kang, J.M. Hur, J.G. Kim, D.H. Ahn, Y.Z. Cho, and E.H. Kim, “Pyroprocessing technology development at KAERI”, Nucl. Eng. Technol., 43, 317-328 (2011).

[3] H.S. Lee, G.I. Park, J.W. Lee, K.H. Kang, J.M. Hur, J.G. Kim, S.W. Paek, I.T. Kim, and I.J. Cho, “Current Status of Pyroprocessing Development at KAERI”, Sci. Tech. Nucl. Install., 2013, 1-11 (2013).

Development of a Fuel Assembly Model for Spent Nuclear Fuel Transportation

Joongjin Kim*, Youngik Yoo, Jinseon Kim, Ohjoon Kwon, Kyounghong Kim,
Kyoungbo Eom, and Hyeongkoo Kim
KEPCO Nuclear Fuel, 242, Daedeok-daero 989beon-gil, Yuseong-gu, Daejeon, Republic of Korea
*joongjin@knfc.co.kr

1. Introduction

Spent Nuclear Fuel (SNF) integrity evaluation is based on a regulatory requirement that is described in 10 CFR 71(transportation) and 10 CFR 72(storage) of the U.S. NRC licensing requirement[1]. For this SNF integrity evaluation using a finite element (FE) model, structural, physical, geometrical and material characteristics of each fuel assembly component have to be considered, and many nonlinear parameters affecting SNF behaviors should be defined. In this regard, we have developed a FE model that can accurately simulate the mechanical behaviors of a fresh fuel assembly prior to applying SNF properties. For the validation of the developed model, a series of analysis with fresh fuel assembly material properties were performed, and analysis results were compared with the test results.

2. Fuel assembly model development

The target fuel assembly is a 14x14 type. The FE model of the fuel assembly consists of all major components including skeleton(top and bottom nozzles, top and bottom grids, 5 mid grids, 16 guide tubes) and 180 fuels. Beam and connector elements were used using ABAQUS v6.14[2], as shown in Fig. 1.

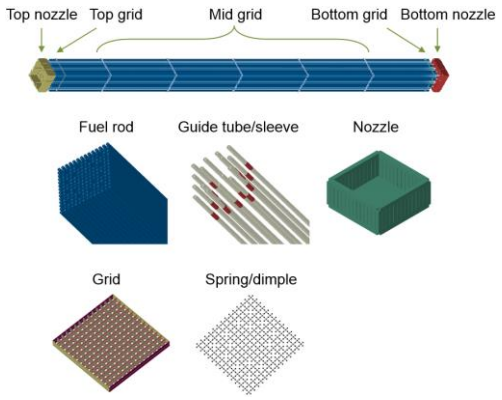

Fig. 1. Fuel assembly finite element model.

3. Model validation

3.1 Modal analysis

The natural frequencies of the fuel assembly are in Fig. 2 which shows that the normalized analyses results are in good agreement with the test results. Therefore, the fuel assembly FE model is considered to be valid from the dynamic viewpoint.

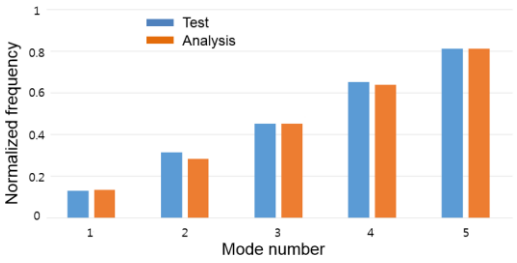

Fig. 2. Experimental setup to verify the developed model.

3.2 Axial deflection analysis

Fig. 3 shows the axial deflection analysis

results. The normalized axial deflection results are in good agreement with the test data at each component position.

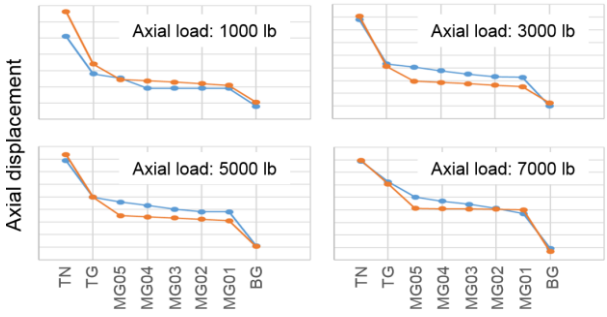

Fig. 3. Axial deflection analysis results.

3.3 Lateral impact analysis

Initial deflection at mid grid 03 increased from 0.1 inch to 0.9 inch in increment of 0.2 inch, and after removing initial deflection condition, reaction forces at rigid surface nodes were measured.

Fig. 4 shows the lateral impact analysis results. As shown in this figure, the analysis results were well matched to the test data

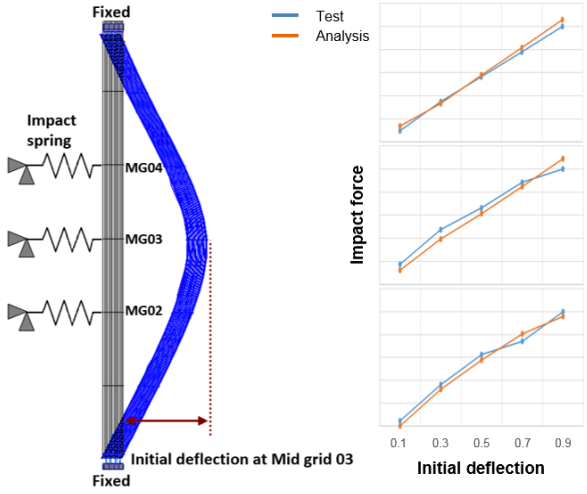

Fig. 4. Lateral impact analysis results.

4. Conclusion

In this study, we developed a three dimensional FE model that can simulate the mechanical behaviors of a fuel assembly using commercial analysis code. A series of analyses were performed with the developed model, and the performance of the model was validated by comparing with the test data. Since the analysis results are in good agreement with test data, the developed model is expected to be suitable for evaluating the fuel assembly integrity reflecting the specific SNF characteristics.

ACKNOWLEDGMENTS

This work was supported by the Korea Institute of Energy Technology Evaluation and Planning (KETEP) grant funded by the Korea government (MOTIE) (20181710201770, Development of Evaluation Technology for Vibration and Shock Load Characteristics and PWR Spent Nuclear Fuel Integrity under Normal Conditions of Road and Sea Transport).

REFERENCES

[1] “Packaging and Transportation of Radioactive Material/Licensing Requirements for the Independent Storage of Spent Nuclear Fuel, High-Level Radioactive Waste, and Reactor-related Greater than Class C Waste”, NRC 10CFR71/72, 2013.

[2] ABAQUS 6.14 Documentation, ABAQUS analysis user’s manual, Dassault Systems, 2014.

Neutron Activation Calculations for DFDF Hot Cell at KAERI

Siwan Noh*, Woo Jin Jo, Gil Sung You, and Seungnam Yu
Korea Atomic Energy Research Institute, 111, Daedeok-daero 989beon-gil, Yuseong-gu, Daejeon, Republic of Korea
*snoh@kaeri.re.kr

1. Introduction

About 26 kgU of spent nuclear fuels are stored in the DFDF (DUPIC Fuel Development Facility) hot cell of IMEF (Irradiated Materials Examination Facility) at KAERI. Spent fuels can emit a small amount of neutrons from (α, n) reactions and spontaneous fissions without chain reactions. The neutrons from spontaneous fissions account for over 98% of total emitted neutrons from spent nuclear fuels and over 98% of spontaneous fissions occurs in ^{244}Cm.

The components, equipment, casks, and structure of DFDF hot cell become activated when irradiated by the neutrons emitted from the spent nuclear fuels. Because the neutron flux density is expected to be very low, radioactivity concentrations by neutron activations may be within clearance criteria level.

In this study, we calculated the radioactivity concentrations by neutron activations for DFDF hot cell using FISPACT computer codes to verify whether the concentrations meet clearance criteria level, which is needed with respect to decontamination and decommissioning. In the activation calculations, the components, equipment, and casks are not considered because the surfaces of them are contaminated a lot and difficult to be decontaminated. For that reason, we calculated the radioactivity concentration only for the hot cell concrete (heavy concrete) and steel (SS304) liner for which it is relatively easy to decontaminate.

2. Materials and Methods

ORIGEN-ARP, MCNP, and FISPACT computer codes are used to calculate neutron source terms, neutron flux density, and radioactivity concentrations, respectively.

The DFDF hot cell stores various types of spent nuclear fuels having different enrichment, burnup, and cooling time, which is used to calculate neutron source terms using ORIGEN-ARP. Using the calculated neutron source terms, neutron flux density is obtained by MCNP. In MCNP calculation, simplified geometry in which all equipment, casks, and spent nuclear fuels are neglected is used and the neutron source terms is assumed to be located homogeneously in the volume of 50×50×50 cm^3 as shown in Figure 1. Because the activation level is heavily dependent on the concrete depth, we calculate the neutron flux density by 1 cm from the surface to 10 cm depth and each section has the volume of 10×10×1 cm^3.

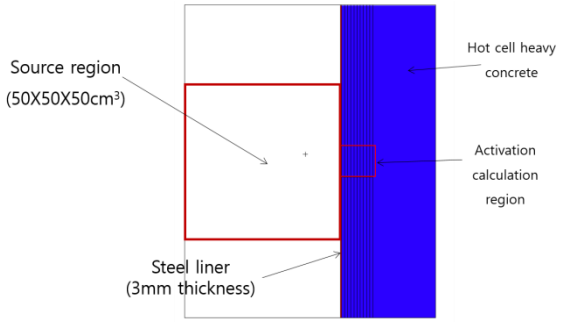

Fig. 1. The simplified MCNP geometry for neutron flux density calculations.

Using the neutron flux density for each section, the radioactivity concentrations are calculated using FISPACT. FISPACT is one of famous computer codes to calculate neutron activation developed by UK Atomic Energy Authority and has been widely used for various fields such as nuclear reactors, nuclear fusion, accelerator, decommissioning. Neutron flux density, material information, and irradiation/cooing scenarios are required to calculate radioactivity concentrations by neutron activation. For material information, a slight amount of impurity in concrete and steel should be considered because impurity materials can have very large neutron absorption cross-section and make relatively long half-life radionuclides. It is well known that Co, Eu, Cs impurities are important for concrete and Co is important for steel. The impurity concentration information is available on a few reference [1-5] but the information has very large deviation. In this study, we used the highest impurity concentrations for each element that are 10 ppm

of Co, 1.3 ppm of Cs, and 1 ppm of Eu in the concrete, and 4000 ppm of Co for SS304. It is assumed that the spent nuclear fuels are stored for 30 years and radioactivity concentrations are calculated for each cooling time of 30 days, 1 year, 5 year, and 10 year. The ratio of the radioactivity concentration to clearance criterial level is calculated in the end.

3. Results and Discussion

Table 1 shows the radioactivity concentrations in the concrete for major radionuclides and the ratio to clearance criteria level at 1cm depth section for cooling time of 30 days. Figure 2 shows the ratio to clearance criteria level by the concrete depth. Table 2 shows the radioactivity concentrations in the steel liner for major radionuclides and the ratio to clearance level for cooling time of 30 days. Table 3 shows the ratio to clearance criteria level by cooling time.

Table 1. The radioactivity concentrations in the concrete for major radionuclides and the ratio to clearance criteria level

Nuclide	Activity Conc. [Bq/g]	Criteria [Bq/g]	Ratio
Mn-54	5.41E-04	0.1	5.41E-03
Sc-46	7.07E-06	0.1	7.07E-05
Fe-59	6.60E-07	1	6.60E-07
Eu-152	2.35E-07	0.1	2.35E-06
Sc-47	2.34E-07	100	2.34E-09
Co-60	1.87E-07	0.1	1.87E-06
Eu-154	1.19E-07	0.1	1.19E-06
Cs-134	9.60E-08	0.1	9.60E-07
		Total	5.49E-03

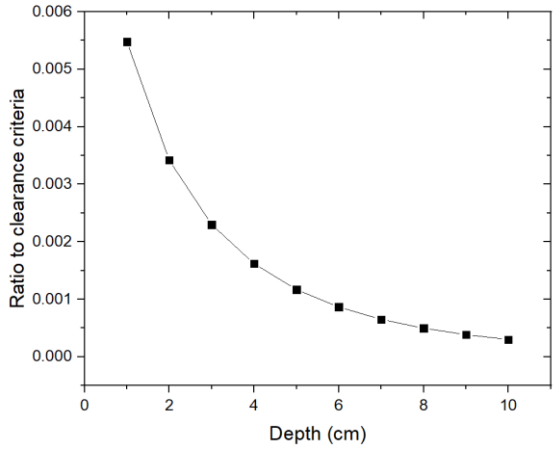

Fig. 2. The ratio to clearance criterial level by concrete depth.

Table 2. The radioactivity concentrations in the steel liner for major radionuclides and the ratio to clearance criteria level

Nuclide	Activity Conc. [Bq/g]	Criteria [Bq/g]	Ratio
Co-58	1.49E-01	1	1.49E-01
Mn-54	9.01E-02	0.1	9.01E-01
Co-60	7.24E-03	0.1	7.24E-02
Co-57	6.22E-04	1	6.22E-04
Fe-59	2.31E-04	1	2.31E-04
		Total	1.12

Table 3. The ratio to clearance criteria level in the steel liner by cooling time

Cooling time	Ratio
30 days	1.12
1 year	0.47
5 years	0.04
10 years	0.009

As shown in Table 1, the ratio to clearance is very smaller than 1, which means that the concrete can be considered as non-radioactive waste. The major nuclide in the concrete is Mn-54. As shown in Table 2, the ratio to clearance for steel liner is slightly 1. However, the ratio become less than 1 within a few months because Mn-54 that is the major nuclide has only 312 days of half-life. Thus, the steel liner also can be considered as non-radioactive waste if the surface of liner is sufficiently decontaminated.

4. Conclusion

In this study, we calculated the neutron activation for the concrete and steel liner in the DFDF hot cell. We confirm that the radioactivity concentration in the concrete and steel liner meets the clearance criteria level and they can be considered as non-radioactive waste. Even though the radioactivity level by neutron activation is very low because of small amount of spent nuclear fuel in this study, neutron activation may become more important problem for long-term and large-scale spent fuel storages.

REFERENCES

[1] T.Zager et. al., J.Nucl.Mat., 335, 379-386 (2004).
[2] K.Masumoto et. al. J.Radioanal. and Nucl. Chem., 255(3), 465-469 (2003).
[3] G.Hampel et. al., WM02 conference, Feb.24-28, Tuson, AZ, US (2002).
[4] KNSSC, MONO120141529 (2013).
[5] US NRC, NUREG-3474 (1984).

Influencing Factors for Assessing the Spent Nuclear Fuel Integrity During Handling and Transportation

Wooyong Choi*, Donghyo Lee, Janghwan Lim, and Seongki Lee
KEPCO Nuclear Fuel, 242, Daedeok-daero 989beon-gil, Yuseong-gu, Daejeon, Republic of Korea
*wychoi@knfc.co.kr

1. Introduction

Nuclear fuel is burned in a reactor for a specified period and then stored in a spent fuel pool. However the storage capacity of spent fuel pool in a nuclear plant cannot accommodate all the spent fuel generated during the operation of a power plant. So, it is inevitable to transfer the spent fuel to a separate storage facility. Since spent fuel contains a large amount of radioactive material, the integrity of the cladding shall be maintained under handling and transport, and the possibility of failure need to be evaluated. Therefore, the purpose of this study is to derive the factors affecting the integrity of cladding tube and to suggest a method for evaluating cladding failure.

2. Influencing factors for evaluating probability of cladding failure

2.1 Cladding temperature

The temperature of the cladding is one of the most important parameters for evaluating the behavior of spent fuel during the dry and transport. It affects the pellet-cladding gap, creep, rod internal pressure, hoop stress, and hydride reorientation.

2.2 Oxidation

Nuclear fuel transfers heat through direct contact with the coolant. In this process, zirconium, the main material of the fuel cladding, reacts with the coolant to form a zirconium oxide on the cladding surface. This oxide film reduces the thickness of the zirconium cladding. Therefore, the oxide film has an influence on the integrity of the fuel cladding.

2.3 Hydrogen

Hydrogen is generated during oxidation of the cladding. Some hydrogen diffused into the cladding is present in solid solution in the zirconium lattice structure depending on the temperature of the cladding, but when it exceeds the solid solution limit, it combines with zirconium to form a hydride. The hydride precipitates increase the brittleness of the cladding to reduce ductility and fracture toughness.

2.4 Rod internal pressure and hoop stress

Fission products are produced by nuclear fuel fission in a reactor. Representative fission products include xenon and krypton, which increase the rod internal pressure as fission gas. Increase in the internal pressure of the rod affects the hoop stress applied to the cladding along with the increase in the temperature of the cladding during the transfer from the spent nuclear pool to the dry storage cask.

2.5 Hydride reorientation

In wet storage, most of the hydrides in the cladding are circumferentially distributed. However, as dry storage begins, hydrides are dissolved into the zirconium lattice as the cladding temperature increase. After this, the hydride is re-precipitated as the decay heat decreases. At this time, if more than a certain level of hoop stress occurs, the hydride can be

precipitated in the radial direction instead of the circumferential direction. This phenomenon is called hydride reorientation, and radial hydrides make the mechanical integrity and fracture toughness of the cladding more vulnerable than circumferential hydrides.

2.6 Gap between pellet and cladding

Because of thermal expansion and swelling of the pellet, the gap between the pellet and the cladding can be reduced and even contact. Contact of the pellet with the cladding can affect failure due to pellet-cladding interaction, hoop stress, and hydride reorientation. On the other hand, when the gap is wide, the probability of failure of the cladding may increase when an external impact occurs. Therefore, the gap between the pellet and the cladding is one of the important factors in calculating the probability of cladding failure.

2.7 Pinch load

Pinch load is an external load acting directly on the spent fuel cladding during handling and transportation. It can be caused by a collision between the fuel rods or an impact between the fuel rods and the cask. It is the most influential factor in evaluating the mechanical integrity of spent fuel. Since the spent fuel impact test is difficult to perform directly, it can be calculated by analytical methods through modeling.

3. Application of the factors for evaluating the spent fuel cladding failure

In order to evaluate the mechanical integrity of spent fuel, the failure probability will be calculated by comparing the critical strain energy density (CSED) for the cladding under various conditions with the strain energy density (SED) due to the pinch load that can occur under design based accident conditions. In order to calculate the CSED, burn-up, cladding temperature, oxide film, hydride, rod internal pressure, hoop stress, etc. will be considered and the SED calculation will take into account the gap between the pellet and the cladding and the pinch load. The calculated CSED and SED will be compared to determine the possibility of the cladding failure.

4. Conclusion

As a result of analyzing the factors that may affect the integrity of the fuel cladding during the handling and transportation of spent fuel, it was confirmed that various factors are closely related to each other. These factors are also greatly influenced by the spent fuel burn-up history when released after being in a reactor. Therefore, it is important to manage the burn-up history of nuclear fuel from the beginning. As a future work, we will develop a probabilistic evaluation method for the cladding failure during handling and transportation through evaluation of spent fuel characteristics of the factors.

ACKNOWLEDGEMENT

This work was supported by the Korea Institute of Energy Technology Evaluation and Planning (KETEP) and the Ministry of Trade, Industry & Energy (MOTIE) of the Republic of Korea (No. 2014171020166C)

REFERENCES

[1] EPRI Document No. 1013448, “Spent Fuel Transportation Applications: Longitudinal Tearing Resulting from Transportation Accidents – A Probabilistic Treatment”, 2006.

Uncertainty Quantification of Thermal Analysis for Dry Storage Cask

Sung Yong Lee*, Jae Hun Ko, Hyo Sub Kim, and Dong Gyu Lee
Korea Nuclear Engineering & Service, 65, Myeongdal-ro, Seocho-gu, Seoul, Republic of Korea
*sylee@kones21.com

1. Introduction

The credibility and predictive capability of computational fluid dynamics (CFD) is greatly enhanced, and CFD can be considered a reliable tool for engineering analysis, if the numerical errors and uncertainties present in the solution can be reliably estimated. Error and uncertainty for a solver and a solution is formally estimated through a verification and validation (V&V) process. In 2009, the American Society of Mechanical Engineers (ASME) published a standard explaining the procedures for code verification, solution verification, and validation of CFD studies. The general objective of the V&V process is to estimate the accuracy of a numerical study.

This study presents the methodology and results from a numerical error estimation analysis performed for thermal analysis of the dry storage cask.

2. Methodology for Uncertainty Quantification

2.1 Solution Verification

According to ASME V&V 20-2009, solution verification refers to the process of estimating the numerical uncertainty for a particular solution of a problem. The two main sources of errors that contribute to numerical uncertainty are the discretization error and the iteration convergence error. The discretization error is the difference between the result of a particular simulation with a specific grid and the results obtained with systematically refined grids. Discretization error can be estimated using a systematic grid refinement analysis, where the numerical solution is expected to asymptotically converge to the exact solution as the mesh size approaches zero. Systematic grid refinement forms the basis of the solution verification process.

2.2 Grid Convergence Index Calculation Method

Discretization error is normally calculated using Richardson extrapolation (RE). RE is formulated to estimate the exact solution to the partial differential equations (PDEs) using the order of accuracy and solutions from two levels of grids. Based on the concept of RE, Roache proposed a method for a numerical uncertainty estimation, known for the grid convergence index (GCI) method. The GCI method was developed as a means of converting the discretization error estimates from the RE into uncertainties. The GCI is an estimated as a 95 percent uncertainty calculated by multiplying the absolute value of the RE error by a factor of safety (Fs). GCI provides the uncertainty of the solutions derived from discretized equations by a numerical and an analytical approach.

3. Uncertainty Quantification for a Concrete Cask for the Dry Storage of Spent Nuclear Fuel

Solution verification for the dry storage cask was performed using four levels of mesh

generated with systematic grid refinement. Simulation was performed for a concrete cask for the dry storage of spent nuclear fuel as shown in Fig. 1.

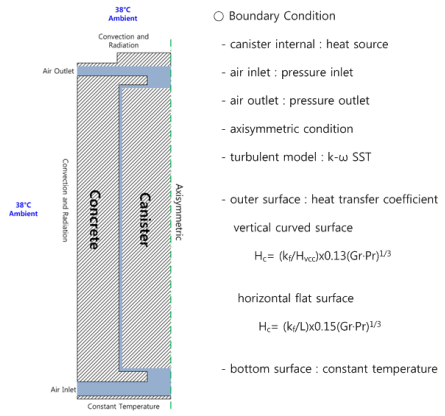

Fig. 1. Analysis model and boundary conditions for uncertainty quantification.

The levels of grids used in the analysis for the concrete cask are provided in Table 1 and Fig. 2. Table 1 also lists the mesh refinement factor between two consecutive levels of grids calculated using the procedure described in Section 2. Simulation for all the levels of grids was conducted with the same input parameters and the same turbulence model that was used for the baseline simulations for the concrete cask.

Table 1. Mesh levels used in GCI analysis of the concrete cask

Mesh Type	Total cell number	Mesh refinement factor (r)
Baseline mesh	18,772	-
Fine mesh 1	23,746	1.2650
Fine mesh 2	51,337	2.1619
Fine mesh 3	125,416	2.4430

Uncertainty quantification was performed for a maximum cladding temperature and average stack velocity using GCI method. It was found that maximum cladding temperature and average stack velocity showed ±2.6[°C] and 0.264[m/s] variation, respectively.

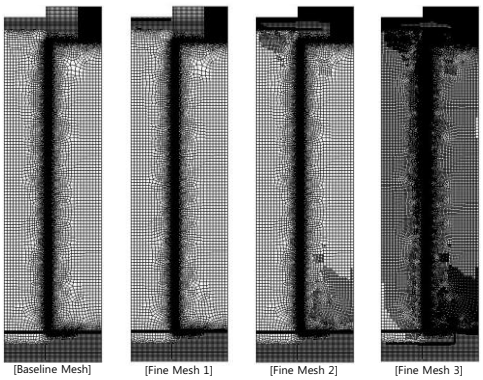

Fig. 2. Four mesh levels for uncertainty quantification.

4. Conclusion

In this paper, the methodology was presented to perform uncertainty quantification and GCI calculation for a thermal analysis of a dry storage cask. Uncertainty for the discretization error in CFD can be quantified by GCI method and furthermore, it can be used as a safety margin calculation tool.

Acknowledgement

This research was supported by the Korea Institute of Energy Technology Evaluation and Planning (KETEP) granted financial fund from the Ministry of Trade, Industry and Energy (MOTIE), Republic of Korea (No. 20171710201750).

REFERENCES

[1] ASME, “Standard for Verification and Validation in Computational Fluid Dynamics and Heat Transfer”, ASME V&V 20-2009, American Society of Mechanical Engineers, New York, 2009.

Response Spectrum Analysis for Selection of Representative Spent Fuel Under Normal Conditions of Transportation

Donghyo Lee*, Hyeongkoo Kim, and Seongki Lee

KEPCO Nuclear Fuel, 242, Daedeok-daero 989beon-gil, Yuseong-gu, Daejeon, Republic of Korea

*donghyo@knfc.co.kr

1. Introduction

Many types of spent fuel have been generated for 40 years and the capacity of spent fuel pool will be saturated in the near future. Transportation of spent fuel is inevitable process for dry storage in this situation. According to 10 CFR 71, the integrity of spent fuel shall be maintained under normal conditions of transportation [1]. It takes much time to evaluate all types of spent fuel, so it is efficient to develop an assessment method with representative spent fuel. Candidate fuel assemblies are 14OFA, 16ACE7, 17ACE7, KSFA. In this paper, response spectrum analysis was performed to choose a representative spent fuel with reference spectrum [2].

2. Response Spectrum Analysis

2.1 Methodology of the Response Spectrum Analysis

Response spectrum analysis is a method of approximating the response of the entire structure as a combination of single-degree-of-freedom natural responses when load changes rapidly over time. Modal analysis must be preceded before the response spectrum analysis. After obtaining the natural frequency from modal analysis, the maximum physical quantities for each mode are calculated using the input spectrum. In this analysis, ABS (Absolute Sum) method is applied for mode combination. The ABS method assumes that maximum response of all mode have same direction at the same time, thus this method is very conservative.

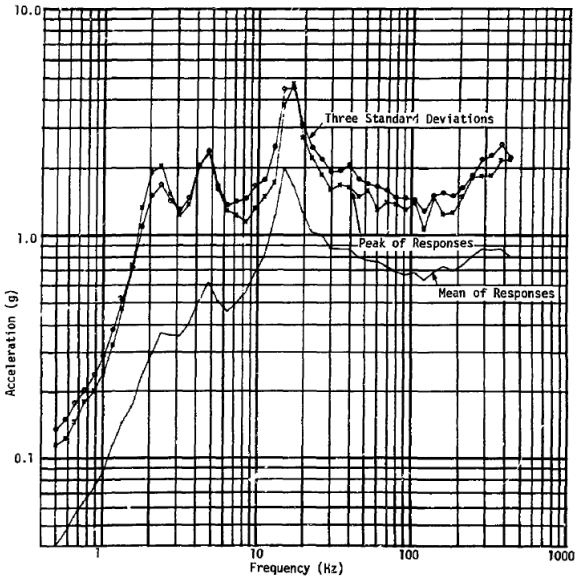

Fig. 1. Reference response spectrum [2].

2.2 Simplified Beam Model

Simplified beam model is composed of mass and beam elements for response spectrum analysis. Mass elements are located at grids and nozzles to reflect mass of fuel assembly. Beam elements are used to simulate the cross sections and materials of claddings, guide tubes, and instrumentation tubes. Fuel assembly model has dynamic characteristic of each fuel assembly.

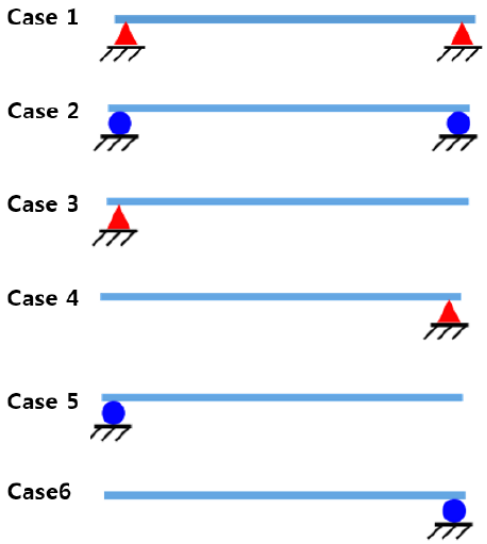

Fig. 2. Boundary conditions of response spectrum analyses.

Under transportation condition, spent fuel is subjected to shock and vibration loads from various road environments. Therefore 6 boundary conditions, e.g. both fixed, both pinned, top fixed, bottom fixed, top pinned, bottom pinned, are considered as shown in Fig. 2. On these 6 cases of boundary conditions, response spectrum analysis is conducted using ABAQUS [3].

3. Results and Discussion

Table 1. Stress results of each fuel assembly types [MPa]

Type	Both fixed	Top fixed	Bottom fixed
KSFA	5.95	2.74	2.14
14OFA	4.52	1.59	2.59
16ACE7	6.81	2.15	2.86
17ACE7	7.87	3.00	3.94

Table 1 shows the stress results of each fuel assembly types. 17ACE7 fuel assembly represents higher stress than other fuel assemblies. That is caused by second smallest area moment of inertia and second largest displacement. The smaller the area moment of inertia and the larger the displacement, the larger stress came out.

4. Conclusion

The integrity of spent fuel shall be maintained under normal conditions of transportation. The first step for evaluating integrity of spent fuel is to select the representative spent fuel. In this research, the response spectrum analysis considering nuclear fuel characteristics was performed. Not only response spectrum analysis, but MMTT (Multi Modal Transportation Test) data acquisition made 17ACE7 selected as representative spent fuel.

ACKNOWLEDGEMENT

This work was supported by the Korea Institute of Energy Technology Evaluation and Planning (KETEP) and the Ministry of Trade, Industry & Energy (MOTIE) of the Republic of Korea (No. 20181710201770).

REFERENCES

[1] Title 10 of the Code of Federal Regulations (10 CFR) 71, “Packaging and Transportation of Radioactive Material”.

[2] C. F. Magnuson, Shock and Vibration Environments for a Large Shipping Container during Truck Transport (Part II), SAND78-0337, Sandia National Laboratory, Albuquerque, NM, May 1978.

[3] ABAQUS, ABAQUS 6.14 Analysis User’s Guide, Dassault Systemes Simulia Corp., Providence, RI, USA, 2014.

Application of the Computer Codes in the Nuclear Fuel Cycle Facility

Woo Jin Jo*, Siwan Noh, Hyo Jik Lee, and Seung Nam Yu
Korea Atomic Energy Research Institute, 111, Daedeok-daero 989beon-gil, Yuseong-gu, Daejeon, Republic of Korea
*wjjo@kaeri.re.kr

1. Introduction

The design of the nuclear facilities requires a variety of disciplines. There are no nuclear reactors in the nuclear fuel cycle facility, but the nuclear fuel behavior should be evaluated because the nuclear fuel cycle facility handles the spent nuclear fuels. In addition, a safety analysis along the route of exposure in the accident or waste disposal is also required. Furthermore, designing the nuclear fuel cycle facilities requires design related to machinery, structure, civil engineering and sites, including design of the hot cell structures.

Unlike the nuclear power plants whose designs are formalized, nuclear fuel cycle facilities require a wide variety of design techniques depending on their locations, handling volume of the spent nuclear fuel, and processing method. Nuclear power plants have very well established computer codes associated with designs or verifications. However, in the case of nuclear fuel cycle facilities, some computer codes for the nuclear power plants may be sued as they are, but some may not.

In this paper, the computer codes that are necessary or applicable for designing nuclear facilities are reviewed and classified. In addition, the applicability of the computer codes to the nuclear fuel cycle facilities was evaluated.

2. Computer codes for design and construction of the nuclear facilities

There are two major computer codes categories that can be applied to the design and construction of the nuclear facilities. The first is a safety analysis codes and the second is an industrial codes.

Safety analysis provides sufficient safety margin considering uncertainty caused by equipment performance, analysis model, and assumptions in the analysis by applying conservative and deterministic criteria. This means that the radiological risk to the facility workers and the public is acceptable. In general, simulations of the design basis accidents and the beyond design basis accidents on the nuclear power plants are evaluated and the safety indicators are derived through computational codes(mostly thermohydraulic analysis codes).

The nuclear fuel cycle facilities are no different from the nuclear power plants. However, as mentioned previously, the nuclear fuel cycle facilities have different characteristics of each nuclear facility unlike the conventional the nuclear power plants. Therefore, applicable safety analysis codes and industrial codes can also be changed.

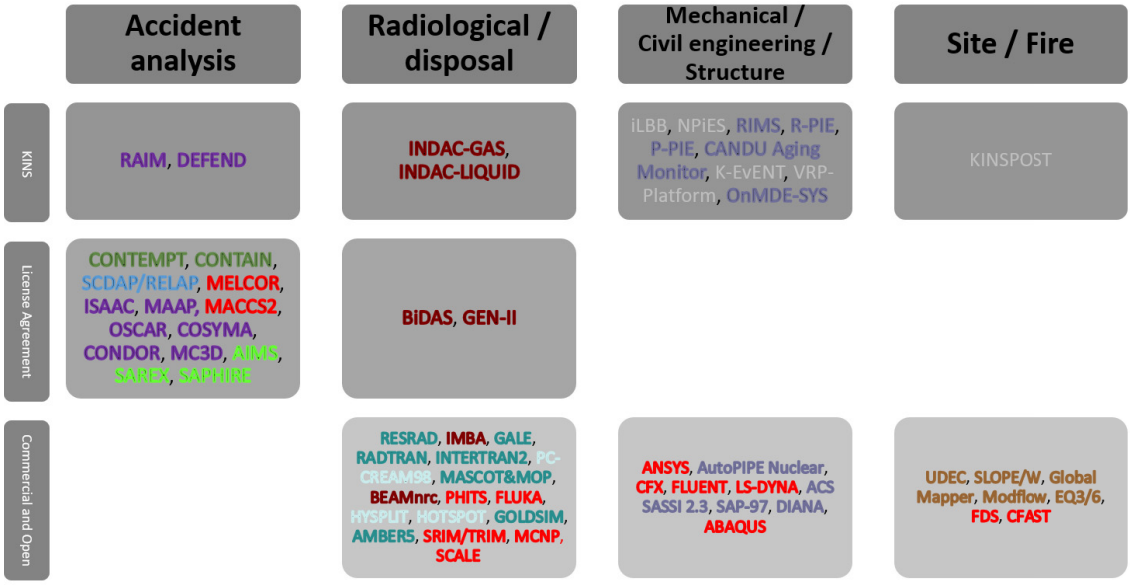

Fig. 1. Applicable the computer codes for the design of the nuclear fuel cycle facilities.

3. Computer codes for the nuclear fuel cycle facility

In the nuclear fuel cycle facilities, most of the codes used to design the nuclear power plants can be used as is. Because most fuel behavior simulation computer codes are applicable to both new and spent nuclear fuel. However, since the nuclear fuel cycle facilities do not have systems such as reactor cores or power generation systems, the nuclear power plants codes are difficult to apply and needs to be selectively applied.

This paper briefly summarizes the computer codes applicable to the nuclear fuel cycle facilities as shown in figure 1. Details will be explained at the conference

4. Conclusion

In this paper, the applicable computer codes for design of the nuclear fuel cycle facilities are investigated and summarized based on the codes used in the nuclear power plants.

The use of each code should be judged by the designer of the facility. However, if an Integrated Safety Analysis procedure for the nuclear fuel cycle facilities is established and the regulatory guides become clear, the result of this paper can be utilized to establish a computer codes systems for the nuclear fuel cycle facilities.

ACKNOWLEDGEMENT

This work was supported by Nuclear Research & Development Program of National Research Foundation of Korea (NRF) funded by Minister of Science, ICT and Future Planning (MSIP).

Modification of Light System in Large Inert Gas Filled Facility PRIDE

Ilje Cho*, Youngkuk Jang, Seonho Noh, and Heeseok Kang
Korea Atomic Energy Research Institute, 111, Daedeok-daero 989beon-gil, Yuseong-gu, Daejeon, Republic of Korea
*hyilje@kaeri.re.kr

1. Introduction

PRIDE is a three-story building and it has a large-scale inert argon gas filled cell (40.3 m length, 4.8 m width, 6.4 m height) at the second floor. PRIDE systems consist of utilities and remote handling systems that provide safe operation for PRIDE. A large argon cell has 17 work stations with several remote handling systems doing test remotely. The remote handling systems of PRIDE comprises 34 pairs of MSMs (Master Slave Manipulators), small and large equipment transfer lock systems, windows, cell lights, feed-through, etc., as shown in Figure 1. All cell equipment have to be carefully installed and maintained to keep the inert gas environment of cell.

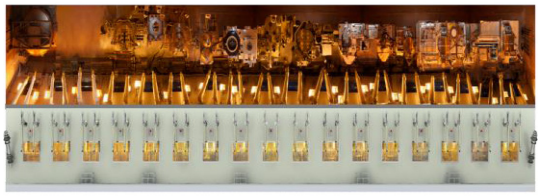

Fig. 1. Bird's eyes view of large inert gas filled cell.

A metal-halide lamp is an electrical lamp that produces light by an electric arc through a gaseous mixture. Because metal-halide lamp has high luminous efficacy and it can produce an intense white light, metal-halide lamp is used for general lighting purposes in a large inert gas cell. Metal-halide lamp requires electrical ballast and ignitor to generate a high-voltage pulse to start the arc inside a bulb. Figure 2 shows light systems and metal-halide bulbs installed in inert gas cell.

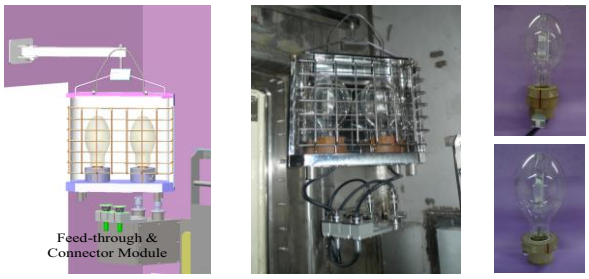

Fig. 2. Cell light systems installed in inert gas cell.

2. Modification of Cell light system

2.1 Two major causes of failure

In the metal-halide lamp used as an argon cell lighting device, 1,500 V or higher voltage is applied in the initial lighting process.

It is observed that the attenuation characteristics of high voltage during initial lighting process with a certain distance between the ballast and lamp are very important due to the characteristic of the ballast of the high voltage. When the ballast is turned on, the ballast starts the metal halide lamp with a high voltage. However, when the distance between the ballast and the lamp is long enough, the metal halide lamp does not start due to the rapid attenuation of the starting voltage. As a result, cell light system is subjected to various electrical problems as it continues to apply a high voltage until it is turned on.

And a short circuit or a discharge inside the cell is highly positive due to the characteristics of argon gas. Breaking of electrical insulation will happen when the applied voltage increases than the breakdown voltage. As a result, the gas will begin to conduct above the breakdown voltage. According to the Paschen's [1] curve

for air and argon, breakdown voltage of argon is less than air and breakdown voltage is increased in proportion to distance between of electrodes.

2.2 Design improvements

In order to fix those problems and improve safety, design improvements have been made on cell light system. In order to minimize the attenuation problem of initial high voltage generation of ignitor, electricity supply line concepts are changed so that the distance between the ballast and the metal-halide lamp is reduced to less than 10 m rather than the pre-existing 40 m. Figure 3 shows the diagrams of the ballast box (stabilizer, ground circuit breaker, and terminal block of metal halide lamp) have been installed at each cell light zone less than 10m from the lamp using beam clamp at the bottom of argon cell H-beam.

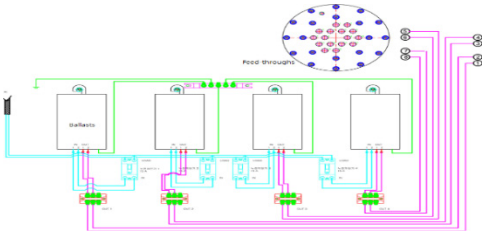

Fig. 3. Ballast box wiring diagram.

And to improve the electrical safety at high voltage of plug in inert argon gas filled cell, the plug design is modified so that the distance between the electrodes of plug is increased and the insulator is introduced inside the bulb socket. Figure 4 shows the plugs, plugs assembly with support guide and bulb sock assembly.

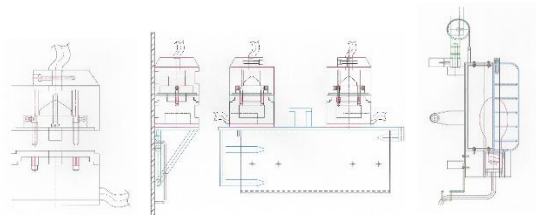

(a) (b) (c)

Fig. 4. Modification of cell light system (a) plug, (b) plugs assembly, (c) bulb socket assembly.

2.3 System installation and performance test

The feed-through has been designed and manufactured to ensure sufficient gas-tight performance, shown in figure 5. And the installation of cell light systems and feed-through while maintaining the inert atmosphere of cell has been finished by utilizing a maintenance glove box that can be attached on windows frame or feed-through frame, as shown in Figure 6.

Fig. 5. Gas-tightness test of feed-through.

Fig. 6. Maintenance glove box system.

3. Conclusions

In order to solve the cell light problems in large inert argon gas cell, modification of light system has been made. By changing the wiring concepts, the attenuation problem of initial high voltage generation of ignitor has been solved. And a short circuit or a discharge problems have been solved by changing the plugs design and reinforcing socket insulation.

REFERENCES

[1] https://en.wikipedia.org/wiki/Paschen%27s_law

Electrolytic Reduction of Nd_2O_3 With Ni Wire Electrode in Molten LiCl at 923 K

Dokyu Kang and Sungyeol Choi*
Korea Advanced Institute of Science and Technology, 291, Daehak-ro, Yuseong-gu, Daejeon, Republic of Korea
*sungyeolchoi@kaist.ac.kr

1. Introduction

During electrolytic reduction process of pyroprocessing, most of U and TRUs oxides are reduced to metal mixtures on the cathode, on the other hand, rare earth oxides shows reduction yields less than 50 % because of their thermodynamic stability in oxide form [1]. When the unreduced rare earth oxides are transferred to electrorefining process, they react with UCl_3 and oxidize it to UO_2 again. Therefore, in this paper, electrolytic reduction of Nd_2O_3 pellet using intermetallic formation with Ni was investigated to improve reduction efficiency of rare earth oxides [2].

2. Method

Nd_2O_3 (99.9% purity, Alfa Aesar) powder was put into a mold and pressed by a uniaxial press with 100 MPa of pressure and a cold isostatic press (CIP) with 300 MPa of pressure. The pressurized pellet was sintered at 500°C for 2 hours and then heated up to 1500°C and stayed for 2 hours.

The fabricated Nd_2O_3 pellet was tied with Ni wire and put into molten LiCl salt at 923 K. The counter electrode was W and Ag wire in LiCl-1 wt.% AgCl solution with mullite membrane was used as reference electrode. Three working electrodes, W wire, Ni wire, and Ni wire tying Nd_2O_3 pellet, were used in cyclic voltammetry. After the cyclic voltammetry, chronoamperometry was conducted with -2.0 V for 1 hours.

3. Preliminary Results

3.1 Cyclic voltammetry with W and Ni wire

The result of cyclic voltammetry with W wire is shown in Fig. 1. Only one sharp redox pair (Li^+/Li reaction) is observed at around -2.2 V.

On the other hand, the result of cyclic voltammetry with Ni wire shows two additional redox peaks except Li^+/Li reaction (Fig. 2). One redox peak appear between 0 V and 0.4 V which is related to Ni^{2+}/Ni reaction. The other redox peak appear around -1.6 V which is expected to be redox reaction of intermetallic compound among Li, Ni, and Nd.

3.2 Cyclic voltammetry and chronoamperometry with Ni & Nd_2O_3 wire

When Ni wire tying Nd_2O_3 pellet is used as working electrode, the result of cyclic voltammetry is shown in Fig. 3. The redox peak of Li^+/Li reaction broaden wire and the other redox peaks are increased, compared to the result of Ni wire. It can be explained by increased surface area of working electrode contacting Nd_2O_3.

The -2.0 V of potential, which is thought to be enough to reduce intermetallic compound was applied to the cathode and the current

measured during the chronoamperometry was shown in Fig. 3. During the first 20 minutes, the current keep decreasing up to about 19 mA and the value is maintained.

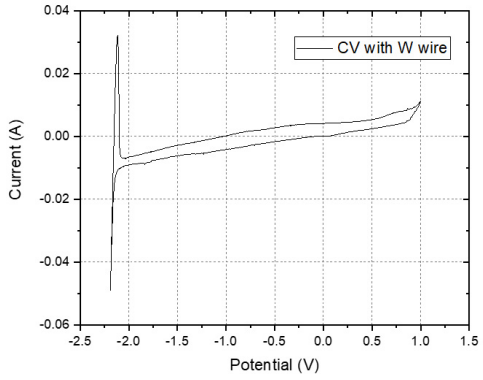

Fig. 1. Cyclic voltammetry with W wire from 1.0 V to -2.3 V.

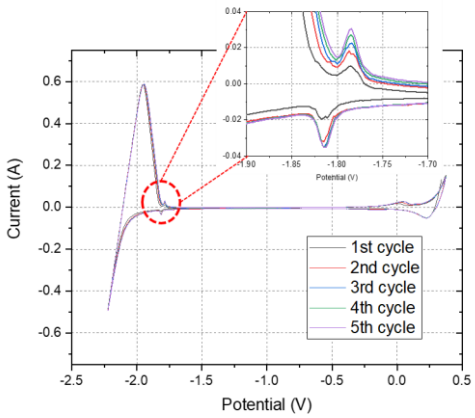

Fig. 2. Cyclic voltammetry with Ni wire from 0.4 V to -2.3 V.

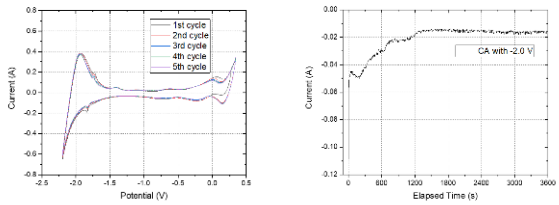

Fig. 3. (left) Cyclic voltammetry with Ni & Nd_2O_3 wire from 0.4 V to -2.3 V,
(right) chronoamperometry with -2.0 V.

4. Conclusion

In this paper, cyclic voltammetry of Nd_2O_3 with three different working electrodes, W wire, Ni wire, and Ni wire tying Nd_2O_3 pellet was conducted and electrolytic reduction has done with -2.0 V.

ACKNOWLEDGEMENT

This work was supported by the National Research Foundation of Korea (NRF) funded by the Ministry of Science and ICT (The grant number: NRF-2016M2B2B1945249).

REFERENCES

[1] S. Herrmann, S. Li, M. Simpson, Electrolytic Reduction of Spent Light Water Reactor Fuel Bench-Scale Experiment Results, Journal of Nuclear Science and Technology, 44 (2007) 361-367.

[2] H.S. Ji, H.Y. Ryu, E.-Y. Choi, S.-W. Cho, M.F. Simpson, S.M. Jeong, Preparation of NdNi5 using an electrochemical reduction of a NiO–Nd_2O_3 mixture in molten LiCl, Journal of Industrial and Engineering Chemistry, 24 (2015) 259-265.

Estimation of On-site SF Storage Capacity With and Without Centralized Interim Storage by Using GoldSim Code

Hong Jang*, Hyo On Nam, and Yong-Soo Hwang
Korea Atomic Energy Research Institute, 111, Daedeok-daero 989beon-gil, Yuseong-gu, Daejeon, Republic of Korea
*janghong@kaeri.re.kr

1. Introduction

In 2016, the government has announced the "Basic Plan on High-level Radioactive Waste Management" including a roadmap to secure a centralized interim storage facility and a permanent disposal facility [1]. However, current government has decided to reexamine the previous government's plan due to insufficient public engagement. Consequently, the interim storage facility expected to operate from 2036 becomes elusive. Therefore, each NPP (nuclear power plant) site might take a bigger responsibility to store and manage the accumulated SFs (spent fuels) until the operation of the interim storage facility or even the disposal facility. For this uncertain situation, it is necessary to identify the maximum capacity of storage to be added at each NPP site.

In this context, we estimated and compared the required capacities of on-site additional storages with and without the centralized interim storage, by using our GoldSim dynamic mass flow analysis code.

2. GoldSim code

We have developed a GoldSim code for quantitative analysis and evaluation of the domestic SF management scenario based on the dynamic mass flows. This GoldSim code includes an UI (user interface) to set several scenarios and check mass flow results for non-professional users. (Fig. 1, 2) In addition, the code can be distributed as a "Player mode" file, which can be opened and played without paid GoldSim licenses.

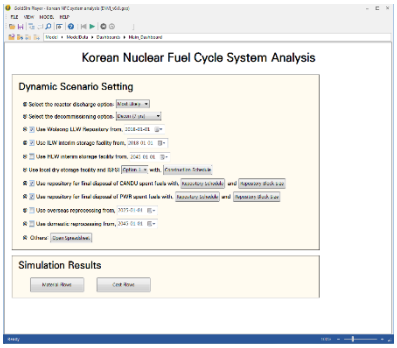

Fig. 1. GoldSim user interface for setting the scenario.

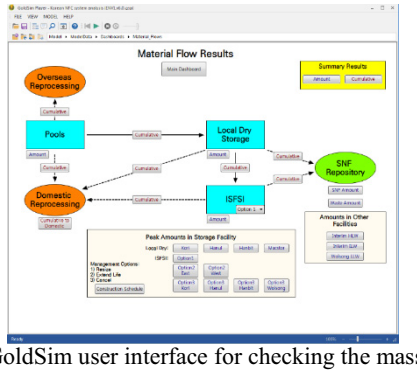

Fig. 2. GoldSim user interface for checking the mass flows.

Current version covers the domestic back-end nuclear fuel cycle ranged from the SF generation to disposal. In compliance with the latest government announcement [1], the domestic back-end nuclear fuel cycle is basically realized with three steps: on-site temporary storage, centralized interim storage, and permanent disposal. In addition to this, the oversea reprocessing and domestic dry processing are considered as options.

The code consists of many complicatedly linked transportation logics and facility mass flow models as "Container" elements (Fig. 3). Due to the space limit, any details about the logics and models are skipped in this paper.

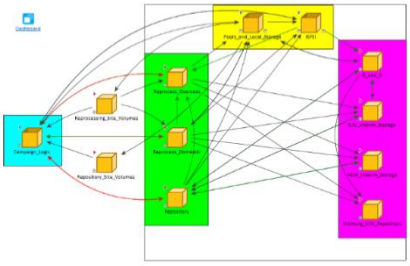

Fig. 3. Linkages of the transportation logics and facility mass flow models.

All input data related to the analysis are arranged in an Excel file and imported to GoldSim. The input data include the information about reactors, fuel cycle facilities, etc., and the user can modify any data through Excel.

3. On-site Storage Capacity Analysis

By using the GoldSim dynamic mass flow analysis code, a case study estimating the required capacities of on-site additional storages

with and without the centralized interim storage was performed. To do this, we set following two scenarios.

1) Scenario 1: on-site temporary storage > off-site centralized interim storage > disposal
2) Scenario 2: on-site interim storage > disposal

The NPP operation follows the "8th Basic Plan on Electricity Demand and Supply (2017~2031)" [2]. It assumes that the on-site additional storages start operation before the saturation of wet storages and the Saeul site shares one additional storage with the Kori site. For Scenario 1, the interim storage is assumed to open from 2036. And for both scenarios, the disposal facility is assumed to open from 2053.

We applied the future SF generation data estimated by the KEEI (Korea Energy Economics Institute). In this estimation, the PHWR SF generation is obtained from the correlation between the past PHWR SF generation and electricity generation. And the PWR SF generation was determined from the fuel reloading and maintenance plan of KHNP (Korea Hydro & Nuclear Power Co,. Ltd.).

After setting each scenario and running the code at the UI in Fig. 1, the dynamic mass flows are obtained as tables or plots at the UI in Fig. 2. To determine the required capacities of on-site additional storages, the peak amounts of the SFs in the storage should be analyzed. As an example, Fig. 4 shows the peak amounts in the additional storage at the Kori site for Scenario 1. In this case, the required capacity was determined as the value at 2035/12/31. And Fig. 5 shows the peak amounts in the additional storage at the Kori site for Scenario 2. In this case, the required capacity was determined as the maximum value of the peak amount curve. The required capacities for other sites were determined in the same way.

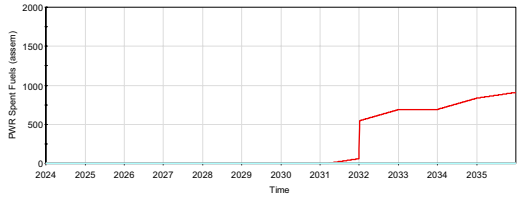

Fig. 4. Peak amounts in the additional storage at the Kori site for Scenario 1.

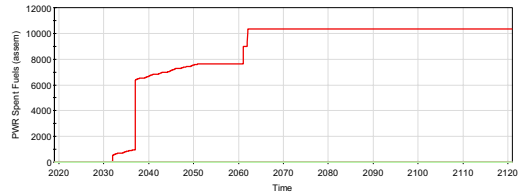

Fig. 5. Peak amounts in the additional storage at the Kori site for Scenario 2.

Table 1 summarizes the required storage capacities for two scenarios. Compared to Scenario 1, Kori, Hanul, Hanbit and Wolsong (PHWR) sites need about 11.3, 8.9, 9.9 and 2.9 times more capacities for Scenario 2, respectively. In case of Scenario 1, the additional storage at the Wolsong site for PWR SFs is not necessary.

Table 1. Required storage capacities for Scenario 1 and 2

Site	Scenario 1 [assembly]	Scenario 2 [assembly]
Kori	910	10,320
Hanul	1,530	13,650
Hanbit	1,120	11,090
Wolsong (PWR)	-	2,640
Wolsong (PHWR)	87,300	253,100
Interim (PWR)	33,730	-
Interim (PHWR)	165,800	-

For the storages for PHWR SFs, the summations of required capacities for Scenario 1 and 2 are equal. For PWR SFs, however, the summations seem different (37,290 vs. 37,700). The reason for this is different transportation logics from the interim storage to the disposal facility. Scenario 1 has only one way from the centralized interim storage to the disposal facility so the logic is simple. However, Scenario 2 has multiple ways from the on-site interim storages to the disposal facility so the logic becomes complicated.

4. Conclusion

In this study, the required capacities of on-site additional storages with and without the centralized interim storage were estimated. In the estimation, our GoldSim dynamic mass flow analysis code, which can realize various domestic back-end nuclear fuel cycle scenarios, was used. As a result, the required capacities of on-site additional storages without the centralized interim storage were higher than those with the centralized interim storage.

Ultimately, the required capacity of on-site additional storage results in the required site area and the cost. The required site area could be used as an evaluation criterion for the public acceptability. And the cost could be used as an evaluation criterion for the economic viability.

REFERENCES

[1] MOTIE, Basic Plan on High-level Radioactive Waste Management (Draft), MOTIE, Seoul, Korea, 2016.
[2] MOTIE, The 8th Basic Plan on Electricity Demand and Supply (2017~2031), MOTIE, Seoul, Korea, 2017.

Preliminary Performance Test of Drying Test System Using Inert Gas

Kyung-Wook Shin[1),*], Gyung-Sun Chae[1)], Geon-Hui Lee[1)], Jae-Seok Park[1)], K.S.Bang [2)], and S.H.Yu[2)]
[1)]SAE-AN ENGINEERING CORPORATION 184, Gasan digital 2-ro, Geumcheon-gu, Seoul, Republic of Korea
[2)]Korea Atomic Energy Research Institute, 111, Daedeok-daero 989beon-gil, Yuseong-gu, Daejeon, Republic of Korea
[*]and9211@sae-an.co.kr

1. Introduction

In order to solve the saturation problem of spent fuel pool, the domestic nuclear power plants are planning to operate dry storage in consideration of the ease of operation and expansion of spent fuel intermediate facilities. In order to change the storage of spent fuel from the wet storage to the dry storage, it is important to secure spent fuel transport and long-term dry storage safety. The process of transferring spent fuel from the wet storage to the dry storage facility is called a short-term loading operations and including drying, backfilling with inert gas, and transfer of the cask to dry storage facility. The removal of the residual water from dry storage container is important during the short-term loading operations, because the oxide and water contents have serious effects on the fuel cladding and structure, system and components of storage system.

2. Drying Test System and Results

2.1 General Information

The basic concept of a forced gas drying process is a dehydration method by blowing a heated and dry gas into a container loaded with spent fuel. The system configuration is shown in Fig. 1.

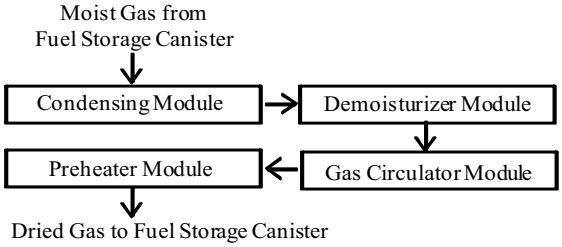

Fig. 1. Flow diagram of forced gas drying process.

The drying test system was designed and manufactured based on this basic concept. The preliminary performance test was performed after filling the drying test system loop with helium.

2.2 Flow Rate

In the drying process, the flow rate is one of the important operating parameters, and in the drying test system, the speed of the circulation pump and the control valve can be controlled. Table 1 shows the test results of flow rate a pressure of 0.1 MPa and setting the speed of the circulation pump to the minimum.

Table 1. Flow rate according to control valve adjustment

Inverter (20Hz)	Control Valve Open				
	10%	20%	30%	40%	50%
m^3/hr	24	26	30	35	37

2.3 Gas Temperature Rise

The heater heats up the cooled inert gas before entering the test container. In the drying test, the inert gas was set at 0.1 MPa and the

heater was set at 200 °C and the temperature need to be maintained 200 °C while circulating the inert gas. It takes time to reach a setting temperature since test starts. The result is shown in Fig. 2. The average flow rate was 36.7 m^3/hr.

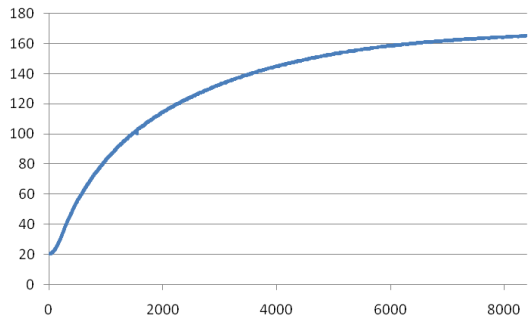

Fig. 2. Inert Gas Temperature with Heating Time.

2.4 Residual Water Removal

The residual water removal test was performed on two simple test containers of 65 L and 130 L. Measured amount of water was poured into the bottom of the container, and connected to a filling test container to form a closed loop. The residual water inside the container was indirectly measured by the change of a dew point and a relative humidity from outlet of the test container. The dryness criteria is less than 3 torr for 30 minutes for the vacuum drying. The dryness criteria of the forced gas circulation drying is equal to 3 torr of vapor pressure. It means that the dew point is less than -6 ° C inside container.

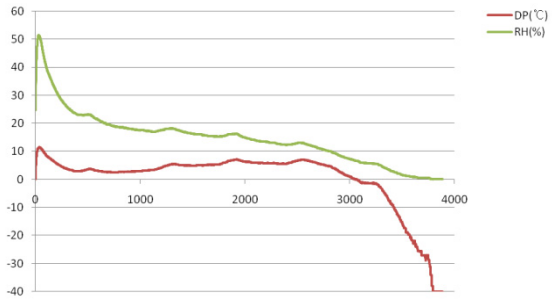

Fig. 3. Dew Point and Relative Humidity Changes (65L).

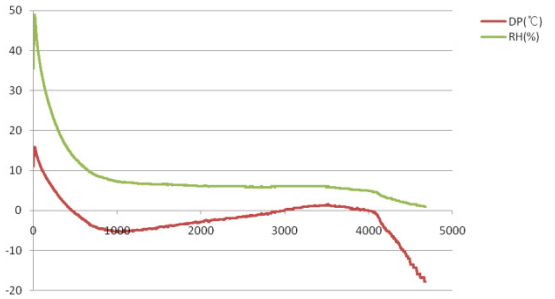

Fig. 4. Dew Point and Relative Humidity Changes (130L).

3. Conclusion

The drying test using drying test system will continue to establish various operating parameters and procedures for the drying process.

Acknowledgement

This work was financially supported by Korea Institute of Energy Technology Evaluation and Planning(KETEP) grant funded by Ministry of Trade, Industry & Energy (20181720201020).

REFERENCES

[1] ASTM C1553-16, “Standard Guide for Drying Behavior of Spent Nuclear Fuel[1]”, ASTM, 2016.

[2] Charles Patterson and etc.,“Dry Storage Handbook Fuel Performance in Dry Storage”A.N.T International, March 2015.

Analysis of Comparison Between Original and Quarter Scale Model of Transport Cask for Large Capacity SNF

Yun-young Yang*, Jongmin Lim, and Woo-seok Choi

Korea Atomic Energy Research Institute, 111, Daedeok-daero 989beon-gil, Yuseong-gu, Daejeon, Republic of Korea

*Yang0124@kaeri.re.kr

1. Introduction

The large capacity CANDU spent fuel transport cask is a container for transporting 360 bundles of spent fuel (SNF). The cask carrying the SNF can be used after obtaining a license, and the record must be submitted by performing a safety test of the cask to obtain the license. The cask safety test includes drop, rupture, fire and flood tests. Since there is no safety test facility for a 100 ton cask, a test is conducted using a reduced model considering similarity. This study analyzed the bolt stress and the carrier spacing by performing 0.3 m drop analysis on the circular cask and the quarter scale model.

2. Main Title

2.1 Model of Transport Cask for Large Capacity CANDU SNF

The 1/4 scale model of the CANDU SNF cask is an actual test model to check the normal operation of the carrier and is preparing for the drop test at the Korea Atomic Energy Research Institute.

The 1/4 scale model of the CANDU SNF cask is the actual test model to check the normal operation of the carrier. This model is currently being prepared for the drop test at the Korea Atomic Energy Research Institute. The 1/4 scale model is simplified in many parts for the purposes of testing. The inner basket and lower impact limiter were designed and manufactured in Lumped mass considering only weight and center of gravity.

The carrier and impact limiter consisted of very thin plates, even in a circular form. By creating scale model, they had thinner plates from 0.7 to 6 t.

The original model weighs 70 tones and the reduced model weighs about 1 ton.

2.2 Analysis Model and Condition

The figure 1 is the 1/4 scale finite element model of large capacity CANDU SNF cask. The quarter reduction model was modeled to its original size using the NMAP function in ABAQUS. In 0.3 m drop analysis of transport cask, ABAQUS/Explicit was used.[01]

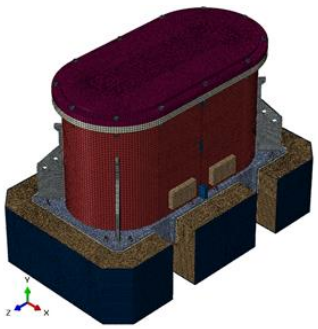

Fig. 1. Transport Cask FE Model.

Bolts are modeled only for bolts in the main position (Cask-Cask Lid, Inner Shell-Lumped mass, Impact Limiter-Cask Body), and other bolts are not modeled and attached by reflecting tie conditions. The material properties were the same for both original and quarter scale models. The flat part of the floor that was to be crashed gave all fix conditions.

Gravity acceleration was applied as the load condition. As the drop speed, 2.5 m/s was applied which corresponds to 0.3 m drop height under normal transport conditions.

2.3 Result

The 0.3 m drop analyzes were performed on original model and quarter scale model. And the following result were compared for both models.

The gap change in the quarter-scale model is compared with the gap change in the original model. For the comparison, the gap change value obtained from the quarter scale was multiplied by the factor value according to the geometrical similarity. Figure 2 and figure 3 show the change in distance from the top and bottom of the carrier to the housing, respectively.

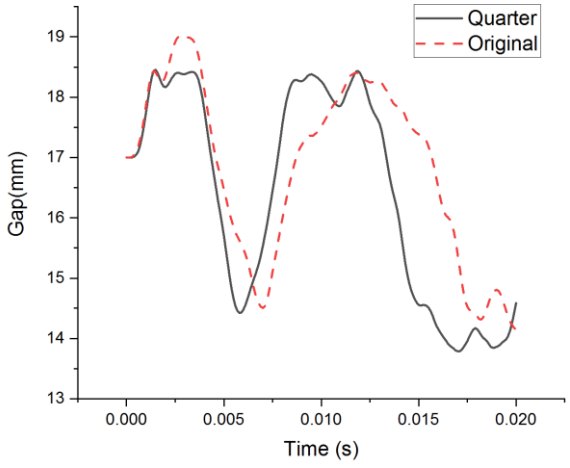

Fig. 2. Gap of Carrier Lower and Housing.

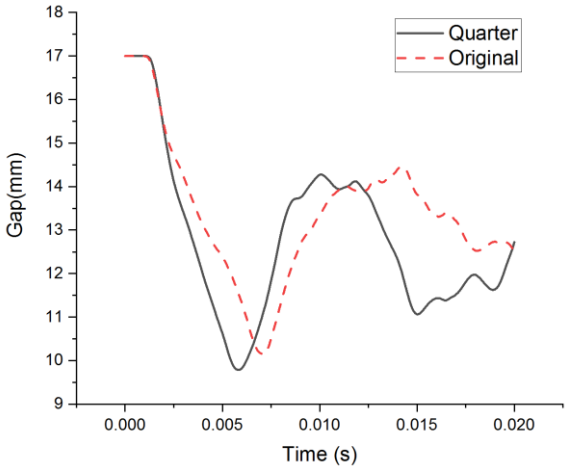

Fig. 3. Gap of Carrier upper and Housing.

3. Conclusion

The drop analysis were performed on two large capacity CANDU SNF cask models with the same conditions and geometrical similarity, and the result are compared.

As a result of comparison of the quarter scale model and the original model, the gap change between the top and bottom parts of the carrier and the housing showed a similar tendency, although the values did not exactly match.

The reason for not exact match is presumably because Carrier is the part receiving the impact derived from the secondary impact, not the part directly receiving the primary impact.

REFERENCES

[1] Nuclear Safety And Security Commission, “Regulation about packing and transportation of radioactive materials”, NSSC notice 2019-07, 2019.

Effect of Surrogate Elements on the Electrochemical Behavior and Deposit Characteristics of U in LiCl-KCl-UCl_3 Molten Salts

Chang Hwa Lee* and Sung-Jai Lee

Korea Atomic Energy Research Institute, 111, Daedeok-daero 989beon-gil, Yuseong-gu, Daejeon, Republic of Korea

*chwalee@kaeri.re.kr

1. Introduction

Pyroprocessing is considered as one of the promising nuclear fuel cycle technologies in which used nuclear fuel is electrochemically treated in a high-temperature molten salt to separate fission products, and U and TRU can be recovered and recycled [1]. In the pyroprocess developing at KAERI, used PWR fuels are supposed to be decladded at the pretreatment step and are converted into metallic forms at the electroreduction process in 650 °C LiCl-Li_2O molten salt. Highly pure metallic U is recovered from the converted fuel using electrorefining process in 500 °C LiCl-KCl-UCl_3 molten salt followed by recovering a U/TRU product from the remaining salt using a liquid Cd cathode in electrowining process.

In the U electrorefining process, several nuclides can be dissolved into the salt by chemical and electrochemical reactions with UCl_3. Consequently, such nuclides can be included as contaminants in the U deposit depending on the applied potential or the concentration of UCl_3, which could affect the purity of recovered U and the deposit characteristics [2].

In this study, we examine the effect of representative surrogate elements on the electrochemical behavior of U in LiCl-KCl-UCl_3 molten salts. In addition, morphological features of the U deposit will be observed in the presence of surrogate elements.

2. Experimental

An anhydrous LiCl-KCl eutectic salt (99.99 wt.%, Sigma-Aldrich) was used as the base electrolyte with the addition of 3.8 wt.% UCl_3 in this study. As representative surrogate elements, $FeCl_2$ that can be dissolved from anode baskets under a high overpotential condition, and $NdCl_3$, and $CeCl_3$ that can be chemically chlorinated by the reaction with UCl_3 in the salt were used in the concentration range between 0.1 wt% to 0.5 wt.%.

Electrochemical measurements in the LiCl-KCl-UCl_3 in the presence of each surrogate element were performed using potentiostat/galvanostat (BioLogics, SP-150) at an operation temperature of 500 °C under a quiescent condition. A tungsten (W) wire (1 mm diameter, 30 mm length) and U metal in a mesh basket were used as a working and counter electrode, respectively. The Ag/AgCl reference electrode where a Ag wire (1 mm diameter) was inserted in a closed-end pyrex tube partially filled with LiCl-KCl-1 mol% AgCl) was used.

The operating temperature was set to 500 °C and all the experiment was performed unde a quiescent condition in an Ar-purging glove box of which moisture and oxygen are controlled within a few ppm.

3. Results and Discussion

For a large scale electrorefining system, a current controlled electrorefining process is preferred due to a continuous increase in the current driven by a constant potential as the surface area increases with time. However, when the reduction yield or conversion ratio of U oxide is relatively low at the oxide-reduction process or U in the basket is depleted at the ER step, anode basket components can be dissolved into the salt and codeposited with U by a significant increase of overpotential at a constant operating current. Therefore, effect of the major corrosion element, $FeCl_2$, was examined using cyclic voltammetric measurement as shown in Fig. 1.

In the absence of $FeCl_2$, cathodic and anodic peaks associated with the reduction and oxidation of U are evident at -1.50 V and -1.33 V vs. AgCl, respectively. For 0.1 wt% $FeCl_2$, additional reduction and oxidation peaks appeared at -1.33 V and -1.13 V, respectively. Also a substantial peak shift of U oxidation to -1.28 V was found, which might be associated with the oxidation of U-Fe alloy compounds. The peak intensities associated with U-Fe alloys are gradually increased with the $FeCl_2$ concentration in the salt. In particular, a positive-feedback current response on the reverse scan at a higher potential region was evident for 0.25 wt.% and 0.5 wt.% $FeCl_2$.

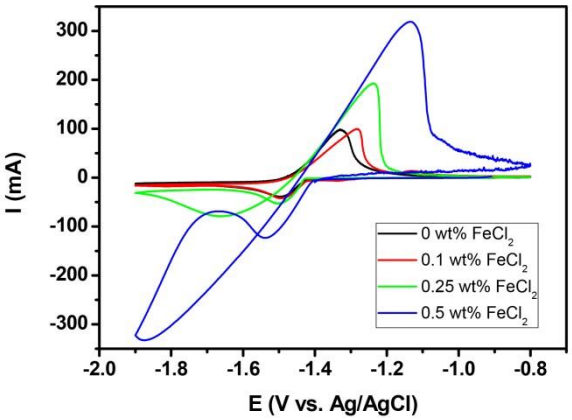

Fig. 1. CV curves in the presence of various concentrations of $FeCl_2$ in 500 °C LiCl-KCl-UCl_3 molten salt.

Additional CV measurement will be performed in the presence of various concentrations of $NdCl_3$ and $CeCl_3$, which could be produced by the following reactions with UCl_3 in the salt.

$$Nd + UCl_3 = NdCl_3 + U \ (\Delta G = -158.90 \text{ kJ}) \quad (1)$$

$$Ce + UCl_3 = CeCl_3 + U \ (\Delta G = -169.68 \text{ kJ}) \quad (2)$$

4. Conclusion

We examined the effect of representative surrogate elements on the electrochemical behavior of U in LiCl-KCl-UCl_3 molten salts. Effect of rare earth surrogates such as Nd and Ce will also be performed in further studies.

REFERENCES

[1] H. Lee et al., “Korean pyrochemical process R&D activities”, Energ. Proc., 7, 391 (2011).

[2] J.-H. Lee et al., “Electrodeposition of Characteristics of U in Molten LiCl-KCl Eutectic and its Salt Distillation Behavior, J. Nucl. Sci., 43, 263 (2006).

Experimental Studies for Two Operation Modes of Drying System of Pyroprocessing Automation Mockup

Jonghui Han* and Seungnam Yu
Korea Atomic Energy Research Institute, 111, Daedeok-daero 989beon-gil, Yuseong-gu, Daejeon, Republic of Korea
*jhan@kaeri.re.kr

1. Introduction

To control humidity level of dry rooms, the pyroprocessing automation mockup has equipped a drying system, which is composed of a dehumidifier, a dry air supply system, and an emergency dry air supply cabinet [1, 2]. This drying system of the mockup has five operation modes: 1) control mode for process operations including heating, 2) drying mode for rapid recovery of dry atmosphere, 3) sustaining mode for maintenance of dry atmosphere, 4) emergency mode for black-out, and 5) suspension mode. In normal situations, 1) to 3) modes can be selected according to the process activities inside the main dry room. The control and drying modes utilize the dehumidifier to control the atmosphere inside the room actively, and the sustaining mode supplies dry air into the dry room to maintain the humidity level with less energy consumption. In the emergency mode, dry air is supplied from a gas cabinet when black-out. In this paper, experimental studies are presented to determine the operation parameters in the drying mode and to evaluate performance of the emergency dry air supply system.

2. Operation conditions for Drying Mode of the Dehumidifier

2.1 Operation modes for the dehumidifier

In the control mode and drying mode, the drying system should make a dry atmosphere inside the room rapidly. In these two modes, the dehumidifier should be operated with proper parameters such as outer air intake rate, circulation flow rate, and exhaust flow rate. Additionally, in the control mode, the temperature of supply air should be controlled in order to restrict the increase of temperature and pressure within the room when process equipment is heated up.

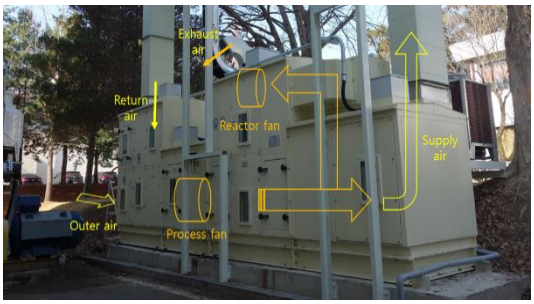

Fig. 1. Dehumidifier of drying system.

In this section, operation parameter studies for the drying mode were conducted.

2.2 Parameter studies for drying mode

In the drying model, the parameters for flow rate are important since the variation of temperature is not so big. Since the flow parameters can affect the pressure of the dry room, those are carefully selected so that the wall is not overly pressurized. The flow rate

related parameters of the dehumidifier are the damper openness of outer air (%, OA, same to the intake rate), speed (Hz) of process and reactor fan (P/F and R/F).

In this study, OA was set from 5 to 20%, P/F and R/F ranged from 40 to 55 Hz, respectively. From the study, the room pressure is in proportion to OA and P/F, but R/F is in inverse. Since the design pressure of the room is less than 15 mmH_2O, 10 %, 45 Hz and 40 Hz were selected for the parameters of the drying mode respectively. In this condition, the room pressure was about 3 mmH_2O and the moisture increased 10 ppm when a worker stayed in the room for 10 minutes.

Fig. 2. Dew point when a worker stays in dry room.

3. Experimental Studies of Drying System in Emergency mode

Fig. 3. Inside of the emergency dry air cabinet.

3.1 Emergency dry air supply system

In the emergency mode, dry air (less than 1 ppm moisture) is supplied from the emergency dry air supply cabinet. The cabinet can load up to 8 cylinders, so dry air can be supplied in 37 hours with a flow rate of 1 m^3/hour.

3.2 Experiments of the emergency mode

In the experiments, two cases were considered: without any supply and supply from the emergency cabinet. After 40 hours, the moisture level of the first case increased 1645 ppm, but that of the second increased about 1349 ppm. It should be noted that the outside humidity of the second was about 4 times higher than the first. Hence, the feasibility of the emergency cabinet was acceptable, but more studies for moisture level is required.

4. Conclusion

In this paper, experimental studies for two operation modes of the drying system of pyroprocessing automation mockup was performed. Further studies for the control mode is planned.

REFERENCES

[1] J. Han, et al., “Construction of Dry Room for Pyroprocessing Automation Verification Mock-up”, Proc. of the KRS 2018 Spring Conference, 2018.

[2] J. Han, et al., “Dry Atmosphere Test of Pyroprocess Automation Mockup Using Dried Air Supply and Drying System Operation”, Proc. of the KRS 2019 Spring Conference, 2019.

Preliminary Evaluation for Efficient Operation of Spent Fuel Pool Cooling System of Kori Unit 2 After Permanent Shutdown

Ha-eun Jeong and Seokyoung Ahn*

Pusan National University, 2, Busandaehak-ro 63beon-gil, Geumjeong-gu, Busan, Republic of Korea

*sahn@pusan.ac.kr

1. Introduction

Kori Unit 2 has started commercial operation in July 1983 (684 MWe, 2-loop, Westinghouse-type pressurized water reactor) and will be permanently shut down in July 2023. The spent fuels withdrawn from the reactor after permanent shutdown are required to be stored wet and cooled for at least five years in accordance with the provisions of the Nuclear Safety Commission for safety. After permanent shutdown, the decay heat from spent fuel decreases rapidly over time. The rapid decrease of decay heat reduces the cooling load and increases the bypass flow rate of component cooling(CC) water in the spent fuel pool(SFP) heat exchanger. And also increases the bypass flow rate of essential service water(ESW) in the CC heat exchanger. Therefore, SFP cooling system which designed to meet the decay heat of spent fuel generated during normal operation becomes inefficient because the heat load decreases tremendously after permanent shutdown. Accordingly, it can be found that nuclear power plants under permanent shutdown abroad operate small size cooling pumps or installed independent new cooling facilities to be suitable for the decreased heat load after shutdown. The purpose of this study is to calculate the heat load of the spent fuel in Kori Unit 2 after the permanent shutdown, and to derive the efficient operation plan of the SFP cooling system to meet the required heat load.

2. Hear load calculation after shutdown

2.1 Decay heat of SFP after shutdown

According to NUREG-800 BTP(Brach Technical Position) ASB 9-2 a decay heat equation was developed to calculate decay heat for nuclear fuel in long-term cooling in light water reactor. The total decay heat of nuclear fuel can be obtained by combining the heat of decay in the nuclear fission product of ^{235}U with the heat of decay produced by ^{239}U and ^{239}Np.

$$\frac{P}{P_0}(t_0,t_s)=(1+K)\left(\frac{1}{200}\sum_{n=1}^{n=11}A_n e^{-a_n t_s}\right)-\frac{P}{P_0}(\infty,t_0+t_s) \quad (1)$$

$$\frac{P(U-239)}{P_0}=2.28\times10^{-3}\times C\frac{\sigma_{25}}{\sigma_{f25}}(1-e^{-4.91\times10^{-4}t_i})(e^{-4.91\times10^{-4}t_s}) \quad (2)$$

$$\frac{P(Np-239)}{P_0}=2.17\times10^{-3}\times C\frac{\sigma_{25}}{\sigma_{f25}}1.007(1-e^{-3.41\times10^{-4}t_i})\times (e^{-3.41\times10^{-4}t_s})-0.007(1-e^{-4.91\times10^{-4}t_i})(e^{-4.91\times10^{-4}t_s}) \quad (3)$$

In consideration of the decay heat decrease of spent fuel drawn out for each cycle as time passes, the decay heat of the spent fuel in the SFP after permanent shutdown can be obtained by using spreadsheet type calculation.

2.2 Intermittent operation of SFP cooling pump due to decrease of decay heat after permanent shutdown

In the intermittent operation, the pump start cycle also decreases as the decay heat decreases after the permanent shutdown period elapses. The decay heat of spent fuel after permanent shutdown is can be assumed as shown in the table below.

Table 1. Temperature increasing rate when SFP cooling pump is stopped

Time After Shutdown	Temperature increasing time when SFP cooling pump stopped(10-40°C)[hr]	Decay heat	
		[MBtu/hr]	[kcal/hr]
1year	39.7	3	755490
2years	59.56	2	503660
4years	99.27	1.2	302196
5years	119.12	1	251830
7years	132.36	0.9	226647

2.3 Make small capacity of SFP cooling equipment (CC,ESWpump)

The ratio of cooling capacity to decrease of decay heat with time after permanent shutdown is shown in the table below. Since this improvement takes a design change, so it would be advantageous in terms of economic feasibility and constructability if it is promoted after exemption of safety level first.

Table 2. Required cooling capacity after permanent shutdown

Time After Shutdown	Required cooling for design[%]		Decay heat	
	CC	ESW	[MBtu/hr]	[kcal/hr]
1year	15.48	15.48	3	755490
2years	13.65	13.65	2	503660
4years	12.19	12.19	1.2	302196
5years	11.82	11.82	1	251830
7years	11.64	11.64	0.9	226647

2.4 Change of cooling method (water to air cooling)

Changing the water cooling system to air-cooling will be a very efficient way, since the CC and ESW systems are not used. In order to change the heat source by the air-cooling method, the preconditions may needed due to the termination of operation and design change of other equipments using the existing equipment which uses water as the coolant is needed. First, considering the economic feasibility and construction, it is necessary to release the safety grade of SFP cooling facilities. And the liquid waste evaporator and gas waste compressor should be terminated. If the instrument air compressor needs to be operated continuously, the cooling source should be switched to raw water.

3. Conclusion

After permanent shutdown, the spent fuel of Kori Unit 2 will be stored in the-SFP and the decay heat of the spent fuel will decrease rapidly with time and cooling load will also decrease afterward. Therefore, using the SFP, CC, ESW after shutdown without any modification can be inefficient so alteration in the cooling and cooling performance adjustment can be economically beneficial.

The efficient SFP cooling system for Kori Unit 2 is proposed by analyzing the operations of SFP cooling system applications. First case is an installation of small capacitance of seawater pump like in Kewaunee nuclear power plant in the U.S. Second case is the intermittent operation of SFP cooling pump like in Hanbit nuclear power plant. Finally the third case is independent air cooling SFP system of Maine Yankee nuclear power plant in the U.S.

REFERENCES

[1] Kyoung-young Ha, "Study on temperature change of spent fuel pool after permanent shutdown of Kori NPP-1", Department of Nuclear Engineering, Pusan National University, 2018, Feb.

[2] US NRC 1981 "NUREG-800 9.2.5 ULTIMATE Heat Sink".

[3] Public Released FSAR KORI unit2, KHNP.

[4] Junki Baik /Chang-Lak Kim, Review for Applying Spent Fuel Pool Island (SFPI) during Decommissioning in Korea, 2015, vol.13, no.2, pp. 163-169 (7 pages), KINGS.

Model Development for Estimating Electrochemical Parameters in a Rotating Disk Electrode System

Kwang-Rag Kim*, Sung-Ki Kim, and Hyo-On Nam
Korea Atomic Energy Research Institute, 111, Daedeok-daero 989beon-gil, Yuseong-gu, Daejeon, Republic of Korea
*krkim1@kaeri.re.kr

1. Introduction

Pyrochemical processing for the treatment of spent nuclear fuel consists of a series of molten-salt electrochemical reactors as the main processes [1]. This process typically involves the dissolution of spent fuel into a molten-salt media and selective deposition of actinides on the electrode in an electrochemical cell.

The rotating disk electrode (RDE) hydrodynamic technique has been used to provide the important kinetic information concerning electrodeposition system. The RDE in laboratory-scale reactors provide well-defined electrolyte hydrodynamics and support fundamental research into material deposition characteristics. This system has found a wide variety of applications in the investigation for the commercial-scaled system design. This investigation is of industrial importance and allows modeling and quantification of electrode reaction rates, when the process limited by the rate of mass transfer.

In this study, a CFD (Computational Fluid Dynamics) modeling approach was used and simulated to compare with a well-known diffusion-limited correlation [2] for RDE in the molten-salt electrodeposition system.

2. Theory

2.1 Mass transport correlation

A RDE is a polished disc surrounded by an insulating sheath of substantially larger diameter. The structure is rotated about an axis perpendicular to the surface of the disc electrode. The RDE system is constructed from a disc of electrode material imbedded in a rod of insulating material. The electrode is attached to a motor and rotated at a certain frequency. This movement of rotation leads to well-defined solution flow pattern, as can be seen Fig. 1.

Levich [2] deduced an expression relating the diffusion layer thickness (δ_{diff}, cm) with experimental variables such as the diffusion coefficient (D_{i}, cm^2/s), kinematic viscosity (ν, cm^2/s) and the rotation speed of the electrode (ω, rad/s):

$$\delta_{diff} = 1.61 \times D_i^{1/3} \times \nu^{1/6} \times \omega^{-1/2} \qquad (1)$$

2.2 CFD model

The mass transfer rate (j_w) per unit area from the bulk electrolyte to the cathode surface may be related with mass transfer coefficient (k_i) and described as:

$$j_w = -D_i \frac{\partial C}{\partial r}\Big|_w = -k_i(C_{bulk} - C_w) \qquad (2)$$

The first term indicates that the concentration gradient in the normal direction can be evaluated at the electrode surface in the CFD platform. Three dimensional CFD simulations are used to solve the local concentration profiles near the electrode surface with electrolyte turbulence model. The local diffusion boundary layer thickness (δ_x) can be obtained from the precedent mass flux equation:

$$\delta_x = \frac{C_{bulk} - C_w}{\frac{\partial C}{\partial r}\Big|_w} \qquad (3)$$

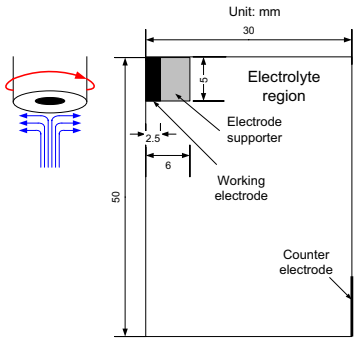

Fig. 1. RDE and schematics of the solution flow towards its surface (left) and flow of the solution near its surface (right). Black area shows the conductive electrode material, and grey area is insulation.

3. Results and discussion

Fig. 2 shows the typical electrolyte flow pattern of the RDE system. The stream lines were tracked in accordance by employing the various rotation speeds. When the electrode is rotated, it pumps electroactive ionic solution from the bulk of the electrolyte onto the disc. There is a thin layer in which only diffusion takes place with no convection. Concentration profiles in this layer were obtained by varying the rotation speed of the RDE.

The diffusion layer thicknesses achieved from the local concentration profiles were almost same across the whole surface of the disc. These values were in good agreement with the Levich correlation.

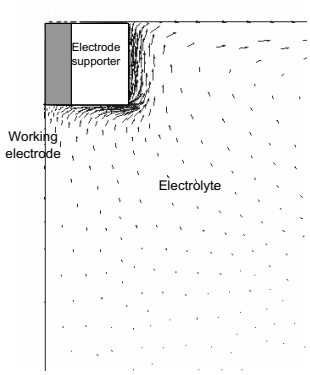

Fig. 2. Velocity vectors of solution flow towards RDE surface.

4. Conclusion

Simulations demonstrated an approach of the coupled solution of electrochemical and mass transport equation in the cell employing a rotating disk electrode. The model implemented here can be useful to improve the accuracy of measurement.

REFERENCES

[1] OECD NEA, “Spent Nuclear Fuel Reprocessing Flowsheet,” NEA/NSC/WPFC/DOC, Paris, 15 (2012).

[2] V. G. Levich, Physicochemical Hydrodynamics, Prentice-Hall, New York, 1962.

Consideration on the Conversion Characteristic of Uranium Ions to Metal in the LiCl-KCl Salt With the Aid of Yttrium Metal

Joon-Bo Shim*, Dal-Sung Yoon, and Sung-Jai Lee
Korea Atomic Energy Research Institute, 111, Daedeok-daero 989beon-gil, Yuseong-gu, Daejeon, Republic of Korea
*njbshim@kaeri.re.kr

1. Introduction

KAERI has developed unique drawdown method to recover most of the actinide elements remained in a spent molten salt by introducing the rare earth metal. [1, 2] The previous experiments on this drawdown method in the uranium chloride salt have shown remarkable results from the viewpoint of minimizing actinides concentration in a molten salt. In this presentation, we investigated and focused on the conversion characteristic of uranium ions to metal based on the bench scale test results conducted using the yttrium metal in a simulated LiCl-KCl salt.

2. Experimental

A simulated LiCl-KCl molten salt mixture containing the uranium and three rare earth metal such as Nd, Ce and La chlorides was prepared in an alumina crucible. For an example, a simulated salt mixture (400 g) was composed of the U (1.16 wt%), Nd (1.43 wt%), Ce (0.96 wt%) and La (0.57 wt%) metal chlorides for a bench scale test. For another test we had used a little changed composition of the simulated salt. One or two yttrium metal rods were introduced into a simulated LiCl-KCl salt contained in the crucible with stirring the salt at 40~70 rpm. The ICP quantitative chemical analysis of the salt samples and the on-line cyclic voltammetry (CV) monitoring of a salt phase were carried out to examine the changes of the salt composition.

3. Results and discussion

The conversion reaction of uranium ions to metal by introducing the yttrium (Y) metal into a molten salt is as follows.

$$Y(s) + UCl_3 + REsCl_3 \rightarrow U(s) + YCl_3 + REsCl_3 \quad (1)$$

The uranium tri chlorides (UCl_3) converts to the yttrium tri chlorides (YCl_3) because of the difference of the Gibbs free energy of formation for the metal chloride. The Gibbs free energy of YCl_3 is larger than that of UCl_3. The stable formation of YCl_3 gives rise to the decomposition of unstable UCl_3. Therefore, the uranium ions are changed into the uranium metals in a salt medium.

In general, we can imagine that the metal ions in a liquid medium can be changed into a very fine metal powders at nanoscale size with an aid of the chemical potential. So, the fine metal powders formed can be distributed into a liquid medium. The purpose of the drawdown in the pyroprocessing process is to recover all the

actinide elements and to reduce the concentration of the actinides at a minimum level in a salt medium.

The bench scale test results have shown that the concentration of the uranium ions contained in a salt mixture decreased from a value more than one weight percent to a very low value due to the chemical reduction of uranium ions according to the chemical potential provided by the yttrium metal in a salt. After 90 minutes the concentrations of uranium in two salt samples decreased to a very low value less than 50 ppm. [2] Also, the concentration of uranium in a salt of the other test's ICP analysis results was measured a value less than 10 ppm. [1]

The uranium ions in a salt were converted to U metals which covered on the surface of basket containing two yttrium rods. These uranium metal particles were easily detached from the basket and recovered into the collection crucible by an up-down vibrating force. After removing the covered uranium particles, the mesh basket was returned to its clean original shape. The color of the salt became white after the drawdown test.

Not only the surface of yttrium rod, but also the stainless steel material basket or wires which were electrically connected to the yttrium rod were covered with the aggregated uranium particles. In the molten salt there are various forces to aggregate the very fine metal powders, such as Van der Waals, gravity, electrical, electrochemical forces etc. We could understand the phenomenon that the uranium particles covered on the surface of stainless steel were formed due to the electrochemical forces generated from the Galvanic effect.

4. Conclusions

The phenomenon that the uranium particles aggregated on the surface of the yttrium rod and stainless steel was clarified.

The concentration of uranium ions in a simulated salt can be decreased to a very low value less than 50 ppm in a salt with an aid of the yttrium metal. The converted uranium metals which were formed due to the electrochemical forces have covered on the surface of the yttrium rod and connected stainless steel material.

ACKNOWLEDGEMENT

This work was supported by a National Research Foundation of Korea (NRF) grant funded by the Korean government (MSIP) (No. 2017M2A8A5015079).

REFERENCES

[1] J. B. SHIM, et al., "Recovery of the Actinides and Content Analysis in the Recovered Product Using Rare Earth Metal Equipped in a Stirring Mesh Basket from a Simulated LiCl-KCl Molten Salt," Proceedings of the Korean Radioactive Waste Society SPRING 2016, p.0240 (2016).

[2] J. B. SHIM, et al., "Collection of Uranium Metal from the Salt Mixture Using Yttrium Metal," Proceedings of the Korean Radioactive Waste Society SPRING 2019, p.0116 (2019).

Economics of a Nuclear Fuel Cycle Under Circumstances of the Energy Transition

Hyo On Nam* and Hong Jang
Korea Atomic Energy Research Institute, 111, Daedeok-daero 989beon-gil, Yuseong-gu, Daejeon, Republic of Korea
*hnam@kaeri.re.kr

1. Introduction

In December 2017, the 8th Basic Plan for Long-term Electricity (BPLE) Supply and Demand (2017-2031) was announced [1]. It is pursuing energy transition by decreasing a share of nuclear and coal, and increasing share of natural gas and renewables. It also includes phase out the use of nuclear energy, because public concerns on the safety of nuclear power plants(NPP) grows after the accident in Fukushima and several earthquakes near Gyeongju and Pohang prefecture. Based on the energy transition policy, life extension of operating NPP is not allowed and no new NPP is going to be constructed.

In September 2019, 21 pressurized water reactors (PWRs) and three pressurized heavy water reactors (PHWRs) are in operation including Shin-Kori unit 4 which recently starts commercial operation. Kori unit 1 was closed in June 2017 after 40 years of service and is waiting to be decommissioned. Wolsong unit 1 is currently taken offline and to be permanently shut down due to the uncertain economic viability of it continued operation.

In this article, a proper method to evaluate the economics of various nuclear fuel cycles under circumstances of energy transition (or phase-out of the nuclear power) is discussed.

2. Deployment of Energy Systems under Circumstances of the Energy Transition

In Korea, researches on pyroprocessing technology in combination of sodium-cooled fast reactor (SFR) technology have been pursued as one of the options to manage the spent fuel by partitioning and burning out toxic transuranic (TRU) elements in the spent fuels. Under circumstances of the Energy Transition policy, it is suggested that several units of burner type SFRs is to be deployed to burn out the TRUs in the PWR spent fuels, and it helps to decrease the toxicity of its inventory and the waste volume.

Based on the 8th BPLE, no new current NPP systems including PWR and PHWR(CANDU) is constructed. However, this study considers special scenario which assumes deployment of several TRU-burner energy systems for the management of spent fuels from PWRs as shown in Fig. 1.

The purpose of the TRU-burner is not the generation of electricity unlike the typical NPP systems under the nuclear phase out policy. In

the economic point of view, then, what is a proper way of assessing the economics of this special nuclear fuel cycle systems?

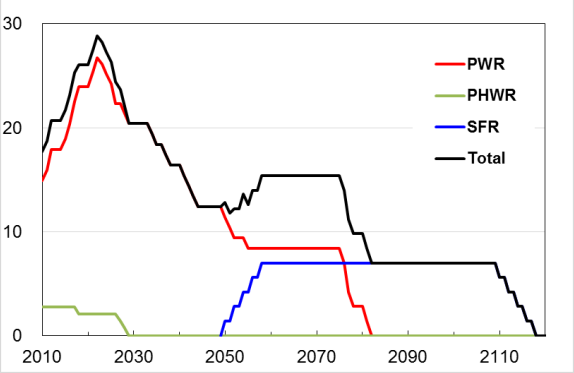

Fig. 1. Assumed capacity of nuclear energy systems.

3. Economics of a Nuclear Fuel Cycle under Circumstances of the Energy Transition

In the study, the economics of TRU-burner scenario (TB) is compared to the once-through (OT) scenario. The overnight cost, net present value (NPV), and levelized unit cost of electricity (LCOE) for two scenarios and the amount of electricity generation is analyzed with a discount rate of 1.5% considering uncertainties in the input unit cost data as shown in Table 1.

Table 1. Comparison of economic metrics between two scenarios

	OT scenario	TB scenario
Overnight Cost (B$)	157	253
NPV (B$)	110	157
Electricity Generation (TWh)	6,524	9,651
LCOE (mills/kWh)	22.72	25.96

It shows a large difference between two scenarios in terms of the amount of an energy generation as well as the expenditure due to the large amount of capital and operation cost of the TRU-burners.

Although the LCOE is a widely used metric to compare economics between different energy generation sources, it can be controversial when the LCOE is used because the purpose of the TRU-burner is not the generation of electricity. Therefore, overnight cost and NPV can be used as an alternative metrics to compare two scenarios. However, in this case, the revenue of the excess electricity generation should be quantified.

4. Conclusion

In this article, special scenario which is assuming deployment of new nuclear energy systems is considered for the nuclear fuel cycle system analysis even under the energy transition policy.

The LCOE should not be the only metric to be used in the special circumstances such as the energy transition, because there is a large difference between two scenarios in terms of the energy generation as well as the expenditure due to the large amount of capital and operation cost.

REFERENCES

[1] Ministry of Trade, Industry and Energy, the 8th basic plan for long-term electricity supply and demand (2017-2031), (2017).

Surface Treatment of Zirconium Contamination Layer Using Laser Ablation

Seong-Jun Ha[a,b], Ki-Hwan Kim[b], Jeong-Yong Park[b], Seoung-Woo Kuk[b], and Young-Kook Lee[a,*]

[a]Yonsei University, 50, Yonsei-ro, Seodaemun-gu, Seoul, Republic of Korea

[b]Korea Atomic Energy Research Institute, 111, Daedeok-daero 989beon-gil, Yuseong-gu, Daejeon, Republic of Korea

[*]yklee@yonsei.ac.kr

1. Introduction

The metallic fuel slugs have been developed as a nuclear fuel for a Sodium-cooled Fast Reactor (SFR). In general, the U-10wt.%Zr metallic fuel is fabricated using an injection casting method having the advantage of remote control. But a considerable amount of metallic fuel scraps has been formed such as the melt residue and the butts of the metallic fuel slugs as a uranium-mixture waste after casting. For this reason, it is necessary to develop the technology which is recycling fabrication of the metallic fuel scrap waste to maximize the utilization of expensive fuel materials and minimize uranium-mixture waste. The objective of this study is to evaluate the feasibility of recycling U-10wt.%Zr metallic fuel scraps using laser ablation technology. The zirconium contamination layer was formed on the surface by carburizing the zirconium plate as a surrogate material to simulate the reactivity with graphite crucible and zirconium. And the surface treatment was performed using laser ablation according to scanning pass. The zirconium plate treated using laser ablation was analyzed for surface topography and structure through Scanning electron microscopy (SEM) to evaluate the feasibility of recycling metallic fuel scrap.

2. Methods and Results

The zirconium plate was prepared for the surrogate material. The contamination layer of the zirconium plate was formed by carburizing in Air atmosphere at 920°C. A cleanLASER equipment was used for all laser ablation treatments. The laser pattern was Gaussian profile with an intensity level of 150MW/cm^2 and a frequency of 110 kHz. Since the laser ablation rate is proportional to the laser scanning pass, five scanning pass were selected such as 1, 2, 3, 7, and 30 times to treat the zirconium plate, as shown in Fig. 1.

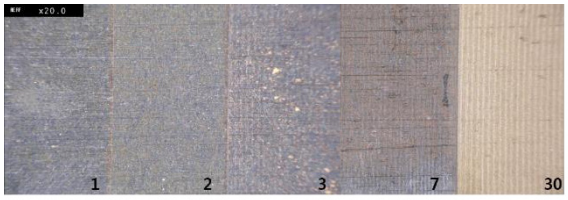

Fig. 1. Stereoscope image of treated zirconium plate according to scanning pass.

A scanning electron microscope (SEM) was used to investigate the effect of laser ablation treatment on the surface topography of zirconium plate. Fig. 2 presents SEM images of treated zirconium surfaces. It can be observed

that laser ablation at the low scanning pass (i.e., 1time) exhibited little influence on the surface topography of the zirconium contamination layer. Moreover, it was found that the surface layer seemed to be melted and continued increases of scanning pass created a significantly rougher surface.

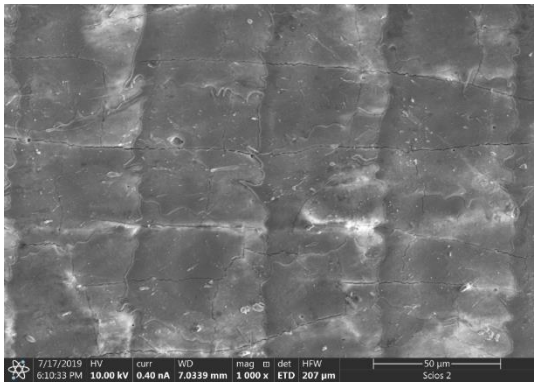

(a)

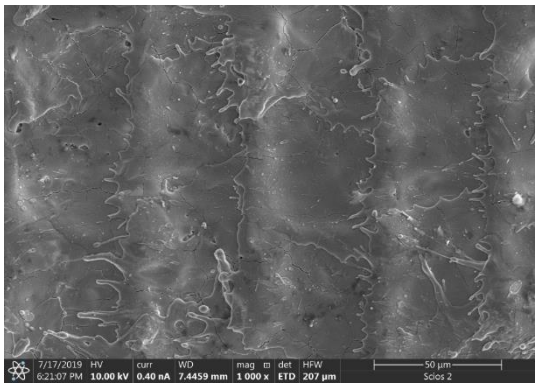

(b)

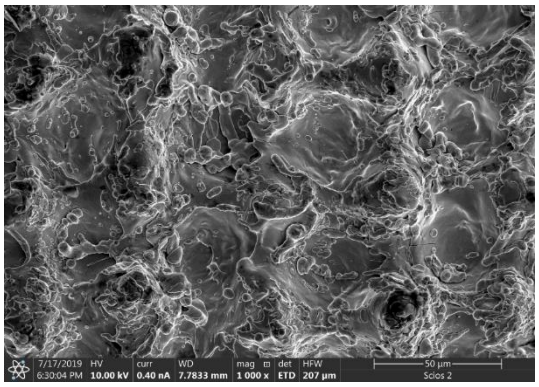

(c)

Fig. 2. Effect of laser ablation treatment on the surface topography; (a) 1, (b) 3 and (b) 30 times.

3. Conclusion

In this work, experiments were conducted to understand the effect of laser ablation treatment on the performance of the removing zirconium contamination layer. The surface of zirconium contamination layer was treated using laser ablation, and laser ablation rate was proportional to the scanning pass. The surface treatment at high scanning pass increased the surface roughness, which is assumed to be a contributing factor to the performance of laser ablation. Hence, the results of this study confirmed the feasibility of recycling fuel scraps.

REFERENCES

[1] S.J. Ha, K.H. Kim, J.Y. Park, and S.I. Hong "Characterization of reused U-10Zr heel residue containing rare-earth elements through surface treatment", Journal of Radioanalytical and Nuclear Chemistry, 316 (2018), 1157-1163.

Radiation Shielding Evaluation for Large Capacity CANDU Spent Fuel Transportation Cask

Jae-Hun Ko*, Dong-Gyu Lee, and In-Soo Jung
Korea Nuclear Engineering & Service, 798-1, Yuseong-daero, Yuseong-gu, Daejeon, Republic of Korea
*kojh4@kones21.com

1. Introduction

Spent fuels generated from Wolsong NPP, which is a CANDU reactor, is temporarily stored in concrete silos and MACSTOR/KN-400 storage modules to secure spent fuel storage capacity. In addition, cask for transporting 120 spent fuels (two baskets transport, one basket : 60 SNFs) to a temporary storage facility on the same site is used. The government is considering disposing of high-level radioactive waste from 2050 and expects to operate a centralized spent nuclear fuel storage facility from 2035[1].

Therefore, instead of 120 spent fuels transport cask currently in operation, a large capacity (6 baskets transport, 360 SNFs) spent fuel transport cask is being developed in which the transport efficiency is increased and the transport cost is reduced. In this study, the radiation safety evaluation of the conceptual model was performed under normal transport condition.

2. Shielding Evaluation of IP-2 container

2.1 Dose Rates Criteria

Under the Normal transport condition, the dose rate at the surface of the spent fuel transport cask is limited to 2mSv/h and one at any point 2m away from the container is limited to 0.1mSv/h.

2.2 Source Terms

The design basis fuel of the large capacity transport cask for the CANDU spent fuel is the same as the design basis fuel for the transport / storage system operating in Wolsong NPP. The characteristics of design basis fuel are as follows :

- Burnup : 7,800MWD/MTU
- Min. cooling time : 6yr
- Enrichment of U-235 : Natural Uranium

The source terms for the design basis fuel were used ORIGEN-ARP module of SCALE6.1 computer code [2]. The spectra of gamma rays and neutrons emitted from the active fuel region are shown Figure 1.

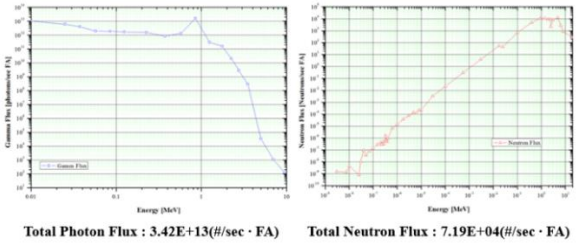

Fig. 1. Gamma & Neutron Spectra for DBF.

2.3 Analysis Model

The main body of the cask is made of steel (SUS 304 & C.S), and shock absorbers are attached to the upper and lower parts to ensure structural safety. The overall shape is a unitary structure that structurally combines two separate cylindrical forged carbon steel bodies and has an interior space. Figure 2 shows a conceptual drawing of a spent fuel transport cask under development. A shielding analysis model for normal transport conditions that applied the dimensions of the conceptual model is shown in Figure 3.

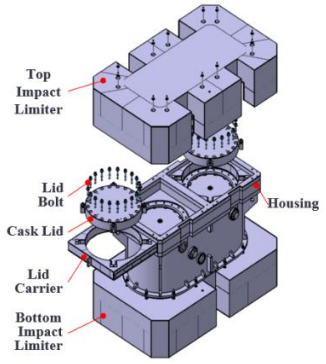

Fig. 2. Conceptual drawing of large capacity transport cask.

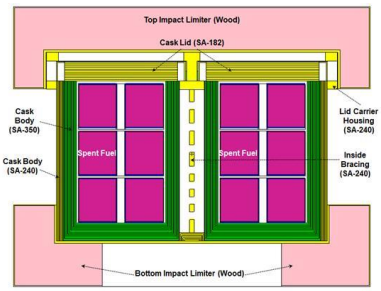

Fig. 3. Shielding Evaluation Model.

2.4 Shielding Evaluation

MCNP6 computer code using the three-dimensional Monte Carlo method has been used to calculate dose rates at the various desired locations of the spent fuel transport cask [3]. The flux-to-dose conversion factor was added to the input data so that it could be expressed as the dose rate at the locations of interest. The dose conversion factors used in this calculation was taken from ICRP-74(1996) [4].

3. Shielding Evaluation Results

In this MCNP calculation, 11 interested regions were placed at the external surface and 2 m position of the transport cask, respectively. Table 1 shows the maximum dose rates at all positions and Figure 4 shows dose rates at calculated points for the side of the spent fuel transport cask. Relative errors of these detectors were 0.01~0.02.

Table 1. Dose Rates Results (Normal Condition)

[Unit : mSv/h]

Cal. Point	External Surface		2m from the Surface	
	Results	Limit	Results	Limit
Top	0.062	2.0	0.012	0.1
Side	0.296		0.065	
Bottom	0.330		0.038	

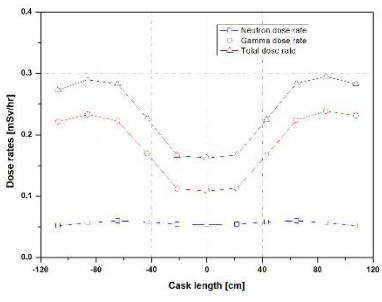

(a) Dose rates at External Side Surface of cask

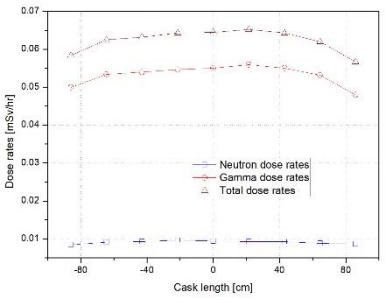

(b) Dose rates at 2m form the Side Surface of cask

Fig. 4. Results of Shielding Evaluation.

4. Conclusion

As a result of evaluation of the maximum radiation dose rate at external (surface and 2m away from surface) of the cask, it was found that the dose rate limitation requirement was satisfied under normal transport conditions. This study is expected to help the approach of radiological safety evaluation in the detailed design of large-capacity spent fuel transport cask and the design of storage facility and system for spent fuel.

ACKNOWLEDGEMENT

This work was supported by the Korea Institute of Energy Technology Evaluation and Planning (KETEP) generated financial resource from the MOTIE, Republic of Korea. (No.20171710201750)

REFERENCES

[1] Ministry of Trade and Industry, "High-Level Radioactive Waste Management Basic Plan (draft)", 2016.05.

[2] ORNL/TM-2005/39, Version 6.1, "Origen-Arp : Automatic Rapid Processing for Spent Fuel Depletion, Decay, and Source Term Analysis", June 2011.

[3] Los Alamos National Laboratory, MCNP –A General Monte Carlo N particle Transport Code, Ver.5, Release 1.40 (2005).

[4] ICRP, Conversion Coefficients for Use in Radiological Protection Against External Radiation, ICRP-74 (1996).

Criticality Analysis for OASIS-24DFC Cask Capable of Loading Damaged Fuel Assemblies

Tae Kyung Lee*, Yong IL Kim, Joon Gi Ahn, and Gyu Cheon Lee
KEPCO Engineering & Construction Company, 111, Daedeok-daero 989beon-gil, Yuseong-gu, Daejeon, Republic of Korea
*tklee85@kepco-enc.com

1. Introduction

KEPCO E&C has already developed OASIS-32D cask model for dual purpose (transport and storage) to load 32 intact fuel assemblies and completed safety analyses for mechanical structure, heating, shielding and criticality. On the other hand, OASIS-24DFC model (Figure 1) which is designed to load 4 damaged and 20 intact fuel assemblies uses the same outer size of the canister for OASIS-32D but different inner basket structure. Four cells for the damaged fuel assemblies are separately located in each quadrant of the X-Y plane of the canister and also adaptable to load the intact fuel assemblies. In this study, criticality safety analysis on OASIS-24DFC is performed.

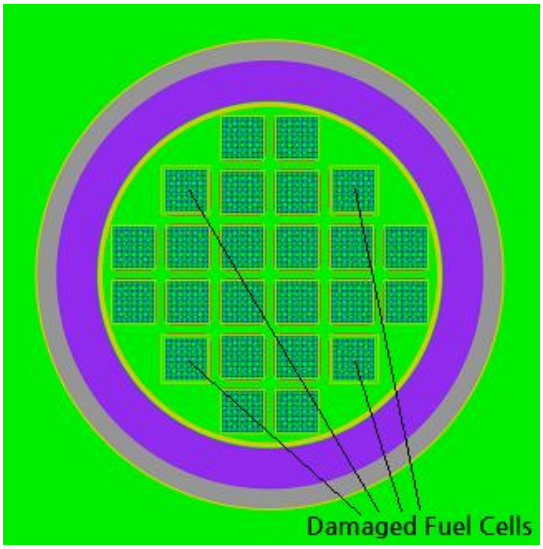

Fig. 1. X-Y Cross Section View of OASIS-24DFC Cask.

2. Methods and Results

SCALE6.2.3 [1] CSAS5 module is used for the criticality safety analysis based on OASIS-24DFC structure presented in Table 1. All loaded fuels including the damaged fuels are conservatively assumed to be 5.0 wt% ACE7 fuels in that the ACE7 has the highest reactivity among various types of fuels generally used in domestic nuclear power plants. Bias and uncertainty analyses for OASIS-24DFC are not yet performed but the result based on the nominal condition is empirically reviewed to investigate whether the calculated effective multiplication factor (k_{eff}) has margin enough to offset the anticipated bias and uncertainty, and meets the criticality safety criteria ($k_{eff} \leq 0.95$) suggested in NUREG-1536 [2] Section 7.4.

Table 1. Dimensions of OASIS-24DFC Inner Structure

Canister Inner Diameter		1735 mm
Cell Pitch (Intact Fuel Cell)		283 mm
Intact Fuel Cell	Inner Width	222 mm
	Thickness	6 mm
Damaged Fuel Cell		
- Canister	Inner Width	222 mm
	Thickness	4 mm
- Basket	Inner Width	245 mm
	Thickness	6 mm
Neutron Absorber	Thickness	3.5 mm
	Width	190 mm
	Sheath Thickness	0.6 mm
Gap between Cells		49 mm
Flux Trap Water Gap		40.8 mm

Enlarged cross section view of the damaged fuel cell is shown in Figure 2. Unlike the intact fuel cells, the damaged fuels are surrounded with 2 plates. 4 mm thick canister and 6 mm thick basket were applied for this analysis.

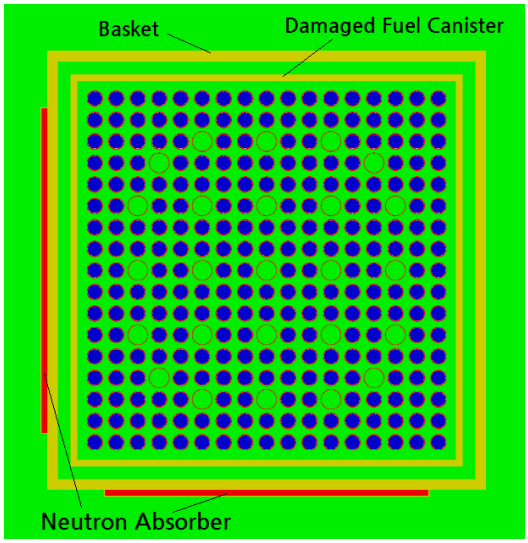

Fig. 2. Enlarged Cross Section View of Damaged Fuel Cell in the First Quadrant.

Materials used for the criticality analysis on OASIS-24DFC are presented in Table 2. On outer surface of each basket facing another cell basket, neutron absorber composed of 3.5 mm thick MAXUS is built and covered with 0.6 mm thick sheath composed of Stainless Steel 304. Reflective boundary condition is applied to cuboid water which is minimum 30 cm thick surrounding the cask.

Table 2. Materials used for OASIS-24DFC model

Fuel	5.0 wt% enriched UO_2
Fuel Cladding and Guide Thimble	ZIRLO
Moderator	Water (H_2O)
Canister Shell, Cask Outer Shell and Cell Baskets	Stainless Steel 304
Neutron Absorber	MAXUS
Cask Shell	Carbon Steel
Neutron Shield	NS-4-FR

The result of the criticality analysis on OASIS-24DFC is summarized in Table 3. The result represents the calculated effective multiplication factor and the statistical uncertainty as a standard deviation due to the use of Monte Carlo method.

Table 3. The Summarized Result of the Criticality Analysis

Effective Multiplication Factor (k_{eff})	Standard Deviation (1σ)
0.91434	0.00021

3. Conclusion

The k_{eff} value for OASIS-24DFC model was evaluated as 0.91434 with statistical uncertainty of ±0.00021. The bias and other uncertainties should be additionally considered to confirm the final criticality safety for OASIS-24DFC. However, based on engineering judgement and profound experiences of many other criticality analyses with ACE7 fuel, it is concluded that OASIS-24DFC sufficiently meets the criticality safety criteria even if all the bias and uncertainties are considered.

REFERENCES

[1] ORNL/TM-2005/39, Ver. 6.2.3, “SCALE Code System,” Oak Ridge National Laboratory, March 2018.

[2] NUREG-1536, Rev.1, “Standard Review Plan for Spent Fuel Dry Storage Systems at a General License Facility,” U.S. Nuclear Regulatory Commission, July 2010.

Zr-based Cladding Fire During Loss-of-Coolant-Accident in a Spent Fuel Pool

Sun Ki Kim* and Dong Hak Kook
Korea Atomic Energy Research Institute, 111, Daedeok-daero 989beon-gil, Yuseong-gu, Daejeon, Republic of Korea
*kimsk@kaeri.re.kr

1. Introduction

The spent fuel pool accident scenario is classified into two kinds of accident initiators. One is a loss of cooling that leads to a boil-off in the spent fuel pool(SFP). The other is a loss of coolant that brings a full or partial drainage in the spent fuel pool. The atmosphere condition would be different in each sequence. In the boil-off scenario, a coolant water becomes evaporated and a steam would be produced. In the loss of coolant accident either in partially or fully, air would be admitted into the pool. Both steam and air would react with zirconium alloy cladding. The air oxidation of zirconium alloy cladding leads to a higher exothermal heat production and a more severe cladding degradation than the steam oxidation of zirconium alloy cladding [1-3]. In this paper, the zirconium fire phenomenon is investigated, which may occur in the spent fuel pool complete loss of coolant accident scenario. If the zirconium fire occurs, the cladding would be severely degraded and it may lead to a massive release of radioactive source terms. Therefore, it is crucial to prevent the zirconium fire phenomenon for the spent fuel pool safety.

In the complete loss of coolant accident, the zirconium alloy cladding would be directly reacted with air. However, a main cause to trigger the zirconium fire was not identified. In order to identify a possible mechanism of the zirconium fire, the integral test data is analyzed, which is a prototypical experimental program of spent fuel pool complete loss of accident.

2. Spent Variation of Spent Fuel Temperature

2.1 Variation of Spent Fuel Temperature

The Spent Fuel Pool Project (hereinafter SFP project) [4-5] is the experimental program to investigate the phenomena of spent fuel pool complete loss of coolant accident using a 17×17 PWR fuel assembly. In this section, the zirconium fire phenomenon which was observed from the SFP project is briefly investigated.

Fig. 1 shows the fuel assembly temperature (i.e. zirconium alloy cladding temperature) and oxygen concentration profile of the SFP project phase-1 ignition test. At around 12.7 hour, the temperature abruptly increased and the oxygen concentration also dramatically decreased. This abrupt temperature escalation is the zirconium fire phenomenon. In order to investigate the mechanism of this zirconium fire phenomenon, behaviors of both temperature and oxygen concentration are carefully compared in the following.

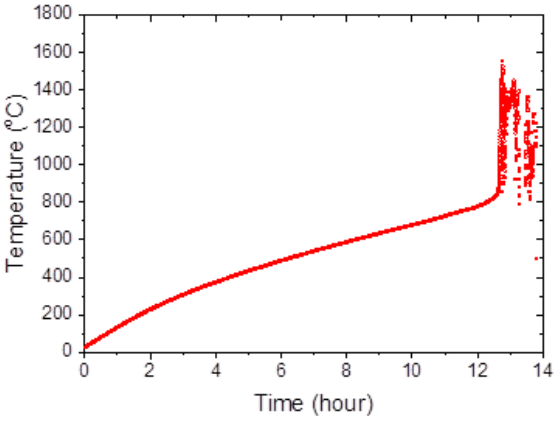

Fig. 1. Fuel assembly temperature of the SFP project phase-1 ignition test.

2.2 Variation of oxygen concentration

As oxygen consumed significantly, the temperature escalates rapidly as shown in Fig. 2. As plotted in Fig. 2, as oxygen consumed dramatically, the cladding temperature increased very sharply up to almost 1600ºC from around

850ºC within less than 10 minutes. After then the thermocouples were failed, so temperature records were scattered. However, the interesting behavior is oxygen concentration profile. Firstly, it was consumed significantly, but after the cladding temperature was reached the maximum, the oxygen concentration was increased to 21% and was decreased again. It seems that the zirconium alloy cladding was fully oxidized within a very short period by consuming oxygen. After zirconium alloy cladding was fully oxidized, the oxygen might be no more consumed in the cladding. However, oxygen concentration was highly decreased again at around 13.3 hour as shown in Fig. 3. It is still questionable why oxygen was consumed again. The more detailed investigation is ongoing to understand better the behavior of oxygen concentration.

It seems that the zirconium fire (i.e. very abrupt increase of zirconium alloy cladding surface temperature) might be induced by a breakaway phenomenon that is a kinetic transition from a parabolic to linear kinetic rate law. However, still the direct cause of zirconium fire phenomenon is investigated by further detailed analysis of SFP project experimental data and other zirconium cladding oxidation test data. This paper presents a preliminary analysis of fuel behaviors regarding the zirconium fire phenomenon that was observed from the SFP project experiment. Further study is ongoing in theoretically and in experimentally to identify the cause of zirconium fire.

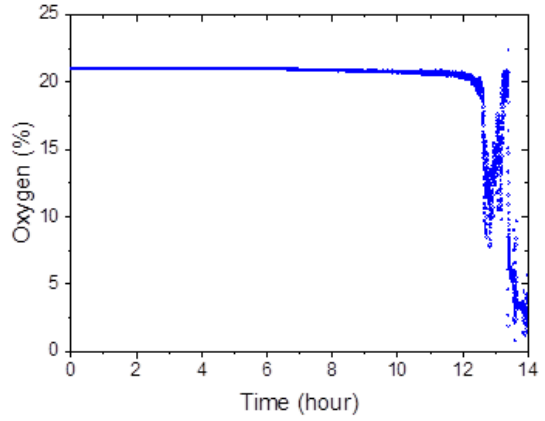

Fig. 2. Oxygen concentration of the SFP project phase-1 ignition test.

3. Conclusion

This paper investigate the data of SFP project experiment and then a mechanism of zirconium fire phenomenon was discussed. It seems that the zirconium fire phenomenon might be a consequence of thermal mismatch between heat generation and dissipation. A large amount of heat might be generated by the air oxidation of zirconium alloy cladding immediately after the kinetic transition which is a breakaway phenomenon. This paper discussed the relationship between the breakaway phenomenon and the zirconium fire in case of air oxidation of zirconium alloy cladding. This paper presents preliminary findings on the zirconium fire phenomenon from the open experiment data of the prototypic spent fuel severe accident scenario. It is expected that these findings would enhance the knowledge of zirconium cladding air oxidation and an understanding of the spent fuel pool accident scenario progression.

REFERENCES

[1] S. Park, Effect of nitriding during air oxidation of zircaloy-4, Proc. of TopFuel 2015, September 13-17, 2015, Zurich, Switzerland.

[2] M. Steinbrück, A. Miassoedov, G. Schanz, L. Sepold, U. Stegmaier, J. Stuckert, Nuclear Engineering and Design 236, 14-16 (2006).

[3] C. Duriez, T. Dupont, B. Schmet, F. Enoch, Journal of Nuclear Materials, 380, 1-3 (2008).

[4] S. G. Durbin, Spent Fuel Pool Project Phase I: Pre-ignition and Ignition Testing of a Single Commercial 17x17 Pressurized Water Reactor Spent Fuel Assembly under Complete Loss of Coolant Accident Conditions, US NRC, NUREG/CR-7215, April 2016.

[5] S. G. Durbin, Spent Fuel Pool Project Phase II: Pre-ignition and Ignition Testing of a 1x4 Commercial 17x17 Pressurized Water Reactor Spent Fuel Assembly under Complete Loss of Coolant Accident Conditions, US NRC, NUREG/CR-7216, April 2016.

Development of a Spacer Grid Model for Spent Nuclear Fuel Assembly

Youngik Yoo*, Kyounghong Kim, Kyongbo Eom, and Joonkyoo Park
KEPCO Nuclear Fuel, 242, Daedeok-daero 989beon-gil, Yuseong-gu, Daejeon, Republic of Korea
*yiyoo@knfc.co.kr

1. Introduction

Predicting and evaluating the integrity of a irradiated spacer grid by experimentally identifying its mechanical behavior is very complicated and requires considerable cost and time. Therefore, the development of a finite element (FE) model that can predict the mechanical behavior of a spacer grid is required to replace such experimental methods.

The objective of this study is to develop a full-size three dimensional (3D) spacer grid FE model. To validate the developed model, spacer grid static compression and dynamic impact tests were conducted, and the test and analysis results were compared.

2. Spacer grid model development

A 3D FE model was developed for the mid spacer grid of a 14×14 nuclear fuel assembly using Abaqus v6.14, as shown in Fig. 1. To simplify the shape of the spacer grid, beam elements were used for the spacer grid, fuel rods, guide tubes, and sleeves, while connector elements that could simulate contact and friction characteristics were used for the springs/dimples of the spacer grid and applied friction force to the fuel rods. These connector elements could set the gap between the fuel rod and spacer grid and could express the slip of the fuel rods that may occur during buckling.

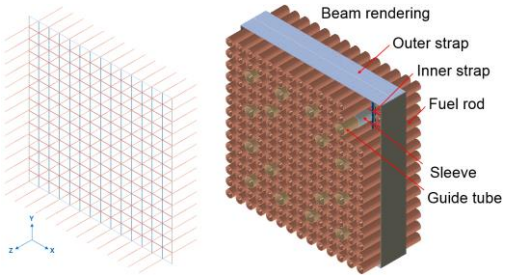

Fig. 1. Spacer grid finite element model.

3. Model validation

To verify the performance of the developed model, static and dynamic spacer grid tests were conducted, as shown in Fig. 2. As-built spacer grid specimens as well as four different cell-sized specimens (Table 1) were used for the tests. The gap between the fuel rod and spring/dimple is known to be the factor that has the greatest impact on the mechanical property changes of end-of-life spacer grids [1].

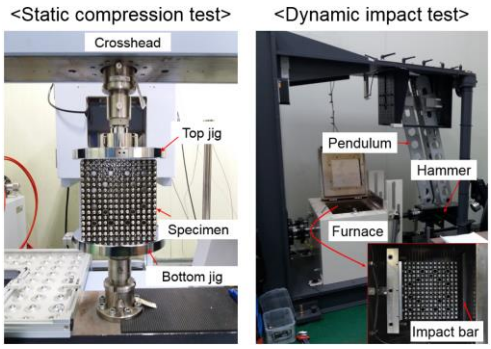

Fig. 2. Experimental setup to verify the developed model.

Table 1. Average gap sizes of spacer grid specimens for tests

Specimen	Gap size (mm)	
	Static test	Dynamic test
As-built	-0.3253(4EA)	-0.3253(4EA)
A	-0.2168(2EA)	-0.2128(4EA)
B	-0.0381(2EA)	-0.0280(4EA)
C	0.0567(2EA)	0.0562(4EA)

3.1 Static compression behavior

Fig. 3 compares the analysis results with the static compression test results according to the gap size. The results obtained using the developed spacer grid model agree well with the experimental static compression behavior and well predicted the buckling load decrease according to the gap size.

3.2 Dynamic impact behavior

Fig. 4 shows the impact test and analysis results according to the gap size. For each specimen, the FE model well simulated the impact load increase with increasing impact velocity, and buckling load. The buckling load of the analysis results was selected as a point at which the load increased by less than 5 % compared to the previous load with a constant impact velocity increment. The developed model accurately predicted buckling load reduction with increasing gap size as shown in Fig. 5.

4. Conclusion

In this study, a 3D FE model that can simulate the static and dynamic mechanical behaviors of a spacer grid was developed. The validity of the developed spacer grid model was verified by comparing the test and analysis results.

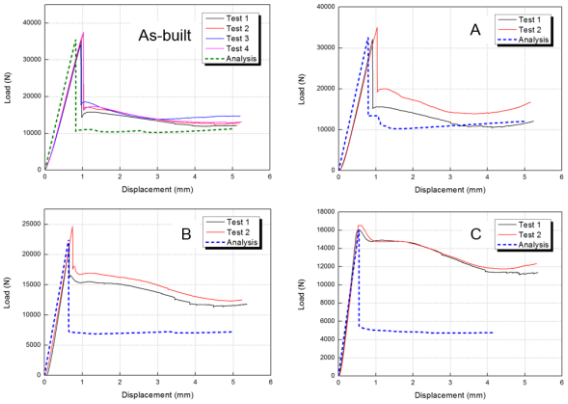

Fig. 3. Static behavior comparison.

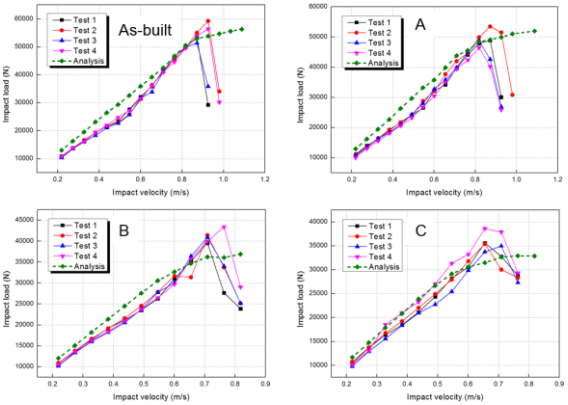

Fig. 4. Dynamic behavior comparison.

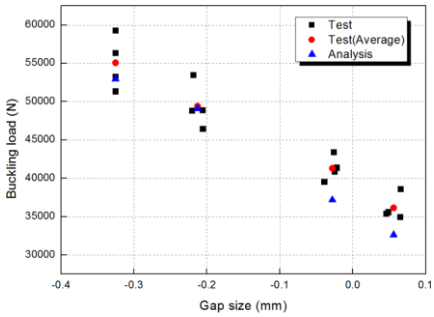

Fig. 5. Dynamic buckling load as a function of gap size.

REFERENCES

[3] ML113470490, “Irradiation effects on fuel assembly spacer grid crush strength”, US NRC Information Notice 2012-09, 2012.

Modal Analysis of KORAD-21 Road and Sea Transport Test Model

Gil-Eon Jeong*, Yun-Young Yang, Jaehoon Lim, Sang Soon Cho, Ki-Seog Seo, and Woo-Seok Choi
Korea Atomic Energy Research Institute, 111, Daedeok-daero 989beon-gil, Yuseong-gu, Daejeon, Republic of Korea
*gejeong@kaeri.re.kr

1. Introduction

The modal analyses for the KORAD-21 transport test model are performed to obtain data for evaluating vibration and shock characteristics when the spent nuclear fuel is transported during the road and sea test with normal conditions.

2. Modeling and analyzing conditions

2.1 Modeling

The KORAD-21 test model [1] is illustrated in Fig. 1. As shown in Fig. 1, the KORAD-21 test model consists of the cask, cradle, and their sub-parts. For each part, the material properties are described in Table 1.

Table 1. Material Properties

	Density [kg/m^3]	Young's modulus [MPa]	Poisson ratio
Cask	8,000	195,000	0.29
Shield	1,760	3,650	0.31
Cradle	7,850	200,000	0.3
Copper	8,940	125,000	0.345
Rubber	2,000	20	0.48

2.2 Analyzing conditions

The analyzing conditions are as follows for each KORAD-21 test model. In the case of the cask, the analysis is conducted without imposing any boundary conditions to identify the features of the model itself. In the case of the cradle, the bottom surface is fixed to describe the road and sea test with normal conditions. Between the cask and cradle, the frictionless contact condition is imposed to support the cask on the cradle.

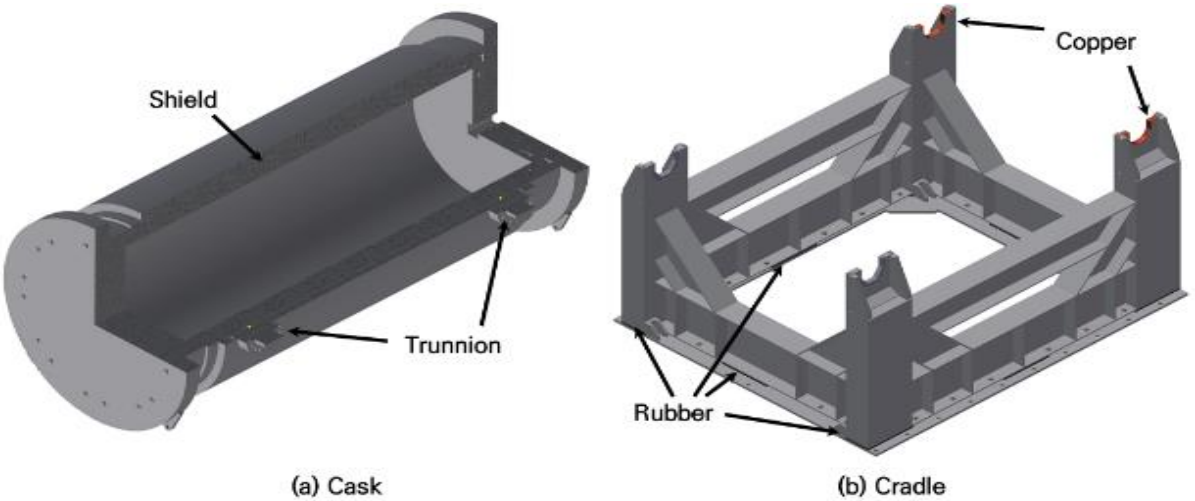

Fig. 1. Schematic descriptions for KORAD-21 test model.

Table 2. Modal analysis results for each model

Model	Frequency (Hz)	Mode Shape	Remark
KORAD-21 Cask	205.66 Hz	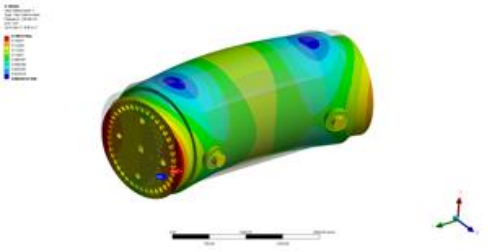	Yaw-Bending
KORAD-21 Cradle	8.47 Hz	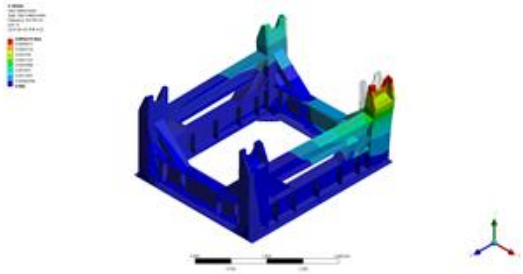	Out-Phase Back Pillars Bending
KORAD-21 test model	41.78 Hz	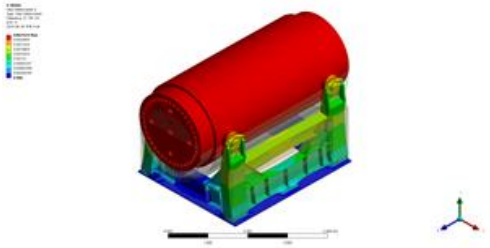	Vertical-Direction Translation

3. Results and discussion for modal analysis

Based on the above-mentioned modeling and analyzing conditions, the modal analyses are conducted using the commercial software ANASYS Workbench [2]. The results for each KORAD-21 test model are illustrated in Table 2.

The mode shape and their frequencies in Table 2 provide the information to obtain data when the KORAD-21 test model is transported during the road and sea test with normal condition.

ACKNOWLEDGMENT

This work was supported by the Korea Institute of Energy Technology Evaluation and Planning (KETEP) and the Ministry of Trade, Industry & Energy (MOTIE) of the Republic of Korea (No. 20181710201770).

RERFERENCE

[1] Gil-Eon Jeong, “Modal Analysis of KORAD-21 Road and Sea Transport Test Model”, KAERI/TR-7721/2019.

[2] ANSYS 19.0 Mechanical User’s Guide.

Deformation Analysis on the Thermal Effect of Vol-oxidizer Reactor

Younghwan Kim*, JuHo Lee, and Yungzun Cho
Korea Atomic Energy Research Institute, 111, Daedeok-daero 989beon-gil, Yuseong-gu, Daejeon, Republic of Korea
*Yhkim3@kaeri.re.kr

1. Introduction

The SF (Spent Fuel) vol-oxidizer function for scale-up design data is an oxidation device that processes the decladding and confrication of SF at the same time making and supplying uniform fine powder of U_3O_8 to electric metal reduction device.

Using the SF rods cutter, which is a head-end process of this device, the nuclear fuel rods were cut with 25 cm interval, and the cut SF rods are inserted into the device. It is a device, for the confrication of the inserted pellet, where a heating device is used to supply high temperature heat and air to SF vol-oxidizer, confrication of UO_2 pellet into the uniform U_3O_8 is performed, and hulls are separated from the powder. Also, during the oxidation process, fissile material is removed from the air atmosphere and vacuum state.

The purpose of the structural interpretation of SF vol-oxidizer is to derive the optimal rotation shaft of SF vol-oxidizer by performing thermal interpretation of SF vol-oxidizer rotating shaft to be able to process high efficiency large volume, and to produce the scale-up design data of this device. As a result of the interpretation, we could set the optimal diameter of the rotating shaft with the calculation of the slag amount by the distributed load of SF vol-oxidizer rotating shaft.

2. Thermal interpretation of rotating shaft

As a program for thermal interpretation, Solid Works Advanced Professional and Solid Works are used. The purpose of the thermal interpretation for the rotating shaft is to interpretate the slag amount by the distributed loads of the temperature and the weight for each rotating shaft diameter (Ø 20, 30, 40, 50, 60mm) under the condition of the temperature of 1250°C, and the weight of about 11kg (mesh, side plate, catching plate, ball, shaft). With the result, the diameter of the rotating shaft without deformation is decided.

In the execution of the purpose of the thermal interpretation stated above, to obtain a highly reliable interpretation value, 3D shape modeling is made based on the designed detail data. Especially, actual material characteristics are reflected to certain parts of the core device of vol-oxidizer which carry out the interpretation.

Each interpretation was made to decide the adequate shaft by deriving the rotating shaft slag amount by the distributed load of the heat transfer according to the temperature condition, material characteristics, and structural characteristics.

3. Interpretation target and condition

Vol-oxidizer is a nuclear fuel oxidation device, and it is composed of the heater, which is the heat generating part, and the chamber, which is the reacting part, including mesh, rotating shaft, and powder semicircle shape tray.

The target model for the interpretation of the slag amount by the distributed load are rotating shaft, and it is as in figure 1, which is composed of mesh, rotating shaft, side plate, and catching plate, the material of the shaft is Inconel 601, and the material of the ball is ceramic (SiC).

The interpretation characteristics condition for each distributed load is stated in Table 1.

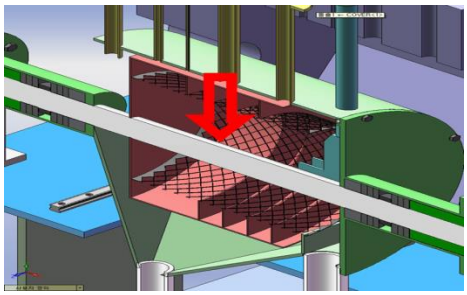

Fig. 1. Deformation analysis of shaft.

Table 1. Analysis condition for distribution stress

Condition \ Diameter	20mm	30mm	40mm	50mm	60mm
Temperature(°C)	1250	1250	1250	1250	1250
Mass(kg)	11	11	11	11	11
Mass condition: Mesh (5kg), Side plate + Catch plate (2.5kg), Ball (310g), Shaft (3kg) = About 11kg					

4. Results of shaft interpretation

The purpose of the slag amount interpretation is to decide the rotating shaft diameter without deformation. As the boundary condition, 1) Material: Inconel 601, SiC (Silicon Carbide), 2) simplifying the weight of the parts fixed to the rotating shaft to total of 11kg distributed load 3) shaft surface temperature that increases the slagging (1250°C), 4) shaft fixing by the parts assembled to the shaft (Flange, Chamber Cover, Bearing, etc.).

Total weight on the rotating shaft is 11kg, and the interpretation was carried out in 1250°C condition. The interpretation results are as in figure 2.

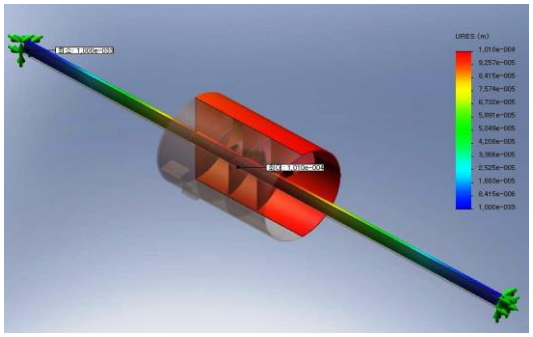

Fig. 2. Total deformation analysis (Φ50mm).

5. Conclusion

The rotating shaft diameter without slag deformation of the shaft by the distributed load is derived. As a result of the analysis, the rotating shaft with the diameter of 30mm ~ 60mm except the case of having the diameter of 20mm was within the limit boundary, and the rotating shaft of the diameter of 35mm was found to be most idealistic for SF vol-oxidizer.

With the above analysis result, the thermal characteristics of SF vol-oxidizer showed the possibility as experimental equipment in the safety and the reliability sector. But, since this analysis is limited to certain parts of the device, there shall be an interpretation through more verifications and comparisons with experiment data in the future.

ACKNOWLEDGEMENTS

This paper is the study carried out with the 2013 funding of the Ministry of Education, Science and Technology and the support from National Research Foundation of Korea (Nuclear Energy Technology Development Project, No. 2012M2A8A5025 696).

REFERENCES

[1] Y. H. Kim, Y. Z. Cho, J. W. Lee, J. H. Lee, S. C. Jeon, and D. H. Ahn, “Engineering Design of a Voloxidizer with a Double Reactor for the Hull Separation of Spent Nuclear Fuel Rods,” Science and Technology of Nuclear Installations, vol. 2017, Article ID 9854830, pages 12, 2017.

3분과

고준위폐기물처분 (Oral)

A Disposal Concept of Spent Nuclear Fuel in Deep Horizontal Drillholes

Kyungsu Kim

Korea Atomic Energy Research Institute, 111, Daedeok-daero 989beon-gil, Yuseong-gu, Daejeon, Republic of Korea

kskim@kaeri.re.kr

1. Introduction

The worldwide predominant disposal concept of spent nuclear fuel is to dispose of in mined repository in a suitable host rock at a depth between 300 m and 1,000 m. Based on this concept, Finland has obtained the world's first permit for the construction of a deep mined repository in Olkiluoto in November 2015.

Korea has not yet determined management policy for spent nuclear fuel, which will have an effect on the waste inventory for geological disposal and the disposal concept that can be considered in our circumstances.

The Korea Atomic Energy Research Institute is carrying out R&D on various disposal concepts. The development of deep mined repository concept is the primary subject in current research phase. In addition, the feasibility on deep vertical borehole disposal concept [1] has been studied in Korean geological condition [2].

This paper introduces the concept of “Deep Horizontal Drillhole Disposal (hereafter, 'DHD')” proposed by Deep Isolation Inc. [3], and reviewed its applicability in Korea.

2. Concept of Deep Horizontal Drillhole Diposal

The concept of DHD is to drill multiple deep horizontal boreholes using off-the-shelf directional drilling techniques available in sedimentary, igneous, or metamorphic rock mass suitable for deep geological disposal. Corrosion-resistant canisters holding individual spent nuclear fuel assemblies are emplaced end-to-end, before the small diameter horizontal drillhole is backfilled, plugged and sealed (Fig. 1). This disposal concept can be suitable in a centralized disposal site and/or a reprocessing facility or nuclear power plant site where high-level radioactive waste is generated.

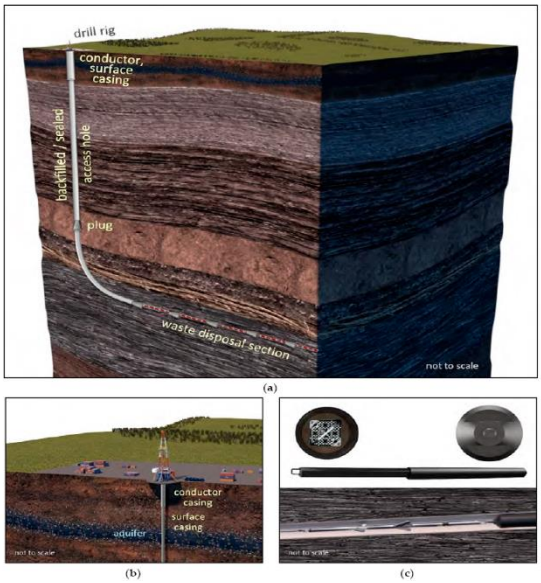

Fig. 1. Schematic of a deep horizontal drillhole repository [3].

The main advantages of the DHD concept compared to the deep mined repository concept are as follows [3];

- Simplicity, low waste density of the concept leads to a more robust and more defensible safety assessment,

- Smaller diameter holes (8” to 30”) reduce the disturbed zone of geological environment,
- No humans need to be underground, long-distance transportation is reduced or avoided and established drilling technology can be used,
- Logistical simplicity increases operational safety and reduces costs.

3. Alternative to Deep Minded Repository Concept

In the United States, approximately 280,000 spent nuclear fuel assemblies from PWR and BWR are stored at 75 sites in 33 states. Placing disposal canisters containing single PWR or BWR assembly into drillholes end-to-end every 6 m amounts to a total disposal-section length of 1,680 km. This means that an average about 22 km of disposal section is required for each of 75 storage sites [3].

In Korea, as of the end of 2017, total 17,707 PWR spent nuclear fuel assemblies were generated in four reactor sites, and it is expected to reach 63,170 assemblies (27,214 tons) when the all reactors are closed [4]. Assuming that the all PWR spent nuclear fuel is disposed of in the DHD concept, approximately 380 km of horizontal drillholes are required, and 190 drillholes are needed if every 2 km are used for disposal zone in each drillhole (83 in Kori, 35 in Hanbit, 60 in Hanul, 12 in Wolsong).

4. Conclusion

For the DHD concept to be a viable solution for permanent disposal of spent nuclear fuel, it must be acceptable to regulators and the public and requires the participation of all stakeholders throughout the conceptualization, development and implementation. This concept will be an applicable option only if the current U.S. Radioactive Waste Policy Act is amended or a new law is enacted. In addition, the U.S. NRC will need to develop regulatory guidelines to accommodate this technology.

In Korea, it may be considered as an alternative disposal option, which is disposing of the spent nuclear fuel in deep horizontal drillholes from the nuclear power plant site towards the sea side continental shelf when it is not possible to select final disposal site in future. Even if a disposal site is selected, comparative analysis with mined repository concept will help determine the more appropriate disposal option when focusing on safety and economic feasibility.

REFERENCES

[1] Brady, P.V. et al., “Deep Borehole Disposal of High-Level Radioactive Waste”, Report SAND2009-4401, Sandia National Laboratories (2009).

[2] Lee Jong Youl et al., “Preliminary Evaluation of Domestic Applicability of Deep Borehole Disposal System”, JNFCWT, 16(4), 491-505 (2018).

[3] Muller, R.A. et al., “Disposal of High-Level Nuclear Waste in Deep Horizontal Drillholes”, Energies, 12(11) (2019).

[4] Lee Jong Youl et al., “An Engineered Barrier Concept of Reference Deep Geological Disposal System for Hi-burnup Spent Fuels”, KAERI/TR-7405/2018 (2018).

Vitrification of the Spent Nuclear Fuel Using Iron Phosphate Glasses

Cheong Won Lee* and Jong Heo
Pohang University of Science and Technology, 77, Cheongam-ro, Nam-gu, Pohang-si, Gyeongsangbuk-do, Republic of Korea
*schwarz@postech.ac.kr

1. Introduction

Spent nuclear fuel (SNF) assemblies of approximately 4.7×10^5 units are temporarily stored inside the nuclear power plants (NPP) in Korea. Spaces for these storages will be near to the saturation by 2024 [1]. Direct disposal has been considered in Korea as one of the options to dispose SNF. We propose the direct vitrification using iron phosphate glass to reduce the amount of SNF that needs to be stored inside the repository.

2. Experimental procedures

2.1 Preparation of the glasses

The nominal composition of the iron phosphate glasses is given in Table I. Starting chemicals of $NH_4H_2PO_4$, Fe_2O_3 and Al_2O_3 were mixed and UO_2. Batch mixtures were calcined in alumina crucibles at 220 °C for 1 hour and melted at 1300 °C for 1 hour. Melts were then quenched by pouring onto brass mold in the air to form glasses black in color.

Table 1. Nominal and analyzed compositions of the iron phosphate glass prepared

Elements	Nominal composition		Analyzed composition
	(mol%)	(wt.%)	(wt.%)
P_2O_5	60	50.63	49.32
Fe_2O_3	15	14.24	14.45
Al_2O_3	5	3.03	2.50
UO_2	20	32.10	33.73
Total	100.00	100.00	100.00

2.2 Analysis

X-ray fluorescence (XRF) spectroscopy was used to analyze the glass composition quantitatively. Density was measured at room temperature by the Archimedes method using deionized water as a medium. Glass transition temperature (T_g) and specific heat (C_p) were determined using a differential scanning calorimetry (DSC) at a heating rate of 10 °C/min and thermal conductivity (k) was measured using laser flash method (LFA).

Chemical durability of the glasses was evaluated using the product consistency test (PCT) [2]. Glasses were crushed and sieved to 75 ~ 150 μm in size. Glass powders were then washed with deionized water and ethanol and 1.5 g of powders were soaked in 15 mL of deionized water inside a Teflon vessel and kept at 90 ± 2 °C for 7 days. The leachate was filtered using syringe with a 0.45 μm filter. Concentrations of elements in the leachate were analyzed using inductively coupled plasma mass spectrometer (ICP-MS). Oxidation state of U in the glass was determined using X-ray photoelectron spectroscopy (XPS).

3. Results

3.1 General properties

Compositions of the glasses analyzed were similar to the nominal composition without any significant loss of individual components (Table 1). The glass contains 33.73 wt.% of UO_2. Normalized elemental release of U was 6.3×10^{-3}

g/m^2 and all other elements were < 0.2 g/m^2 significantly below US regulation of 2 g/m^2. The iron phosphate glasses have T_g = 555±2 °C, C_p = 271.4±1 J/kg ^{o}C and k = 0.29±0.016 W/m K with a density of 3.40 g/cm^3. Most of U in the glass prepared exist as U^{4+} (Fig. 1) and it is chemically more durable than U^{5+} and U^{6+} [3].

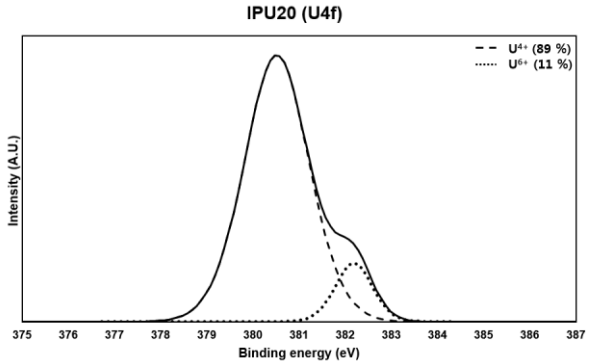

Fig. 1. XPS spectra of U4f from the glass. Dashed line is U^{4+} peak and dotted line is U^{6+} peak.

4. Conclusion

Iron phosphate glasses containing UO_2, were developed as a potential waste form for immobilization of SNF. The waste loading of UO_2 in the glass was 33.7 wt.%. Normalized elemental releases of all elements were < 0.2 g/m^2, well below the US regulations. Chemically durable U^{4+} is dominant species in the glass.

ACKNOWLEDGEMENT

This research was supported by Basic Science Research Program through the National Research Foundation of Korea (NRF) funded by the Ministry of Science and ICT (NRF-2017R1A2B4006754).

REFERENCES

[1] B.H. Park, “Assessment of spent nuclear fuel amounts to be managed based on disposal option in Republic of Korea”, Annals of Nuclear Energy, 109, 199-207 (2017).

[2] The Product Consistency Test (PCT), C 1285-02, ASTM International, West Conshohocken, PA, 2008 <www.astm.org>.

[3] N.C. Sturchio, M.R. Antonio, L. Soderholm, S.R. Sutton, and J.C. Brannon, Science, 281(5379), 971-973 (1998).

Sorption Characteristics of Strontium and Nickel on Container Corrosion Products Under the Disposal Conditions: Case Study for Mackinawite in Alkaline Conditions

Chung-Kyun Park*, Tae-Jin Park, Seung-Yup Lee, and Jae-Kwang Lee
Korea Atomic Energy Research Institute, 111, Daedeok-daero 989beon-gil, Yuseong-gu, Daejeon, Republic of Korea
*ckpark@kaeri.re.kr

1. Introduction

Strontium(Sr-90) has quite a large portion of radioactivity in the radioactive waste, and nickel(Ni-59) has a long half-life of 76,000 years. Thus they should be dealt importantly for the safe disposal. To retard movement of nuclides with groundwater in underground, it worthy of notice that some minerals generated from the corrosion of the waste containers have a good chemical interaction with nuclides. Mackinawite(FeS) is selected as a candidate mineral in this study, which is a kind of iron and sulfur compound. A sorption experiment carried out with Sr and Ni for the mackinawite under anoxic and alkaline conditions. pH dependence on the sorption and reversibility of the sorption will be investigated.

2. Sorption experiment

$SrCl_2$ and $NiCl_2$ were used as the sorbates and mackinawite was used as a corrosion product. In the sorption test, 50 ml of the experimental solution was put into 1 g of the target mineral, and 0.01 M of sodium hydrosulfite ($Na_2S_2O_4$) was added to maintain the reducing conditions. The initial concentrations of Sr and Ni were about 1 mM. In order to investigate the pH effect in the alkaline condition, the pH of the solution was divided into four different regions: 8.4, 10.3, 11.4 and 12.4. The NaOH was used to adjust the pH of the system. After the two weeks of the sorption reaction, the sample solution was centrifuged at 8600 rpm for 20 minutes and then filtered through a 0.2 μm filter. The mineral that reacted with Sr & Ni were separately collected and the amount of nuclides was determined using the sequential chemical extractions with 0.1 M $CaCl_2$ and KCl on the minerals collected.

3. Results and Discussion

3.1 Sorption of Sr and Ni onto the mackinawite and pH dependence of the sorption

Experimental results were arranged as distribution coefficient (K_d) in table 1. Nickel was highly sorbed on the mackinawite, while strontium was not. And K_d values of the two nuclides were increased as pH was increasing. When pH is increasing, the OH^- ions are increasing in the solution and detach cations on the mineral surface. Thus, cations such as Sr and Ni can sorb easily on the detached sites.

Table 1. K_d values of Sr and Ni

unit [ml/g]

pH	Strontium	Nickel
8.4	0.12	1216
10.3	0.8	2164
11.4	1.78	3015
12.4	185	6000

3.2 Chemical extraction and sorption reversibility

Fig. 2 shows the ratios of the amount of Sr

desorbed by each extraction agent onto the minerals for each test of pH. The extracted ratios by $CaCl_2$ were not shown a distinctive difference according to the pH values. Weakly sorbing cations like the alkaline earth ions such as Ca^{+2} and Sr^{+2} do not generally form covalent bonds, and sorption of these ions are influenced by electrostatic forces. Thus, Sr sorbs on the outer sphere of the surface complex. This indicates that the reversible sorption is the main sorption mechanism for Sr.

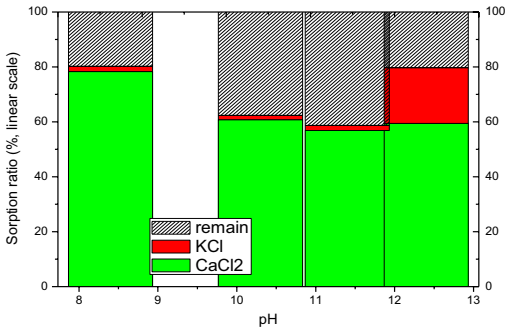

Fig. 1. Extraction result for Sr according to pH.

Fig. 2 shows the same plot for Ni. Only minor amounts of Ni were extracted for the whole extraction steps and all pH ranges. Transition metal cations such as Mn^{+2} and Ni^{+2} can be strongly sorbed against electrostatic repulsion. These ions tend to react with the hydroxyl groups on the mineral surface. They sorb on the inner sphere of the surface complex. This indicates that Ni sorbed strongly and irreversibly on the mackinawite [1,2].

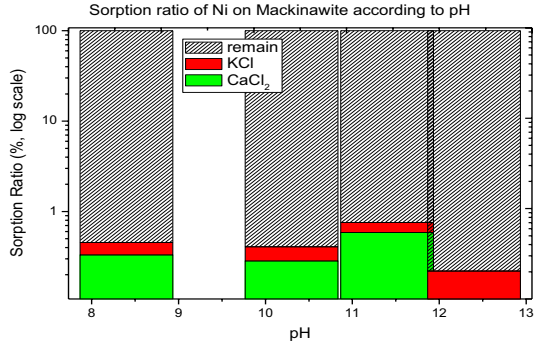

Fig. 2. Extraction result for Ni according to pH.

4. Conclusion

The result of sorption experiment under anoxic and alkaline conditions by reflecting deep underground environments show that mackinawite is a good retarding media for nuclides. Especially, nickel sorbed highly and irreversibly on mackinawite. And as pH increases in the solution, as distribution coefficients (K_d) are increased for both nuclides, other words, when an alkalinity goes stronger, a plenty of hydroxy group on the mineral surface attracts the cationic nuclides of Sr and Ni. Our results suggest that mackinawite, which can be the secondary minerals from corrosion of the steel container, can retard the nuclide migration under alkaline environments.

ACKNOWLEDGEMENT

We acknowledge the Korean Government, Ministry of Science, ICT and Future Planning (MSIP), for support (No. 2017M2A8A5014859).

REFERENCES

[1] R.T. Wilkin, D.G. Beak, “Uptake of nikel by synthetic mackinawite”, Chemical Geology, 462(6), 15-29 (2017).

[2] J. Morse, T. Arakaki, “Adsorption and coprecipitation of divalent metals with mackinawite”, Geochim. Cosmochim. Acta 57, 3635-3640 (1993).

The Removal of Arsenic and Uranium From Aqueous Solution by Sorption Onto MgO-coated Waste Coal

Bong-Ju Kim[1,*], Soonjae Lee[2], and Jang-Soon Kwon[1]

[1]Korea Atomic Energy Research Institute, 111, Daedeok-daero 989beon-gil, Yuseong-gu, Daejeon, Republic of Korea

[2]Korea University, 145, Anam-ro, Seongbuk-gu, Seoul, Republic of Korea

[*]kbj7878@kaeri.re.kr

1. Introduction

Magnesium oxide (MgO), which is known as non-toxic and eco-friendly material, has high efficiency for the removal of various toxic chemicals dissolved in an aqueous solution.

Because of its high removal activity, the applicability as a commercial sorbent has been investigated, but the field treatment using MgO is still facing several problems including mass manufacturing, effectiveness, efficiency, cost, etc. To solve the problems in this study, we synthesized high-reactivity waste coal coated with magnesium oxide (MgO) by soak-calcination method.

2. Materials and Methods

2.1 Adsorbent (GWCs)

The waste coal used in this study was collected from the area of Hwasun-gun, Jeollanam-do, Korea. After crushing, the granulated waste (GWCs)coal was separated into 2.8-4.0 mm particle size and washed before the synthesis.

And then, MgO coated GWCs (hear after is called Mg-GWCs) were synthesized by a sequence of soaking, drying, calcination (in N_2), washing and drying.

2.2 Adsorbates

In this study, hexavalent uranium (U(Ⅵ)) and trivalent arsenic (As(Ⅲ) were used as adsorbates. Natural U(Ⅵ) containing groundwater samples used in this study are derived from KAERI underground research tunnel (KURT) and its initial concentration of U is 0.7 mg L^{-1}. As(Ⅲ) is prepared as stock solution of 1000 mg L^{-1} by dissolving appropriate amounts of $NaAsO_2$ in deionized water.

2.3 Experimental method and Analysis

The sorption experiments were performed at 1:10 sorbent-sorbates ratio, and the initial concentrations of U(Ⅵ) and As(Ⅲ) were 0.7 and 50 mg L^{-1}, respectively.

The synthesized Mg-GWCs were characterized by XRD, SEM, XPS and FT-IR. XRD result shows that the mineral phases of Mg-GWCs consist of quartz and clay minerals such as chlorite and illite mainly (Fig. 1).

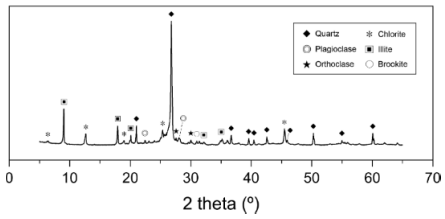

Fig. 1. XRD Patten of granulated waste coals (GWCs).

3. Results

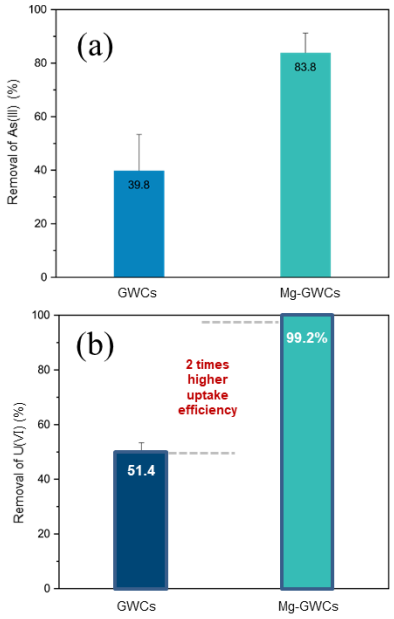

Fig. 2. Removal of As (a) and U (b) by Mg-GWCs.

The results of batch experiments by Mg-GWCs showed removal efficiencies of 83.8% and 99.2% for As(Ⅲ) and U(Ⅵ), respectively (Fig. 2). After the reaction, the additional XPS analysis for the Mg-GWCs revealed the presence of arsenic and uranium on the crystal surface. And the results suggest that the removal mechanisms of U(Ⅵ) and As(Ⅲ) onto the Mg-GWCs are quite distinct by adsorption and precipitation, respectively (Fig. 3). Basically, the removal as a precipitation crystallized onto the medium surfaces has the advantage for the immobilization of pollutant.

In the near future, XAS analysis using the particle accelerator will be used to identify the bonding states of arsenic and uranium with the microscopic approach of atomic-molecular units and to confirm the removal mechanism of arsenic and uranium onto the Mg-GWCs.

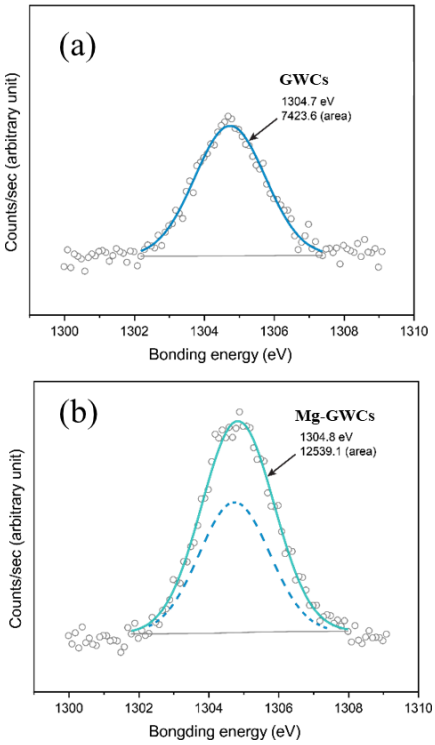

Fig. 3. XPS spectra of GWCs (a) and MgO-GWCs (b) catalysts.

Throughout this preliminary sorption study, it is expected that the synthesis of highly reactive medium by reforming of waste material could be a realistic alternative as a sorbent for removal of chemical pollutants in the field.

ACKNOWLEDGEMENT

We acknowledge the Korean Government, Ministry of Science, ICT and Future Planning (MSIP), for support (No. 2017M2A8A5014859).

Numerically Investigating Effect of Dispersivity Ratio on Heat Transport in Fully Saturated Porous Medium

Byeong-Hak Park[1] and Kang-Kun Lee[2,*]

[1]Korea Atomic Energy Research Institute, 111, Daedeok-daero 989beon-gil, Yuseong-gu, Daejeon, Republic of Korea

[2]Seoul National University, 1, Gwanak-ro, Gwanak-gu, Seoul, Republic of Korea

[*]kklee@snu.ac.kr

1. Introduction

Thermal dispersion represents heat spreading in longitudinal and transverse directions due to heterogeneous velocity field. It has been underestimated in the subsurface heat transport modeling [1]. Recent studies, however, demonstrate that thermal dispersivity for dispersion effects plays a significant role on predicting thermal plumes evolving from the thermal use of shallow aquifers [2 and references therein]. In this context, this work investigates the influence of thermal dispersivity ratio on the plume propagation through steady-state and transient simulations.

2. Heat Transport Modeling

2.1 Finite Element Model

Based on thermal tracer tests [3], 3-D model domain was constructed in FEFLOW® 5.3 [4] with the same dimensions of 1.0 m × 0.6 m × 0.6 m ($L \times W \times H$) as the transport experiments. The numerical model was discretized on the basis of space and time according to the previous results [2].

2.2 Initial and Boundary Conditions

Initial condition for hydraulic head was set to be 0.6 m over the entire domain. Dirichlet boundary conditions (BCs) for that were assigned on left and right boundaries to satisfy observed hydraulic gradients of 0.041 to 0.118 [3], and then steady-state simulations were conducted to calculate the head distribution. Initial temperature of the model was set equal to that of background water right before the tracer tests, and then Dirichlet BC for temperature was set on left boundary where the background water flows in. To represent warm water injection in the laboratory experiments, two BCs (i.e., mean injection rate and temperature) were set at an injection point.

2.3 Case Simulations

The developed model was validated by comparing the results with observed temperature–time series data. The validated model was employed to investigate the effect of anisotropy ratio between longitudinal and transverse thermal dispersivity on the subsurface heat transport processes. In the case simulations, the dispersivity ratio was varied from 1 to 10. Because injection of warm water can disturb flow field and thus affect dispersive transport of heat [3, 5], three injection rates of 26, 50, and 75 ml/min were also considered in the simulations.

3. Results and Discussions

3.1 Effect of Dispersivity Ratio

Numerical results show that the ratio of longitudinal to transverse dispersivity have an influence on plume dimensions, especially for background flow direction. This seems to be related with the disturbed flow field by injected water. This result suggests that thermal plumes from an injection well can be underestimated or overestimated depending on the dispersivity ratio.

3.2 Effect of Injection Rates

Since thermal dispersion increases with flow velocity [3 and references therein], its influence can be greater in the enhanced flow velocity by warm water injection [3, 5]. The simulation results indicate that the effect of dispersivity ratio also increases particularly for background flow direction as the injection rate increases.

4. Conclusion

Because thermal dispersion phenomenon has been underestimated when modeling the heat transport processes in shallow aquifers, thermal dispersivity values and their ratio have been assumed. The numerical results of this study, however, indicate that the thermal dispersivity ratio can affect the thermal impact assessment from an injection well and its effect can be greater with higher injection rates.

Acknowledgments

This work was supported by the National Research Foundation of Korea (NRF) grant funded by the Ministry of Science and ICT (MSIT) of South Korean government (No. 2017R1A2B3002119).

REFERENCES

[1] N. Molina-Giraldo, P. Bayer, and P. Blum, “Evaluating the influence of thermal dispersion on temperature plumes from geothermal systems using analytical solutions”, International Journal of Thermal Sciences, 50 (7), 1223-1231 (2011).

[2] B. H. Park, B. H. Lee, and K. K. Lee, “Experimental investigation of the thermal dispersion coefficient under forced groundwater flow for designing an optimal groundwater heat pump (GWHP) system”, Journal of Hydrology, 562, 385-396 (2018).

[3] B. H. Park, “Experimental and numerical investigation of thermal dispersion and its significance for designing groundwater heat pump (GWHP) systems”, Ph.D. Dissertation, Seoul National University, Seoul, Republic of Korea (2019).

[4] H. J. G. Diersch, “Reference Manual for FEFLOW”, WASY GmbH, Berlin, Germany Journal of Hydrology, 562, 385-96 (2005).

[5] B. H. Park, G. O. Bae, and K. K. Lee, “Importance of thermal dispersivity in designing groundwater heat pump (GWHP) system: Field and numerical study”, Renewable Energy, 83, 270-279 (2015).

Spectroscopic Properties of Natural Organic Matters in KURT Groundwater

Euo Chang Jung*, Tae-Hyeong Kim, Jang-Soon Kwon, Wansik Cha, and Min Hoon Baik
Korea Atomic Energy Research Institute, 111, Daedeok-daero 989beon-gil, Yuseong-gu, Daejeon, Republic of Korea
*ecjung@kaeri.re.kr

1. Introduction

It is necessary to know the concentrations and compositions of several species such as cations, anions and natural organic matters (NOMs) existing in groundwater to understand the migration behavior of uranium in the geochemical condition. The concentrations and compositions of the cations and anions in groundwater can be measured without difficulty. The interaction of these species with U(VI) (hexavalent uranium) is widely investigated. For example, the U(VI) exists in the form of Ca-U(VI)-carbonate complexes in KURT groundwater [1]. In contrast, the information on the interaction of U(VI) with NOMs is not as well-known because the chemical speciation of NOMs is more complicated. In the western country, the relevant studies are concentrated on the interaction of U(VI) with humic substances. In KURT groundwater extracted from a borehole in granite bedrock formation, the concentration of humic substances is very low (approximately less than 5%). Until now, the chemical speciation of the NOMs in KURT groundwater has rarely been studied.

In the present study, the spectroscopic properties of NOMs in KURT groundwater are investigated using various techniques for the chemical speciation of NOMs. The excitation and emission spectra of NOMs were primarily measured using the excitation emission matrix (EEM) spectroscopy. The EEM characteristics of NOMs in KURT groundwater were compared with those of known NOMs. The interaction of U(VI) species with NOMs were examined using time-resolved laser-fluorescence spectroscopy (TRLFS).

2. Experimental Conditions

Several groundwater samples were collected from a borehole with a depth of 500 m in granite rocks (DB-1 and DB-3) located at the KURT. All the groundwater samples were kept in an Ar-conditioned glove box. The EEM spectra were acquired by scanning the excitation spectrum of the sample while simultaneously acquiring the fluorescence emission spectrum at each excitation wavelength using spectrofluorimeter (Horiba, model Aqualog). The experimental apparatus of TRLFS was described in detail in the previous study [2]. The luminescence spectra of U(VI) were measured at low temperatures (one degree celcius in this study) to enhance the luminescence intensities.

3. Results and Discussion

Fig. 1 shows representative EEM spectrum measured from the groundwater sample named S5, in which the concentration of the dissolved organic carbon (DOC) is approximately 1.7 mg/L. The existence of NOM is usually verified by the measurement of total organic carbon (TOC), DOC, and absorption of UV light.

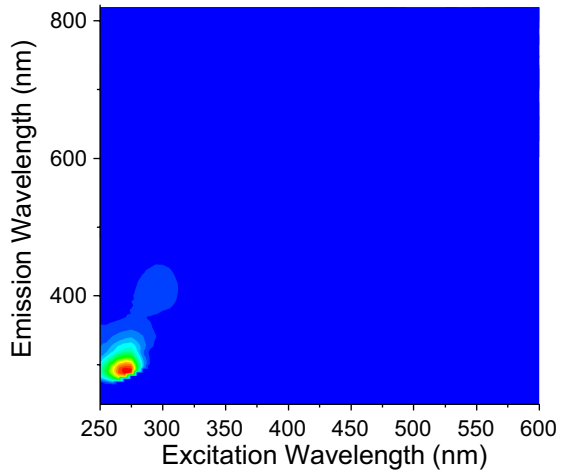

Fig. 1. Representative EEM measured from the groundwater sample named S5, in which the concentration of the DOC is approximately 1.7 mg/L.

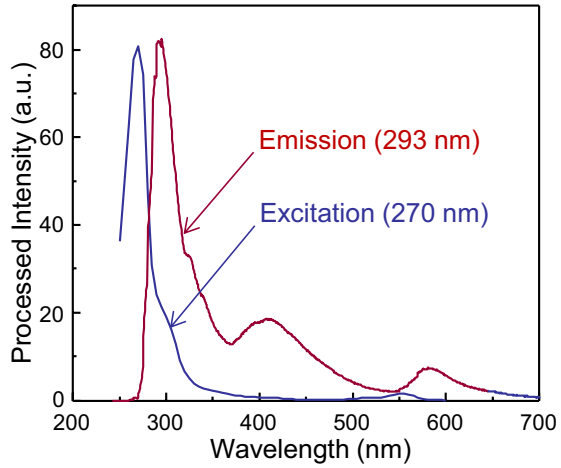

Fig. 2. Excitation and emission spectrum derived from the data in Fig. 1.

Fig. 2 represents the excitation and emission spectrum derived from the data in Fig. 1. The mean positions of excitation and emission maxima were observed at 270 and 293 nm, respectively. These values were compared with those of other well-known NOMs in Table. 1. The observed EEM characteristics do not coincide exactly with those of well-known NOMs. Although the EEM characteristics are similar with those of tyrosine-like, protein-like NOMs, further study should be performed for the detailed speciation of NOMs in KURT groundwater.

Table 1. Major EEM peaks for water samples [3]. Asterisk means the observed wavelengths in KURT groundwater.

Excitation (nm)	Emission (nm)	Component type
270−280*	310−320*	
270−285	340−360	Tyrosine-like, protein-like
310−325	400−450	Fulvic-like
310−325	380−420	Humic-like (marine humic-)
330−390	420−500	Humic-like

The interaction of U(VI) with NOM in KURT groundwater was also investigated.

4. Summary

It is observed that the EEM spectra of the NOM in KURT groundwater are much different from those of humic-like and fulvic-like substances. The present study is the beginning point of the chemical speciation of NOMs in groundwater. The spectroscopic properties of various functional groups of organic substances should be collected as a reference data for the comparison purpose.

ACKNOWLEDGEMENT

This work was supported by a grant from the Nuclear Research and Development Program of the National Research Foundation of Korea funded by the Korean Ministry of Science and ICT (Grant code: 2017M2A8A5014719).

REFERNCES

[1] M. H. Baik, E. C. Jung, J. Jeong, J. Radioanal. Nucl. Chem. 305, 589−598 (2015).

[2] E. C. Jung, M. H. Baik, H-R. Cho, H. Kim, W. Cha, J. Nucl. Fuel Cycle and Waste Technol. 15(2), 101-116 (2017).

[3] A. Matilanian, E. T. Gjessing, T. Lahtinen, L. Hed, A. Bhatnagar, M. Sillanpää, Chemosphere, 83 1431−1442 (2011).

Saturated Hydraulic Conductivity Model for the Korean Compacted Bentonite Installed in In-DEBS

Seunghun Park[1,2], Seok Yoon[2], Sangki Kwon[1,*], and Geonyoung Kim[2]
[1]Inha University, 100, Inha-ro, Michuhol-gu, Incheon, Republic of Korea
[2]Korea Atomic Energy Research Institute, 111, Daedeok-daero 989beon-gil, Yuseong-gu, Daejeon, Republic of Korea
[*]kwonsk@inha.ac.kr

1. Introduction

In the deep disposal repository, it is essential to prevent the release of radionuclides for tens of thousands of years using disposal containers. The engineered barrier system (EBS) with the aim of delaying the movement of radionuclides consists of a disposal canister, a buffer material and near-field rocks. Among them, a buffer material plays an important role in the long-term stability and integrity of high-level radioactive waste disposal (HLW). The hydraulic conductivity of the buffer is a property that needs to be understand because it is associated with the control of nuclide transport and groundwater penetration. Many researchers have investigated the hydraulic properties of the bentonite using Kyungju bentonite (KJ-1), a buffer material candidate in Korea [1,2]. However, KJ-1 bentonite is not produced at present, and KJ-2 bentonite mined in Kyungju, which has similar components, is being used for disposal studies.

The Korea Atomic Energy Research Institute (KAERI) has carried out a demonstration study using the In-DEBS which is the long-term in-situ test on the EBS. The buffer block of KJ-2 bentonite was installed in In-DEBS equipment. In order to understand the hydraulic behavior of the buffers and the In-DEBS modeling, the hydraulic study of the bentonite needs data analysis based on laboratory experiments. Studies on thermal behavior under various conditions (water content ratio, dry density, temperature change, etc.) using KJ-2 bentonite have secured prediction equation of thermal properties, verification of significance, and laboratory data [3,4]. On the other hand, the study of the hydraulic behavior of KJ-2 bentonite under various conditions is insignificant compared to the thermal behavior study. Therefore, this study aims to propose a hydraulic conductivity estimation model for various dry densities and constant temperature using KJ-2 bentonite blocks.

2. Experimental Setup

2.1 Hydraulic conductivity test

The hydraulic conductivity of the saturated compacted bentonites (KJ-2) was measured using GDS Advanced Pressure/Volume Controller (ADVDPC), based on the constant head method [1]. This device consists of the gauge which can be measured and controlled to the pressure of fluid, the volume change, as shown in Fig. 1. The fluid from this device can be injected to water and oil and the additional device is needed to inject the air. The hydraulic conductivity can be calculated using Eq. (1)

$$K = \frac{Q \times L}{A \times H} \quad (1)$$

Where K is the hydraulic conductivity (m/s), Q is the volumetric flow rate (m^3/sec), A is the surface area of specimen (m^2), L is the length of specimen (m) and H is the hydraulic gradient (m/m). The saturated compacted bentonite were installed in the stainless steel cell (Fig. 1), and they were heated from the heating tape during the experiment in order to consider temperature change. After heating, the compacted bentonite was cooled naturally at a constant temperature.

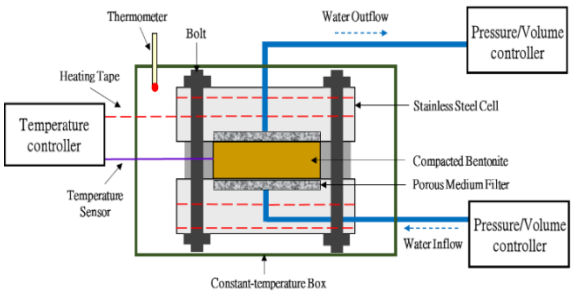

Fig. 1. Concept of hydraulic conductivity test.

2.2 Results

Fig. 2 shows hydraulic conductivity variation of the saturated compacted bentonites according to dry densities change at the constant temperature. Hydraulic conductivity range of KJ-2 is 8.5×10^{-14} ~ 4.8×10^{-12}(m/s). There was about 2 orders decrease of thermal conductivity with respect to dry density increase. A decrease of the hydraulic conductivity was inversely proportional to the increase in dry density. This reason is considered to be contributed to the compressibility of the bentonite particles by increasing the dry density.

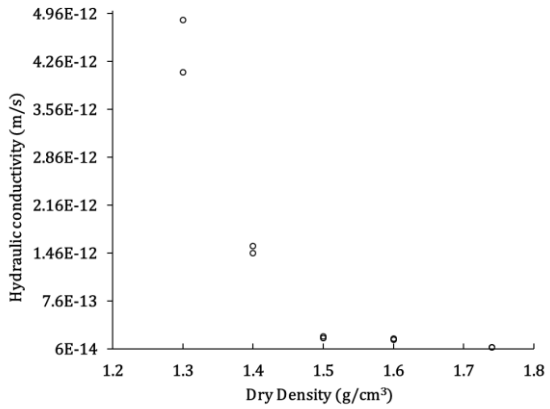

Fig. 2. Hydraulic conductivity of different dry densities of KJ-2 at a constant temperature.

$$\log K = -3.9645\gamma_d - 6.3396 \quad (2)$$

Eq. (2) indicates the predicted model of the hydraulic conductivity (K) according to dry density (γ_d) on the KJ-2 bentonite. The correlation coefficient is 0.9126, which is considered to be significant in terms of the dry density and the hydraulic conductivity.

3. Conclusion

This study measured the hydraulic conductivity of saturated compacted bentonites with various the dry densities. The hydraulic conductivity of the different bentonite was 8.5×10^{-14} ~ 4.8×10^{-12} (m/s). The hydraulic conductivity was inversely a proportional to dry density increase. And a decrease of the saturated hydraulic conductivity can be explained that bentonite has compact particles with dry density increase. Thus, it is necessary to analyze saturated hydraulic conductivity for the compacted bentonite on variety aspect of dry densities in order to design the buffer in real repository condition.

ACKNOWLEDGEMENT

This research was supported by the Nuclear Research and Development Program of National Research Foundation of Korea (NRF) funded by the Minister of Science, ICT and Future Planning.

REFERENCES

[1] Yoo, M.G.B.G.B.N.L., Choi, H.J., Lee, M..S, Lee, S.Y., Chemical and mineralogical characterization of domestic bentonite for a buffer of a HLW repository, KAERI/TR-182 (2015).

[2] Cho, W.J., Lee, J.O., Chun, K.S., The temperature effects on hydraulic conductivity of compacted bentonite, Applied Clay Sci. 14 (1999), 47-58.

[3] Lee, J.W., Choi, H., Lee, J.Y., Thermal conductivity of compacted bentonite as a buffer material for a high-level radioactive waste repository, Ann. Nucl. Energy 94 (2016a), 848-855.

[4] Yoon, S., Lee, M.S., Kim, G.Y., Lee, S.R., Kim, M.J., A prediction of thermal conductivity for compacted bentonite buffer in the high-level radioactive waste repository, J. Korean Geotech. Soc. 32 (2017), 55-64.

Hydrogeochemical Investigation in the Geological Repository Site for LILW Disposal During Construction in Korea

Jang-Soon Kwon* and Yong-Kwon Koh
Korea Atomic Energy Research Institute, 111, Daedeok-daero 989beon-gil, Yuseong-gu, Daejeon, Republic of Korea
*jskwon@kaeri.re.kr

1. Introduction

Underground isolation of radioactive waste is considered a safe and reliable method, and therefore, it was adopted in several countries [1], and in Korea, the geological repository for low and intermediate low radioactive waste (LILW) is operating in the southeastern coastal area. The geological repository (bottom at -130 m a.s.l.) for LILW disposal in Korea was constructed from 2008 to 2014, and got the licensing for its operation by Dec. 2014. In order to understand the hydrogeochemical variation of bedrock aquifer during underground space construction for the LILW repository, various graphical methods including multiple-component plots and chemical trends were used to estimate the mixing rate between seawater and freshwater and to investigate the evolution of water quality in this study.

2. Monitoring Program

Nuclear facilities related to radioactive waste require a site monitoring program at different periods during its lifetime according to the International Atomic Energy Agency [2] and Nuclear Safety Act [3]: 1) during the preoperational period to obtain baseline data to characterize the site; 2) during the operational period to obtain data to verify the characterization of the site, safety evaluation, and design; and 3) during the post-closure period to acquire data for the early warning with respect to radionuclide releases from the disposal site and to verify the characterization of the site and safety evaluation. According to the [3], at least quarterly hydrogeochemical monitoring should be continued during construction and over 60 years during operation until closure as shown in Table 1.

Table 1. Hydrogeochemical surveillance function

Classification		Item	Places	Period (construction)
Stream water		·Geochemistry	3 EA	quarterly
Groundwater	In site	·GW level	7 EA	continuous
		·GW level ·EC	3 EA	continuous
		·Hyd. Pres.	8 EA : Boreholes installed MP system	continuous
		·Geochemistry		quarterly
		· Infrow rate to Silo	6 EA : Effluents	continuous
		·Geochemistry		quarterly
	Within a radius of 10 km	·GW level ·Geochemistry	13 EA	quarterly
Seawater		·Tide	Tidal station	continuous
		·Geochemistry	2 EA	quarterly

* Geochemistry includes water quality (Temp., pH, Eh, EC, DO) and concentrations of inorganic constituents.

And figure 1 shows the monitoring points for surveillance function around the Wolsung LILW repository site.

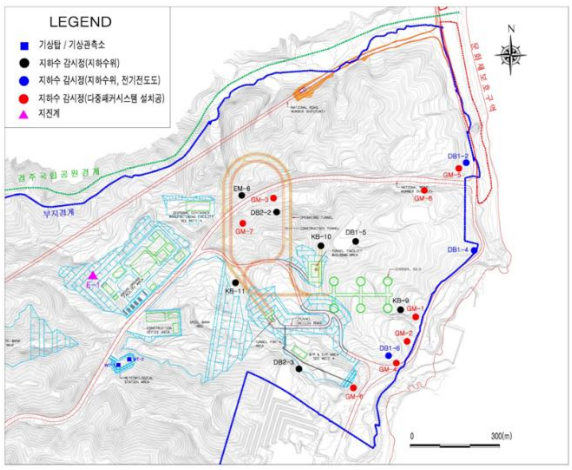

Fig. 1. Monitoring points for surveillance function around the Wolsung LILW disposal site.

3. Results

3.1 Stream water

The three stream water around the repository site showed the total dissolved solids ranged of 88~395 mg/L and water chemical type of Ca-Na-HCO_3, which no seasonal variations. And the tritium has been detected less than the MDA.

3.2 Groundwater in BHs installed MP

Underground space construction can cause dramatic changes in groundwater quality as well as groundwater flow direction due to the level decline. During construction, the groundwater level decreased and upper groundwater flow in the southeastern area reversed. In this point, the variations of the groundwater chemistry and groundwater level differ depending on the depth, even in wells, because of fracture networks. Especially, the groundwater chemistry in monitoring wells located along the coastline was classified as Na-Cl type, Na-HCO_3 type, and Ca-Cl type due to the influence of the seawater intrusion. And hydrogeochemical and isotopic data show that local freshwater is subjected to geochemical processes, such as reverse ion-exchange.

3.3 Seawater

Tidal variation shows periodic behavior, and there are no significant variation for seawater chemistry during construction.

3.4 Silo groundwater

The six Silo seepage groundwaters in the construction cave have a different chemical type each other, which are fresh, brackish, high ferrous and high alkaline. The pH in the section considered effect of grouting was measured higher than 11, and in the specific section the influence of seawater intrusion and geochemical reaction such as ion-exchange were observed.

REFERENCES

[1] N.T. Rempe, “Permanent underground repositories for radioactive waste”, Prog. Nucl. Energy, 49, 365-374 (2007).

[2] IAEA, “Disposal of Radioactive Waste”, IAEA Safety Standard Series, SSR-5, 40-41 (2011).

[3] NSSC, “Guidelines for the Preparation of Site Characteristic Report for Low- and Intermediate Low-Level Radioactive Waste Disposal Facilities”, No. 2014-57 (2014).

3분과

고준위폐기물처분 (Poster)

Hydrogeochemical Characteristics of the Deep Environment for Granitic and Gneissic Lithologies in South Korea

Jang-Soon Kwon[1,*], Yong-Kwon Koh[1], and Soonyoung Yu[2]

[1]Korea Atomic Energy Research Institute, 111, Daedeok-daero 989beon-gil, Yuseong-gu, Daejeon, Republic of Korea

[2]Korea University, 145, Anam-ro, Seongbuk-gu, Seoul, Republic of Korea

[*]jskwon@kaeri.re.kr

1. Introduction

In order to understand the control of different lithologies (granite and gneiss) on hydrogeochemical conditions, bedrock groundwater was investigated in the two study areas (AH and BH, respectively) (Fig. 1a). In the two areas, a total of 5 boreholes (AH-1, 2 and BH-1, 2, 3) were drilled up to 500 m below ground surface (BGS). Hydrological tests and groundwater sampling for chemical constituents and isotopic compositions were performed at about 50 m intervals during drilling and where wet fractures were found after the borehole drill was completed. In addition, rock and fracture-filling materials were analyzed to determine major minerals and geochemical compositions. The relation between hydrological, hydrochemical and geochemical results was discussed in this study.

2. Study area

The AH area is located on the Jurassic Daebo granite that was intruded by dike swarms, and the main rock type in this area is two-mica granites (Fig. 1b). The BH area is located on the northeastern Yeongnam Massif, which consists of Paleoproterozoic metasedimentary rocks and metagranitoids and Phanerozoic cover rocks and granitoid plutons (Fig. 1c), and several varieties of gneiss and marble were observed in this area.

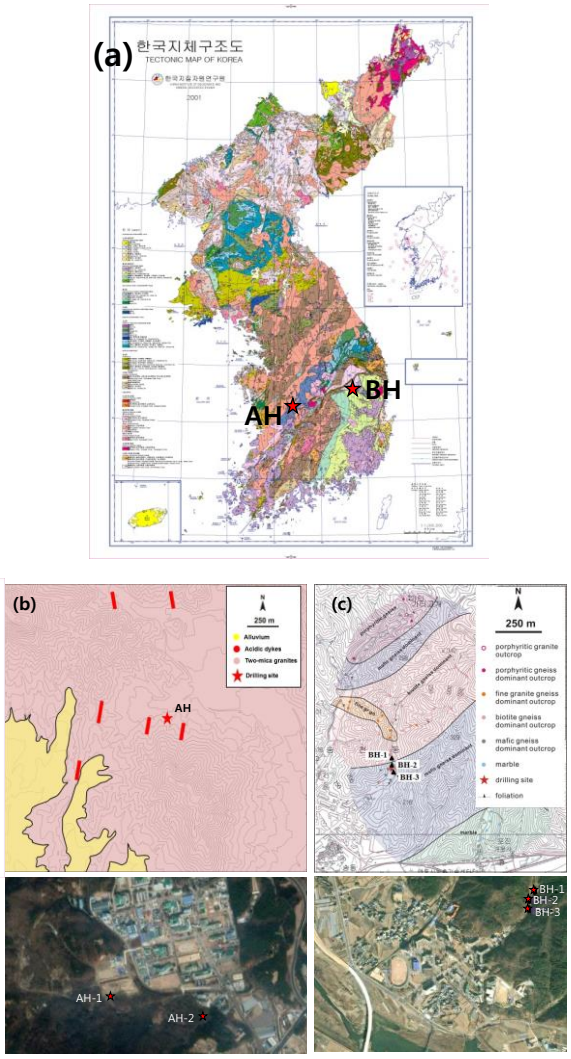

Fig. 1. Study areas (AH and BH) and the locations of boreholes.

3. Results

3.1 Hydrology and mineralogy

AH and BH showed the hydraulic conductivity (K) from 1.83×10^{-11} to 4.73×10^{-7} m/sec and from 1.15×10^{-10} to 1.27×10^{-6} m/sec, respectively.

As fracture-filling minerals, illite was frequently observed in AH while chlorite in BH. Rocks from BH showed higher CaO, MgO, P_2O_5, TiO_2, Cr, Sc, Ni, Cu and EU while rocks from AH showed the higher Be, Rb, Mo, Pb and U.

3.2 Field measurements

Most of the groundwater samples showed pH higher than 7, and most of the field measurements did not show a distinct variation with depth. It is noticeable that the AH area showed the high temperature and DO and relatively low EC in 300~351.7 m BGS (AH-2-3), while high EC but low Eh and DO in 186~210.7 m BGS (AH-2-2) during drilling. AH-2-2 included the grouting depth of 191~202 m BGS, while AH-2-3 included the fracture zone of 330~341 m BGS.

3.3 Major and minor compositions

Both AH-2-2 and AH-2-3 samples showed a Na-HCO_3 water type. In BH, a sample ((BH-3-2 from 60~91.4 m BGS during drilling) showed pH larger than 10. Groundwater from BH showed the higher TDS (210±18 mg/L) than AH (144±26 mg/L). In particular, Na, Mg, Sr, SO_4, HCO_3 and F were higher in BH, and the Na-HCO_3 water type was more distinct in BH. Meanwhile the minor elements such as Fe, Al, Be, Cd and Cs were more frequently detected in AH where the high concentrations of Mn (122 ppb), Li (up to 87 ppb), Co (84 ppb), Zn (209 ppb), Ba (1,140 ppb) and U (385 ppb) were also observed.

3.4 Isotopic compositions

D and ^{18}O were plotted along the global meteoric water line in both areas, but AH showed higher D and ^{18}O. ^{34}S was higher in AH groundwater with lower SO_4 concentrations. $^{13}C_{DIC}$ values were similar in both areas, although AH showed a wide range. Higher tritium concentrations were observed in AH while older groundwater ages were observed in BH, regardless of depth.

4. Summary

AH and BH showed different hydrochemical properties. Major compositions seem to be affected by reaction times rather than lithologies, while minor elements by lithologies.

Acknowledgement

Dataset used in this study were provided by the Nuclear Core Technology of the KETEP grant funded by the Korean government MOTIE (No. 20171510300670). We also acknowledge the Korean government MSIP (No. 2017M2A8A5014859) for support to interpret.

Enhancement of Bayesian Belief in Flow Rates in the Repository for SNFs by Sequential Updating of the Hydraulic Conductivity Distribution

Youn-Myoung Lee* and Dong-Keun Cho
Korea Atomic Energy Research Institute, 111, Daedeok-daero 989beon-gil, Yuseong-gu, Daejeon, Republic of Korea
*ymlee@kaeri.re.kr

1. Introduction

For conceptual HLW repository for spent nuclear fuels (SFs) from both PWR and CANDU reactors, GSTSPA (GoldSim[1] Total System Performance Assessment) has been developed and used for assessment of the repository. This program has been proven to be suitable for such an evaluation of nuclide transports in the near- and far-field of a repository as well as a transition among biosphere compartments under various release scenarios associated with FEPs identified. Although almost all required parameter values associated with the repository system are usually assumed or sometimes overestimated and still far from being highly reliable, such methodology results from the probabilistic models are believed to be reliable and informative not only for safety assessment of the repository, but also for its design feedback. Uncertainties nested in nuclide transport modeling around the repository are mainly dominated by parametric uncertainty, involved in input parameter values, aside from intrinsic model uncertainty. Reliable estimate of the parameter values commonly expressed as probability density functions (PDFs) always require a large amount of measured data. These PDF distributions are used as input to the probabilistic assessment program through Monte Carlo simulation to quantitatively provide possible uncertainty of the results. However, in most cases, especially in the safety assessment of the repository which is typically related with both long time span and wide modeling domain, inefficient observed data from the field measurements are common, making conventional probabilistic calculations rather uncertain. Therefore, in most cases, although estimation of the distributions successfully expressed as PDFs or other types, parametric uncertainty could still remain. Since Bayesian approach is known to be especially powerful and efficient in the case of lacking of available data measured, such short data could be compensated by coupling with a priori belief, reducing uncertainty. By allowing the a priori knowledge for incorporating insufficient observed data, which include expert' elicitation, their beliefs and judgment regarding the parameters as well as recent site-specific measurements, based on the Bayes' theorem, the older parameter distributions, "prior" distribution can be updated to a rather newer and reliable "posterior" distribution. Newer distributions are not necessarily expressed as PDFs for probabilistic calculation. These updates could be done even iteratively as many times as data values are sequentially available, which calls sequential Bayesian updating, making belief of posterior distributions become much higher by reducing parametric uncertainty. To show a possible way to enhance the belief as well as to reduce the uncertainty involved in parameter for the Bayesian scheme, hydraulic conductivity that is directly connected to the flow rate in and around the repository was exclusively chosen among many others involved in nuclide transport in fractured rock medium to investigate the results. The algorithm and module that have been developed and implemented in GSTSPA through current study was shown to work well for all assumed prior, three sequential posterior distributions and likelihoods,

2. Sequential Bayesian Updating

Bayesian framework allows us to update our beliefs iteratively every time new data from measurements and observations continuously come in. At time n, we may have an updated distribution of parameters to its posterior as

$$p(\vec{\theta}|\boldsymbol{D}_{n+1}) \propto \mathcal{L}(\boldsymbol{D}_{n+1}|\vec{\theta}) \cdot p(\vec{\theta}|\boldsymbol{D}_n) \quad (1)$$

For Bayesian updating described above, despite of its advantage in buildup of belief for the parameter distribution, practical application

is still limited due to difficulty to get a posterior distribution analytically. Markov Chain Monte Carlo (MCMC) sampling algorithm was adopted, by which posterior distribution could be sampled.

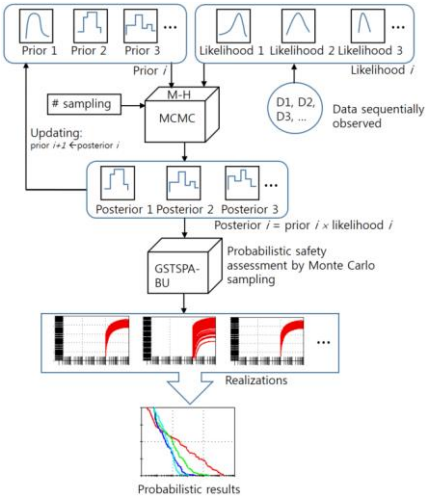

Fig. 1. Probabilistic safety assessment procedure with MCMC algorithm.

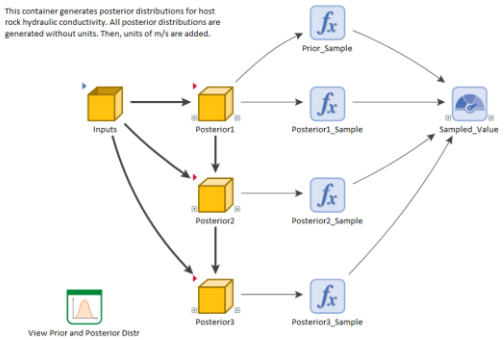

Fig. 2. GSTSPA Bayesian updating module.

3. Illustration with Bayesian Module

A Bayesian updating module has been developed is shown in the flowchart in Fig.1, and then implemented in the GSTSPA GoldSim template program by utilizing a Metropolis-Hastings (M-H) algorithm has been implemented as a GoldSim module into the GSTSPA as shown in Fig. 2. Values sampled from either the prior distribution and multiple posterior distributions are then ready to be used as inputs to the GSTSPA model for probabilistic Monte Carlo safety assessments of the repository. Breakthrough curves for 3 selected representative nuclides such as ^{79}Se, ^{135}Cs, and ^{226}Ra are shown for the dose rates in Fig. 3. Comparatively than other nuclides, ^{226}Ra is shown to have distinctly wider widths of the varying breakthrough curve bundles, as shown in 4. This seems to be due to its relatively higher distribution factor value, which retard its transport along the fracture.

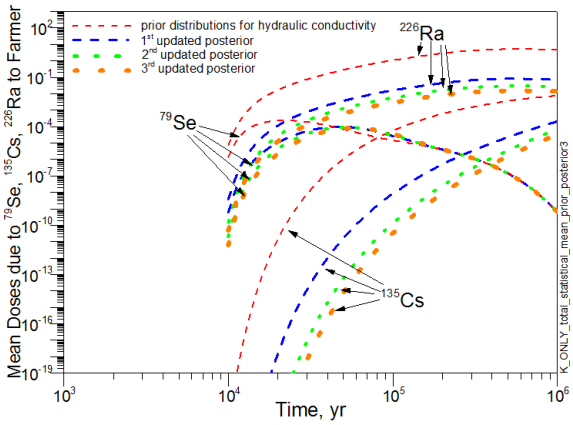

Fig. 3. Dose rates due to ^{79}Se, ^{135}Cs, and ^{226}Ra, probabilistically calculated for each prior and each of 3 updated posterior distributions and compared among each other.

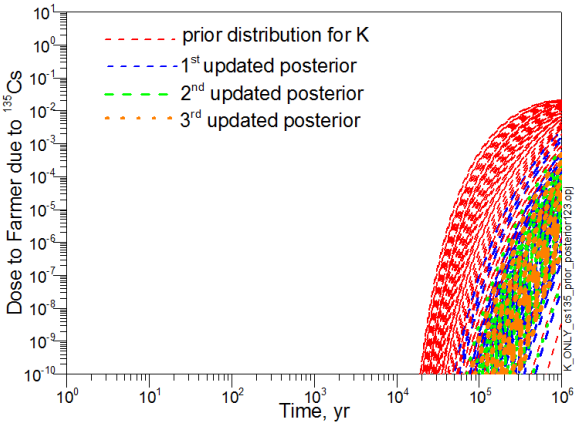

Fig. 4. Exposure dose rates due to ^{226}Ra for prior and three updated posterior distributions.

REFERENCES

[1] GoldSim, GoldSim Contaminant Transport Module User's Guide, Version 12.1, www.goldsim.com/Web/Customers/Education/Documentation, GoldSim Technology Group, Seattle, U.S.A. (2018).

[2]Youn-Myoung Lee et al., "An evaluation of an earthquake scenario for a pyroprocessed waste repository," Progress in Nuclear Energy 66, pp.133-145(2013).

Effect of Geochemical Conditions on the Sorption of Radionuclides by Granite

Jae-Kwang Lee*, Min-Hoon Baik, Jongtae Jeong, and Ji-Hun Ryu
Korea Atomic Energy Research Institute, 111, Daedeok-daero 989beon-gil, Yuseong-gu, Daejeon, Republic of Korea
*jklee1@kaeri.re.kr

1. Introduction

The primary purpose of the deep geological disposal of radioactive waste is to isolate the radionuclide from human. Radionuclides included in a radioactive waste have a considerably long half-life and their harmful effects can persist for a long time if released to ecosystems.

If radionuclides released from the deep geological environment of the radioactive waste repository, they can interact with minerals and groundwater in natural barriers. Hence, the geochemical reaction of radionuclides in natural barriers should be considered to the safety assessment of radioactive waste disposal. The sorption of radionuclides in the underground media plays an important role in retardation of radionuclides in the natural barrier[1].

In this work, we measured distribution coefficients (Kd) of actinides (U, Am, Np) and anionic radionuclides (I, Se, Tc) for granite, and the effect of geochemical factors on the sorption of radionuclides was also evaluated.

2. Materials and Methods

The sorption experiments were carried out using fresh granite and groundwater sampled from KURT(KAERI underground research tunnel) at the Korea Atomic Energy Research Institute. Granite samples were crushed by a hammer mill and a disk type crusher, followed by sieving by particle size, and granite powder of $0.15 \leq \Phi < 0.3$ mm was washed and dried. The sorption experiments were carried in a glove box maintained in a N_2 atmosphere.

3. Results and Discussion

3.1 Sorption of actinides (U, Np, Am)

The sorption of U by granite was measured to be in the range of $1.7\times10^{-2} \sim 7.0\times10^{-2}$ m^3/kg and $1.9\times10^{-2} \sim 3.4\times10^{-2}$ m^3/kg under the reducing and oxidizing conditions, respectively. The Np was in the range of $1.1\times10^{-1} \sim 2.6\times10^{-1}$ m^3/kg (Eh = ~-0.3 V) and $8.4\times10^{-3} \sim 2.2\times10^{-2}$ m^3/kg (Eh = ~+0.3 V). On the other hand, the Kds of Am were measured very high.

When the pH of the solution increased from pH 3.46 to pH 8.56, the Kd of Np increased from in the range of $2.3\times10^{-2} \sim 3.6\times10^{-2}$ m^3/kg to 1.1×10^{-1}~2.6×10^{-1} m^3/kg respectively. Am sorption by granite was in the range of $2.8\times10^{-2} \sim 4.4\times10^{-2}$ m^3/kg at pH 3.08 and increased to pH 8.13, which increased the Kd of Am to 4.1 ~ 15.2 m^3 / kg. It confirmed that the pH effect on the sorption of Am by granite was greater than that of Np.

Table 1. Sorption of Actinides by Granite: Eh Effect

Nuclide	Eh (V)	pH	Kd (m^3/kg)
U	-0.3	9.32±0.03	$(4.4±2.6)×10^{-2}$
	+0.3	9.13±0.01	$(2.7±0.8)×10^{-2}$
Np	-0.3	8.56±0.04	$(1.8±0.7)×10^{-1}$
	+0.3	8.70±0.08	$(1.5±0.7)×10^{-2}$
Am	-0.3	8.13±0.11	11.2±6.2
	+0.3	8.59±0.15	6.3±2.6

Table 2. Sorption of Actinides by Granite: pH Effect

Nuclide	Eh (V)	pH	Kd (m^3/kg)
U	+0.3	3.57±0.57	$(1.1±0.7)×10^{-2}$
		6.92±0.17	$(8.3±2.5)×10^{-2}$
		9.2±0.04	$(2.9±0.2)×10^{-3}$
Np	-0.3	3.46±0.54	$(2.8±1.3)×10^{-2}$
		5.67±0.40	$(4.2±1.7)×10^{-2}$
		8.56±0.04	$(1.8±0.7)×10^{-1}$
Am	-0.3	3.08±0.09	$(3.3±0.4)×10^{-1}$
		6.01±0.45	4.5±3.3
		8.13±0.11	11.2±6.2

Table 3. Sorption of Anionic Radionuclides by Granite: Eh Effect

Nuclide	Eh (V)	pH	Kd (m^3/kg)
I^-	-0.35	8.83±0.04	$(2.0±2.0)×10^{-4}$
	+0.35	8.83±0.03	$(3.0±2.0)×10^{-4}$
$Se^{IV, IV}$	-0.35	8.65±0.14	$(1.7±1.4)×10^{-3}$
	+0.35	8.74±0.07	$(2.2±1.5)×10^{-3}$
Tc^{VII}	-0.35	8.51±0.10	$(3.0±0.6)×10^{-2}$
	+0.35	8.67±0.07	$(3.0±3.3)×10^{-3}$

Table 4. Sorption of Anionic Radionuclides by Granite: pH Effect

Nuclide	Eh (V)	pH	Kd (m^3/kg)
I	-0.35	3.01±0.02	$(5.0±2.0)×10^{-4}$
		6.63±0.70	$(6.0±1.0)×10^{-4}$
		8.83±0.04	$(2.0±2.0)×10^{-4}$
$Se^{IV, IV}$	-0.35	2.67±0.24	$(1.4±2.1)×10^{-1}$
		5.99±0.33	$(8.4±9.5)×10^{-3}$
		8.65±0.14	$(1.7±1.4)×10^{-3}$
Tc^{VII}	-0.3	2.96±0.06	$(5.8±4.1)×10^{-3}$
		5.45±0.65	$(4.8±1.2)×10^{-3}$
		8.67±0.07	$(3.0±3.3)×10^{-3}$

3.2 Sorption of anionic radionuclides (I, Se, Tc)

The sorption of I by granite was measured very low regardless the redox conditions and the solution pH with the Kd values range between $2.0×10^{-4}$ ~ $6.0×10^{-4}$ m^3/kg. The low Kd values of I for granite might be attributed its low reactivity with minerals[2]. While the redox potential of solution had an insignificant effect on the Se sorption by granite, pH had a great effect on its sorption. In an acidic condition, Kd values of Se were measured in the range of $4.0×10^{-3}$ ~ $5.5×10^{-1}$ m^3/kg. Except for the Kd values at acidic condition, sorption of Se was measured very low. A large variation of Kd values of Se is attributed to the redox state of Se such as selenite(Se^{IV}) and selenite(Se^{VI}). The sorption of Tc was sensitive to the redox condition, however the effect of pH on the sorption of Tc was in significant.

4. Conclusion

Kd values commonly used for the safety assessment of geological disposal repository for radioactive waste. Sorption of radionuclides could differently react with surrounding minerals when the geochemical conditions were changed. Kd values for various geochemical conditions should be considered for the safety assessment.

REFERENCES

[1] N. Chapman, I. McKinley, and M. Hill, “The Geological Disposal of Nuclear Waste”, John Wiley & Sons, Chichester (1987).

[2] D. Kaplan, R. Serne, K. Parker, and I. Kutnyakov, “Iodine Sorption to Subsurface Sediments and Illitic Minerals”, Environ. Sci. Technol., 34, 399-405 (2000).

Shearing Technology of Simulated Nuclear Fuel Rod Using Colling and Notching

Younghwan Kim*, Yungzun Cho, and Jinmok Hur

Korea Atomic Energy Research Institute, 111, Daedeok-daero 989beon-gil, Yuseong-gu, Daejeon, Republic of Korea

*Yhkim3@kaeri.re.kr

1. Introduction

The wet process shearer has problems such as mass oil waste when the simulated spent fuel rods are sheared by tools, and it has low product ability because of change time of oil and tools. Also, when spent fuel rod is sheared by shearer, round shape is crushed. In order to solve these problems, simulated spent fuel rods (Zry-4 tube+pellet) were manufactured and shearing test was conducted. Also, we selected a method of liquefied nitrogen with a roller blade for a fine circular type, and consisted of shearing module, rotation module and cooling module. We selected a nozzle spray method of cryogenic coolant on the pipe for shearing test. In the results, the problems of wet process shearer such as oil contamination and low product ability were solved by the nozzle spray method of cryogenic coolant. Also, a circular shape of shearing section was maintained by the cutting blades, nozzle splaying and lever. In the case of high speed shearing, tool life was largely affected by tool cooling than pipe cooling, if low speed of shearing, highly effective by it.

2. Existing wet shearer

The shearer of wet method is the device to shear anisotropic material. This device has the problem of continuously generating oil as during the shearing. Also, during the shearing by the shearer, the cross section of the anisotropic material was deformed from the original form.

3. Cryogenic dry shearer

Concept design, design supplementation, and basic design were carried out as in figure 1(a). For this, cryogenic shearing method using liquid nitrogen and roller blade method to maintain the original form were selected. This method cools the shearing part with the liquid nitrogen in the storage space installed at the back of the tool or on the tool holder with thermal conduction. At the same time of supplementing the design of the tube cryogenic dry shearer as in figure 1(b), test product of the tube dry shearer was made, which is composed of the cooling part, shearing part, and driving rotation part. The shearing length is decided by the micro meter on the left, and when the anisotropic tube of 25cm is manually inserted into the universal chuck of the driving rotation part, clamping is done by the fixed chuck wrench with uniform length. At this time, while rotating and forwarding with the tube shearing blade's needle handle, adjust the shearing depth.

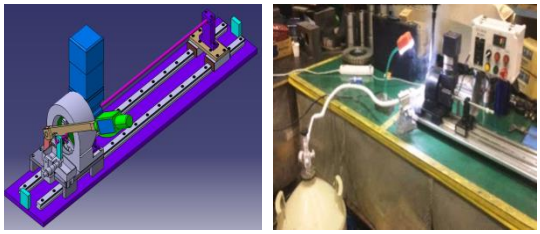

(a) Design (b) Device

Fig. 1. Cryogenic dry shearer design.

4. Shearing test

Tube cryogenic dry shearer was used to carry out the shearing test. The material of the target tube was SUS 316, length was 250mm, diameter was Φ 9.5mm on the outside and 8.3mm on the inside with white cement filled and solidified on the inside wall. The shearing length is adjusted to 30 mm with a micros meter, and the target

tube was fixed to the universal chuck and rotated. At this time, the variable number of rotations of the universal chuck was 15 rpm. The needle handle of the tube shearing blade was changed to 50°, 70°, and 90° to adjust the shearing depth. As in figure 2(a) liquid nitrogen of 300cc/min was sprayed by positioning the nozzle on the sheared scratched notch surface. At the same time, the tube was sheared using the principle of lever as in figure 2(b).

(a) Cooling (b) Shearing

Fig. 2. Shearing of cryogenic dry shearer.

5. Shearing test result

Figure 3 shows the sheared tubes. Also, it shows the result of the cross section of the sheared tube by comparing to the original form. With the comparison to the previous original shape before the shearer, the original form was not distorted. Table 1 shows the tool lifespan, productivity, and the surface illumination result of wet shearing and dry shearing.

Fig. 3. Results of cryogenic dry Shearing.

Table 1. Comparison of wet and dry process

Wet method	Dry method
○ Tool lifespan shortened by continuous processing - Tool lifespan during the shearing : 1	○ Tool lifespan extended for continuous processing - Shearing tool lifespan compared to previous lifespan : 4
○ Increased frequency of cutting oil and tool replacement - Reduced productivity by tool replacement	○ Improved productivity by reduced tool replacement time - 20% productivity increase by reduced tool
○ Use of cutting oil - Soil and water quality contamination by mass waste generation	○ Cryogenic cooling shearing technology - Prevention of environment contamination with cryogenic shearing method

6. Conclusion

The shearer shearing an anisotropic tube has the difficulty of distorted form from the original form of the anisotropic tube after the shearing. For this, the simulated rod-cuts were made for the shearing of the simulated nuclear fuel rods. Also, cryogenic shearing method using liquid nitrogen and roller blade method to maintain the original form were selected. The cryogenic cooling shearing test was carried out. As a result, the original form of the cross section of the tube was maintained with shearing blade, liquid nitrogen nozzle spray, and shearing by lever. Especially, in the cryogenic machine processing, as the shearing speed is higher, the tool cooling had bigger influence on the tool lifespan than the cooling of the processing subject, and as the shearing speed is lower, cooling the tools had much more effect on the tool lifespan.

ACKNOWLEDGEMENTS

This paper is the study carried out with the 2013 funding of the Ministry of Education, Science and Technology and the support from National Research Foundation of Korea (Nuclear Energy Technology Development Project, No. 2012M2A8A5025696).

REFERENCES

[1] J. A. King, T. J. Malewitz, S. M. James, and B. D. Simmons, “Mechanical Decladding of Irradiated FFTF Mixed Oxide Fuel Rods,” Transactions of the American Nuclear Society, Vol. 117, Washington, D.C., OCT.–NOV., pp. 333, 2017.

Simulations of Dipole Flow Tracer Test for Estimating Locally Variable Hydraulic Property

Nak-Youl Ko*, Kyung-Woo Park, and Sung-Hoon Ji
Korea Atomic Energy Research Institute, 111, Daedeok-daero 989beon-gil, Yuseong-gu, Daejeon, Republic of Korea
*nyko@kaeri.re.kr

1. Introduction

It can be expected to damage walls of boreholes for investigating underground environment and constructing underground facilities for deep geological disposal of radioactive wastes. It is important for safety of the disposal because radionuclide transport at the near-field can be facilitated by formation of short-cuts. In this study, numerical simulations of in-situ DFTT (Dipole Flow Tracer Test) was conducted in order to predict the effects by the damaged structures and to design effective field tests.

2. Method

With hydraulic data obtained from the field tests at boreholes in Research Gallery #6 of KURT, numerical simulations of DFTT were performed. The detailed hydraulic field tests were conducted and hydraulic conductivities of each test interval were assigned according to the results of field tests at the boreholes [1]. A local structure with different hydraulic conductivity, which represents damaged structures by excavation, was assumed to be located between the upper and lower chamber (Fig. 3).

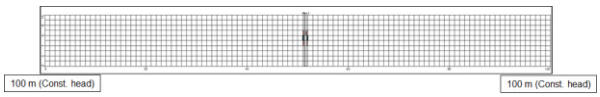

Fig. 1. Discretized modeling domain.

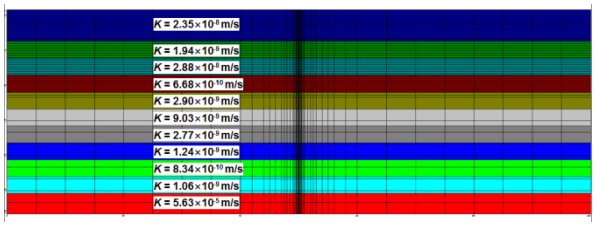

Fig. 2. Distribution of Hydraulic conductivity in the modeling domain by the detailed field tests.

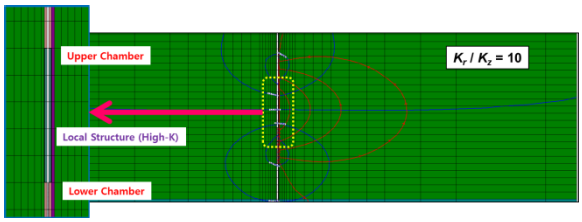

Fig. 3. Overview of two chambers for DFTT and location of locally damaged zone.

3. Results

3.1 Spatial Distribution of Tracers

Spatial distribution of tracers was simulated in the basic condition, which was assumed that the hydraulic conductivity of the local structure is 10^{-5} m/s (Fig. 4). The local structure had a role of a short-cut for injected water and tracers at the lower chamber. The difference of

hydraulic conductivities of each layer caused different spreading of tracers.

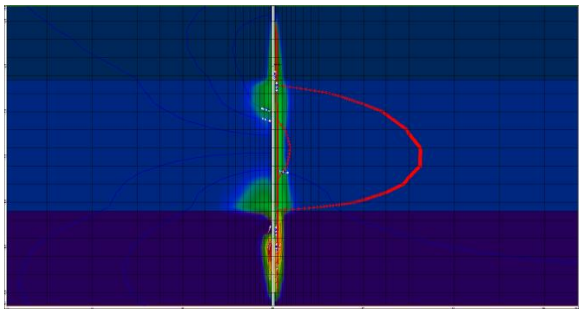

Fig. 4. Distribution of tracers under the basic condition.

3.2 Breakthrough Curves for Different Hydraulic Conductivity of the Local Structure

From the simulation results, when the hydraulic conductivity of the local structure was larger than a certain level, about 20 times that of the surrounding layer in this study, most of tracers moved through the local structure and the peak time of tracer concentration became shorter (Fig. 5).

4. Conclusions

To identify effects of local structure on a borehole wall due to damaged zone, numerical simulations of DFTT were performed. The arrangement of hydraulic conductivity in the modeling domain constructed from the data of field test had influence on a pattern of tracer breakthrough curves. Analysis of the pattern may give a representation occurred by local structures caused by excavation. The results of this study can be applied to design effective in-situ test of a dipole flow tracer test.

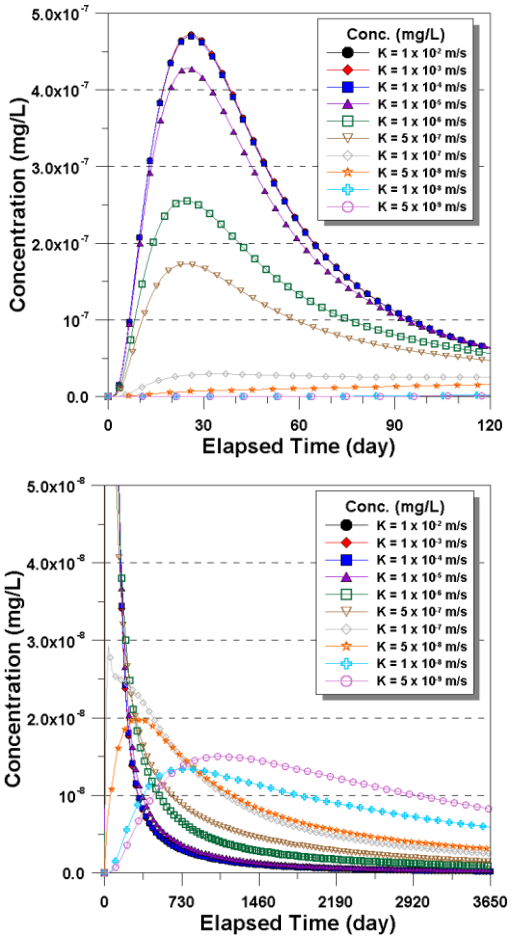

Fig. 5. Breakthrough curves of tracer concentrations for each hydraulic conductivity of the local structure.

ACKNOWLEDGEMENT

This work was supported by the Ministry of Science, ICT and Future Planning within the framework of the national long-term nuclear R&D program (NRF- 2017M2A8A5014858).

REFERENCES

[1] Korea Atomic Energy Research Institute (KAERI), Assessment of Hydrogeological Characteristics in BDZ-2 Borehole, KAERI/TR-7668/2019, KAERI, 2019.

Investigation Plan for the Geological Environment for URL Site in Korea

Jin-Wook Kim and Chang-Lak Kim*

KEPCO International Nuclear Graduate School, 658-91, Haemaji-ro, Seosaeng-myeon, Ulju-gun, Ulsan, Republic of Korea

*clkim@kings.ac.kr

Introduction

Detailed site investigation and characterization span the final stages of a siting process provides recommendations particularly for the detailed site characterization stage leading to site confirmation [1]. Based on the experience of Mizunami Underground Research Laboratory (URL) of JAEA, investigation plan for URL site in Korea is considered in this paper. Purpose of URL investigation is understanding of the geological environment and its long-term transition of the selected place. Geology and geological structures, groundwater flow, chemical properties, mechanical properties, etc. in a few kilometers square and below few hundred meters deep is needed to investigate. The investigation plan is intended to be formulated in three phases.

Phase 1. Surface-based Investigation

Purpose of surface-based investigation is understanding initial condition of geological environments. In this phase, literature survey, airborne and ground geophysical survey, surface geological investigations, reflection seismic investigation, and core borehole investigation, social feasibility study will be conducted. Results of surface-based investigation will be geological model and hydrochemical conceptual model.

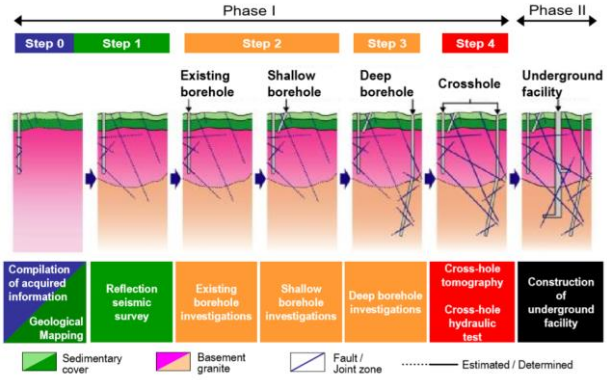

Fig.1. Investigation steps of Mizunami URL [2].

Phase 2. Investigation during Construction

During construction of the URL, investigation of geological environments around shafts and galleries will be conducted. Verification of geological environment models constructed in phase 1 and measurement of construction impact will be investigated through geological mapping, rock sampling, geophysical investigation and monitoring. Result of investigation during construction is evaluation of accuracy of geological model.

Phase 3. Investigation in Drift

Purpose of investigation in drift is understanding long-term behavior of geological environments. Monitoring in boreholes, in-situ experiments, groundwater recovery experiment will be conducted. Results of investigation in drift are development of countermeasure technologies for reducing groundwater inflow, development of modelling technologies for mass transport, development of drift backfilling technologies, and development of disposal safety cases. So that technologies, experiences and data for licensing and construction of actual disposal repository can be accumulated.

Conclusion

This paper introduced a plan to investigate the geological environment of URL in Korea through the case of Japan. The geologic environment can be defined sequentially in three phases to obtain information on long-term geological environment changes until the actual disposal site is operated and closed. Since only geological and hydrological studies can be conducted through a generic URL, such as MIU in Japan, therefore investigation using a site-specific URL will be required to apply for licensing of an actual disposal sites.

ACKNOWLEDGEMENTS

This research was supported by the 2019 Research Fund of the KEPCO International Nuclear Graduate School (KINGS), the Republic of Korea.

REFERENCES

[1] IAEA, Geological Disposal Facilities for Radioactive Waste, IAEA Specific Safety Guide No. SSG-14, 2011.

[2] JAEA, Sythesized Research Report in the Second Mid-term Research Phase, JAEA-Review-2016-014, 2016.

Physical and Mineralogical Changes of the Compact Bentonite in Underground Environment

Minsoo Lee* and Sung-Hoon Ji
Korea Atomic Energy Research Institute, 111, Daedeok-daero 989beon-gil, Yuseong-gu, Daejeon, Republic of Korea
*minm@kaeri.re.kr

1. Introduction

Compact bentonite buffer is generally installed around a disposal canister to suppress a nuclide transport and fix the canister at a borehole place. The installed buffer can change its physical and mineralogical properties for various reasons in underground environment. One of reasons considered is dissolving off of the mineral component such as feldspar or silica in hot underground water [1], and another thing is the precipitation of corrosion product on the bentonite particles. The metal ion from the corrosion product is reported to induce a cation exchange reaction with alkali cations in bentonite layer [2] which cause a considerable decrease of the swelling pressure. Therefore the survey of physical and mineralogical changes of the disposed buffer could be very important since which are directly related with the barrier performance of the bentonite buffer. In this paper, the bentonite buffers from the 3.1 and 6.5 year old KURT corrosion experiment were studied to know that there is any change in density, mineral component, and swelling index.

2. Experiment

Two kinds of bentonite buffers were selected from KURT long term corrosion experiments with different test periods of 3.1 and 6.5 years old. The bentonite blocks were used as the buffer materials of cast nodular iron and stainless steel 304 (Fig. 1).

XRD analysis was done to know the mineral composition change in bentonite buffers. ICP-OES and EPMA analyses were done to deduce the diffusion thickness of metal ions within the bentonite buffer. The apparent densities of the buffer blocks were estimated using a newly devised mineral oil impregnation method to know any other mineral loss or gain in the buffers. And the barrier performance change was also estimated by measuring a swelling index of the buffers.

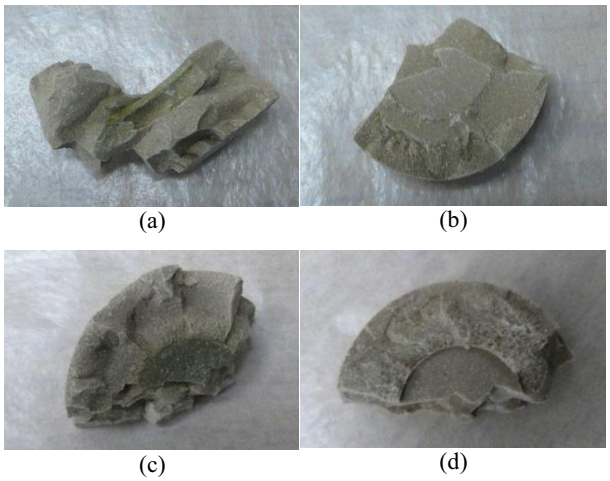

Fig. 1. Bentonite blocks from KURT long term corrosion experiment; (a) 3.1 year old-cast nodular iron test, (b) 3.1 year old-stainless steel test (c) 6.5 year old-cast nodular iron test, and (d) 6.5 year old-stainless steel test.

3. Result

3.1 XRD

The bentonite buffers of 3.1 and 6.1 years old did not exhibited any distinguishable change in the mineral composition. Some bentonite showed slight loss of Albite, but the montmorillonite content was nearly the same with the original bentonite for all samples.

3.2 ICP-OES, EPMA

The buffer used for cast nodular iron corrosion test showed high iron content to a depth of 2.5 mm. The permeation depth of iron was nearly the same of around 2~3 mm for the 3.1 and 6.5 year old buffers.

3.3 Apparent Density

The apparent density was about 1.72 g/cm^3 for all the 3.1 and 6.5 year old buffers which was nearly the same with the apparent density 1.76 g/cm^3 of the original buffer.

3.4 Swelling Index

The swelling index was influenced by the exposure time to underground water. The 3.1 year old buffer showed lower swelling index than that of the original buffer, but higher than that of the 6.5 year old buffer.

4. Conclusion

The 3.1 and 6.5 year old of bentonite buffers at KURT underground water were analyzed in the aspect of mineral composition, apparent density, and swelling index. There were not any noticeable changes in mineral composition and its density, but the swelling index was slowly decreased with the exposure time.

ACKNOWLEDGEMENT

This work was supported by the Ministry of Science, ICT and Future Planning within the framework of the national long-term nuclear R&D program (NRF- 2017M2A8A5014858).

REFERENCES

[1] C.W. Parmelee and A.J. Monack, "The solubility of feldspars in water", Journal of the American Ceramic Society, Volume 13, Issue 6, Version of Record online: 2 JUN 2006.

[2] A.E. Milodowski, M.R. Cave, S.J. Kemp, H. Taylor, B.P. Vickers, K.A. Green, C.L. Williams, R.A. Shaw, "Mineralogical investigations of the interaction between iron corrosion products and bentonite from the NF-PRO Experiments (Phase 1)", SKB Technical Reposrt, TR-09-02 (2009).

Groundwater Chronology in Fractured Granitic Bedrock in South Korea

Jihye Jeong*, Jang-Soon Kwon, Yong-Kwon Koh, and Jae-Kwang Lee
Korea Atomic Energy Research Institute, 111, Daedeok-daero 989beon-gil, Yuseong-gu, Daejeon, Republic of Korea
*yz0201@kaeri.re.kr

1. Introduction

In the repository sites for the high level radioactive waste (HLW), it is important to identify the groundwater characteristics because unplanned leakage of radionuclides from canister can transport along the groundwater movement eventually. So far, a number of studies have been conducted to investigate hydrochemical and biogeochemical properties of groundwater [1]–[3], but researches on the age evaluation of groundwater in fractured granitic bedrock in South Korea are little. The purpose of this study is to evaluate geochemical characteristics of groundwater and to discuss the age-tracers in fractured granitic bedrock in South Korea.

2. Study area

The groundwater samples were collected from the two representative granitic bedrocks (A and B sites) in the central region of South Korea. The geology of the A site is composed of Mesozoic Triassic, Jurassic and Cretaceous granites, while the B site consists of granite intruded by the Mesozoic Triassic. The elevation is 400 m and 680 m above sea level (a.s.l.) at the A and B area, respectively. And the land surface is mainly used for forest and grassland suggesting no anthropogenic source from mankind activities.

3. Methods

CFCs and SF_6 in groundwater were analyzed by Gas Chromatography with Electron Capture Detection in GNS science of New Zealand. The apparent ages of CFCs and SF_6 were determined by using the "CFC Report 2020" program. And the North American air curves for CFC-11, CFC-12, and CFC-113 were used to quantify the groundwater apparent aging in this study. Analysis of the absolute age for the groundwater used Tracer LPM program distributed by USGS and estimated optimal groundwater age (tracer) with error rate.

4. Results and Discussions

4.1 Hydrochemical characteristics

The quantitative sequence of major ions in the both A and B sites was in the order of HCO_3 > NO_3 > Cl > SO_4 > F. And in case of cations, calcium was the highest in both sites. Major ions and trace elements from the study areas showed not exceed the drinking water quality standards.

4.2 Age-dating of groundwater

Multiple analytical methods of CFC-12, CFC-

113 with the lowest error rate, showed the greatest accuracy (with a range of 10% ± 5). In the case of groundwater in the A site, the average age is estimated to be 25.1 years, which was recharged from 1988 to 1996. In the case of a B sites groundwater, the average age is 24.8 years, the average age was interpreted as a groundwater recharged from 1986 to 1996. Basically, in this study, the absolute age was originally determined using two kinds of analysis methods (CFCs, SF_6), but SF6 was excluded from the absolute age analysis due to its high error rate (average 80.4%). Originally, SF_6 has excellent advantages as an environmental tracer, but there are many limitations [4]: 1) the potential for inflow into groundwater through artificial contaminated routes; 2) inflow of contamination caused by the construction of the well; 3) the origin of natural generation. In this study, high fluorine concentration were observed in the groundwaters from the two sites, and these are might hesitate SF_6 age-dating.

5. Conclusions

The dominant constituents in the groundwater within granitic bedrock aquifer in this study were calcium and bicarbonate for cation and anion, respectively. The ages of groundwater are 25.1 and 24.8 years for the area A and B, respectively. This is the result calculated using the Multiple parameter tracers of CFC-12 and CFC-113. The reasons why SF6 cannot be used in determining age in granite groundwater are as follows: 1) the potential for inflow into groundwater through artificial contaminated routes; 2) inflow of contamination caused by the construction of the well; 3) the origin of natural generation.

ACKNOWLEDGEMENT

This work was supported by the MSIT within the framework of the national long-term nuclear R&D program (NRF-2017M2A8A5014859).

REFERENCES

[1] J.-H. Ryu, J.-S. Kwon, G.-Y. Kim, and Y.-K. Koh, “Geochemical Characterization of Rock-Water Interaction in Groundwater at the KURT Site,” J. Nucl. Fuel Cycle Waste Technol., vol. 10, no. 3, pp. 189–197, 2012.

[2] N.-Y. Ko, K. W. Park, K. S. Kim, and J. W. Choi, “Groundwater Flow Modeling in the KURT site for a Case Study about a Hypothetical Geological Disposal Facility of Radioactive Wastes,” J. Nucl. Fuel Cycle Waste Technol., vol. 10, no. 3, pp. 143–149, 2012.

[3] S. Y. Lee, Y. Roh, and J. T. Jeong, “Changes of the Oxidation/Reduction Potential of Groundwater by the Biogeochemical Activity of Indigenous Bacteria,” Econ. Environ. Geol., vol. 47, no. 1, pp. 61–69, 2014.

[4] Busenberg, E., & Plummer, L. N. (2000). Dating young groundwater with sulfur hexafluoride: Natural and anthropogenic sources of sulfur hexafluoride. Water Resources Research, 36(10), 3011-3030.

Investigation of Thermal Conductivity for the Bentonite Particles

Seok Yoon[1,*], Seunghun Park[2], and Geonyoung Kim[1]
[1]Korea Atomic Energy Research Institute, 111, Daedeok-daero 989beon-gil, Yuseong-gu, Daejeon, Republic of Korea
[2]Inha University, 100, Inha-ro, Michuhol-gu, Incheon, Republic of Korea
[*]syoon@kaeri.re.kr

1. Introduction

The concept of an engineered barrier system (EBS) is suggested to dispose high level waste (HLW). EBS is composed of a disposal canister with packed spent fuel, a buffer material, backfill material, and near field rock mass [1]. A buffer material is very essential to guarantee the disposal safety of HLW, and play a very important role to protect the waste and canister against any external mechanical impact. Furthermore, it requires high thermal conductivity to release as much decay heat as possible from the spent fuel [2]. The thermal conductivity of the buffer material is a very important thermal property that determines the temperature change owing to decay heat from spent fuel. There have been many researches to investigate the thermal conductivity of bentonite buffer materials or many types of soils. However, there is a lack of research on the specific evaluation of the thermal conductivity of bentonite particles considering temperature variation. Therefore, this paper measured thermal conductivity of the dried compacted bentonite considering temperature variation.

2. Experimental Setup

2.1 Transient hot wire method

Fig. 1. Specimen and probe.

The thermal conductivity of the dried compacted bentonites produced in Gyeongju region of Korea was measured using QTM-500 (Kyoto Electronics Manufacturing Company, Japan), based on the transient line source method [2]. An impulse of thermal flow is supplied by hot wire into the compacted bentonite, and temperature rise is measured within a certain time. The thermal conductivity can be measured using Eq. (1)

$$\lambda = \frac{Q}{4\pi\Delta T}\ln(\frac{t_2}{t_1}) \quad (1)$$

where λ is the thermal conductivity ($W \cdot m \cdot K^{-1}$), Q is the heat capacity per unit length ($W \cdot m^{-1}$), T is the temperature (K), and t is the time (s). The dried compacted bentonite and probe were

sealed with heat resistance tape (Fig. 1), and they were placed in the furnace during the experiment in order to consider temperature variation.

2.2 Results and Discussion

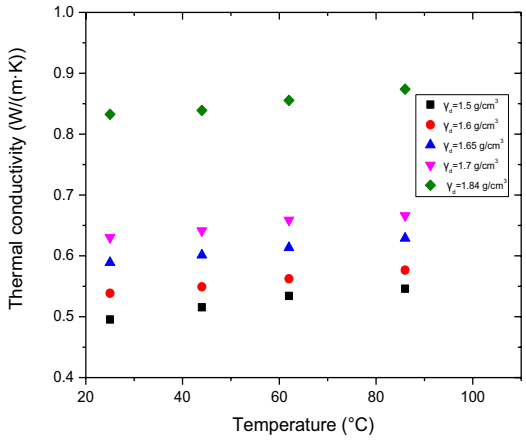

Fig. 2. Thermal conductivity variation (w=0%).

Fig. 2 shows thermal conductivity variation of the dried compacted bentonites according to temperature increase. There was 4~10% increase of thermal conductivity with respect to temperature increase. In dry condition, there are just air and soil particles. The thermal conductivity of air is 0.025~0.3 W/(m·K) under the temperature range 20 to 90 °C [2]. Since the thermal conductivity of air is very small in comparison with water or bentonite particles, it is thought that bentonite particles can contribute to the increase of thermal conductivity for the dried compacted bentonite.

3. Conclusion

This paper measured thermal conductivity of dried compacted bentonites with different dry densities according to temperature increase. Temperature range was between 20 and 90 °C. Thermal conductivity was a little proportional to temperature increase, and it can be referred that thermal conductivity of bentonite particles can be increased with temperature increase. Therefore, it is necessary to analyze thermal conductivity for the compacted bentonite at different degrees of saturation of dry densities in order to consider real repository condition.

ACKNOWLEDGEMENT

This research was supported by the Nuclear Research and Development Program of National Research Foundation of Korea (NRF) funded by the Minister of Science, ICT and Future Planning.

REFERENCE

[1] Lee, J.W., Choi, H., Lee, J.Y., Thermal conductivity of compacted bentonite as a buffer material for a high-level radioactive waste repository, Ann Nucl Energy 94 (2016a), 848-855.

[2] Yoon, S., Lee, M.S., Kim, G.Y., Lee, S.R., Kim, M.J., A prediction of thermal conductivity for compacted bentonite buffer in the high-level radioactive waste repository, J. Korean Geotech Soc 32 (2017), 55-64.

[3] Lee, M.S., Choi, H.J., Lee, J.W., Lee, J.P., Improvement of the thermal conductivity of a compact bentonite buffer, KAERI/TR-5311 (2013).

[4] Cengel, Y.A. and Ghajar, A. J., Heat and mass transfer: fundamentals and applications, Fourth edition, McGraw Hill Education.

A Study on Concept Development of a Horizontal Disposal for CANDU Spent Fuels

Jong-youl Lee*, Hyun-a Kim, In-young Kim, Heui-joo Choi, and Dong-keun Cho
Korea Atomic Energy Research Institute, 111, Daedeok-daero 989beon-gil, Yuseong-gu, Daejeon, Republic of Korea
*njylee@kaeri.re.kr

1. Introduction

There are two types of reactors, Pressurized Water Reactor (PWR) and Pressurized Heavy Water Reactor (PHWR or CANDU), in Korea. For the CANDU type, four nuclear power reactors have been operated in Wolsung site and about 665,000 bundles of CANDU spent fuels are estimated to be generated from these four CANDU reactors. The characteristics of CANDU spent fuels are quite different from PWR spent fuels. Therefore, a disposal concept for CANDU spent fuels should be developed like PWR spent fuels disposal concept.

Generally, the KBS-3V (Vertical) type disposal in deep geological disposal options has been considered as a reference concept and currently under the stage of licensing. However, there are many methods as alternative concepts to the reference concept. The horizontal disposal concept can be one of the alternative concepts.

In this study, a reference disposal concept for CANDU spent fuels was reviewed and preliminary study on the development of a horizontal disposal concept was described. In addition, thermal analysis for a horizontal disposal concept was carried out. Lastly, preliminary disposal efficiency was analyzed.

2. Reference CANDU SF Disposal Concept

In Korea, there is no site-specific activity for HLW disposal. Therefore, Figure 1 showed a generic reference disposal concept for CANDU spent fuels that was vertical disposal type called KBS-3V. This reference concept has multiple barrier. They are natural barrier that is host rock and engineered barrier that are disposal canister and buffer block. Because the concept has a thermal requirement (buffer temperature<100°C), the thermal analysis was carried out to check the design requirement. Figure 2 showed the thermal analysis results. As shown in the figure, the disposal system met the thermal requirement.

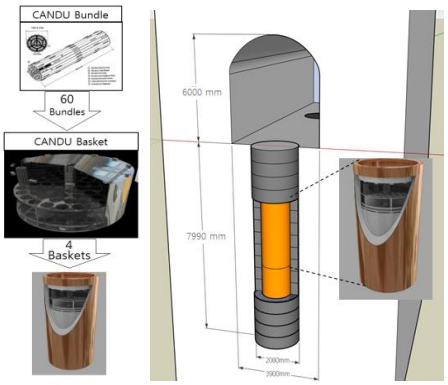

Fig. 1. Reference disposal concept for CANDU SNF.

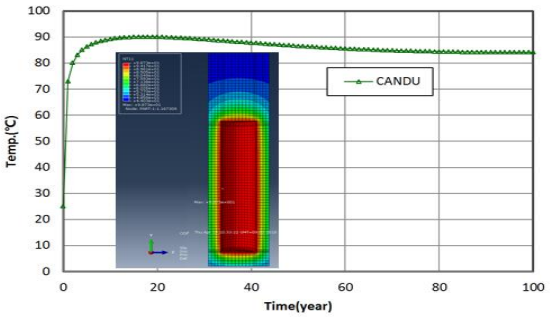

Fig. 2. Thermal analyses and results.

3. Horizontal Disposal Concept for CANDU SF

Development of alternative disposal concepts to improve the efficiency and safety of the reference concept suitable for various environments in each country is necessary. To do this, alternative disposal concepts were analyzed by reviewing the status of disposal concept in various countries. In this paper, the KBS-3 type horizontal disposal concept was studied preliminarily based on the results of the review results.

A horizontal type disposal concept for CANDU spent fuels is a kind of modified KBS-3H type disposal concept.

In this concept, an integrated module with disposal container and bentonite block box which was called buffer box was adopted. Figure 3 showed the concept of disposal container and buffer box. In addition, the

disposal tunnel section was shown in the figure.

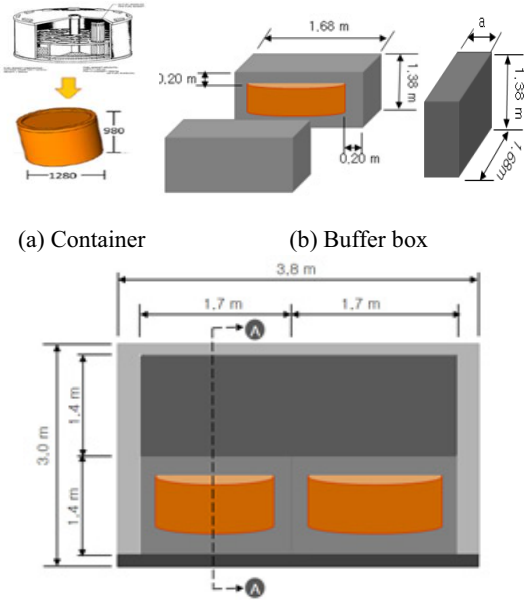

(a) Container (b) Buffer box

(c) A concept of disposal tunnel

Fig. 3. Horizontal disposal concept for CANDU SF.

To check the thermal requirement of the disposal concept, the thermal analysis was carried out preliminarily. Figure 4 showed the model and the result of the analysis.

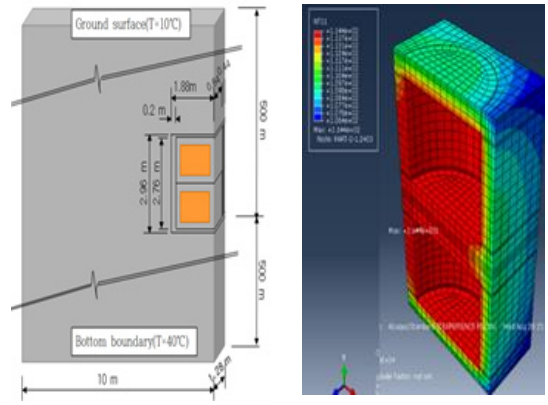

(a) Thermal analysis model (b) Results

Fig. 4. Thermal analysis for horizon disposal.

From the thermal results, horizontal disposal concepts for CANDU spent fuels were shown in the table 1. Preliminary results of disposal efficiencies analyses were shown in table 2. As shown in the table 2, the horizontal disposal concept for CANDU spent fuels could have a reduced disposal area about 20 ~ 30 % depend on the tunnel spaces.

Table 1. Concepts of horizontal disposal for CANDU SF

Cool. T.	Tunnel S.	Container S.	Max. Temp.
30 yr.	25 m	2.56 m	99.8 °C
40 yr.	25 m	2.56 m	97.6 °C

Table 2. Disposal efficiencies

	Ref. Concept	Horizontal Concept	
Total SF	664,637	664,637	664,637
Tunnel S.	40 m	25 m	30 m
Container S.	5 m	2.56 m	2.56 m
Unit D. A	200 m^2	64 m^2	76.8 m^2
Disposal A	276,932 m^2	177,236 m^2	212,683 m^2
Efficiency	1.00	0.64	0.77

4. Conclusion

In this study, for efficiency of the disposal area of CANDU spent fuels, a preliminary study on the development of a horizontal disposal concept was carried out. In addition, thermal stability and efficient analysis for a horizontal disposal concept were analyzed. Analyses that are more detailed should be carried out with real site data later.

The results of this study can be used as an input data for the next step of disposal concept development and for establishment of national policy on spent fuel management.

ACKNOWLEDGEMENT

This work was supported by the Ministry of Science and ICT within the framework of the national long-term nuclear R&D program (NRF-2017M2A8A5014856).

REFERENCES

[1] SKB, Horizontal emplacement technique of super container and distance blocks, SKB R-08-43 (2008).

[2] J. LEE, H. CHOI, An Engineered Barrier Concept of Reference Deep Geological Disposal System for Hi-burnup Spent Fuels, Technical Report, KAERI/TR-7405/2018 (2018).

[3] J. Noronha, Deep Geological Repository Conceptual Design Report, NWMO. APM-REP-00440-0015 (2016).

Fracture Study Using Borehole Dara and Microstructural Analysis of Fracture Filling Minerals Around KURT Site

Soolim Jung*, Sung-Hoon Ji, and Kyung-Su Kim

Korea Atomic Energy Research Institute, 111, Daedeok-daero 989beon-gil, Yuseong-gu, Daejeon, Republic of Korea

*sljung@kaeri.re.kr

1. Introduction

In order to evaluate long-term safety of disposal facilities for radioactive waste, it is necessary to understand the geological characteristics of natural barrier and its long-term evolution history around the disposal site. Fracture network is one of the key characteristics in terms of disposal site investigation. Open fractures developed underground intrusive granite body are the most probable pathways for groundwater flow, and the groundwater flow could carry the hazardous nuclides from the deep underground facility to subsurface ecosystem. In addition, relatively weak fracture surfaces have high potential to occur seismic slip under the excessive stress field than intact rock, which can cause serious disturbances to the facility. In this study, distribution of fractures around KURT site were investigated and microstructures of fracture filling minerals were observed to understand the history of fracture generation. The development history of fracture could contributes to better estimation of underground fracture networks.

2. Study area

The research was performed around KURT (Korea Atomic Energy Research Institute Underground Research Tunnel), Daejeon, Korea. The KURT is located in the boundary between Okcheon Belt and Kyunggi Massif. The area is mostly composed of Mesozoic intrusive granite body. The major rock type consisting KURT area is two-mica granite[1].

To understand the geological information around the research area, structural analysis of the exposed outcrop and flat-cut surface inside KURT were investigated. Relatively fresh outcrops located in the several research modules of the KURT were observed to interpret the fracture networks.

The borehole geophysical surveys have been performed for several drillholes adjacent to the KURT to collect geological information of the deep underground. Drilling core samples were taken from the host rocks and fracture fillings to observe microstructures and then characterize the fracture networks.

3. Results

According to the previous study, most of distinctive joint sets were corresponded to approximately 6 sets of joints recognized in the outcrop of KURT, including three major sets of joints measured from the regional scale field survey[2]. The fracture systems observed in the borehole are almost correlated with the major joint sets from field survey. The microstructures of fracture filling minerals indicate the evidences of several hydrothermal events during the cooling stage of intrusive granite body in the research area. NW-SE trend fractures which direction is similar with hydrothermal fluid intrusion, could be formed by extensional fracturing at higher depth and temperature, and some hydrothermal alterations might be overlapped for a long geological period through the granite body uplifting. Further absolute age dating and chemical and microstructural analysis for fracture fillings are required to construct detailed development history of fractures and corresponding fracture networks of the research area.

ACKNOWLEDGEMENT

This work was supported by the Ministry of Science, ICT and Future Planning within the framework of the national long-term nuclear R&D program (NRF- 2017M2A8A5014858).

REFERENCES

[1] H.-I. Park, J.-D. Lee, and J.G. Jeong, “Geological map of Korea: Yuseong sheet”, Korea Institute of Geoscience and Mineral Resources (1977).

[2] S. Jung, K.-W. Park, S.-H. Ji, and K.-S. Kim, “Interpretation of Geological Deformation History by Integrated Analysis of Field and Borehole Survey around KURT Area”, Proc. of the KRS 2019 Spring Conference, 17(1), May 8-10, 2019, Busan.

Analysis on Characteristics of Structural Materials in the PLUS7 PWR SNF

In-Young Kim* and Dong-Keun Cho

Korea Atomic Energy Research Institute, 111, Daedeok-daero 989beon-gil, Yuseong-gu, Daejeon, Republic of Korea

*iykim@kaeri.re.kr

1. Introduction

For safe disposal of SNFs in Korea, the KRS concept had been developed in 2000s based on a low burn-up reference fuel. Recently, two kinds of SNFs are considered as reference fuels because of change in projection of SNF generations after KRS development. For the Westinghouse-type reactors, a KSFA with 4.5 wt. % of initial enrichment, 55 GWd/MtU of burn-up, and 50 years of cooling time is selected. For the Korean-type reactors, a PLUS7 SNF with 4.5 wt. % of initial enrichment, 55 GWd/MtU of burn-up, and 45 years of cooling time is selected [1]. In this study, characteristics of cladding and structural materials of PLUS7 PWR SNF were analyzed as a part of quantitative analysis of a PLUS7 reference fuel.

2. Methods and Results

2.1 Analysis Models

To evaluate characteristics of structural and cladding materials of a PLUS7 reference fuel, activation and decay calculation was conducted using Origen-arp. The major compositions of each materials are described in the Table 1. Although bottom and top region fluxes are much lower than core region, activation fluxes are assumed to be same as fuel rod conservatively.

Table 1. Materials for PLUS7 assembly [2]

Material	Component	Weight [kg]	Major composition
Zirlo	Cladding	105.7	Zr: 97.8 Sn: 1.0 Nb: 1.0
	Outer guide tube and post center, Center guide tube, Sleeve	19.1	
SS-304	Inner extension, Flow plate, Bottom nozzle assembly	81.4	Fe: 68.8 Cr: 19.0 Ni: 8.9
Inconel-718	Hold down spring, Strap, Washer	6.7	Ni: 52.0 Cr: 20.0 Fe: 18.0

2.2 Results

From Fig.1 to Fig. 6 shows decay heat and radioactivity from 1kg of activated Zirlo, SS-304, and Inconel-718 in the PLUS7 fuel. The major nuclides of the Zirlo are Sb-125, Nb-93m, Nb-94, Zr-93. The Fe-55, Co-60, Ni-63, Ni-59, C-14 are major nuclides for SS-304. For Inconel-718, Co-60, Ni-63, Nb-94, Ni-59 are major nuclides. The decay heat of Zirlo, SS-304, and Inconel-718 are 0.03%, 1.0%, 6.1% of 1kg SNF fuel rod respectively. The radioactivity of Zirlo, SS-304, and Inconel-718 are 0.1%, 2.3%, 13.7% of 1kg SNF fuel rod. Despite insignificant decay heat and radioactivity, nuclide inventories of cladding and structural material must be considered because of high content of PA nuclides such as C-14, Tc-99 affecting exposure dose of DGR.

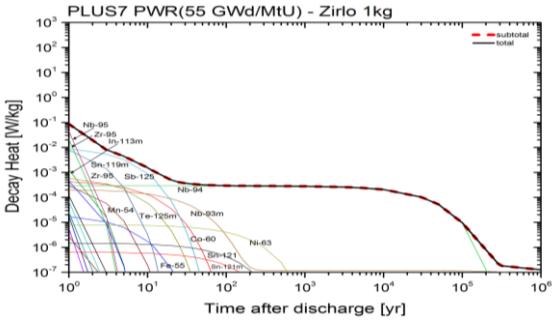

Fig. 1. Decay heat from 1 kg Zirlo in PLUS7 SNF.

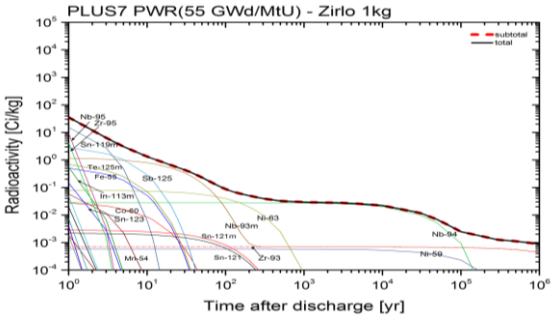

Fig. 2. Radioactivity from 1 kg Zirlo in PLUS7 SNF.

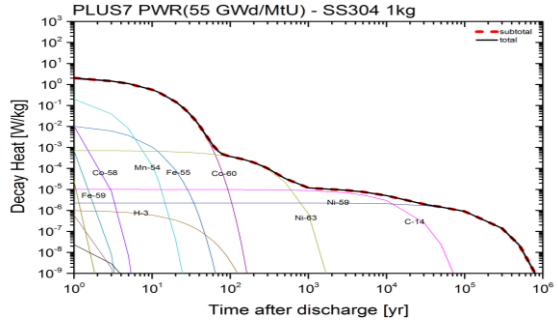

Fig. 3. Decay heat from 1 kg SS-304 in PLUS7 SNF.

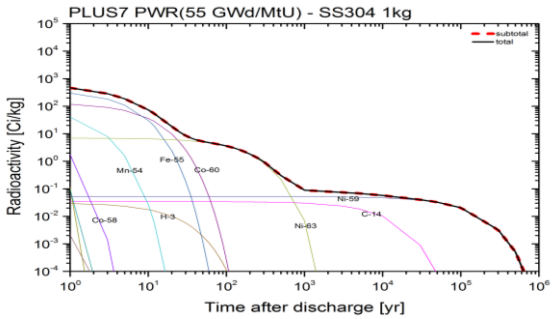

Fig. 4. Radioactivity from 1 kg SS-304 in PLUS7 SNF.

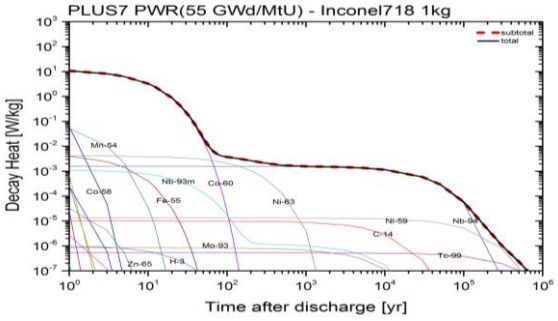

Fig. 5. Decay heat from 1 kg Inconel-718 in PLUS7 SNF.

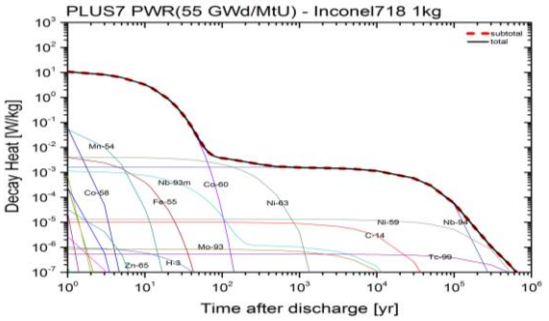

Fig. 6. Radioactivity from 1 kg Inconel-718 in PLUS7 SNF.

3. Conclusion

In this study, characteristics of cladding and structural materials are evaluated assuming activation in core region conservatively. Decay heat and radioactivity of Zirlo, SS-304, and Inconel-718 are very low comparing SNF fuel rods. Major nuclides of each materials are defined. The nuclide inventory of cladding and structural material must be considered in TSPA of DGR because of high content of PA nuclides such as Tc-99 and C-14. Results of this study would be used as design data for amelioration of KRS.

REFERENCES

[1] Dong-Keun Cho et. al., Investigation of PWR SF for the Design of DGR, progress in the publication process.

[2] Chang Je Park et. al., Radiation Analysis for Skeleton of SNF Assembly, KAERI/TR-4171/2010, KAERI.

Development of an Input Database for the Post-closure Safety Assessment of a Radioactive Waste Repository

Jongtae Jeong* and Dong-Keun Cho
Korea Atomic Energy Research Institute, 111, Daedeok-daero 989beon-gil, Yuseong-gu, Daejeon, Republic of Korea
*jtjeong@kaeri.re.kr

1. Introduction

The post-closure safety assessment of a radioactive waste repository is a fundamental part of the development of radioactive waste management program. Large amounts of input data are necessary for the post-closure safety assessment of a radioactive waste repository. The development of an input database may be very useful for the efficient practice of a safety assessment. In this paper, we developed a database management system using Microsoft Access program [1] for the safety assessment of a radioactive waste repository.

2. Development of a database

2.1 Tables and Fields of PCSA Input Database

Microsoft Access is a relational database system designed for home or small business usage. Access is known as a desktop database system because its functions are intended to be run from a single computer.

We developed a PCSA (Post Closure Safety Assessment) Input Database using Microsoft Access program. We divided input data for the safety assessment into three categories; inventory and source tern, near field, and far field. The tables and fields in each table are summarized in Table 1. This lists of tables and field data of inventory are shown in Fig. 1.

We collected input data from many references such as input data for K-PAM code and safety assessment reports of Sweden [2], Finland [3], USA, and Canada.

Table 1. Tables and fields in PCSA input database

Inventory and source term	Inventory	PWR, CANDU, Pyro Metal Wastes, Pyro Ceramic Wastes, YMP SF, CANDU-NWMO
	Instant Release Fraction	SKB(Lower/Central/Upper), POSIVA(EPR, VVER), NWMO(CANDU)
	Activity Release Rates	Time(Max), Release Rate
Near Field	Diffusion coefficient	KAERI(Water, Effective, Apparent), POSIVA(Buffer, Backfill), SKB(Effective, Upper, Lower)
	Distribution coefficient	KAERI(Buffer, Rock, Backfill, Soil, River, Sea), POSIVA(Backfill, Buffer, Rock), SKB, NWMO, Swiss
	Solubility	KAERI(Mode, Min, Max), POSIVA(Buffer, Backfill, Water), SKB(Saline, Bentonite, Ice Melting), NWMO(Solubility, SD, Distribution Type)
Far Field	Dose coefficient	KAERI(Ingestion, Inhalation, External), SKB(Ingestion, Inhalation, External), POSIVA
	Soil to plant concentration factor	Rice, Grain, Fruit, Root Vegetable, Green Vegetable, Pasture
	Transfer coefficient to animal product	Beef, Pork, Chicken, Mutton, Cow Liver, Cow Milk, Chicken Liver, Chicken Egg
	Weathering rates	Rice, Grain, Fruit, Root Vegetable, Green Vegetable, Pasture)

2.2 Forms and Reports of PCSA Input Database

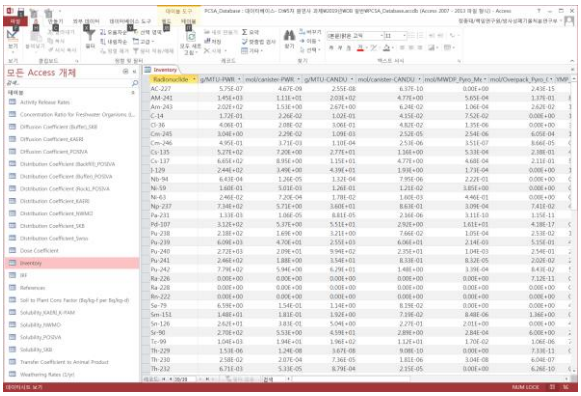

Fig. 1. Screenshot of PCSA Input Database.

Access forms provide non-technical users the ability to add and modify data to the database. In the PCSA Input database, we made access forms such as diffusion coefficient input form, distribution coefficient input form, inventory input form, solubility input form, and transfer coefficient to animal product input form. As an example, the inventory input form is shown in Fig. 2. With these input forms we can add and update data.

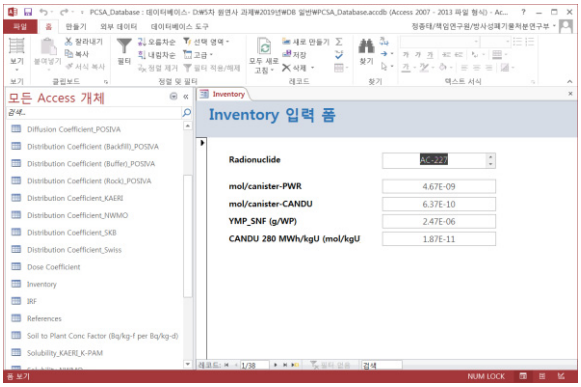

Fig. 2. Screenshot of the Inventory Data Input Form.

A report in the Access database is a database object that is used to organize and display data pulled from tables and queries. We made reports for the display of diffusion coefficients, distribution coefficients, inventories, solubilities, and transfer coefficients to animal products. As an example, the report for the spent fuels and pyro-wastes is shown in Fig. 3.

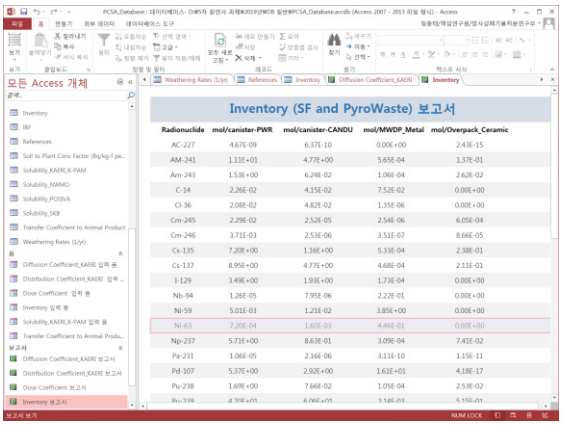

Fig. 3. Screenshot of a Report for Inventory Data.

3. Conclusions

We are developing a PCSA Input Database using Microsoft Access program for the purpose of collecting, managing, and updating of input data for the post closure safety assessment of a radioactive waste repository. Although it is now under development, it can be very useful for the management of input data for the safety assessment.

ACKNOWLEDGEMENT

This work was supported by the National Research Foundation of Korea Nuclear Research and Development Program (2017M2B2B1072407, 2017M2A8A5014856) funded by the Ministry of Science and ICT.

REFERENCES

[1] Microsoft Official Academic Course Microsoft Access 2016 (2016).

[2] SKB, SR-Can Data and uncertainty assessment, SKB-TR-04-18, Sweden (2004).

[3] POSIVA, Radionuclide Release and Transport - RNT-2008, Finland (2008).

Thermal Behavior of Montmorillonite in Korean Bentonite Under the KURT Groundwater Saturated Conditions

Tae-Jin Park[1,*] and Donghoon Seoung[2,‡]
[1] Korea Atomic Energy Research Institute, 111, Daedeok-daero 989beon-gil, Yuseong-gu, Daejeon, Republic of Korea
[2] Chonnam National University, 77, Yongbong-ro, Buk-gu, Gwangju, Republic of Korea
[*]etjpark@kaeri.re.kr, [‡]dseoung@jnu.ac.kr

1. Introduction

The host-guest interaction and structural configuration of water molecules inside montmorillonite interlayers under the controlled thermal conditions are of importance in understanding the performance of high-level radioactive wastes buffer system especially under the conditions that the spend nuclear fuels generate decay heats [1,2,3].

The volume expansion and contraction via hydration and dehydration of the buffer are accompanied by the configuration of water layers inside montmorillonite [4,5]. Thus, we have conducted in-situ X-ray powder diffraction experiments as a function of temperature for the Korean bentonite (*e.g.*, the Gyeongju bentonite) under the dry as well as the KURT groundwater saturated conditions and report the thermal behavior of montmorillonite in Gyeongju bentonite obtained under the KURT groundwater saturated conditions.

2. In-situ synchrotron X-ray powder diffraction

2.1 Method

In-situ synchrotron X-ray powder diffraction on montmorillonite was performed at beamline 3D at Pohang light source (PLS-II) at Pohang accelerator laboratory (PAL). For the in-situ sample heating environments, a sealed capillary with a diameter of 700 ㎛ surrounded by nickel-chrome resistance heating coils was heated from RT to 250°C as a function of temperature.

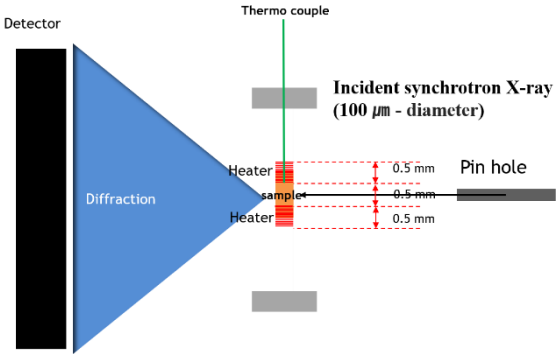

Fig. 1. A schematic of in-situ synchrotron XRD experiments of montmorillonite in Gyeongju bentonite.

2.2 Thermal behavior of montmorillonite under the KURT groundwater saturated condition

In case of dry condition for comparison, the water layers inside montmorillonite abruptly change from 2 layers to no water layers at 120°C concomitant with 35.4% of volume contraction due to its hydrogen bond breaking with oxygen atoms of aluminosilicate layers (Fig. 2(a)). As a counterpart, ground water saturated montmorillonite shows changes from 4 water layers to 2 layers as a function of increasing temperature via *d*-spacing change from 19.02 Å to 16.11 Å. After its abrupt collapse, water layers configuration gradually decreases from 2 layers to single layer until 225°C via d-spacing change from 16.11 Å to 13.65 Å.

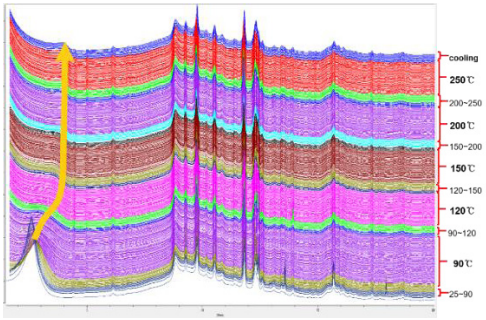

(a)

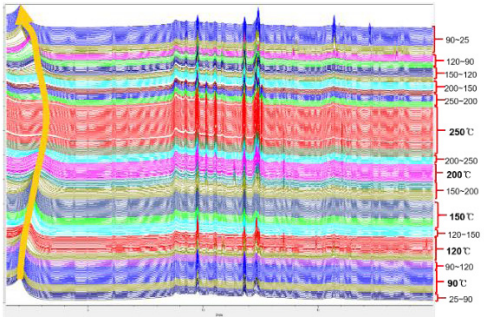

(b)

Fig. 2. Changes in the d-spacing (Å) of montmorillonite (001) reflections (a) without water condition (b) under water saturated condition as a function of temperature.

3. Conclusions

We experimentally established an approach to study the thermal behavior and water layer configurations of montmorillonite at the elevated temperatures. This includes both hydrothermal and dry conditions that show particular contraction of the montmorillonite at 120°C and 250°C with dehydration sequence concomitant with changes of water layers configuration.

ACKNOWLEDGEMENT

We acknowledge the Korean government, Ministry of Science and ICT, for support No. 2017M2A8A5014859 and NRF-2017R1D1A1B03035418.

REFERENCES

[1] Park, T.-J., Ryu, J.-H., Cho, W. H., and Lee, J.-K., "Buffer retardation experiments for radionuclides under the elevated temperature conditions: Strategy and methodology development for the Korean bentonite", Proc. Kor. Rad. Waste Soc., 16(2), 203-204 (2018).

[2] Seoung, D. and Park, T.-J., "Buffer retardation experiments for radionuclides under the elevated temperature conditions: In-situ synchrotron X-ray powder diffraction study for the Korean bentonite under the KURT groundwater saturated conditions", Proc. Kor. Rad. Waste Soc., 17(1), 149-150 (2019).

[3] Park, T.-J., Ryu, J.-H., Lee, J.-K., and Seoung, D., "Buffer retardation experiments for radionuclides under the elevated temperature conditions: In-situ synchrotron X-ray powder diffraction study for the Korean bentonite under the dry conditions", Proc. Kor. Rad. Waste Soc., 17(1), 147-148 (2019).

[4] Ewing, R.C., "Long-term storage of spent nuclear fuel", Nature Materials, 14(3): p. 252-257 (2015).

[5] Sellin, P. and O.X. Leupin, "The use of caly as an engineered barrier in radioactive-waste management - A review", Clays and Clay Minerals, 61(6): p. 477-498 (2013).

Development of Far-field Hydraulic Module of APro

Jung-Woo Kim[1),*], Minjeong Kim[1),2)], Jaewon Lee[1)], Kyung Woo Park[1)], and Dong-Keun Cho[1)]
[1)]Korea Atomic Energy Research Institute, 111, Daedeok-daero 989beon-gil, Yuseong-gu, Daejeon, Republic of Korea
[2)]Ulsan National Institute of Science and Technology, 50, UNIST-gil, Eonyang-eup, Ulju-gun, Ulsan, Republic of Korea
[*]jw_kim@kaeri.re.kr

1. Introduction

KAERI has been developing a process-based total system performance assessment model for a geological disposal system, which is the so called "APro". In this context, the modeling interface was designed and set up using MATLAB, COMSOL, and PHREEQC, and EBS-related modules, such as radioactive decay heat and thermal transfer, canister corrosion, and radionuclide release, were developed in the previous study.

The hydraulic characteristics (e.g. groundwater flow) in the host rock around the repository are very important as a major inducer of radionuclide transport, which is a key element of the safety assessment of the disposal system. In this study, therefore, the far-field hydraulic module was developed based on the KURT data and embedded into APro.

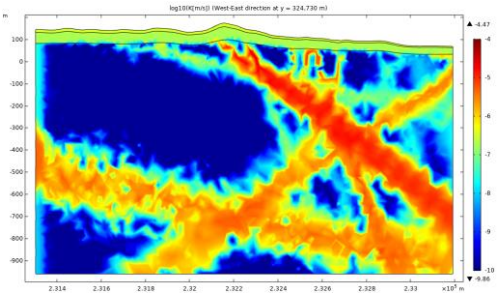

Fig. 1. Distribution of hydraulic conductivity around KURT ($\log_{10}$(K[m/s]) at y = 324,730 m).

2. Hydraulic Data around KURT

2.1 Hydraulic conductivity

Based on the hydraulic characteristics, the rock around KURT were divided into 3 zones: weathered zone (WZ, 15 ~ 30 m depth), upper highly fractured rock (UHFR, 22.5 ~ 84.2 m depth), and lower sparsely fractured rock (LSFR, below 84.2 m depth). The hydraulic conductivities of WZ and UHFR were homogeneously defined as 1.83×10^{-7} m/s and 1.05×10^{-7} m/s, respectively. The anisotropic hydraulic conductivity of LSFR, which includes several major fracture zones, was simulated as an equivalent continuous porous medium (ECPM) model based on the discrete fracture network (DFN) model (Fig.1).

2.2 Hydraulic head

Hydraulic head around KURT was estimated by the interpolation of several borehole data measured (Fig.2). From the result, is could be predicted that the west side (higher head) is recharge area and the east side (lower head) is discharge area.

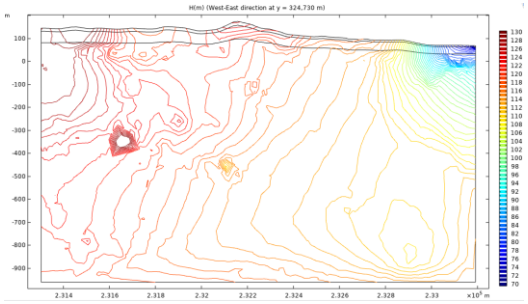

Fig. 2. Contour of hydraulic head around KURT (H[m] at y = 324,730 m).

2.3 Surface Infiltration

Surface Infiltration rate around KURT was estimated based on the meteorological data (Fig. 3).

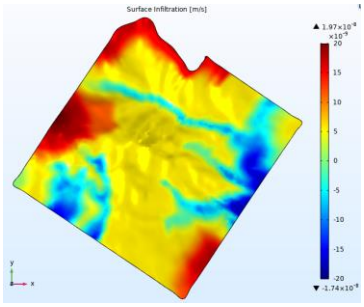

Fig. 3. Distribution of surface infiltration rate around KURT (Q[m/s]).

3. Far-field Hydraulic Module of APro

3.1 Model setup

The far-field host rock was regarded as a saturated porous media, and thus the groundwater flow in the far-field was computed by using Darcy's Law, and the initial and boundary conditions were set up using the

hydraulic head data (shown in Fig. 2), except the upper boundary condition which is the inflow boundary condition using the surface infiltration data (shown in Fig. 3).

3.2 Darcy's velocity

Since constant head boundary condition was applied in the model, the hydraulic results were reached to the steady state, immediately (Fig. 4).

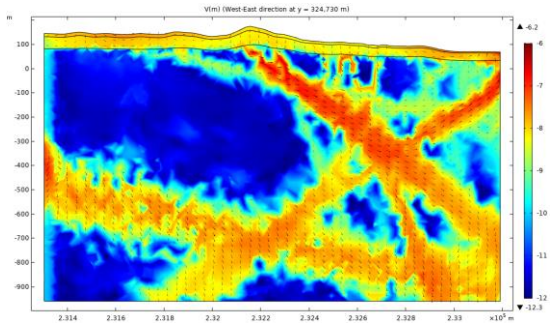

Fig. 4. Distribution of Darcy's velocity around KURT (H[m] at y = 324,730 m).

4. Optimization of Repository Location

Based on the hydraulic characteristics of the repository site, the optimal repository location was recommended.

4.1 Optimization parameter

Optimization parameter, which is the function of hydraulic conductivity and distance, was defined as follows

$$O = \frac{\sum_i^n \frac{1}{K_i L_i}}{n} \quad (1)$$

where, O is the optimization parameter at a position (x,y,z), K_i and L_i are the hydraulic conductivity and distance around the position, respectively. The optimal repository location can be recommended as the location where O is maximized.

4.2 Optimal location

Based on the hydraulic conductivity data around KURT with two assumptions: i) radius of the repository is 200 m, ii) the optimal depth is between -550 m and -450 m, the optimal location was computed as (232,061 m, 324,471 m, -530 m) (Fig. 5). From the result, it was confirmed that the optimal location was well avoided the area where the groundwater flow actively occurs.

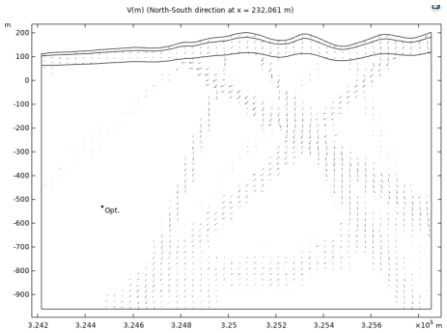

(a) North-South direction at x = 232,061 m

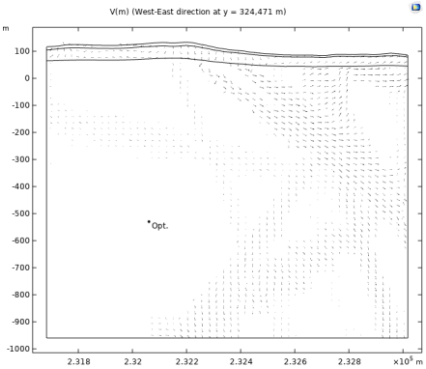

(b) West-East direction at y = 324,471 m

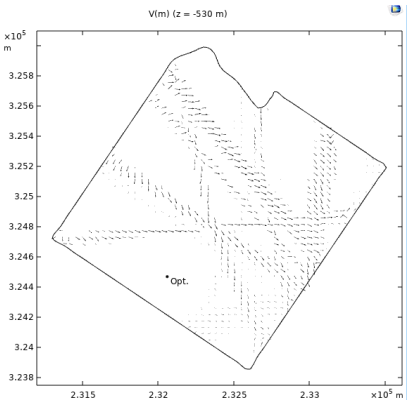

(c) Plane view at z = -530 m

Fig. 5. Optimal location of the repository and Darcy's velocity around KURT.

5. Conclusion

The far-field hydraulic module of APro developed in this study, will be coupled with the near-field modules of APro by using component coupling technique.

ACKNOWLEDGEMENT

This work was supported by the National Research Foundation of Korea Nuclear Research and Development Program (2017M2A8A5014856) funded by the Ministry of Science and ICT.

Characteristic Sorption of Iodine by Heat-treated Samples of Cu_2S Under Anaerobic Conditions

Hyo-Jin Seo*, Seung Yeop Lee, Heejae Ju, and Jae-Kwang Lee

Korea Atomic Energy Research Institute, 111, Daedeok-daero 989beon-gil, Yuseong-gu, Daejeon, Republic of Korea

*hjseo@kaeri.re.kr

1. Introduction

High-level radioactive wastes should be safely disposed in a metal disposal container in a deep underground site to isolate them from ecosystems. Generally, the disposal metal containers are composed of iron (Fe) and copper (Cu) so that they can maintain geochemical stability. However, corrosion of the disposal canisters could occur by the effects of oxidation-reduction change, activity of microbes, and radiation. When the canisters are corroded, there may occur some by-products such as chalcocite (Cu_2S), chalcopyrite ($CuFeS_2$) and mackinawite (FeS) [1]. These corrosion by-products may affect the chemical behavior of radionuclides that are leaching through them.

In this study, we investigated the sorption of iodine (I), which is one of major nuclides, by the heat-treated corrosion product (Cu_2S) under anaerobic condition.

2. Materials and methods

2.1 Heat treatment on metal corrosion product

The Cu_2S sample used in this study is purchased from Sigma-Aldrich.

The corrosion product was heated at high temperature for the later investigation of nuclide sorption. The Cu_2S sample was heated in dry state under an oxidation condition. 10 g of the sample was placed in 125 ml-FED bottles and heated to 60, 90, 120 °C for 5 days.

2.2 Sorption of Iodine

To investigate the sorption of iodine by the Cu_2S, which was heated to 60, 90, and 120°C were prepared. Four samples including raw material were added to each 125ml-serum bottles in an amount of 100mg. Distilled water of 100 mL was added to the bottles, and they were purged with N_2 gas for 40 minutes to remove oxygen in the solution. Iodine was injected to the solution to be 5 ppm. The bottles were placed in a shaking incubator for 3 days (100 rpm). During the reaction, the supernatant was sampled after 1 and 5 hours, and 1, 2, and 3 days and analyzed by ICP-MS to determine the sorption concentrations of iodine and the dissolution amount of copper over time. After the experiment, the solid samples were precipitated by the centrifugation (5,000rpm and 5 minutes) and freeze-dried. They were investigated by SEM-EDS to observe the nuclide sorption onto their surface.

3. Results and discussion

Sorption of iodine was observed for the heat-treated sample (Fig. 1). The iodide (I^-) sorption

gradually increased with time. The iodine sorption capacity was especially good for the dry-heated sample (120°C).

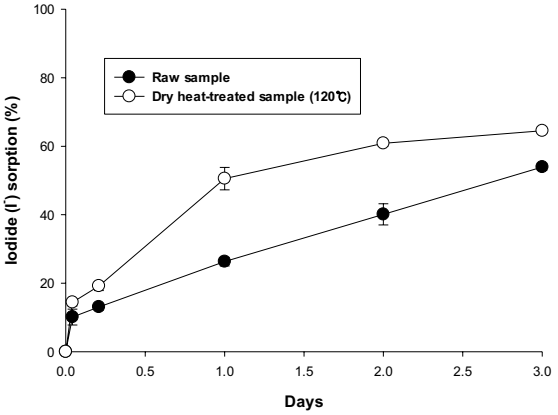

Fig. 1. Characteristic iodide (I^-) sorption curves by the raw and heat-treated Cu_2S samples.

There are assumptions for adsorption isotherms, in general [2].

1) The solute may be adsorbed onto a medium as single or double layers. That is, it can adsorb only to a limited surface.

2) At equilibrium, a rate of adsorption is equal to a rate of desorption at a surface of a medium.

Equilibrium is usually reached within 24 hours in most adsorption experiments. However, it is difficult to apply the isotherm in this study because the iodide sorption continued with time.

The dissolution of Cu from the Cu_2S was also observed in our study. The dissolved copper affected the iodide sorption behaviors by its concentrations.

4. Conclusion

The sorption of iodine by the heat-treated metal corrosion product was investigated under anaerobic conditions. It seemed that iodine may be sorbed onto the surface of metal product by chemically bonding with it. The dissolved amounts of copper also affect the sorption quantity of iodine in our study.

ACKNOWLEDGEMENT

This research was supported by National Research Foundation of Korea (NRF) funded by the Ministry of Science, ICT and Future Planning (The nuclear research and development program No. 2017M2A8A5014859).

REFERENCES

[1] J.K. Lee et al., Complex Behavior of Radionuclides in a Deep Geological Environment, KAERI/TR-6547/2016, 2016.

[2] Ruthven, D. W., Principles of adsorption and adsorption process, JOHN WILEY & SONS, U.S.A., 1984.

Heat Transfer Modelling of A-KRS on the Contact Condition

Seunghyun Kim*, Sanghwan Lee, and Sangjin Lee
Korea Radioactive Waste Agency, 174, Gajeong-ro, Yuseong-gu, Daejeon, Republic of Korea
*shkim@korad.or.kr

1. Introduction

A-KRS is a concept to dispose of pyroprocessing waste developed by Korea Atomic Energy Research Institute. High-level radioactive waste is minimized by pyroprocessing, and the final generated high-level radioactive waste is produced in the form of monazite ceramic. Monazite ceramic waste is permanently disposed of at the site and generates heat. The generated heat raises the temperature of the buffer that protects the waste and is limited to design temperature of 100 °C. The temperature can be controlled by the distance between disposal spaces and has been modelled by Korea Atomic Energy Research Institute. Since the boundary condition interpreted by Korea Atomic Energy Research Institute assumes perfect contact, the temperature distribution due to the thermal resistance caused by the gap generated at the initial disposal is unknown. In order to compensate for this, we performed the heat transfer analysis by the interval that existed at the initial disposal. The analysis was done using COMSOL multi physics and compared with the results of previous studies.

2. Numerical approach

2.1 Heat Transfer equation

Numerical Analysis Heat Transfer Equation Heat transfer is mainly achieved by the thermal conduction of the buffer and the rock. The three-dimensional numerical analysis of heat transfer is as follows based on the unsteady-state equation.

$$k \cdot \left[\frac{\partial^2 T}{\partial x^2} + \frac{\partial^2 T}{\partial y^2} + \frac{\partial^2 T}{\partial z^2}\right] + e^{gen} = \rho c \frac{\partial T}{\partial t} \quad (1)$$

e^{gen} is the decay heat of monazite, k is the thermal conductivity, ρ is the density, and c is the specific heat. The temperature distribution by thermal analysis modelling is determined by the thermal properties and boundary conditions of the material such as decay heat and the thermal conductivity. For more accurate heat transfer analysis, heat transfer by radiation should be considered, but only heat transfer equation is considered in this study.

2.2 Boundary conditions

The thermal properties of the material were applied in the same way as in the previous study as shown in Table 1. The temperature distribution of 500 m underground was increased by 30 °C/km, and the surface temperature was set to 10 °C as in the previous study.

Table 1. Material properties in the modelling [1]

Material	Properties	Values
Nodular cast insert	Density (kg/m^3)	7200
	Thermal conductivity (W/m°C)	52
	Specific heat (J/kg°C)	504
Copper outer shell	Density (kg/m^3)	8900
	Thermal conductivity (W/m°C)	386
	Specific heat (J/kg°C)	383
Ca-bentonite buffer	Density (kg/m^3)	1970
	Thermal conductivity (W/m°C)	0.8
	Specific heat (J/kg°C)	1380
Backfill	Density (kg/m^3)	2270
	Thermal conductivity (W/m°C)	2
	Specific heat (J/kg°C)	1190
Rock	Density (kg/m^3)	2600
	Thermal conductivity (W/m°C)	3
	Specific heat (J/kg°C)	900

3. Results and discussion

3.1 Buffer temperature distribution

The hottest position in the cushioning material of the disposal hole is the part directly in contact with the top of the overpack. This part is in perfect contact with the canister and is directly affected by the heating element.

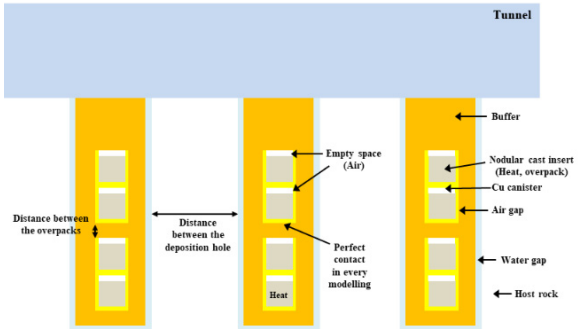

Fig. 1. The vertical disposal concept for A-KRS.

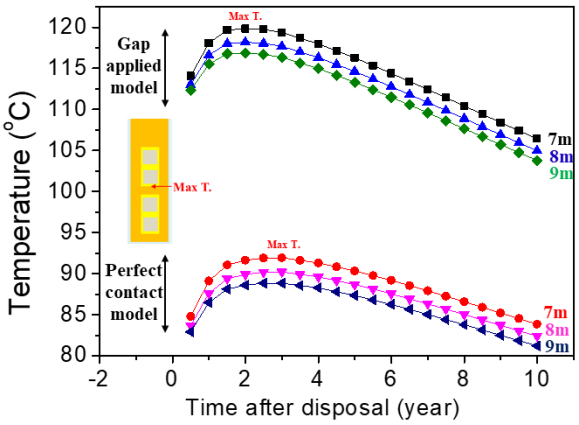

Fig. 2. The maximum buffer temperature after disposal with gap applied and the perfect contact applied model.

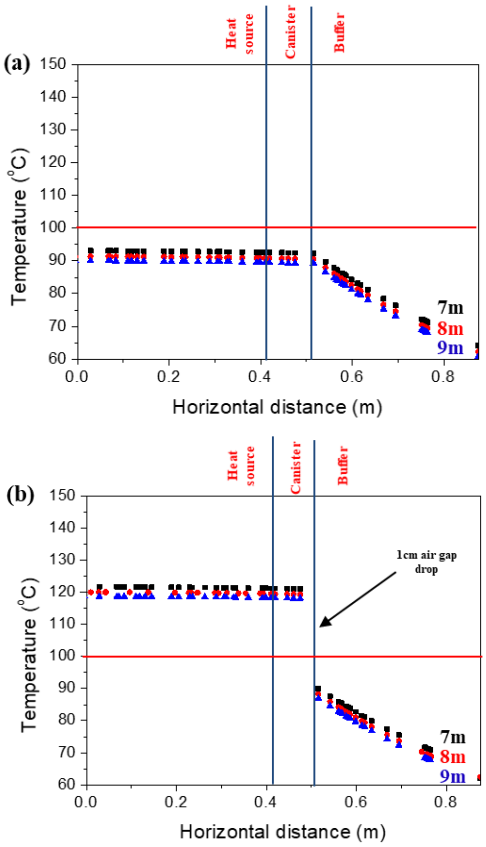

Fig. 3. Horizontal temperature distribution according to the perfect condition model (a) and the gap applied model (b).

4. Conclusion

In this study, modeling was performed by applying gaps that may exist at disposal to compensate for this in the analysis of contact conditions. the maximum buffer temperature in the horizontal direction is lower than the perfect contact condition due to the gap.

REFERENCES

[1] J. Y. Lee, M. S. Lee, H. J. Choi, D. S. Bae, K. S. Kim, “A Study on the Conceptual Development for a Deep Geological Disposal of the Radioactive Waste from Pyro-processing”, JNFCWT, 10, pp. 219-228 (2012).

Geochemical Model for the Oxidative Dissolution UO_2 in a Geological Repository

Heejae Ju*, Ji-Hun Ryu, Seung Yeop Lee, and Jae-Kwang Lee
Korea Atomic Energy Research Institute, 111, Daedeok-daero 989beon-gil, Yuseong-gu, Daejeon, Republic of Korea
*heejaeju@kaeri.re.kr

1. Introduction

Understanding degradation process of spent fuel in a geological repository is significant for the safety assessment of spent fuel (SF) disposal. The oxidative dissolution of uranium (IV) dioxide by radiolysis products would be a key process determining the release of radioactive nuclides from the geological repository.

The objective of this study is to develop a process model for the oxidative dissolution of UO_2. The model should address the long-term behavior of SF in an ambient geochemical condition reasonably. For this reason, we carefully incorporate thermodynamic and kinetic features in the model.

2. Methodology

2.1 Transition state theory

The saturation state of leachate significantly affects the dissolution rate of UO_2. For this reason, we used the transition state expression.

$$R = R_{+}[1 - \exp(\Delta G/RT)] \qquad (1)$$

Here, R is the net rate of the dissolution reaction, R_{+} the forward reaction rate, and ΔG the Gibbs free energy of the reaction.

For the forward dissolution rate of UO_2 in oxic condition, we used the rate equation proposed by Pablo et al [1].

2.2 Description of the model

Fig. 1 simply depicts the UO_2 dissolution model. The model incorporates the surface dissolution and precipitation of UO_2 and the diffusion of U(VI) species through bulk solution. There are several possible U(VI) solid phases. In this study, we considered meta schoepite ($UO_3 \cdot 2H_2O$) as solubility limiting solid phase (SLSP) to determine the saturation state.

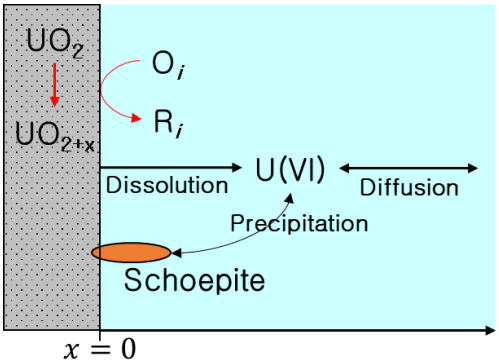

Fig. 1. Simple scheme of the dissolution model. The surface reaction and the diffusion of [U] are incorporated.

2.3 Geochemical modeling tool: PHREEQC

The model was simulated by a geochemical simulation program PHREEQC. The qualified thermodynamic database developed by Lawrence Livermore National Laboratory was used (thermo.com.V8.R6.230).

3. Results

We compared the model in this study with the model developed by Cera et al [2].

Fig. 2 shows the dissolution behavior of UO_2 over 1,000 days. Three cases are compared: the results of this study with and without diffusion, and the result of Cera's model.

Fig. 3 shows the estimated [U] over 10,000 days. The estimated [U] in this study approaches to the saturation state while the result by Cera's model dose not.

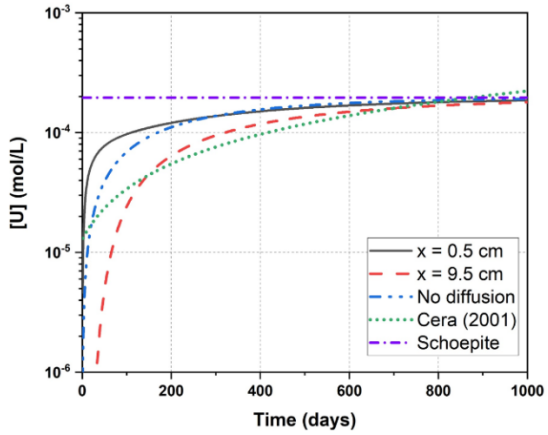

Fig. 2. The estimated [U] over 1,000 days. The effects of saturation and diffusion are compared.

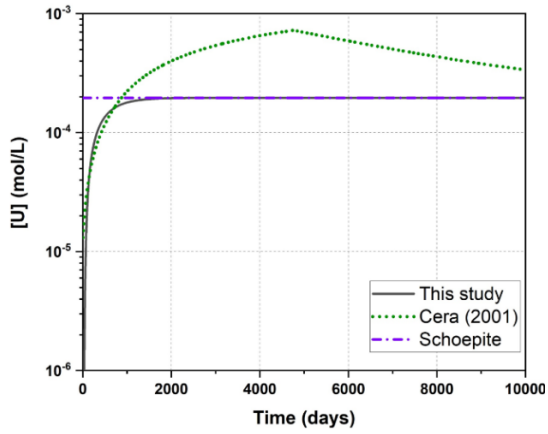

Fig. 3. The estimated [U] over 10,000 days.

4. Discussion and Conclusion

The difference between the case without diffusion and the case with diffusion shows saturation effect of leachate (Fig. 2). The [U] at 9.5 cm from the surface well matches with the Cera's modeling result. This implies that the transport process should be incorporated in UO_2 dissolution model.

The estimated [U] by Cera et al linearly increases until UO_2 completely dissolves and then decreases to the solubility limit of schoepite (Fig. 3). From this, we can conclude that the result in this study is more reasonable.

ACKNOWLEDGEMENT

This research was supported by National Research Foundation of Korea (NRF) funded by the Ministry of Science, ICT and Future Planning (The nuclear research and development program No. 2017M2A8A5014859).

REFERENCES

[1] J. E. Pablo et al., "The oxidative dissolution mechanism of uranium dioxide. I. The effect of temperature in hydrogen carbonate medium", Geochimica et Cosmochimica Acta, 63 (19/20), 3097-3103 (1999).

[2] E. Cera et al., "Modelling of UO_2 dissolution mechanisms in synthetic groundwater solution", POSIVA 2001-03 (2001).

A Comparative Study of Using Single-component and Multi-components for a Geological Disposal System in APro

Minjeong Kim[1, 2,*], Jung-Woo Kim[2], Jaewon Lee[2], Kyung Woo Park[2], and Dong-Keun Cho[2]
[1] Ulsan National Institute of Science and Technology, 50, UNIST-gil, Eonyang-eup, Ulju-gun, Ulsan, Republic of Korea
[2] Korea Atomic Energy Research Institute, 111, Daedeok-daero 989beon-gil, Yuseong-gu, Daejeon, Republic of Korea
[*]paekhap0835@kaeri.re.kr

1. Introduction

Process-based total system performance assessment models enable a time-dependent and multi-physics simulation for a geological disposal system. However, it necessarily requires a long computation time, as complex processes are sequentially computed in a single model component. It can help reducing a computation time to separate computing memory for components of the near-field (~several hundred meters) and far-field (~several kilometers).

The objectives of this study are 1) to compare computation speeds of single-component and multi-component models, and 2) to examine potential errors induced by component coupling.

2. Method

2.1 Model description

The APro model was developed in MATLAB programming language with combining COMSOL and PHREEQC [1]. It provides four physics modules including thermal, hydraulic, mechanical and chemical processes. Additionally, it has two options of single or multiple components.

The option of a single component created a single component (called 'DS') including both near-field and far-field. On the other hand, the option of a multi-component generated single far-field component (called 'FF') and multiple near-field components (called 'NF'), separately. The 'Identity Mapping' function in COMSOL was used for component coupling. It exchanged the boundary information of near-field components with the corresponding boundary information of a far-field component.

2.2 Model set-up

The thermal and hydraulic processes were simulated for 4,000 years, while the chemical process was predicted for 100 years due to its relatively fast temporal variation.

Model domains are described in Figure 1. The near-field component consisted of a single tunnel, borehole, and canister. Free tetrahedral mesh was generated for canister, buffer, backfill, near-field rock and far-field rock, whose maximum mesh sizes were 0.4, 0.3, 0.6, 5 and 100 m, respectively. The DS, FF, and NF had 314,251, 69,898, and 193,466 domain mesh elements, respectively. Model performances were evaluated based on the simulation results at four sample points (Figure 1).

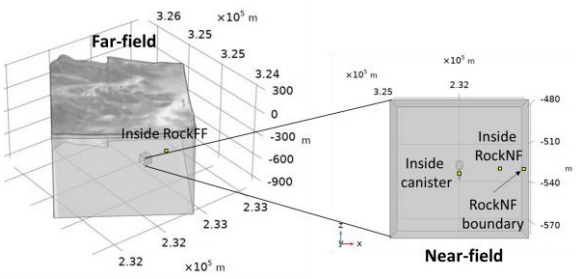

Fig. 1. Model domains with locations of four sample points for model comparison.

3. Results and discussion

3.1 Computation speed

The single-component model required 3.53 hours, while the multi-component model required 3.07 hours. In short, the multi-component model reduced the computation time by 13.2%. The percentage of a time reduction would be greater if there are more near-field

components or if more processes are additionally simulated for the near-field component.

3.2 Thermal transfer

The multi-component model showed identical temporal variation of temperature (degC) to the single-component model.

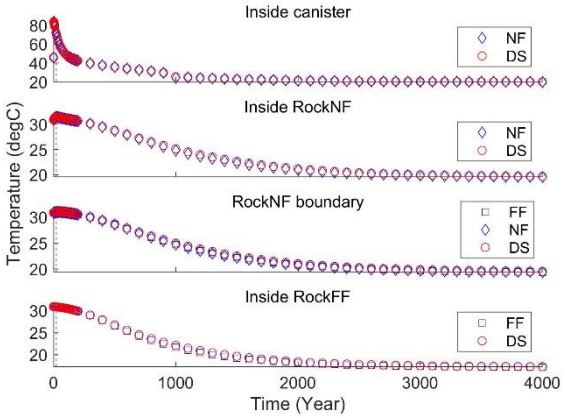

Fig. 2. The simulated temperature (degC) at four locations by the single-component (DS) and multi-component (NF and FF) models.

3.3 Groundwater flow

The pressure (MPa) simulated by the multi-component model had up to $5 \cdot 10^{-4}$ MPa error to one computed by the single-component model.

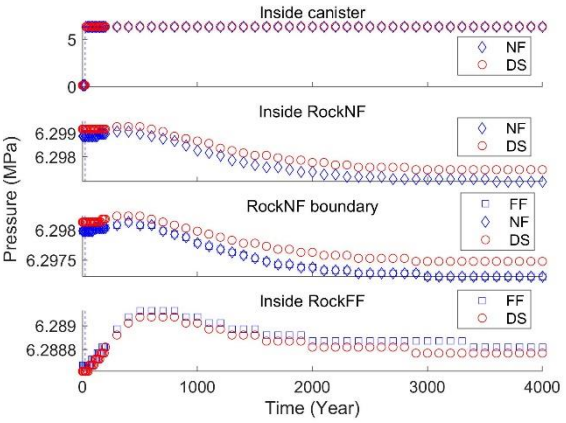

Fig. 3. The simulated pressure (MPa) at four locations by the single-component (DS) and multi-component (NF and FF) models.

3.4 Conservative solute transport

The simulated concentration of chloride was normalized from 0 to 1. At the 'Inside canister' point, the multi-component model showed the identical temporal variation to the single-component model. However, the multi-component model had up to $3 \cdot 10^{-4}$ mol m^{-3} error at the rest of sample points. This error was presumably propagated from the error existing in simulating groundwater flow.

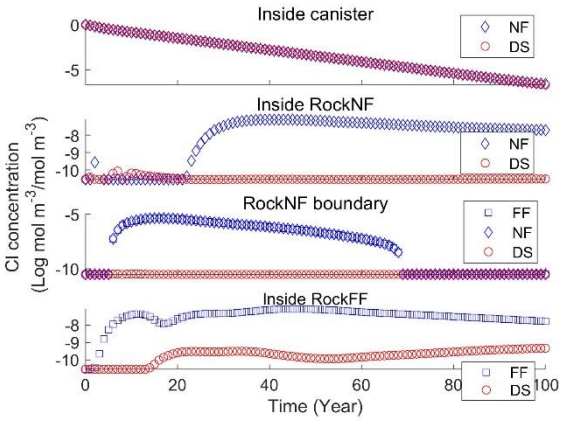

Fig. 4. The simulated concentration of chloride (Log mol m^{-3} / mol m^{-3}) at four locations by the single-component (DS) and multi-component (NF and FF) models.

4. Conclusion

The multi-component model required less computation time than the single-component model. The error induced by component coupling was negligible for thermal, hydraulic, and chemical processes.

ACKNOWLEDGEMENT

This work was supported by the National Research Foundation of Korea Nuclear Research and Development Program (2017M2A8A5014856) funded by the Ministry of Science and ICT.

REFERENCES

[1] Kim, J. W., Lee, J., & Cho, D. K. (2019). Development of User-friendly Modeling Interface for Process-based Total System Performance Assessment Framework (APro) for Geological Disposal System of High-level Radioactive Waste. JNFCWT, 17(2), 227-234.

Development of Two-phase Transport Model of Radionuclides in Porous Media Using COMSOL Multiphysics

Jaewon Lee*, Jung-Woo Kim, and Dong-Keun Cho
Korea Atomic Energy Research Institute, 111, Daedeok-daero 989beon-gil, Yuseong-gu, Daejeon, Republic of Korea
*jwl@kaeri.re.kr

1. Introduction

The main role of engineered and natural barriers in high-level radioactive waste disposal is to isolate radionuclides from leaking into the ecosystem [1]. In this context, it is very important to identify the mechanisms of migration of radionuclides. In the early stage of disposal, two-phase flow phenomena occurs due to decay heat and groundwater. If radioactive materials leak from the canister, radionuclides move along the two-phase flow. Therefore, radionuclides transport model in porous media considering two-phase flow is required.

Recently, KAERI proposed the concept of the process-based total system performance assessment model for a geological disposal system which is called APro [2]. Since COMSOL Multiphysics is one of APro's main codes, therefore, we developed a two-phase transport model of radionuclides in porous media using COMSOL Multiphysics in this study as one of the alternative processes.

2. Governing equation

2.1 Basic assumptions

Basic assumptions for the governing equation of two-phase fluid flow in porous media and two-phase transport of radionuclides are defined as follows:

- Local thermodynamic equilibrium
- Compositional model which allows a transfer of components from one phase into the other
- Negligible effect of radionuclides transport on fluid flow
- Negligible influence of thermal effect

2.2 Two-phase fluid flow in porous media

Mass balance equation for arbitrary subdomain V_n of the flow system which is bounded by the closed surface Γ_n is as follows:

$$\frac{d}{dt}\int_{Vn} M^{\kappa} dV_n = \int_{\Gamma n} \mathbf{F}^{\kappa} \bullet \mathbf{n} d\Gamma_n + \int_{Vn} q^{\kappa} dV_n \quad (1)$$

where κ is the mass component (water and air).

Mass accumulation term M^{κ} is as follows:

$$M^{\kappa} = \phi \sum_{\beta} S_{\beta} \rho_{\beta} X_{\beta}^{\kappa} \quad (2)$$

where β is fluid phase (liquid and gas), Φ is porosity, S_{β} is saturation of phase β, ρ_{β} is density of phase β, and X_{β}^{κ} is mass fraction of component κ present in phase β.

Only advection is considered for mass flux term F^{κ} based on multi-phase Darcy's law.

$$\mathbf{F}^{\kappa}\Big|_{adv} = \sum_{\beta} X_{\beta}^{\kappa}\mathbf{F}_{\beta} \tag{3}$$

$$\mathbf{F}_{\beta} = \rho_{\beta}\mathbf{u}_{\beta} = -k\frac{k_{r\beta}\rho_{\beta}}{\mu_{\beta}}(\nabla P_{\beta} - \rho_{\beta}\mathbf{g}) \tag{4}$$

Where $\mathbf{u}_{\beta}$ is Darcy velocity (volumetric flux) in phase β, k is absolute permeability (intrinsic permeability), $k_{r\beta}$ is relative permeability to phase β, and μ_{β} is viscosity in phase β.

2.3 Two-phase transport of radionuclides

Two-phase transport of radionuclides follows mass balance equation (Equation 1).

Mass accumulation term M^{κ} is as follows:

$$M^{\kappa} = \phi\sum_{\beta} S_{\beta}c_{\beta} + (1-\phi)\rho_R c_l K_d \tag{5}$$

where c_{β} is concentration of phase β, ρ_R is bulk density of rock mass, and K_d is aqueous phase sorption coefficient.

Advection and dispersion are considered for mass flux term F^{κ}.

$$\mathbf{F}^{\kappa}\Big|_{adv} = \sum_{\beta} c_{\beta}\mathbf{u}_{\beta} \tag{6}$$

$$\mathbf{F}^{\kappa}\Big|_{diff} = \sum_{\beta} \phi\tau_0\tau_{\beta}d_{\beta}^{\kappa}\nabla c_{\beta} \tag{7}$$

Where d_{β}^{κ} is diffusion coefficient of component κ in phase β, $\tau_0\tau_{\beta}$ is tortuosity which includes a porous medium dependent factor τ_0 and a coefficient that depends on phase saturation S_{β}, $\tau_{\beta} = \tau_{\beta}(S_{\beta})$.

We considered the decay of radionuclides as follows:

$$\frac{dM^{\kappa}}{dt} = -\lambda_{\kappa}M^{\kappa}\ , \quad T_{1/2} = \frac{\ln 2}{\lambda_{\kappa}} \tag{8}$$

where M^{κ} is the mass of radionuclide κ per unit volume, and the decay constant λ_{β} is related to the half life ($T_{1/2}$).

3. Conclusion

In this study, we developed a two-phase transport model of radionuclides in porous media using COMSOL Multiphysics in this study as one of the alternative processes. For further work, comprehensive verifications and validations will be conducted.

ACKNOWLEDGEMENT

This work was supported by the Nuclear Research and Development Program (No. 2017M2A8A5014856) of the National Research Foundation of Korea (NRF) funded by the Ministry of Science and ICT (MSIT).

REFERENCES

[1] IAEA, “Geological disposal facilities for radioactive waste”, IAEA Specific Safety Guide No. SSG-14 (2011).

[2] J.-W. Kim et al., “Development of Modeling Interface for a Process-Based Total System Performance Assessment of a Geological Disposal System”, Proceeding of 2018 KRS Spring Meeting (2018).

Geological Environments for Deep Disposal of Radioactive Wastes in Korea

Won-Jun Choi[1], Seongjin Ryu[2], and Chang-Lak Kim[3,*]

[1] Pusan National University, 2, Busandaehak-ro 63beon-gil, Geumjeong-gu, Busan, Republic of Korea

[2] Pukyong National University, 45, Yongso-ro, Nam-gu, Busan, Republic of Korea

[3] KEPCO International Nuclear Graduate School, 658-91, Haemaji-ro, Seosaeng-myeon, Ulju-gun, Ulsan, Republic of Korea

[*]clkim@kings.ac.kr

1. Introduction

The continuous increase in spent fuel and radioactive waste due to the development of the nuclear industry is inevitable. In Korea, the issue of disposal of radioactive waste is also emerging. And we need to select a repository site for the treatment of High Level Radioactive Waste (HLW). In order to select a site, various geological factors such as rock type, geological structure, lineament structure, earthquake, and should be considered. therefore, basic research was conducted to find out. It was performed as a part of the "Experimentation and practice program of radioactive waste deep geological disposal" supported by KONICOF (Korea Nuclear International Cooperation Foundation).

2. Geological Environment Feature

To understand the geological features of Korea, it is necessary to understand the topography of the surrounding countries. In Figure 1, around South Korea, South Korea is parallel with China's Wuyi Mountains and Siberia's Central Sikhote-Alin Mountains. Taiwan and Japan are also in the same direction. This confirms that Korea is at the edge of the Eurasian continental plate.

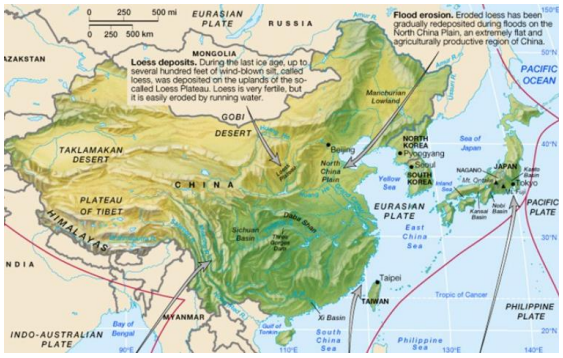

Fig. 1. Landscape regions of East Asia [1].

2.1 Geology Distribution

In Korea, there are various strata and rocks created from the Precambrian to the Cenozoic era. The metamorphic rocks of the Precambrian and plutonic rocks of the Mesozoic, which are shown in red color in Figure 2, occupy more than half of Korea's geological area.

Fig. 2. Geological Distribution Map of Korea [2].

2.2 Lineament Structure

The lineament structure data of KIGAM, which has been studied in the past, is shown in Figure 3, and a preliminary analysis for the selection of wide area was conducted. According to this data, there are 5676 linear structures in South Korea. In addition, more than about 50% of the linear structure belongs to less than 4 km, and more than about 30% of the linear structure belongs to 4km ~8km. The lineament structure was generally dominated by north-east-south-south to north-east-south and west-west-east-east.

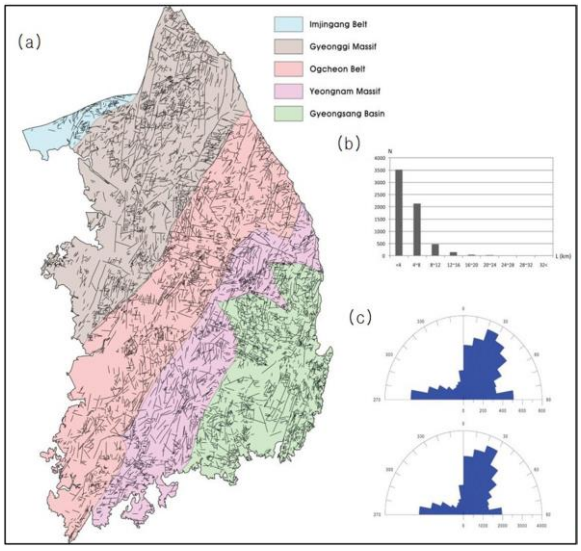

Fig. 3. Lineament data from KIGAM [3].

2.3 Seismic Activity and Active Fault

In Korea, the most distinctive volcanic activity occurred at Mt. Baekdu and Mt. Halla. Not only those two regions, some large and small volcanoes have recently occurred inland. In addition, the number of earthquakes tends to increase over time. In particular, earthquakes occurred along the Active faults in the southeastern region where nuclear power plants are located.

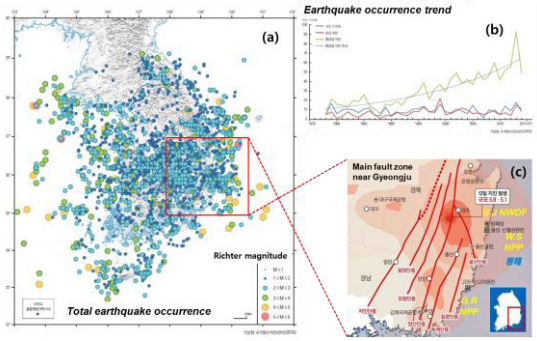

Fig. 4. Seismic Activity and Active Faults [4].

3. Conclusion

In this study, we summarized the geological characteristics of Korea to establish a repository site for high level radioactive waste (HLW). Selecting the repository site is very important for structural integrity, so more detailed information needs to be obtained and analyzed than now. In addition, long-term safety assessment should be conducted through studies of radiochemical and radionuclide migration and retardation, natural barriers, artificial barriers, as well as geological information.

ACKNOWLEDGEMENT

This work was supported by a grant from by the Korea Nuclear International Cooperation Foundation.

REFERENCES

[1] Kaley Lillywhite , “East Asia. China Japan N.Korea S.Korea Taiwan Communist bloc Capitalist economy” (2015).

[2] KIGAM, “Tectonic Map of Korea” (2019).

[3] KIGAM, “Development of quantitative assessment technology for long-term geological safety factors” (2012).

[4] Korea Meteorological Administration “Domestic and International Earthquakes” (2016).

Assessment of Hydrogeological Characteristics in BDZ Boreholes in KURT

Kyung-Woo Park*, Sung-Hoon Ji, and Nak-Youl Ko
Korea Atomic Energy Research Institute, 111, Daedeok-daero 989beon-gil, Yuseong-gu, Daejeon, Republic of Korea
*woosbest@kaeri.re.kr

1. Introduction

This paper describes the derivation of the hydrogeological characteristics of a three-inch diameter borehole (BDZ-1, BDZ-2) in KURT to observe the short-term evolution of the granitic rock due to the extension of the borehole from 3-inch to 4-inch. For this purpose, the geological investigation and hydraulic tests were conducted at BDZ boreholes in 2018 and 2019. Especially, in the hydraulic test, 5 meters interval and the more detailed 1.45 meters interval tests were carried out in BDZ boreholes.

2. Study area

The study area is located at a northern part of Daejeon city. The topography of the study site is well characterized as rolling hills surrounded by upland of EL. 300-500m and the lowland of about EL. 50m. The geology of the study area is mainly composed of Mesozoic plutonic rock, Precambrian metamorphic rock, and a dike. The geologic formation of the Mesozoic plutonic rock is Jurassic schistose granite and two-mica granite. The Cenozoic alluvium is distributed over a wide area through the surface basin system in the research area with a 3-11m depth.

3. Results

3.1 Geological characteristics

In BDZ boreholes, concrete is distributed and can be distinguished by the base rock of the upper layer and lower part of the KURT surface. In granite, which is a base rock, quartz, and meteorites are partially calculated as quartz, quartz, and dike, in which tissues are visible to be constructed or assembled.

The results observed through drilling cores show partly vertical fractures, some quartz vein appears, and the dike is developed by vertical direction. Host rock can be classified as hard rock based on weathering, strength, and interval of fracture. A total of 33 and 63 fractures can be identified in drilling cores in BDZ-1 and BDZ-2. It is possible to identify the section of fracture zones in BDZ boreholes by comparing the fracture frequency in a unit meter.

Geophysical loggings such as full-wave sonic, natural gamma, electrical conductivity and temperature of groundwater also were conducted. The results of the geophysical logging help for identification of groundwater conducting fracture zones in BDZ borehole.

3.2 Hydrogeological characteristics

The slug was carried out at intervals of 5 m and 1.45 m using the double-packer system at the BDZ boreholes. In the slug test at 5 m intervals, the average of transmissivities was derived from 3.71×10^{-7} m^2/sec in BDZ-1 and 2.27×10^{-6} m^2/sec. Among the test sections, the highest permeable sections and lowest permeable sections were analyzed in two BDZ boreholes.

The detailed hydraulic test was carried out after finishing the 5 m test at the BDZ boreholes. The detailed hydraulic test results show that the average of transmissivity derived from the BDZ-1 borehole is 1.47×10^{-8} m^2/sec, which is less than 1 order compared to the results of the 5 m interval test. The average of transmissivity derived from the BDZ-2 borehole is 1.08×10^{-8} m^2/sec, which is less than 2 order compared to the results of the 5 m interval test.

The results of the detailed hydraulic test are different from the results of 5m intervals test, the difference between transmissivity of the highest and the lowest permeable section is derived by about 5 order and shows typical hydrogeological heterogeneity dominated by a fracture on the crystalline rock.

4. Conclusion

Based on the results of the hydraulic test conducted at the BDZ boreholes, the hydraulic conductivities were calculated based on the transmissivity derived from each test section. The hydrogeological characteristics were strongly related with the geological properties at hydraulic test section in each borehole and hydraulic connectivity to KURT, which is considered as a hydrogeological boundary around the study area. Especially, we also found the relation between the transmissivity and hydraulic head in BDZ boreholes.

In the middle of 2019, the extension from 3-inches to 4-inches diameter was completed in two BDZ boreholes. The geophysical logging and hydraulic test will be continued to observe the short-term evolution of the granitic rock due to the extension of the borehole.

ACKNOWLEDGMENT

This work was supported by the Nuclear Research and Development Program of the National Research Foundation of Korea (NRF-2017M2A8A5014858).

Parameter Determination for the Mechanical Constitutive Model (BBM) of Bentonite Buffer: Saturated Material Constants

Jae Owan Lee*, Seok Yoon, and Geon Young Kim
Korea Atomic Energy Research Institute, 111, Daedeok-daero 989beon-gil, Yuseong-gu, Daejeon, Republic of Korea
*jolee@kaeri.re.kr

1. Introduction

The buffer is one of the key components of an engineered barrier system in an HLW repository. The mechanical constitutive model of the buffer is essential for the performance evaluation and design of engineered barrier system. The BBM (Barcelona Basic Model) presented by Alonso et al. [1] is widely used as a mechanical constitutive model of unsaturated and saturated buffer. This model however is difficult in concept, and the experimental apparatus for measuring model parameters is complicated and not standardized yet. Experience and systematic approach are needed to determine reliable model parameters from experimental results. This paper reviews the principal concept of the BBM, tri-axial test methods and how to determine the saturated material constants of the BBM from the measured experimental results.

2. Principal Concept of BBM

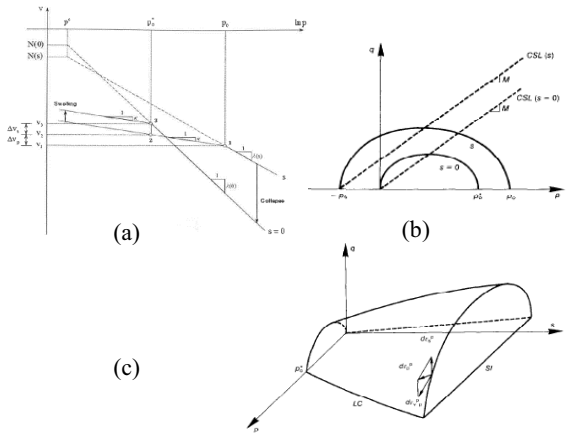

Fig. 1. BBM concepts: (a) Compression curves, (b) yield surfaces in (p, q) space, (c) 3-D yield surfaces in (p, q, s) space for saturated and unsaturated soils.

The BBM uses mean net stress (total stress reduced by the value of air pressure) p, deviator stress q and suction s as stress variables. The BBM assumes that saturated conditions are achieved whenever s is zero, and at this limit it approaches the Modified Cam Clay Model (MCCM) for saturated soils [2]. In this model, the relationship of void ratio e (or specific volume v) versus logarithm of mean net stress is linear. Different stiffness (line slope) for elastic states within yield locus and elasto-plastic loading are used, and the slope of the elasto-plastic virgin compression line depends additionally on the current value of suction (Fig. 1(a)). The BBM assumes that the yield locus expands when suction increases and contracts when suction decreases. The size of the BBM yield locus is determined by the preconsolidation stress for saturation conditions and suction (Fig. 1(b)). A three-dimensional view of the yield surfaces in the (p, q, s) space is given as shown in Fig. 1(c). The later improved BBM takes into account the stress-strain relationship to temperature changes.

3. Determination of Saturated Material Constants Using Triaxial Cell Test

3.1 Triaxial cell test

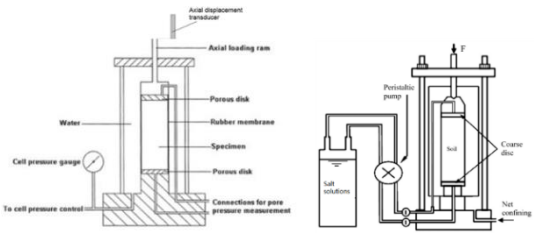

Fig. 2. Tri-axial test apparatuses for the measurement of BBM parameters: conventional one (left) and one with suction-controlling device (right).

Triaxial cell test is to measure the consolidation and shear properties of the porous medium allowing independent control of the loading (stress) in three perpendicular directions. The three dimensional loading produces a total volume change (strain) of the sample. Fig. 2 represents triaxial test apparatuses for the measurement of BBM parameters. The left is a conventional one which is widely used for saturated soils, and the right is the one with suction-control, which can be used for unsaturated and saturated soils while drying and wetting. Both the test apparatuses have several variations: Consolidated Drained (CD), Consolidated Undrained (CU), Unconsolidated Undrained (UU). The saturated material parameters of BBM are measured using any of these test apparatuses. However, the left conventional apparatus has a limitation for its application to unsaturated soils where suction control is required.

3.2 Determination of saturated material constants

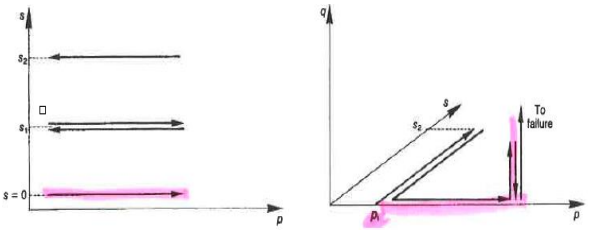

Fig. 3. Suitable stress paths (pink colored) to determine the saturated material constants of BBM.

The saturated material constants of 10 BBM parameters, as also called MCCM constants, are five: $\lambda(0)$ – slope of the virgin normal compression line (NCL) in the log (p) - ν plot, κ – slope of the elastic loading – unloading line in the ln (p) - ν plot, M – slope of the critical state line (CSL) in the $p-q$ space, G – shear modulus and N(0) – specific volume for virgin compressed soil reached reference mean stress p^c. An initial value of the hardening parameter $p_0{}^*$ must be given before the starting of the test. When conducting the triaxial cell tests, $\lambda(0)$, κ, N(0) should be measured under isotropic stress states, while G and M should be measured under triaxial stress states. Alonso et al. suggested suitable stress paths (pink-colored) as experimental conditions for the measurement of the saturated material constants (Fig. 3).

4. Summary and Conclusions

This paper reviewed BBM, triaxial cell tests, determination of saturated material constants from measured experimental results. Two types of triaxial test apparatuses are available for the measurement of saturated material constants: conventional one only for saturated soils and suction-controlling one for both unsaturated and saturated soils. Among the saturated material constants, $\lambda(0)$, κ, N(0) are measured under isotropic stress states, while G and M are measured under triaxial stress states. However, the experimental apparatus is complicated and standardized procedures for determining model parameters have not been established yet. Experience and systematic approach are required to determine reliable model parameters from experimental results.

ACKNOWLEDGEMENT

This work was supported by Nuclear Research & Development Program of the National Research Foundation of Korea (NRF) Grant funded by the Ministry of Science, ICT and Future Planning (MSIP).

REFERENCES

[1] Alonso, E.E., Gens, A., and Josa, A., “A constitutive model for partially saturated soils”, Geotechnique 40(3), 405-430 (1990).

[2] Roscoe, K.H., Burland J.B., “On the generalized stress-strain behavior of 'wet' Clay”, Engineering Plasticity (J. Heyman, Leckie F.A. eds), Cambridge University Press, Cambridge, 535-609 (1968).

Hydrothermal Analysis of a Double-layered Bentonite in Two-layered Repository Using TOUGH2 Code: High Performance Buffer

Jin-Seop Kim*, Won-Jin Cho, and Geon-Young Kim
Korea Atomic Energy Research Institute, 111, Daedeok-daero 989beon-gil, Yuseong-gu, Daejeon, Republic of Korea
*kjs@kaeri.re.kr

1. Introduction

Thermal criteria of an EBS (Engineered Barrier System) is one of the key factors influencing the design of a geological waste disposal system. Recently, there are growing interests and demands on the increase of disposal efficiency, which is inevitable issues especially for the small countries compared to the number of nuclear reactors in operation.

The objective of this study is to evaluate the double-layered concept of bentonite buffer to increase the heat transfer from spent fuel to near-field rock mas. This concept was applied to KRS (Korea Reference disposal System) in which EDZ (Excavation Damaged Zone) was taken into account in a deposition hole.

2. Approach

With regard to the double-layered buffer, the highly thermal-conductive layer and insulating layer were taken into account in the performance assessment of EBS in this study. The hydrothermal behaviors of this concepts were simulated by TOUGH2 code.

For the mass transport in a buffer and backfill, the gas phase diffusion of water and air is considered, and the water vapor and air in the gas phase are assumed to be a binary mixture. The two-phase relative permeability and the capillary pressure are calculated by using the Fatt and Klikoff function and the van Genuchten function.

3. Model setup

A summary of material properties used in hydrothermal modeling are listed in Table 1 below. Fig. 1 shows the model geometry and dimensions used for the model simulations.

Table 1. Input parameters for hydrothermal model

	Parameter	Unit	Value
Buffer	dry density	Mg/m^3	1.6
	porosity	-	0.42
	absolute permeability	m^2	1.5×10^{-20}
	specific heat	J/kg.°C	966.0
	pore compressibility	Pa^{-1}	1.0×10^{-8}
	pore expansivity	1/°C	1.0×10^{-6}
	Klingenberg slip factor	Pa	3.24×10^{6}
	vapor diffusion coefficient	m^2/s	2.58×10^{-5}
	wet thermal conductivity of add. layer I	W/m.°C	2.618
	wet thermal conductivity of add. layer II	W/m.°C	0.654
	wet thermal conductivity of buffer	W/m.°C	1.309
Host rock	dry density	Mg/m^3	2.70
	porosity	-	0.10
	absolute permeability	m^2	1.0×10^{-18}
	specific heat	J/kg.°C	820.0
	pore compressibility	Pa^{-1}	1.0×10^{-8}
	pore expansivity	1/°C	1.0×10^{-6}
	Klingenberg slip factor	Pa	6.86×10^{5}
	vapor diffusion coefficient	m^2/s	2.58×10^{-5}

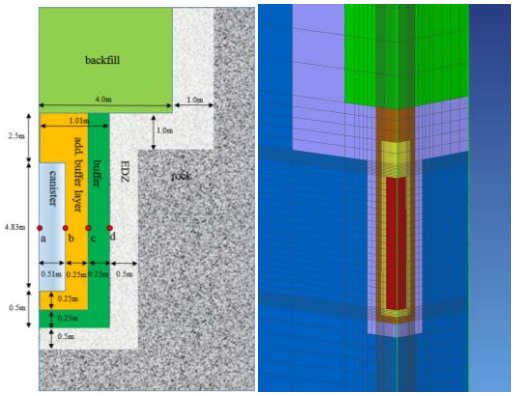

Fig. 1. Concept of double-layered buffer and model geometry based on KRS.

4. Main Results

The variations of saturation, temperature and pressure of EBS including near-field rock are presented in Fig. 2-6.

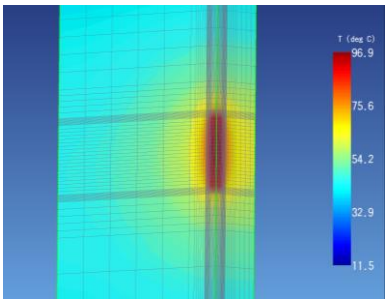

Fig. 2. Temperature distribution after 10 years (add. buffer layer I).

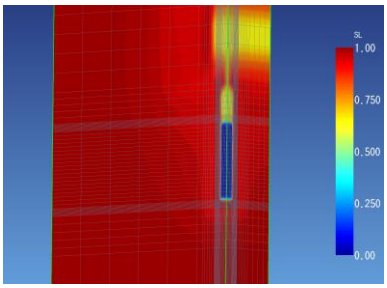

Fig. 3. Saturation distribution after 10 years (add. buffer layer I).

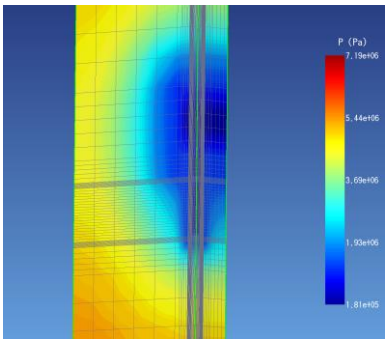

Fig. 4. Pressure distribution after 10 years (add. buffer layer I).

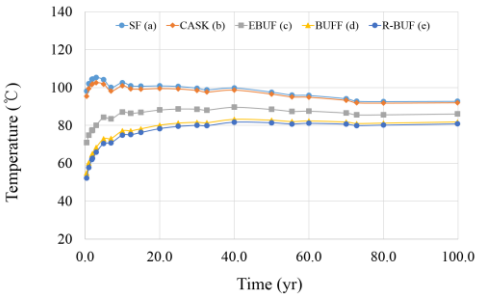

Fig. 5. Temperature variation for different locations with time.

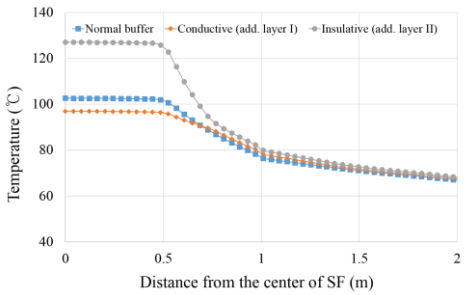

Fig. 6. Temperature variation along a distance from the SF for different additive buffer layers.

5. Conclusion

When it comes to the disposal efficiency in Korea, it is worth to take into account the insertion of thermally modified-bentonite layer in a design of buffer. The workability for a high performance buffer still remains to be solved from more study.

REFERENCES

[1] Heui-Hoo Choi and Jongwon Choi, “Double-alyered buffer to enhance the thermal performance in a high-level radioactive waste disposal system, Nuclear Engineering and Design, 238, 2815-2820 (2008).

[2] Won-Jin Cho, Jin-Seop Kim, and Heui-Joo Choi, “Hydrothermal modeling for the efficient design of thermal loading in a nuclear waste repository, Nuclear Engineering and Desing, 276, 241-248 (2014).

[3] Won-Jin Cho, Jin-Seop Kim and Geon-Young Kim, “Effects of Excavation Damaged Zone on Thermal Analysis of Multi-layer Geological Repository”, JNFCWT, 17(1), 75-94 (2019).

4분과

중저준위폐기물관리 (Oral)

The Structural Stability Analysis of a 16-pack Disposal Container Disposed of in Gyeongju LILW Repository

Hyeongjin Byeon, Gwan Yoon Jeong, Yeonghwan Jeon, Hyewon Shin, and Jaeyeong Park*
Ulsan National Institute of Science and Technology, 50, UNIST-gil, Eonyang-eup, Ulju-gun, Ulsan, Republic of Korea
*jypark@unist.ac.kr

1. Introduction

The waste acceptance criteria of the Gyeongju LILW repository exploited the criteria of the U.S, operating different types of waste repository with Korea. Therefore, the expected loading to the repository is different between Korea and U.S as the crushed granite and shotcrete are backfilled in Gyeongju repository while sand is backfilled in U.S repository.

In this study, the compatibility of the current waste acceptance criteria was checked by applying the Drucker-Prager yield criterion which is widely used to calculate plastic behavior of brittle materials. Also, the modification model for disposal strategy was suggested to improve the safety of disposal container and solidified waste.

2. Method

2.1 Structural details

The geometry of 16-pack disposal container containing 16 waste drums was applied to the COMSOL. The 8 by 8 structural steel rebars with 2.4 cm radius and 2.5 m length were assumed, shown in Fig. 1. The other structural details of the disposal container are shown in Fig. 2.

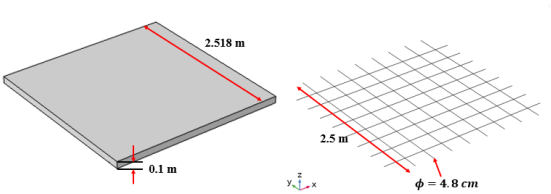

Fig. 1. The geometry of the concrete cover (left) and 8 by 8 structural steel rebars (right).

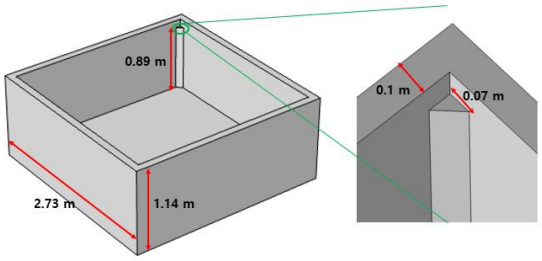

Fig. 2. The geometry of the disposal container (left) and supporting triangular pole (right).

2.2 Drucker-Prager yield criterion

The Drucker-Prager yield criterion is widely implemented to the pressure-dependent materials like soil, rock, and concrete, etc., which is available in COMSOL. The Drucker-Prager model adopts the following functions:

$$\sqrt{J_2} = A + B\,I_1 \qquad (1)$$

I_1 is the first invariant of the stress tensor, J_2 is the second invariants of deviatoric stress tensor. By assuming that the Drucker-Prager yield

surface circumscribes the Mohr-Coulomb yield surface, the constants A and B are:

$$A = \frac{6\,c\cos\phi}{\sqrt{3}(3-\sin\phi)}, B = \frac{2\sin\phi}{\sqrt{3}(3-\sin\phi)} \quad (2)$$

3. Results

The pressure of 15 kPa less than expected loading was applied to the empty disposal container and the yielding points, shown in Fig. 3, was checked due to the stress concentration near the supporting columns.

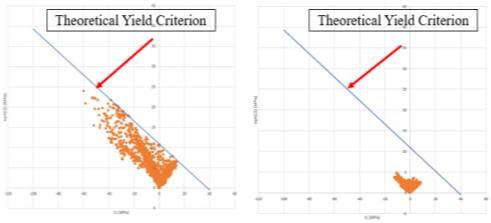

Fig. 3. Drucker-Prager plotting result for empty box model under 1.5 kPa pressure (left), revision model under 0.25 MPa pressure (right).

Thus, under the expected pressure, 0.25 MPa, the broken shape of the cover was assumed. The modeling result shows that the maximum stress in a vertical direction, 6.68 MPa, on the solidified waste is larger than the compressive strength.

To avoid stress concentration near the supporting pillars, the modified disposal container model was tested. As the number of supporting pillars increases, the stress and deformation were dramatically decreased and plastic strain on the container are checked shown in Fig. 3.

4. Conclusion

The structural instability of the disposal container was checked by the modeling calculation. Also, by assuming the cover of container is broken, the stress on wastes was estimated larger than the compressive strength criteria. Therefore, the design of the disposal container or the waste acceptance criteria needs to be revised considering the expected loading.

ACKNOWLEDGEMENTS

This work was supported by the Nuclear safety Research Program through the Korea Foundation Of Nuclear Safety(KoFONS), granted financial resource from the Nuclear Safety and Security Commission(NSSC), Republic of Korea. (No. 1903005)

REFERENCES

[1] Pul, Selim, et al. "Experimental Determination of Cohesion and Internal Friction Angle on Conventional Concretes." ACI Materials Journal 114.3 (2017).

A Study on the Dose Assessment Methodology for Worker by Radioactive Waste Clearance Recycling Scenario

Ji Young Song*, Ki Baek Shin, and Junhyuck Im
Korea Atomic Energy Research Institute, 111, Daedeok-daero 989beon-gil, Yuseong-gu, Daejeon, Republic of Korea
*jysong1994@kaeri.re.kr

1. Introduction

In Korea, it is necessary to satisfy the regulatory requirements of radioactivity concentration or exposure dose for radioactive waste clearance. Generally, commercial program is used to assess radiation doses to worker arising from exposure due to clearance. In case of recycling scenario, RESRAD-RECYCLE has been normally used. However, since 2005, this code has no longer been available and no updated. Consequently, RESRAD-RECYCLE does not meet those Korea regulatory guidelines established in 2005. Therefore, it is necessary to develop new program considering the circumstances in Korea. The objectives of this study is to develop worker dose assessment program about recycling scenario.

2. Dose Assessment Methodology of External Exposure

2.1 RESRAD-RECYCLE

RESRAD-RECYCLE uses external dose conversion factor (DCFs) to calculate radiation doses to workers. The DCFs are dependent upon the material in the radiation source, size of the source, and distance between the receptor and the source. In addition, they are based on the latest EPA external DCFs. This algorithm is confidential. The external radiation dose incurred by the receptor is calculated by

$$E = C_i \times DCF \times ED \times Constant \quad (1)$$

where C_i denotes the concentration of a radionuclides and ED denotes exposure duration.

2.2 New Approach

In this study, an equation has been newly derived to evaluate the external radiation dose incurred by the receptor in the case of cylindrical radiation source. During developing the new equation, we assumed that cylinder is became when the circle or disk is continuously connected (see Fig. 1).

Equation (2) is a formula for the concentration of radiation of a cylindrical radiation source at the receptor (that is, the concentration of radiation at location *P* in Fig. 1) — the formula was derived by incorporating the formula for the concentration of radiation of a disk source at the receptor [that is, Eq. (3)]. A part of Eq. (2) was simplified for convenience of calculation.

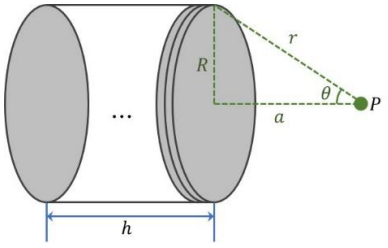

Fig. 1. Schematic Diagram of a Cylindrical Radiation Source for Deriving the Formula.

$$S_{cylinder} = \frac{S_A \times \rho}{2 \times h}\left[\left\{h \times ln\left(\frac{\sqrt{(a+h)^2+R^2}+\sqrt{a^2+R^2}}{2}\right)\right\} - \{(a+h)\times \ln(a+h) - (a+h)\} + \{a \times \ln(a) - a\}\right] \quad (2)$$

$$S_{plane} = \frac{S_A}{2} \ln\left(\frac{r}{a}\right) \quad (3)$$

The external radiation dose incurred by the receptor is given by the following equation:

$$E = S_{cylinder} \times DCF \times Constant \quad (4)$$

3. Verification of New Approach

We have compared the results with the commercial program to verify newly developed equation. As a comparative program, we selected RESRAD-RECYCLE and Microshield because this programs could evaluate exposure situation about recycling scenario. In case of Microshield, we evaluated the radiation dose with buildup factor and those without buildup factor to analyze effect of buildup factor. Figure 2 shows that the results calculated by developed equation were found to be between those by RESRAD-RECYCLE and by Microshield with buildup factor. Since the developed equation takes into account the buildup factor, the results of developed equation were found to be most similar to results of the Microshield with buildup factor.

It was confirmed that the developed equation is valid and the newly developed equation will can be used develop worker dose assessment programs according to recycling scenario.

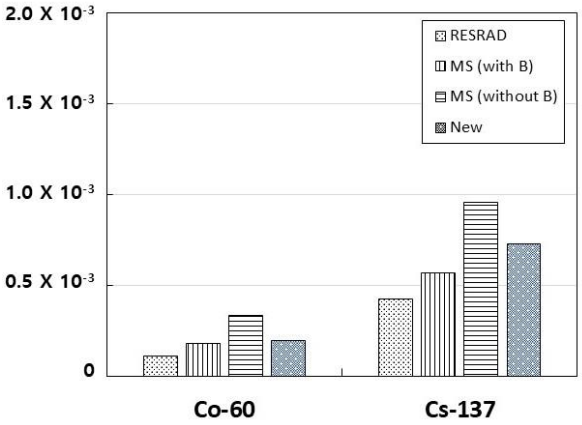

Fig. 2. Comparison of Dose Assessments Result between the Commercial Program and Developed Equation in the case of a Scrap Cutter Scenario.

4. Conclusion

In this paper, a dose assessment methodology of external exposure has been developed. A radiation concentration formula for a cylindrical source at the receptor has been derived by integrating that for a disk source at the receptor. In addition, the newly developed equation has been verified by comparing with commercial programs.

The proposed external exposure dose assessment methodology can be used to develop worker dose assessment programs according to recycling scenario.

REFERENCES

[1] John R. Lamarsh, Anthony J. Baratta, “Introduction to Nuclear Engineering”, 3rd Edition.

[2] ANL, “RESRAD-RECYCLE” (2000).

[3] EPA, “External Exposure to Radionuclides in Air, Water, and Soil”, Federal Guidance Report No.12 (1993).

ISO/PWI 24389-1 Through 4, The Pre-disposal and Disposal for L&IL Radioactive Waste From Decommissioning

Kwangyoung Sohn [a,*], Changhwan Cho [a], Sungjong Kim [a], and Namchan Cho [b]
[a]MIRAE-EN Co., Ltd., 17, Techno 4-ro, Yuseong-gu, Daejeon, Republic of Korea
[b]KEPCO Nuclear Fuel, 242, Daedeok-daero 989beon-gil, Yuseong-gu, Daejeon, Republic of Korea
[*]kwangyoung.sohn@mirae-en.co.kr

1. Introduction

Due to the absence of comprehensive and implementable waste management guideline for L&IL (Low and Intermediate Level) radioactive waste in ISO[1] community as well as national standard, there have been attempts to establish standard on this topic in ISO TC85 SC5 WG5 "characteristics and waste management" since 2016. Eventually this topic was registered as ISO/PWI 24389 in 2019.

This PWI topic being led by MIRAE-EN Co., Ltd. is in the centre of roadmap in Fig. 1, and the following has more of this standardization.

2. Background of WG5 standardization

2.1 The roadmap of ISO TC85 SC5 WG5

In 2019, Berlin, ISO TC85 SC5 WG5 established the standardization roadmap partly for "characteristics and waste management" as indicated in Fig. 1.

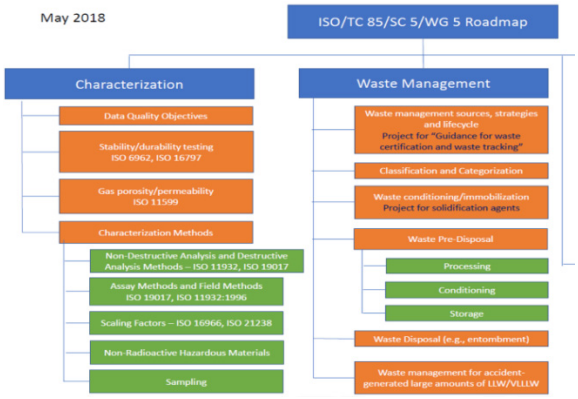

Fig. 1. Roadmap of WG5 (excerpted).

2.2 IAEA document analysis

For pre-disposal and disposal process or steps for L&IL waste management considering protection of public and environment is conceptually addressed in IAEA DSS 477.

According to this roadmap in Fig. 1, standardization plan based on predisposal management was discussed. For preliminary analysis of IAEA position, documents pertaining to radioactive waste management has been reviewed, and SSG-40 [2] provides more specific requirements for pre-disposal and disposal waste management process.

3. The series of ISO/PWI 24389

This PWI, as indicated in Fig. 2, is organized in accordance with the roadmap in Fig. 1 and IAEA position for pre-disposal and disposal of waste.

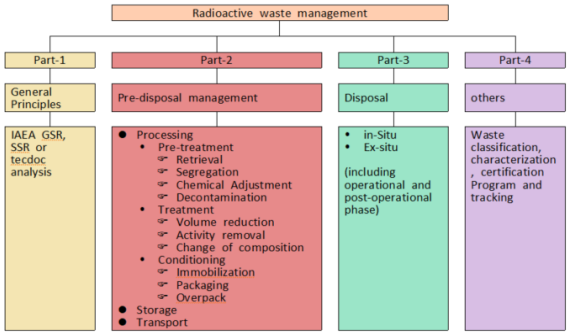

Fig. 2. The structure of ISO/PWI 24389 series.

Despite some references in IAEA, there is no umbrella standard commensurate with SC5 WG5 technical roadmap. Also, it is identified that there are some gaps and/or mismatches among pre-disposal process and lack of details to implement this in the field.

This is one of the reasons to write standard and these things have been reviewed as one of the topics for "de facto standard" of ISO/PWI 24389. ISO/PWI 24389 Part-1 is delivering the general and fundamental requirements for L&IL radioactive waste management.

3.1 Part-2 pre-disposal process management

3.1.1 Radioactive waste management planning. According to PWI, the plan and preparation for waste management shall be established for systematic and transparent guideline as a basis

[1] International Organization for Standardization. https://www.iso.org.

for managing radioactive waste life cycle. It needs to provide the comprehensive waste management and certification that should be adhered to throughout the waste management process. Also, all the risks and its emergency, mitigation or recovery plan shall be considered and prepared to cope with the unexpected events during radioactive waste management life cycle.

3.1.2 Waste characterization. Waste shall be characterized physically, biologically and chemically to ensure the safety of waste package, which also determines the subsequent process for waste management necessary. However, the limit and level of depth for characterization shall be outlined in reasonable level.

3.1.3 Waste segregation, collection, and pre-treatment. This could be divided into sub-process such as pre-treatment and treatment process depending on the specific waste stream. It may involve collection, segregation, decontamination and chemical adjustment for waste collection.
The characteristics of raw radioactive need to be well defined with care in a sense that the various type of characteristics of raw waste stream can determine a series of further treatments such as burning as incineration, pyrolysis and solidification by eliminating a liquid, gaseous and pyrophoric compound etc., and of characteristic performance testing for conformity. All the data gathered in this process need to be recorded and reviewed for approval.

3.1.4 Waste treatment and conditioning. In the predisposal management of radioactive waste, decisions often must be made at a time when no disposal facility is available and the waste acceptance criteria for disposal are unknown. A similar situation would arise if radioactive waste were to be stored over long periods of time for reasons of safety or for other reasons [1]. In both cases, consideration must be given to whether, for the purposes of safety, the radioactive waste will be stored in a raw, a treated or a conditioned form.

3.1.5 Radioactive waste packaging and delivery. These two (2) processes has been covered under SC5 WG4 of “transportation of radioactive materials”.

3.2 Part-3 disposal (in/ex-situ)

As in Fig. 2, part-3 will address the various disposal techniques, maintenance and its requirements for implementation.

3.3 Part-4 waste certification, characterization and tracking etc.

As in Fig. 2, part-4 will provide the detail guideline for Waste Acceptance Criteria (WAC), certification, tracking, characterization and other supporting technologies for waste management and disposal.

4. IoT application

When implementing the waste management process, the application of Internet Of Thing (IoT) is an attempt to achieve the efficiency, and the following is one of the those applications [3];

1) Digital data upload directly without intervention
2) Digital location tracking
3) Remote handling and manipulation
4) Condition monitoring and Inspection (CM&I) for storage as well as disposal
5) Smart Package with IoT
6) Storage and disposal management operation using AR (Augmented Reality) and VR (Virtual Reality)

5. Government (KEIT) support for FDIS

In 2019, this PWI being led by MIRAE-EN Co., Ltd. is accepted as KEIT’s standard R&D project [3] to develop standard until 2022.

6. Conclusion

All the topics mentioned so far is an attempt to achieve the traceability and safety of radioactive wastes management regardless of the waste stream and level of activity. These topics would play a great role to establish the baseline for Waste Certification Program (WCP), ensuring the integrity of waste package with the help of WAC and Waste Tracking System (WTS).

REFERENCES

[1] IAEA GSR Part 5, predisposal management of radioactive waste, 2009
[2] No. SSG-40, Predisposal Management of Radioactive Waste from Nuclear Power Plants and Research Reactors
[3] KEIT Proposal No: 20006891, The requirements for L&IL radioactive waste life cycle from decommissioning, 2019.7.

Leaching Behaviors of Co_2, Cs, and I From Geopolymer and Cement Waste Forms Containing High-sulfate Sludge Waste

Seongye Kwon*, Jinmo Ahn, and Wooyong Um
Pohang University of Science and Technology, 77, Cheongam-ro, Nam-gu, Pohang-si, Gyeongsangbuk-do, Republic of Korea
*mole1130@postech.ac.kr

1. Introduction

Alkali activated geopolymers have attracted increasing attention on recent years for their potential application. It can be used as cementitious binders to overcome and replace the problems of Ordinary Portland cement (OPC) [1]. The OPC has disadvantage in stability due to formation of secondary sulfate mineral such as ettringite. Therefore, geopolymer can form reinforced radioactive waste forms with sulfate as an alternative to cement waste form.

The leaching test (ANSI/ANS16.1) is an important part of the performance evaluation of a radioactive waste form that is included in the acceptance criteria. The objective of this study was to synthesize the stable waste form for radioactive waste with high sulfate ions, and to test the capability of solidification and stabilization of cement and geopolymer waste forms.

2. Methods

2.1 Materials

Metakaolin (MK) was prepared by calcination of kaolinite at 750°C for 4h. Cement waste forms were formulated using OPC (Type I). The high-sulfate sludge waste (HSW) was obtained from Hydrazine Based Reductive metal Ion Decontamination (HyBRID) process developed by Korea Atomic Energy Research Institute (KAERI). The chemical compositions of MK, OPC, and HSW determined by X-ray fluorescence (XRF) are shown in Table 1. For surrogates of radioactive Cs-137 and I-129, stable CsI (CAS number 7789-17-5, Sigma Aldrich) was used for this study.

Table 1. Compositions of MK, OPC, and HSW (wt%)

	SiO_2	Al_2O_3	BaO	SO_3	LOI*
MK	54.8	39.5	<0.02	N.D**	3.40
OPC	20.2	5.01	N.D	2.39	3.59
HSW	21.5	1.15	43.03	21.9	0.29

* LOI: Loss of Ignition, **N.D: Not detected

2.2 Designs of geopolymer and cement waste forms

Geopolymer waste forms with containing 40 wt% of HyBRID waste were formulated with molar ratio of Si/Al, K/Al, and H_2O/Al fixed at 1.6, 1.0, and 1.0, respectively. Besides, Cs and I (~15,000 ppm) were added to the dry mixture, which is similar to Co concentration in HSW. Cement waste forms were prepared by mixture of OPC (18.6 wt%), HSW (40 wt%), CsI (3 wt%), and DIW (41.4 wt%). All mixture samples were poured into cylindrical polyethylene mold (diameter 2.3, height 4.6 cm), and cured in the clean bench at room temperature for 7days.

2.3 Mechanical strength of geopolymer and cement waste forms

Compressive strength of geopolymer and cement waste forms was measured by using universal testing machine (ST-1001, Salt Inc., South Korea) at a loading rate of 0.3 MPa S^{-1} according to ASTM C39 procedure.

2.4 Leaching test

The leaching test was conducted according to ANSI/ANS16.1 method. A total sampling time was 10 times with 2hr, 7hr, 1day, 2days, 3days, 4days, 5days, 19days, 47days, and 90days. Two types of leachates were used, deionized water

(DI) and sea water (SW) with 10.0±1.0 ratio of total volume of leachate to surface area of waste form. The leachability index (LI) was calculated by Eq. 1.

$$L_i = \frac{1}{n} \cdot \sum_1^n [log(\beta / Di)]_n \quad (1)$$

L_i: The leachability index of a nuclide, i
n: Total sampling days
β: A defined constant (1.0 cm^2/s)
D_i: The effective diffusivity of nuclide

3. Results and Discussion

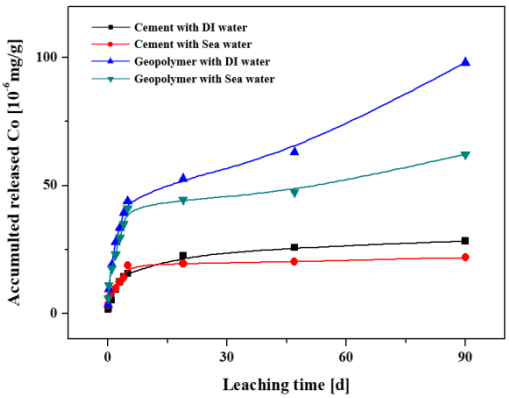

Fig. 1. Leaching test results of Co.

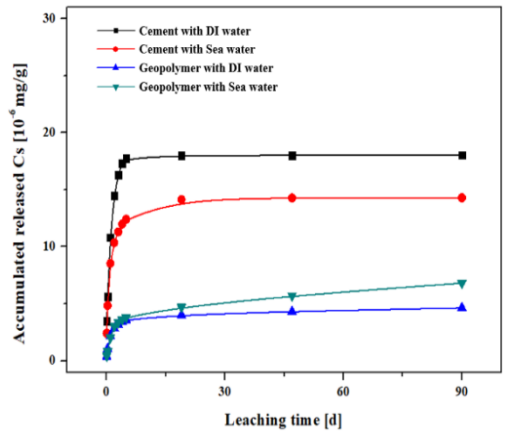

Fig. 2. Leaching test results of Cs.

The results of compressive strength of geopolymer (GP) and cement (CM) waste forms after leaching test were 20.37 Mpa (DI-GP), 3.845 Mpa (DI-CM), 16.96 Mpa (SW-GP), and 4.711 Mpa (SW-CM), respectively. They are higher than 3.44 Mpa, which is the acceptance criteria for waste form in repository.

Comparing leachability of four tests (Fig. 1 and 2), each LI of Co and Cs were calculated as 18.54 and 8.29 (DI-CM), 18.89 and 7.96 (SW-CM), 17.66 and 8.47 (DI-GP), 17.94 and 8.17 (SW-GP), respectively. LI of I was lower than LI of Co and Cs. They were calculated as 7.05 (DI-CM), 5.07 (SW-CM), 7.06 (DI-GP), 5.37 (SW-GP), respectively.

4. Conclusion

Solidification and stabilization of geopolymer and cement waste forms contained HSW were evaluated by ANSI/ANS 16.1 leaching test method. Based on the results from compressive strength and leaching test, both geopolymer and cement waste forms are appropriate for immobilization of the HSW. The calculated LIs of Co, Cs, I in DI leachate were higher than 6.0 and satisfied the waste form acceptance criteria in repository.

ACKNOWLEDGEMENT

This work was supported by the Korea Atomic Energy Research Institute (KAERI) granted financial resource (NRF-2018M2A8A5024109).

REFERENCES

[1] D. Peter et. al., “The role of inorganic polymer technology in the development of ‘green concrete’”, 37(12), p. 1590-1597 (2007).

[2] Ahn, J., WS. Kim, and W. Um, “Development of metakaolin-based geopolymer for solidification of sulfate-rich HyBRID sludge waste”, Journal of Nuclear Materials, 518, 247-255 (2019).

Verification of Efficiency Calculation for an Overpack 320 L Drum Containing Compressed 200 L Radioactive Waste Drum

Sang Mo Ham[1, 2,*] and Sung Yeop Jeong[2]
[1] Kyung Hee University, 1732, Deogyeong-daero, Giheung-gu, Yongin-si, Gyeonggi-do, Republic of Korea
[2]Godo-tech Co.,Ltd., 150, Jojeong-daero, Hanam-si, Gyeonggi-do, Republic of Korea
[*]hsm@godo-tech.com

1. Introduction

Most of the low and intermediate radioactive wastes generated by nuclear power plants are disposed of by the Korea Radioactive Waste Agency in the form of 200 L drums. However, recently, due to the saturation of waste temporary storage in nuclear power plants, overpack 320 L drums containing two or more compressed 200 L drums are disposed to reduce the volume and quantity of waste generated. In the case of overpack 320 L drum, the radioactivity was measured by performing the calibration under the geometric condition in which one 200 L drum was re-packed with the 320 L empty drum.

However, the overpack 320 L drum containing two or more compressed 200 L drums, has a different measurement geometry and requires a new calibration method to improve measurement accuracy. These drums are underestimated in their radioactivity because the geometric conditions change when measuring radioactivity using the efficiency calculated by current calibration method. Therefore, in this study, the correction factor was determined by reflecting the shielding increase effect of the compressed 200 L drums, and the measurement accuracy was evaluated by comparing the radioactivity specified in the source certification value with the measured activity applied with the correction factor.

2. Materials and Methods

Non-destructive Assay for radioactive waste drum is dependent on drum density and container thickness. Therefore, it is necessary to compensate for matrix attenuation (density) and thickness of shield. Since the density increases as the weight becomes heavier, the tare weight for one 200 L drum applied under existing calibration geometry should be changed to the weight corresponding to the number of compressed 200 L drums. However, density is not considered because the effect of matrix attenuation is corrected using Tx correction or Multi-efficiency method in operation software. Therefore, this study only considers the change of shield thickness. Drums compressed at high pressure will increase the shield thickness of the drum side by reduced volume.

The increase in shielding thickness was calculated using the X-ray image data of overpack 320 L drum, and finally, a calibration accessary corresponding to the increased shielding thickness was produced.

Figure 1 shows a calibration accessary that reflects shield thickness increments. It has a thickness equivalent to four compressed 200 L drums and can be covered on 200 L calibration drum and centered in 320 L empty drum to reproduce the measurement geometry of an overpack 320 L drum.

Fig. 1. Calibration accessary designed for accuracy evaluation.

The accuracy evaluation was performed using a calibration accessary, a 200 L particle drum (0.72 kg/l), sand drum (1.67 kg/l) and concrete drum (3.03 kg/l) and 320 L empty drum to ensure that accuracy was maintained for the entire density distribution of overpack 320 L drums and

it was measured three times for each density.

In this measurement, radioactivity was calculated using three different method to compensate for the increase in shielding thickness. The first method is to use the current calibration efficiency, and second method is to apply the correction factor derived from the mass attenuation coefficient. The last method is to apply the correction factor calculated using the ISOCS code. The radioactivity calculated using these three methods were compared with each other, and the accuracy evaluation.

3. Results and Discussion

The 1st acceptance criteria was applied to the radionuclide concentration validity criteria of the Korea Radioactive Waste Agency, and the 2nd acceptance criteria was applied to the accuracy table of Tomographic Gamma Scanner (TGS) provided by Canberra Industries, Inc.

We calculated the results by considering only four compressed 200L drums. This is because more than 90% of overpack 320 L drums are compressed with three or four 200 L drums. The result of the accuracy evaluation causes overestimation of about 4 % when the number of internal compressed 200 L drums is greater than three. but if multiple analysis modes exist, the operation time is reduced due to the increased calibration time for operation. Therefore, minimal calibration procedures are required as long as accuracy is maintained.

Table 1 shows the results of accuracy evaluation according to the 1st and 2nd acceptance criteria As a result of the calculation, the current calibration method, the mass attenuation coefficient method, and the ISOCS code method all met the first acceptance criteria However, only the method using the ISOCS code met the 2nd acceptance criteria and the rest of methods exceeded the acceptance criteria.

4. Conclusion

On the basis of the above measurements, we confirmed that the method using ISOCS code calculation is effective for radiological characterization of overpack 320 L drum containing compressed 200 L drums.

Consequently, considering the shielding thickness, if the calibration drums is manufactured and calibration is performed, the accuracy of the quantitative analysis on the overpack 320 L drum will be improved.

ACKNOWLEDGMENTS

This work was supported by a grant from “Development of calibration method and accuracy evaluation for overpack 320 L drum containing compressed 200 L drums” carried out by Korea Hydro & Nuclear Power Co., Ltd.

REFERENCES

[1] NIST, “Tables of X-ray mass Attenuation Coefficients and Mass Energy-Absorption Coefficients 1 keV to 20 MeV for Elements Z=1 to 92 and 48 Additional Substances of Dosimetric Interest”, NISTIR 5632 (1995).

Table 1. Result of Accuracy test for an overpack 320 L drum containing compressed 200 drums (■: Pass ■: Fail)

		Current calibration method		Mass attenuation coefficient method		ISOCS code		1st acceptance criteria		2nd acceptance criteria	
Quantity of Compressed 200 L drum	Drun density	Co-60	Cs-137	Co-60	Cs-137	Co-60	Cs-137	Co-60	Cs-137	Co-60	Cs-137
4	Low density (0.72 kg/l)	68 %	61 %	84 %	82 %	89 %	90 %	50 % ~ 150 %	30 % ~ 250 %	88 % ~ 112 %	88 % ~ 112 %
	Medium density (1.67 kg/l)	67 %	62 %	83 %	82 %	89 %	90 %	50 % ~ 150 %	30 % ~ 250 %	86 % ~ 124 %	86 % ~ 124 %
	High density (3.03 kg/l)	75 %	70 %	93 %	94 %	100 %	103%	50 % ~ 150 %	30 % ~ 250 %	77 % ~ 123 %	77 % ~ 123 %

Dynamic Changes of Groundwater Chemistry in the LILW Disposal Facility Along the Coastal Area

Eunhye Kwon, Jonghoon Park, and Nam C. Woo*
Yonsei University, 50, Yonsei-ro, Seodaemun-gu, Seoul, Republic of Korea
*ncwoo@yonsei.ac.kr

1. Introduction

The LILW disposal facility in Wolsung area is located close to the shoreline, and groundwater chemistry of the facility has been monitored from the beginning of the facility construction. In this study, we present the results of groundwater monitoring activities from the facility from 2015 to 2017.

2. Methods

For this study, quarterly field monitoring had been performed from June 2015 to Dec. 2017 during the operation stage of the facility. We sampled groundwater from six monitoring wells screened at multi-depths in discrete intervals (GM-1, GM-2, GM-4, GM-5, GM-6, GM-7; Fig. 1, Fig. 3), and sea waters at two points north and south of the facility boundary. Observations from GM-7 well were used as backgrounds comparatively to the other five wells.

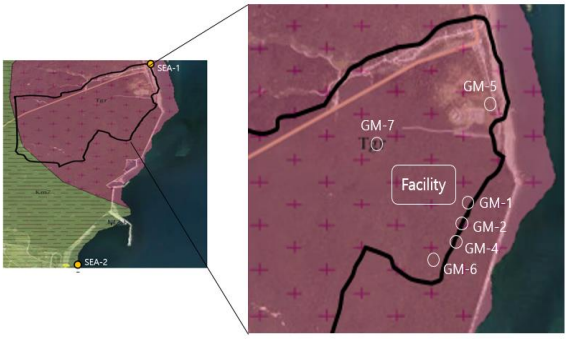

Fig. 1. Geology map & sampling point of study area (modified Kim et al., 2018).

Table 1. Monitoring wells and their information on elevations, total depths and sampling intervals

Well ID	Ground elevation (m)	Well depth (m)	Sampling depth (m, a.s.l)					
			#1	#2	#3	#4	#5	#6
GM-1	18.4	301	-59.6	-116.6	-155.6	-225.6		
GM-2	17.6	302	-86.4	-136.4	-190.9	-267.4		
GM-4	22.4	300	-67.6	-107.6	-156.6	-215.6	-244.6	-268.6
GM-5	19.5	228	-78.4	-109.9	-140.4	-163.4	-191.4	-199.4
GM-6	19.0	300	-117.0	-173.0	-217.0	-241.0	-265.0	
GM-7	76.0	302	-48.0	-82.0	-104.0	-131.0	-155.0	-202.0

Samples were measured on site and in laboratory for field parameters and chemical compositions with stable isotopic signatures. Using charge balance, chemical data was verified for their analytical qualities. During the pre-operational period of the underground facility from 2010 to 2014, results of quarterly monitoring of groundwater were presented in Kim et al. [1], and results of this study was interpreted in the perspective of continuous groundwater flow.

3. Results and Discussion

3.1 Spatio-temporal changes of groundwater chemistry – Grouping

EC values of each monitoring wells were plotted in time in Fig.2, and groundwater was subdivided into several groups based on its water type and the pattern of temporal change. GM-1 and GM-7 wells have no change in time indicating background groundwater. Some groundwater shown EC changes that started increasing since 2012-1Q, became to the maximum with EC values of 16 mS/cm, and remained as steady conditions, so classified as Group 1. Others having EC type of rise-and-

decline temporal changes through the monitoring period, called as Group 2. Lastly, wells of GM 5 shown that EC values increased fast from 2010-3Q, reached to the maximums within two years and sustained with mostly saline to brackish water-type, named as Group 3.

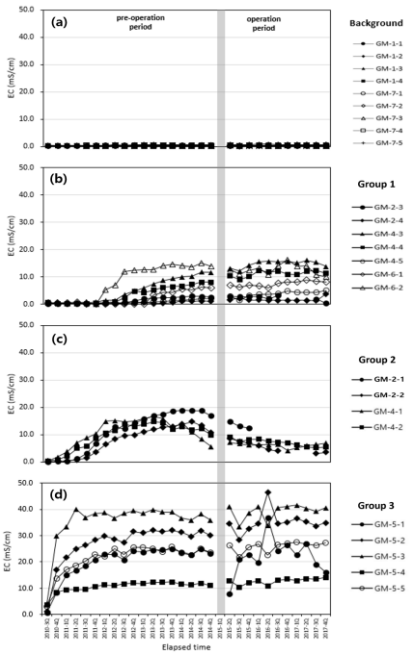

Fig. 2. Groundwater EC in time from the pre-operation to the operation period and subsequent grouping.

These changes of water chemistry appeared to be varied in depths as well (Fig.3), implying those reactions occur along the connected groundwater flow paths, such as fractures.

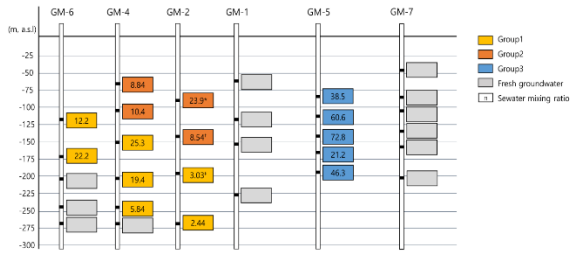

Fig. 3. Spatial variation of groundwater chemistry in groups.

3.2 Changes of hydrogeochemical reactions along the flow paths

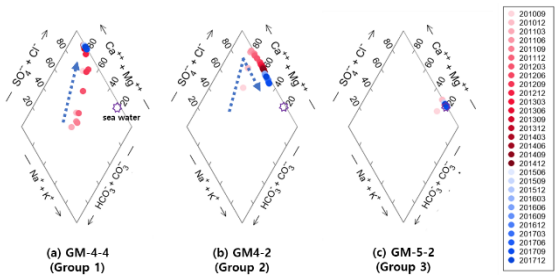

Fig. 4. Quarterly changes in groundwater composition of GM-4-4, 4-2, and 5-2 representing Group 1, 2, and 3, respectively. Red and blue colors indicate those before and after construction stages, respectively.

Groundwater in the GM-4-4 well, representing Group 1 in Fig.4(a), shows dominant changes in composition through the ion exchange process along the sea-water intrusion (SWI). The exchange of Ca^{2+} and Na^{+} between aquifer matrix and intruding sea water is noted as an arrow [2]. GM-4-2 groundwater representing Group 2 in Fig.4(b) shows water-chemistry change following ion exchange and mixing processes. Groundwater in the GM-5-2 well representing Group 3 have shown direct mixing with sea water, even though the mixing ratios are various in depths (Fig.4(c)), implying the groundwater in the aquifer at GM-5 well location maintains its connections to sea water.

4. Conclusion

Construction of the underground facility initiated the changes. During the operational stage, some wells show on-going changes, some returned to become steady, and some no changes. Thus, systematic and continuous monitoring is warranted for the safety of the facility.

REFERENCES

[1] Kim et al., 2018, Hydrogeochemistry in the coastal area during construction of geological repository. Jour. of Hydrology, 562, 40-49.

[2] Appelo, C.A.J., Postma, D., 2005. Geochemistry, Groundwater and Pollution, second ed. Balkema, Rotterdam, Netherlands.

Study on the Establishment of Grouping Analysis Range for KAERI's Radioactive Waste Using Concentration Averaging Method

Dong-Ju Lee, Junhyuck Im*, Dae-Seok Hong, and Il-Sik Kang

Korea Atomic Energy Research Institute, 111, Daedeok-daero 989beon-gil, Yuseong-gu, Daejeon, Republic of Korea

dongju15@kaeri.re.kr

1. Introduction

Radioactive Waste Chemical Analysis Center at the Korea Atomic Energy Research Institute (KAERI) has used the grouping analysis method for the analysis efficiency of contaminated trash (e.g. combustible waste, HEPA filters). In this study, we have assessed the optimum amount of drum for grouping the waste samples using concentration averaging method proposed by US Nuclear Regulatory Commission (NRC) [1].

2. Background of the assessment

According to the NRC standards, KAERI's radioactive contaminated trash is classified as "blendable waste" because it is not expected to contain durable items with significant activity. NRC suggests a volume threshold which allows radionuclide concentration averaging of blendable waste and we applied the threshold as the number of drums that can be grouped.

Table 1. thresholds for demonstrating adequate blending

Characteristics of most concentrated influent waste stream	Volume of Mixture in m^3(ft^3)		
	Class A Mixture	Class B Mixture	Class C Mixture
Sum of fractions < 10	No Limit	No Limit	No Limit
10≤Sum of fractions< 20	No Limit	No Limit	50 (1800)
20≤Sum of fractions<30	60 (2100)	No Limit	20 (700)
30≤Sum of fractions<50	20 (700)	No Limit	6 (210)
50≤Sum of fractions<100	6 (210)	40 (1400)	2 (70)

3. Method and result of the assessment

3.1 Determination of the radionuclide inventories of reference waste drum and waste classification

The major nuclides used in the evaluation are the 11 nuclides proposed by the final repository as disposal limits. Nuclide inventories were assessed by the results of radionuclide concentrations analyzed for disposal from 2015-2018. For conservative assessment, the maximum values for each nuclide were applied and volume of 1 drum was set to 0.17m^3 based on the minimum void fraction allowed for disposal (15%). The determined nuclide inventories for assessment are shown in table 2.

Table 2. nuclide inventories of reference waste drum

Radionuclide	Half Life (Y)	Inventory (Ci/m^3)
Gross-α	24110	1.051E-01
H-3	12.33	2.345E+00
C-14	5730	4.347E-02
Co-60	5.271	4.036E-02
Sr-90	28.74	1.637E-01
Nb-94	20300	1.106E-02
Tc-99	211100	7.162E-02
I-129	15700000	1.023E-03
Cs-137	30.04	2.224E-01
Ni-59	76000	9.142E-03
Ni-63	100.1	1.558E-01

As a result of the waste classification according to the method proposed in NRC 10CFR 61.55 "Waste Classification"[2], the reference drum which contains the determined nuclide concentration (table 2) was classified as class C.

3.2 Determination of the radionuclide inventories of hot spot waste drum and waste classification

To establish the most conservative situation, we set up a situation that all major nuclides correspond to disposal concentration limits (i.e. hot spot waste drum). The determined nuclide inventories are shown in table 3.

Table 3. nuclide inventories of hot spot waste drum

Radionuclide	Half Life (Y)	Inventory (Ci/m^3)
Gross-α	24110	1.549E-01
H-3	12.33	4.646E+01
C-14	5730	9.293E+00
Co-60	5.271	1.549E+03
Sr-90	28.74	3.098E+00
Nb-94	20300	4.646E-03
Tc-99	211100	4.646E-02
I-129	15700000	1.549E-03
Cs-137	30.04	4.646E+01
Ni-59	76000	3.098E+00
Ni-63	100.1	4.646E+02

As a result of the waste classification, the hot spot waste drum slightly exceeded class C limit.

3.3 Set up the hot spot inflow scenario

Based on the evaluation of 3.1 and 3.2, we assumed a “hot spot inflow scenario”. The hypothetical situation is the continuous grouping of a certain number of hot spots (slightly above Class C) into the Class C radioactive waste. In this situation, the maximum allowable drum quantity is evaluated.

3.4 Result

When a certain amount of hot spot inflows into one reference drum, the allowable 200L drum quantity based on the table 1 thresholds (m^3) was evaluated as shown in table 4.

Table 4. result of allowable drum quantity evaluation

Hot spot drum quantity (200L)	Sum of fractions	Volume of mixture (m^3)	Table 1. threshold (m^3)	Result
4	2.313E+01	0.85	20	satisfied
6	3.436E+01	1.19	6	satisfied
7	3.998E+01	1.36	6	satisfied
10	5.684E+01	1.87	2	satisfied
11	6.245E+01	2.04	2	dissatisfied

According to the results, although up to 10 hot spot drums are included and a total of 11 drums are grouped, it can be seen that the NRC criteria is satisfied. However, from the 7 hot spot drums inflow scenario, the final waste class exceeded class C, which is not suitable for the disposal of low-level radioactive waste on the NRC standards. In other words, the maximum allowable amount of radioactive waste that satisfies the NRC threshold was evaluated as 7 drums (inflow of 6 hot spot drums).

4. Conclusion

In this study, we applied the allowable grouping range of KAERI’s radioactive waste (contaminated trash) by using concentration averaging method of blendable waste. Conservative assessment has shown that KAERI’s radioactive waste can be grouped up to 7 drums on NRC basis. If this approach is established appropriately by additional reviews of domestic and international literatures and conducting verification experiments, the analysis efficiency of KAERI’s radioactive waste can be increased. And also transportation of radioactive waste to the final repository can be promoted.

REFERENCES

[1] U.S. NRC, “Concentration Averaging and Encapsulation Branch Technical Position, Revision 1”, Vol.1, February 2015.

[2] U.S. Nuclear Regulatory Commission, 10CFR Part 61.55, “Waste Classification”.

A Proposal of "Innerpack" Design Concept for Efficient Transport and Disposal of Radioactive Waste

Moonoh Kim*, Wooyoung Kim, and Nakhoon Sung
Korea Nuclear Engineering & Service, 65, Myeongdal-ro, Seocho-gu, Seoul, Republic of Korea
*mokim@kones21.com

1. Introduction

The radioactive waste generated during operating nuclear power plants has been temporarily stored in 200 or 300-liter drums, and then packed by eight units in an IP-2 type packaging and transported to a disposal facility. Due to the various radioactive levels of decommissioning waste, however, it is expected that there may be limitations in transporting various dismantled wastes to the current transport system carried by as single packaging: the increase of thickness and weight of container and difficulty to disposal. To overcome those difficulties, in this study, the design concept of "Innerpack" was proposed and the design requirements for transporting various radiation levels of decommissioning wastes efficiently and economically.

2. Shielding Design with Radiation Levels

2.1 Radioactive Levels of Decommissioning Waste

The most important factor in the shield design of packaging is the specific radioactivity of Co-60 in the radioactive waste. According to the classification criteria of radioactive material [1], the maximum specific radioactivity of Co-60 of low-level radioactive waste is $3.7x10^7$ Bq/g. However, the specific radioactivity of Co-60 in miscellaneous radioactive solid waste is known to be about $10^2 \sim 10^3$ Bq/g [2], and in the spent filter or spent resins is more than 10^4 Bq/g [2]. Therefore, the design of packaging for transporting decommission waste, even for low-level radioactive waste, should be performed to enable coping with various radiation levels.

2.2 Shielding Design of Packaging

Radioactive waste would be transported in Type-L, A or B packaging according to the A value of radioactive waste and Low Specific Activity (LSA) materials could be in Type-IP-1,2 or 3 packaging with their specific radioactive density.

As shown in Table 1, the minimum thicknesses of IP-2 packaging with dimensions of 1.46m(W) × 1.46m(L) × 0.95(H) required to shield the radioactivity of radioactive wastes with various Co-60 radiation levels were evaluated by MCMP5 code using the three-dimensional Monte Carlo method.

Under the normal transport conditions, the requirement for shielding should meet the following [3],[4]:

- Dose rate at surface below 2mSv/hr
- Dose rate at any point 2m away from the container below 0.1mSv/hr

As shown in Table 1, it was found that metallic material with thickness of 120mm was required to shield radiation from radioactive waste with concentration of $1.0x10^5$ Co-60 Bq/g.

As a result, in order to shield the radiation from Co-60 with a concentration of about 10^5 order, the weight of container with 1.2m x 3.4m x 1.6m in size made of a metallic material with a thickness of at least 120 mm, shall be about 20 tons.

Table 1. Minimum Thickness according to Concentration of Co-60

Concentration of Co-60 (Bq/g)	Minimum Thickness of Metal (mm)
1.3×10^3	5
1.5×10^3	10
4.0×10^3	30
6.8×10^3	50
1.0×10^5	120

3. Concept of Innerpack

When transporting radioactive waste with high doses of radiation, the thickness of the packaging is inevitably thickened to meet the requirements associated with shielding. Therefore, it is difficult and inefficient to transport and dispose of thick and heavy containers made of metallic material. To overcome those problems, a new concept container called "Innerpack" is proposed as shown Fig.1. An Innerpack is a container with minimum requirements that meet the acceptance criteria for disposal. It is transported to the disposal container for disposal or direct disposal by the packaging. If radioactive waste is

packaged in Innerpack and transferred by packaging, the shielding thickness to satisfy the transport requirements is shared between the Innerpack and the packaging. By reducing the thickness of the Innerpack that is finally disposed of, it can contribute to the improvement of economics as well as the safety of the repository.

The Innerpack should be designed to meet the minimum requirements such as Waste Acceptance Criteria of the repository [5]. The Innerpack proposed in this study has the following design requirements.

- Dose rate at surface below
  - 2mSv/hr (Non-Exclusive)
  - 10mSv/hr (Exclusive)
- 5-stage Stacking
- Lifting Requirement to support its mass

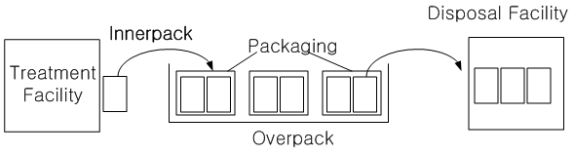

Fig. 1. Concept of Innerpack.

The shielding requirement such as surface dose rate below 2mSv (Requirement of surface dose rate) of the Innerpack are the same as that of the packaging [4]. However, the packaging must meet the additional requirement that the maximum radiation level should be less than 0.1mSv at a distance of 2m (Requirement of distance dose rate).

Table 2 shows the change in the thickness of the container according to the shielding requirements. As shown in Table 2, the requirement of distance dose than that of surface dose has a greater effect on the shielding design; minimum thickness for shielding packaging is calculated to reflect not only requirement of surface dose rate but also that of distance dose rate. Therefore, applying only requirement of surface dose to the shield design of the Innerpack reduces the thickness of the container by 40-60% compared to the packaging designed with requirements of surface and distance dose rate.

From Table 2, metal material of thickness of 120mm is required to transport the wastes with 10^5 Bq/g concentrations of Co-60 for transporting by a single packaging. However, thickness of 76 mm for Innerpack and thickness of 44 mm for packaging are required, respectively, for transporting by a combination of those. The packaging with reduced thickness by about 60% could be reused after transporting the Innerpack to the disposal site and Innerpack with reduced thickness by about 40% compared to the use of a single packaging would be disposed of at the repository site.

Table 2. Comparison the thickness of Innerpack with that of Packaging according to Concentration of Co-60

Concentration of Co-60 (Bq/g)	Minimum Thickness of Metal (mm)	
	Innerpack	Packaging
$1.0x10^4$.	25mm	60mm
$1.0x10^5$	76mm	120mm

4. Conclusion

In this study, a new concept of radioactive waste container called “Innerpack” was proposed. When radioactive waste with high dose rate was transported, it was found to reduce the thickness of packaging by using the Innerpack and packaging together. Consequently, the improvement of economics for manufacturing container as well as the safety of the disposal site could be expected by applying the Innerpack reduced thickness container.

Acknowledgement

This work was supported by the Korea Institute of Energy Technology Evaluation and Planning (KETEP) granted fund by MOTIE, Republic of Korea. (No.20181510300870)

REFERENCES

[1] NSSC, Regulations for Classification Criteria and Clearance of Radioactive Material, No. 2017-65 (2017).
[2] Kang Il Jung et al, Prediction of Radionuclide Inventory for the Low- and Intermediate-Level Radioactive Waste Disposal Facility by the Radioactive Waste Classification, JNFCWT Vol. 14, No. 1, pp.63-78, 2016.
[3] NSSC, Regulations on the Technical Standards for Radiation Safety Control, No-20 (2018).
[4] NSSC, Regulations for Packaging and Transportation of Radioactive Material, No. 2017-56 (2017).
[5] KORAD, Safety Analysis Report for Low and Intermediate Leve Radioactive Waste Disposal Facility on the Planning Phase (2008).

4분과

중저준위폐기물관리 (Poster)

A Study on the Input Data for Radionuclides Behavior Assessment of Combustible Radioactive Waste in Decommissioning Nuclear Power Plants

Sang Heon Lee[1,*], Jong Soon Song[1], Jung Suk Park[2], Chang Hyun Ryu[2], and Cheol Hyun Hwang[2]

[1]Chosun University, 309, Pilmun-daero, Dong-gu, Gwangju, Republic of Korea

[2]KEPCO Nuclear Fuel, 242, Daedeok-daero 989beon-gil, Yuseong-gu, Daejeon, Republic of Korea

[*]leesanghoen@naver.com

1. Introduction

A large portion of the radioactive wastes, generated in nuclear facilities, is organic materials, and the volume reduction ratio during incineration or pyrolysis is known to be considerably big. Incineration is a process of burning combustible organic wastes. Chemically, it is a process of reacting the wastes with oxygen, making carbon dioxide and vaporizing them. On the other hand, pyrolysis is a reduction reaction that dissolves organic matters with high heat without any oxygen. It is different from the incineration technology in that it vaporizes organic matters, which have oxygen, hydrogen, nitrogen, etc. attached to carbon atoms, with high heat. This study was a basic research for evaluating the behavior of radionuclides depending on temperature. It examined the current status of the organic waste treatment technology, the types of organic wastes generated in the nuclear power plant and the chemical forms of key nuclides.

2. Technology Status of Volume Reduction

2.1 Incinerator of continuous pyrolysis

The heat necessary for pyrolysis can be obtained in two ways: first, off-gas with a low oxygen concentration is re-circulated, and the residual heat is used, and second, the heat, generated during direct oxidation by the mixed air consisting of re-circulated off-gas and fresh air, is used. A guide fan is used to send the gas, generated by pyrolysis, to the combustion chamber, and it is completely combusted at about 900°C in the state of excess air.

2.2 Incinerator of batch pyrolysis

The heat necessary for pyrolysis is obtained through partial oxidation of wastes (by limiting the air supply to 30~50% of the air necessary for complete combustion). To keep a consistent exit temperature, the auxiliary propane burner interworks with a temperature controller to control exit temperature so that all gaseous and particulate matters can be completely combusted.

3. Combustible Radioactive Waste in NPP

Looking at the amount of each type of low and intermediate level radioactive wastes, generated by Korea Hydro & Nuclear Power Co. Ltd., dry active waste accounts for about 65% of the total, the largest amount. Dry active waste is classified into combustible and non-combustible according to the classification standard.

Table 1. Type Combustible Waste

Classfication	Waste type
Cotton	Clothing, Gloves, Socks, etc.
Paper	paper, other paper, etc.
Vinyl	Tape, other vinyl, etc.
Plastic	PVC, Bottles, etc.
Wood	Wood scaffolding, woods, etc.
other	rubber, bag, nylon, etc.

4. Derivation of Chemical Form by Radionuclides

To evaluate the behavior of radionuclides according to temperature, key nuclides must be determined, and the chemical properties of nuclides must be identified.

13 nuclides, suggested by the radioactive waste acceptance criteria, were selected as key nuclides. The chemical forms for evaluating the behavior of radionuclides were identified using a HSC chemistry 9.0 code as shown in Table 2.

Table 2. Abbreviated Chemical Form of Nuclides

Nuclides	Chemical Form
H	H(g), H_2(g), H_3(+g), $HAlO_2$(g), $HAsO_2$(a), $HAuBr_4$(a), HBN(g), etc.
C	C, C(g), C(A), C(D), C_2(g), C_2(-g), C_2(+g), C_3(g), C_4(g), CS(g), C_6(g), etc.
Fe	Fe, Fe(g), FeAl, $FeAl_2O_4$, FeAs, $FeAsO_4$, FeAsS, FeB, FeBr(g), etc.
Co	Co, Co(g), Co_2(g), CoAl, $CoAl_3$, CoAs, $CoAs_2$, Co_2As, CoB, Co_2B, etc.
Ni	Ni, Ni(g), Ni_2(g), NiAl, NiAs, NiB, NiBr(g), $NiBr_2$, Ni_3C, $Ni(CN)_2$, etc.
Sr	Sr, Sr(g), Sr_2(g), $Sr(AsO_2)_2$, $SrBO_2$(g), $SrBeO_2$(g), $SrBi_2O_4$, SrBr(g), etc.
Nb	Nb, Nb(g), NbB_2, $NbBr_5$, $NbBr_5$(g), NbC, Nb_2C, Nb_3C, $NbCl_2$, $NbCl_3$, etc.
Tc	Tc, Tc(g), TcC(g), $TcCl_3$, $TcCl_5$, TcF_3, TcF_4, TcF_5, TcF_5(g), TcF_6(g), etc.
I	I, I(g), I_2, I_2(g), I_2(a), IBr, IBr(g), ICl, ICl_2, ICl_3, IF(g), INO_2(g), IO(g), etc.
Cs	Cs, Cs(g), Cs_2(g), $CsAlH_4$, $CsAlO_2$, $CsAlSiO_4$, $CsAsO_2$, CsAu, etc.
Ce	Ce, Ce(g) Ce_2(g), Ce(+g), $CeAlO_3$, CeAu(g), CeB_4, CeB_6, $CeBr_3$, etc.

5. Conclusion

This study investigated the basic data for evaluating the behavior of radionuclides when the volume of combustible wastes is reduced. The behavior of radionuclides will be evaluated by selecting volatile nuclides from the 13 nuclides above.

REFERENCES

[1] Kim JK, “Oxygen Incineration Process for Treatment of Alpha-contaminated Wastes”, KAERI/TR-1886, 2001.

[2] NIER, “Integrated Pollution Prevention and Control Reference Document on Best Available Techniques for the - Waste Incineration”, NIER-GP2013-452, 2013.

[3] Jung KI, “Comparison of Radionuclide Inventory Between Predicted and Measured Activity of Dry Active Waste From Korea Nuclear Power Plant”, Journal of Nuclear Fuel Cycle and Waste Technology Vol.15 No.3 pp.281-299 (2017).

[4] Diaz S, “ Trace element evaporation during coal gasification based on a thermodynamic equilibrium calculation approach”, Journal of Fuel Vol.82 pp.137-145 (2003).

Dissolution Characteristics of Silver Tellurite Glass Containing ^{129}I

Cheong-won Lee*, Bansuk Yu, and Jong Heo
Pohang University of Science and Technology, 77, Cheongam-ro, Nam-gu, Pohang-si, Gyeongsangbuk-do, Republic of Korea
*schwarz@postech.ac.kr

1. Introduction

^{129}I is one of the fission products and poses significant issues in the waste treatment, because of its long half-life (~1.57×10^7 y), high volatility, high solubility and mobility in water [1, 2]. Most of ^{129}I is captured as an AgI form in off-gas treatment system during the reprocessing because of its high trapping efficiency for the gaseous iodine [3].

Glasses containing silver oxide can accomodate a large amount of AgI [4]. Tellurite glasses have low melting temperatures (700~800 °C), good chemical durability and network flexibility. Therefore, tellurite glasses mixed with silver oxides can be a suitable waste form to immobilize ^{129}I. Dissolution behavior of these silver tellurite glasses are investigated following the long-term dissolution test.

2. Experimental procedures

2.1 Preparation of glass specimens

Nominal composition of the glasses in Table 1 was prepared by mixing TeO_2 (Kojundo, 99.9%), Ag_2O (Kojundo, 99%), Bi_2O_3 (Kojundo, 99.9%) and AgI (Alfa aesar, 99%). Batch mixtures were heated in alumina crucibles at 700 °C for 30 min and quenched by pouring melt onto brass molds in the air.

Table 1. Nominal and analyzed compositions of the glass obtained by X-ray fluorescence (XRF) spectroscopy

Elements excluding oxygen	Nominal composition	Analyzed composition
Te	37.18	35.99 ± 0.85
Ag (combined)	38.16	39.38 ± 0.84
Bi	11.45	11.99 ± 0.40
I	13.21	12.64 ± 0.02
Total	100.00	100.00

2.2 Characterization

XRF spectroscopy was used to analyze glass composition. Density was measured by Archimedes method in deionized water (DIW) as a medium. Chemical durability of the glasses was evaluated using the product consistency test (PCT). Glasses were crushed and sieved to 75 ~ 150 μm in size. Glass powders were then washed with deionized water and ethanol and 1.5 g of powders were soaked in 15 mL of deionized water inside a Teflon vessel and kept at 90 ± 2 °C for 7 days. The leachate was filtered using syringe with a 0.45 μm filter. Concentrations of elements in the leachate were analyzed using inductively coupled plasma mass spectrometer (ICP-MS).

2.3 Evaluation of the long-term leaching properties

Long-term leaching tests were conducted to investigate dissolution behavior of silver tellurite glasses. Bulk and powdered specimens

were leached in DIW and 0.1 M acetic acid (pH 2.88), respectively. ICP-MS was used to analyze leachate. Time of flight secondary ion mass spectrometry (ToF-SIMS) and scanning electron microscope-energy dispersive spectroscopy (SEM-EDS) were used to analyze depth profile of bulk specimen.

3. Results

3.1 General properties

The glass contains 12.64 wt.% of I in the composition excluding oxygen as shown in Table 1, i.e. I retention was 95.7 %. This result indicates that I content was 11.21 wt.% of all elements in glasses including oxygen.

The values for the normalized elemental releases of all elements were < 4.0 x 10^{-2} g/m^2 and it was well below US regulation of 2 g/m^2.

3.2 Dissolution behavior

Elemental leaching from the glass in DIW was extremely low. Therefore, we focused on glass dissolution in low pH solution. Ag was the most leached element from the glass. Then Ag precipitated on the surface (Fig. 1). Ag leaching is still ongoing after 64 days.

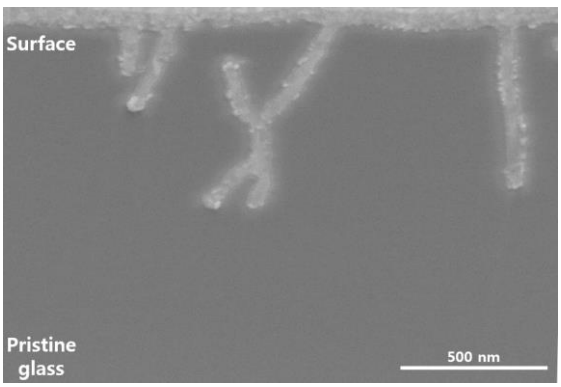

Fig. 1. Cross-section of the glass 64-days leached in low pH solution. Silver precipitated layer is formed on the surface.

Acknowledgement

This research was supported by Basic Science Research Program through the National Research Foundation of Korea (NRF) funded by the Ministry of Science and ICT (NRF-2018M2A7A1074894).

REFERENCES

[1] H.S. Lee, G.I. Park, K.H. Kang, J.M. Hur, J.G. Kim, D.H. Ahn, Y.Z. Cho and E.H. Kim, "Pyroprocessing Technology Development at KAERI", Nuclear Engineering and Technology, 43(4), 317-328 (2011).

[2] D.R. Haefner and T.J. Tranter, "Methods of Gas Phase Capture of Iodine from Fuel Reprocessing Off-Gas", INL/EXT-07-12299 (2007).

[3] J.H. Yoo, C.S. Seo, E.H. Kim and H.S. Lee, "A conceptual study of pyroprocessing for recovering actinides from spent oxide fuels", Nuclear Engineering and Technology, 40(7), 581-592 (2008).

[4] S. Rossignol, J.M. Reau, B. Tanguy, J.J Videau and J. Portier, "Glass Formation and Conductivity in the AgI-$AgO_{0.5}$-TeO_2 System", Journal of Non-Crystalline Solids, 155, 77-84 (1993).

Assessment of the Near Surface Disposal Facility According to Disposal Containers Usage Plan

Hyungoo Kang*, Changmin Shin, Sanghwan Lee, and Hoseog Dho
Korea Radioactive Waste Agency, 174, Gajeong-ro, Yuseong-gu, Daejeon, Republic of Korea
*kanghyungoo@korad.or.kr

1. Introduction

The near-surface disposal facility can be classified into a case of filling only the disposal container and disposing of the gap of the disposal container with backfill material. In the latter case, a structural analysis is needed to withstand the load (i.e. self-weight of the container), depending on the long-term life of the disposal container material. This study describes the results of the structural analysis of the backfill part that resist the load due to container loading.

2. Main condition of the disposal facility

2.1 Assumption of the disposal

Considering the size of the disposal facility, the disposal container arrangement was consider-ed to accommodate a weight of 125,000 tons and a volume of 32,825 m^3. Each container is placed at the cell of the backfill structure.

Table 1. Information of the disposal container

Name	Specification
SC 1	1.5m × 1.5m × 0.95m / 19ton
SC 2	1.6m × 3.4m × 1.2m / 35ton

2.2 Numerical analysis

The analysis was performed using ABAQUS, a finite element analysis software. The near-surface disposal facility was set to rigid conditions for considering the pure structural behavior at the backfill concrete structure. The upper load of the backfill structure was imposed using an equivalent rigid element (1,420tons of 200L drum, the concrete cover of the disposal structure and upper soil weight). Also, the analysis reflects the container load as the virtual distribution load. Table 2 shows the properties of the backfill concrete structure.

Table 2. Information of the backfill material

Material	Concrete
Elastic modulus	28,730MPa
Poisson's ratio	0.2
Mass density	2.3×10^{-9}N/mm^3
Compressive strength	37MPa

3. Result of the numerical analysis

3.1 Emplacement scenario

The emplacement scenario took into account the distance between disposal containers and the inner spacing of the single disposal facility. Two scenarios were calculated with 726EA SC1 disposal container and 300EA SC2 disposal container. After all containers have been loaded,

1,420EA 200L drums are loaded on the upper floor.

3.2 Performance of the backfill structure

Fig. 1 shows the stress evaluation at the backfill concrete structure reflecting the two container emplacement scenarios. The maximum compressive stress was 8.5MPa (Case SC1) and 13.9MPa (Case SC2). The second result exceeds the allowable compressive stress (25% of the design strength), so further consideration is required.

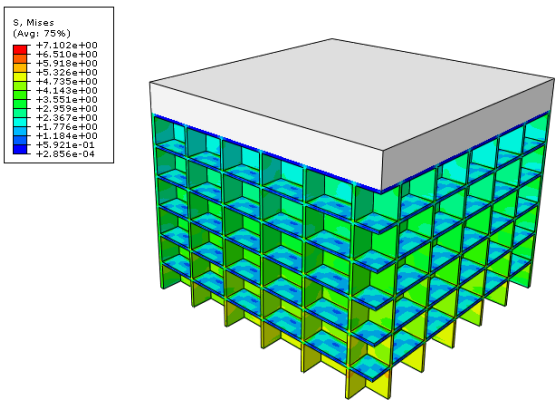

(a) Case 1 : SC1 loading

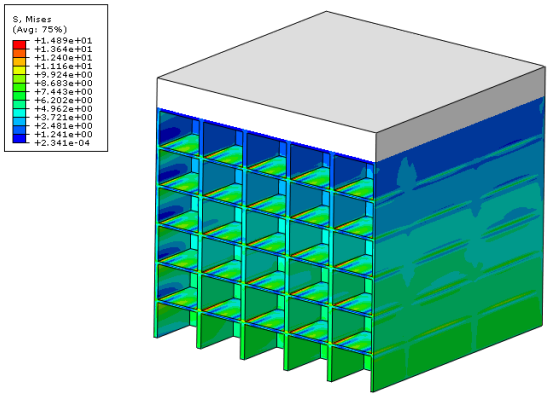

(b) Case 2 : SC2 loading

Fig. 1. Von-Mises stress distribution at the backfill.

4. Conclusion

This study analyzed the conditions under which two radioactive waste disposal containers were disposed in near-surface disposal facilities. As a result of analyzing the structural performance of the concrete backfill material in the disposal facility, the using condition of the SC1 container shows enough performance of capability. However, the SC2 disposal container usage conditions showed a maximum vertical displacement of about 4 mm. Therefore, requires further review of the SC2 disposal container usage scenario.

ACKNOWLEDGEMENT

This research was supported by the Korea Institute of Energy Technology Evaluation and Planning (KETEP), (No. 20181510300870).

REFERENCES

[1] Fillmore, D. L, “Literature Review of the Effects of Radiation and Temperature on the Aging of Concrete (No. INEEL/EXT-04-02319)”, Idaho National Laboratory (INL), 2004.

[2] IAEA Safety Standard No. SSG-29, “Near Surface Disposal Facilities for Radioactive Waste”, International Atomic Energy Agency, 2014.

[3] Jaechul Ha, Jeonghwan Lee, and Jeonghyoun Yoon, “Simulation of Unsaturated Fluid Flow on the 2nd Phase Facility at the Wolsong LILW Disposal Center”, Journal of Nuclear Fuel Cycle and Waste Technology, 15(3), 219-230 (2017).

Increased Homogeneity of Epoxy Solidifications by Ball-mill Treatment

Seonggon Ryu, Misuk Jang, and Seoung Rae Kim
Nuclear Engineering Services & Solutions, 756-27, Daedeok-daero, Yuseong-gu, Daejeon, Republic of Korea
*nessrnd@ness.re.kr

1. Introduction

Ion exchange resins (IERs) are used to remove radioactive material from liquid wastes through the exchange of ions between the liquid phase and the solid IERs in nuclear power plant.

Spent IERs should be treated as a form of low and intermediate level radioactive waste. Spent IERs are considered as a presenting a problem solid waste and are required special treatments to satisfy the waste acceptance criteria for a disposal site in Korea.

The homogeneity of solidification is one of the important acceptance criteria for final disposal site. To meet the waste acceptance criteria for a disposal site, the NESS conducted a study on solidification methods for effective disposal of IERs. Various materials can be selected to solidify IERs [1-3]. Solidifications were made using epoxy that has high adhesiveness and waterproofness, so it can be expected to have high leaching resistance. And epoxy also has good durability and high strength [4].

In this paper, the NESS presents the results of the homogeneity of the solids to spent IERS.

2. Experimental methods

Co and Cs were adsorbed on MB106 for 4 hours using a solution of $CoCl_2$ and $CsCl{\cdot}6H_2O$. After adsorption, it was cleaned several times with distilled water then dried at 90°C for overnight. Ball milling times of dried MB-106 were set differently to compare the characteristics of ion exchange resin according to the particle size after solidification. Ball milling times are 0 hour ,1 hour , 3 hour, and 5 hour.

Binder and curing agent are epoxy and iso-phorone diamine(IPDA), respectively. The ratio of binder and IERs are 5:5.

Fig. 1. Schematic diagram of solidification making process.

Various analyses were conducted, such as leaching test, heat circulation test, and compressive strength test, to confirm whether the acceptance criteria of the made solidification were met or not. The leaching test was carried out according to ANS16.1 method, and the heat cycle test took 30 cycles. One cycle means one hour at -40°C and one hour at 80°C.

3. Results and discussions

The initial Co and Cs concentration of the prepared solidification was calculated using the Co and Cs on IERs measured by ICP-MS (inductively coupled plasma mass spectrometry).

The waste acceptance criteria for a disposal site in Korea as follows [4]:

- leaching index of Co and Cs : ≥6
- compressive strength(CS) : ≥3.45 MPa
- heat circulation : CS 3.45 Mpa after 30 cycles

For five-day leaching test, the leaching index of Co and Cs was shown met the acceptance criteria as shown on Fig. 2. The compressive strength (CS) test results of solidifications measured before and after the heat circulation test (HCT) met the acceptance criteria(≥3.45 MPa) as shown on Fig. 3.

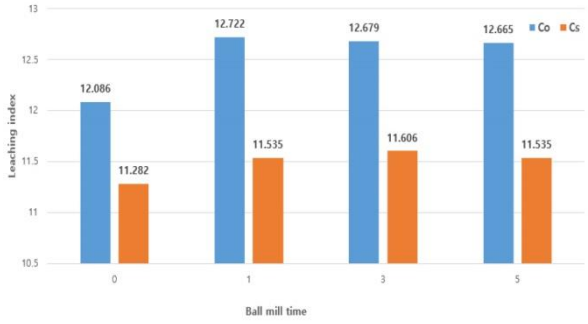

Fig. 2. Leaching index of Co, Cs.

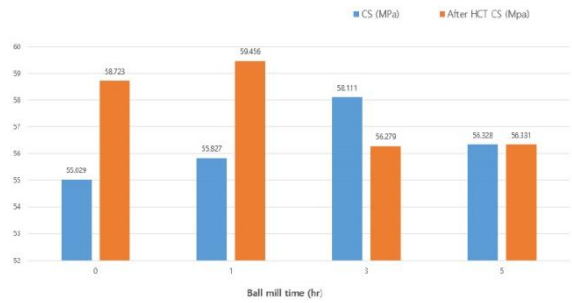

Fig. 3. Compressive strength of solidifications.

As a result of confirming the homogeneity according to the ball milling time, the non-ball milled solidification was not uniformly distributed because the resin sank during the solidification process. Fig. 4 shows the homogeneity of solidifications according to the ball milling time. As shown in this figure, the probable ball milling time for the production of homogeneous solidification was estimated to be 3 hours or more.

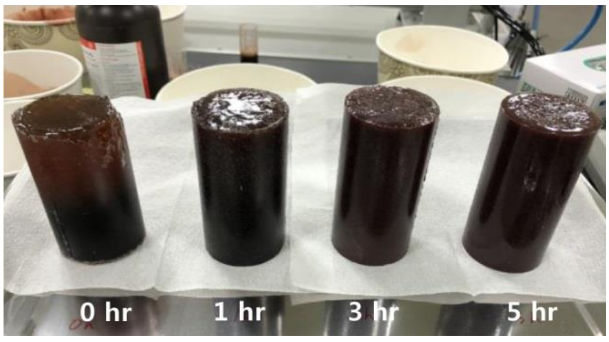

Fig. 4. Homogeneity of solidifications.

4. Conclusions

As a result of this study, it was confirmed that the homogeneity of the solidification could be increased by ball milling and the optimum ball milling time is 3 hours or more.

And various analysis results showed that all prepared solidification met the acceptance criteria for leaching test, compressive strength test, and heat circulation test.

ACKNOWLEDGEMENTS

This work was supported by the Korea Institute of Energy Technology Evaluation and Planning (KETEP) and the Ministry of Trade, Industry & Energy (MOTIE) of the Republic of Korea (No. 20171520000410).

REFERENCES

[1] Kim.J.M., “Relationship between Compressive Strength and Dynamic Modulus of Elasticity in the Cement Based Solid Product for Consolidating Disposal of Medium-Low Level Radioactive Waste”, Journal of the Korea Concrete Institute, 25 (3), 2013, pp.321 ~ 329.

[2] J. F. Li, J. L. Wang, “Advances in cement solidification technology for waste radioactive ion exchange resins: A review”, Hazard. Mater, 135 (1-3), 2006, pp. 443–448.

[3] I. Plecas, A. Peric, S. Glodic, A. Kostadinovic., “Comparative leaching studies of 60Co from spent radioactive ion-exchange resin incorporated in cement” Cement Concrete Res., 25 (2), 1995, pp.314–318.

[4] “Leach Testing of Immobilized Radioactive Waste Solids, A Proposal for a Standard Method,” International Atomic Energy Agency, E. D. Hespe, Ed., At. Energy Rev.,9, 1 (1971).

A Study on the Management of Radioactive Waste in Major Countries for Exporting Nuclear Power Plants

Ji-woon Lee*, Jin-kyu Choi, and Eun-young Kim.
KEPCO Engineering & Construction Company, 269, Hyeoksin-ro, Gimcheon-si, Gyeongsangbuk-do, Republic of Korea
*cloud25@kepco-enc.com

1. Introduction

It is the basic policy of all countries who operates nuclear power plants (NPPs) to safely manage and dispose of radwaste, a byproduct of nuclear power generation. In order to safely and economically dispose of radwaste, the countries that operate NPPs establish their own radwaste classifications considering their disposal site characteristics and environmental conditions. The Czech Republic and Saudi Arabia, which have recently been pushing to export NPPs, cannot be an exception. This paper investigates the radioactive waste management systems and policies of major countries, and tries to derive what should be considered from the perspective of radwaste management for the export of NPPs.

2. Investigation of Waste Classifications

2.1 Classification of Radwaste in Korea

The radioactive wastes generated in Korea are classified into five categories: High Level Waste (HLW), Intermediate Level Waste (ILW), Low Level Waste (LLW), Very Low Level Waste (VLLW), and Exempt Waste (EW). The detailed information about definition and numerical limits for each category is presented in Nuclear Safety and Security Commission (NSSC) Notice 2017-65. Figure 1 shows the conceptual illustration of waste classification scheme.

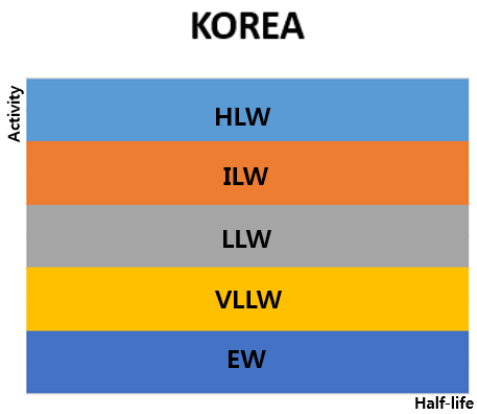

Fig. 1. Classification of Radwaste in Korea.

This classification scheme is developed based on the IAEA safety guide for radioactive waste classification. Figure 2 shows the IAEA classification scheme.

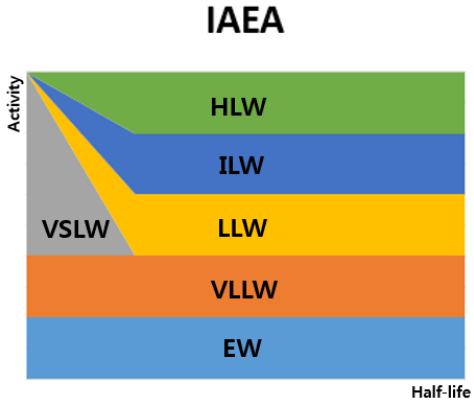

Fig. 2. Classification of Radwaste in IAEA.

2.2 Classification of Radwaste in EU

European Atomic Energy Community (EURATOM) which is organization for nuclear safety and radiation protection in European Union (EU) establishes the standard for radwaste classification. However, the standard has not been considered as legally binding requirement for all countries in EU. Each EU nation has their own classification scheme for radioactive waste.

There are five basic categories in EU: HLW, LILW-Short Lived, LILW-Long Lived, VLLW, and Transition Waste. Transition Waste is mainly medical wastes that is equivalent to the Very Short-Lived Level Waste (VSLW) in IAEA scheme. Figure 3 shows the EU classification scheme.

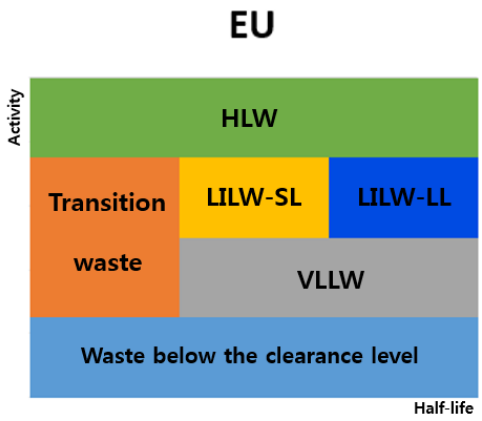

Fig. 3. Classification of Radwaste in EU.

2.2.1 Classification of Radwaste in Czech Republic. Czech Republic has recently changed their classification scheme for radioactive waste. In Decree No. 377/2016 Coll., there are five categories: Temporary Radioactive Waste, which after storage for at most 5 years exceeds radioactivity lower than clearance levels, VLLW, LLW, ILW, and HLW. Czech Republic classifies the radioactive waste by its activity level, but especially, ILW and LLW are determined by amount of long lived radionuclides. Figure 4 shows the Czech Republic classification scheme.

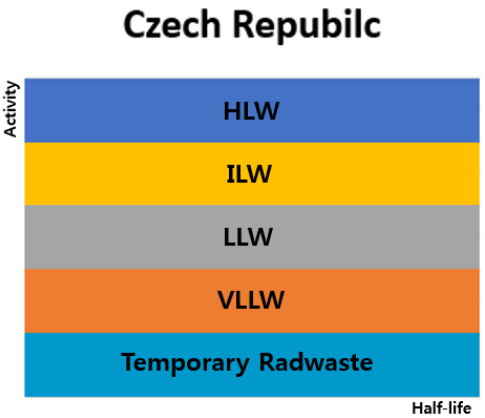

Fig. 4. Classification of Radwaste in Czech Republic.

2.3 Classification of Radwaste in Saudi Arabia

Radwastes in Saudi Arabia are generated from various applications such as medical, industrial, and research institutions. These wastes are mainly considered as LLW. They are planning to construct the Nuclear Power Plants, and also enact laws of Radwaste accordingly.

3. Comparison for Radwaste classification

The classification schemes described above have consistency in a view that :

- The radioactive waste is classified by its activity and concentration of radionuclides.
- In addition to the consideration above, HLW is determined by its heat generation rate.

However, the detail of its implementation is different. IAEA and EU classifies separately the radioactive waste by its half-life such as VSLW, Transition Waste, LILW-SL, and LILW-LL. Korea and Czech Republic, on the other hand, does not. And also, Czech Republic has no specific numerical limit for the heat generated by HLW. Saudi Arabia has not established their own classification scheme yet.

4. Conclusion

As previously discussed, it is confirmed that the countries with experiences in operation NPPs have systematic radwaste classifications, while in the Czech Republics and Saudi Arabia, our export destinations, the radwaste classifications are not clearly established. Therefore, if we prove that radwaste packages processed by NPPs can be safely and economically disposed of under the comprehensive disposal sites and environmental conditions based on our experiences and technologies, it is expected that the technology superiority of our NPPs will be verified and help our export of NPPs. In addition, such efforts are expected to be accompanied by not only exports of NPPs, but also additional effects such as to establish the radwaste classification scheme and to secure the superiority in terms of exporting of final disposal facilities.

REFERENCES

[1] Notice of Nuclear Safety and Security Commission (NSSC) No. 2017-65. (Radwaste 16), NSSC, 2019.
[2] The Safety Case and Safety Assessment for the Disposal of Radioactive Waste, Specific Safety Guide, No. SSG-23, IAEA, 2012.
[3] Classification of Radioactive Waste, General Safety Guide, No. GSG-1. IAEA, 2009.
[4] The Czech Republic National Report, SUJB, 2018.
[5] The Czech Republic National Report, SUJB, 2005.

Reviews of the Technologies to Carry Out the Development Project of NPP Decommissioning Radioactive Waste Certification Program (WCP)

Tae-man Kim*, Jae-chul Ha, Ji-seon Jang, and Chun-hyung Cho
Korea Radioactive Waste Agency, 174, Gajeong-ro, Yuseong-gu, Daejeon, Republic of Korea
*tmkim@korad.or.kr

1. Introduction

At 2017, Korea has formulated an energy conversion (the phase-out of NPPs) policy aims to abolish new NPPs and prohibiting the extension of old NPPs and presented a roadmap to phase out 15 of the 24 NPPs currently in operation [1]. Accordingly, starting in 2017, Kori Unit 1 will be permanently stopped, and it is expected that about 16 nuclear plants will be permanently suspended by 2030, including Kori 2-4, etc. By 2100, about 435,000 drums of decommissioned LILW are expected to be dismantled based on 30 NPPs. This is equivalent to 62.5% of the estimated total level of LILW, and the very low-level waste accounts for more than 67%. For this reason, systematic waste management is required as nuclear decommissioning is in full swing.

The purpose of this study is to analyze the status of the technology development carried out at domestic and abroad to develop the waste certification program (WCP) with quality assurance system and the requirements for the whole-cycle management of decommissioning wastes generated in a short amount of time.

2. Technology Status Analysis

2.1 Acceptance Criteria (WAC)

In Korea, the 2005 Notification No. 2005-12 'Technical Standards for Operation of LILW Disposal Facilities' was established, and the basic details of the acceptance criteria (WAC) related to disposal were derived. In addition, the criteria for accepting the phase 1 disposal facilities have been set forth in the Regulations on the Delivery of LILW (No. 2017-60). The WAC for the phase 2 disposal facility are proposed in the SAR for surface facility operation licenses and are currently under review by the regulatory body (as of April 2019). The WAC for the phase 3 disposal facility has not yet been derived. Therefore, it is necessary to prepare WAC for very low-level wastes and establish the basis for the WAC through research projects according to the construction schedule of the disposal facilities.

The US Nevada Waste Land Acceptance Criteria (DOE / NV 325-16-00, 2016) addresses waste generator approval processes, waste standards, characterization, quality assurance requirements for certification programs, and transportation. The UK LILW Disposal Acceptance criteria address acceptable waste, waste volume, radioactive properties, packaging, and transport requirements [2].

As such, the low-level radioactive waste acceptance criteria verification method deals with waste generator certification programs. And the Low-Level Waste Collection Plan deals with the characteristics of the waste, the requirements for the type of the waste, the classification of the acceptance inspection, the process of approval of the generator and the waste, and the acceptance of the waste [3][4]. However, these reports on the WAC do not deal with the acceptance criteria for the decommissioning solidification wastes of nuclear power plants at the stage of the process.

2.2 Waste Certification Program (WCP)

In 2004, the first, technical standards and applicability review tasks for the development of a radioactive waste certification system were undertaken. After that, waste generators and managers were separated, and in 2011, the KORAD ordered the development of a WCP development guideline and evaluation system. In 2015, KHNP went on to develop 'WCP' (Phase 1), but only from the point of view of waste management that occurred during the operation of NPPs [5].

Verification for acceptance of radioactive waste by ANDRA in France is carried out through document verification, waste package quality inspection, WCP audit, tracking system, destructive and non-destructive inspection. The UK NDA's radioactive waste management is managed at the stages of forecasting, characterization, quality assurance, acquisition request, delivery, and acceptance. The management of radioactive waste in Belgium's ONDRAF/NIRAS is governed by the WAC, the accreditation system of the waste generator, and the acceptance process. The US NEVADA permits disposal operators to review the conditions and characteristics of the waste generator's request for disposal, as well as the qualifications to request disposal. And the HANFORD Site has established a waste certification program and applied it to solidification waste.

3. Result

In the event of decommissioning of the NPPs, the establishment of requirements for acceptance wastes may not be appropriate, or if the established requirements are not applied, a large amount of nonconforming waste may be generated in the acquisition. Therefore, there is a need for research and development on the methodology for establishing and applying for the radioactive waste certification program.

In June 2019, KORAD began research on the development of WCP requirements for nuclear decommissioning radioactive waste as part of the MOTIE / KETEP project. Several private companies, research institution and educational institution will participate in the research. The main research items are 'Evaluation of radwaste source-term', ' Nuclide inventory verification system', 'Method of applying acceptance criteria for verification of Disposal Compliance', 'Acceptance methodology and criteria of disposal application by disposal facility' and 'development requirements for WCP establishment'. In the future, this analysis will be used to promote the development of acceptance criteria and the development of waste certification programs for the efficient and safe disposal of solid waste generated by decommissioning of NPPs.

Acknowledgement

This work was supported by the Korea Institute of Energy Technology Evaluation and Planning (KETEP Project No. 20193210100060) and the Ministry of Trade, Industry & Energy (MOTIE) of the Republic of Korea.

REFERENCES

[1] MOTIE, Nuclear Power Plant Decommissioning Waste Safety Management Technology Development Project Planning Report (2018).

[2] LLW Repository Ltd, Waste Acceptance Criteria for LLW disposal (WSC-WAC-LOW – Version 5.0 Issue 1) (2016).

[3] DOE, Methods for Verifying Compliance with Low-Level Radioactive Waste Acceptance Criteria (1993).

[4] WASTE CONTROL SPECIALISTS LLC, “Waste acceptance plan for low-level radioactive waste land disposal facilities” (2014).

[5] KHNP, Development of Radioactive Waste Certification Program (Phase 1) (2015).

A Study on the Analytical Method for Clearance of Decommissioning Waste

Younggook Kim and Jae Yong Oh*

KHNP Central Research Institute, 70, Yuseong-daero 1312beon-gil, Yuseong-gu, Daejeon, Republic of Korea

kim.090909@khnp.co.kr, *jaeyongoh@khnp.co.kr

1. Introduction

The wastes generated by the decommissioning of nuclear power plants (NPPs) can be classified into radioactive wastes and activated wastes based on the source. In general, activated wastes are caused by neutron irradiation and because of volume contamination, contamination cannot be removed. The main source of radioactive waste is pipeline, equipment and structures contaminated by deposition of radioactive corrosion products or fission products. Generally, clearance waste is composed of about 88% of total waste, about 12% is LLW, about 0.03%is LILW, and about 0.0007% is GTCC waste[1].

The disposal of such a large amount of clearance waste is very important. Also, in Korea, decontamination is essential to minimize the volume of decommissioning waste. If it is treated as clearance waste through decontamination, waste can be disposed of by recycling, landfilling, incineration, etc. in accordance with Korea nuclear regulations. The purpose of this study is to examine the analysis method for clearance waste among decommissioning wastes that can be generated in a large amount in a short time due to the decommissioning of NPPs.

2. Method and Regulation of Clearance

2.1 Analysis on Clearance in Korea

In Korea, it is excluded from the application of the Nuclear Safety Act that the concentration of nuclear species in radioactive wastes is less than the allowable concentration of clearance in accordance with the NSSC Notice 2017-65[2]. Non-radioactive waste can be managed by incineration, landfilling or recycling. For clearance of wastes, at least 1 EA sample per 1 m^2 should be analyzed for surface contamination waste. If the surface condition is difficult to measure for radioactivity using direct or indirect measurement, each 1 kg of sample per 200 kg or 1 m^2 is required. In the case of volume-contaminated waste, radioactive analysis should be conducted by directly sampling the target waste through a method such as coring. When conducting radiological analysis by sampling, approximately 1 kg of representative sample per 200 kg should be collected. In the case of liquid wastes such as waste oil, 1 L of representative sample per 200 L should be collected[3].

2.2 Process for Clearance waste in U.S

The waste generator characterizes the waste and sends the data to the BSFR(Bulk Survey for Release) facility.

The BSFR facility performs the following: ① Document, Manifest Check, ② Dose Measurement, ③ ISOCS(In Situ Object Counting Systems) Analysis, ④ Vehicle Radiation Measurement and Export. If a nuclide other than the generator record is present or concentration is exceeded, the generator is notified and incinerated or returned(Less than about 10%).

There are two measuring equipment. There are Box Assay System for measuring such as Metal Debris and Guardian System for measuring concrete and soil. Transfer waste to a B-25 container to measure metal debris. The four sides outside the rectangular box are measured with a hand held measuring instrument. Then place it on the Box Assay System and measure the bottom of the box using the ISOCS inside Box Assay System. Three ISOCS are installed to measure the radioactivity concentration in each box. The measurement time depends on the volume and mass but usually ends in a few minutes.

The Guardian System, which measures concrete and soil waste, is installed on two trailers, with trucks carrying waste between trailers. The trailer is equipped with three types of instruments. At the front is a plastic scintillator for the scanning survey, and three ISOCS (High Purity Ge Detector) are located inside the trailer.

At the end there is a NaI detector. After the truck passes the trailer, the waste is sent to designated clearance waste disposal site.

3. Conclusion

Even if the disposal costs are low in the United States, it is inefficient to dispose of all wastes generated during nuclear decommissioning as waste. In the United States, there is no Clearance system like Korea. However, Tennessee has a BSFR system similar to clearance waste disposal. In many states, large quantities of concrete and soil waste from decommissioning NPPs are sent to Tennessee for measurement and disposal of clearance waste. There are four companies in the state of Tennessee that perform like BSFR, including Bear Creek. Decommissioning waste that meets the BSFR criteria is disposed of at a designated landfill for clearance. However, there is an implication in that the measuring method proceeds very quickly in the form of direct measurement rather than collecting 1kg of representative samples per 200 kg as in Korea. In Korea, the clearance waste whose radioactivity has been verified to be below the clearance standard should be thoroughly reviewed for the application of the direct measurement method.

REFERENCES

[1] Mark Kirshe, “Waste Management During Decommissioning”, ReNuke Assuming DECOM (2019).

[2] Notice of Nuclear Safety and Security Commission, 2017-65 (2017).

[3] KINS, “Safety Analysis on Clearance of Radioactive Waste”, RG-N12.08 (2015).

A Study on the Reduction Method of Radioactive Liquid Waste Using Outdoor Air Control Unit With Heat Pipe System

Youngwoo Kwon*, Heeseok Kang, Youngkuk Jang, Seonho Noh, and Ilje Cho
Korea Atomic Energy Research Institute, 111, Daedeok-daero 989beon-gil, Yuseong-gu, Daejeon, Republic of Korea
*kyw@kaeri.re.kr

1. Introduction

The Korea Atomic Energy Research Institute operates the Nuclear Cycle Experimental Research Facility which has radiation controlled area in the laboratory with the aim of realizing pyroprocessing technology. During the summer, the facility should maintain proper temperature and humidity to manage analysis and experiment equipment. However, about few tons of condensate are generated every year due to the cooling load.

It considered reducing the amount of liquid radioactive waste by using OAC with Heat Pipe System.

2. OAC with Heat Pipe System

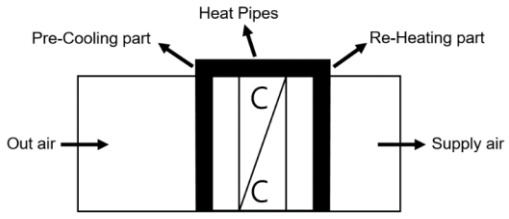

Fig. 1. OAC with Heat Pipes System.

The OAC with heat pipe system is a system that can achieve pre-cooling and pre-heating for free of charge using natural convection. Briefly, the outdoor air is pre-cooled through heat exchanging with heat pipe. Then, the pre-cooling air passes through the cooling coil and becomes very humid and low temperature air. Lastly, the air passes through the heat pipe again before air supply. The air is re-heating and has the proper temperature and humidity.

2.1 Original OAC vs OAC with Heat Pipe

Original OAC is a system that focuses on Cooling loads, while OAC with heat pipe is the system that concentrates on dehumidification. The original OAC is cooled for temperature and humidity control. It is the system that requires a lot of energy consumption. On the other hand, OAC with Heat Pipe reduces load of cooling coil through pre-cooling. It is free for Reheating load to maintain proper relative humidity and temperature. It is the system that saves more energy due to higher energy absorption during the rainy season.

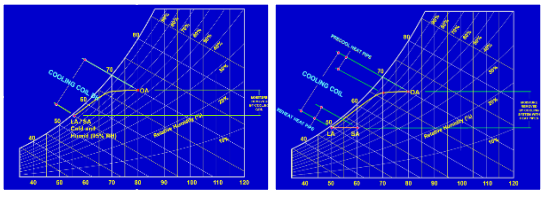

Fig. 2. (a)Original OAC, (b)OAC with heat pipe.

The X-axis represents the dry bulb temperature, the Y-axis is the absolute humidity, and the relative humidity is shown on the charts.

Pre-cooling and re-heating sections are made free of charge by using heat pipes. As a result, total cooling load (cooling coil part) and the

difference in absolute humidity were both increased. The amount of condensation water will also increase. Because of the absolute humidity difference between the OA(Outdoor Air) and the SA(Supply Air).

3. Simulation Results

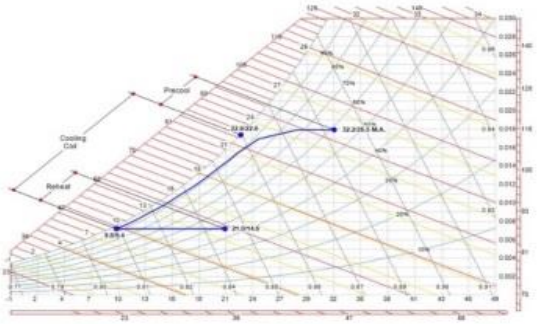

Fig. 3. Psychometric chart.

3.1 Equations

$$L = G(x_2 - x_1) = \gamma Q(x_2 - x_1) \quad (1)$$

$$q_T = G\Delta h = q_S + q_L = GC_p\Delta t + G\Delta h = \gamma QC_p\Delta t + \gamma Q\Delta h \quad (2)$$

Table 1.

Outdoor air conditions	32.2 °C 58.8 %RH
Air volume	10,000 m^3/h
Precool	38,024 W
Cooling coil	130,000 W
Reheat	38,024 W
Condensate	122,5 kg/h
Total Energy Saving	76,048 W

The psychometric chart shows the results of a simulation based on the Nuclear Cycle Experimental Research Facility. The condition of outdoor air was based on the average temperature and humidity during the summer of the Daejeon, and the air volume was assumed to be 10,000 m^3/h. Total energy savings and condensate generation were calculated by using Psychometric Analysis.

As a result, a condensate of 122.5 kg/h will be collected. This shows how much moisture can be removed from the laboratory per hour. Air temperature of supply will be 21 degrees Celsius and the relative humidity will be 46.3 percent. A total of 76,048W of energy can be saved by pre-cooling and re-heat processes.

4. Conclusion

According to the data, if OAC with Heat Pipe dehumidification system is applied to radiation controlled area, the amount of radioactive liquid waste can be dramatically reduced. Highly sensitive equipment in the area can be managed at appropriate humidity and temperature. The pre-cooling process saves about 32 kcal/h of energy, so the compressor capacity can be reduced. Re-heated energy can be used for free (32 kcal/h), so there is no need to install boilers or electric heaters.

This system is expected to be excellent for reducing condensate due to excellent moisture removal in radiation controlled area.

REFERENCES

[1] John Dieckmann, 2003, Dedicated Outdoor Air Systems, ASHRAE Journal, May 2003.

[2] ANL-7959 Hot Fuel Examination Facility /North Facility Safety Report, February 1975, Argonne National Laboratory pp. 42-53.

Analysis of Disposal Container and Waste Acceptance Criteria for Landfill Disposal of Very Low Level Waste

K.H. Park*, K.H .Lee, U.J. Lee, and S.W. Chung

ORIONENC Co., Ltd., Suite 1306, 37, Seongsui-ro 22-gil, Seongdong-gu, Seoul, Republic of Korea

*khpark@orionenc.com

1. Introduction

Domestic 3rd Step Landfill Disposal Facility is under construction for accepting total 104,000 very low level radioactive waste(VLLW) which come from decommissioning site mainly during May 2019 till February 2026(total budet:224.6 billion won) in 1st step plan. After then total 260,000 drums including 104,000 drums will be stored in 5 trench type facilities (34,076m^2 area). Now KORAD is preparing for waste acceptance criteria for this VLLW and disposal containers. Comparing to cavern type disposal, 3rd step landfill disposal site shall accept bigger size and weight containers for efficient management of radioactive waste. This paper presents the analysis of anticipated disposal containers for VLLW disposal together with anticipated Waste Acceptance Criteria (WAC) to give how the VLLW is managed in 3rd step landfill disposal site in near future.

2. Disposal Container and Waste Acceptance Criteria

2.1 Description of packing container

Generally, the packing containers used in operating NPPs in Korea are given in Table 1 and some of them are shown in Figure 1. Several types of containers are used in operating NPPs for DAW, spent Resin, spent filter, concentrated wastes, consumable parts which were produced during Calandria replacement work at Wolsung 1, etc. But these containers are partly used for decommissioning waste, because these are not efficient to handle and manage VLLWs come from decommissioning site in size and weight point of view.

Fig. 1. Type of containers used in NPPs.

Table 1. Type of packing containers

Division	TYpe of Packing Container			Dimension(Outer) Diameter or L/W(m)		H(m)
1	Steel Container		200LDrum	0.615		0.884
2			320LDrum	0.713		0.955
3			1,296L Steel Box	0.800	2.600	0.610
4			1,760L Steel Box	1.100	1.600	1.000
5			2,508L Steel Box	1.200	1.900	1.100
6			2,950L Steel Box	1.400	3.110	0.950
7	Concrete Container	Circular	Hanul C1type concrete container	1.400		1.300
8			Hanul C2type concrete container	1.400		1.300
9			HanulC4type concrete container	1.100		1.300
10			Kori circular concrete container	1.060		1.370
11		Rectangular	Kori 4-pack concrete container	1.460	1.460	1.180
12	Special container		FE-HIC container	1.181		1.289
13			PE container	1.194		1.296
14			PC-HIC container	unknown		unknown

2.2 Plan of Disposal container for decommissioning waste

During decommissioning, bulky soil and concrete wastes are mainly generated as VLLW waste, so the containers will be prepared as the efficient and economical way for these wastes. Table 2 shows the plan of VLLW waste container for 2nd and 3rd step landfill disposal. In this table, the purpose means the purpose of containers for packing, transportation and disposal. For example, packing/disposal means that the can be used for packing at site as well as for transportation to disposal site. As shown in Table 2 the max. weight and size of containers are bigger than previous containers.

Table 2. Plan of containers for decommissioning waste

step	type	purpose	Dimension (WxLxH,m)	Max. weight (ton)	Level	container type	Remark
2nd step	metal	packing/transport/disposal	1.5x1.5x0.95	19	VLLW / LLW	IP2	six stages storage
			1.6x3.2x1.2	35			
			2.3x4.7x1.2	35			
			2.3x4.7x2.4	35			
3rd step	soft bag	packing/disposal	2.2x1.1x1.1	4-6	VLLW	IP2	
	ISO container	disposal	6.1x2.5x1.3	about 20	VLLW	-	

Table 2 shows that the soft bag and ISO container will be expected to be used for decommissioning waste towards soil and concrete (pieces of concrete and scabbling concrete) waste.

2.3 Waste Acceptance Criteia for VLLW in 3rd Step Landfill Disposal Site

At present, total 23 items (radioactivity concentration, nuclei investigation, surface radiation dose, weight, etc.) were used for judgment criteria for accepting disposal waste at cavern type disposal site. But for 3rd step landfill disposal site, the WAC will be prepared by KORAD soon. At this moment it is expected that most judgment criteria are adopted, but more simple and efficient criteria for bulky decommissioning waste, etc. will be modified. Figure 2 and Figure 3 shows Movilliers site in France and El Gabril site in Spain for VLLW how the disposal of VLLW is managed in simple and efficient way.

Fig. 2. Movilliers site for VLLW.

Fig. 3. El Gabril Site for VLLW.

Based on the study towards foreign countries' experiences and applications, Table 3 shows the expectation of WAC modifications for VLLW disposal.

Table 3. Modifications of WAC for VLLW

Present WAC	Modifications
Unit weight of container (below 10 tons for concrete) (below 1ton for steel)	In consideration of new containers more weight is will be adopted. (over 20tons)
Unit dimension of container Min.:0.5m(D)×0.5(W) ×0.8(H) Max.: 1.5m (D) ×1.5m(W) ×1.5m(H)	In consideration of new containers bigger size will be adopted. (6.1×2.5×1.3m)
Immobilization needed for non-homogeneous nuclei having more than half-life 20 years (total radioactivity more than 74,000Bq/g).	Immobilization needed for non-homogeneous nuclei without options.
Internal volume of container occupancy : over 85% (HIC is not applied)	over 97%
Container type Concrete/steel possible	Concrete/steel/soft bag
Solidification needed for homogeneous waste	Soil and Scabbling Concrete are exempted
Disposal concentration Limit by nuclei -11 items	Modification adopting foreign cases (level down)

3. Conclusion

3rd step landfill disposal site will store VLLW in near future for targeting decommissioning waste. According to the terms and conditions in 3rd step landfill disposal site the container for disposal and WAC will be prepared. Because 3rd step landfill disposal site is for VLLW, so the WAC and containers for disposal need more flexibility than present site terms and conditions, especially in weight, size and inner volume occupancy, radioactivity concentration limit by nuclei, immobilization condition, etc.

ACKNOWLEDGEMENT

This paper was supported by KETEP Energy Technology Development R&D titled "Development of Waste Acceptance Criteria Application and WCP Requirements for Disposal of NPP Decommissioning Radioactive Waste Solidification Treatment".

REFERENCES

[1] DOE, "Licensing Requirements of Land Disposal of Radioactive Waste" (10CFR61, 2017).
[2] OECD/NEA, "Radioactive Management Programmes in OECD/NEA Member Countries" (2000).
[3] IAEA, "Strategy and Methodology for Radioactive Waste Characterization" (TECDOC-1537, 2007).

The Implementation Scenario for Waste Certification Program (WCP)

Sungjong Kim [a,*], Jin-hang Lee[b], Jung-bo Yang[b], and Seung-hoon Han[b]
[a]MIRAE-EN Co., Ltd., D403, 17, Techno 4-ro, Yuseong-gu, Daejeon, Republic of Korea
[b]KEPCO Nuclear Fuel, 242, Daedeok-daero 989beon-gil, Yuseong-gu, Daejeon, Republic of Korea
[*]sungjong.kim@mirae-en.co.kr

1. Introduction

The objective of WCP is to ensure the integrity of waste, relieve the burden of disposal facility and temporary storage owner as well as waste generator from the legal responsibility, and simplify the waste acceptance in transparent way. Thus, this paper provides the practical and implementable WCP in conceptual and strategical level with the support of Waste Tracking System (WTS) and Waste Acceptance Criteria (WAC).

2. IAEA hierarchy for waste certification

IAEA documents mention high level requirement of WCP [1]. Based on this, a suitable WCP procedure should be elaborated for safety and integrity of radioactive waste management and disposal.

Unlike acceptance criteria of the quantitative compliance limits, it is not easy to establish specific program to evaluate the characteristics for unknown pre-treatment and conditioning technology, the qualitative acceptance limits like visual inspection, which means that there should be continuous development and update for WAC for new technology and its validation in WCB (WAC Consultation Board), an authorized and dedicated organization with support of expert consulting group as in Fig. 1. Also, there should be strategy for decision making guideline, which is now being developed in ISO TC85 SC5 WG5, to cope with ambiguous and unprecedented circumstances, and the approval of historical waste.

As in Fig. 1, the core of WCP is WAC, and WCP shall cover the technology management via quality management strategy, WTS, and its detail plan and procedure as one of the QA programs. This is fundamental to deliver the waste to disposal and storage including Dry Active Waste (DAW) and any other conditioned wastes such as solidification and vitrification etc.

If necessary, the owner of disposal facility and storage could/should activate the 3rd party independent certification (assessment) of waste package, which includes the site inspection.

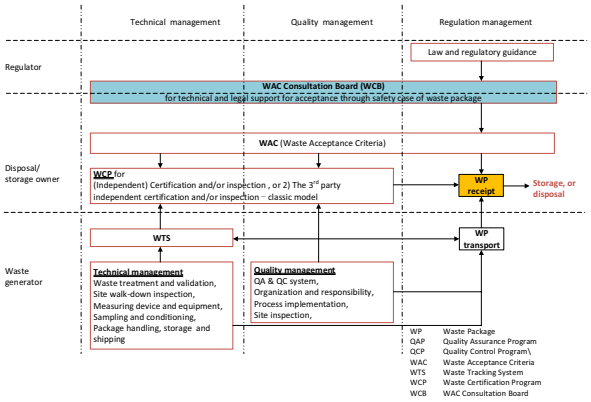

Fig. 1. WCP implementation scenario.

3. The requirements for waste certification

3.1 Technical management

3.1.1 Process management. WCP sometimes needs generator site inspection to see if they implement the waste management process as described in ISO/PWI 24389 series of standard including data and acceptance criteria review on desk. This should be done for each waste stream normally [2].

3.1.2 Pre-treatment and conditioning technology. It is necessary to establish a conformity and acceptance criteria for still unknown pre-treatment and conditioning technology and its validation (ex: solidification and/or vitrification and its acceptance criteria for qualitative and quantitative), which should be developed and updated with a relative plan/procedure and its commitment by authorized organization continuously. See § 4.1.

3.1.3 Resource management. All the resources of process, product and people should be managed transparently for traceability of waste management. The implementation of waste management process, organization and staff qualification and training, waste package handling is a typical resource management.

3.1.4 Sampling. The sampling method that is not specified in the guidance shall be justified with appropriate rationale. However it is

recommended that each independent test be conducted on one separate stream for each testing.

3.2 Quality management

3.2.1 Organization and responsibility. The implementation of radioactive waste qualification requires people have the appropriate range of skills and knowledge to provide capability across all relevant disciplines involved in the waste management life cycle and waste management strategy.

3.2.2 Quality assurance program (QAP). QAP based on international, national or other guidance acceptable to the competent authority shall be established and implemented through the radioactive waste management processes and inspection of all radioactive waste management life cycle to ensure compliance with the relevant provisions of regulations.

3.2.3 Training. Personnel involved in waste management and certification shall receive appropriate training regarding radiation protection and safety.

3.2.4 Document control. The organization shall establish and maintain procedures to control all documents that form part of its management system (internally generated or from external sources), such as regulations, standards, other normative documents, the methods utilized in each waste management life cycle process, as well as drawings, software, specifications, instructions and manuals. WTS and decommissioning information system may cover this.

3.3 Regulation management

For waste acceptance, the regulation management and control are undisputedly important to implement WCP in practical and reasonable way considering that waste management is one of destruction engineering processes. Also, it is necessary to remind that typically the geological disposal facility had been designed and constructed based on defense-in-depth (DID) concept for safety. Through explicit acceptance criteria, there should no responsibility burden of organization and/or staff in certifying waste through well-defined procedure.

The role and responsibility of each stakeholder involved in waste management shall be clearly defined and delegated, and the safety cases for WAC should be continuously developed and updated on a case by case basis.

4. The supporting element for waste certification

4.1 WAC for qualitative acceptance criteria

Qualitative and quantitative acceptance criteria for various waste stream need to be established for public acceptance and exempt waste for self-disposal. In case of ambiguous circumstances difficult to make decision of waste integrity, it's recommended to consider the application of ISO/PWI 23580[1] to support decision making process in waste characterization and management of radioactive waste.

4.2 Approval of historical waste

There may arise occasions when waste packages are prepared for disposal, at least in part, prior to the establishment of fully approved waste package QAP. Historical waste that does not meet the requirements of the waste acceptance criteria may need to be considered further, and acceptability can only be judged on a case by case [1] using probably safety case of waste package. For approval of historical waste, WCB as in Fig. 1 may be necessarily organized and utilized to manage the many cases of waste packages.

5. Conclusion

It is very important to develop the safety cases of WAC, and delegate the waste certification activity to authorized organization like WCB to manage the various cases of waste package.

REFERENCES

[1] IAEA TECDOC-1129, Inspection and verification of waste packages for near surface disposal, 2000, Jan.
[2] The plan and procedure for low and intermediate level of radioactive waste certification program, 2016. 11. MIRAE-EN Co., Ltd., internal document.

[1] Under development with risk-based approach to develop Data Quality Objectives by UK Sellafield Ltd. to support decision-making process for characterization and waste management etc.

The Economic Evaluation of Liquid Radioactive Waste Management System for SMART

Jin-Kyu Choi*, Han-Jeong Na, and Jae-Hwa Yoon
KEPCO E&C, 269, Hyeoksin-ro, Gimcheon-si, Gyeongsangbuk-do, Republic of Korea
*cjk@kepco-enc.com

1. Introduction

The System-integrated Modular Advanced ReacTor (SMART) is the integral type of a pressurized water reactor. The SMART pursues safe, simple and cost-effective nuclear power reactor.

After Standard Design Approval (SDA) for SMART, the optimization works for Chemical & Volume Control System (CVCS) and radioactive waste management system have been conducted to enhance simplicity and cost-effectiveness of SMART.

This paper presents the result of economic evaluation between applicable liquid radioactive waste management technologies.

2. Overview of applicable technologies

There are many kinds of liquid radioactive waste management technologies used for conventional nuclear power plant. Among the various technologies, the Reverse Osmosis (R/O) and ion exchange (IX) technology has been widely adopted to recent nuclear power plants.

R/O and IX technology can also be applicable to SMART, so these technologies are selected for this evaluation.

The schematic diagrams that show overall configuration of two possible technologies are as follows:

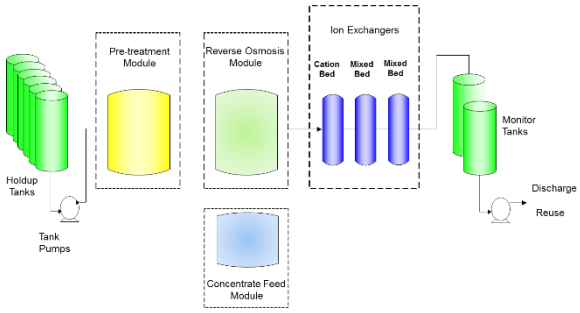

Fig. 1. Schematic diagram in case of using R/O.

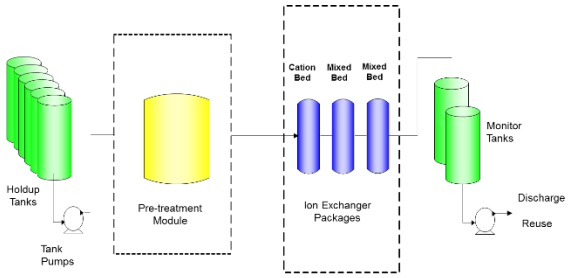

Fig. 2. Schematic diagram in case of using IX.

In general, liquid radioactive waste management system consists of holdup tanks/pumps, treatment system, and monitor tanks/pumps. The dotted-line boxed portion of diagram above presents the configuration of treatment system.

IX package consists of pre-treatment module and ion exchangers. Pre-treatment module removes insoluble contents in liquid influents by filtering prior to IX process.

R/O package generally consists of pre-treatment module, R/O module, concentrate feed module, and post-treatment module using ion exchangers.

Spent filter cartridge and microfilter membrane are generated from pre-treatment module as solid radioactive waste. Spent R/O membrane and concentrate are generated from R/O module. Spent resin is generated from ion

exchangers. The amount of these secondary solid radioactive wastes resulting from each treatment system is one of major factors for this economic evaluation. The secondary waste types from each treatment system are summarized below.

Table 1. List of secondary radioactive wastes

Treatment System	Waste Type
Reverse Osmosis	- Filter cartridge - Microfilter membrane - R/O membrane - R/O concentrate - Spent resin
Ion Exchange	- Filter cartridge - Microfilter membrane - Spent resin

Since the R/O concentrate is additionally generated from R/O treatment system in comparison with IX package, the special treatment and solidification system for R/O concentrate is required in case of adopting R/O package in liquid radioactive waste system. Of course, it has been verified that both technologies can meet the regulatory limits for liquid effluents by separate analysis.

3. Economic Evaluation

Economic evaluation has been performed to estimate the total costs for each technology during 40 years plant operation and based on cost factors such as purchase, construction, installation, utility, labor, media/solidification agent consumption, waste drum generation, disposal, and etc.

The cost factors which have not been determined yet such as purchase cost, agent/media consumption are assumed applying reasonable approach by referencing similar treatment system of operating nuclear power plant in Korea. In addition, for R/O package, the cost estimation for the subsequent R/O concentrate treatment system and associated solidification system are additionally included.

The costs for utility, labor, and disposal are estimated according to the latest notice from KEPCO (for electricity), KENCA (Korea Engineering & Consulting Association, for labor), MOTIE (Ministry of Trade, Industry and Energy, for disposal).

The evaluation does not take into account about the opportunity cost corresponding to public radiation dose reduction resulting from liquid and gaseous effluents. The cost evaluation including public dose factor will be conducted after the investigation of site characteristics for SMART is finalized.

4. Conclusion

The Figure 3 shows the cost comparison between the application of R/O and IX package in liquid radioactive waste system. As a result, the IX package is evaluated to be much cost-effective waste treatment technology and adopted for SMART.

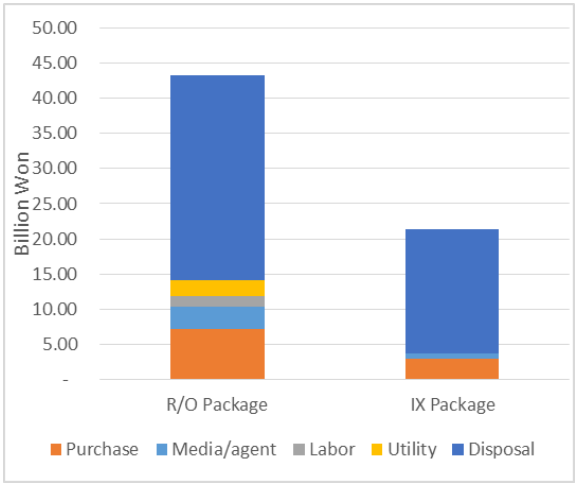

Fig. 3. The Result of Economic Evaluation.

REFERENCES

[1] Design Documents for SMART PPE Liquid Radioactive Waste Management System, KEPCO E&C.

A Study on Evaluation and Prediction of the Radionuclide Inventory for Efficient Operation of the Combined Disposal Facility

Sun Il Kim, Ki Tae Yang, and Jong Soon Song*
Chosun University, 309, Pilmun-daero, Dong-gu, Gwangju, Republic of Korea
*jssong@chosun.ac.kr

1. Introduction

As various radioactive wastes are expected to be generated due to the permanent shutdown and decommissioning of 30 nuclear power plants by 2094 according to the 8th Basic Plan for Long-term Power Supply and Demand and the intermediate and low-level radioactive waste management implementation plan for 2018, a safe and efficient method of operating combined disposal facilities is necessary.

As the disposal facilities in Stage 1 (rock cavern disposal), stage 2 (near surface disposal), stage 3 (landfill disposal) and stage 4 (near surface disposal) have different radioactivity limits, it is necessary to efficiently operate the combined disposal facility by calculating and predicting the intermediate and low-level radionuclide inventory.

2. Necessity of radionuclide inventory prediction

2.1 Review of laws

To establish and implement the combined disposal facility management plan, it is essential to predict all the radionuclide inventory to be disposed in the site.

The domestic Nuclear Safety and Security Commission notification specifies that 'radionuclides that constitute more than 95% of the radioactivity included in the waste must be investigated, and the concentration of the following radionuclides must be investigated.'

2.2 An example of the delivery test

Table 1. Intermediate and low-level radioactive waste disposal test report

	2016	2017	2018
1st	·Direct analysis and scale factor(Wolsong)	·Scale factor (Hanul)	· Destructive analysis and evaluation method (KAERI)
2nd	· Direct analysis and scale factor (Hanbit)	·Scale factor (Hanul/Wolsong)	· Indirect evaluation using the scale factor (Hanbit)
3rd	· Direct analysis and scale factor (Wolsong)	·Scale factor (unit)	· Indirect evaluation using the scale factor (Hanul/Wolsong/unit) ·Direct measurement method by collecting samples (RI)
4th	·Direct analysis evaluation method (KAERI, RI)	·Non-destructive analysis and scale factor (Wolsong/Hanul/unit) ·Non-destructive analysis method (KAERI)	·Indirect evaluation using the scale factor (Kori/Wolsong/Hanul)
5th	-	·Scale factor (KAERI)	-

3. Radionuclide inventory evaluation method

Table 2. Radionuclide inventory evaluation method

Evaluation method	Type	Remarks
Direct evaluation methods	Destructive method	Analyzing radionuclides using the radiochemical analysis method by collecting samples after opening package
	Non-destructive method	Measurement is taken outside of the package.
Indirect evaluation method	Scale factor method	It is used most often, and only key radionuclides are measured to predict DTM.
Non-destructive analysis methods	Neutron Techniques	The neutrons from radioactive materials are measured.
	Gamma Techniques	A representative measurement method is HRGS.
	Assay System	A representative measurement method is SGS

4. Analysis of the Basic Plan for Long-term Power Supply and Demand

Table 3. The 6th, 7th and 8th Basic Plan for Long-term Power Supply and Demand

	NPP	Remarks
The 6th Basic Plan for Long-term Power Supply and Demand(2013~2027)	·For 34 nuclear power ·Operational waste (100 drums/year) · decommissioning waste (14,500 drums/unit)	·Assuming 2,000 drums/unit due to replacement of equipment during continued operation · Predicting about 800,000 drums
The 7th Basic Plan for Long-term Power Supply and Demand (2015~2029)	·For 36 nuclear power plants ·Operational waste (100 drums/year) ·decommissioning waste (14,500 drums/unit)	· The continued operation of the 34 nuclear power plants continued operation excluding Kori Unit No. 1 and Wolsong Unit No. 1 is not reflected. ·Predicting about 800,000 drums
The 8th Basic Plan for Long-term Power Supply and Demand (2018~2031)	·For 30 nuclear power plants ·Operational waste (100 drums/year) · decommissioning waste (14,500 drums/unit)	·The construction of 6 new units according to the 7th Basic Plan for Long-term Power Supply and Demand was cancelled and the life extension of 10 old NPPs was stopped. ·Predicting about 708,000 drums

5. Radionuclide inventory prediction method

To predict the radionuclide inventory, the drum data and average specific activity value of each institution are necessary. And this data can predict the radionuclide inventory until all nuclear facilities are decommissioned in 2094 through the following formulas.

1. KAERI: [Existing cumulative specific activity value (Bq/g) + (radionuclide inventory (bq/g) × drums (200L) × 364 drums (200L)/year)] × remaining period (year)
2. KNFC: [Existing cumulative specific activity value (Bq/g) + (radionuclide inventory (Bq/g) × drums (200L) × 320 drums (200L)/year)] × remaining period (year)
3. RI waste: [Existing cumulative specific activity value (Bq/g) + (radionuclide inventory (Bq/g) × drums (200L) × 33 drums (200L)/year)] × remaining period (year)
4. Nuclear power plants in operation: [Existing cumulative specific activity value (Bq/g) + (radionuclide inventory (Bq/g) × drums (200L) × 100 drums (200L)/year)] × remaining period

During operation of 30 NPPs planned according to the 8th Basic Plan for Long-term Power Supply and Demand, 100 drums (unit) were generated per year, and 14,500 drums (unit) were generated during the decommissioning of NPPs, and about 364 drums were generated per year at KAERI, and about 350 drums were generated per year at KNFC, and about 30 drums of RI waste were generated per year.

6. Conclusion

If the amount of radioactive wastes and the radionuclide inventory are calculated using such values as KAERI, KNFC, RI waste, and the average specific activity of the radionuclide inventory of NPPs in operation by radionuclide, it is believed that the combined disposal facilities will be operated efficiently.

Acknowledgements

This work was supported by Korea Institute of Energy Technology Evaluation and Planning (KETEP Project no.20193210100110) and Ministry of Trade, Industry and Energy, Republic of Korea.

REFERENCES

[1] Korea Radioactive Waste Agency, Management plan for Low- and Intermediate –Level Radioactive Waste (2015).

A Study on Fractional Release Rates of Nuclides for Normal and Earthquake Scenarios From a Concrete Vault of Near-Surface Disposal Facility

Hyosub Kim*, Moonoh Kim, Beomho Park, Kihyun Kim, Jaewoo Park, Jae-Hun Ko, Dong-gyu Lee, Suk-Nam Lim, Nakhoon Sung, and Young-Sun Jang
Korea Nuclear Engineering & Service, 65, Myeongdal-ro, Seocho-gu, Seoul, Republic of Korea
* hyosubk@kones21.com

1. Introduction

Approximately 800,000 drums for low- and intermediate-level radioactive waste (LILW) are scheduled to be accommodated at Gyeongju repository in Korea [1]. Therefore safety of the radioactive waste disposal facility is important for the protecting people and environment.

To demonstrate the performance of a near-surface disposal facility, radionuclide release into a biosphere under various scenarios should be evaluated. However, studies on the effects of earthquakes for the repository have been relatively lacking in previous performance assessments. That is why the importance of earthquake damage assessment for the disposal facility has been growing continuously since Korea is no longer regarded as a safe place from earthquake.

In this paper, a study for fractional release rates of the nuclides under normal and earthquake scenario from the concrete vault of near-surface disposal facility is conducted.

2. Conceptual Model

Generally, the multi-barrier approach is adopted for the radioactive waste management: an engineered barrier and a natural barrier, etc. In this study, a single concrete vault for radioactive waste packages is assumed to demonstrate the effects of radionuclides release through a surface crack at the concrete vault under earthquake damage.

A schematic diagram of groundwater pathway for a single concrete vault in the near-surface disposal facility is depicted in Fig. 1. During the radionuclide migration through the concrete vault in the direction of groundwater flow in Fig. 1, all the essential nuclide transport characteristics such as radioactive decay, partition (or sorption) coefficient, solubility and porosity of each medium are considered from a conservative point of view.

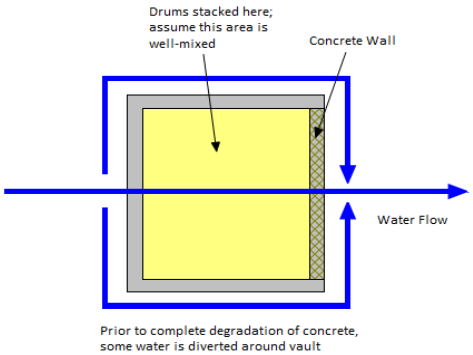

Fig. 1. Schematic diagram of groundwater pathway for a concrete vault in the near-surface repository.

Mostly, contaminants dissolved in groundwater are transported by two mechanisms: diffusion and advection [2]. In this study, specifically, diffusion is mainly considered for the nuclide migration from the vault to surrounding circumstance and advection is additionally considered for the surface crack in the wall of concrete vault. Therefore, advection is supposed to be dominant only at the crack in the vault wall under earthquake damage. The direction of groundwater flow is assumed to be horizontal.

3. Earthquake Scenario Release Model

The radionuclide release model of concrete vault in earthquake scenario is newly developed using GoldSim's commercial contaminant transport module [3]. In this model, the wall of disposal vault will crack just after the end of institutional control period due to the severe earthquake. The degree of crack at the concrete wall under earthquake damage is assumed to be equal to the thickness of the wall.

An iteration number and time of this numerical model for each scenario are 100 and 1,000 years, respectively. And the inventory is selected based on the nuclide list of LLW concentration limit from NSSC notice No. 2017-65 [4]. A mass of each radionuclide is assumed to be 1 g for the analysis of the fractional release rate of each nuclide.

4. Model Simulation Results

Using the radionuclide release model for the single concrete vault above, the fractional release rates for normal and earthquake scenario are illustrated as follows.

Normal scenario in Fig. 2 shows that the major released nuclides at intact surface of the concrete vault are ^{129}I, ^{3}H and ^{137}Cs. However, as for earthquake scenario in Fig. 3, the major released nuclides through crack in the concrete vault are ^{129}I, ^{14}C and ^{59}Ni.

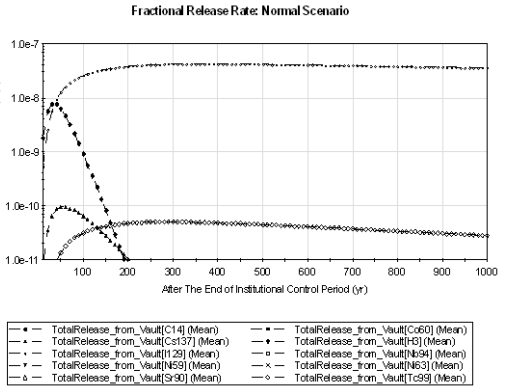

Fig. 2. Fractional release rate of major nuclides in normal scenario.

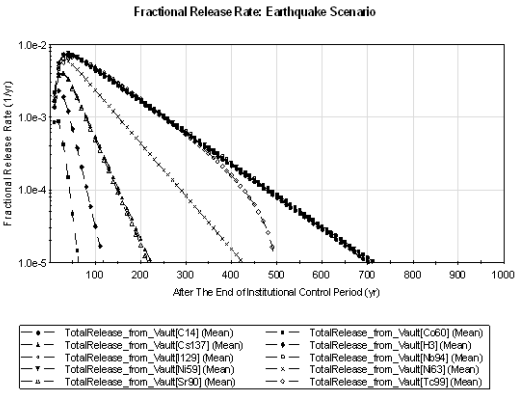

Fig. 3. Fractional release rate of major nuclides in earthquake scenario.

Although the simulation results would be a little bit different depending on the input data, it could be confirmed that when the mass of each nuclide is identical, it is possible to compare the distinction of release rate for each nuclide based on the specific characteristics of the radionuclides even in various scenarios.

From the results above, it could be speculated that the maximum released nuclide for both scenarios, ^{129}I (half-life: 1.57E+7 yrs), and ^{14}C (half-life: 5,730 yrs) should be regarded significantly since their fractional release rates are faster than any other nuclides due to the long half-life if the sorption does not work properly at surrounding media. It could be an important factor for the safety of near-surface disposal facility.

5. Conclusion

The radionuclide release model of concrete vault under earthquake damage is newly developed focusing on the fractional release rates for normal and earthquake scenario. It could be identified that which radionuclides is well released and which would be a significant impact on biosphere depending on each scenario. It is also estimated that if the concrete vault cracks on the wall, the fractional release rates especially for ^{129}I and ^{14}C are faster than usual due to earthquake. Therefore the inventory of these hazardous nuclides at near-surface repository should be limited and managed carefully.

The results of this study would be utilized as a technical basis to support the establishment of a guide for the radionuclide release assessment of near-surface disposal facility in earthquake scenario.

Acknowledgement

This work was supported by the Korea Institute of Energy Technology Evaluation and Planning (KETEP) granted funds by Ministry of Trade, Industry and Energy (MOTIE), Republic of Korea. (No. 20181510300870 & No. 20193210100040)

REFERENCES

[1] Kang Il Jung et al., “Comprehensive Development Plans for the Low- and Intermediate-Level Radioactive Waste Disposal Facility in Korea and Preliminary Safety Assessment”, JNFCWT, Vol. 14(4), p.385-410, 2016.

[2] C. Bucur et al., “Radionuclide Diffusion in Geological Media”, Rom. Journ. Phys., Vol. 51, p. 469-478, 2006.

[3] GoldSim Technology Group, “GoldSim Contaminant Transport Module Version 7.1”, User’s Guide, Version 12.1, GoldSim Technology Group, Seattle, USA, 2018.

[4] NSSC, “Regulation on Classification of Radioactive Waste and Clearance Standards”, NSSC Notice No. 2017-65 (Dec. 26, 2017), Republic of Korea, 2017.

Development of Equipment for Removing Free Water in Radioactive Waste Using Low-temperature Dry Air

Hyung kwon Jeong*, Dong kyu Jang, Cheol yeong Jeong, and Jeong won Park
Actrmt Co., Ltd., 219, Gasan digital 1-ro, Geumcheon-gu, Seoul, Republic of Korea
*Jhk0502@actrmt.co.kr

1. Introduction

Atomic Energy Commission Notice NO. 2017-60, "Delivering low-level radioactive waste regulations" requires limiting the free water in radioactive waste as much as possible. Recently humidity is recognized as an important element as well as temperature conditions when drying wastes generated in nuclear power plants. Although free water in radioactive waste is regulated less than 0.5% of the waste volume, the free water in the package is currently checked by visual inspection to determine the integrity of the drum. As a conventional method for drying facilities have been designed by measuring moisture in drums and have dried wastes at high temperatures. However, drying method using this sort of things is possible with fire hazard.

In order to solve the problems of the conventional drying method, we developed drying facilities using low-temperature dry air.

2. Development of removing free water in the radioactive waste package

2.1 General Information of equipment

- Air circulation pump for circulating air in the radioactive waste package through a flow path connected to one side of the package
- The instrument of measuring temperature and humidity for measuring the temperature, relative humidity and dew point of the air flowing from air circulation pump
- Plate heat exchanger with heat transfer as Freon gas with different temperature flows between thin plates in opposite direction
- Air separator installed on low temperature side of Plate heat exchanger and thermostat installed on high temperature side.

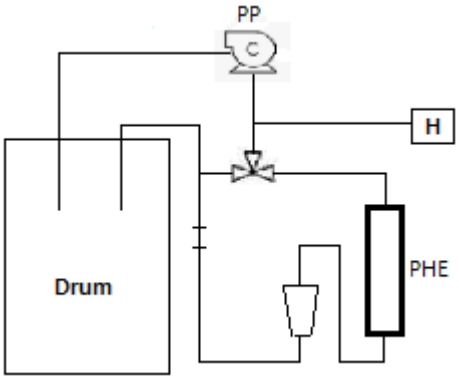

Fig. 1. Basic configuration of drying device.

2.2 Plate Heat Exchanger

The plate heat exchanger is fixed by numbers of thin and corrugated heat transfer plate, hanged between the carrying bar on the above and the guide bar on the below. These heat transfer plate provide flow channels for two kinds of fluid, and the chevrons on the heat transfer plate make the turbulent flow and play a role to support the plate against the pressure difference between the two fluids. There are 4

holes on the PHE using Freon gas R as a fluid in Fig. 2. Hot leg is connected to entrance of drum. On the other hand Cold leg is connected to exit of drum.

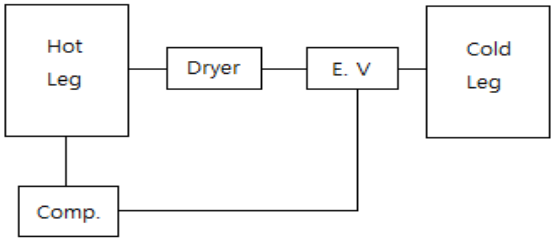

Fig. 2. Schematic diagram of tube side in Plate Heat Exchanger.

3. Characteristic of Low-temperature Dry Air

Lowering air temperature decrease the air's ability to hold moisture. Thus, the air can be made drier by cooling it. To remove large amounts of water by cooling the air, over-cooling and subsequent reheating are required. As shown in Fig 3, the relative humidity chart shows that the relative humidity vary with temperature. Relatively hot air is injected into the drum to dry the drum because the higher temperature of the air is able to take more moisture.

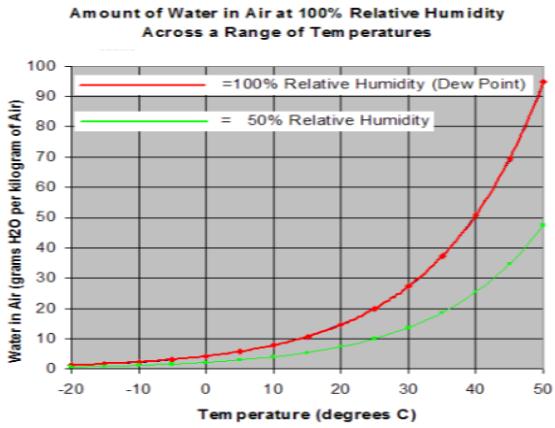

Fig. 3. Relative Humidity Diagram.

4. Conclusions

The use of nuclear energy for electricity generation can be considered extremely safe. It is important to set up a reasonable method for drying waste, because being able to determine the integrity of the drums.

Newly developed radioactive waste drum drying apparatus makes it possible to perform drum drying safely without risk of fire hazard.

In addition, this system is not necessary housing to maintain high temperature, drying operation would be very convenient and easy in tight working environment.

REFERENCES

[1] Yim SungPaal, Lee HoJin, "A method and equipment for measuring and removing free water in the radioactive waste package", KAERI.

[2] Jin Ho Ha, Hyun Chae Song, Myeong Ho Kim, "Development of Radioactive Waste Drum Cutting System Using STD-11 Cutter", Journal of Korean Radioactive Waste Society (2018).

[3] B.L.Miller, M.S.Lee, J.W.Hughes and Y.Pom. 1981. Measuring high moisture content of cereal grains by pulsed nuclear magnetic resonance. Cereal Chem. 57(2):126-129.

Safety Comparison of Marine and Land Transport for Low and Intermediate Level Radioactive Waste

JeongMi-Lee*, ByeongMok-Park, AhRan-Cha, CheolWan-Park, and SangJin-Lee
SAE-AN ENERTECH CORP, #923, 184, Gasan digital 2-ro, Geumcheon-gu, Seoul, Republic of Korea
*davi1009@sae-tec.com

1. Introduction

Korea Radioactive Waste Agency (hereinafter referred to as the "KORAD") began its full-scale operation in July 2015 with the first disposal of low and intermediate level radioactive waste underground silos.[1] As a result, transport of low and intermediate level radioactive waste to KORAD is being carried out. The release of radioactive materials due to collisions, abalone, fires and sinking during the transport of low and intermediate level radioactive waste can have a serious impact not only on workers directly involved in transport, but also the general public and the surrounding environment. Therefore, safe transportation of radioactive waste should be prepared in accordance with the Nuclear Safety Act and the Enforcement Decree and Enforcement Regulations for the Nuclear Safety Act.

In this paper, the present situation of marine transportation and land transportation of low and intermediate level radioactive waste of nuclear power plant will be examined and its safety will be compared and analyzed.

2. Main Subject

In the Nuclear Safety Act, the transport of radioactive waste is applied in the same way as the transport of radioactive materials.[2]

Hanul, Kori and Hanbit nuclear power plant radioactive wastes are transported on sea (transportation from the temporary storage of each nuclear power plant to the lighters wharf of each nuclear power plant, and from Wolsong nuclear power plant to the storage building of the acquisition are transported on land), Wolsong nuclear power plant and Daejeon RI Wastes are transported on land. The marine transport of low and intermediate level radioactive waste to the KORAD was 4,100 drums in 2017, 3,000 drums in 2018, and land transport was 1,700 drums in 2017 and 750 drums in 2018.[3]

2.1 Comparison of Transportation Means and Safety Devices in Marine and Land Transport

2.1.1 Marine transport ship and safety devices. Currently, there is CheongJeongNuriHo in Korea, and it was designed and built in accordance with international standards such as the International Maritime Organization and domestic standards such as domestic Ship Safety Act and Nuclear Safety Act. CheongJeongNuriHo belongs to INF Grade 3 in Article 5 of the「Safety Standards for Radioactive Materials Transport Ships」of the Ministry of Oceans and Fisheries Notice No. 2015-93. The grade is a ship carrying spent nuclear fuel, radioactive waste and plutonium that does not limit total radioactivity. The hull arrangements (watertight bulkheads, double bottoms, cargo spaces), resilience in case of non-damage and damage, fire safety, temperature control of cargo spaces and cargo securing devices, power supply, etc. shall be in accordance with the Ministry of Oceans and Fisheries Notice No. 2015-93.[4]

To ensure safety, operations are prohibited in case of adverse weather conditions, and to minimize contact with other ships, the operation will be conducted on the shortest route from the lighters wharf to baseline of the territorial sea, and then run along baseline of the territorial sea. And Vessel Traffic Service is utilized to secure real-time maritime traffic information and check shipping routes. Two radiation safety managers and one KORAD transport manager board the ship. During the transport, 10 radiation monitors in the ship monitor real-time radiation leakage and prepare for an emergency accident.[1]

2.1.2 Land transport vehicle and safety devices. According to the Nuclear Safety And Security Commission Rule No. 23「Regulations on Technical Standards for Radiation Safety Management and the like」, land transport vehicle has multiple safety devices such as a hydraulic fixing fastening device to prevent

accidents such as falling of a carrying object, a warning light for confirming the normal conclusion of the carrying object, a multi sensor for sensing, and a vehicle and a rear monitoring CCTV. Radiation shields were installed in the driver's seat for driver radiation protection.
In order to ensure safety, the vehicle is transported along the designated route, and the general staff and the vehicle are controlled by installing signs. The radiation safety manager boards the transport vehicle first, and safety is ensured through the provision of driver's pre-training and radiation protection items (one or more radiation and radiation contamimation measuring devices each, personal dosimetry at least the number of people on board the vehicle, Rope, radiation signs, communication equipment, and equipment necessary for decontamination).[1]

2.2 Transport Procedure Comparison

In case of marine and land transportation, emergency preparedness plan and emergency response procedures are established in accordance with the Nuclear Safety Act in preparation for any accident, strengthening the emergency response capability through periodic repetitive training, and conducting the radiation impact assessment on the transportation route in advance.[2] In order to pre-check the route during transportation to a certain distance, the marine transport operates the leading ship and is escortde by the marine police. Land transport also operates the leading vehicle and is escorted by the police.

2.2.1 Marine Transport Procedure. Confirmation of Satisfaction with「Regulations on Technical Standards for Radiation Safety Management ane the like」→ transport document argument → Transport worker safety training → Transport vehicle safety check → Land Transport on the lighters wharf → Loading a Package on Ship → Contamination inspection of empty transport vehicles → Satisfaction of ship transport standard → Safety training and ship safety inspection → Ship operation declaration → Maritime transportation to the Wolsong Nuclear Power Plant lighters wharf → cargo unloading and vehicle loading → Check of loading status and transport conditions → Land transport to KORAD → cargo unloading → Contamination inspection for packages, transport workers and vehicles

2.2.2 Land Transport Procedure. Confirmation of Satisfaction with「Regulations on Technical Standards for Radiation Safety Management ane the like」→ transport document argument → Transport worker safety training → Transport vehicle safety check → Land transport to KORAD → cargo unloading → Contamination inspection for packages, transport workers and vehicles

3. Conclusion

In this paper, it was confirmed that the transportation procedure is partly the same, although there is a difference in safety devices due to the difference in route between the marine and the land transport. Land movement between the nuclear power plant (or KORAD) and the lighters wharf is included in marine transport but follows the procedures for land transport. It can be seen that it is possible to perform land transport with the ability of marine transport, but not vice versa.

Marine transport can be carried in large quantities (1,000 drums per transport), but there is a risk of major accidents. On the other hand, land transport, which is loaded with 16-drums per vehicle(1.6% of the marine transport), is less affected by weather changes and has no concern about sinking, so safety can be secured by relatively simple transportation procedures and safety devices compared to marine transportation.

Using these advantages and disadvantages in transporting low and intermediate level radioactive wastes in the future, it will be more efficient to use and operate marine and land transport appropriately.

4. Reference

[1] Korea Radioactive Waste Agency, https://www.korad.or.kr/korad/index.do.
[2] Nuclear Safety Act and the Enforcement Decree and Enforcement of the Act, Nuclear Safety And Security Commission Notice.
[3] Waste Comprehansive Information Database, http://wacid.kins.re.kr.
[4] Ship Safety Act, Ministry of Oceans and Fisheries Notice.

Development of Cement Waste Form for Decommissioning Wastes of Nuclear Power Plant

Ju-hyeok Lee*, Jaeeun Kang, Jaehyuk Kang, Wonseok Kim, and Wooyong Um

Pohang University of Science and Technology, 77, Cheongam-ro, Nam-gu, Pohang-si, Gyeongsangbuk-do, Republic of Korea

*jhlee5489@postech.ac.kr

1. Introduction

Recently, various disposal methods have been developed for large amounts of decommissioning radioactive wastes released from nuclear power plants (NPPs). These decommissioning wastes could occur in large quantities over a short period of time with various forms and radiation levels. To dispose these wastes, the waste loading is one of the important factors to solidify and immobilize the large amount of the decommissioning wastes in the limited volume of waste forms.

So far, cement, glass, ceramics, and hardening treatments are applied to the immobilization and stabilization methods to safely dispose of the radioactive wastes. Among them, the cement-based waste form is widely used because of the low cost and applicability to various waste types.

In this study, we developed the cement waste form using Ordinary Portland Cement (OPC), Blast Furnace Slag (BFS), and Fly Ash (FA) with various ratios to find the optimized waste loading for different types of the decommissioning wastes such as soil, metal, concrete, sludge, etc.

2. Experimental

2.1 Materials

As the ingredient materials, OPC, BFS, and FA are used to formulate the cement waste form. BFS can develop strength of cement waste form over long period, leading to reduced permeability and improved durability [1]. FA has features that improve liquidity and decrease the drying shrinkage of waste form [2]. Both BFS and FA were obtained from SUNGSHIN Cement Co., and used without further treatment. Soil waste (SW) was collected from site adjacent to Gori NPP unit 1 and used after size separation (< 2 mm). The SUS304 metals with various shapes like plate, cubic, pipe, and ring were obtained from YMS company and used for the simulated wastes. Other wastes such as concrete, concentrated waste solution, and sludge waste were also prepared based on the physical and chemical properties of the waste composition provided by the Korea Hydro & Nuclear Power Co. (KHNP).

2.2 Formulation of cement waste form

Various ratios of OPC, BFS, and FA were tested to find an optimized ratio that increased the waste loading with suitable viscosity and stability using different water to dry ingredients (OPC, BFS, and FA) ratios (W/D). The waste loading gradually increased and the compressive strength of samples was measured to compare, depending on the dry ingredient, W/D ratios, and waste loading. After mixing materials, the slurry was transferred into the plastic mold (diameter 2.5 × length 5 cm). While the slurry was being poured into the mold, air bubbles were removed from the slurry in the mold using the vibrator for 15 minutes. Finally, the cement slurry within the mold was cured for 28 days under appropriate moisture condition (relative humidity=~80-100%). All the formation process of the cement waste forms was prepared in duplicate.

2.3 Characterization

X-ray fluorescence (XRF) was used to analyze the component of waste form. X-ray diffraction (XRD) and Fourier Transformed infrared spectroscopy (FT-IR) were used to identify the mineral phase and vibrational structure, respectively. In addition, compressive strength was measured to check whether the results could meet the acceptance criteria for low and medium-level radioactive waste disposal or not.

3. Results and Discussion

3.1 Compressive strength

Table 1. Compressive strength depending on soil loading

Containing Soil Waste		
Cement	Soil loading (wt.%)	Water to Dry Mix Ratio
		0.5
		Compressive strength (MPa)
K-stone	10	20.76
	15	22.98
	20	18.06
	25	22.52
	30	16.45

The cement waste forms composed of 20% OPC, 40% BFS, 40% FA (hereafter, abbreviation as K-stone) were measured for compressive strength (Table 1). Even though the soil waste loading increased from 10 to 30%, the compressive strength exceeds the acceptance criteria of 3.44 MPa.

3.2 Composition & Crystalline patterns

Table 2. XRF results

OPC	CaO	SiO_2	Al_2O_3	MgO	Fe_2O_3	SO_3
	61.9	21	4.37	3.67	3.27	2.53
BFS	CaO	SiO_2	Al_2O_3	MgO	SO_3	TiO_2
	43.21	33.1	13.5	3.22	1.85	0.666
FA	SiO_2	CaO	Al_2O_3	Fe_2O_3	SO_3	MgO
	42.1	23.6	18.6	4.204	4.12	2.31
SW	SiO_2	Al_2O_3	Fe_2O_3	CaO	K_2O	Na_2O
	65.19	15.8	6.471	3.16	2.91	2.29

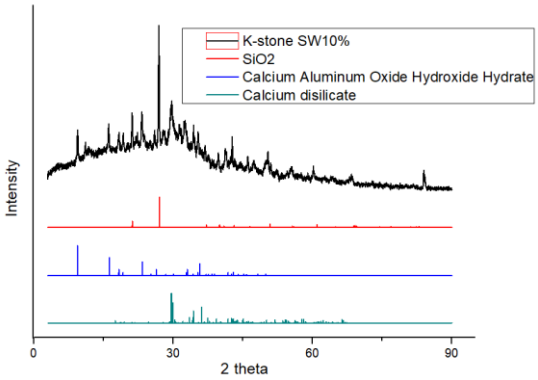

Fig. 1. XRD pattern of cement waste form.

The XRF results showed that CaO, SiO_2, and Al_2O_3 were dominant with minor amounts of MgO, Fe_2O_3, SO_3, and TiO_2 in the ingredients of the cement waste form (Table 2). The XRD pattern of final cement waste form with soil waste (10wt%) also indicates three major mineral phases (SiO_2, $Ca_6Al_2O_6(OH)_6$-$32H_2O$, and $CaSi_2O_5$) (Fig. 1) consistent with the XRF results.

4. Conclusion

Cement waste forms prepared with K-stone composition showed higher compressive strength. Moreover, even though the soil waste loading increased in cement waste form, the results showed a high compressive strength that sufficiently could meet the acceptance criteria of low and medium-level radioactive waste disposal facilities. In the future, we will conduct additional experiments to solidify and immobilize the various wastes such as waste filters, spent resin, and concrete.

ACKNOWLEDGEMENT

This work was supported by the Korea Institute of Energy Technology Evaluation and Planning (KETEP) and the Ministry of Trade, Industry & Energy (MOTIE) of the Republic of Korea (No. 20181510300870).

Application of ED-XRF Measurement on Uranium Contaminated Soil Waste for Regulatory Clearance

Mal-Go-Bal-Gae-Bit-Na-La Yoo*, Ji-Young Park, Jong-Myoung Lim, Won-Hyuk Jang, and Dae-Seok Hong
Korea Atomic Energy Research Institute, 111, Daedeok-daero 989beon-gil, Yuseong-gu, Daejeon, Republic of Korea
*yoo1707@kaeri.re.kr

1. Introduction

According to the regulation, radioactive waste can be classified into High Level radioactive Waste (HLW), Intermediate Level radioactive Waste (ILW), Low Level radioactive Waste (LLW), and Very Low Level radioactive Waste (VLLW). The radioactive wastes should meet permissible criteria on nuclide concentration or dose for clearance. Currently, the Korea Atomic Energy Research Institute (KAERI) is conducting an analysis by regulatory guidelines of Korea Institute of Nuclear Safety (KINS) [1] for regulation clearance of uranium contaminated soil generated from the parking lot site that had been constructed during the remodeling process.

In this study, a representative sampling procedure and an analysis of the soil samples were described. In addition to that, the maximum value was used as RESRAD code parameter and the ED-XRF method has been finally approved for clearance from a regulatory body.

2. Methods and Results

2.1 Materials

The building, which was used as a refining research laboratory for uranium ore in the past, was remodeled including the parking lot around the building from 2013 to 2014. About 68 tons of the contaminated soil from the parking site was not cleared. They are expected to be contaminated with uranium since they were found close to facilities that deal with uranium ore.

2.2 Temporary radiation management zone setting and procedures

In order to dispose of the uranium contaminated soil in KAERI, the site was designated as temporary radiation management zone in accordance with procedures for radiation protection of the research institute. Procedures for performing radiation work including sampling, collection and transportation should be submitted to the Radiation Safety Management Department. The two greenhouses one for work space and the other for storage space were installed [Fig. 1].

Fig. 1. Work (A) and storage (B) greenhouses.

2.3 Sample collection and preparation

For sampling from soil pile were taken, compact excavator and shovels were used. The quantity of the soil that the excavator could collect at a time was about 50 kg, of which about 250 g of sample was taken. By repeating this procedure approximately five times, representative sample of 1 kg per 200 kg of soil in accordance with regulatory guide was obtained. Totally of 340 representative samples were collected and analyzed by sieving to

ensure homogeneity of the representative samples and reproducibility of analysis [Fig. 2].

Fig. 2. The representative samples over 1 kg (A) and the analysis samples (B).

2.4 Analysis of soil using ED-XRF

The Energy Dispersive X-ray fluorescence analysis (ED-XRF, Xepos HE, Spectro, Kleve, Germany) is applied by the geochemistry trace powder method for environmental and mineral sample measurement.

The measurement for the uranium contaminated soils took approximately 30 min per sample under the analytical conditions of ED-XRF determination of a tube voltage of 39.7 kV, current of 0.8 mA, He gas flow rate 70-80 L/h and the secondary targets such as cobalt, molybdenum, aluminum oxide, and zinc. The calculation for converting the mass concentration of the nuclides (ppm) into the radioactive concentration is indicated in Equation 1.

$$m = \frac{A \times M \times t_{1/2}}{ln2 \times N_A} \quad (1)$$

Where m is the mass of analytical nuclide (g), A is the decay rate (Bq), M is the molar mass (g/mol), $t_{1/2}$ is the half-life (s), and N_A is the Avogadro's number (mol^{-1}).

The maximum uranium concentration was 0.0734 Bq/g for 340 samples as shown in Fig. 3. The value was used as a parameter of the RESRAD code, and the results of the exposure dose assessment showed that the individual dose was 7.77×10^{-1} μSv / year and the collective dose was 1.37×10^{-2} man·Sv / year, which satisfies the clearance dose criteria.

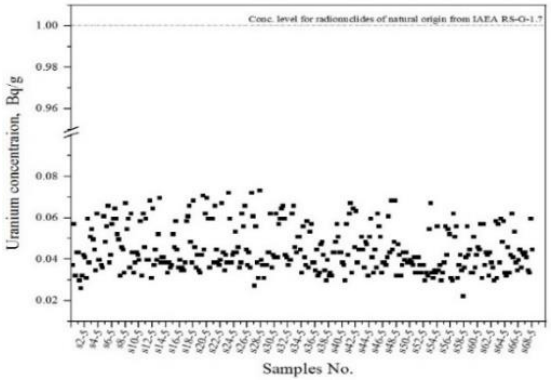

Fig. 3. The uranium concentrations of 340 samples measured by ED-XRF.

3. Conclusion

The ED-XRF method applied for the determination of uranium concentration in soil is useful as a non-destructive and fast routine measurement of samples in addition to avoid pretreatment. Based on the methodology on this study, KAERI could obtain approval for clearance from the regulatory body because the methodology was successfully used to prove that the soil was meet domestic dose criteria such as individual dose < 10 μSv/year and collective dose < 1 man·Sv/year as well as the allowable concentration for clearance suggested by the IAEA[2].

REFERENCES

[1] Korea Institute of Nuclear Safety/RG-N12.08, Radioactive Waste Self-disposal Safety Assessment, KINS, 2015.

[2] Application of the Concepts of Exclusion, Exemption and Clearance, Vienna, Austria, IAEA Safety Standard Series No. RS-G-1.7, 2004.

Investigating the Necessity of a Waste Certification Program (WCP) to Manage Radioactive Waste From Decommissioned NPPs

Hyeongmin Park, Sooyeun Park, Suri Park, Heekyung Kim, Eunsuk Choi, Sangkoo Han, Dongsik Jin, Heesoo Bae, and Yongho Hong*
ACT Co., Ltd., 1434, Yuseong-daero, Yuseong-gu, Daejeon, Republic of Korea
*saintzeno@actbest.com

1. Introduction

The oldest commercial reactor in Korea, i.e., the Kori-1 Nuclear Power Plant (NPP), was decommissioned in 2017. Additional 12 NPPs will also be permanently decommissioned by the year of 2030 [1]. Because large quantities of radioactive waste are expected to be generated, successful NPP decommissioning requires an appropriate waste treatment

The IAEA estimates that the amount of decommissioning waste per unit of 1,000 MW of PWR will be 19,000 drums. Therefore, 600 MW of PWR can generate 14,000 drums [2].

Figure 1 shows the process of radioactive waste disposal according to the current transfer procedures.

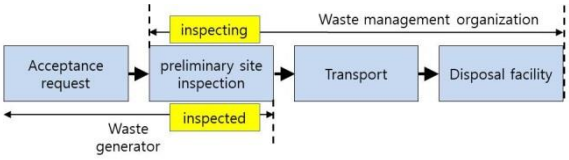

Fig. 1. Transfer procedure for disposal of radioactive waste.

Current radioactive waste transfer procedures entail significant economic losses, and preparation for preliminary inspection of the target area requires a large amount of manpower, time, and human exposure.

Considering this, a waste certification program (WCP) is expected to provide the methods for effective management of nuclear waste.

2. Related Laws and the Necessity of WCP

2.1 Korean WCP – related legislation

The WCP is defined in Article 3 (Definition) of the Regulations on the Acceptance of Radioactive Waste according to the notices of the Ministry of Trade, Industry, and Energy. Article 13 suggests that waste producers can establish and operate a WCP [3].

2.2 Institutional issues for WCP establishment

Mandatory control must be prepared for successful operation of WCP.

2.3 Expected effects of applying a WCP

Figure 2 shows the procedure for nuclear waste removal following WCP application. Producers can minimize personnel and material resource costs by obtaining an exemption from preliminary inspection, which occurs before the waste is transferred to the disposal facility.

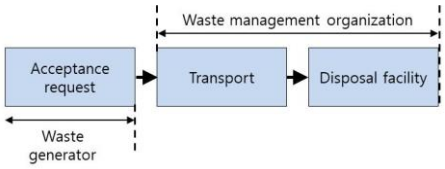

Fig. 2. Transfer procedure for disposal of decommissioned waste after the application of the WCP.

The disposal compliance evaluation will be applied to the processes of waste generation, classification, treatment, packaging, storage, and disposal. This process will also help to ensure that improper waste generation methods, i.e., methods that have not been recognized as safe, are not employed. Therefore, it will be possible to minimize the amount of nuclear waste that is reprocessed and repacked by ensuring that the generated waste can be appropriately treated. [4].

3. Conclusion

Legislation that includes regulations for NPP decommissioning must be prepared to ensure that proper compensation and safety can be confirmed. A WCP is expected to have the following effects.

1) The target producer can be exempted from undergoing a preliminary inspection before the nuclear waste is transferred by conducting disposal compliance assessments. The acceptance criteria will cover the collection, sorting, treatment, and packaging processes.

2) Waste treatment efficiency will be increased as a result of analyzing the results of required facility assessments and managing waste acquisition.

3) Cost reduction and less nonconforming waste generation as a result of producers performing disposal compliance evaluations for their decommissioned waste procedure.

Acknowledgment

This work was supported by Korea Institute of Energy Technology Evaluation and Planning (KETEP) grant funded by the Korea government (No. 20193210100060).

REFERENCES

[1] KAERI, Nuclear report 2018-5 “Nuclear decommissioning industry advancement” (2018).

[2] KRS, “Decommissioning waste management scenario analysis” (2013).

[3] Ministry of Trade, Industry and Energy Notice No. 2016-230, “Regulations on the acceptance of radioactive waste” (2016).

[4] KPS, “The phase 1 development of the KHNP WCP(Waste Certification Program) applicable to the KORAD” (2015).

Experimental Study of the Cement Waste Forms With Concrete Waste

Donghee An*, Hyunkook Choi, and Jaeyoung Kim

SungShin Cement Research and Development, 48-37, Bugangoecheon-ro, Bugang-myeon,

Sejong-si, Republic of Korea

*anzilda@sscem.com

1. Introduction

Concrete materials are the main component of the waste occurs during the decommissioning of nuclear power plants. In most case, radioactive waste in the a low-radioactive concrete is the cement paste.

The purpose of this study is to obtain the basic data for developing a method to make cement waste forms using separated cement paste in a low-radioactive concrete waste.

2. Experiments

2.1 Materials

In this study we used concrete over 20 years old. Concrete specimens are crushed to several centimeters using con-crusher and crushed to several millimeters using jaw-crusher(Fig. 1). And they were dried at 100°C to remove moistures. After drying we separate powder using standard sieve(0.15 millimeters). Powders were measured for weight loss at 600°C and analyzed for CaO contents by XRF.

2.2 Experiment methods and items

In order to get CaO content of the powder separated from concrete, we use X-ray fluorescence analysis method (XRF, Rigaku, Japan, ZSX Primus II) and measurements of loss on ignition at 600°C for 90 min. using the electric furnace.

To estimate cement pastes contents in the powder, we used CaO content which get from XRF analysis results and weight loss of mixtures.

2.3 Compressive strength test

Mortar compressive strength was measured according to KS L ISO 679 for evaluation of mechanical properties of cement waste forms.

Cement waste forms for testing of compressive strength were prepared by two different method. The First method is calcinations of powder at 600°C and the other is additions of solidifying agent. The solidifying agents is based on cement materials and superplasticizer.

2.4 Result of Paste Content calculation

The results of the XRF analysis and loss on ignition at 600°C for the powder are shown in table 1.

We estimate cement pastes contents in the powder with this results and graph get from previous research. We found that measure values of CaO in XRF analysis results and ignition loss of powder at 600°C showed good relationship for cement paste contents in the previous research.

Fig. 1. Crushed concrete and Powder from concrete waste.

Table 1. Results of the analysis of the powder

Calculated Paste content (wt.%)	Chemical Composition (%)		
	CaO	SiO_2	Al_2O_3
60~70%	44.46	36.72	6.67

Table 2. Test results for compressive strength

Cement waste forms	Compressive Strength (MPa)		
	7 Day	28 Day	91 Day
Origin	X	X	X
Calcination At 600°C	X	5.1	7.4
Additions of solidifying	X	13.0	17.4

X : compressive strength is not measured

Calculated paste contents in the powder is about 60% using the result according to CaO contents of XRF analysis. And it is about 70% using the result of weight loss of mixtures at 600°C.

In the previous studies for determining cement paste content in mortar, there are a few differences XRF analysis method and weight loss method. But in this study differences between two method are some increased. We tried to found the reason of this difference and new test method of determining cement paste contents in concrete waste.

Test results for compressive strength of cement waste forms are shown Table 2. As shown Table 2. powders separated from waste concrete cannot be used to cement waste forms by itself as to it does not have sufficient hydraulic properties. Therefore we should consider add to some process including calcinations of powder at high temperatures or using solidifying agents base on cement materials.

The calcinations of the powders separated from concrete waste at 600°C increase compressive strength of cement waste forms, but the rise of strength is not satisfactory.

Additions of solidifying agents to concrete waste powder makes remarkable increasing in the strengths of the cement waste forms.

3. Discussion and Conclusion

In this study, we use powders separated from concrete waste over 20 years old. We thought this makes some differences as compared to the results of previous study.

The results of this study showed properties of cement waste forms using calcinations method could be affected by not only cement paste contents but also the service life of concrete. We thought it is due to cement hydration products are changed by chemical reactions of cement and environmental influences.

In the high temperatures, hydration products are decomposed at certain temperature conditions. For examples, one of the main hydration products of cements, calcium hydroxide decomposed to Calcium Oxide and water at 450°C approximately. These decomposed compound might have a hydraulic properties but its effectiveness is not noticeable.

In comparison, additions of the solidifying agent based on cement materials affected a few by the cement paste contents in concrete waste or service life of concrete. Because solidifying agent based on cement materials could enhance strength of the cement waste forms.

Acknowledgement

This work was supported by the Energy Technology Program of the Korea Institute of Energy Technology Evaluation and Planning(KETEP) granted financial resource from the Ministry of Trade, Industry & Energy, Republic of Korea (No. 20161510300420).

REFERENCES

[1] Jang Jong-Ho, “A Study on the Fundamental Properties and Application as Cementious Admixture by heating Temperature of Recycled Powder”, Proceeding of Korea Concrete Institute, May 12, 635-40, (2001).

[2] Ahn JC, Lee JH, Kang BH, “Properties of Recycle Cement made of Cementitious Powder from Concrete Waste by Conditions of Burning”, Journal of Architectural Institute of Korea, Nov,19(11):109-12, (2013).

[3] Mun YB, Choi HK, “A Fundamental Study for Development of Radioactive Waste Content and Solidifying During the Dissolution of Concrete in Decommissioning Nuclear Power Plant” Proceedings of the Korean Radioactive Waste Society, Vol.16, No. 1, 2018, 295-296.

[4] Ahn DH, Kim JY, Choi HK, “Experimental Study of the Analysis Method for Paste Contents in the waste Concrete” Proceedings of the Korean Radioactive Waste Society, Vol. 17, No. 1, 2019, 295-296.

Conceptual Design of Radioactive Waste Classification Using an Object Recognition Technologies

Sung-Chan Jang, Dong-Ju Lee, Il-Sik Kang, Jeong-Guk Kim, Dae-Seok Hong, and Hee-Seoung Park*
Korea Atomic Energy Research Institute, 111, Daedeok-daero 989beon-gil, Yuseong-gu, Daejeon, Republic of Korea
*parkhs@kaeri.re.kr

1. Introduction

The management of radioactive waste under high levels of safety, capability and reliability requires a high disposal cost. In order to reduce costs, a technique for managing radioactive waste through systematic classification is essential. The segregation of radioactive waste is completely done by manual laborers which is less efficient, time-consuming and not completely feasible due to large amount of waste [1].

This paper proposes conceptual design of a radioactive waste classification technologies based on deep learning to detection and recognition. The technologies detect and identify Radioactive waste directly in monitoring system using a computer vision and deep learning technology.

2. Background

2.1 Overview

Radioactive waste contains various kinds of radioactive material and generated as a by-product of nuclear facility operation and other applications of nuclear fission or nuclear technology, such as research and medicine. It can be hazardous to be exposed to radioactive waste and it should be regulated by regulatory bodies in order to protect human health and the environment.

Radioactivity decays out over time, so radioactive waste has to be isolated and confined in appropriate disposal facilities for a sufficient period until it no longer poses a threat. The time for radioactive waste to be stored depends on the type of waste and radioactive isotopes. Current approaches to manage radioactive waste have been segregation and storage for short-lived waste, near-surface disposal for low and some intermediate-level waste.

The management of radioactive waste is a very important part of the nuclear industry. In the future of the nuclear industry, the safe management of radioactive waste is an essential technology and the demand for that will increase. In particular, many technologies are needed to efficiently dispose of radioactive waste at space-limited disposal facilities.

2.2 Comparing conventional methods and new technologies

For proper management, radioactive waste has to be handled, segregated, transported and disposed so as to reduce the risks to public lives. One of the big problems of radioactive waste is that it occurs in industrial, research, hospital, power plant waste, etc., and has a variety of types and radioactive materials. As such, there is a need for good classification of radioactive waste to reduce disposal costs.

Some industries do follow semi-automatic waste segregation process and it needs some manual work, which leads to health hazards [1]. Deep learning is a class of machine learning algorithm that uses multiple layer of data representation and feature extraction. Using convolution neural network, a class of deep, feed-forward artificial neural network has successfully been applied to analyze the image [2]. Thus, in waste segregation using deep learning involves acquiring images from camera

with detection, object recognition, prediction and classification into categories [3].

2.3 Advantages of deep learning for classification of the radioactive wastes

Deep learning technology has become a buzzword nowadays due to the state-of-the-art results obtained in the domain of image classification, object detection, natural language processing. The reasons behind popularity of deep learning are two folded, viz. large availability of datasets and powerful Graphics Processing Units. As deep learning requires large datasets and powerful resources to perform training, both requirements have already been satisfied in this current era [3].

Object detection is the procedure of determining the instance of the class to which the object belongs and estimating the location of the object by outputting the bounding box around the object. Detecting single instance of class from image is called as single class object detection, whereas detecting the classes of all objects present in the image is known as multi class object detection. Different challenges such as partial/full occlusion, varying illumination conditions, poses, scale, etc are needed to be handled while performing the object detection [2].

The ubiquitous and wide applications like scene understanding, video surveillance, robotics, and self-driving systems triggered vast research in the domain of computer vision in the most recent decade. Being the core of all these applications, visual recognition systems which encompasses image classification, localization and detection have achieved great research momentum. Due to significant development in neural networks especially deep learning, these visual recognition systems have attained remarkable performance. Object detection is one of these domains witnessing great success in computer vision. This paper demystifies the role of deep learning techniques based on convolutional neural network for object detection. Deep learning frameworks and services available for object detection are also enunciated. Deep learning techniques for state-of-the-art object detection systems are assessed in this paper.

3. Conclusion

Great progress has been made in target detection and recognition based on vision and artificial intelligence, but it requires a lot of computing resources, and it is difficult to meet the requirements of the embedded video surveillance front-end module. At the same time, the model is used to make target box dimensional clustering, classification network pre-training improvement and lightweight processing to facilitate the transplantation of embedded systems. Finally, narrow-band Internet of Thing has been used to do communication among thousands of monitoring terminals and background servers. Although we have made reasonable simplification for the algorithm, the real-time capability should be made further improvement. This study will provide the ability to visually identify wastes in sealed radioactive waste drums through augmented reality (AR) technologies.

REFERENCES

[1] Ying Liu, Zhishan Ge, Guoyun Lv, Shikai Wang, “Research on Automatic Garbage Detection System Based on Deep Learning and Narrowband Internet of Things”, Journal of Physics, 1069, 012032 (2018).

[2] X H Fang, W Xiong, B J Hu, LT Wang, “A Moving Object Detection Algorithm Based on Color Information”, Journal of Physics, 48, 384-387 (2006).

[3] Ajeet Ram Pathak, Manjusha Pandey, Siddharth Rautaray, “Application of Deep Learning for Object Detection”, Procedia Computer Science, 132, 1706-1717 (2018).

Development of Glass for Vitrification of Fukushima Liquid Waste With Cold Crucible Induction Melter

Sunghoon Hong[a,*], Young Hwan Hwang[a], Jung-Su Jung[a], and Toshiro Oniki[b]

[a]KHNP Central Research Institute, 70, Yuseong-daero 1312beon-gil, Yuseong-gu, Daejeon, Republic of Korea

[b]IHI Yokohama Engineering Center, Kanagawa 235-8501, Yokohama-shi, Isogo-ku, Shin-Nakahara-cho, Japan

[*]sunghoon.hong@khnp.co.kr

1. Introduction

The site of a Fukushima Daiichi power plant after the accident, massive radioactive waste is in storage outside. The radioactive wastes are consist of solid waste (such as stone, wood, dry active waste, and etc.), contaminated water treated by Cs/Sr removal facilities, and sludge-type second radioactive waste generated by Cs/Sr removal process. Among of the radioactive wastes, the intermediate and low level radioactive sludge-type waste contained Cs and Sr is difficult to store due to highly radioactive and corrosive properties.

Many countries are looking into solidification treatment using vitrification [1], geo-polymer concrete, and polymer technology as a solution for treatment of the sludge-type waste. Currently, as shown in the Fig. 1, in the KHNP CRI, with CCIM (Cold Crucible Induction Melter), vitrification demonstration test has been performed to confirm the applicability of treatment of sludge-type waste. Especially, it is very important to develop the glass composition in view of commercial application such as time and electric power consumption.

Therefore, in this study, properties (viscosity and electro-conductivity) depending on temperature with various glasses were evaluated using Glass form 1.1 program. The calculated properties are discussed in the view of the criterion for determining which glass is suitable for the commercial use.

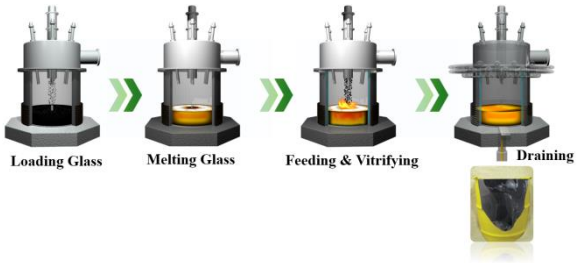

Fig. 1. Vitrification process by using CCIM [2].

2. Development of candidate glass

The development procedure of optimum glass composition for vitrification is shown in Fig. 2. The computer simulation using code Glass Form 1.1 is used to achieve the optimum glass composition with chemical composition of slurry. The computer simulation using code Glass Form 1.1 enables development of chemically stable glass composition, in terms of phase stability and leach rate, with viscosity of ≤70 poise and electrical conductivity of ≥0.4 S/cm at a CCIM operation temperature of 1,150°C using inorganic materials composition, waste loading, etc.

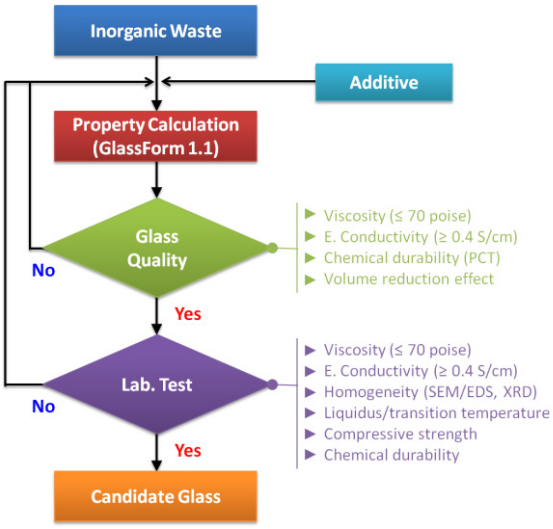

Fig. 2. Procedures for development of candidate glass.

3. Results and discussion

The Fig. 3 shows the viscosity with respect to the temperature. The viscosity at 1150 °C of all candidate glasses are similar. However, viscosity at low temperature, 900 °C, are very different. It seems that the high viscosity of G1 at low temperature hinders the thermal energy transfer during the startup process and results in slow glass melting behavior, which is not adequate in commercial CCIM operation. As shown in the Fig. 4, G1 glass was partially melted in spite of long time operation. G2, G3, G4, and G5 glasses were suggested for the commercial use. The calculation result shows that the viscosity of G3 and G4 were 607 poise and 653 at 900 °C, respectively. Accordingly, not only the operating temperature but also the low temperature of glass properties should be considered for CCIM vitrification process.

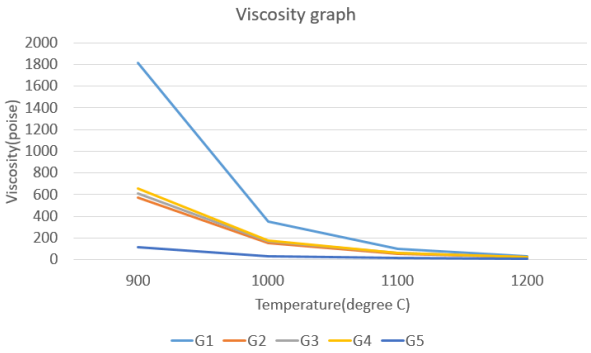

Fig. 3. Calculated viscosity using Glass form 1.1.

Fig. 4. Partially melted G1 glass on CCIM test.

4. Conclusion

The results of glass form 1.1 indicates that the slope of viscosity with respect to temperature also need to be considered when develop the glass formation for the smooth startup of CCIM and it is also found the low level of slope is preferred.

REFERENCES

[1] C.W. Kim, et al., “Chemically Durable Iron Phosphate Glasses for Vitrifying Sodium Bearing Waste (SBW) Using Conventional and Cold Crucible Induction Melting (CCIM) Techniques”, Journal of Nuclear Materials (2003).

[2] C.W. Kim, “Vitrification Technology for Radioactive Waste Treatment”, Korea Atomic Industrial Forum (2011).

Preliminary Evaluation of the Surface Dose Rate for the Waste Package Type of Low and Intermediate Level Radioactive Waste

Rin-Ah Kim*, Ho-Seog Dho, and Tae-Man Kim

Korea Radioactive Waste Agency, 174, Gajeong-ro, Yuseong-gu, Daejeon, Republic of Korea

*krina26@korad.or.kr

1. Introduction

Radioactive waste is managed through several stages from generation to final disposal. The regulator is verified the various stages of radioactive waste management for safety-related aspects and regulatory control. In order to ensure the waste management system under international safety standards, classification of radioactive waste is divided into intermediate level waste (ILW), low level waste (LLW), very low level waste (VLLW). In this study, the surface dose rate was calculated for the waste package type of low and intermediate level waste using MCNP code whether it satisfies the waste acceptance criteria.

2. Dose rate calculations of the waste packages

2.1 Source term

The source term is necessary to calculate the dose rates of the waste packages. The radionuclide considered in this study is Co-60 among the 14 radionuclide that require of radionuclide identification. Co-60 can be evaluated conservatively because of its high energy and strength among key radionuclides emitting gamma rays. Specific radioactivity of Co-60 that is derived by waste streams is shown in Table 1.

Table 1. Concentration limits of Co-60 (Bq/g)

Material	EW	VILW	ILW
PWR Spent resin	7.13E-03	7.13E-01	3.70E+07
PHWR Spent resin	4.10E-02	4.10E+00	3.70E+07
PWR Concentrated wastewater	3.31E-02	3.31E+00	3.70E+07
PWR Spent filter	6.82E-03	6.82E-01	3.70E+07
PHWR Spent filter	6.36E-03	6.36E-01	3.70E+07

2.2 Main technical specification of the waste packages

In this study, the type of material is classified into spent resin, concentrated wastewater, spent filter. These wastes have not been acquired currently at the disposal site.

There are presently six types of container specified in the safety analysis report.

The main technical specification of the waste packages, which are summarized in Table 2, quotes from the physical properties of the material in Reference [1].

Table 2. The main technical specification of the waste packages

Materials	Container	Density (cm^3/g)	Internal volume (cm^3)	Weight (kg)
Cement solidification of spent resin	200L Drum	1.32	124,052	165
Dry spent resin	200L Drum	0.76	211,180	165
Spent resin	C1 concrete	1.32	900,502	1,200
	C2 concrete	1.32	312,557	420
	HIC-FE	0.76	1,272,574	970
Paraffin solidification of concentrated wastewater	200L Drum	1.15	211,579	245
Cement solidification of concentrated wastewater	200L Drum	1.73	211,579	370
Concentrated wastewater	C1 concrete	1.73	900,502	1,600
	C2 concrete	1.73	312,557	550
Spent filter	200L concrete Drum	2.38	18,761	50
	C2 concrete	2.38	312,557	750
	C4 concrete	2.38	467,690	1,150

2.3 MCNP calculation

The dose rates are calculated using MCNP code. The virtual detectors (F4 tally) for MCNP calculation were located 10 mm above the top and side on the surface of the waste package. It is assumed that Co-60 is a homogeneously distributed in radioactive material. The flux to dose rate conversion factors applies ICRP 74. The analysis accuracy was confirmed the relative error about the statistical results of the MCNP code. The dose rates should be demonstrated to be below maximum dose rate levels in 10mSv/h [2]. Figure1 shows the MCNP modeling of the waste packages.

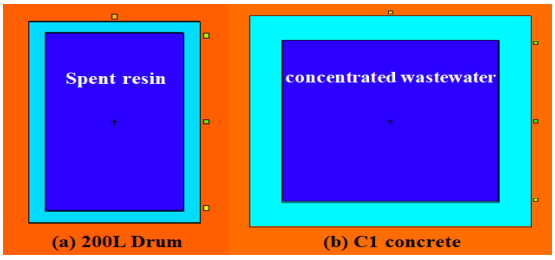

Fig. 1. MCNP modeling.

2.4 Results

Table 3 shows the lower limits of the dose rate according to the waste classification.

Table 3. The dose rate of the waste packages (mSv/h)

Materials	Container	Dose rate (mSv/h)		
		VLLW	LLW	ILW
PWR Cement solidification of spent resin	200L Drum	6.50 E-07	6.50 E-05	9.20 E+00
PWR Dry spent resin	200L Drum	1.18 E-06	1.18 E-04	1.67 E+01
PWR Spent resin	C1 concrete	2.58 E-07	2.58 E-05	3.68 E+00
	C2 concrete	1.14 E-07	1.14 E-05	1.62 E+00
	HIC-FE	1.12 E-06	1.12 E-04	1.60 E+01
PHWR Dry spent resin	200L Drum	6.77 E-06	6.77 E-04	3.16 E+00
PWR Paraffin solidification of concentrated wastewater	200L Drum	9.05 E-06	9.05 E-04	1.17 E+02
PWR Cement solidification of concentrated wastewater	200L Drum	1.16 E-05	1.16 E-03	1.50 E+02
PWR Concentrated wastewater	C1 Concrete	1.21 E-06	1.21 E-04	1.57 E+01
	C2 Concrete	5.54 E-07	5.54 E-05	7.18 E+00
	200L Drum	1.50 E-07	1.50 E-05	4.27 E+00
PWR Spent filter	C2 Concrete	1.23 E-07	1.23 E-05	3.52 E+00
	C4 Concrete	2.49 E-07	2.49 E-05	7.07 E+00
PHWR Spent filter	200L Drum	1.40 E-07	1.40 E-05	1.06 E+00

3. Conclusion

In this study, the surface dose rate of the waste packages was calculated. The dose rate of VLLW and LLW are satisfied with the waste acceptance criteria. However, ILW of PWR with dry spent resin (200L), spent resin (HIC-FE), paraffin solidification of concentrated wastewater (200L), cement solidification of concentrated wastewater (200L), concentrated wastewater (C1 concrete) are not satisfied with the waste acceptance criteria. As a result, remote control equipment is necessary to effectively control these waste packages for radioactive waste management.

ACKNOWLEDGEMENT

This research was supported by the Korea Institute of Energy Technology Evaluation and Planning (KETEP), (No. 20181510300870).

REFERENCES

[1] Korea Radioactive Waste Agency, “Final Report on Comprehensive Disposal Plan for Radioactive Waste Management”, 2014.
[2] Korea Radioactive Waste Agency, “Safety Analysis Report (SAR)”, Capture 8, 2016.

Preliminary Radiation Shielding Evaluation of the Conceptual Disposal Container for the Decommissioning Waste

Ho-Seog Dho*, Taeman Kim, and Chun-hyung Cho

Korea Radioactive Waste Agency, 174, Gajeong-ro, Yuseong-gu, Daejeon, Republic of Korea

*ehghtjr@korad.or.kr

1. Introduction

In order to promote the decommissioning business of Kori Unit 1, it is necessary to develop a new container considering the characteristics of decommissioning waste. Dismantling wastes occur in large quantities in a short period time and come in a variety of forms and levels. Currently, Korea Radioactive waste Agency (KORAD) is designing a large disposal container that reflects the characteristics of Low-Level Radioactive wastes, which are targeted for wastes generated during operation and decommissioning wastes.

In this study, the evaluation of shielding analysis for the conceptual disposal container was carried out for the solidified filter, solidified sludge and dry active waste.

2. Shielding Evaluation of the Conceptual Disposal container

2.1 Dose Rates Criteria

There are no domestic and international technical standards for the surface dose rate of waste disposal containers. In Korea, KORAD, the agency of the disposal of radioactive wastes, has established and applied the wastes acceptance criteria in consideration of low and low-level waste disposal sites and operation facilities. KORAD's acceptance criteria for wastes limits the surface dose rate to 10mSv/h. However, considering the operating system of the interim storage facility, it is desirable to satisfy the surface dose rate of the disposal container to be less than 2mSv/h.

2.2 LLW Package

According to previous assessments of radionuclide inventories for operational waste, waste filters and sludge generated during operation are classified into Mid-Level, Low-Level, and Very Low-Level and the dry active waste are classified into Low-Level and Very Low-Level [1]. Conceptual disposal containers are used in a 2nd disposal facility for Low / Very Low-Level waste. The maximum allowable weight of a radioactive waste package is 35tons. External dimensions of the conceptual disposal container are 1.6 m(W) × 3.4 m(L) x 1.2 m(H) and thickness of it is 0.012 m and the weight of the conceptual disposal container is 3.6tons, the maximum allowable weight of the radioactive waste is 31.4tons. The calculated radioactivity of the LLW in the conceptual disposal container is shown in Table 1.

Table 1. Radioactive of LLW

Radioactive waste	Specific Activity [Bq/g]	Activity [Bq]	Weight [Ton]
Solidified filter	8.09E+03	1.19E+11	14.7
Solidified sludge	5.19E+02	5.56E+09	10.7
Dry active waste	2.48E+02	1.28E+08	5.1

2.3 Source Terms

The LLW used as the radiation source is assumed to be uniformly distributed inside the disposal container. Fig. 1 shows the model of disposal containers with LLW for shielding evaluation. The volume inside the disposal container is 6.19 m^3. The weight was derived by applying the density (Solidified filter: 2.38T/m^3, Solidified sludge: 1.73T/m^3, Dry active waste: 0.83T/m^3) of each low-level waste, and it was

assumed that 100% of the container was filled with contents. Alpha and beta releasing nuclides were excluded from the shielding calculation, and only ^{60}Co, the major gamma radiation releasing nuclides, was considered.

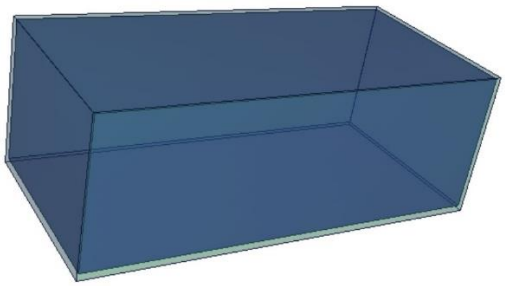

Fig. 1. Shielding Evaluation Model.

2.4 Shielding Evaluation

MCNP5 computer code using the three-dimensional Monte Carlo method has been used to calculate dose rates at the various desired locations of the conceptual disposal container [2]. The flux-to-dose conversion factor was added to the input data so that it could be expressed as the dose rate at the locations of interest. The dose conversion factors used in this calculation were taken from ICRP-74(1996) [3].

The assumptions applied in radiation shielding calculations are as follows.

- Around the container to form an air layer to reflect the skyshine effects
- It is saturated by the proper volume considering the total weight of radioactive contents inside the container, and there are no voids in the stack.
- F5 tally (point detector) applied

3. Shielding Evaluation Results

In this MCNP calculation, 15 detectors were placed at the external surface of the conceptual disposal container, respectively. Table 2 shows the maximum dose rates at all positions in the conceptual disposal container for each LLW. The relative errors of these detectors were 0.01~0.02.

Table 2. Dose Rates of disposal container

[Unit : mSv/hr]

Radioactive waste	External Surface		Limit
	Results		
	Top	Side	
Solidified filter	0.45	0.46	2.0
Solidified sludge	0.02	0.02	
Dry active waste	0.0005	0.0005	

4. Conclusion

Evaluation of the radiation shielding of the conceptual disposal container for LLW, such as solidified filter, solidified sludge and Dry active waste was performed. The conceptual disposal container satisfies the radiation dose limits presented in the waste acceptance criteria. Based on the results of this study, the structural safety assessment reflecting the specifications of the 2nd disposal facility can be used to determine the application. Also, it would be possible to improve the utility of the conceptual disposal container by checking the availability of the shielding analysis based on the RV / RVI source term of Kori Unit 1.

ACKNOWLEDGEMENT

This work was supported by the Korea Institute of Energy Technology Evaluation and Planning (KETEP) generated financial resource from the MOTIE, Republic of Korea. (No.20181510300870)

REFERENCES

[1] Kyung Hee University, Analysis of Total Disposal Plan for Radioactive Waste Management (2014).

[2] Los Alamos National Laboratory, MCNP –A General Monte Carlo N particle Transport Code, Ver.5, Release 1.40 (2005).

[3] ICRP, Conversion Coefficients for Use in Radiological Protection Against External Radiation, ICRP-74 (1996).

Technology Development Status of High Integrity Container in Domestic and International

Mi-Hyun Lee*, Young Hwan Hwang, and Ji-Hoon Lee
KHNP Central Research Institute, 70, Yuseong-daero 1312beon-gil, Yuseong-gu, Daejeon, Republic of Korea
*mihyun.lee@khnp.co.kr

1. Introduction

Low and intermediate level radioactive waste generated in the nuclear industry should be safe and rigid enough to meet regulatory requirements for treatment and disposal. Radioactive waste from nuclear power plants is classified into very low level, low level, intermediate level and high level waste. Radioactive waste, except high level waste, must meet the acceptance criteria for disposal. Among them, concentrated liquid waste and spent resin should be solidified or disposed using high integrity container (HIC)[1].

In this paper, the technology development status of HIC in domestic and international is discussed.

2. Current Status of HICs

2.1 High Integrity Container (HIC)

The HIC is a radioactive waste packaging container capable of maintaining integrity for more than 300 years under the general underground environment and disposal conditions in Korea. In the US, it was first commercialized for waste disposal.

Domestic waste disposal regulations state that the waste should be solid, physically and chemically stable and non-flammable. Liquid wastes should be solidified homogeneously. The solidified form should meet several requirements, including compressive strength over 500 psig with pristine sample/irradiated sample/thermal cycled sample, leaching index over 6 for Cs, Sr, Co, etc.

2.2 Technology Development Status of HIC

2.2.1 Domestic Status. Recently, the application of the polymer concrete-HIC is approved. The 860L polymer concrete HIC for concentrated liquid waste is licensed. The KHNP is pursuing application of 510L PC-HIC for spent resin for silo disposal facility.

2.2.2 International Status. Currently, most countries, except the US, Korea, and China, do not use the HIC. In addition, waste classification and stabilization requirements vary from country to country. However, it seems that they must maintain integrity for more than 300 years at the disposal site.

2.3 Internationally Licensed HICs

The HIC developed and used in international is shown in Fig1-Fig3, and most of them have various sizes by container type.

2.3.1 Polyethylene Container. Polyethylene is a thermoplastic used to store many chemicals because of its high corrosion resistance. The wall thickness of the container is 11-19 mm.

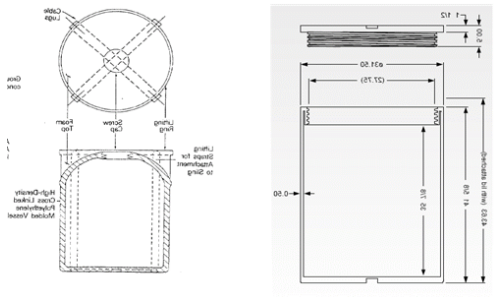

Fig. 1. PE-HIC model [2].

2.3.2 Rebar Concrete Container. The container body is cylindrical shaped made of rebar concrete. High density polyethylene is fixing to protect the corrosion protection coating during loading, handling and transportation.

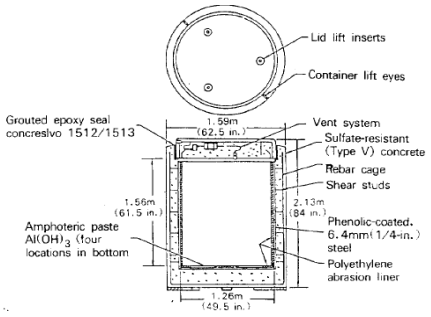

Fig. 2. Rebar Concrete HIC model [3].

2.3.3 Overpacking HIC. The main material is rebar concrete, which is strong mechanical strength and low permeability properties. The metallic fiber is added as a reinforcing materials. It is cylindrical and cubical type, and has various sizes such as height 1.2-5 m and diameter 0.84-4 m. The wall thickness is 20-30 cm.

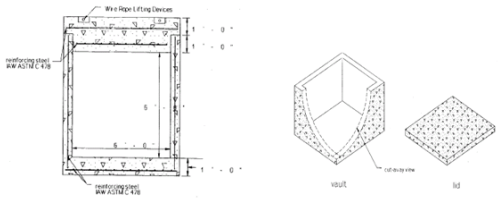

Fig. 3. Overpacking HIC model [4].

3. Conclusion

Various HICs, including PE-HIC, and rebar concrete HIC are discussed in this paper. Since the HIC allows high safety and integrity, it seems that the demand for HIC is increasing when considering waste acceptance criteria.

In consideration of disposal safety and economic feasibility, it is necessary to dispose of high-dose waste resin and concentrated liquid waste in a timely manner by proving the long-term integrity of domestically developed HIC or internationally commercialized HIC.

The detailed safety analysis will be followed including structural analysis using computer code, material radiation resistivity, and shielding property.

REFERENCES

[1] Luc Marlet High Performance Fibre Reinforced Concrete Containers (2004).

[2] RWE NUKEM, Products and Services.

[3] Kim, Technical Status of HIC, KAERI (1993).

[4] W.S. Josephson, High Integrity Container Evaluation for Solid Waste Disposal Burial Containers, Westinghouse Hanford Company.

Leaching Behavior of Two Waste Glass Forms (Iodine-Tellurite and Rhenium-Tellurite) Under Radioactive Waste Repository Conditions

Samiratu Atibun Isa*, Jaeeun Kang, Jueun Kim, Sangsu Park, HyunJu Kim, Cheong Won Lee, Jae-Young Pyo, Jong Heo, and Wooyong Um
Pohang University of Science and Technology, 77, Cheongam-ro, Nam-gu, Pohang-si, Gyeongsangbuk-do, Republic of Korea
*mirasey2019@postech.ac.kr

1. Introduction

Understanding of the glass dissolution is important in determining the behavior of nuclear waste glass forms for safe long-term disposal in geological repositories. The aim of this study was to investigate the leachability of two waste glass forms, Rhenium-Tellurite (Re-Te) and Iodine-Tellurite (I-Te) glass for evaluating their sustainability inside radioactive waste repositories using Materials Characterization Center (MCC-1) and Single-Pass Flow-Through (SPFT) standard leaching test methods.

2. Method

2.1 Glass preparation

I-Te glass was prepared by mixing powders of TeO_2 (41.29wt %), Ag_2O (25.69 wt %), Bi_2O_3 (11.33 wt %) and AgI (21.69 wt %) (with purities > 99%). Similarly, Re-Te glass was prepared by weighing and mixing powders of TeO_2 (74.047 wt %), Al_2O_3 (8.131 wt %), B_2O_3 (5.047wt %), Na_2O (2.908 wt %), CaO (3.466 wt %), and K $(ReO_4)_2$(6.40wt %) powders. X-ray fluorescence spectrometer was used to analyze the glass compositions quantitatively [1, 2]. Synthetic groundwater based on Gyeongju repository groundwater was prepared and used as leachate for both tests in this study.

2.2 Dissolution tests

MCC-1 static leach test was conducted at 90°C for 28 days. Re-Te and I-Te monolith (surface area of 400mm^2 each) glass samples were prepared and used. Solution samples (10 ml each) were collected at 3, 7, 14, and 28 days for analysis using ICP-MS. Measured pH and EC were 8.75-8.96 and 0.3-0.5 mScm^{-1}, respectively for the collected solutions. The SPFT test is an ongoing long-term leaching test in close reaction vessels at 70°C. Re-Te monolith glass (surface area of 449 mm^2) and I-Te monolith glass (surface area of 443.5 mm^2) samples were prepared and used. The filtered samples from the reaction cell's output solutions (50 ml each) were collected at 2h intervals for 12h, then 1, 3, 5, 7, 14, 21, 30 days and analyzed using ICP-MS. Measured pH and EC were 8.0-8.6 and 0.4-0.5 mScm^{-1}, respectively for the collected solutions. The test was performed in duplicates and the average was taken. Mass of the collected output solutions will be used to calculate the flowrate (q) and nominal glass dissolution rate (r) using equation (1) below. This will explain further the leachability of the two glasses with respect to their surface area.

$$rate = \frac{[C_i(i) - C_i^\circ] \cdot \left(\frac{F}{S^\circ}\right)}{f_i} \quad (1)$$

3. Results and Discussion

3.1 MCC-1 leach test

As seen in Fig. 1 and 2, a normalized linear increase in Te concentrations for both glasses with time was observed. The target radionuclides, I and Re showed a low release into solution (as low as 0.009 and 7.308 gm^{-3}, respectively). Other elements were very low except Na and Ca in Re-Te glass. The leachate composition also might have contributed to high releases of Na and Ca. [3, 4].

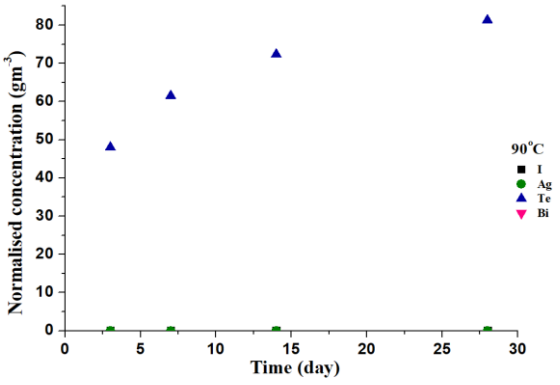

Fig. 1. Normalized concentrations of dissolved components in solution at 90°C for Iodine-tellurite glass.

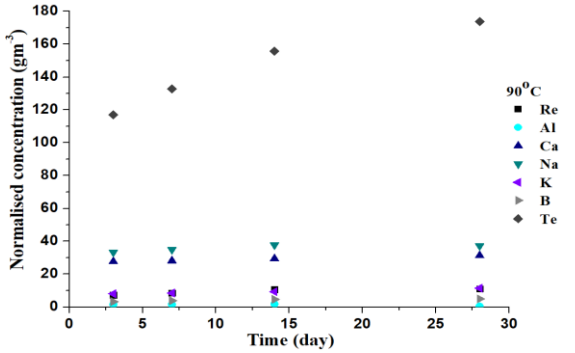

Fig. 2. Normalized concentrations of dissolved glass components in solution at 90°C for Rhenium-tellurite glass.

3.2 SPFT Leach test

As seen in Fig. 3, a normalized linear increase in Te concentration with time (up to 14 days) was observed but decreased after 15 days. Sudden increase in iodine concentration (0.552 gm^{-3}) at day14 could be due to error from ICP analysis as the measured iodine concentration before and after day 14 were significantly different.

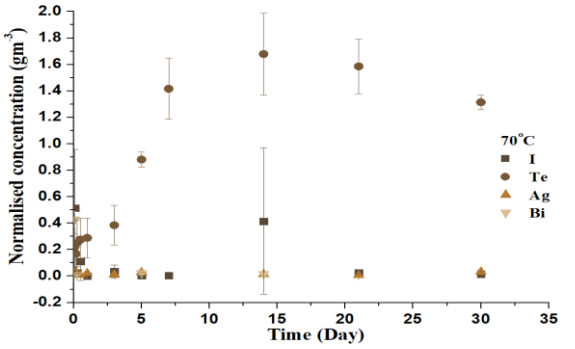

Fig. 3. Normalized concentrations of dissolved components as a function of time at 70°C for Iodine-tellurite glass.

In Fig. 4, an initial increase of Te release at 1 day was observed followed by a steady decrease. Re release was very minimal and steady with time (as low as 0.032 to 0.044 gm^{-3}), whereas other elements were very high except B and Al

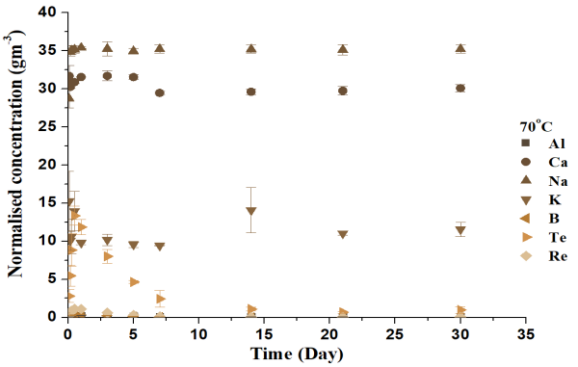

Fig. 4. Normalized concentrations of dissolved components as a function of time at 70°C for Rhenium-tellurite glass.

4. Conclusion

MCC-1 and SPFT test were conducted to evaluate the leachability of Iodine-tellurite and Rhenium-tellurite glasses. A low steady release of I and Re was observed, whiles Te release increased with time only at the early stage of leaching in both glasses. This observation could be due to the wash-off process for Te at the surface layer of glass exposed to the leaching solution with time and the effect of freshly exposed glass surfaces from sample preparation (sawing) [3]. These low I and Re releases in both tests indicate that they are well immobilized in the glass network formed [1, 2]. The dissolution rate of components in glass will be also calculated to give more insights to the glass leaching behavior for the long-term storage.

Acknowledgement

This research was supported by the National Research Foundation of Korea (NRF) grant funded by the Korean government. (NRF-2018M2A7A1074894).

References

[1] J.Y. Pyo, C.W. Lee, H.S. Park, J.H. Yang, W Um, and J. Heo, “Tellurite glasses for vitrification of technetium-99 from pyrochemical processing”, Journal of Nuclear Materials, 493, pp.1-5 (2017).

[2] Lee, C.W., Pyo, J.Y., Park, H.S., Yang, J.H. and Heo, J., “Immobilization and bonding scheme of radioactive iodine-129 in silver tellurite glass”, Journal of Nuclear Materials, 492, pp.239-243 (2017).

[3] J. J. Neeway, R. M. Asmussen, E. A Cordova, C. E. Lonergan, B. D. Williams, I. I. Leavy, and E. M. McElroy, “FY2017 ILAW Glass Corrosion Testing with the Single-Pass Flow-Through Method”, Pacific Northwest National Lab. (PNNL), Richland, WA (United States), No. PNNL-27098 (2018).

[4] D. M. Strachan, “Results from long-term use of the MCC-1 static leach test method." Nuclear and Chemical Waste Management 4, no. 2, pp.177-188 (1983).

Stabilization of UF_6 in KAERI : Focused on D-UF_6 Sampling

YuJeong Choi*, Jongjin Kim, Jeong-Guk Kim, and Dae-Seok Hong
Korea Atomic Energy Research Institute, 111, Daedeok-daero 989beon-gil, Yuseong-gu, Daejeon, Republic of Korea
*choiyj@kaeri.re.kr

1. Introduction

KAERI adopted UF_6 from United States on 1980s for research purpose. Some of UF_6 were used for experiments and lefts are stored as Depleted UF_6 (D-UF_6) form in Neutron Science Auxiliary Building. Total quantity of stored D-UF_6 are 185tons in 15 units of 48Y cylinders and a 30 inch cylinder. For longer and safer storage, KAERI will de-convert UF_6 into more stabilized form UO_2.

1st phase of sampling process design was finish last August. The following 2nd phase detailed design will be started in this October (5 month projects, plan). In this phase, material balance and detail of equipment will be discussed.

2. UF_6 stabilization

2.1 The Characteristic of UF_6

General characteristic of UF_6 is shown in the following phase diagram (Fig.1). UF_6 is solid colorless crystalline mass at 1.0 atm and room temperature [1]. When the temperature increased over 56.5°C, it becomes gaseous state and unstable to store. UF_6 is low specific activity material itself [1]. However, when it reacts with water in the air, it generates HF (Fluoric acid, Eq. 1). HF is weak acid (pKa 3.2) but highly corrosive and chemical toxic material that can cause lung inflammation, vomiting and etcs [2]. It can corrode cylinder and release uranium compounds (UF_6, HF, UO_2F_2) into the atmosphere.

$$UF_6 + 2H_2O \rightarrow UO_2F_2 + 4HF \qquad (1)$$

Therefore, KAERI will de-convert D-UF_6 into UO_2 more suitable form for long term storage.

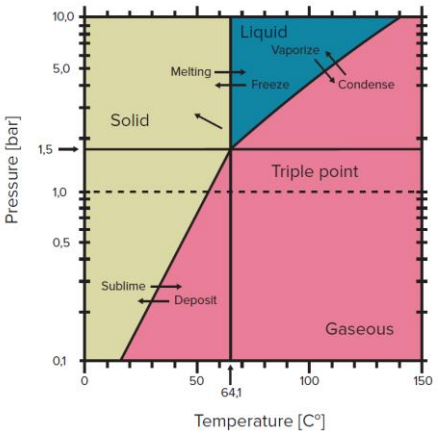

Fig. 1. Phase diagram of UF6 [1].

2.2 Sampling

The D-UF_6 sampling method suggested in this paper is based on phase change of UF_6 depending on temperature [1]. Sampling system will be installed at UF_6 cylinder storage, i.e., the Neutron Science Auxiliary Building and used for drawing small amounts of sample from each cylinders. The details of sampling process are shown in Fig.2.

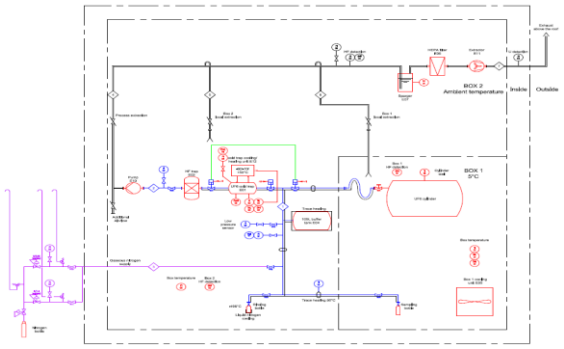

Fig. 2. Schematic diagram of D-UF_6 sampling [4].

The rough processes are as following.

- Pumping the contents of the cylinder plenum to a buffer tank. The gases extracted are composed of UF_6, HF and air (mainly N_2 and O_2).
- Trap the UF_6 in a cold trap and the HF in an aluminum oxide trap.
- Transfer the trapped UF_6 to a sampling bottle,[1]

The moist air will react with UF_6 as following reaction:

$$UF_6 + 2H_2O \rightarrow UO_2F_2 + 4HF \qquad (2)$$

In the HF trap, the aluminum oxide will capture the HF contained in the flow as following reaction:

$$Al_2O_3 + 6HF \rightarrow 2AlF_3 + 3H_2O \qquad (3)$$

The residual HF from the vents will be captured in the sparger E07 with sodium carbonate as following reaction:

$$Na_2CO_3 + 2HF \rightarrow 2NaF + CO_2 + H_2O \qquad (4)$$

3. Conclusion

KAERI is willing to manage the 17 cylinders UF_6 form to stable form as U_3O_8 in ORANO sites. To confirm the acceptance of transport and such cylinders de-conversion in Orano Cycle Plant, the sampling will be operated under regulatory body's permission [5].

REFERENCES

[1] WNTI, Fact Sheet Uranium Hexafluoride (UF6), [online access: https://www.wnti.co.uk /media/76713/WNTI%20%20FS%20UF6% 20-%20FINAL%20FINAL%205%208%2015% 20-JK%20approved.pdf].

[2] Massoud Mohsendokht, Risk assessment of uranium hexafluoride release from a uranium conversion facility by using a fuzzy approach, Journal off Loss Prevention in the Process Industries (2017).

[3] J. MALBOS, ORANO Projects GA 1277_ENG_Rev.C-02.18 KAERI- Detailed Design SYSTEM Description, ORANO (2019).

[4] M. Michel, SH 102004010001A KAERI Detailed Design PID, ORANO (2019).

[5] Services contract between Korea Atomic Energy Research Institute & Orano cycle, 2019 [confidential].

[1] J. MALBOS, ORANO Projects GA 1277_ENG_Rev.C-02.18 KAERI- Detailed Design SYSTEM Description, ORANO ,2019, p.8

Co^{60} & Eu^{152} Removal From Dissolved Concrete Liquor: Initial Precipitation Studies

Richard I. Foster*, Maengkyo Oh, Kwang-Wook Kim, and Keunyoung Lee
Korea Atomic Energy Research Institute, 111, Daedeok-daero 989beon-gil, Yuseong-gu, Daejeon, Republic of Korea
*rifoster@kaeri.re.kr

1. Introduction

Concrete is the main building material used for the construction of nuclear power plants and other nuclear related facilities. Large volumes of concrete wastes containing low levels of radioactivity are generated from decommissioning activities of nuclear power stations and require appropriate waste management strategies.[1] Wet chemical processes offer one possible approach, yet, often generate secondary wastewaters of considerable volume which require further treatment. A treatment option already widely used and understood for wastewater treatment is precipitation followed by coagulation-flocculation before either sedimentation or filtration.

We have assessed the effectiveness of such an approach for the removal of cobalt and europium from dissolved concrete liquors (DCL); synthetic of real concrete wastes generated during wet chemical treatment processes. In this preliminary study we have assessed precipitation with appropriate separation methods for treatment of DCL.

2. Experiment

2.1 Method

Active and non-active simulant DCLs were prepared. Both were studied independently.

Approx. 100 mL of liquor was placed into a beaker along with a magnetic stirrer bar. The solution pH was adjusted by the addition of NaOH (5 M, 1 M or 0.1 M) with a target screening range of between 3 – 11. Adjustments were made under fast mixing conditions (240 rpm). Once the required pH was reached the liquor was separated via centrifuge. The separated supernatant was then filtered through a 0.22 μm syringe filter before being returned to the beaker. The procedure was repeated until a final pH > 11 was reached prompting the precipitation of Ca.

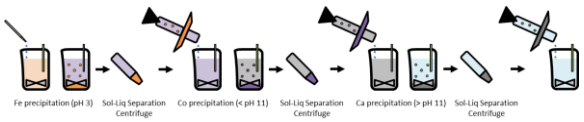

Fig. 1. Experimental procedure.

3. Results and discussion

3.1 Non-active DCL

The major component of DCL is calcium, found to be at a concentration of ≥ 10,000 ppm (mg/L). The isolated removal of Co and Eu (either together or separate) from Ca potentially offers a large volume reduction of radioactive waste requiring disposal.

Precipitation of Eu, Co and Ca were confirmed to occur at pH 6, 8 and > 11, respectively. In the case of Eu and Co substantial removal of both contaminants occurred before pH 10 with Ca

precipitation beginning at pH 11, thus a target pH of 10 is suitable for the separation of Eu and Co from Ca.

The removal of Al, Fe and Si occur prior to pH 10 and are likely to aid in the removal of Eu and Co by co-precipitation or a surface adsorption mechanism.

3.2 Active DCL

Initial active tests confirmed the removal of Co^{60} and Eu^{152} independent of calcium is possible by pH controlled precipitation and filtration. Adjustment to pH 10 affords a removal percentage of 99.8 %, corresponding to a DF of over 500 for Co^{60}.

Table 1. Removal of Co^{60} from DCL

Contaminant / pH	[Co^{60}] Concentration (Bq/mL)	[Co^{60}] Removal (%)
Initial (pH 0)	3.890	-
pH 3	3.023	22.3
pH 10	0.007	99.8
pH 13	N.D	100.0

4. Conclusions

Initial precipitation studies indicate that it is possible to separate both Eu and Co from Ca found in DCL. Further trials are required with for process optimization with particular focus on suitable solid-liquid separation, waste immobilization and disposal.

REFERENCES

[1] K. Y. Lee et al., “Trend in Technology Development for Radioactive Concrete Waste”, J. Nucl. Fuel Cycle Waste Technol., 16, 93-105 (2018).

Removal of Antimony From Effluents Generated During the Korean SENSEI Process: Iron Precipitation & Coagulation-Flocculation-Filtration Studies

Richard I. Foster*, Maengkyo Oh, Kwang-Wook Kim, and Keunyoung Lee
Korea Atomic Energy Research Institute, 111, Daedeok-daero 989beon-gil, Yuseong-gu, Daejeon, Republic of Korea
*rifoster@kaeri.re.kr

1. Introduction

The Selective Extraction of Non-radioactive Species, Encapsulation and Immobilization (SENSEI) process for the volume reduction of a spent uranium-antimony catalyst has recently been proposed.[1] Targeted removal of the uranium component has been confirmed thus eliminating the radiological hazard. However, a significant concentration of environmentally toxic antimony (Sb) remains in the process effluent. Such is the toxicity of Sb that permissible Sb concentrations in drinking water have been set by many of the worlds regulatory bodies including the World Health Organization (5 ppb). Release limits for industrial effluents are also in force. A limit of 0.2 mg L^{-1} (0.2 ppm) has been set in Korea.

In water Sb(III) is stable under reducing conditions while Sb(V) is stable under oxidizing conditions. Antimony is present in the catalyst in the +3 oxidation state.[2] However, the SENSEI process is oxic [1], thus, it is likely that the chemistry of antimony in the effluent is predominated by Sb(V) and not Sb(III). Following treatment of the catalyst the remaining effluent contains upto 50 mg L^{-1} antimony and requires final treatment before release.

Precipitation and coagulation-flocculation followed by either sedimentation and/or filtration have been considered for antimony removal. Commonly aluminum, iron or calcium based coagulants are employed however it has been shown that aluminum is ineffective for Sb removal while the kinetics of calcium removal are prohibitively slow. This therefore leaves iron coagulants, the most common of which being ferric chloride ($FeCl_3$), as the focus of this study for antimony removal. We have looked into the ability to remove Sb from effluents in which initial Sb concentrations far exceeds the 0.2 mg L^{-1} release limit. By considering dosage, pH, precipitation kinetics and interfering ions we have assessed the feasibility of iron chloride addition for the removal of antimony from effluents stemming from the SENSEI process for the volume reduction of the uranium-antimony spent catalyst.

2. Experiment

2.1 Method

Working solutions of Sb(III) and Sb(V) (50 mg L^{-1}) in chloride and sulfate media (0.5 M) were prepared and used throughout. Ferric chloride was dosed in range between 0 and 10 mg L^{-1}. Phosphate was also dosed $[PO_4^{3-}]/[Sb] = 0.5 – 10$ in selected experiments. Dosing was performed under fast mixing conditions (240 rpm). The solution pH was adjusted by the addition of NaOH (5 M, 1 M or 0.1 M) with a target screening range of between 3 – 11. Mixing was reduced to slow mixing (60 rpm) for 15 minutes to induced coagulation-flocculation. Antimony concentrations were analyzed via ICP-OES and removal percentages determined. Solution turbidity was measured using HI 98703 Hanna instruments turbidity meter and pH measurements using Orion star A215 pH meter – Ross Ultra pH/ATC Triode Electrode 8157BNUMD.

3. Results and discussion

3.1 pH Screen

Addition of $FeCl_3$ (10 mM) has a large effect on Sb removal (Figure 1). Sb(III) is removed to below release limit from Cl and SO_4 media. Sb(III) removal from SO_4 media occurs over a wide pH range (pH = 4 – 10). Sb(V) removal from Cl media similar trend to Sb(III) removal; But the pH window for optimal removal is narrower by 1 – 2 pH units (pH = 4 – 7). Sb(V) removal from SO_4 media is poor failing to reach the release limit at any pH (Figure 2).

3.2 Iron Dosage

The removal of both Sb(III) and Sb(V) is improved by an increase of $FeCl_3$ dose. Sb(III) at an initial concentration of 50 mg L^{-1} requires an [Fe] of ≥ 8 mM equivalent to an [Fe]/[Sb(III)] ≥ 20. Sb(III) removal from chloride or sulfate media follows the same trend. Sb(V) removal is also improved by an increase in [Fe] but required higher concentrations. Sb(V) removal from sulfate significantly poorer requiring iron dosages far in excess of 10 mM.

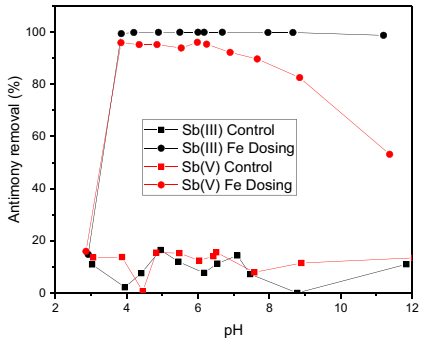

Fig. 1. Percentage removal of antimony from sulfate media with and without iron dosing.

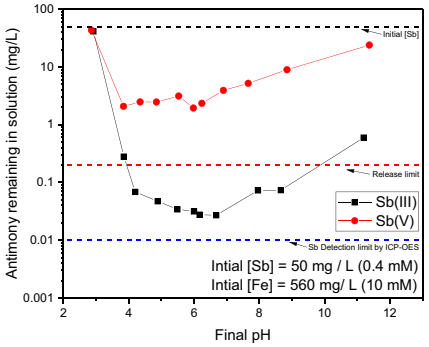

Fig. 2. Remaining antimony concentration in sulfate media as a function of pH.

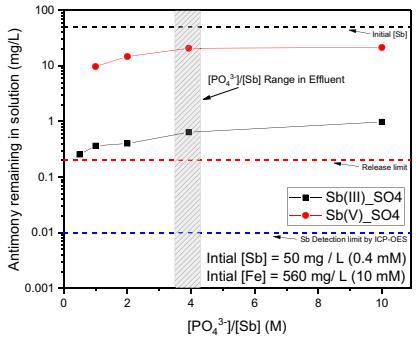

Fig. 3. Remaining antimony concentration in the presence of phosphate (sulfate media).

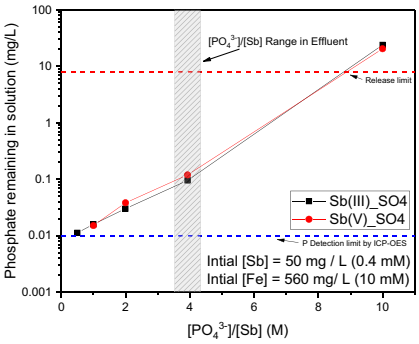

Fig. 4. Remaining phosphate concentration in the presence of phosphate (sulfate media).

3.3 Kinetics

The formation of iron precipitates occurs rapidly at pH 5.0 regardless of media (confirmed visually). Sb(III) removal occurs rapidly from both chloride or sulfate media with removal under 5 minutes. Sb(V) removal also occurs rapidly from both media. Sb(V) removal from sulfate media fails to reach the release limit even after 1 hour reaction time.

3.4 Phosphate dosage

Removal of both Sb(III) and Sb(V) are hindered by the presence of PO_4^{3-}. Sb(V) removal is significantly affected by phosphate vs Sb(III). The PO_4^{3-} anion competes with $Sb(OH)_6^-$ anion for surface binding sites through an inner-sphere binding mechanism, thus reducing the Sb removal efficiency.

Removal of excess [PO_4^{3-}] is effective with a [Fe] dose of 10 mM. Removal of upto 3 mM [PO_4^{3-}] ([PO_4^{3-}]/[Sb] = 8) can be achieved without additional iron. [PO_4^{3-}] is expected to be approximately 1.6 mM.

4. Conclusions

Addition of ferric chloride has a significant impact on antimony removal. Removal of Sb(III) is possible from both Cl and SO_4 media (pH = 5.0, [Fe] = > 10 mM, ΔT = 5 minutes). Removal of Sb(V) is possible from Cl media only (pH = 5.0, [Fe] = > 10 mM, ΔT = 5 minutes). Removal of Sb(V) from SO_4 media is only possible at significantly higher ferric dosages. Phosphate significantly affects Sb(V) removal from both chloride and sulfate media. Simultaneous Sb & P removal is possible but requires significant iron doses due to competition for surface binding sites.

REFERENCES

[1] K. W. Kim et al., 2018. “Development of a treatment process and immobilization method for the volume reduction of uranium-bearing spent catalyst for final disposal”, J. Nuc. Sci. & Tech., 1516578.

[2] K. W. Kim et al., “Glass-ceramic composite wasteform to immobilize and stabilize a uranium-bearing waste generated from treatment of a spent uranium catalyst”, J. Nuc. Mater., 516, 238-246.

Development of Hazardous Chemicals Treatment Technology in Radiation Management Area

Jeongsu Jeong*, Sunghoon Hong, and Mi-Hyun Lee

KHNP Central Research Institute, 70, Yuseong-daero 1312beon-gil, Yuseong-gu, Daejeon, Republic of Korea

*happytiger13@khnp.co.kr

1. Introduction

Among radioactive wastes generated by nuclear power plants, the amount of untreated radioactive wastes that are not suitable for disposal delivery is increasing. The disposal of radioactive wastes and storage space in the plant are required.

Hazardous chemical wastes generated in radiation controlled area are chemically hazardous to human health and/or the environment and need to be developed to ensure the safety of treatment/disposal and minimize waste generation.

In this study, we would like to develop a technology to treat hazardous wastes stored in radiation controlled area by applying plasma thermal decomposition technology.

2. Waste types subject to treatment

Hazardous chemicals stored in nuclear power plant radiation controlled area are generated during structural inspection and facility maintenance. The representative species of them are organic/ fluorocarbons, sodium triphosphate, cleaning agents, and grease.

It also has various characteristics such as oxidation, ignitability, and flammability, so processing is necessary through development of separate treatment technologies.

Fig. 1. Fluorescence Waste (left), Sodium triphosphate (right).

Fig. 2. Gypsum (left), Grease (right).

3. Hazardous chemical treatment technology

Various methods are applied for the disposal of hazardous chemicals, but incineration techniques are most commonly applied. The incineration is a combustion method that uses air to process temperatures between 700 ~ 1,100 °C.

Alternative technologies are being developed/ applied as many harmful environmental pollutants(such as NOx. CO) are generated during processing.

Melting technology using plasma is a technology that can handle the physical

characteristics of radioactive wastes (solid, liquid) without distinction, and the target waste is hotly degraded/ molten at a temperature of 1,600 °C. Create a solid substance suitable for disposal. In addition, waste preprocessing is unnecessary and facilities can be constructed with a small amount of mobility.

4. Design of Plasma Torch System Mockup

Considering the type of waste stored in the nuclear power plant radiation management zone, the amount of storage and the installation/ operating space of the plasma melt facility. It is designed with plasma torch and power supply facilities for waste thermal decomposition and melting, as well as exhaust treatment facilities for removal of radioactive materials and environmental pollutants (NOx, SOx, CO and HCl). The molten furnace processing capacity is 10-20 kg/h, and the torch is an airtight type that allows continuous operation for up to 1,000 hours and prevents external leakage of exhaust gas and is composed of modular types that are easy to disassemble and move.

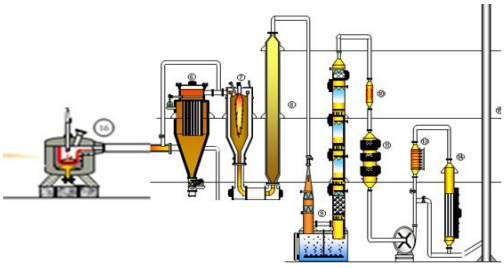

Fig. 3. Plasma Torch Melting System.

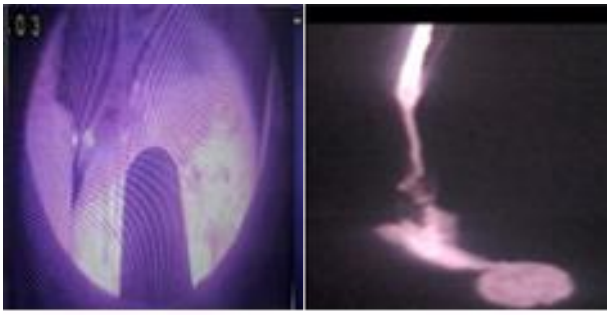

Fig. 4. Plasma melting (left), Pouring (right).

5. Conclusion

The plasma melting technology enables significant reduction and stabilization of radioactive wastes. It is also believe that the technology attributes to the secure of waste storage space and minimization of environment harmness.

REFERENCES

[1] Mi.Hyun Lee, Hyun.Je Cho “Development of Plasma Melter for Melting & Volume Reduction” (2018).

[2] Dong Wha Park “Decomposition Chlorinated Methane by Thermal Plasma” (2007).

[3] H.S Hong “ Development of arc plasma for removal of high concentration VOCs” (2017).

An Analysis on Waste Treatment Research Trend for Designing a New Rad Waste Treatment Facility

San Chae*, Jongjin Kim, Jeong-Guk Kim, and Dae-Seok Hong

Korea Atomic Energy Research Institute, 111, Daedeok-daero 989beon-gil, Yuseong-gu, Daejeon, Republic of Korea

*schae@kaeri.re.kr

1. Introduction

A radioactive waste generated during the operation of research institute was organized various forms of liquid, solid, gaseous and multiphase waste streams with different physical and chemical characteristics. A number of conditioning technologies of various waste forms were identified for treatment of waste. However, despite recognized international research, there are still many challenges in institutional radioactive waste management, only cement solidification technology is widely used in the world until now. Because cement has economic feasibility that it applies for LILW (Low and Intermediate Level Waste).

The Korea Atomic Energy Research Institute (KAERI) will design the new radioactive waste volume reduction facility (tentative name) for effective management technique of the various radioactive wastes produced from the institute. Within this paper, therefore, a literature survey was performed for designing the new facility.

2. Waste Condition Technology

Selection of a solidification/stabilization form depends on the physical and chemical characteristics of the radioactive waste and the acceptance criteria for the storage and disposal facilities. The main features and limitations of conditioning technologies are summarized in Table 1. And additional details are shown in following sections.

Table 1. Features of wasteforms

	Features	Limitations
Glass	- proven to liquid HLW - high reliability - high durability - small volume	- high initial cost - not economical for LILW - limited experience
Ceramics	- possible to actinides - more stable and durable than glass - suitable for long term isolation	- limited experience - no economical verification
GCM's	- High waste loading - high stability	- limited experience
Cements	- Already widely used for LILW - low cost - high radiation stability	- increase of volume - low retention of some fission products - poor compatibility
Bitumen	- Already widely used for LILW - high waste loading - high flexibility	- high temperature process - low fire resistance

2.1 Glass (vitrification) and Glass composite materials

Vitrification is one of the immobilization techniques for high-level radioactive waste. In vitrification process, radioactive waste can be converted to bulk glass blocks for long term

storage and waste volume is reduced to about 1/3 of the original volume. The glass form waste is durable for thousands of year, relatively cheap and good mechanical properties, nevertheless, these glasses are not ideal at this time for immobilization. One of the limitations is that it doesn't have economical to apply to LILW.

2.2 Ceramics

Most widely studied ceramics as S/S waste form are titanate-based ceramic. These materials as waste form are more stable and hence are more durable than glass. Therefore, it can be expected to be suitable for long term isolation since it simulates natural rocks. However, it cannot be generally verified economical for LLW and ILW, because S/S equipment by using ceramics is not present commercial installations in operation.

2.3 Cements and bitumen

Cements and bitumen are mostly used for variety of LLW and ILW due to high flexibility, high radiation stability, impact and fire resistance. And these are proven economic for waste form.

2.4 Other conditioning materials

Other waste conditioning materials are metals and glass-ceramic material. Each of these techniques has drawbacks; in particular. It can be difficult to find appropriate composition and process to apply current situation. In other words, these techniques have a limitation until now.

3. Conclusion

In a nuclear facility, Needs for waste treatment facility increase due to numerous generation of waste during the operation time. Therefore, KAERI is designing the new waste treatment facility, a finding of appropriate waste conditioning technologies of LLW and ILW is important.

REFERENCES

[1] Neslihan Yanikomer et al., "New Solidification Materials in Nuclear Waste Management", International Journal of Engineering Technologies, 2, 76-82 (2016).

[2] IAEA-TECDOC-1817, "Selection of Technical Solution for the Management of Radioactive Waste", IAEA, 2017.

Review on the Treatment and Disposal of Long-Term Decayed High-Dose Spent Filter in Nuclear Power Plant

Hang-Rae Cho* and Sung-Hoon Hong
KHNP Central Research Institute, 70, Yuseong-daero 1312beon-gil, Yuseong-gu, Daejeon, Republic of Korea
*hrcho6795@khnp.co.kr

1. Introduction

Kori nuclear power plant Unit 1, whose permanent shutdown had been decided in June 2017 after 40 years of commercial operation, is scheduled to be dismantled from June 2022.

For a smooth decommissioning project, a timely treatment and disposal plan for untreated radioactive waste generated during operation and stored for a long time should be established.

The spent filters generated form the reactor coolant system and the spent fuel purification system are stored in dedicated storage areas such as preliminary filter room according to the policy of post-decay treatment due to high radioactivity.

Therefore, we have sought a way to develop a remote control robot system that safely draws out the stored filters and sorts them by dose group. In addition we have reviewed the method to secure disposal suitability after packing them with reduced volume through ultra-high pressure compression.

2. Storage status

The surface dose measured at the generation of the Kori Unit 1 spent filters ranged from 0.03 to 800 mSv/hr and averaged 15 mSv/hr. According to the dose distribution of the spent filters, as shown in the Fig. 1, the RCP Seal Injection filter accounted for 91%, and above 2, RC filter (38%), Cavity filter (24%), and RCP seal injection filter (20%) occupies most of it.

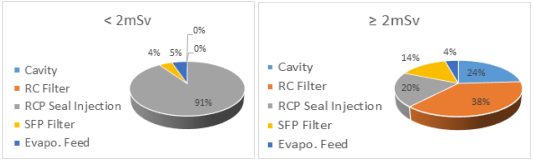

Fig. 1. Spent filter distribution by dose rate.

The quantity of each dose group is similar at 52% and 48% as shown Fig. 2 (left) for less than 2 mSv/hr and more than 2 mSv/hr, respectively. In addition, the distribution by filter type according to the storage location is as shown in the Fig. 2 (right). The RCP seal injection filter is the most stored as 63% in the filter room.

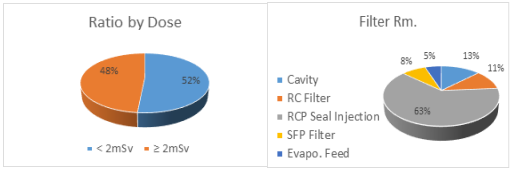

Fig. 2. Spent filter ratio by dose (left) and storage (right).

The spent filter is in the form of a cartridge as shown in the Fig. 3, and the materials of the structure and the media are STS304 and Glass fiber, respectively.

Fig. 3. RCP seal injection (left) & RC filter (right).

In the past, spent filters were treated by cement solidification to steel or concrete drums as shown in the Table 1.

Table 1. Spent filter treatment status [1]

Type	Quantity(drum)	Remark
Cement solidification	1,018	200 L
Cement solidification	176	320 L
Concrete drum (C2)	10	Hanul NPP 1
Concrete drum (C4)	506	Hanul NPP 1

3. Treatment strategy

3.1 Development of a robot system

In order to treat high-dose spent filters, they must be safely and efficiently withdrawn from storage with a robot arm like as Fig. 4 while minimizing the worker's radiation exposure. In a high-radiation environment, a remote control

robot system with 4th industrial technology that can take out and handle spent filters on behalf of an operator will be needed.

Therefore, investigation of domestic and foreign special environmental robot technology and field conditions and collection of opinions from experts and field workers will be need to establish a concept design for excellent field applicability that include a method and level of remote control for taking out spent filters and measuring the radiation dose, and sorting them by dose.

Based on the concept design, it is possible to develop an algorithm for drawing out, handling the spent filters and measuring doses of them.

Fig. 4. Concept of robot arm.

Overseas, remote robotic systems are being developed that can access hazardous areas such as highly radioactive areas. One example is the OCRobotics snake-arm robot in the UK, where various utilities such as dosimeter, camera, gripper can be installed [2].

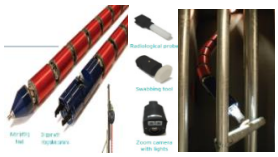

Fig. 5. OCRobotics Snake-arm robot.

3.2 Compression and packing

In order to meet the waste treatment, transportation and disposal criteria of the spent filters, it is necessary to study the method to secure a proper volume reduction ratio and filling ratio in drum considering the compression ratio and radiation dose.

Fig. 6. Shield drum (left) and compactor (right) [3].

3.3 Evaluation of radioisotope inventory

It is necessary to evaluate the radioisotope inventory of each drum in order to dispose drums filled with compressed spent filters to satisfy fill rates and surface doses.

It is necessary to secure a reliable radioisotope inventory and a demonstration of disposal suitability, which can be recognized by waste disposal agency and regulatory agency such as gamma nuclide analysis with drum nuclide analyzer and radioactivity evaluation of difficult-to-measure nuclide with scale factor.

4. Conclusion

Radioactive waste generated during operation, such as high-dose spent filters, should be disposed of in a timely manner for the smooth dismantling of Kori Unit 1.

Therefore, a special robot system should be developed that can safely take out the spent filters and measure the radiation dose, and sort by dose. In addition, it will be necessary to secure an ultra-high pressure compression system that can compress the spent filters with compression vessels of various sizes according to the dose in conjunction with the robot system and various shielding drums that can accommodate the compressed spent filter bundles at various sizes.

These technologies will contribute not only to the timely disposal of the Kori Unit1 spent filters, but also to the advancement of the treatment technology for high radioactive spent filter in preparation for the sequential dismantling of NPPs with design life according to the energy conversion policy.

REFERENCES

[1] K. I. Jeong, et al., Prediction of radionuclide Inventory for the Low-and Intermeddiate-Level Radioactive Waste Disposal facility by the Radioactive Waste Classification, JNFCWT (2016).

[2] OCRobotics, www.ocrobotics.com (2012).

[3] Westinghouse Electric Company, www.westinghousenuclear.com (2017).

Shielding Evaluation of 860L PC-HIC for Packaging of Concentrated Liquid Waste

Jong-seon Jeon[1,*], Hong-goo Lee[1], Jong-Min Park[2], Ki-Ho Park[3], and Byung-Yoon Min[1]

[1]Kyelim Co.,Ltd, 66, Gangnam-daero 30-gil, Seocho-gu, Seoul, Republic of Korea

[2]Korea Hydro and Nuclear Power, 696-13, Donghaean-ro, Yangnam-myeon, Gyeongju-si, Gyeongsangbuk-do, Republic of Korea

[3]Soosan ENS, 10, Bamgogae-ro 1-gil, Gangnam-gu, Seoul, Republic of Korea

[*]jsjeon@polycon.co.kr

1. Introduction

Concentrated liquid waste generated during the operation of a nuclear power plant is intended to be packed and disposed of in Polymer Concrete-High Integrity Container (PC-HIC) for disposal according to requirements. Shielding evaluation of the container was performed to ensure that the packaging and disposal requirements for the radioactive waste were met.

For shielding evaluation of PC-HIC, dose constraint of the surface dose rate was confirmed and evaluation methodology was established. MCNP computational model was created and shielding evaluation was performed. Verification test was performed using Ir-192 isotope(point source).

2. Shielding Evaluation of PC-HIC

2.1 Acceptance Criteria

Transport dose constraint is follow to the Nuclear Safety Commission regulations 2019-7 Article 22 (14).

- Surface dose rate of container is less than 2 mSv/hr, exclusive use is less than 10 mSv/hr.

2.2 Evaluation Methodology

The shielding of the PC-HIC is mainly performed by the container body and the upper container cover. Shielding evaluation was performed using MCNP code (v2.5). Evaluation of the maximum dose rate at each weak point was performed by computer simulation. To verify the shielding evaluation of modeling, the shielding performance test result was obtained using the point source and the computational modeling results were corrected.

2.3 Radiation Source

Source term was used as radioactivity of the concentrated liquid waste below 10 mSv/hr of the surface dose rate of the Hanul power plant. The Specific activities of major nuclides are shown in Table 1.

According to the design, the concentrated liquid waste loading capacity of the container is 8.17E+05 cm^3 and density of the concentrated liquid waste is 0.969 g/cm^3. The resulting waste weighs 7.92E+05 g.

2.4 Shielding Performance Test

Ir-192 source was used as a radiation source for shielding performance test. The radioactivity of the source used for the test was 1.74 Ci.

Table 1. Activity of concentrated liquid waste

Nuclides	Specific Activity [Bq/g]	Activity [TBq]
Co-58	6.73E+03	5.33E-03
Co-60	2.18E+04	1.72E-02
Cs-137	1.80E+03	1.42E-03
Nb-94	6.43E+00	5.09E-06

2.5 MCNP Modeling

The source of concentrated liquid waste should be redefined as a gamma source to be applied to the computational model. Gamma-ray energy and emission fractions of gamma-emitting nuclides contained in radioactive waste differ depending on the nuclide. The weight and nuclide fraction of the concentrated liquid waste were calculated. The gamma source term in the actual container was calculated. This is converted into a form for use in computer modeling.[1] Gamma radioactivity in concentrated liquid waste is 2.40E+10 Bq.

2.6 Material and Container Structure

PC-HIC consist of a metal shell, a high-density polyethylene(HDPE) inner shell, and a polymer concrete forming an intermediate body.

Geometry of MCNP computer model reconstructed based on the drawing of the 860L PC-HIC is shown in Fig. 1.

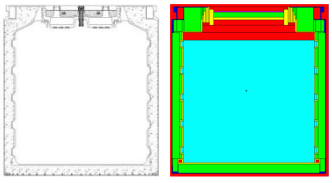

Fig. 1. PC-HIC and MCNP model structure.

2.7 Shielding Dose Calculation

After the flux of the measurement position was calculated in the MCNP code, dose was calculated using Flux-to-Dose Rate Conversion Factors (ICRP-74)[2]. Dose is shown in Fig. 2.

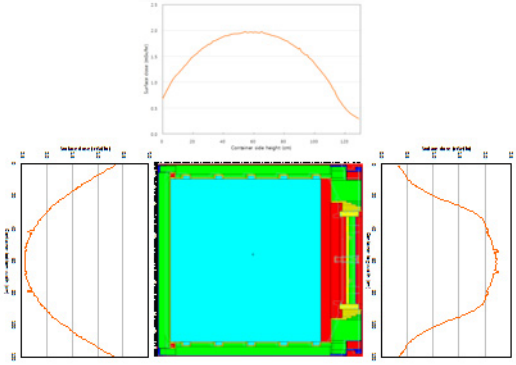

Fig. 2. Results of the shielding evaluation.

3. Conclusion

The Surface doses rates of the concentrated liquid waste PC-HIC, which was calculated through the derivation of the correction coefficient and MCNP computational modeling, were 0.33 to 2.26 mSv/hr in cover, 0.66 to 2.43 mSv/hr in bottom, and 0.30 to 1.97 mSv/hr in vertical section.

REFERENCES

[1] Los Alamos National Laboratory, MCNPX User's Manual, Ver.2.5 (2005).

[2] ICRP, Conversion Coefficients for Use in Radiological Protection Against External Radiation, ICRP-74 (1996).

Treatment System of Clearance Waste at KAERI

Won Hyuk Jang*, MalGoBalGaeBitNaLa Yoo, Tae Su Song, Joone Hee Lee, Jeong Guk Kim, and Dae Seok Hong
Korea Atomic Energy Research Institute, 111, Daedeok-daero 989beon-gil, Yuseong-gu, Daejeon, Republic of Korea
*whjang@kaeri.re.kr

1. Introduction

As a result of self-inspection, clearance waste of about 1,000 ton has been founded in nuclear & radiation facility, RI laboratory and radwaste storage facility at KAERI.

In order to treat these wastes, RMC (Radwaste Management Center) was organized for integrated managing and treating operational waste, clearance waste and decommissioning waste.

Waste treatment process have to be dealt with in accordance with internal manual of KAERI, legislation and guides of regulatory body.

2. Background

2.1 Overview

Most clearance wastes are stored at radwaste storage facility and managed under RMC control. The other clearance waste stored in nuclear & radiation facility and RI laboratory has been treated by waste generating division until now. But waste treatment process is very complex and need a lot of technical knowledge, IRM (Integrated Radwaste Management team) supports the clearance waste treatment following the treatment process of clearance waste (Fig. 1.). Although main agent of clearance waste treatment is a waste generating division because of evaluation system, treatment budget and so on, IRM supports most process.

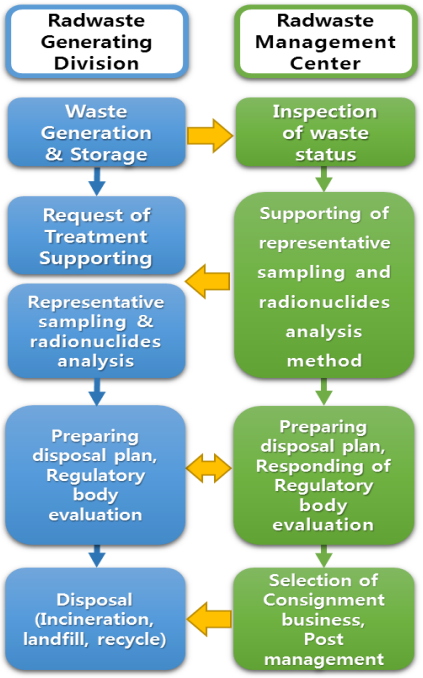

Fig. 1. Treatment process of clearance waste at KAERI.

2.2 Organization for clearance waste treatment

RMC was organized for integrated managing and treating operational waste, clearance waste and decommissioning waste at KAERI. IRM was especially organized for supporting reducing of waste generation division (Fig. 2.).

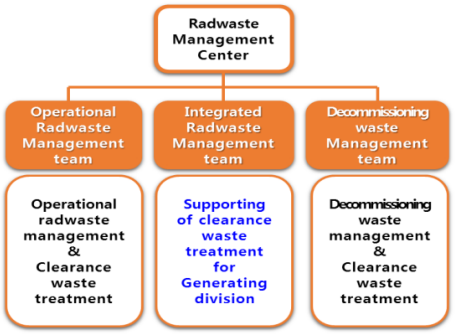

Fig. 2. Organization chart for clearance waste treatment.

2.3 Definition of a new term for clearance waste management

To efficiently manage radwaste, we definite a new term, ‘clearance waste (expected)’. It means that radwaste is managed in radiation controlled area but has a very low surface contamination or surface radiation dose rate, so it could be treat as clearance waste (expected) (Fig. 3.).

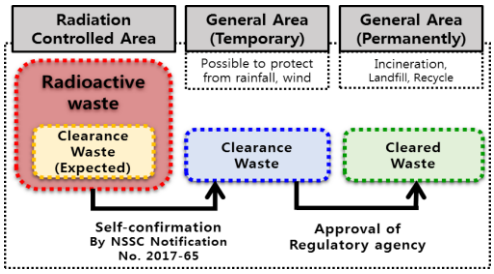

Fig. 3. Relation chart for clearance waste treatment.

3. Clearance waste treatment system

Waste treatment process have to be dealt with in accordance with internal manual of KAERI and notification No. 2017-65 of NSSC (Nuclear Safety and Security Commission) [1].

3.1 Examination of waste generic information

Waste generic information is very important to start treatment process. We ask information such as expected & permitted radionuclides of waste generating facility or laboratory, management period since the waste generation for evaluating possibility of treatment.

3.2 Representative sampling scheme & radionuclides analysis

We’re going to develop a proper representative sampling and radionuclides analysis scheme with radiochemical analysis team considering waste type, size and distribution of contaminated radionuclides.

3.3 Preparing for disposal plan & responding for regulatory body evaluation

We support preparing a disposal plan included waste generation history, representative sampling method, radionuclides analysis results and assessment results of radiation dose. We also support responding for questions during evaluation by regulatory body.

3.4 Management of clearance waste storage facility

Clearance waste storage facility was constructed in 2018. The waste identified as clearance waste under notification No. 2017-65 of NSSC could be stored in clearance waste storage facility until approval of regulatory body.

4. Conclusion

In order to safely treat clearance waste (expected), proper treatment process and specialized organization are necessary. And cooperation of many division is needed for developing of representative sampling and analysis method.

We continuously have contact with waste generating division and are proceeding with work for treatment under the regulation. We are trying to decrease clearance waste stored at KAERI through expanding treatment capability and diversification of treatment method.

REFERENCES

[1] Nuclear Safety and Security Commission, “Regulation of radwaste classification and regulatory clearance standard”, Notification No. 2017-65.

Expansion of Deregulation System for Very Low-Level Waste (VLLW)

Jeong-Guk Kim*, Won Hyuk Jang, MalGoBalGaeBitNaLa Yoo, and Dae-Seok Hong
Korea Atomic Energy Research Institute, 111, Daedeok-daero 989beon-gil, Yuseong-gu, Daejeon, Republic of Korea
*jungkim@kaeri.re.kr

1. Introduction

Clearance, one of the deregulation system for very low-level waste (VLLW), is the very useful system to reduce the amount of material disposed as waste, thereby reducing cost. However, if clearance criteria are not established or have too restrictive clearance level values, resources will be waste. In decommissioning, clearance criteria are also needed to determine the decommissioning endpoint (when decommissioning is finished). In this article, the IAEA recommendation for clearance will be discussed with the Korean clearance system, and then the more expansion to application also will be suggested.

2. Establishment of Radionuclide-Specific Clearance Levels Recommended by IAEA

2.1 Effects of Clearance System

Clearance system impacts on the amount of material to be disposed of and affects operators. And, inappropriate clearance criteria can result in previously-cleared material becoming the focus for further remediation [1].

Therefore, the establishment of clearance criteria and its level must be prepared with considerations of radiological background as well as relationship with waste classification scheme and disposal option [2].

2.2 Derivation of Clearance Level

Regulatory body either directly gives or approves clearance levels, according to the derivations by IAEA [3]. For the artificial radionuclides, the typical exposure situations are 1) using realistic parameters values and a dose criteria of 10 μSv/y, 2) using low probability parameter values and a dose criteria of 1 mSv/y, and 3) dose criteria to the skin of 50 mSv/y. For the naturally occurring radionuclides, worldwide distribution of activity concentration by United Nations Scientific Committee on the Effects of Atomic Radiation (UNSCEAR) [4] is based.

2.3 Application of Clearance

The procedure to apply the clearance to radioactive materials is as follows: 1) location of clearance instruments in low-background area, 2) acquisition of material history, 3) setting on clearance levels based on volumetric and surface contamination.

The clearance of porous material and the materials that are suspected to be alpha-contaminated is actually difficult. The clearance also needs to monitor for compliance with clearance criteria. To do this monitoring, measurements, collection and analysis of samples, and management system must be prepared.

3. Korean Clearance System

3.1 Regulatory Framework

Recently, Nuclear Safety and Security Commission (NSSC) revised the regulation provision, which stipulated the "Clearance Procedures and Methods of Radioactive Waste" in decree of Nuclear Safety Act, and the "Classification and Clearance Criteria of Radioactive Waste" in notice of NSSC. Radioactive waste is classified into four: high-level, medium-level, low-level and very low-level waste (VLLW). Among VLLW, the radioactive waste below clearance level can be disposed on its own, which is called stylistically 'self-disposable waste'.

3.2 Clearance Procedure

In order to dispose clearance-level waste, it is necessary to prove to meet the permissible dosage for clearance: less than 10 μSv per year for individual and less than 1 man·Sv per year for group [3]. And, it also needs to management not to mix with other radioactive wastes in controlled area until it is proved to meet the individual and collective effective dose criteria. After the proof, it can be stored in uncontrolled area. The grant for clearance is allowed by NSSC according to evaluation for the clearance procedures such as clearance strategy, waste characterization, surface contamination, proof method, clearance method, record, and the attached clearance documents. This kind waste is then cleared by one of the specified clearance methods such as landfill, incineration and recycle.

4. Summary

Clearance of radioactive material is based on trivial risk (de-minimis): 10 μSv per year for individual and 1 man·Sv per year for group. Korea has accepted IAEA's recommendation for clearance concept, and stipulated the clearance system for VLLW.

However, the Korean clearance system needs an expansion for clearance of VLLW under clearance-level. Since there is no class of exempt waste (EW), it is impossible to exempt the waste at generation stage. Especially, policy to consider any waste from a controlled area as radioactive waste makes great increase of the amount of VLLW generated. Therefore, it is also necessary to apply the EW broadly.

REFERENCES

[1] IAEA Presentation, "Concepts Exemption and Clearance", IAEA.

[2] IAEA General Safety Guide No. GSG-1, "Classification of Radioactive Waste," International Atomic Energy Agency, Vienna, 2009.

[3] IAEA Safety Standards No. GSR Part 3, "Radiation Protection and Safety of Radiation Sources: International Basic Safety Standards," International Atomic Energy Agency, Vienna, 2014.

[4] Unites Nations, Sources and Effects of Ionizing Radiation (Report to the General Assembly), Scientific Committee on the Effects of Atomic Radiation (UNSCEAR), UN, New York, 2000.

A Preliminary Study on the Availability of Big Data for Isotopic Scaling Factor Effect on Radioactive Waste Storage Drum

Seung Uk Yoo* and Chang Je Park
Sejong University, 209, Neungdong-ro, Gwangjin-gu, Seoul, Republic of Korea
*yooswok@sju.ac.kr

1. Introduction

Scaling factor is introduced to define the quantity of difficult to measure (DTM) radioactive nuclides in the spent fuel by comparing the ratio of concentration with DTM and key (KEY) nuclides such as Co-60 and Cs-137.[1]

In this study, a test is performed by the various conditions in pressurized water reactor (PWR) for low and intermediate-level radioactive wastes. The analysis is proceeded by ORIGEN-S[2] code and ORIGEN-ARP[2] code. The results contains a huge quantity of nuclides data. In order to investigate the applicability for the big data for the scaling factors, these data are organized with R studio, which is the program compile with R code and is a widely used platform for the big data analysis recently.[3]

2. Conditions

The calculation was done by using a fuel assembly library in the ORIGEN-S code and ORIGEN-ARP code for the Westinghouse 17×17 fuel assembly of which characteristics is givne in Table 1. In this study, various conditions of enrichment and burnup were applied to the calculations such as given in Table 2.

Table 1. Characteristics of Fuel Assembly

Condition	Value
Fuel Type	Westinghouse 17×17
Weight of Uranium (MTU)	1
Cycles	3
Cooling Time (years)	30
Power Density (MW/MTU)	40.17082

Table 2. Enrichment and Burnup Conditions

Cases	Enrichment (wt%)	Burnup (MWD/MTU)
1	1.5	35000
2	1.5	40000
3	2.0	35000
4	2.0	40000
5	3.0	35000
6	3.0	40000
7	3.0	45000
8	4.0	35000
9	4.0	40000
10	4.0	45000
11	5.0	35000
12	5.0	40000
13	5.0	45000

From Ref. 4, the measured activity data from dry active waste (DAW) are tabulated and saved as input file for R code as given in Table 3. The total number of data set including calculation is 130 sets per nuclides, which means 1690 data sets for the whole cases,

3. Results

To establish the method of handling the massive data set from the dry active waste, it is calculated ~~out~~ all the data sets from the conditions above, and is compared the tendency or the data set with the reference case as provided in Table 2. By using R code and R studio, it is able to make a database much faster than before.

Table 3. Measured Scaling Factor

	VLLW	LLW
^{3}H	1.48E+00	2.41E+00
^{14}C	4.10E-02	5.81E-02
^{55}Fe	9.43E-01	1.05E+00
^{58}Co	4.98E-03	2.95E-04
^{60}Co	1.00E+00	1.00E+00
^{59}Ni	7.82E-02	1.27E-01
^{63}Ni	3.96E+00	3.75E+00
^{90}Sr	1.22E-02	3.89E-02
^{94}Nb	1.92E-03	2.07E-03
^{99}Tc	3.16E-01	3.27E-01
^{129}I	1.58E-04	1.78E-04
^{137}Cs	3.20E-01	3.63E-01
^{144}Ce	1.42E-01	1.08E-02
Gross Alpha	6.94E-02	6.87E-02
Total	8.37E+00	9.20E+00

After the calculations for each case, with the script with R code, the data sets are rearranged for the analysis.

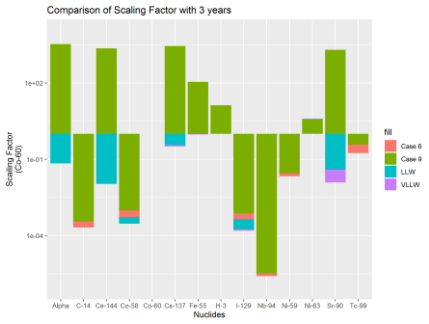

Fig. 1. Comparison of Scaling Factor with 3 years.

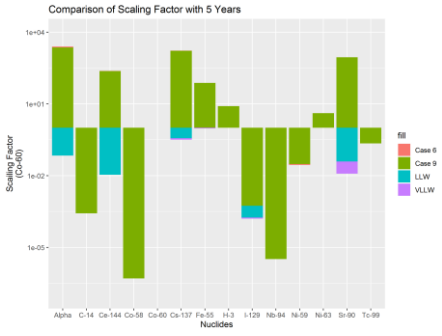

Fig. 2. Comparison of Scaling Factor with 5 years.

For the first analysis, the scaling factor change as a cooling time such as Fig. 1 for 3-year cooling and Fig. 2 for 5-year cooling, respectively.

As shown in Fig. 1 and Fig. 2, some differences are found for various isotopes because calculation results ignored the process of making DAW. From the trend analysis, the importance of waste process is recognized in this preliminary test.

4. Conclusion

By computing the data sets and drawing the graph with R studio, the time with organizing the data sets and drawing graphs were decreased. From this preliminary study on handling big data with R studio, it may be useful for the application of radioactive waste management part which treats thousands isotopes and millions burn data for different enrichments and discharge burnups, and cooling times.

REFERENCES

[1] “Determination and Use of Scaling Factors for Waste Characterization in Nuclear Power Plant”, IAEA Nuclear Energy Series, No. NW-T-1.18, 2009.

[2] S. M. Bowman, I. C. Gauld, “OrigenArp Primer: How to Perform Isotopic Depletion and Decay Calculations with SCALE/ ORIGEN”, Oak Ridge National Laboratory, April 2010.

[3] W. N. Venables, D. M. Smith, the R Core Team, “An Introduction to R”, Version 3.6.1, July 2019.

[4] Kang Il Jung, Jin Hyeong Kim, Noh Gyeom Jeong, and Jin Beak Park, “Comparison of Radionuclide Inventory Between Predicted and Measured Activity of Dry Active Waste From Korea Nuclear Power Plant”, JNFCWT Vol. 15 No.3 pp.281-289, September 2017.

Development of Candidate Porous Materials to Extract Alkanes From Liquid Radwastes

Jongjin Kim[1,*], Junhyuck Im[1], Hyungwoo Kim[2], and Donghoon Seoung[2]
[1]Korea Atomic Energy Research Institute, 111, Daedeok-daero 989beon-gil, Yuseong-gu, Daejeon, Republic of Korea
[2]Chonnam National University, 77, Yongbong-ro, Buk-gu, Gwangju, Republic of Korea
[*]jjkim@kaeri.re.kr

1. Introduction

Organic liquid radwastes produced in KAERI are temporarily stored in radioactive waste treatment facilities. About 67% of this organic hybrid waste consists of alcohol, acetone, TBP, Dodecane, etc. The best disposal option for processing organic liquid waste is incineration, but it is not easy to get approval from the government due to social issues.

In this study, polymer candidates that can selectively adsorb only organic substances in mixed solutions were selected. The surface treatment of melamine sponge was carried out to selectively adsorb organic substances using polymer candidates. Through this process, the amphiphilic melamine sponge was changed to hydrophobic properties. The experiment was performed to confirm the adsorption of organic materials selectively using the corresponding materials in water and organic solution. To understand the structure and properties of the synthesized candidates, Density Functional Theory (DFT) [1] calculation techniques and adsorption energies for common organic materials

The final goal of this study is to develop a technique for separating organic compounds and inorganic materials from organic hybrid waste liquids using microporous polymer polymers and graphene-sponge materials.

2. Method

The surface is treated with three functional groups that can selectively adsorb organic material to the sponge of melamine foam. After 12 hours of exposure to melamine foam sponge in NH4OH, 60 ° C for 12 hours, H20-EtOH treatment was used to surface the surface with two functional groups: Octyl and Fluorooctyl, Figure 1 shows a schematic of the surface treatment using functional groups.

Two coated sponges were immersed in dodecane, water, and mixed solution, and then tested for adsorption capacity for water and dodecane through mass change.

For theoretical verification, the dodecane and binding energy of each functional group were calculated using the DFT calculation.

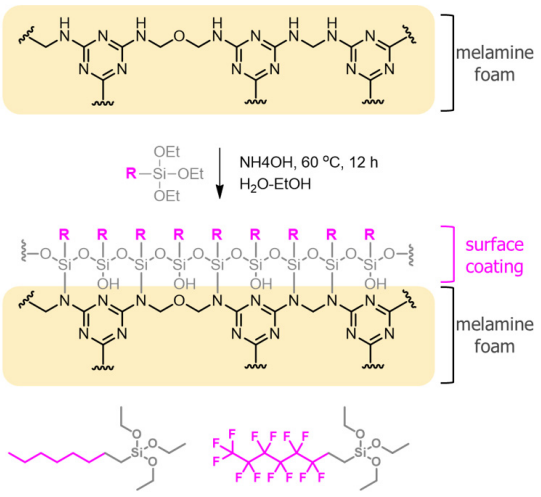

Fig. 1. Schematic of the surface treatment using functional groups.

3. Results and discussion

Figure 2 shows the weight percent changes of each surface-coated sponge in water and dodecane solution.

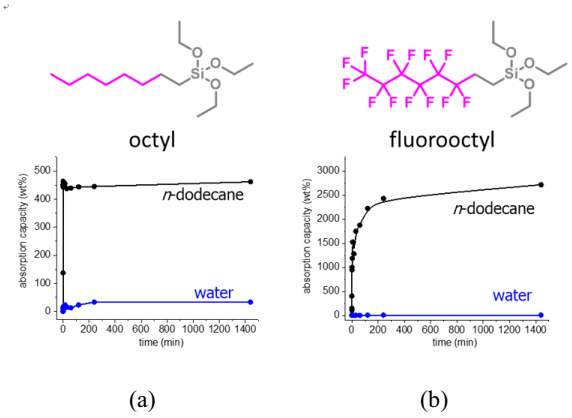

(a) (b)

Fig. 2. weight percent changes of surface-coated sponge in water and dodecane : (a) coated by octyl, (b) coated by fluorooctyl.

Both the ocyl and fluorooctyl coated sponges showed a marked increase in weight percent in the dodecane solution.

It can be seen that more dodecane is adsorbed when the melamine sponge is coated with fluorooctyl group and, in both cases, almost all adsorption was confirmed in 200 minutes.

The calculated binding energies between dodecane with octyl and fluorooctyl were summarized in Table 1.

Table 1. Binding energy between dodecane and each functional group

Functional Group		Binding Energy
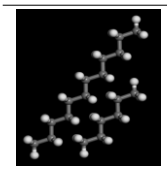	Octyl	-1.01E-2 (eV)
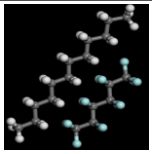	Fluoroocyl	-1.36E-2 (eV)

All calculations were calculated assuming that each molecule is located at the optimal distance between molecules. The binding energy of fl fluorooctyl was calculated to be 30% higher than that of octyl functional group. The high binding energy can be considered to be more capable of adsorption. However, since the current calculation is a simple intermolecular calculations, it must be calculated considering the multi-molecular interactions for theoretical verification, which will be further calculated.

4. Conclusion

We developed a sponge candidate material that selectively absorbs dodecane, one of the organic substances, through the surface coating of melamine sponge, and verified through theoretical calculations. We plan to continue experimenting and verifying by applying more organic materials and multi-molecules.

REFERENCES

[1] Hohenberg, P. and Kohn, W: Pysical Review B, 136, pp 864-871 (1964).

Radiological Dose Assessment for Regulatory Clearance of Soil Radioactive Waste at KAERI

Ki-Baek Shin*, Won-Hyuk Jang, Malgobalgaebitnala Yoo, Junhyuck Im, and Dae-Seok Hong
Korea Atomic Energy Research Institute, 111, Daedeok-daero 989beon-gil, Yuseong-gu, Daejeon, Republic of Korea
*kbshin@kaeri.re.kr

1. Introduction

At Korea Atomic Energy Research Institute (KAERI), nuclear facilities have generated various radwastes that have extremely low levels of radioactivity. Thus, reducing the amount of radwastes by regulatory clearance has become one of the most important task for radwaste management.

In this study, radiological dose assessment for regulatory clearance about soil radioactive waste generated from KAERI is described.

Radiological dose assessment for should be performed for regulatory clearance. And, the assessment results must meet the dose criteria set by Nuclear Safety Act of Korea (individual dose < 10 μSv/year, collective dose < 1 man×Sv/year). RESRAD-onsite code and its parameters were used for assessment. [1]

2. Generation and Analysis

2.1 Generation of Soil Radioactive Waste

About 68 tons of soil radioactive waste was generated during the construction of nuclear facility and parking lot in KAERI from 2013 to 2015. The concept of the regulatory clearance has been applied to the soil waste due to conservative disposal even though the contamination possibility of the soil waste is extremely low.

2.2 Analysis of soil Radioactive Waste

U-238 was characterized as the target nuclide because of uranium ore history. ED-XRF (Energy Dispersive X-ray Fluorescence) was used for the chemical analysis of the soil waste. And, the maximum radioactivity concentration of U-238 in the soil waste was represented (Table 1).

Table 1. Activity Concentration of Soil Radioactive Waste

Type	Nuclide	Maximum Activity [Bq/g]
Soil	U-238	7.34E-02

3. Radiological Dose Assessment

3.1 RESRAD (onsite) Code

RESRAD has been well known as a computer model designed to estimate radiation doses and risks from RESidual RADioactive materials. RESRAD has used widely by U.S. Department of Energy (DOE), U.S. Environmental Protection Agency (EPA), U.S. Nuclear Regulatory Commission (NRC), etc. for deriving limits for radionuclides in soil. [2]

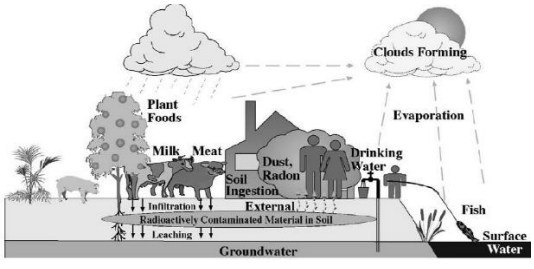

Fig. 1. Exposure pathways in RESRAD-onsite.

3.2 Major Input of Variables and Parameters

Most inputs of variables and parameters are default values. All input of variables and parameters is line with U.S. standard.

So, some of the domestic data that can be found applied to the assessment. Major input of the domestic data were represented (Table 2). [3]

Table 2. Major input of variables and parameters

Item	Value[1)] [unit]
Radionuclide transformations	ICRP 38
Internal dose library	ICRP 72
External dose library	ICRP 60
Nuclide	U-238
Concentration	0.07 [Bq/g]
Area of contaminated zone	22.67 [m^2]
Thickness of contaminated zone	2 [m]
Length parallel to aquifer flow	5.37 [m]
Cover depth	0.6 [m]
Inhalation rate	7400 [m^3/y]
Mass loading for inhalation	6.0E-6[g/m^3]
Fruit, vegetable and grain consumption	138 [kg/y]
Leafy vegetable consumption	100 [kg/y]
Milk consumption	32 [L/y]
Meat and poultry consumption	24 [kg/y]
Fish consumption	41.4 [kg/y]
Other seafood consumption	13.4 [kg/y]
Drinking water intake	138 [L/y]
Contaminated fractions	1
Livestock water intake for milk	60 [L/d]
Mass loading for foliar deposition	4.0E-4[g/m^3]
Length of growing season (Leafy)	0.17 [y]
Weathering removal constant	18 [y]

1) Adult standard

3.3 Dose Assessment Results

After a series of processes, the assessment result showed that the maximum individual dose was 7.77E-01 μSv/year and the collective dose was 1.37E-02 man·Sv/year (population standards near landfill).

4. Conclusion

There were about 68 tons of radioactive soil waste in KAERI. In this study, we have assessed the radiological dose of the soil waste using RESRAD-onsite code for regulatory clearance. In the radiological dose assessment, some codes have been adapted to the domestic situation. As a results of the assessment, the dose rate of the soil waste meet the criteria of the regulatory clearance on the Nuclear Safety Act of Korea.

REFERENCES

[1] “Nuclear Safety and Security Commission”, Notification No. 2017-65.

[2] “User’s Guide for RESRAD-Onsite Code”, Version 7.2, ANL/EVS/TM-18/1.

[3] “Development of Regulatory Requirements for Clearance of Radioactive Waste”, KINS/RR-144.

5분과

제염해체 (Oral)

Development of the Pushing Type Cutting Device to Dismantle Biological Shield Concrete for Decommissioning of Nuclear Power Plant

Bong-Jae Lee*, Yong-Kyu Kwon, Chang-Dong Hong, and Kyong-Nam Min
Sejong Engineer & Construction Co., Ltd, 23, Oncheonbuk-ro, Yuseong-gu, Daejeon, Republic of Korea
*bjlee550@naver.com

1. Introduction

The biological shield of Kori unit 1 is composed of rectangular upper part and cylindrical lower part with about 500 tons weight. In order to dismantle it safely, we have developed the pushing type equipment with isolation cover collecting dust and also cooling liquid can be supplied for the frictional heat generated by diamond wire saw. The operation of fabricated cutting device and the leakage of dust were tested.

2. Design of equipment

The wire saw of equipment wraps the front side of concrete structure and move forward for depth direction. The cutting operation can be performed by the dry method or the cooling liquid supply method. The shape of fully designed equipment is shown in Fig. 1 and Fig. 2. The cutting equipment developed in this study is divided by 6 parts. The pulley part has 7 pulleys to transfer power to diamond wire saw and controls its tension.

The various liquid can be injected through the cooling liquid supplying part. The isolation cover part has function to minimize external release of dust or sludge. The coring instrument part was installed.

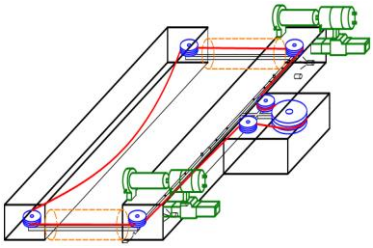

Fig. 1. External shape of the designed equipment.

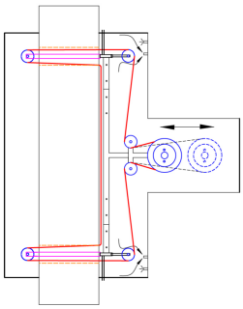

Fig. 2. Locations of 7 pulleys and diamond wire saw.

The external apparatus part was designed. Dust collected within isolation cover is accumulated into the container outside. The sludge in used liquid is cleaned through a purifier and liquid is sent to cooling liquid tank for recycle. The controller part was developed to control whole cutting process. The dry method or the moisture method can be selected through the controller.

3. Operation and dust collection test

3.1 Operation of the fabricated equipment

The fabricated equipment is installed on the concrete wall to test operation as shown Fig. 3. The pulley parts were installed on the both sides of wall. Two pulleys were inserted into two holes made by the coring instrument. The driving power suppler was used as shown Fig. 3. As a performance test result, it was confirmed that the fabricated equipment works well.

Fig. 3. The fabricated device installed on the concrete.

3.2 Leakage rate of dust

The test place was covered by 4 m width × 6 m depth × 4 m height with tents. Two air samplers were located by the certificated company as shown Fig. 4. Table 1 shows the result of test. The leakage rate of dust is about 1.7 % and the dust is collected more than 98% in total. The release of dust can be decreased more by adding other means.

Fig. 4. Inside and outside position of air samplers.

Table 1. The analysis results of dust samples.

Conditions	Results(μg/m^3)		Measuring Time	Analysis method
	Inside	Outside		
with cover	75.4	28.1	13: 30 ~ 16:00	weighting
without cover	4,4221	114.8		

4. Conclusion

It was confirm that cutting operation was carried out very well and the leakage rate of dust appeared very low also. The fabricated equipment can be set up on horizontal or vertical side of concrete structure easily. The exposure dose of workers is minimized due to adoption of pushing method. It will be utilized as a cutting apparatus for dismantling not only any various reinforced concrete structure but biological shield for decommissioning of nuclear power plant.

REFERENCES

[1] Kwang-Soo Park et al., “A Study for Dismantling Method of Bio-shield in Kori Unit 1 Nuclear Power Plant”, Proc. of the KRS 2019 Spring Conference, 17[1], May 8-10, 2019, Pusan.

Removal of Cobalt From the Radioactive Concrete Waste Using Sink-Float Separation

Seok-ju Hong, Sangsoo Han, Seongsik Nam, Won-Seok Kim, and Wooyong Um*
Pohang University of Science and Technology, 77, Cheongam-ro, Nam-gu, Pohang-si, Gyeongsangbuk-do, Republic of Korea
*wooyongum@postech.ac.kr

1. Introduction

Radioactive concrete waste now becomes one of the most important problem in the nuclear power plant's decommissioning procedure. Because of its large amount and huge volume, it should be reduced in volume through the selective decontamination process. However, selective removal of cobalt, which is one of the main radionuclides in the concrete waste, is very difficult, because the cobalt concentration in concrete waste is very low (~ppm) and the pH of the concrete waste is very high (~12).

In the concrete waste, cobalt is divided into contaminated cobalt and radiated cobalt. Among them, contaminated cobalt has been proven in our previous research that it exists in the form of a cobalt oxide after the thermal treatment. Until now, almost all of decontamination process used chemical digestion by strong acids. However, this would result in a large amount of secondary liquid waste, and the volume reduction of concrete waste cannot be achieved.

In this study, we tried to remove the cobalt from concrete waste by applying the sink-float separation process that has used in mining. The application of this process can remove not only oxide form of contaminated cobalt, but also radiated cobalt. Furthermore, because we didn't use the acids, the decontamination cost would be lower, and the volume reduction of the concrete waste can be achievable through minimizing the generation of secondary wastes.

2. Materials and Methods

2.1 Concrete preparation and thermal treatment

Concrete coupons were made with 37g of sand, 24g of aggregates, 21g of Portland cement (Type I/II), 13g of DI water, and 5g of fly ash. Cobalt nitrate hexa-hydrate ($Co(NO_3)_2 \cdot 6H_2O$) was used to contaminate the concrete coupons. From our previous study, an optimized thermal treatment condition was 550°C for 1hour. After the thermal treatment, Co phase was changed into oxide form.

2.2 Sink-float separation process

Sink-float separation is also called as heavy liquid separation. This separation is based on the density difference of two materials. Separation by density difference is spontaneous and very accurate. Thus, we don't need to give an additional process, and furthermore it doesn't matter whether the target material's concentration is low or high.

There are various types of heavy liquids. But we used sodium polytungstate (SPT) solution, because we need a heavy liquid with a density of ~3g/cm^3. SPT solution is favorable to a large-scale process, due to its non-toxic, and reusable characteristics.

2.3 Carbonation of cement paste

Before applying the sink-float separation, free Ca^{2+} ion should be minimized for preventing the formation of $CaWO_4$. Inhere, industrial CO_2 gas was used to precipitate the Ca^{2+} ion as $CaCO_3$ solid phase.

3. Results and Discussions

3.1 Contaminated cobalt removal test

After the CO_2 carbonation, concrete waste would have a lot of $CaCO_3$. Therefore, $CaSiO_3$,

$CaCO_3$, and sand (SiO_2) that are concrete were each thoroughly mixed with cobalt oxide powder to simulate the concrete waste [Fig. 1].

Although simulated concrete waste and cobalt oxide powder were mixed well, they were separated clearly [Fig. 2], because the density of $CaSiO_3$ (2.6g/cm^3) and $CaCO_3$ (2.7g/cm^3) are lower than SPT solution (3.0g/cm^3), while the CoO (6.44g/ cm^3) is much higher. Therefore, only cobalt oxide sink, and other materials could float on SPT solution.

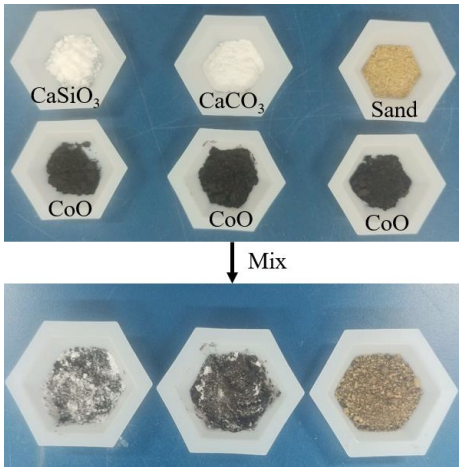

Fig. 1. Simulated cobalt-contaminated concrete waste.

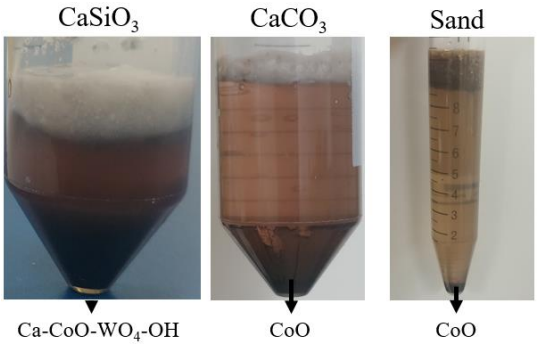

Fig. 2. Sink-float separation test with simulated waste.

3.2 Potential removal of radiated cobalt

Most of the radiated cobalt is Co-60 produced by reaction between the neutron and Co-59. Actually in nature, cobalt cannot exist as a free element. It normally exists in cobalt containing minerals with high density [Table 1]. As a result, if we can separate those minerals with sink-float separation, we also can remove radiated cobalt.

Table 1. Representative cobalt containing minerals

Mineral phase	Chemical form	Density
Cobaltite	CoAsS	6.33
Glaucodot	(Co,Fe)AsS	5.9
Linnaeite	Co_3S_4	4.8
Smaltite	$(Co,Ni,Fe)As_2$	6.5
Skutterudite	$CoAs_3$	6.5
Erythrite	$Co_3(AsO_4)_2 \cdot 8H_2O$	3.06
Safflorite	$(Co,Ni,Fe)As_2$	7.2
Cattierite	CoS_2	4.82
Spherocobaltite	$CoCO_3$	4.13

4. Conclusions

The sink-float separation method which is already proven in the mining industry has been tested to separate radioactive solid concrete waste. In addition, separation process used in mines have already proven for the large scale application. Therefore, this sink-float separation process is expected to efficiently use for separating the radioactive concrete waste generated during decommissioning and decontamination processes.

Acknowledgement

This research was supported by Advanced Nuclear Environment Research Center (ANERC) from the National Research Foundation of Korea (NRF), NRF-2017M2B2B1072374 and NRF-2017M2B2B1072404.

REFERENCES

[1] MURRAY R. GREGORY & KEITH A. JOHNSTON (1987) A nontoxic substitute for hazardous heavy liquids — aqueous sodium polytungstate ($3Na_2WO_4.9WO_3.H_2O$) solution (Note), New Zealand Journal of Geology and Geophysics, 30:3, 317-320.

Underwater Cutting of Thick Stainless Steels With High-power Fiber Lasers Aimed at Dismantling Nuclear Facilities

Jae Sung Shin*, Seong Yong Oh, Hyunmin Park, Gwon Lim, Taek-Soo Kim, Lim Lee, Chin-Man Chung, and Jonghwan Lee

Korea Atomic Energy Research Institute, 111, Daedeok-daero 989beon-gil, Yuseong-gu, Daejeon, Republic of Korea

*jsshin12@kaeri.re.kr

1. Introduction

Laser cutting has many advantages in dismantling nuclear facilities, such as ease of remote control, secondary waste reduction, and low reaction force. In particular, it is one of the most powerful tools for dismantling reactor pressure vessels and their internals in nuclear power plants. Practical application of laser cutting to dismantling of nuclear power plants requires a technique capable of cutting at least 100 mm thick for steel [1]. In addition, underwater cutting is also required. Therefore, techniques for cutting underwater as well as cutting thick steels through high-power lasers have been developed [1-6]. In the previous works, cutting in the air was possible up to 300 mm using a 30 kW fiber laser [1], while underwater laser cutting remained at less than 40 mm [2]. Recently, our group successfully made cuts of stainless steel up to 60 mm thick but needed to cut thicker steel [6].

In this work, underwater laser cutting of stainless steel thicker than 60 mm was performed, and up to 100 mm thick using 9 kW of laser power.

2. Underwater laser cutting

2.1 Experimental procedure

Figure 1 shows the views of underwater laser cutting experiment.

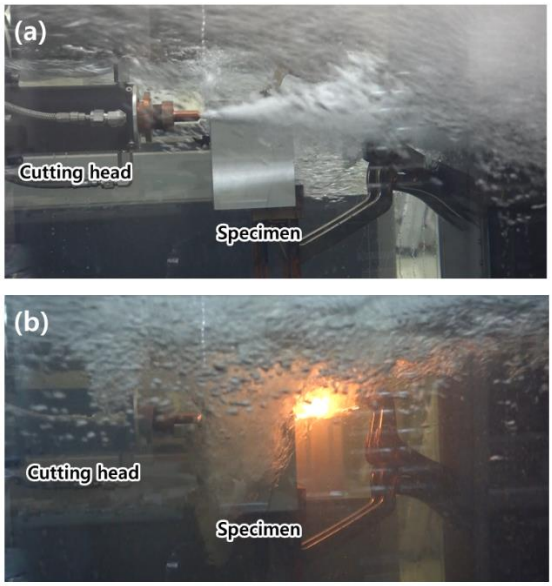

Fig. 1. Views of underwater laser cutting experiment: (a) before cutting, (b) cutting in progress.

A 6-kW level fiber laser (YLS-6000, IPG Photonics) and a 10 kW fiber laser (YLS-10000, IPG Photonics) were applied as the laser sources. The laser beam was delivered through the 20 m long process fiber and enter the cutting head. With high pressurized assist gas (compressed air), the laser cutting was started. SUS304L stainless steel plates were used as the specimens.

2.2 Results and discussions

When using 16 bar of assist gas, cutting was well up to 70 mm thick. On the other hand, in the thickness of 80 mm or more, even if the assist gas pressure was increased to 21 bar and a laser power of 9 kW was applied, the cutting was not possible. The problem was overcome with the help of a double nozzle, and cutting up to a thickness of 100 mm was successfully done.

3. Conclusion

Study on underwater laser cutting was performed aimed at dismantling nuclear facilities. With a power of 9-kW, the stainless steels were cut up to a thickness of 100 mm.

ACKNOWLEDGEMENT

This research was supported by the Nuclear Research and Development Program through the National Research Foundation of Korea (NRF), funded by the Ministry of Science and ICT (grant no.: NRF-2017M2A8A5015146), Republic of Korea.

REFERENCES

[1] K. Tamura, R. Ishigami, and R. Yamagishi, “Laser cutting of thick steel plates and simulated steel components using a 30 kW fiber laser,” Journal of Nuclear Science and Technology, 94, 244-247 (2017).

[2] P. A. Hilton, and A. Khan, “Underwater cutting using 1 μm laser source,” Journal of Laser Applications 27, 032013 (2015).

[3] C. Chagnot, G. de Dinechin, and G. Canneau, “Cutting performances with new industrial continuous wave ND:YAG high power lasers: for dismantling of former nuclear workshops, the performances of recently introduced high power continuous wave ND:YAG lasers are assessed,” Nuclear Engineering and Design, 240, 2604–2613 (2010).

[4] J. S. Shin, S. Y. Oh, H. Park, C.-M. Chung, S. Seon, T.-S. Kim, L. Lee, and J. Lee, “Laser cutting of steel plates up to 100 mm in thickness with a 6-kW fiber laser for application to dismantling of nuclear facilities,” Optics and Lasers in Engineering, 100, 98-104 (2018).

[5] J. S. Shin, S. Y. Oh, H. Park, C.-M. Chung, S. Seon, T.-S. Kim, L. Lee, and J. Lee, “Cutting performance of thick steel plates up to 150 mm in thickness and large size pipes with a 10-kW fiber laser for dismantling of nuclear facilities,” Annals of Nuclear Energy, 122, 62-68 (2018).

[6] J. S. Shin, S. Y. Oh, H. Park, T.-S. Kim, L. Lee, C.-M. Chung, J. Lee, “Underwater cutting of 50 and 60 mm thick stainless steel plates using a 6-kW fiber laser for dismantling nuclear facilities,” Optics and Laser Technology, 115, 1-8 (2019).

Introduction a Case Study for Radio-cesium Fallout Pattern for Determination of Optimum Decontamination Depth in Forest Soil

Seongjoo Kang[1,*], Minoru Yoneda[2], Seungil Kim[1], and Dukwon Kang[1]
[1]Elim-Global Co. Inc., 767, Sinsu-ro, Suji-gu, Yongin-si, Gyeonggi-do, Republic of Korea
[2]Kyoto University, Kyoto daigaku-katsura, Nishikyo-ku, Kyoto, Japan.
[*]seongjoo.kang@elim-global.com

1. Introduction

Due to the accident of the Fukushima Daiichi nuclear power plant in 2011, many radioactive materials were released and causing widespread contamination in northeastern Japan. In particular, almost 70 percent of Japan's land is made up of mountainous areas, which seriously affects the lives of timber-related industries and residents around forests. It has been reported that radioactive cesium has been strongly adsorbed to soil within 10cm of the surface layer for more than several decades since the Chernobyl accident in 1986 [2]. The release of radioactive materials into the outside of the forest ecosystem has known to be released into rivers by floating soil due to heavy rains during typhoons and monsoon rains, but less than 1 percent of the total forest inventory. At the same time, however, without artificial decontamination, it will have a serious impact on forest ecosystems and forest-based residents and forestry workers for a fairly long period of time. Therefore, it is essential to continuously monitor and observe based on site data as to where and how fast radioactive materials will be transported and accumulated in developing decontamination measures based on mid- and long-term prospects.

We are currently developing a decontamination technology based on the soil washing process as a Korea Institute of Energy Technology Evaluation and Planning (KETEP) project. To this end, we are reviewing the methodologies for the estimation of the optimal decontamination range of contaminated soils. And among them, we introduced a cesium behavior monitoring study in two types of forest soil and how radioactive cesium is distributed spatially and vertically for each location in forests near Fukushima one year and seven months after the accident.

2. Methods

2.1 Migration depth and migration rate

To calculate the migration rates of ^{137}Cs in soil, we used the migration center and the migration rate [1]. With monitored depth distribution information, Eq.1 and Eq.2, it is possible to obtain the corresponding mean migration rate. where qi is the ^{137}Cs fraction in the layer i, C_i is the activity distribution (Bq/m^2) in the layer and Ct is total activity distribution (Bq/m^2) in the soil. The mean migration depth (X, cm) is calculated using Eq. (2)

$$q_i = \frac{C_i}{C_t} \quad (1)$$

$$\sum_{k=1}^{n}(X - X_i)\, q_i = 0 \quad (2)$$

2.2 Gamma spectrometry and calculation of radioactive cesium concentrations

^{134}Cs and ^{137}Cs of soil samples were analyzed by high resolution gamma spectrometry system configured with a p-type coaxial hyper pure Ge-detector (HPGe, EG & G ORTEC). Standard geometries were used which is come from JSAC (The Japan Society for Analytical Chemistry). The detector which was properly calibrated using certified reference standards samples in the same geometry as the measured samples. All measured activities were corrected for radioactive decay between sample collection and radiation detection.

$$\varepsilon(E) = N(E)/(A \cdot P\gamma \cdot C) \times 1000(g/kg) \quad (3)$$

ε(E) = Counting efficiency
N(E) = Counting rate of E
A = Radioactivity, Bq
Pγ= Emission provability
C = Weight of Standard

$$S = 1000(g/kg) \cdot N(E) / \varepsilon(E) \cdot P\gamma \cdot m \qquad (4)$$

S = Radioactivity per weight (Bq/kg)
m = Weight of Sample (g)

3. Results

The distribution pattern of ^{137}Cs was quite varied regardless of species and geological difference. Total inventory of deciduous tree's case is more highly distributed compared to Coniferous tree.

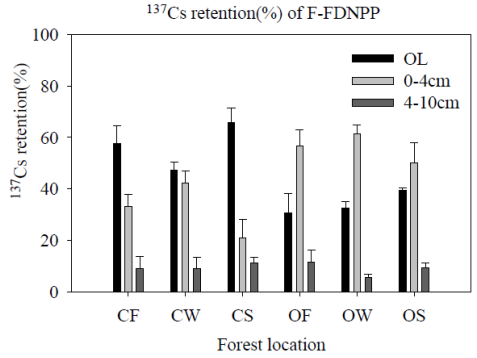

Fig. 1. ^{137}Cs retention in topsoil fallout from Fukushima nuclear power plant-derived based on ^{137}Cs inventory data.

Table 1. Migration rate and migration center of both Fukushima derived and Nuclear Weapon Test derived ^{137}Cs source after 1.6 year of Fukushima accident

Site (year)	FDNPP-Derived		NDT-Derived	
	Migration rate (cm/y-1)	Migration Center (cm)	Migration rate (cm/y-1)	Migration Center (cm)
CS (1.6y)	1.69	2.68	0.14	7.56
OS (1.6y)	1.08	1.71	0.13	7.36
MW (1.6y)	1.40	2.22	0.10	5.73

4. Conclusion

The inventory of radioactive cesium monitoring results showed that the total inventory of radio-cesium fell into the forest one year and seven months after the accident was slower to the coniferous forest than in the deciduous forest. Similar to the situation in Chernobyl, Japan also has confirmed that forests maintain an ecosystem that retains almost 85% of radioactive cesium within upper 4 cm depth. Migration rate of ^{137}Cs in soil of two species was about 10 times faster in derived from Fukushima than Nuclear Weapon Test. Based on this monitoring results, it is thought that these behavioral evaluation studies of cesium may be useful in assessing the depth calculation and behavior of contaminated soil that may occur in the event of future nuclear emergency accidents and decommissioning of Nuclear Power Plant.

Acknowledgement

This work was supported by the Korea Institute of Energy Technology Evaluation and Planning (KETEP) granted financial resource from the Ministry of Trade, Industry and Energy, Republic of Korea (No. 20181510300800).

REFERENCES

[1] Arapis, G., Petrayev, E., Shagalova, E., Zhukova, O., Sokolik, G., & Ivanova, T. (1997). Effective migration velocity of ^{137}Cs and ^{90}Sr as a function of the type of soils in Belarus. Journal of Environmental Radioactivity, 34, 171-185.

[2] Hird, A. B., Rimmer, D. L., & Livens, F. R. Factors affecting the sorption and fixation of caesium in acid organic soil. European Journal of Soil Science 1996; 47: 97-104.

Application of Gross Alpha Determination in Radioactive Waste Characterization

Hyuncheol Kim*, Mee Jang, Jong-Myoung Lim, Ji-Young Park, Ha-Jin Song,
Young-Gun Ko, and Sang-Bum Hong
Korea Atomic Energy Research Institute, 111, Daedeok-daero 989beon-gil, Yuseong-gu, Daejeon, Republic of Korea
*hckim3@kaeri.re.kr

1. Introduction

In the characterization of RW generated from nuclear facility operation and its decommissioning process, the license holder should present the level of gross alpha in RW according to nuclear safety act notice (2017-60).

Gross alpha determination is widely used, but not for quantitative analysis. In other words, the value of gross alpha in the sample is not necessarily equal to the sum of individual alpha emitters.

In this study, we presented the limitations of gross alpha for characterization of RW. The gross alpha of soil generated from the decommissioning process was analyzed. The analysis of uranium (U) in the soil was followed and, then compared with the value of gross alpha.

2. Experimental

2.1 Sample and Apparatus

The soil contaminated with U was prepared for this test. TRU resin (Eichrom, USA) was used for chemical separation U from the matrix. Gross alpha was analyzed by *S5XLB* (Canberra). The source of ^{241}Am was obtained from NIST and U from AccuStandard. The isotopic activity ratio of U was analyzed by ICP-MS (Spectro) and was 1:0.77:0.04 (^{238}U:^{235}U:^{234}U).

2.2 Determination of counting efficiency

The known activity of ^{241}Am and U was taken into the stainless steel planchet (47 mm), respectively. Ammonium bi-oxalate solution was added in the source, resulting in varying the weight of the deposit after dry. It was dried under an infrared lamp. The planchet was weighed before the addition of the radio-source and after dry. The counting efficiency was determined by following the equation: ε- counting efficiency, N_{net}- net count rate (cps), A- activity (Bq)

$$\varepsilon = \frac{N_{net}}{A} \quad (1)$$

2.3 Analysis of gross alpha and U in soil

One gram of soil sample was ashed at 450^{o}C overnight. It was utterly dissolved by alkali fusion method, then followed an extraction chromatography using TRU. Uranium was eluted with 0.1M ammonium bi-oxalate. Then an aliquot of it was taken for gross alpha determination. The analysis of U by ICP-MS was followed.

3. Result and discussion

3.1 Counting efficiency of ^{241}Am and U

Fig. 1. shows the counting efficiency of ^{241}Am and U with the amount of deposit. The counting efficiency of ^{241}Am is 1.5 times higher than that of U.

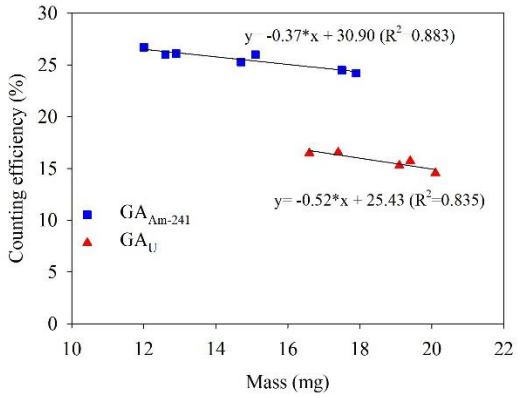

Fig. 1. Counting efficiency with mass of the deposit using ^{241}Am and U standard.

3.2 Comparison of gross alpha and U activity in soil sample

Fig. 2. shows the activity of U determined by ICP-MS (U_{ICP-MS}), the gross alpha based on the counting efficiency determined by ^{241}Am (GA_{Am-241}) and U standard solution (GA_{Ustd}), respectively. The ratio of U_{ICP-MS} and GA_{Am-241} is averagely 1.5. GA_{Am-241} was underestimated. But, the ratio of U_{ICP-MS} and GA_{Ustd} is approximately 1.1. It is resulting from the dependence of counting efficiency in gross alpha against alpha energy. ^{241}Am is widely used as a source to determine counting efficiency. If the sample contains other alpha emitters besides of ^{241}Am, gross alpha analysis could not clarify the alpha content of it as shown in Fig. 2.

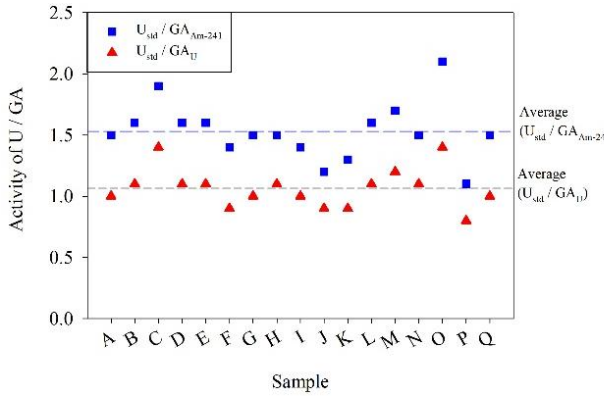

Fig. 2. Ratio of activity of U and gross alpha (GA) using ^{241}Am and U standard source.

4. Conclusion

Gross alpha is widely used for characterization of RW because it is a rapid and simple method. However, it is crucial to ensure that gross alpha analysis is not absolute determinations of alpha contents in RW. It is limited so it could not equal to the sum of individual alpha emitters. Therefore, gross alpha determination should be recommended as a just screening technique.

ACKNOWLEGDEMENT

This work was supported by the National Research Foundation of Korea (NRF) granted financial resource from the Ministry of Science, ICT and Future Planning of Korea (No. 2017M2A8A5015143).

REFERENCES

[1] ISO 10704, Water quality – Measurement of gross alpha and gross beta activity in non-saline water – Thin source deposit method.

Analytical Method for Determination of ^{41}Ca in Concrete

Yong-Jin Lee[1], Ji-Young Park[1], Jong-Myoung Lim[1], Sang-Bum Hong[1], Hyuncheol Kim[1,*], and Jin-Hong Lee[2]
[1]Korea Atomic Energy Research Institute, 111, Daedeok-daero 989beon-gil, Yuseong-gu, Daejeon, Republic of Korea
[2]Chungnam National University, 99, Daehak-ro, Yuseong-gu, Daejeon, Republic of Korea
[*]hckim3@kaeri.re.kr

1. Introduction

Characterization of radioactive waste (RW) generated from decommissioning nuclear facilities is crucial for the safety management of RW. According to nuclear safety act, 14 radionuclides(e.g., ^{3}H, ^{14}C, ^{55}Fe, ^{63}Ni, ^{59}Ni, ^{90}Sr, ^{99}Tc, ^{129}I and some gamma emitters) in RW should be clarified for the disposal. In the nuclear facilities, concrete is mainly used as core shield and its dominant element is calcium. Since ^{41}Ca, which have a long half- life over 100,000 years, is produced by neutron activation of ^{40}Ca in concrete, being like ^{55}Fe and ^{63}Ni and ^{41}Ca, it have been classified the important monitoring radionuclide in terms of the safety disposal of RW.

In this study, we presented the evaluation results of the developed analytical procedure of ^{41}Ca from concrete. It is crucial to chemically separate Ca from the sample matrix. Especially, other neutron activated radionuclides (e.g ^{55}Fe and ^{63}Ni) should be removed to avoid the overestimation in the measurement by LSC. Additionally, alkali earth metal such as ^{90}Sr and ^{140}Ba should be separated from the matrix due to its similar chemical behavior with Ca. Alkali fusion method is applied to extract Ca from the concrete sample, because acid leaching is often not able to extract neutron activated radionuclides from the matrix. Then, Ca is purified by applying consecutive precipitation based on the difference of solubility product between Ca and other interferences. We carried out the various performance tests of this method using ^{45}Ca instead of ^{41}Ca, which is generated by same mechanism.

2. Experimental

2.1 Sample and Pretreatment

ED-XRF (Xepos HE, SPECTRO) was used for the qualitative analysis of the elements in concrete. The concrete sample was completely dissolved through the alkali fusion method with 1.5 g of $LiBO_2$, 1 g of concrete sample and 0.25 g of LiBr under at 1000^{o}C.

2.2 Procedure

The initial concentration of elements in the molten sample was determined by ICP-OES. First, NaOH was added to adjust pH to 7. Fe and Ni was completely precipitated as hydroxide precipitates. The pH of the supernatant was adjusted to 10, and Na_2CO_3 was sufficiently added to precipitate alkaline-earth metals. The precipitate was dissolved with conc. HCl, and then NaOH was added to dilute the solution to 1 M NaOH. At this circumstance, only Ca in alkaline earth metals is precipitated as

hydroxide form. The separated Ca was dissolved in weak acid and measured by LSC. The precipitation process was based on the Ksp value (Table 1). The overall experimental procedure is shown in Fig. 1.

Table 1. The solubility product(Ksp) of metals with hydroxide and carbonate

	Hydroxide	Carbonate
Fe^{3+}	2.79E-39	-
Ni^{2+}	5.48E-16	-
Sr^{2+}	6.40E-03	5.60E-10
Ba^{2+}	2.55E-04	2.58E-09
Ca^{2+}	5.05E-06	3.36E-09

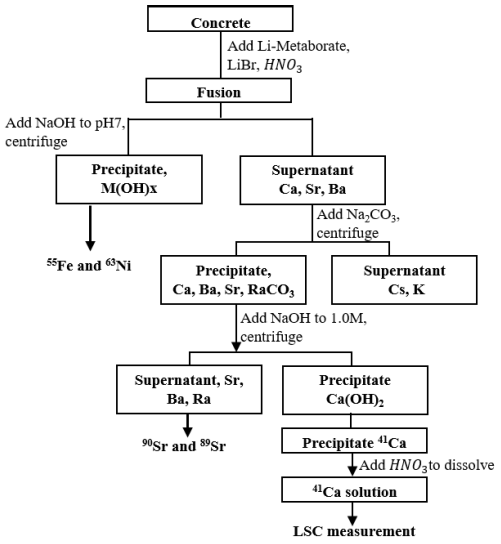

Fig. 1. Analytical procedure of Ca in concrete.

3. Result and discussion

The test using fusion blank containing Ca, Fe, Ni, Sr and Ba showed approximately 87 % for recovery of Ca. However, the test using concrete sample showed approximately 50 % through whole procedure. The loss of Ca could be attributed to the first precipitation step (pH 7) from the matrix. At this condition, silicon in the concrete sample was precipitated as silicate, and consequently some of Ca was co-precipitated with it. Other alkali earth metal such as Sr and Ba was clearly separated from Ca in the solution of 1 M NaOH, showing decontamination factor of 10^2-10^3.

4. Conclusion

The method for separation of Ca in the concrete sample need to be modified to achieve higher recovery of Ca. The modified method could be linked with the sequential separation of Fe and Ni from the same sample.

REFERENCES

[1] Xiaolin Hou, “Radiochemical analysis of radionuclides difficult to measure for waste characterization in decommissioning of nuclear facilities”, JRNCA, Vol. 273, No.1 43-48 (2007).

[2] Mee Jang, Jong Myoung Lim, Hyun Chul Kim, Chang-Jong Kim “Inventory Estimation of ^{36}Cl and ^{41}Ca in concrete of Kori Unit 1”, JNFCWT, Vol.17, No.1 121-126 (2019).

Chemical Decontamination Process for Primary Coolant System in Nuclear Facility

Jungsoon Park[1,2], Hee-Chul Eun[2], Seonbyeong Kim[2,*], So-Jin Park[1] , Changhyun Roh[2,†], and Bumkyoung Seo[2]
[1]Chungnam National University, 99, Daehak-ro, Yuseong-gu, Daejeon, Republic of Korea
[2]Korea Atomic Energy Research Institute, 111, Daedeok-daero 989beon-gil, Yuseong-gu, Daejeon, Republic of Korea
[*]sbkim@kaeri.re.kr, [†]chroh@kaeri.re.kr

1. Introduction

The nuclear power plant operates for a long-time under high temperature and pressure. And, corrosion products of Cr, Fe and Ni will be gradually generated on the inner surface of the system. The corrosion products include active elements such as Co-58 and Co-60, which cause problems of radiation field build-up and poor heat transfer efficiency. To overcome these problems, chemical decontamination of the system is important issue to use [1,2].

The decontamination is one of the most important technologies at the time of dismantling the nuclear power plant, and it can reduce worker's exposed to radiation and reuse some parts of the power plant. Therefore, decontamination techniques with excellent decontamination efficiency are steadily being developed, as the level of radioactivity may be reduced to levels not subject to regulatory application through decontamination [3].

KAERI has been developing a SP-HyBRID representing new inorganic acid based on decontamination process. This process consists of two steps of oxidation (SP) and reduction (HyBRID) [4].

In the oxidation step, the chromium oxide is dissolved to destroy the lattice, and in the reduction step, the iron oxide is dissolved to remove the oxide from the surface of the contaminated area.

A typical chemical decontamination system is HP-CORD using oxalic acid which is an organic acid. However, this system has a defect that inter-granular attack in the material after decontamination, and oxalic acid is formed at this stage, making it difficult to treat the waste water.

A general chemical decontamination system is composed of a multi-step system that undergoes oxidation and reduction step, and the oxidizing agent is regenerated and used as a reuse agent. In the case of HP-CORD, it is also regenerated by using oxalic acid [5].

However, in the conventional system, the decontamination agent after oxidation and reductive decontamination is discharged and separated into waste water, and there is a problem that massive amounts of waste water are generated while decontamination is repeated.

In this study, we developed new integrated process system such as SP-HyBRID process based on inorganic acid to complement the problems of the conventional method and seeking a method to reduce the amount of waste water generated.

2. Methods and Results

2.1 Decontamination solution

The composition of the decontamination solution, which is used for an oxidative and reductive decontamination, is shown in Table 1. The oxidation solution contains $KMnO_4$ could be triggered to the oxidation of Cr(IV) to Cr(III) from Cr oxide, and the optimal acidity was pH 2.3 adjusted by H_2SO_4 and operating condition was 95°C. The reductive solution contains N_2H_4 could be triggered to the reduction of Fe(III) to Fe(II) from Fe oxide and Cu(II) ions to facilitate the reductive dissolution. The optimal acidity was pH 3 adjusted by H_2SO_4 and operating condition was 95°C.

Table 1. The description for decontamination solution

Process	Concentration of component and experimental condition	Values
Oxidation (SP)	Volume	0.2L
	[$KMnO_4$]	6.33mM
	Temp.	95 °C
	pH	2.3
Reduction (HyBRID)	Volume	0.2 L
	[N_2H_4]	0.05 M
	[Cu(II)]	0.5 mM
	Temp.	95 °C
	pH	3

2.2 The evaluation of Cr and Fe oxide dissolution by SP-HyBRID

In order to investigate the SP-HyBRID process, a simulated oxide film composed of Cr and Fe was manufactured and decontaminated, and the results are shown in Fig. 1 and Fig. 2.

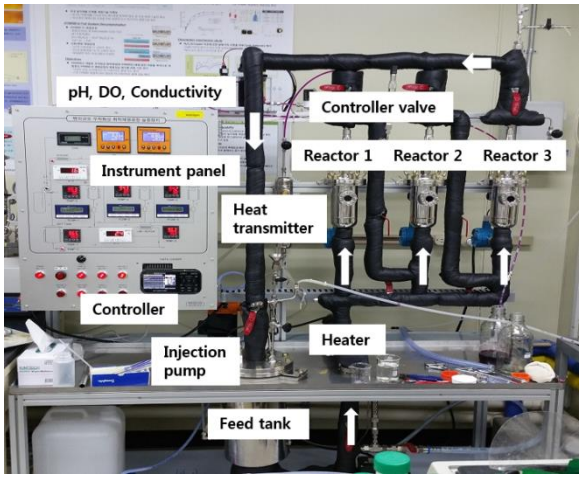

Fig. 1. Bench scale for decontamination equipment.

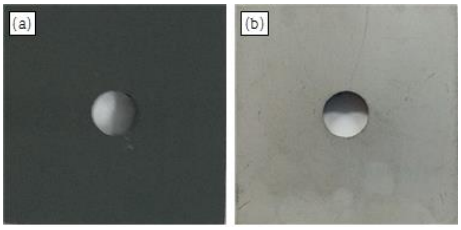

Fig. 2. Decontamination of Cr and Fe oxide film image; before (a) and after decontamination (b).

2.3 Integrated SP-HyBRID process test

An integrated decontamination process is shown to reduce the amount of waste water generated by regenerating the decontamination agent after an oxidation-reduction step different from the conventional system that treats waste water after the oxidation and reduction steps, and the results are shown in Fig. 3.

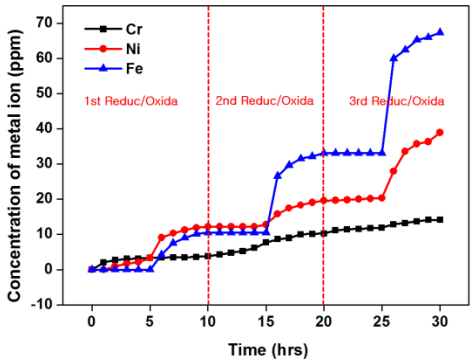

Fig. 3. Integrated decontamination performance of Cr, Fe and Ni oxide.

As a result, a total of three cycles (1cycle = oxidation and reduction step) were carried out, and the dissolution rate was 78% Cr, 96% Fe and 100% Ni. And, the possibility of integrated decontamination process could be confirmed.

3. Conclusion

The newly developed SP-HyBRID with an inorganic acid base was evaluated to complement the problems of the general system with an organic acid base. Integrated decontamination evaluation results, the volume of waste water that can be generated in the general system can be considerably reduced, and decontamination performance is also excellent. The results could be confirmed from the feasibility of the integration process.

REFERENCES

[1] R. Riess, S. Odar and J. Kysela, “Decontamination and Steam Generator Chemical Cleaning”, ANT International Krongiutarvagen 2C, SE-730. 50 Skultuna, Sweden (2009).

[2] N. Bojinov, VTT Research Report, TUO 75-056-5 (2006).

[3] J.S. Song, M.Y. Jung, S.H. Lee, “A Study on the Applicability for Primary System Decontamination through Analysis on NPP Decommission Technology and International Experoence”, Technical Paper (2016).

[4] S.B. Kim, H.J. Won, J.K. Moon, W.K. Choi, “Magnetite Dissolution using Hydrazine-Acid Solution for Chemical Decontamination”, Transactions of the American Nuclear Society, Vol 115, Las Vegas, NV, November 6–10 (2016).

[5] P. Kinnunen, “ANTIOXI Decontamination Techniques for Activity Removal in Nuclear Environments”, Research Report, VTT-R-00299-08 (2008).

Synthesis of Chalcogenide Sorbent for Cs Removal

Sangsu Park*, Jaehyuk Kang, and Wooyong Um
Pohang University of Science and Technology, 77, Cheongam-ro, Nam-gu, Pohang-si, Gyeongsangbuk-do, Republic of Korea
*pss33823012@postech.ac.kr

1. Introduction

Metal sulfide ion exchanger has been studied to selectively capture soft ions in typical ion exchange reactions. The metal sulfide materials such as $A_2Ga_2Sb_2S_7$ (A = amine based cation), KMS-1, and KMS-2 (potassium based cation exchanger) show a unique characteristic which is known as the selective capture for soft-Lewis acid cations such as Cs^+, Sr^{2+}, and Ni^{2+} retained in nuclear wastes. In addition, chalcogenide layered material MoS_2 is expected to have high adsorption affinity for soft acid cations based on Hard and Soft Acid and Base (HSAB) theory [1]. However, although these metal sulfide ion-exchanger showed high removal capacity and selectivity to Cs^+, it is hard to distinguish that the capacity and selectivity is derived from functionalized sulfur, not oxide counterparts (MoO_x), because ion exchange is strongly affected by ion size and sorbent structure.

In this study, we synthesized amorphous chalcogenide sorbent to investigate how the chalcogenide material removed the radionuclide and metal ions. The main objective was to synthesize inorganic sorbents (chalcogenide material) to remove the radionuclide and metal cations from solution wastes and understand the removal mechanism compared to oxide sorbents.

2. Experimental section

2.1 Synthesis of molybdenum sulfide chalcogenide

MoS_x was synthesized using solvothermal synthesis method using methanol with $(NH_4)_2MoS_4$. The synthesis method has advantages with leaving building blocks of chalcogenides 0.52 g of $(NH_4)_2MoS_4$ was sealed in Parr reactor (25 mL) with 10 mL of methanol and heated at 170 ˚C for 2 days. Then, black gel was obtained and washed three times using 4:1 (ethanol:DIW) solution. After centrifugation, finally obtained black powder was dried in vacuum oven at 80 ˚C for 1 day.

2.2 Cesium removal experiment

A typical adsorption experiment was carried out in a 20-mL glass vial with the total concentration of 1 ppm of Cs^+ prepared using CsCl in 10 mL of DIW and 10 mg of MoS_x added (solid to solution ratio = ~1 g/L). Subsequently, the sample mixture was completely reacted in 180 rpm of shaker. All experiments were prepared in duplicate.

Independent experiment for adsorption kinetics were carried out in advance with different times of reactions monitored at 3, 5, 10, 20, 30, 60, 120, 180, 360, and 720 min. Adsorption Isotherm was also carried out using various initial Cs^+ concentrations ranged from 1 to 400 ppm within 3 hours. All other experimental conditions were prepared and conducted equally to the typical adsorption experiment conditions mentioned above.

3. Results and Discussion

The XRD pattern of synthesized MoS_x indicates general MoS_3 crystalline pattern even though the result contains amorphous peak (Fig. 1) [2].

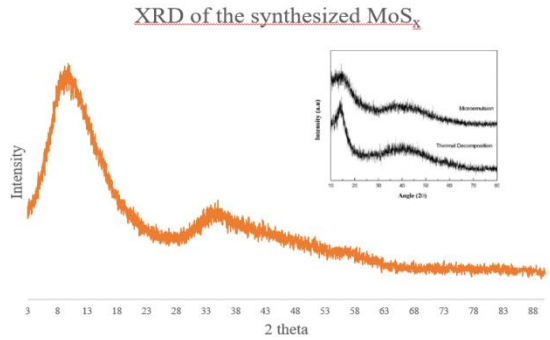

Fig. 1. XRD patterns of the synthesized chalcogenide material with reference, MoS_3.

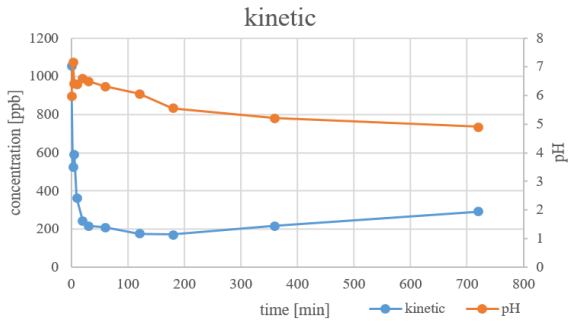

Fig. 2. Kinetic results for Cs^+ removal using MoS_x.

In the kinetic results (Fig. 2), the MoS_x indicates rapid Cs^+ removal and high removal efficiencies (about 83 %) in spite of the low solid to solution ratio (1 g/L). Especially, the maximum removal was reached at around 2-3 hours with little pH changes (from pH=6.0 at 0 min to 5.6 at 180 min).

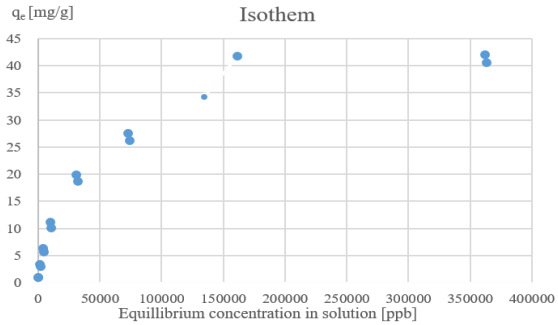

Fig. 3. Cs^+ adsorption isotherm results using MoS_x.

In the isotherm results (Fig. 3), the maximum q_e value (q_m) of the MoS_x was calculated to ~ 40 mg/g which is considerably high q_m compared with activated carbon adsorbent (~19% Cs removal with an initial concentration of 1.16 ppm at pH 7 in deionized water) [3].

4. Conclusions

The amorphous chalcogenide material, MoS_x, was synthesized and investigated for the effect of sulfide toward Cs^+ adsorption. The fast kinetic within 3 hours and relatively high adsorption capacity of MoS_x could result from the presence of sulfide on MoS_x. Although more characterization would be required, the chalcogenide sorbent can provide insight of potential use for radionuclide removal as the efficient sorbent.

ACKNOWLEDGEMENT

This work was supported by KOREA HYDRO & NUCLEAR POWER CO., LTD (No. 2017-Tech-07).

REFERENCES

[1] Zhongying Wang et al., “Removal and Recovery of Heavy Metal Ions by Two-dimensional MoS_2 Nanosheets: Performance and Mechanisms”, Environmental Science & Technology 52 (17), 9741-9748 (2018).

[2] Wang, J. et al., “Characterization of nanosize molybdenum trisulfide for lithium batteries and MoS_3 structure confirmation via electrochemistry”, Electrochemical and Solid-State Letters, 10 (9), A204-A207, (2007).

[3] S. R. H. Vanderheyden et al., “Adsorption of cesium on different types of activated carbon”, J. Radioanal. Nucl. Chem., 310, 301-310 (2016).

5분과

제염해체 (Poster)

Magnetic Separation of ^{133}Cs-illite From Soil Using Surface Functionalized Fe_3O_4 Nanoparticles

June-Hyun Kim[1,2], Sung-Man Kim[2], In-Ho Yoon[2], and Ilgook Kim[2,*]

[1] Kyungpook National University, 80, Daehak-ro, Buk-gu, Daegu, Republic of Korea

[2] Korea Atomic Energy Research Institute, 111, Daedeok-daero 989beon-gil, Yuseong-gu, Daejeon, Republic of Korea

*ilgook@kaeri.re.kr

1. Introduction

After the Fukushima accident, the surrounding soil of Fukushima was severely contaminated by radioactive Cs. Once released to soil, Cs isotopes have accumulated at the top-5 cm soil because of their strong affinity with clay minerals in soil. It is well known that the clay minerals have highly selective sorption for Cs because of their large specific surface area, high charge density, and presence of frayed edge site. In particular, micaceous phyllosilicate minerals such as illite, which have high selectivity and irreversible adsorption property toward Cs due to frayed edge site. In order to reduce the volume of contaminated soil, therefore, it is desirable to effectively separate clay from soil. In the present work, we used cationic magnetic nanoparticles (MNPs) for the selective separation of Cs-contaminated from soil. Because the surface charge of clay minerals is negative, the cationic MNPs can selectively adsorb onto clay [1]. The surface-modified magnetic nanoparticles (MNPs) by polyethylenimine (PEI) which is known for its high density of positive charge, were used to separate clay having a negative charge. Also, illite was selected because of its aforementioned highly selective and irreversible Cs sorption.

2. Materials and methods

2.1 Separation of illite from solution

The PEI-coated MNPs were mixed with different mass ratio (0.005:1, 0.01:1, 0.05:1, 0.1:1, 0.2:1, 0.4:1, 0.8:1, and 1:1 MNPs·g/clay·g) of ^{133}Cs-illite (0.029 mmol·Cs/g·illite). After mixing, the PEI-coated MNPs-illite complexes were separated from solution by permanent magnet for 10 min. Separation efficiency (SE%) of ^{133}Cs-illite from solution was calculated using SE% =100% - (m_f/m_0 × 100%), where m_0 is the initial clay mass in the suspension and m_f is the final clay mass in the solution.

2.2 Selective separation of illite from soil

The ^{133}Cs-illite was mixed with surrounding soil (0.038~2 ㎜ soil) in DI water. The PEI-coated MNPs were mixed with the soil mixture at a 0.05 g·PEI-coated MNPs/g·illite mass ratio for 10 min. After separation, magnetic soil with PEI-coated MNPs was separated from non-magnetic soil by magnetic separation. The particle size distribution of each soil fraction was analyzed by a wet sieving method. The samples were divided into 5 distributions: sand (2.0-0.5, 0.5-0.2, and 0.2-0.075 mm), silt (0.075-0.038), and silt-clay (<0.038 mm).

3. Results and discussion

3.1 Separation of illite from solution

Fig. 2 indicates that the separation efficiency (SE%) of clay minerals increased with the increase of the mass ratio between the PEI-MNPs and illite. When the mass ratio of PEI-coated MNPs to ILT was 0.04 g/g, the maximum SE was 100%. Thus, the PEI coating enhanced the adhesion between MNPs and clay mineral due to the functional amine groups that

are available for adsorbing negatively charged clay minerals. Also, Fig. 1c shows that the PEI-coated MNPs easily separated illite from solution within 60 s in a magnetic field.

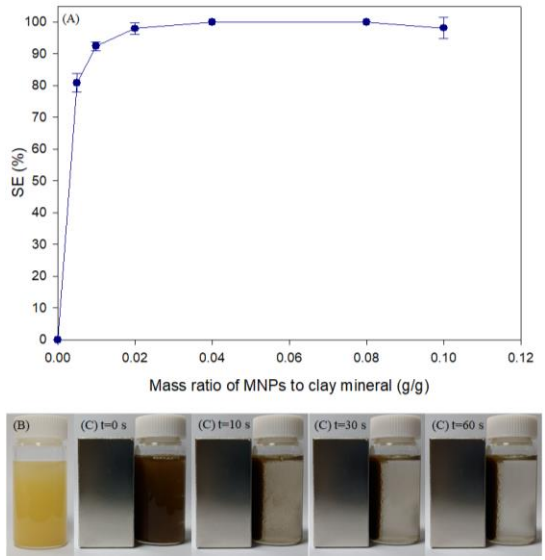

Fig. 1. (a) separation efficiency of illite with different mass ratios of MNPs to illite at pH 7, and photographs of (b) illite in solution and (c) magnetic separation of the PEI-coated MNPs-illite complexes at the different time (0 to 60 s).

3.2 Selective separation of clay from soil

The raw soil has 12.6% of silt- and clay-sized soil particles (< 0.038 mm), showing a predominance of the sand-sized fraction (0.075-2 mm) with 83.9%. In the magnetic soil fraction, the soil particles below 0.038 mm represented the largest proportion of 84.3%, whereas it exhibits low fraction with 1.7% in the non-magnetic soil. These results indicate that the PEI-coated MNPs can be selectively separate clays including silt sized fine particles even in the presence of a large amount of sand, at a low dose and without pH control.

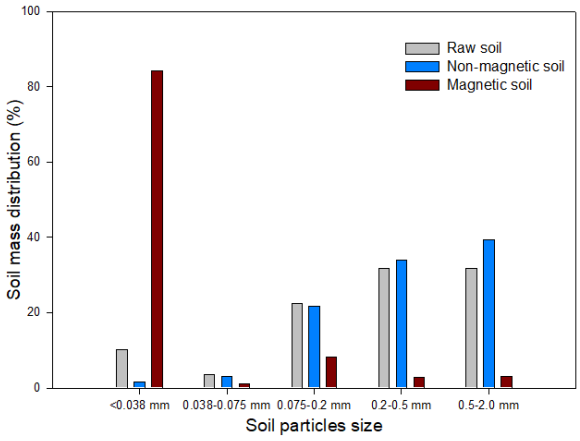

Fig. 2. Particle size distribution of raw soil, non-magnetic and magnetic soil.

4. Conclusion

The PEI-coated MNPs enabled the highly selective separation of clay at their low dose without pH control. After magnetic separation of clay from soil, the particle size distribution showed that the clay- and silt-sized soil particles (< 0.038 mm) represented the largest proportion in the magnetic soil, suggesting the fine particles were successfully separated in magnetic fraction. Hence, the PEI-coated MNPs with magnetic separation provide a promising method for efficient separation of clay minerals.

ACKNOWLEDGEMENT

This work was supported by a National Research Foundation of Korea (NRF) grant funded by the Korean government (Ministry of Science and ICT) (NO.2017 M2A8A5015148).

REFERENCES

[1] T. Wang, W. L. Yang, Y. Hong, Y. L. Hou, Magnetic nanoparticles grafted with amino-riched dendrimer as magnetic flocculant for efficient harvesting of oleaginous microalgae, Chem. Eng. J. 297 (2016) 304-314.

Review of Evaluation of Robotics and Automation for Decommissioning Task Applications

Jihwan Yu* and Jungwun Kim

KHNP Central Research Institute, 70, Yuseong-daero 1312beon-gil, Yuseong-gu, Daejeon, Republic of Korea

*liu20893283@khnp.co.kr

1. Introduction

Currently, most of the work activities are manually conducted and remote operation systems (robotics) and automation systems are limitedly utilized during decommissioning project of NPPs. The advanced robotics and system automation are taken account of various advantages of the radiation reduction and decommissioning work activities during decommissioning project. That's way that these systems also have significant advantages for worker safety and radiation exposure [1].

This review introduces Scoring Metrics to quantitatively assess the applicability of robotics and system automation. In addition, a summary of the decommissioning task list is provided to evaluate the technical applicability of robotics and automation for decommissioning work tasks.

2. Application method

2.1 Technical development

In operation of NPPs, are being used for existing remote operation equipment for operation or fuel replacement. Due to the high radiation effects, the failure of the robot system is considered a risk factor for some decommissioning contractors [2].

In the case of automated systems, for example, automated decontamination and welding are performed for repetitive work activities, which are effective to difficult tasks and cut cost.

2.2 Desirable Attributes for Technologies

The following are the characteristics that requires robotics and automation.

- The system should be user-friendly and intuitive. Workers should be able to training in a reasonable time.
- The system should be flexible and easily adaptable to operational and operational requirements.
- Preventive maintenance should be optimized and the operator can be easily maintained.
- The system should perform faster than the existing technology in equipment installation time, periodic maintenance and demolition.

2.3 Evaluation of decommissioning Task

The work breakdown structure was used as a typical decommissioning task list based on the EPRI Report [1]. Four criteria were considered complexity of the task, impact on the schedule and cost of project, radiological and industrial safety and repeatability of the task. The metrics for determining the ranking applicable to robotics and automation are as shown in Table 1 and Table 2.

Table 1. Ranking Table for the Use of Robotics

Potential for Robotics	
Attribute	Score
Work Complexity of Task	Maximum of 10 points
Impact on Schedule/Cost	Maximum of 10 points
Radiological/Industrial Safety	Maximum of 10 points
Repetition	Maximum of 10 points
Maximum Total of 40 point	
30 – Option should be pursued, 15 ~ 30 – consider the option, <15 – do not consider further.	

Based on robotics metrics, the following items should be pursued (total score more than 30).

- Load spent fuel canisters and transfer to ISFSI (35).
- Segmentation, package and dispose of reactor internals (35).
- (Spent fuel pool) remove and dispose of class B and C waste (30).

Table 2. Ranking Table for the Use of Automation

Potential for Automation	
Attribute	Score
Work Complexity of Task	Maximum of 5 points
Impact on Schedule/Cost	Maximum of 20 points
Radiological/Industrial Safety	Maximum of 5 points
Repetition	Maximum of 20 points
Maximum Total of 50 point	
38 – Option should be pursued, 19 ~ 38 – consider the option, <19 – do not consider further.	

Based on automation metrics, the following items should be pursued (total score of more than 38).

- Segments, package and dispose of reactor internals (46).
- Load spent fuel canisters and transfer to ISFSI (45).
- (Spent fuel pool) Remove and dispose of class B and C Waste (40).

As a result, the 1st to 3rd priority tasks for robotics and automation applications match. These tasks are complex and radiation-effective, and are generally the critical path for decommissioning projects. This assessment can be used as a guide to prioritize the use of robotics or automation systems.

3. Conclusion

Review of evaluation of robotics and system automation for decommissioning applications method was suggested.

We also improve the evaluation method of automation and decommissioning work and will take account of Wolsung#1(PHWR Type) decommissioning project and impact on the cost of project, radiological safety and repeatability of the task in the future.

REFERENCES

[1] Evaluation of System Automation and Robotics for Decommissioning Application, EPRI, Palo Alto, 3002010599 (2017).

[2] Application of Non-Nuclear Robotics to Nuclear Industry Decommissioning, EPRI, Palo Alto, Ca:, 1009571 (2004).

An Approach to the Strategic Implementation for Stakeholder Involvement Management During Decommissioning of Nuclear Facilities

KwanSeong Jeong*, InHye Hahm, JaeHyun Ha, SangBum Hong, and BumKyoung Seo
Korea Atomic Energy Research Institute, 111, Daedeok-daero 989beon-gil, Yuseong-gu, Daejeon, Republic of Korea
*ksjeong1@kaeri.re.kr

1. Introduction

Factors for creating effective stakeholder relations are organizational readiness, planning, stakeholder relations and communications, openness and transparency, developing effective process, and evaluation. In decommissioning projects, the primary decision-making criteria are protection of human health and environment, compliance with legal requirements, and costs. Table 1 presents four typical steps in the involvement of stakeholders.

Table 1. Types of stakeholder involvement

Approach	What is meant by this	Aim
Information giving	Where we give information to people, for example, raising awareness of an issue, alerting people to opportunities for getting involved, telling people of a decision.	To ensure that those who want or need it are in receipt of relevant information.
Information gathering	Using survey methods to gather information. Usually used where we need to understand the opinions of a large number of people.	To generate information to inform the decision-making process.
Consultation	Giving people the opportunity to consider and respond to proposals, issues and options that we have developed.	To generate clearer understanding of people's concerns and opinions
Dialogue	Where we bring smaller numbers of key stakeholders together to discuss and deliberate together with us, before decisions are made.	To create opportunities to build shared understanding and agreement

2. Factors that may influence stakeholder involvement during decommissioning

Stakeholder involvement should be an integral part of the management of nuclear facilities from their conception through final closure and decommissioning. The cycle of planning, implementing, evaluating and adjusting can be represented in many ways, such as represented in Fig. 1.

Fig. 1. The learning cycle of stakeholder engagement.

In decommissioning projects, the primary decision-making criteria are protection of human health and environment, compliance with legal requirements, and costs. Other factors include but are not limited to schedule impacts, local economic impacts, institutional preferences, local social preferences, and environmental.

In fact, the national/local context in which decommissioning decision making will take place is a relevant factor for stakeholder interactions, but the converse is also true and stakeholders determine the decommissioning environment. Certain issues, such as local social and economic conditions, and regulations, are embedded within both a national and local socio-cultural context, and will shape the way in which the process is played out. The context of decision making will shape both the overall objectives of a decommissioning project within the framework of competing societal goals, as well as generate constraints on the decision making process including stakeholder contributions. Most decisions do not exist in isolation, but are built on decisions that have already been taken and affect the choices that will be available in the future. The timing of a decision may, therefore, also be an important factor, since the circumstances surrounding the decision will determine the external constraints, any other factors to be taken into account, and the people who should be involved. The measure of a decision is not just whether it is made efficiently and economically, but whether the decision making process has sufficient legitimacy, the decision sufficient acceptability and the subjects are sufficiently motivated to permit implementation

3. The strategic implementation for stakeholder involvement during decommissioning

In decommissioning projects, the primary decision-making criteria are: protection of human health and environment, compliance with legal requirements, and costs. Other factors include but are not limited to: schedule impacts, local economic impacts, institutional preferences, local social preferences, and environmental impacts. It is obvious that some of these factors are pertinent to the stakeholder interactions presented in this report. In fact, the overall scenario is further complicated by the presence of different – and often conflicting- groups of stakeholders. While a generic recipe for the resolution of strategic issues cannot be given, it is worth mentioning that a multi-attribute analysis is a possible mechanism offering some measure of objectivity. Installation of a quantitative decision aiding system allows implementing the complex process of decision-making in a way transparent to all stakeholders.

A powerful tool that may be used is the multi criteria decision analysis, which is both an approach and a set of techniques, with the goal to provide an overall ordering of options, considering monetary and non-monetary objectives. This approach breaks the problem into more manageable pieces. Objectives and criteria have to be identified, scored and weighted. The results have to be examined and the decision can then be taken after having performed a sensitivity analysis.

Methodology for Calculating the Internal Exposure Dose of Workers on Decommissioning Nuclear Power Plant

Changyeon Yoon* and Kirim Kim

KHNP Central Research Institute, 70, Yuseong-daero 1312beon-gil, Yuseong-gu, Daejeon, Republic of Korea

*Changyeon.yoon@khnp.co.kr

1. Introduction

In 2017, Kori-1 was permanently shut down and the Final Decommissioning Plan(FDP) for Kori-1 must be submitted to the regulation authority in accordance with relevant regulations. Various contents about decommissioning will include in the FDP, and quantitatively calculated exposure dose to workers by decommissioning operations should be described in Radiation Protection part. Since workers are expected to perform various decommissioning operations depending on the stage of decommissioning and the areas, it is essential to predict exposure dose of workers that inevitably occurs in this process.

2. Materials and Methods

To assess internal exposure dose for workers, a long half-life radioactive crud which remains in system and/or pipe is used for source term. Remaining radioactive crud inside the system or pipe can be dispersed in the working area by cutting process. Afterward, dispersed radioactive materials can be inhaled into the human body through breathing.

For conservative assessment, long half-life radioactive materials are used for calculation. Since the longer half-life, the greater effect on the human body

Inputs of internal exposure calculation are shown in Table 1.

Table 1. Inputs of internal exposure calculation [1-2]

Diameters of pipe	1, 2, 3, 4, 5, 6, 8, 10 inch
DF	50, 100
Floating rate	5%
Respiration rate	3.50E+04 m^3/sec
Diffusion factor	1

Schedule No. 40 stainless pipes are used for calculation. Each pipes with eight different diameters are used for calculation since there are various kind of pipes which have different sizes in the nuclear power plant.

For conservative calculations, assumptions which workers do not wear radiation protective equipment, and do not operate heating, ventilation, and & air conditioning(HVAC) for removing floating radioactive materials are applied.

Since decontamination will be performed on several systems prior to decommissioning, decontamination factor (DF) is applied to the internal exposure calculation.

Floating rate, respiration rate and diffusion

factor are used to calculate how much radioactive materials are inhaled in the human body through respiration.

3. Results

Equation of internal exposure calculation is shown in Equation (1).

$$D = L \times A \times R \times C \quad (1)$$

Where,

D : Internal exposure dose for worker(mSv)

L : Dose of floating radioactive materials(Bq)

A : Diffusion factor(sec/m^3)

R : Respiration rate(m^3/sec)

C : Dose conversion factor(mSv/Bq)

Calculation results of internal exposure dose are shown in Table 2.

Table 2. Calculation results of internal exposure dose

Diameter of pipe	DF 50(mSv)		DF 100(mSv)	
	Primary	Secondary	Primary	Secondary
1 in	5.2E-05	5.5E-06	2.6E-05	2.6E-06
2 in	1.0E-04	1.0E-05	5.2E-05	5.2 E-06
3 in	1.5E-04	1.5 E-05	7.7E-05	7.7 E-06
4 in	2.0E-04	2.0 E-05	1.0E-04	1.0 E-05
5 in	2.5E-04	2.5 E-05	1.3E-04	1.3 E-05
6 in	3. E-04	3.0 E-05	1.5E-04	1.5 E-05
8 in	4.0E-04	4.0 E-05	2.0E-04	2.0 E-05
10 in	5.0E-04	5.0 E-05	2.5E-04	2.5 E-05

Internal exposure dose varies according to the diameter of pipe and DF. As the diameter of pipe increases, so does internal exposure dose. In addition, the internal exposure dose of the primary system is greater than that of the secondary system. Comparing calculation result of DF 50 and DF 100, the internal exposure dose is lower when DF is 100.

4. Conclusion

The internal exposure dose by pipe cutting is 2.6E-06 to 5.0E-04mSv, which is very low.

The bigger diameter of pipe, the higher the internal exposure dose since there are more radioactive materials inside. The higher DF, the lower the internal exposure dose since more radioactive crud is removed. In addition, internal exposure dose for the primary system is higher since the primary system is more contaminated by radiation materials than secondary system.

REFERENCES

[1] “Reg 1.195(Methods and Assumptions for Evaluating Radiological Consequences of Design Basis Accidents at Light-Water Nuclear Power Reactors)”, US Nuclear Regulatory Commission (2003).

[2] “Size Distribution and Rate of Production of Airborne Particulate Matter Generated During Metal Cutting”, US Department of Energy (2001).

Development of a Program to Calculate External Exposure Dose of Workers on Decommissioning Nuclear Power Plant

Changyeon Yoon* and Kirim Kim

KHNP Central Research Institute, 70, Yuseong-daero 1312beon-gil, Yuseong-gu, Daejeon, Republic of Korea

*Changyeon.yoon@khnp.co.kr

1. Introduction

In 2017, the first commercial nuclear power plant in Korea, Kori-1 was permanently shut down in about 40 years. Under the Nuclear Safety Act, the Final Decommissioning Plan(FDP) for Kori-1 must be submitted to the regulation authority. In the FDP, exposure dose of workers during decommissioning process and radiation protection should be included.

Since the working areas change from time to time during decommissioning, it is difficult to obtain source information. Therefore, it is necessary to develop an algorithm and a program to calculate workers' external exposure dose with minimal information.

An algorithm for calculating dose rate using measured source information is developed by Electric Power Research Institute(EPRI)[1]. In this research, algorithm and program to calculate workers' external exposure dose based on the EPRI algorithm has been developed.

2. Materials and Methods

Intensity of the source is estimated based on measured dose rate, and external exposure dose of workers is calculated. Shielding effect of radiation, and attenuation effect according to distance are applied in the algorithm. In addition, the information of shielding materials between the source and the measurement position is applied to the attenuation formula of radiation. The flow of the dose calculation algorithm is shown in Fig. 1.

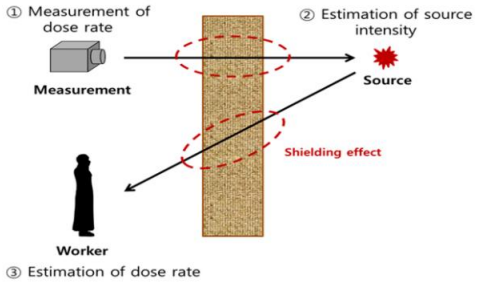

Fig. 1. Dose calculation algorithm.

The 3D Building Information Modeling (BIM) of Kori-1 is developed[2] and integrated with the algorithm to construct an external exposure dose calculation program. Furthermore, all areas of Kori-1 BIM are divided into several detailed work areas, one work area could be selected and enlarged within the program. Based on this 3D building information, detailed work process of workers can be applied into the program and the external exposure dose is accurately calculated.

3. Results

The program is consist of control box and viewer. Name of work area and 3D preview are shown in control box. After selecting one work

area, it is possible to input source position, measured dose rate of source, measured position, working hour, working position, movement of workers and number of workers. In viewer, selected work area is enlarged in 3D. Furthermore, moving line of workers and entered information of source are shown. Figure of control box and viewer are shown in Fig. 2.

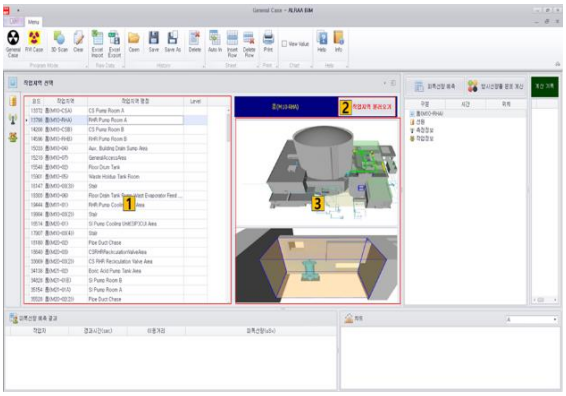

(a)

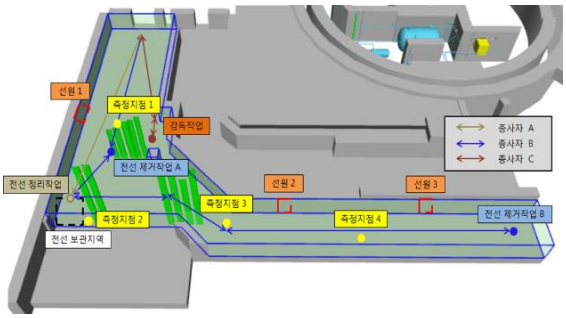

(b)

Fig. 2. Figure of external exposure dose calculation program (a) control box (b) viewer.

Even if several workers perform different works at the same time, respective exposure dose for every workers can be calculated easily. In addition, removed or newly created structures during the decommissioning process can be applied in the program.

Since all work areas are expressed in 3D, it is possible to reflect wherever the worker works. Furthermore, radioactive decay of nuclides is also reflected.

In program, external exposure dose of workers is calculated for every step of work process and statistical error is estimated to evaluate the accuracy of the results.

4. Conclusion

The program is developed to calculate workers' detailed external exposure dose during the decommissioning process of Kori-1. Calculated result by program will be used for the Kori-1 FDP.

To increase user convenience, all areas of Kori-1 are expressed in 3D. Users can check in real time to see if the entered information is properly applied in program.

REFERENCES

[1] "3D Radiation Field Estimation Algorithm", EPRI (2013).

[2] "Development of decommissioning quantity evaluation program for nuclear power plant", KHNP (2010).

Redistribution of WBS-based Korean NPP Decommissioning Cost by ISDC

Jae Yong Oh*, Jungwun Kim, and Hyung-woo Seo
KHNP Central Research Institute, 70, Yuseong-daero 1312beon-gil, Yuseong-gu, Daejeon, Republic of Korea
*jaeyongoh@khnp.co.kr

1. Introduction

Decommissioning has been attracted to a lot of publics from Permanent Shutdown of Kori-1 Nuclear Power Plant (NPP) in Korea. Decommissioning cost is especially highlighted issue due to its generality, universality and accessibility of corresponded information. And also, decommissioning cost estimation and comparison with the previous cases are essential for the safe and economic efficiency of the upcoming decommissioning enterprise. To achieve this purpose, OECD/NEA has developed the International Structure of Decommissioning Costing (ISDC) with IAEA and European Commission.

Meanwhile, in Korea, decommissioning cost is estimated by Work Breakdown Structure (WBS) as suggested in AIF/NESP-036 report. By utilizing this method, it is favorable to make a project management and expenses plan. However, it is hard to compare with other decommissioning cost cases. In this study, WBS-based decommissioning cost usually estimated in Korea is analyzed and redistributed by ISDC matrix.

2. Methods & Current States

ISDC is established to make a comparison conveniently between a variety of WBS-based decommissioning costs because of the site and project specific structure and data [1].

Fig. 1 describes outline processes from raw data to WBS-based decommissioning cost and redistribution to decommissioning cost by ISDC.

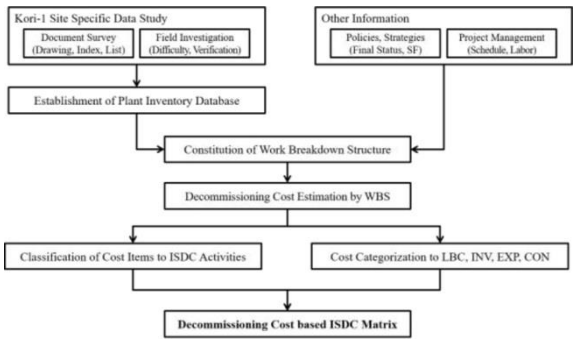

Fig. 1. Flowchart of decommissioning cost redistribution.

2.1 Established Decommissioning Cost in Korea

2.1.1 WBS-based Cost Estimation. Most of the decommissioning cost estimation in Korea are based on Work Breakdown Structure (WBS) [2]. Each cost items related with work activities in decommissioning project such as dismantling, demolition, decontamination and survey for structure, system and components (SSCs).

2.1.2 Decommissioning Appropriation Fund. Korean Government, Ministry of Trade, Industry and Energy (MOTIE), notices decommissioning appropriation fund per each Korean NPPs is 751.5 billion Won [3]. To estimate the appropriation fund, considered structure is composed of cost categories as stated in Table 1.

Table 1. Structure of decommissioning appropriation fund

Category	Sub-categories
D&D Project Mngmt.	Project Management, Waste Processing Facility, Others
Waste Disposal	Radioactive Waste Disposal, Contingency

2.2 Overview and Outline of ISDC Matrix

In ISDC, all the decommissioning cost items are being separated as characteristic and performance time of relevant activities in decommissioning project. Principal activities, Hierarchical Activity Level 1, in ISDC are listed in Table 2. Each detailed cost item consists of labour costs, investment costs, expenses and contingency composite as shown in Fig. 2.

Table 2. Principal activities in ISDC

No.	Activities Description
01	Pre-decommissioning actions
02	Facility shutdown activities
03	Additional activities for safe enclosure or entombment
04	Dismantling activities within the controlled area
05	Waste processing, storage and disposal
06	Site infrastructure and operation
07	Conventional dismantling, demolition and site restoration
08	Project management, engineering and support
09	Research and development
10	Fuel and nuclear material
11	Miscellaneous expenditures

Table 3. Outlines of ISDC matrix

Hierarchical Activity Level	Cost Category				
	Labour	Investment	Expenses	Contingency	Total
Principal Activity (Level 1)	L_{01}	I_{01}	E_{01}	C_{01}	$L_{01}+I_{01}+E_{01}+C_{01}$
Activity Group (Level 2)	$L_{01.0100}$	$I_{01.0100}$	$E_{01.0100}$	$C_{01.0100}$	$L_{0.000}+I_{0.000}+E_{0.000}+C_{0.000}$
Typical Activity (Level 3)	$L_{01.0101}$	$I_{01.0101}$	$E_{01.0101}$	$C_{01.0101}$	$L_{0.001}+I_{0.001}+E_{0.001}+C_{0.001}$

2.3 Transition of Decommissioning Cost Structure

In case of decommissioning appropriation fund, sub-categories of decommissioning cost can be changed to ISDC activities. Project management in appropriation fund can be regarded as Principal activities 08. And, waste processing facility and radioactive waste disposal costs are considered as principal activities 05, respectively.

3. Conclusions

Redistribution of decommissioning cost to ISDC is anticipated to simplify the comparison with various overseas cases. And therefore, costs would be validated for the existing cases and estimated for the following cases in Korea.

REFERENCES

[1] OECD/NEA, “International Structure for Decommissioning Costing (ISDC) of Nuclear Installations”, NEA No. 7088 (2012).

[2] Thomas S. LaGuardia, etc., “Guidelines for Producing Commercial Nuclear Power Plant Decommissioning Cost Estimates”, AIF/NESP-036, Volume 1 (1986).

[3] Notice of Ministry of Trade, Industry and Energy, 2017-195 (2017).

Development of 5D Program for Decommissioning Schedule, Waste Quantity and Cost

Jae Yong Oh[a,*], Younggook Kim[a], Jihwan Yu[a], Taesik Yun[a], Jae-Gon Lee[a], Kyeongmin Song[b], Ilsoo Park[b], Nak-Hoon Sung[c], and Seunghyuk Jung[c]

[a]KHNP Central Research Institute, 70, Yuseong-daero 1312beon-gil, Yuseong-gu, Daejeon, Republic of Korea

[b]WIBTEL, 10, Seongnam-daero 43beon-gil, Bundang-gu, Seongnam-si, Gyeonggi-do, Republic of Korea

[c]Korea Nuclear Engineering & Service, 65, Myeongdal-ro, Seocho-gu, Seoul, Republic of Korea

[*]jaeyongoh@khnp.co.kr

1. Introduction

Decommissioning is one of the most important process in the back-end lifecycle of Nuclear Power Plant (NPP). Decommissioning can be conceptually opposite to commissioning or construction. However, due to the existence of radiological characteristics, decommissioning of NPP should not be progressed in reverse order of construction. Decommissioning of NPP is more difficult and exquisite project to manage without problems.

Thus, management on decommissioning of NPP is convoluted but have to be carried out thoroughly. In order to facilitate management and analysis on decommissioning project, 5D management program (3D waste quantity based on Building Information Modeling (BIM), project schedule as 1D and cost regarded as 1D) is investigated. In this paper, developed 5D management program for decommissioning schedule, waste quantity and cost is introduced.

2. Methodologies and Results

2.1 Decommissioning Project Schedule

Project schedule as a function of time is the most fundamental factor in decommissioning. Schedule is susceptible to alternatives, policies, strategies, stakeholder and characteristics of NPP. Meanwhile, schedule affects labor force and cost in decommissioning project. In 5D management, schedule is illustrated as 1D schedule (time) information. And also, schedule in program can be edited by changing process and printed out as Gantt chart viewer.

2.2 3D Building Information Modeling

BIM is comprehensive information and model for building structures established with 3D design, construction and operation data as depicted in Fig. 1 [1].

In this study, inventories or decommissioning wastes of structure, system and components (SSCs) are realized as objects in BIM model with information such as 3D location, related building, system, drawings, material, dimension, radiological characteristics and etc. All objects have also information on cost for work activities, and so, reflects to waste quantity analysis and cost estimation as stated later.

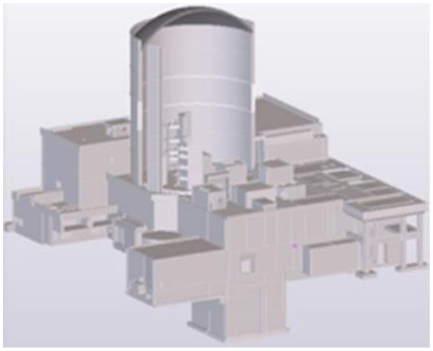

Fig. 1. Example of 3D building information model.

2.3 Decommissioning Waste Quantity Analysis

For waste quantity analysis, not only 3D BIM model but also additional databases are required to evaluate detailed waste information. Based on 3D BIM model and additional established database, waste quantity can be analyzed totally or by various categories, system, area, waste level and user-defined, in 5D management program.

2.4 Decommissioning Cost Estimation

Similar with decommissioning waste quantity analysis, waste-dependent cost is estimated by work activities and unit cost factors from extra database in 5D management program. Moreover, 5D management program estimate cost based on DeCAT-Pro program [2].

2.5 Development of 5D Management Program

KHNP and some of software experts have developed 5D management program to support the safe and economical decommissioning for Kori-1 in recent years. As described above, decommissioning project schedule, waste quantity and cost are managed and verify comprehensively in 5D management program. Table 1 lists the available menus and functions in 5D management program.

Table 1. Menus and functions in 5D management program

Menu	Functions
System Management	Make/Open/Save project, options
DB Management	Viewer mode, search object/data
Waste Analysis	Total/Conditional waste analysis
Cost Estimation	Total/Conditional cost estimation
Schedule Mngmt.	Gantt schedule edit/simulation
Report	Summary report for waste/cost

3. Conclusions

KHNP has developed the 5D comprehensive decommissioning management program based on 3D BIM model, waste quantity and decommissioning cost. It is expected that 5D management program is going to support decommissioning project management.

REFERENCES

[1] Kim, J., et. al., “Development of 3D-based Nuclear Power Plant Decommissioning Waste Quantity Estimation Program”, Proc. of the KRS 2016 Autumn Conference, 14(2), Oct. 12-14, Jeju (2016).

[2] Kim, H., et. al., “Development of Computer Program for Estimating Decommissioning Cost”, 2011 ICEM, Sep. 28 (2011).

Preparation of Project Management in Final Decommissioning Plan

Jae Yong Oh*, Jin-Won Son, and Jungwun Kim
KHNP Central Research Institute, 70, Yuseong-daero 1312beon-gil, Yuseong-gu, Daejeon, Republic of Korea
*jaeyongoh@khnp.co.kr

1. Introduction

Decommissioning is the last phase in the life cycle of Nuclear Power Plant (NPP) since the permanent shutdown of the operation phase. Kori-1 NPP is under permanent shutdown since 2017, and also Wolsong-1 NPP was shut down permanently in 2018. Furthermore, in cases of Kori NPPs, Wolsong NPPs, and etc., in current trends, decommissioning is going to be extended explosively in the near future.

In order to commence the decommissioning in Korea, the NPP licensee, KHNP, must prepare and submit the Final Decommissioning Plan (FDP) which needs to be approved by the regulatory body. Notice of Nuclear Safety and Security Committee (NSSC) states the preparation structure and standard of Decommissioning Plant [1].

Due to the importance for the economical decommissioning, project management, Chapter 2 in the FDP, includes organization, personnel, cost and funding plan. In this paper, preparation of project management in the FDP for Korean NPPs is stated.

2. Project Management in FDP

Project management in decommissioning documents could be differed with each other but basically, IAEA recommended that organization, responsibilities, training and etc. are included in project management, and also, cost and funding mechanisms should be explained [2]. Thus, in Korea, project management in the FDP describes the organization, personnel, cost and funding plan for decommissioning [1].

2.1 Final Decommissioning Plan

Regulation of Korean Nuclear Safety and Security Commission specifies a few articles about organization, cost, strategies, facilitation, safety analysis, radiation protection, radioactive waste management, environmental impact assessment and quality assurance in nuclear facility decommissioning [3]. Based on the regulation and notice, KHNP is carrying out the preparation of the FDP to acquire the licensing approval for decommissioning.

2.2 Constitution of Project Management in FDP

As mentioned in the notice, decommissioning project management depicts the plan and methods to conduct the safe and economical decommissioning project. In this point of view, organization, personnel, cost and funding plans are made out in the same chapter of the FDP. Preparation guidance and methodologies for

each items of project management are listed in Table 1.

2.2.1 Organization. Responsibilities and authorities required for each department as a function of status and phases should be written, and also, they could be related with quality assurance documents. Procedures related with decommissioning must be prepared in this section, as well.

2.2.2 Personnel. In this part, Licensee draws up the personnel and labor operating plan of decommissioning, for example, compositions of decommissioning organization and education and training plans.

2.2.3 Cost. Decommissioning cost have to be quantitatively estimated applying the site and facility characteristics, strategies, physical inventory, radiological inventories, and etc. Also, main assumptions, reasons, procedures and methods for decommissioning cost estimation ought to be suggested in this paragraph.

2.2.4 Funding Plan. This subchapter announces information about funding plan to secure the decommissioning cost as known in the above section. Therefore, the assessment of financial status of organization and comparison of funding with cost estimation results would be explained.

Table 1. Methodologies of project management in FDP [1]

Section	Description
Organization	- Responsibilities and Authorities Required for Decommissioning - Procedures Related to Administration, Operation, Test and Maintenance for Decommissioning
Personnel	- Personnel Composition According to Decommissioning Organization - Training Plans Required for Decommissioning
Cost	- Quantitative Estimation of Decommissioning Cost Considering Site and Facility Characteristics - Reasons, Procedures, Methods and Assumptions for Cost Estimation
Funding Plan	- Comparison and Assessment between Financial Status and Estimation Results of Decommissioning Cost - Funding Plan to Secure the Decommissioning Cost Until License Termination of NPP

3. Conclusions

Project management, Chapter 2 in the FDP for Korean NPPs, states organization, personnel, cost and funding plan for the safe and economical decommissioning. Since FDP including project management is completed and approved, Korean NPP such as Kori-1 are going to be decommissioned as planned in FDP. Finally, project management in FDP for Kori-1 would be anticipated to contribute the FDPs for the following cases.

REFERENCES

[1] Notice of Nuclear Safety and Security Commission, 2018-10 (2018).

[2] International Atomic Energy Agency, “Standard Format and Content for Safety Related Decommissioning Documents”, Safety Reports Series No. 45 (2005).

[3] Regulation of Nuclear Safety and Security Commission, 22 (2019).

Efficient Removal of Cesium Ions From Aqueous Solution Using Alginate/Prussian Blue Composite Hydrogel Bead

Seung Han Woo[1,2,*] and Ohemeng–Boahen. Godfred[1]

[1]Hanbat National University, 125, Dongseo-daero, Yuseong-gu, Daejeon, Republic of Korea

[2]Life Green Technology Co., Ltd., 505, Yuseong-daero 875, Yuseong-gu, Daejeon, Republic of Korea

[*]shwoo@hanbat.ac.kr

1. Introduction

Cesium (Cs) is an integral part of most functioning nuclear power plants (NPPs). However, due to its high radioactivity and relatively longer half-life (30.2 years) [1], its presence in the environment (especially aquatic bodies) as a result of direct or indirect disposal from NPPs may undeniable impede the overall wellbeing of the inhabitants of the ecosystem. As such, treatment of radioactive wastewater containing Cs is very prudent and of upmost importance to researchers and other stakeholders alike.

Adsorption is well-known as the most favorable means of removing several contaminants (even at low contaminant concentration) from wastewater due to its high removal efficiency, low operational cost, simplicity and little to no generation of by-production [2]. Although the use of Prussian blue (PB) for the Cs removal from aqueous solution is prevalent, its commercialization is somewhat difficult due to hydrodynamic issues such as channeling (for granular PB), dispersion of the PB, low hydrodynamic conductivity, pressure drop as well as the high cost in post-treatment separation of the PB powder and the treated water [3]. Hence, the impregnation of PB powder into alginate (Alg), a biocompatible, biodegradable biopolymer will greatly enhance its applicability in adsorption columns as well as eliminate the environmental issues associated with the handling of powdered matter. Herein we, report an Alg/PB composite hydrogel bead (Alg-PB) generated by crosslinking Alg-PB mixture with Ca^{2+}. The Alg-PB was tested for its applicability in Cs removal from aqueous solution.

2. Materials and Methods

2.1 Materials

Alginic acid sodium salt (Alg), Prussian blue and Cesium nitrate were purchased from Sigma Aldrich. Calcium Chloride was purchased from Duksan Pure Chemical Co., Korea.

2.2 Preparation of adsorbents

One gram of Alg powder was added to 100 ml of deionized water and the resulting mixture was placed in a shaking incubator at 150 rpm, 30 °C for 24 h to make the 1 wt.% Alg solution used in this work. The Alg-PB was produced by

dropwise addition of a homogenized mixture of Alg/PB (with known amount of PB) into the coagulation bath (aqueous $CaCl_2$ solution; 0.2M). After 3 h, the Alg-PB were extensively washed with DI water and preserved in DI water for further studies. Physicochemical properties of the Alg-PB were also studied.

2.3 Adsorption Experiment

Ten wet Alg-PB beads were added to 10 ml of 500 mg Cs^+/L aqueous solution and the mixture was kept in the shaking incubator at 30 °C and 150 rpm. The concentration of Cs after 24 h was measured using inductively coupled plasma mass spectrometer (ICP-MS).

3. Results and Discussion

Instantaneous gelation occurred when the sodium alginate droplet contacted the $CaCl_2$ solution. Complete gelation was achieved over time due to the progressive diffusion of the Ca^{2+} into the core of the Alg drop (unreacted sodium alginate)[4]. Fig. 1 shows a 91.24% increase in mass-based adsorptive capacity ($q_{e,\ m}$; mg Cs^+/mg adsorbent) of Alg-PB hydrogel beads relative to the pristine alginate bead (Alg-B).

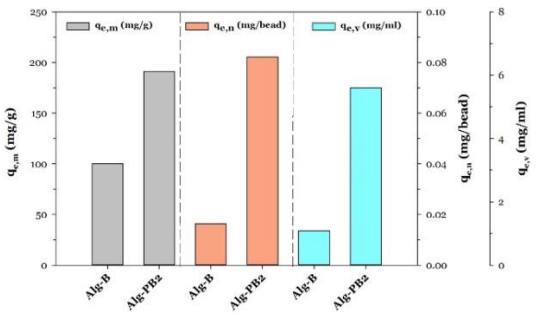

Fig. 1. Adsorption capacity of composite hydrogel beads.

4. Conclusion

1) Prussian blue powder were successfully impregnated into calcium alginate beads.
2) There was synergistic effect in adsorption of Cs^+ upon PB impregnation into the alginate beads.

REFERENCES

[1] X. Liu, G.-R. Chen, D.-J. Lee, T. Kawamoto, H. Tanaka, M.-L. Chen and Y.-K. Luo, Bioresour Technol, 2014, 160, 142-149.

[2] S. Chatterjee, H. N. Tran, O.-B. Godfred and S. H. Woo, ACS Sustain Chem Eng, 2018, 6, 3604-3614.

[3] B. Wang, B. Gao and Y. Wan, J.Ind. Eng. Chem., 2018, 61, 161-168.

[4] H.-S. Kim, Korean J Chem Eng, 1990, 7, 1-6.

Evaluation of Radionuclide Inventory in Concrete of Kori Unit 1

Mee Jang*, Hyunchul Kim, Chang Jong Kim, Ji Young Park, and Jong Myoung Lim
Korea Atomic Energy Research Institute, 111, Daedeok-daero 989beon-gil, Yuseong-gu, Daejeon, Republic of Korea
*mjang@kaeri.re.kr

1. Introduction

The radionuclide inventory prediction of a nuclear power plant can help establish decommissioning plan by providing information of radiation environment. In this study, we calculated the possible radionuclide inventory in bio concrete of Kori Unit 1 using MCNPX and ORIGEN2.

2. Methods and Results

2.1 Activation Products in Bio Concrete

The basic composition of the bio concrete is as shown in Table 1. [1] If there are impurities, the type and content of impurities of concrete can be changed according to the factors such as manufacturing process and added aggregate. Not considering the impurities, we evaluated the amount of possible radionuclide inventory based on the basic composition of the bio concrete. The possible radionuclides and characteristics are shown in Table 2.[2] As shown in Table 2, ^{41}Ca, ^{39}Ar and ^{55}Fe can be produce by Ca, K and Fe. For example, ^{39}K is 93.3% abundant in natural potassium which is present in concrete. ^{39}Ar is can be produced by the reaction ^{39}K(n,p)^{39}Ar with a cross-section of about 0.1b. In the case of ^{41}Ca, we calculated the possible inventory in the earlier study. [3] ^{55}Fe can be produced by the ^{54}Fe(n,γ)^{55}Fe reaction in the 5.9% abundant stable iron isotope ^{54}Fe with a cross-section of 2.25b.

Table 1. Composition of the bio concrete without impurity

Element	Weight Fraction (%)
H	0.55
O	49.83
Si	31.57
Ca	8.26
Na	1.70
Mg	0.26
Al	4.55
S	0.13
K	1.91
Fe	1.23

Table 2. Physicochemical characteristics of possible radionuclide in bio concrete

Parent	^{39}K	^{40}Ca	^{54}Fe
Nuclear Reaction	(n,p)	(n,γ)	(n,γ)
Daughter Nuclide	^{39}Ar	^{41}Ca	^{55}Fe
Principal Emission	β-	EC	EC
Half-life(y)	269	103000	2.73

2.2 Neutron Flux

To evaluate radionuclide inventory of ^{39}Ar, ^{41}Ca and ^{55}Fe in bio concrete, it is necessary to calculate average neutron flux in each zone of reactor. In this research, we simplified the geometry of Kori Unit 1 and calculated the

averaged neutron flux in each zone using MCNPX code. The results are shown in Table 3.

Table 3. Neutron flux in each region of Kori Unit 1

	Zone	Neutron Flux(#/cm^2-s)
1	Baffle	7.79E+12
2	Barrel	4.41E+11
3	Bypass	2.70E+10
4	Thermal shield	3.59E+10
5	Downcomer	1.28E+10
6	RPV	7.40E+08
7	Air	3.10E+08
8	Bio concrete	1.34E+07

2.3 Effective Cross section and Inventory

Using the calculated neutron flux, we estimated the effective cross section ^{39}K, ^{40}Ca and ^{54}Fe as shown in Table 4. We calculated the radionuclide inventory using ORIGEN2 and effective cross section. The total activity of ^{39}Ar, ^{41}Ca and ^{55}Fe in concrete are shown in Table 5.

Table 4. Effective Cross Section of ^{39}K, ^{40}Ca and ^{54}Fe

Radionuclide	^{39}K	^{40}Ca	^{54}Fe
Reaction Rate (MCNPX, #·(cm^3-s)$^{-1}$	3.781×10^{24}	9.153×10^{24}	2.026×10^{23}
Effective Cross Section (barn)	8.687×10^{-4}	3.147×10^{-4}	9.716×10^{-3}

Table 5. Total activity of ^{39}Ar, ^{41}Ca and ^{55}Fe

Radionuclide	^{39}Ar	^{41}Ca	^{55}Fe
Radioactivity	4.725×10^{8}	2.533×10^{6}	1.588×10^{8}

3. Conclusion

In this research, we estimated the inventory of ^{39}Ar, ^{41}Ca and ^{55}Fe using the effective cross section and activation calculation code ORIGEN2. These results can be used for decommissioning plan.

REFERENCES

[1] International Atomic Energy Agency, “Radiological Characterization of Shut Down Nuclear Reactors for Decommissioning Purposes”, Technical Reports Series No. 389 (1998).

[2] Gil Yong Cha, Soon Young Kim, Jae Min Lee and Yong Soo Kim, “The Effects of Impurity Composition and Concentration in Reactors Structure Material on Neutron Activation Inventory in Pressurized Water Reactor”, Journal of Nuclear Fuel Cycle and Waste Technology, 14(2), 91-100 (2016).

[3] Mee Jang, Jong Myoung Lim, Hyun Chul Kim, and Chang Jong Kim, “ Inventory Estimation of ^{36}Cl and ^{41}Ca in Concrete of Kori Unit 1”, Journal of Nuclear Fuel Cycle and Waste Technology, 17(1), 121-126 (2019).

Logistical Simulation Prerequisites for a Soil Remediation Process Scheduling

Eui-taek Lee, David Kessel, and Chang-Lak Kim*

KEPCO International Nuclear Graduate School, 658-91, Haemaji-ro, Seosaeng-myeon, Ulju-gun, Ulsan, Republic of Korea

*clkim@kings.ac.kr

1. Introduction

In previous study [1], we developed a simulation model that can be used for logistics planning for site remediation of the Kori 1 reactor site. Through a FlexSim discrete event simulation, the applicability for a soil washing process was demonstrated. The site remediation of Kori unit 1 Nuclear Power Plant (NPP) is scheduled for 2 years duration and will end in 2032. In order to meet the planned site remediation schedule, it is essential to identify bottlenecks in the soil washing system and enhance the bottlenecked processors to avoid negative effects on the schedule. In addition to the previous simulation conditions, in this paper, we introduced some prerequisites for the soil remediation scheduling management such as input amount estimation and processor set values. Furthermore, it was suggested that a continuous simulation model, which acts as a discrete event simulation model, should be applied for simulating the large number of items, operations and instances.

2. Previous simulation model

In the previous study, the soil washing process was chosen for contaminated soil treatment as shown in Figure 1. This model depicts that the excavated soil from the contaminated site is fed to the feed hopper and the soil that has been cleaned through dry separation is sent to each queue according to the grain size i.e. rubble, gravel, sand, silt and sludge/clay [1].

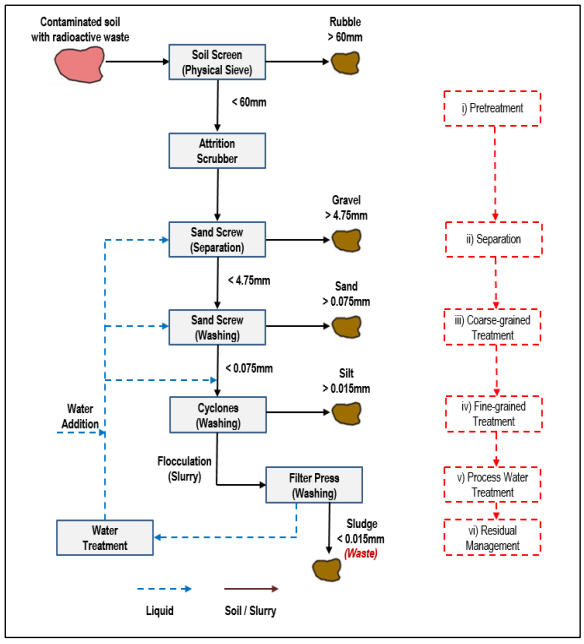

Fig. 1. Soil washing process model [1].

Since it is necessary to meet radioactive waste management requirements that prohibit mixing of wastes with different classifications, the discrete-event model was simulated by using FlexSim which is widely used for simulation of logistics planning in various industries [1].

3. Additional prerequisites

For calculating duration and evaluating or improving the soil washing process system with the previous simulation model, it is necessary to estimate the input amount, to set the processor

capacity, and to select a proper simulation method.

When the excavated area of site is multiplied by depth, the estimated input soil volume can be obtained. The soil volume can be converted to weight by applying volume conversion factors in accordance with the standards for construction estimates [2].

In order to evaluate or improve the system, input capacity, cycle time and process rate should be identified for each processor as can be seen in Table 1. The processors should be selected from representative equipment that is widely used in the construction field.

Table 1. List of processor set values

Item	Input	Cycle time	Rate
	(per cycle)	(min)	
Processor 1	- ton	-	- ton/hr
Processor 2	- ton	-	- ton/hr

Lastly, the soil washing simulation which is subjected to the large number of items, operations and instances should be performed using a continuous simulation model since the computation effort and the software operation instability resulting from large data processing may be concerns [3]. Although a continuous simulation model should be used, this model may act as a discrete-event model by allocating the process delay time as the discrete-event conditions.

These measures will enable identifying bottlenecks in the soil washing system and enhancing these bottlenecks by increasing processor quantity to avoid negative effects on the schedule. Consequently, it is expected to allow for evaluating and enhancing the performance of the soil washing system.

4. Conclusion

This paper introduced some prerequisites for simulating a soil washing system in terms of the scheduling management. In order to meet the planned schedule, the system optimization should be achieved by establishing input amount and processor set values. In contrast to the previous study, we suggested a pseudo continuous simulation model for smooth simulation. Including these measures, the enhanced model will be established and simulated.

Acknowledgements

This research was supported by the Nuclear Safety Research Program through the Korea Foundation of Nuclear Safety (KOFONS), granted financial resource from the Nuclear Safety and Security Commission (NSSC), Republic of Korea (No.1605008).

REFERENCES

[1] D. S. Kessel, C. L. Kim, J. H. Jeon and E. T. Lee, "Simulation Modeling for Planning a Soil Remediation Process," in KRS 2019 Spring Conference, Busan, 2019.

[2] Construction Research Center, "Part 1. Civil Works," in 2014 Standards of Construction, Seoul, Construction Research Center, 2014, pp. 71-73.

[3] M. Beaverstock, A. Greenwood and W. Nordgren, Applied Simulation: Modeling and Analysis Using Flexsim (Fifth Edition), Seoul: Cho-Ah Publishing Company, 2018.

Evaluation of Decommissioning Applicability of the Requirements for the Spread of Contamination and Minimization of Radioactive Wastes

Hyo Jin An[1,*], Seung Kook Park[2], Jin Ho Park[2], and Hyung Gon Jin[1]

[1]Korea Atomic Energy Research Institute, 111, Daedeok-daero 989beon-gil, Yuseong-gu, Daejeon, Republic of Korea

[2]NUDECOMM, 530, Daedeok-daero, Yuseong-gu, Daejeon, Republic of Korea

[*]dks6948@naver.com

1. Introduction

The Nuclear Safety and Security Commission Notice No. 2015-08 defines a number of measures to minimize contamination and ensure ease of decommissioning, except for decommissioning process. But U.S. NRC Regulatory Guide and the Korea Institute of Nuclear Safety (KINS) demand application to full cycles that include decommissioning. Therefore, initial decommissioning plans submitted during construction or operation should be presented by reflecting it.

2. Background

This study categorizes and analyzes the detailed requirements according to the applicability of NRC Reg Guide 4.21, especially additional applications during dismantling.

Consideration of decommissioning is so conceptual that cannot be applied in its entirety. So, the paper studied how this should be applied in practice, according to following four sections.

3. Application to Decommissioning

3.1 Minimize Facility Contamination

Due to variation of radiated level depending on the type of facility, installing compartments and minimizing its' interfaces are essential. Monitoring radiation against possible leakage, including outside of the facility is also effective for rapid detection and identification of current conditions. Management of leaked solutions, detection of leakage must be considered, too.

On the other hand, consideration of pollution-related considerations, such as prevention of source accumulation and decontamination, and the consideration of materials, equipment types and facilities outside the control area are sufficient for operational considerations and require no further action.

3.2 Minimize Environmental Contamination

The installation of CSM (Conceptual Site Model) is considerable when uses little solution during decommissioning of facilities. Also, the prevention of possibility of contamination, depending on the physical character of waste, is needed for decommissioning considerations. Monitoring underground water pollution and estimating of pollutants are not required to be reported in full report form, but the surveillance data must be maintained until the facility is decommissioned.

However, consideration of these requirements, such as the installation of barriers, monitoring of

leaks, backfilling of facilities, reduction of groundwater and on-site disposal of radioactive materials, are sufficient for construction and operational considerations, so they do not need to be taken into account when dismantling.

3.3 Ease of Decommissioning

The types of documents that must be kept until decommissioning include matters relating to the construction and modification of the facility, operating data, radiation safety management data and accident records of the facility. Facility data for ease of decommissioning explains about embedded pipe and device. It is divided into 3 types like pure buried, penetrated, and located in an independent shield compartment type. Choosing right methods for exchanging, repairing and dismantling equipment, depending on its locations and sizes of devices, is important. The transfer route of the decommissioning can be shown in above methods, but the size of the unit, transfer truck and the specifications of the cutting equipment need to be analyzed more precisely in the final decommissioning plan.

3.4 Minimize Radioactive Wastes

In terms of waste management concept, an increase in the amount of waste is not expected due to differences in the management concept and capacity of waste during operations and decommissioning. Therefore, it can be minimized by thorough management, according to their occurrence and treatment characteristics. Decontamination is an essential task, which can reduce workers' exposure, environmental impact and the amount of radioactive waste generated by leakage of radioactive materials out of the workplace. More radioactive waste is generated during decommissioning than operation, so the classification of waste disposal facilities is important. In the modular structure concept, not all structures are constructed as modular structures. However, since only one system having one operation characteristic is installed in one room, rooms in which devices of the same system are installed can be dismantled at the same time.

4. Conclusion

By analyzing the methods applicable to the decommissioning, each consideration can be reflected in the initial decommissioning plan submitted during construction or operation, and is currently applied to the initial decommissioning plan of 14 facilities within the KAERI.

REFERENCES

[1] Regulatory Guide 4.21, “Minimization and Radioactive Waste Generation Life-cycle Planning” (2008).

[2] Nuclear Safety and Security Commission, “Nuclear Safety Act” No. 13078 (2015).

Permanganate Self-decomposition Behavior in the HyBRID Oxidative Decontamination Process by Using Cr_2O_3 Pellets

Yoon-Ji Park*, Hyun-Kyu Lee, Seungyeop Han, Wonzin Oh, and Sang-June Choi

Kyungpook National University, 80, Daehak-ro, Buk-gu, Daegu, Republic of Korea

*qkrdbswl2@knu.ac.kr

1. Introduction

In the oxidative decontamination process of HyBRID technology, the self-decomposition of oxidative decontamination process of $KMnO_4$ was carried out using Cr_2O_3 pellets [1]. A study on the water-phase self-decomposition of $HMnO_4$ is reported in Lee (2018) [2]. The self-decomposition characteristics can be represented by the particle generation model in the supersaturated solution. This reaction is independent of the initial concentration and is presented as a correlation through the characteristic experiment according to the temperature and acidity change.

In this study, the self-decomposition of $KMnO_4$ during Cr_2O_3 dissolution was investigated. In the oxidative decontamination process, MnO_4^- of $KMnO_4$ not only oxidizes water but also oxidizes Cr^{3+} of Cr_2O_3 to Cr^{6+} [3]. The product of these two reactions is MnO_2 precipitates. Therefore, the self-decomposition of MnO_4^- was confirmed when the Cr_2O_3 dissolution reaction was accompanied under the HyBRID oxidative decontamination conditions using $KMnO_4$ and Cr_2O_3 pellets.

2. Experiments

2.1 Chemicals

$KMnO_4$ (min. 99.3%), Cr_2O_3 (min. 99%), and H_2SO_4 (min. 98%) were purchased from DAEJUNG company Korea.

2.2 Method

The volume of the reactor was 300 mL and experimented according to the number of Cr_2O_3 pellets. The reaction temperature is 90 °C and the reaction time is 3 hours. Sampling time was 0, 5, 10, 20, 30, 60, 90, 120, 180 minutes. Mn analysis was measured by UV-vis Spectrophotometer (libra, biochrom, USA) and Cr analysis by ICP-OES (OPTIMA 2100 DV, PerkinElmer Pty. Ltd, USA). The experimental conditions are shown in Table 1.

Table 1. Experimental conditions

Concentration	Pellet
6.33 mM $KMnO_4$ + 3.25 mM H_2SO_4	0
	3

3. Results and discussion

The chromium oxidative dissolution and water oxidation reactions by $KMnO_4$ in the acidic condition are well known to produce MnO_2 particle with the 1 to 1 stoichiometry. And therefore, the consumption of MnO_4^- concentration, ΔMnO_4^-, can be expressed with the Cr dissolution concentration, $[HCrO_4^-]$ and MnO_4^- self decomposition by water oxidation $[MnO_4^-]_{SD}$, as follows:

$$\Delta MnO_4^- = [HCrO_4^-] + [MnO_4^-]_{SD} \quad (1)$$

In case of no self-decomposition of MnO_4^-, the amount of chromium dissolution is the same amount of manganese concentration change as follows:

$$\Delta|MnO_4^-| = \Delta|HCrO_4^-| \quad (2)$$

Fig. 1 shows the self-decomposition (SD) behavior of MnO_4^- at the HyBRID oxidative decontamination condition using 0 and 3 Cr_2O_3 pellets respectively. Self-decomposition, $[MnO_4^-]_{SD}$

estimated by equation of (1) shows that there were no self-decompositions with and without Cr dissolution, considering the permissible experimental errors.

The chromium dissolution behavior using 3 Cr_2O_3 pellets in the Fig. 2 shows that the dissolution rate decreased remarkably after 30 minutes. And the MnO_4^- reduction product of MnO_2 inherent from the oxidative dissolution of Cr_2O_3 oxide was found to be deposited on the surface of Cr_2O_3 pellets as in the Fig. 3, which is thought to interfere the Cr dissolution reaction.

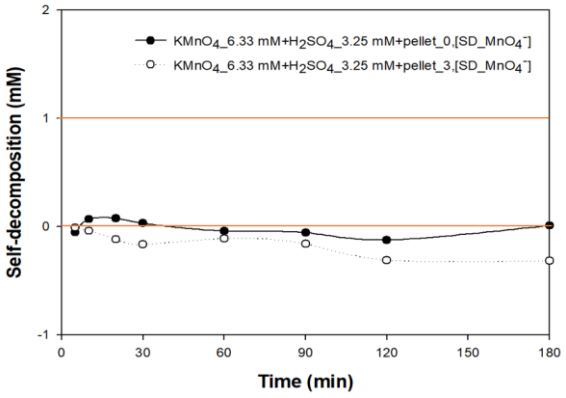

Fig. 1. Self-decomposition of $KMnO_4$ and with without pellet dissolution.

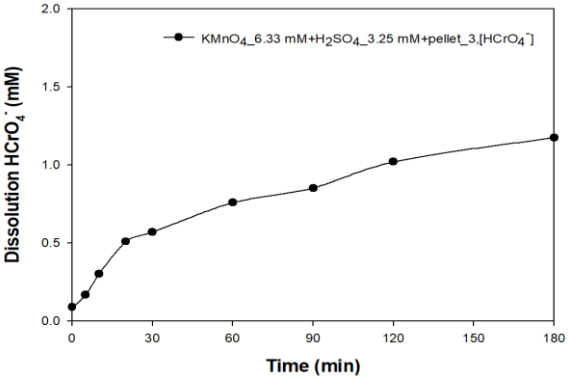

Fig. 2. Cr dissolution behavior in the HyBRID oxidative decontamination condition.

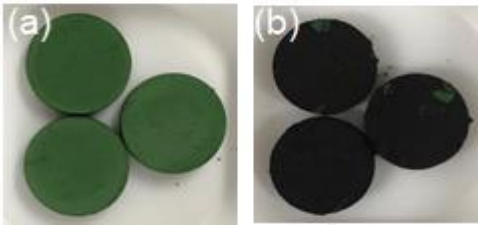

Fig. 3. (a) before and (b) after deposition of MnO_2 particles on the surface of Cr_2O_3 pellets.

4. Conclusion

The following conclusions were obtained from the study on the manganese self-decomposition and Cr dissolution behavior in the HyBRID oxidative decontamination condition by using Cr_2O_3 pellets.

1. Few manganese self-decomposition occurs in the HyBRID oxidative decontamination condition with and without Cr ion dissolution.

2. MnO_2 particles accumulated on the Cr_2O_3 pellet surface takes a role to retard the chromium dissolution rate.

Acknowledgement

This work was supported by the National Research Foundation of Korea(NRF) and the Ministry of Science and ICT(MSIT) of the Republic of Korea. (No. 2017M2A8A5041776)

REFERENCES

[1] W.Z. Oh., et al., “Theory and Application of Decontamination Technology for Dismantling Nuclear Facilities”, Korea Nuclear Export Industry Association (2016).

[2] H.K. Lee., et al., “Spontaneous reductive decomposition behavior of hydrogen permanganate in water for chemical decontamination of nuclear power plants”, Journal of Radioanalytical and Nuclear Chemistry, 317, 1361–1366 (2018).

[3] W.K. Choi., et al., “A Study on the Dissolution Reaction Characteristics of chromium(Ⅲ) Oxide.”, Korean Chemical Engineering Research, 25(6), 634-641 (1987).

Case Study of Hanford Site-specific Hydrologic Parameter Establishing Procedure

SangJune Park*, Jihyang Byon, and Seokyoung Ahn
Pusan National University, 2, Busandaehak-ro 63beon-gil, Geumjeong-gu, Busan, Republic of Korea
*xelidake2@pusan.ac.kr

1. Introduction

In the decommissioning of highly radioactive nuclear facilities, various radionuclides are expected to exist and residual radioactivity is expected to be high. The Hanford site in the US is a highly radioactive nuclear facility that has undergone many nuclear weapons developments, and many cases of decommissioning studies have been conducted. Therefore, this study aims to provide data on highly radioactive nuclear facility research through case study of Hanford nuclear facility decommissioning.

2. Hanford site-specific parameters for RESRAD analyses

In this section, the information about parameters that could be used as Hanford-specific specific parameters are discussed. The key parameters of particular interest to RESRAD vadose zone flow and transport analyses include the hydrostratigraphy and associated flow and transport parameters. The hydrostratigraphy and associated flow and transport parameters can be various according to site.

2.1 Unsaturated zone hydrologic parameters

The hydrologic parameters needed for all unsaturated zone layers for RESRAD analyses include as follow: bulk density (ρ_b), total porosity (P_t), effective porosity (P_e), field capacity (θ_{fc}), saturated hydraulic conductivity (K_s), soil-specific exponential (pore-interaction) parameter (b).

For the bulk density (ρ_b), recent Hanford assessment have defined the best-estimate values as the average of the individual values selected to be representative of the specific model domain sample.

For the total Porosity (P_t), the most reliable estimates for Hanford Site sediments are calculated by equation (1) from measured bulk and particle densities of measured bulk densities and average particle densities.

$$P_t = 1 - \frac{\rho_b}{\rho_s} \quad (1)$$

Where ρ_b is bulk density and ρ_s is particle density.

The best-estimate values for the RESRAD were derived by averaging the total porosity values reported by Freeman and Last (2003) [1], Freeman (2004) [2], Khaleel (2004) [3] and Last et al. (2006) [4].

For the effective porosity (P_e), best-estimates for the Hanford Site are calculated by subtracting the residual volumetric water content from the total porosity. Thus, the best-estimate effective porosity values for the RESRAD are derived by taking the averaged values of the total porosity minus the residual water content as reported by Freeman and Last (2003), Freeman (2004), Khaleel (2004) [1-3], Khaleel et al. (2006a, 2006b) [5, 6], Last et al. (2006) [4], and Khaleel (2007) [7].

For the field capacity (θ_{fc}), best-estimate values for Hanford-specific values for input in RESRAD analyses have been estimated from existing van Genuchten (1980) model water retention parameters. For transport calculations, RESRAD calculates water content values for the unsaturated zone with infiltration rate and the "b" parameter.

For the saturated hydraulic conductivity (K_s), best-estimate values for Hanford-specific RESRAD analyses are based on those defined for selected hydrostratigraphic units and geographic areas for use in specific assessments, in keeping with Khaleel et al. (2001) [8], Khaleel (2004, 2007) [3, 7], Khaleel et al. (2006a, 2006b) [5, 6], and Last et al. (2006) [4].

For the b parameter, there is few data for Hanford sediments. The b parameter can be obtained from the available raw data. This parameter has not been estimated routinely for Hanford Site, and no database currently exist for this parameter. Also, b parameter is derived empirically in a power function model of water retention characteristics by Campbell (1974) [8].

2.2 Hanford site-specific parameters

Through this procedure, the Hanford-specific hydrologic parameters for RESRAD analysis are derived. Table 1. Shows list of the hydrologic parameters and values [9].

Table 1. Hanford site-specific hydrologic parameters

	Bulk density	Total porosity	Effective porosity	Field capacity	Hydraulic conductivity	b parameter
1	1.81	0.34	0.30	0.10	7.27×10^{-4}	2.63
2	2.01	0.21	0.16	NA	5.70×10^{-4}	NA
3	1.67	0.38	0.32	0.18	7.53×10^{-5}	2.63
4	1.70	0.36	0.32	0.12	8.00×10^{-4}	2.31
5	1.64	0.39	0.37	0.07	2.54×10^{-3}	2.03
6	1.91	0.31	0.27	0.08	4.38×10^{-4}	2.53
7	1.95	0.24	0.22	0.06	9.33×10^{-4}	2.96
8	1.99	0.29	0.26	0.06	5.40×10^{-4}	2.95
9	1.66	0.41	0.36	0.13	2.14×10^{-4}	1.77
10	1.69	0.34	0.29	0.14	7.93×10^{-4}	3.54

1. Total average, 2. Backfill average, 3. Silty sand average, 4. Fine sand average, 5. Coarse sand average, 6. Gravelly sand average, 7. Sandy gravel average, 8. Gravel average, 9. Silt average, 10. Caliche average

3. Conclusion

To derive the site-specific hydrologic parameters for RESRAD analysis, following procedure is adapted:

1) Identifies the needed RESRAD parameters; 2) Identifies the raw data sets for the parameter basis; 3) Summarizes the best-estimates parameters used in recent Hanford site assessments; 4) Update the best-estimate parameters.

In the case of Hanford site, there is a lot of site-specific hydraulic data. The raw data sets are derived primarily from borehole geologic and geophysical log data and laboratory analyses.

Compile and verify raw data, stratigraphic units and assessment of the estimate-parameter. In addition, evaluate sensitivity and uncertainty of estimate parameters should be performed. The parameter that lead to the greatest uncertainty in assessment results should be targeted for additional measurement to reduce the uncertainty. Also, it is important to continue to measure the concerned parameter.

The key point is traceability between best-estimate and existing documentation and/or the raw data. Also, the consistency, defensibility and reproducibility of parameter should be ensured. All parameters must belong to database. The database will be maintained and updated.

In this research, the methodology of obtaining the hydrologic parameter for application to RESRAD code from raw data was studied.

For the Countries with few experiences in decommissioning of nuclear power plants, it will be able to acquire and experience relevant knowledge by studying decommissioning cases and methodologies of leading countries.

ACKNOWLEDGEMENT

This work was was supported by the National Research Foundation of Korea grant funded by the Korea government [No. NRF-2018M2B2B1065637]; and was supported by the nuclear research and development program through the National Research Foundation of Korea funded by the Ministry of Science and ICT(MSIT, Korea). [NRF-2019M2C9A1057807].

REFERENCES

[1] Freeman EJ and GV Last, “Prototype Vadose Zone Properties Database and Users Guide”, WMP-17524, Rev. 0, Fluor Hanford, Richland, Washington (2003).

[2] Freeman EJ. “Hanford Vadose Hydraulic Properties Database Update for FY 2004”, Pacific Northwest National Laboratory (2004).

[3] Khaleel R, “Far-Field Hydrogeology Data Package for the Integrated Disposal Facility”, RPP-20621, Rev. 0, CH2M HILL Hanford Group, Inc., (2004).

[4] Last GV, EJ Freeman, KJ Cantrell, MJ Fayer, GW Gee, WE Nichols, BN Bjornstad, and DG Horton, “Vadose Zone Hydrogeology Data Package for Hanford Assessments”, PNNL-14702, Rev. 1, Pacific Northwest National Laboratory (2006).

[5] Khaleel R, MP Connelly, and WJ McMahon, “Modeling Data Package for an Initial Assessment of Closure of the S and SX Tank Farms”, RPP-17209, Rev. 1, CH2M HILL Hanford Group, Inc. (2006a).

[6] Khaleel R, MP Connelly, WJ McMahon, and MI Wood, “Modeling Data Package for an Initial Assessment of Closure of the C Tank Farm”, RPP-13310, Rev. 1, CH2M HILL Hanford Group, Inc., (2006b).

[7] Khaleel R, “Far-Field Hydrology Data Package for the RCRA Facility Investigation”, RPP-RPT-35222, Rev. 1,Fluor Government Group (2007).

[8] Campbell GS, “A Simple Method for Determining Unsaturated Conductivity from Moisture Retention Data”, Soil Science (1974).

[9] Last GV, Murray CJ, Rockhold ML, Cantrell KJ, “Selection and traceability of parameters to support Hanford-Specific RESRAD Analyse”, Pacific Northwest National Laboratory (2009).

Readiness Review of APR1400 Decommissioning Design for UK Export

Hye-Young Shin* and Dae-Jun Kim†

KHNP Central Research Institute, 70, Yuseong-daero 1312beon-gil, Yuseong-gu, Daejeon, Republic of Korea

*shinehyshin@khnp.co.kr, †smilekdj@khnp.co.kr

1. Introduction

Global demand for nuclear power plants is increasing among existing NPP operating countries which would replace their older reactors and emerging nuclear energy countries which are considering, planning or starting nuclear power programs. Since the first export to UAE in 2009, the Korean export type reactor APR1400 has continuously improved its design in order to re-enter overseas and finally obtained EUR (European Utility Requirements) Certification in 2017, Standard Design Acceptance from US NRC in 2018.

The UK, planning 16GW new construction of nuclear power plants by 2030 in order to replace older reactors permanently shut down before 2025 (this corresponds to the half of the UK nuclear capacity), is one of the targeting countries for exports of APR1400.

This paper introduces UK regulations on new nuclear reactor design, reviews precedent application cases, and evaluates the readiness of APR1400 to apply UK licensing process for obtaining Design Acceptance Confirmation (DAC) from ONR (Office for Nuclear Regulation), the UK regulatory body, from the view point of decommissioning.

Table 1. GDA Progress Status of New Reactors

Reactor	Designer	Application	DAC
UK EPR	EdF/Areva	2007.04	2012.12
AP1000	Westinghouse	2007.04	2017.03
UK ABWR	Hitachi-GE	2013.01	2017.12
UK HPR1000	GNS Ltd	2017.01	On-going (Step 3)

2. UK GDA Process and Regulation

UK Government established a new process called GDA (Generic Design Assessment) based upon 2006 Energy Review for permitting for new nuclear power stations. The GDA process is composed of 4 steps; preparation of the design, safety case and security submissions (step 1), fundamental design, safety case and security claims overview (step 2), overall design, safety case and security arguments review (step 3) and detailed design, safety case and security evidence assessment (step 4). 4 advanced reactors completed or is undergoing each GDA process so far. Table 1 shows the GDA progress status of the reactors.

ONR's regulatory decision making in the nuclear permissioning process is based upon SAPs (Safety Assessment Principles) for nuclear facilities and the supporting guides TAGs (Technical Assessment Guides). Regarding decommissioning, SAPs has 9 principles and 53 provisions. As the review result on the principles and provisions, 5 principles are identified as the regulatory baseline to be satisfied with from the GDA stage in the life cycle of a new nuclear power plant as shown in Fig. 1.

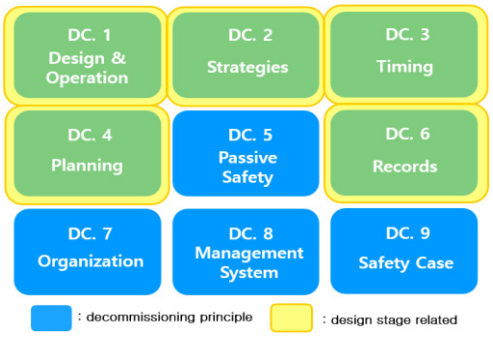

Fig. 1. Decommissioning Related SAP Principles and Design Stage Related Principles.

Table 2. Conformance with Decommissioning Principles

Principle	AP1000	UK ABWR	UK HPR1000
Design & Op.	◎	◎	◎
Strategies	◎	◎	◎
Timing	○	○	◎
Planning	◎	◎	◎
Records	-	◎	◎
[Extra] # of TR*	6	7	1

* Topical Report or Technical Report

3. Case Studies

Main document required to be submitted for GDA process, especially for step 3 and 4, is a generic PCSR (Pre-Construction Safety Report) and all the submitted PCSRs are available on the ONR website. Decommissioning parts of each PCSR for three new reactors except UK EPR have been reviewed for case studies. All the decommissioning chapters contains the required information on the compliances of five principles to each reactor type even though the level of details is different. Especially, UK-ABWR has several topical reports supporting the principles and providing technical aspects such as decommissioning (DC) techniques, impact of construction techniques on DC, DC waste management, and DC safety assessment. The other two reactors also have some separate technical reports as references [1, 2, 3]. Table 2 shows the comparison of SAP decommissioning principle compliances of the new nuclear reactors.

4. Conformance of APR1400 Design

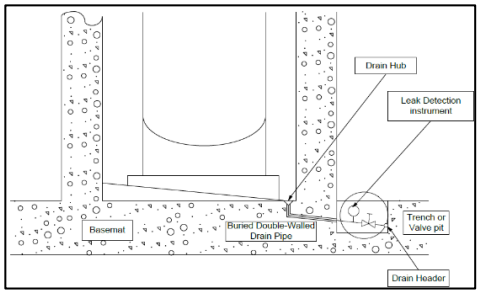

Fig. 2. Typical Design Details of Drainage and Leak Detection Configuration.

APR1400 has mature design features considering decommissioning: US-APR1400 satisfies Reg. Guide 4.21 with the design for minimizing contamination of the facility/environment, minimizing waste generation, and facilitating decommissioning [4]. Fig. 2 presents one example of physical design details for preventing unintended contamination to the environment and for easy removal. EU-APR has the well-developed IDP (Initial Decommissioning Plan) meeting European Utility Requirements [5], and Shin-Kori Unit 3 (the first operating APR1400) has the decommissioning design criteria [6] and the preliminary decommission-ing plan for the operational stage. These are evaluated to satisfy the SAP principles for GDA application.

5. Conclusion

APR1400 has good design features for facilitation of decommissioning and a well-organized decom- missioning plan including strategy, timing, and record aspects satisfactory with the related SAP principles. Therefore APR1400 decommissioning design is ready for an entrance to UK nuclear market.

REFERENCES

[1] Westinghouse, AP1000 PCSR, Chapter 27, UKP-GW-GL-793NP, Rev. 0, Jan. 2016.
[2] HITACHI, UK ABWR GDA, Generic PCSR Chapter 31, DCE-GD-0007. Rev. B, 2015.
[3] GNS Ltd, UK HPR1000 GDA, PCSR, Chapter 24, Rev.0, Dec. 2018.
[4] KEPCO/KHNP, APR1400 DCD Tier 2, Chapter 12, Rev. 3. Aug. 2018.
[5] KHNP, Topical Report, “EU-APR Initial Decommissioning Plan”, 1-035-N495-103, Jan. 2017.
[6] KHNP, Shin-Kore Unit 3 FSAR, Chapter 12, nsic.nssc.go.kr/dta/reguResultlList.do, 2019.

Removal of Manganese Ion in the HyBRID Decontamination Process Using Electrochemical Method

J.H. Sim*, S.Y. Park, and S.B. Kim
Korea Atomic Energy Research Institute, 111, Daedeok-daero 989beon-gil, Yuseong-gu, Daejeon, Republic of Korea
*jhsim@kaeri.re.kr

1. Introduction

KAERI is conducting research on the HyBRID (Hydrazine Base Reductive metal Ion Decontamination) process as the primary system chemical decontamination technology of nuclear power plants [1]. In this process, to oxidize the major metal oxides, potassium permanganate is used as an oxidizing agent. After the oxidation process, it remains as manganese ions in the decontamination solution. In particular, manganese ions react with permanganate to form manganese oxide, which negatively affects the continuous decontamination process. Therefore, it is necessary to remove manganese ions from the decontamination solution. In this study, the mechanism and the efficiency of removing manganese ion was analyzed using the electrochemical techniques.

2. Experimental

All experiments were performed in a specially designed 1L electrolytic cell considering the electrode position. An aqueous 10 mM H_2SO_4 + 1 mM $MnSO_4$ solution was used as a electrolyte, and for this purpose, 97 % purity H_2SO_4 and 99 % purity $MnSO_4$(Sigma-Aldrich) were prepared. A platinum electrode was taken as the working electrode (WE) and the counter electrode (CE). An Ag/AgCl electrode was used as the reference electrode. The experiments were performed at room temperature with a ZIVE LAB MP3 potentiostat/galvanostat system.

3. Results and Discussion

3.1 Mechanism of manganese ion oxidation

Fig. 1 shows the CV (cyclic voltammetry) curves measured in aqueous 10 mM H_2SO_4 + 1 mM $MnSO_4$ solution. According to this, when only H_2SO_4 is present, the redox reaction of hydrogen occurs at -0.2 to 0 V, and redox reaction of oxygen occurs at 0.4 to 0.6 V. However, when $MnSO_4$ added, new peak current appears at about 0.9 V and 1.2 V, indicating that redox reaction of manganese ions occurs.

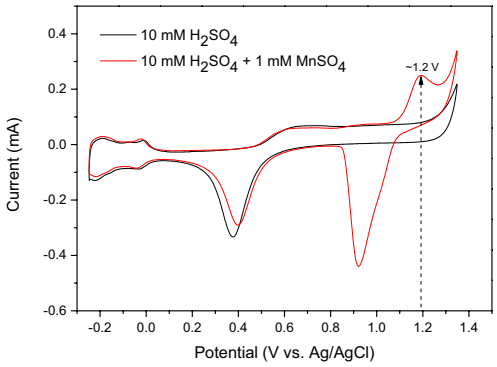

Fig. 1. CV curves of aqueous solution.

For a more detailed analysis, DPV (differential pulse voltammetry) was measured for the oxidation direction and shown in Fig. 2. It is found that three oxidation peak currents are observed between 0.4 V to 1.2 V. This shows that oxidation of manganese ion occurs in three steps. Wenxin Huang et al. was found that the oxidation of manganese ions undergoes a three step reaction as follows [2].

$Mn^{2+} \rightarrow Mn^{3+} + e^-$

$Mn^{3+} + H_2O \rightarrow MnOOH + 3H^+$

$MnOOH \rightarrow MnO_2 + H^+ + e^-$

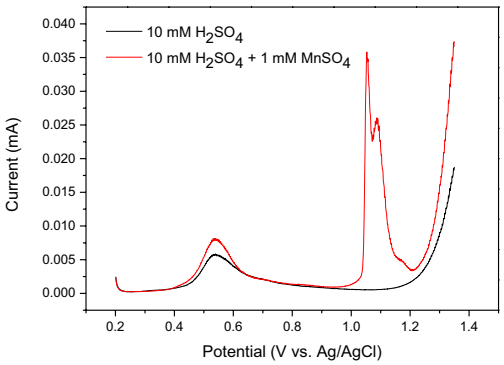

Fig. 2. DPV curves of aqueous solution.

Therefore, it is thought that the manganese ions are oxidized and electrodeposited as manganese oxides according to the above reactions in this experiment.

3.2 Electrodeposition of manganese ion

Considering the CV and DPV results the electrodeposition experiment by the chrono-amperometry was performed at 1.35 V for 1 hour. Also, the electrodeposition by chrono-potentiometry was performed for 1 hour with adjusting the current value (21.54 mA) to apply the same amount of charge as the constant potential experiment. After the test, the concentration analysis was performed for each of the results. At first, Fig. 3 shows that black colored manganese oxide was electrodeposited on the electrode surface after the experiment, unlike before the experiment.

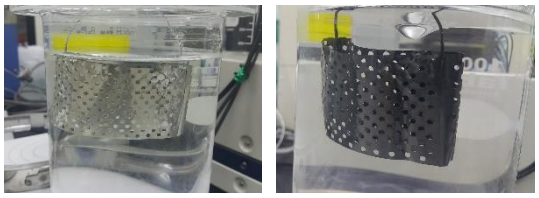

Fig. 3. Electrode surface before & after test.

According to the concentration analysis results in Table 1, it is found that both the potentiostatic method and the galvanostatic method are effective for removing manganese ions in the solution. Especially in the case of potentiostatic method, the removal efficiency for 1 hour is nearly 50 % and current efficiency is about 83 % compared to the theoretical value. Therefore, it is possible to remove most of the manganese ions in the decontamination solution if sufficient electrode area is secured.

Table 1. Results of concentration analysis

Contents	Potentiostatic	Galvonostatic
Initial con.(mM)	0.8109	0.8109
After test (mM)	0.4587	0.5060
Deposit (%)	43.43	37.60
Efficiency (%)	83.85	75.84

4. Conclusion

An electrochemical experiment was carried out to remove manganese ions in decontamination solution of HyBRID process under research and development at KAERI. It is found that manganese ions can be effectively removed by oxidizing them to manganese oxide using the potentiostatic and galvanostatic methods. Also, it is important to secure sufficient electrode area for high removal capability.

REFERENCES

[1] W.K. Choi et al., “Development of Advanced Decontamination Technology for Nuclear Facilities”, KAERI/RR-4230/2016.

[2] Wenxin Huang, Jun Li, Yunhe Xu, “Nucleation and Growth of Porous MnO_2 Coatings Prepared on Nickel Foam and Evaluation of Their Electrochemical Performance”, Materials, 11(716), 1-19 (2018).

Production of Zr Metal by Decomposition of ZrCl at High Temperature

Jungho Hur, Gwan Yoon Jeong, Younghwan Jeon, Hyeongjin Byeon, Hyewon Shin, and Jaeyeong Park*

Ulsan National Institute of Science and Technology, 50, UNIST-gil, Eonyang-eup, Ulju-gun,

Ulsan, Republic of Korea

*jypark@unist.ac.kr

1. Introduction

Zirconium is being broadly used in the nuclear industry such as material for pressure tube, calandria tube, and fuel cladding. After an operation, the electrochemical process has been developed to recover zirconium using chloride molten salt system. However, ZrCl, insoluble formation, was co-deposited with Zr metal during the process [1,2]. To solve this fundamental problem in chloride system, basic study for reduction from ZrCl to Zr metal was performed.

2. Experimental Setup

2.1 General Experimental plan

Firstly, ZrCl has to be produced for reduction process experiments. ZrCl can be made by potentiostatic electrorefining process. The Peak of ZrCl formation from Zr^{4+} was configured from previous studies [2,3]. In this study, -1.1V vs. 1wt.% Ag/AgCl reference electrode was applied due to small different condition.

Secondly, thermogravimetric analysis and differential scanning calorimetry (TGA/DSC) analysis was performed to investigate the decomposition reaction of ZrCl in high temperature.

2.2 Electrolysis

LiCl-KCl eutectic salt and $ZrCl_4$ with the purity of 99.99% were provided from Sigma-Aldrich. AgCl with the purity of 99.99%, 3.175mm diameter of tungsten rod with the purity of 99.95% and 4mm diameter of tungsten rod with the purity of 99.96% was provided from Alfa Aesar.

Table 1. Condition of electrolysis for ZrCl production

Variables	Value
Temperature	450°C
Salt composition	LiCl-KCl-2wt.%$ZrCl_4$ 32.56g
Electrode	WE: W(D=3.175mm) CE: W(D=4mm) x 2 RE: 1wt.% Ag/AgCl
Applied potential	-1.1V vs. RE
Working height	2.3 cm

2.3 TGA/DSC

STA 449 F5 Jupiter model from NETZSCH was used for TGA/DSC experiments.

Table 2. Experimental condition for TGA/DSC

Variables	Value
Temp. range	100-1000°C
Temp. rate	10K/min
Atmosphere/Pressure	Ar/1atm

3. Results

3.1 Electrolysis

After 24 hours of electrolysis experiment to

deposit ZrCl on the electrode, High Power XRD was utilized to analyze chemical composition. In Fig. 1, only ZrCl peak could be observed. Other peaks stand for LiCl and KCl which is used as electrolyte. No Zirconium metal peak was shown.

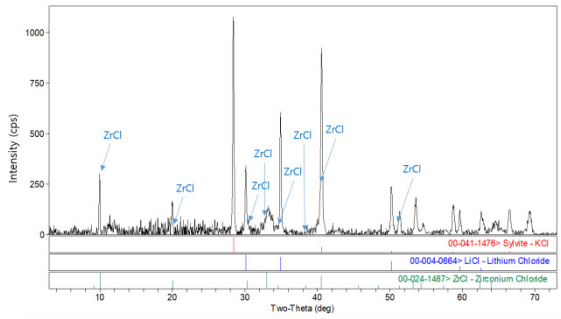

Fig. 1. XRD pattern for deposition.

3.2 TGA/DSC

TGA/DSC analysis was performed for deposition and residual electrolyte after electrolysis. In Fig. 2, melting point of LiCl-KCl eutectic was observed at about 350°C. After about 700°C, region 1 which shows different slope in deposition result was observed. It is inferred that ZrCl reduction reaction:

$$4ZrCl \rightarrow ZrCl_4 + 3Zr \qquad (1)$$

It is also inferred that LiCl-KCl eutectic and residual $ZrCl_4$ were evaporated at region 2.

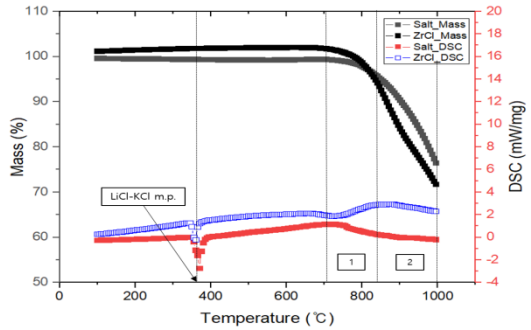

Fig. 2. TGA/DSC results for ZrCl and electrolyte.

4. Conclusion and Future work

In this paper, ZrCl was produced and TGA/DSC analysis for ZrCl and electrolyte was performed to investigate the feasibility of reduction process from ZrCl to Zr metal. To consolidate and visualize the potential of process, further experiments have to be conducted. TGA/DSC for pure LiCl-KCl and LiCl-KCl with different concentration of $ZrCl_4$ will be performed to define reaction in region 1 and 2 concretely. Bulk distillation experiments of ZrCl under reduced pressure will be performed and chemical composition of product will be investigated.

REFERENCES

[1] S. J. Sohn, J. Y. Park, and I. S. Hwang, “Electrolytic Recovery of High Purity Zr from Radioactively Contaminated Zr Alloys in Chloride Salts”, International Journal of The Electrochemical Science, 13, 3897-3909 (2018).

[2] C. H. Lee, K. H. Kang, M. K. Jeon, C. M. Heo and Y. L. Lee, “Electrorefining of Zirconium from Zircaloy-4 Cladding Hulls”, Journal of The Electrochemical Society, 159(8), D463-D468 (2012).

[3] J. Y. Park, S. Y. Choi, S. J. Sohn, K. R. Kim and I. S. Hwang, “Cyclic Voltammetry on Zirconium Redox Reactions in LiCl-KCl-$ZrCl_4$ at 500°C for Electrorefining Contaminated Zircaloy-4 Cladding”, Journal of The Electrochemical Society, 161(3), H97-H104 (2014).

Considerations of Hazardous Materials in Decommissioning of Nuclear Power Plant

Su-Hee Lee* and Hye-jin Jung

KHNP Central Research Institute, 70, Yuseong-daero 1312beon-gil, Yuseong-gu, Daejeon, Republic of Korea

*suhee.lee@khnp.co.kr

1. Introduction

Regulations on radioactive or hazardous materials during operating/dismantling phase of nuclear power plant are well established and normatively defined in most countries. However, there are no specific rules and regulations when radioactive materials and hazardous substances present together in Korea.

According to dismantling activity cases, the problems of hazardous materials with low radioactivity surfaced after the nuclear power plant decommissioning plan had sufficiently developed, schedule and budget have already established. This unexpected problem could cause significant time delays at the dismantling process and impact on the main activities of radioactive components' disassembly, resulting in considerable cost overruns. So these mixed wastes require a specific management strategy.

To prevent hazardous materials from being contaminated by radiation during dismantling or decontamination, we need to figure out how to these materials are managed. In this paper, we will define which hazardous materials that have to be considered during decommissioning nuclear power plant and it could possibly be radioactively contaminated wastes.

2. Non-radioactive Hazardous Materials in Nuclear Power Plants

During decommissioning periods, hazardous materials of concerns in overseas are listed in Table 1 [1]. There are two types of non-radioactive hazardous materials to be cared.

Table 1. Hazardous materials of concern in overseas

Classification	Examples
Organic compounds	·Volatile organic compounds (VOCs) ·Semi-volatile organic compounds (PCBs, Dioxins, furans, Pesticides/herbicides), etc.
Hazardous metals	·Lead ·Mercury, etc.
Special, Universal and Solid Wastes	·Asbestos Containing Materials(ACM) ·Oil ·Petroleum Hydrocarbon based products ·Batteries ·Solid waste, etc.

2.1 Non-radioactive Hazardous Materials on SSCs

In nuclear power plant, there are many System, Structures and Components, which surfaces are on non-radioactive materials such as paints, PCBs and asbestos. This type of materials can be scattered into the air during the dismantling and decontamination process and needs to be managed in terms of worker occupational safety.

2.2 Non-radioactive Hazardous Materials in Radiation Controlled Area

It includes non-radiological hazardous substances that have been, are being used, stored, or disposed of during the operation of the present or past in the plant. Table 2 shows the non-radioactive hazardous materials [2] used in the radiation management area of domestic nuclear power plants operating and most of them are managed and treated in terms of suitability for disposal of radioactive waste drums after use.

Table 2. Major Hazardous substances used in power plants

Classification	Examples
Flammable	·Adhesive, Gasket remover, lubricants, paint, thinner, etc.
Explosive	·Butane gas, etc.
Strongly oxidized	·Batteries ·Chemicals, etc.
Hazardous substance	·Sealants, Fireproof silicone, etc.
Chelating agents and Oxidative	·Detergents, etc.

3. Conclusion

There is a need for specific management plans for mixed waste (radioactive materials and hazardous substances are present) to minimize dismantling process delays and cost overruns. Before this, it is a priority to prevent the affection by managing non-radioactive hazardous materials in the nuclear power plant.

During the decommissioning periods, it is necessary to examine where the non-radioactive elements are essential for the disassembly process of the radioactive inclusions, or where they are concentrated or dispersed. This should be conducted prior to the historical site assessment or, if possible, permanent suspension in the preliminary stage of dismantling.

REFERENCES

[1] R.Reid. “Guidance for Management of Hazardous Materials during Decommissioning”, EPRI, Palo Alto, CA: 2017.3002010592.

[2] Ministry of Environment, Industrial Safety and Health Act, 2018.

Prediction of Waste From Site Remediation for Kori 1

Kyung-Min Go and Chang-Lak Kim*

KEPCO International Nuclear Graduate School, 658-91, Haemaji-ro, Seosaeng-myeon, Ulju-gun, Ulsan, Republic of Korea

*clkim@kings.ac.kr

1. Introduction

As the number of nuclear power plants that have reached the end of their lifetime has increased, an interest in dismantling of nuclear power plants has been increased throughout the world. In Korea, the first commercial NPP, Kori Unit 1, was permanently shut down in 2017, and has already progressed in decommissioning stage. Therefore, preparations for dismantling and site restoration technology and safety regulations are urgently required. The final goal of decommissioning of NPP is to terminate the facility's operating license and to eliminate any residual contaminants in the site boundary allowing the site and building to be reused for other purposed. To reach the goal, we should investigate and eliminate all contaminated materials remaining in the site boundary, so that the site can be finally reused limitedly or unlimitedly. There are various kinds of site remediation technologies which can be applied to Kori unit 1 decommissioning project and future decommissioning projects in Korea. In this study, we derived the predictable waste generated through the site remediation according to the review of remediation technologies which can be applied to Kori unit 1 decommissioning project.

2. Remediation Technologies

When we choose proper technologies, we need to consider several factors to deal with or mitigate environmentally contaminating cases. IAEA recommended that the technology evaluation factors will be provided to make appropriate decisions when it comes to the choice of suitable technology. The required factors which shall be considered are such as performance of the technology, reliability, availability, safety, suitability, and regulatory acceptance etc. [1].

Followings are various remediation technologies which can be applied to Kori unit 1 decommissioning project.

- Natural Remediation
- Containment Technology
- Stabilization Technology
- In Situ Technology
- Thermal Treatment Technology
- Removal Technology
- Ex Situ Technology

Natural remediation is covering any technology or strategy that utilizes natural processes such as absorption, retardation and radioactive decay. Containment technology utilizes physical barriers or specific equipment to isolate contaminants and to restrict any movement. Stabilization is the general term for a process that reduces the mobility of contaminants and hazardous substances by using physical or chemical methods. In situ technology is biological, physical, and chemical treatment that removes or degrades contaminants without excavating or removing soils. Thermal treatment technology will remove or fully destroy the element of contaminated

material. Removal technology will completely eliminate and transport contaminants to do additional treatment and/or disposal. Ex situ technology eliminates contaminated material to a disposal area or treatment facility [1, 2].

3. Prediction of Remediated Waste

We reviewed various kinds of remediation technologies. Each technology has different characteristics and leaves or generates different types of remainders which need to be moved into disposal facilities. Table 1 shows the main remainders or wastes by adopting preferred remediation technologies.

Table 1. List of waste from remediating works

Waste Remainder	Related Technology
Soils, groundwater, concrete, metals etc.	Natural Remediation
Caps, barriers, walls, soils, water, hydraulic system or equipment etc.	Containment Technology
Block of contaminant encapsulated, consolidated waste etc.	Stabilization Technology
Residuals from biological/physical/chemical treatment, treatment system	In Situ Technology
Vitrified material, gases, water, thermal treatment system etc.	Thermal Treatment
Typical excavation equipment*, protective equipment, filters etc.	Removal Technology
Typical excavation equipment*, vitrified material, precipitator, filters, ion exchange resins	Ex Situ Technologies

* Excavation equipment can be re-used. It depends on the circumstances and uses protective covers to protect radioactive material exposure.

4. Conclusion

This paper introduced some applicable remediation technology for Kori unit 1 decommissioning project and future decommissioning projects in Korea. It also derives the different types of remediated wastes according to the introduced remediation technology. We suggest that the secondary waste shall be considered when a decommissioning plan will be prepared. Because they will be transported to a disposal facility which has limited capacity.

Acknowledgement

This research was supported by the Nuclear Safety Research Program through the Korea Foundation of Nuclear Safety (KOFONS), granted financial resources from the Nuclear Safety and Security Commission (NSSC), Republic of Korea (No. 1605008).

REFERENCES

[1] IAEA, Technologies for remediation of radioactively contaminated sites, IAEA-TECDOC-1086, June 1999.

[2] X.H. Zhang, EOLSS Publications, Point Sources of Pollution: Local Effects and their Control - Volume II, Remediation Techniques for Soil and Groundwater, 2009.

Deep Soil Remediation and Regulatory Case in the U.S.

Won-Jae Shin and Chang-Lak Kim*

KEPCO International Nuclear Graduate School, 658-91, Haemaji-ro, Seosaeng-myeon, Ulju-gun, Ulsan, Republic of Korea

*clkim@kings.ac.kr

1. Introduction

Since Korea Hydro & Nuclear Power Co., Ltd. (KHNP) decided to permanently cease the operation of Kori 1 nuclear power plant (NPP) in June, 2015, the Korean government and associated organizations have been conducting preliminary studies for the first decommissioning of a large-scale commercial NPP. Decommissioning includes not only the physical demolition, but the entire procedures from preparation decontamination and dismantling to site remediation. Although the Korean government has immediate dismantling (DECON) plan on Kori1, further studies on decommissioning seem to be still needed due to a lack of experience.

In this study, the overall site remediation process and remediation cases are reviewed focusing on deep soil remediation in the United States. In addition, regulatory cases on soil remediation which were regulated by the regulatory body are reviewed to derive considerations to set Kori 1 remediation strategy.

2. Soil Remediation Process

RESRAD (RESidualRADioactive materials) code and MARSSIM (Multi-Agency Radiation Survey) are widely used for site remediation in the U.S. The U.S. Nuclear Regulatory Commission (NRC) sets the TEDE (Total Effective Dose Equivalent) limit as 0.25 mSv/yr for unrestricted use, and 1 mSv/yr with ALARA for restricted use.

In the translation process, site release criteria is converted into corresponding site-specific DCGL (Derived Concentration Guideline Level) levels for each radionuclide by using RESRAD modeling. Then the site-specific data set is collected during the measurement process with Historical Site Assessment (HSA) and characterization survey. The decision process provides the confidence to verify compliance of data obtained from final status survey (FSS). Because information from each process affects adjacent processes, processes are iteratively performed to improve the quality of the results.

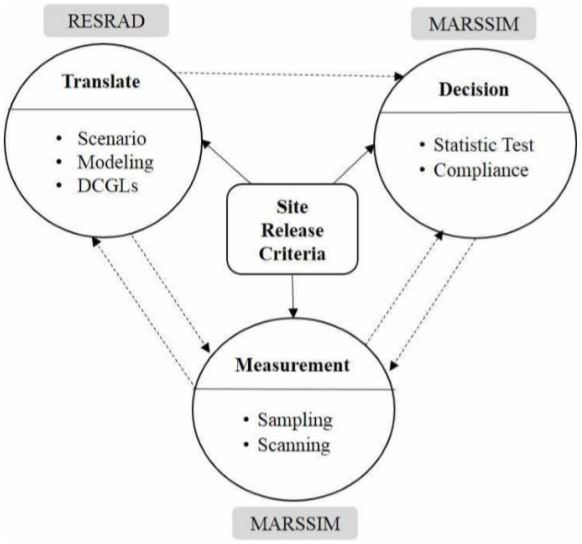

Fig. 1. Site Remediation Process Concept [1].

NUREG-1757 provides detailed guidelines for soil remediation process as below.

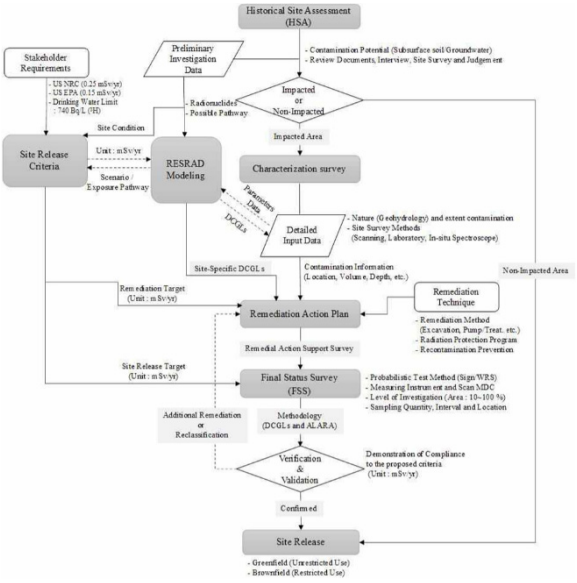

Fig. 2. Soil Remediation Process [1].

3. Case Study

3.1 Soil Remediation Case

Maine Yankee and Haddam Neck nuclear power plant have been chosen to review the soil remediation and regulatory cases considering the type of reactor and site conditions.

In MY site, most of soil contaminations were associated with Processed (or Primary) Water Storage Tank (PWST), Refueling Water Storage Tank (RWST) and Shielded Radiological Waste Storage Area in Radiologically Restricted Area (RRA), and excavation has been performed with maximum of 1 meter depth mainly using excavator [2].

In case of HNP, various radionuclides were detected in RCA and adjacent soil, and the licensee implemented a graded approach to classify the deep soil from Class A to C. Remediation works were performed up to 12.2 meters using excavators and high flow rate vacuum trucks [3].

3.2 Regulatory Case

After reviewing the FSS report, U.S. NRC issued Request of Additional Information (RAI) and asked licensee to provide more detailed information.

Table 1. RAI issued by U.S. NRC

NRC RAI
U.S. NRC Letter to Maine Yankee dated January 5, 2005, Request for Additional Information (RAI) Regarding Final Status Survey (FSS) Supplement No.4
U.S. NRC Letter to Haddam Neck Plant dated March 19, 2001, Request for Additional Information (RAI) Regarding The License Termination Plan (LTP)

4. Conclusion

In this study, overall site remediation process and the case in the U.S. were reviewed.

Although U.S. has a lot of experience on soil remediation, operators and the regulatory body sometimes have had different perspective of view on deep soil remediation criteria since the evaluation methodology on deep soil has not been established yet. Therefore, further study on RESRAD modeling assuming source term in deep soil with uncontaminated surface soil cover is needed as well as the international experiences on site remediation.

Acknowledgement

This research was supported by the Nuclear Safety Research Program through the Korea Foundation of Nuclear Safety (KOFONS), granted financial resources from the Nuclear Safety and Security Commission (NSSC), Republic of Korea (No. 1605008).

REFERENCES

[1] United Federal Agencies, "NUREG-1575, Multi-Agency Radiation Survey and Site Investigation Manual (MARSSIM), Rev. 1" NRC, EPA, DOE and DOD, 2000.

[2] Maine Yankee Atomic Power Company, "Maine Yankee's License Termination Plan. Revision 5" MYAPC, MN-09-005, 2009.

[3] Connecticut Yankee Atomic Power Company, "Haddam Neck Plant License Termination Plan, Revision 4" CYAPC, 2006.

A Conceptual Study for the Separation of Clean Aggregate From Radioactive Concrete Waste

Keunyoung Lee[1,*], Maengkyo Oh[1,2], and Bum-Kyoung Seo[1]

[1]Korea Atomic Energy Research Institute, 111, Daedeok-daero 989beon-gil, Yuseong-gu, Daejeon, Republic of Korea

[2]Yonsei University, 50, Yonsei-ro, Seodaemun-gu, Seoul, Republic of Korea

[*]lky@kaeri.re.kr

1. Introduction

Radioactively contaminated and/or activated concrete waste might be a predominant waste generated from the decommissioning of nuclear facilities, along with radioactive metal waste. In Korea, the final cost for the disposal of radioactive waste is extremely high, which is the reason that various treatment and volume reduction methods are being developed to better performance and efficiency. The separation of clean aggregate from the concrete waste has been a typical method for the volume reduction of radioactive concrete waste [1]. In the present study, we investigated the properties of aggregate separation by thermomechanical treatment and chemical dissolution, and the possibilities of treated aggregate as a clearance waste.

2. Materials and Methods

2.1 Concrete

An artificially contaminated concrete waste was prepared by adding radionuclides, Co-60 and Cs-137, into a normal concrete waste. The crushed concrete with the size of less than 40 mm was used, and the initial radioactivity of around 40 Bq/g was applied.

2.2 Heating and Grinding

The concrete sample was heated at 550 ^{o}C for 40 min in a muffle furnace, as the condition optimized previously [2]. The sample was grinded in a milling jar with and without grinding ball media, after cooling the sample at a room temperature. The sample amount was varied from 150g to 450g, and the milling time was 1hr to 6hrs. The residual cement contents in the treated concrete aggregates with the size of larger than 1 mm were analyzed to evaluate the separation performance of heating and grinding processes.

2.3 Chemical Dissolution

After the thermomechanical treatment, the residual cement in the concrete aggregates larger than 1 mm was dissolved in the acid solution with 0.4 M of hydrochloric acid at different temperatures. The acid concentration for the dissolution of residual cement was decided by measuring the residual cement contents and radioactivities of samples from each step.

2.4 Analysis

The residual cement contents were measured by dissolving cement in a concentrated acid solution with high temperature around 95 ^{o}C. Except for a minor content of silica, most of

calcium and other metals are dissolved in the condition. The radioactivities of Co-60 and Cs-137 were analyzed by gamma spectroscopy.

3. Results and Discussion

3.1 Cement Separation Properties

The residual cement contents in the aggregates larger than 1 mm of different grinding conditions were compared (Table 1). The conventional ball milling showed 10.19% of residual cement in the aggregate. Although the rotary mill (without ball media) for longer treatment time showed higher cement content than ball mill, the cement content could be lowered by increasing the treatment amount by three times (9.13% of cement with 450g use).

Table 1. Residual cement contents (wt%) in the treated concrete aggregates

Conditions	Cement contents (wt%) dissolved from aggregates
150g, Ball mill, 1hr	10.19
450g, Rotary mill, 6hr	9.13
300g, Rotary mill, 6hr	12.07
150g, Rotary mill, 6hr	14.68
450g, Rotary mill, 4hr	8.49
450g, Rotary mill, 2hr	9.78
450g, Rotary mill, 1hr	9.85

3.2 Radionuclide Separation Properties

It is too difficult to ideally separate the pure aggregate by thermomechanical method. In order to remove radionuclides from the treated aggregate, the acid dissolution can be applied for the dissolution of residual cement as well as target radionuclides. Our experimental results demonstrated that the diluted acid solution could be applied for the removal of Co-60, but it was not enough condition for the clearance of waste containing Cs-137. More effective method should be considered for the separation of aggregate with high Cs contamination.

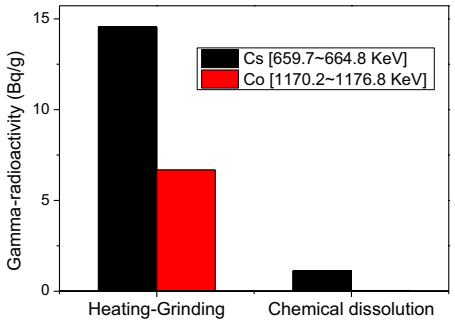

Fig. 1. Variation of gamma-radioactivity of the aggregates after the treatment steps for separation.

REFERENCES

[1] K.Y. Lee, et. al., "Trends in technology development for the treatment of radioactive concrete waste", Journal of Nuclear Fuel Cycle and Waste Technology, 16(1), 93-105 (2018).

[2] M.K. Oh, et. al, "Preliminary study on the heating and grinding method for volume reduction of radioactive concrete waste from decommissioning process", Proc. of the KRS 2018 Autumn Conference, Oct. 31-Nov. 1, 2018, Jeju.

Process-Based Approach for Verification, Validation, and Testing (VVT) of Waste Stream in Comprehensive NPP Radioactive Waste Processing Facility

Sun-Kee Lee* and Chang-Lak Kim†

KEPCO International Nuclear Graduate School, 658-91, Haemaji-ro, Seosaeng-myeon, Ulju-gun, Ulsan, Republic of Korea

*penda1226@naver.com, †clkim@kings.ac.kr

1. Engineered System Structure for the Processing Facility

Engineered system consists of the end products that make up the processing facility and the enabling products from life-cycle perspectives. As shown in Figure 1, end products consist of a number of structures, systems and components, enabling products include management, technology, deployment, operation and VVT for development, production, use/maintenance and disposal.

Structures, systems and components may be classified into safety-related and non-safety-related. Radiation exposure, industrial accident and structural defect may cause safety problems, which VVT may prevent.

Design description of the processing facility are reflected in design documents, which define the functions and requirements derived from development stage. If the designed functions of structures, systems and components are not secured, it is not possible to guarantee the safety of waste stream as well as the processing facility.

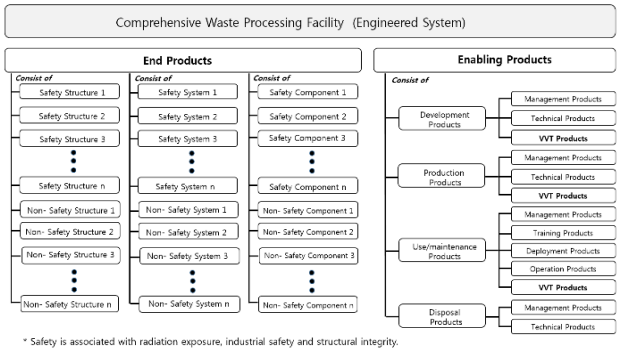

Fig. 1. Engineered System Structure of Waste Processing Facility.

Table 1. Waste Stream Grouping (Steel, Concrete)

Waste Group	type	Radiactive Waste Level prior to processing	Comprehensive NPP Decommissioning Radioactive Waste Processing Facility								
			Cutting	Measurement	Decontamination	Measurement	Melting		Compression	Packing	Immobilization	Evaluating package characteristics
							Plasma Torch	Induction				
Reactor Prseesure Vessel	Head Cover, Vessel Flange, Low Head, etc/ activated	LLW										O
		VLLW										O
Reactor Internals	Upper structure, Lower structure, Connected equipment, etc/ activated	LLW										O
		LLW										O
		VLLW										O
Large Equipment	S/G, Pressurizer, RCP, etc.	LLW	O	O	O	LLW	O				O	O
		VLLW	O	O		VLLW		O			O	O
	SG tube	LLW	O	O					O		O	O
		VLLW	O	O					O		O	O
Small Metals	Piping, Valve, Pump, Tank, Motor, HE, Duct, etc.	LLW	O	O	O	LLW	O				O	O
		VLLW	O	O		VLLW		O			O	O
SF storage Rack		LLW	O	O	O	LLW	O				O	O
		VLLW	O	O		VLLW		O			O	O
Scabbled Concrete	Scabbled waste of structure surface /Dust type	LLW		O			O				O	O
				O							O	O
		VLLW		O							O	O
Concrete Debris	Stucture demolition scrap, etc.	LLW		O			O				O	O
				O							O	O
		VLLW		O							O	O
Boilshield Concrete	Cut piece of biological shield concrete/ activated	LLW		O							O	O
		VLLW		O							O	O

2. Waste Stream and Treating Process in the Processing Facility

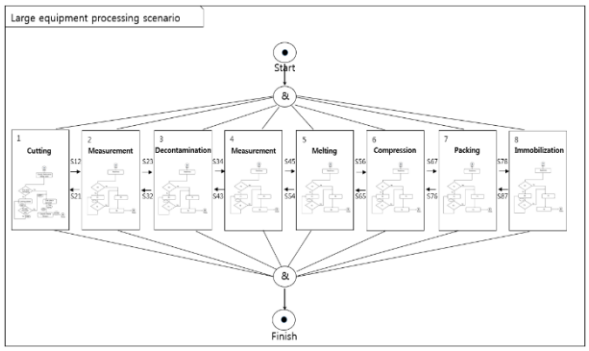

Fig. 2. Large equipment processing scenario.

The decommissioning works are performed on equipment located places and in the processing facility. Large equipment, small metals, and spent fuel storage rack are cut and/or removed at the dismantling places, and then transferred to the facility for cutting, measurement and decontamination, etc. as shown in Table 1.

Table 1 shows the decommissioning waste stream groupings for metals and concrete. Waste treating processes are planned and combined into scenario to reflect each waste stream. When all the processes in the scenario are finished, the scenario ends and stream processing is completed.

Figure 2 depicts large equipment processing scenario in the facility. This diagram may be used to plan the input/output relationship between the work processes in the facility for large equipment processing and the start and end conditions of the processing scenario. Process-based approach to waste stream enables logistic simulation, which is expected to contribute to the systematic implementation of VVT on waste stream as well as operation of the processing facility.

3. Conclusion

Comprehensive NPP Decommissioning Radioactive Waste Processing Facility is a product for end users. We define this product as an engineered system which incorporates end products and enabling products. The end products consist of structures, systems and components that are subject to disposal after development, production and use/maintenance.

VVT is carried out in development, production and use/maintenance phases. The functions and requirements for waste processing shall be separated and tracked by process unit, which may enhance the process-based VVT for waste stream. This paper depicts applicable waste streams and process-based approach in the processing facility.

ACKNOWLEDGMENTS

This work was supported by the Korea Institute of Energy Technology Evaluation and Planning (KETEP) grant funded by the Korea government (MOTIE) (20193210100060, Development of waste acceptance criteria application and WCP requirements for disposal of the NPP decommissioning radioactive waste solidification treatment).

REFERENCES

[1] Avner Engel, Verification, Validation, and Testing of Engineered Systems, p.12, WILEY (2010).

[2] Sun-Kee Lee, Heon Kim, Chang-Lak Kim, “Process Based Decommissioning Scenario Design for PWR and CANDU 6 NPPs”, Transactions of the KNS 2018 Autumn Meeting, Oct 25-26, 2018, Yeosu.

Analysis of Uranium Contaminated Soil Characterization

Seung Su Shin*, Chang Heon Lee, Pu Reun Kim, and Seung Min You
Nuclear Decommissioning Research Institute, 20-13, Yulliyeonghae 2-gil, Cheongnyang-eup, Ulju-gun, Ulsan, Republic of Korea
*tlstkwns@gmail.com

1. Introduction

There are physical, chemical and biological techniques of effectively decontaminating soil contaminated by uranium. As each of the technologies, which have been developed until now, has unique strengths and weaknesses, there is no unique decontamination technique which can removed uranium from contaminated soils with various physical and chemical characteristics.

An important factor to be considered during soil decontamination is that we must correctly know the uranium chemical species that change depending on the physical/chemical state, environmental conditions of the soil. After that we must develop an appropriate new decontamination technology, or select one of the technologies, which have been developed previously, that is thought to be the most appropriate. This paper described the chemical properties of uranium absorbed in the soil or retained in the soil water, and pH and oxidation/reduction potential that can influence retention and mobility of uranium.

2. Chemical Properties of Uranium in Soil

2.1 Factors Involved in Uranium Contamination

The retention and mobility of the uranium in the soil vary depending on the physical/chemical properties of the soil and the stability of the uranium complex, which is formed in the underground water, in the soil water or in the pores of the soil particles, and they are influenced by pH, oxidation/reduction potential and complex ion concentration [1].

2.2 Changes in the Uranium Chemical Species and Solubility

In an acid solution, UO_2^{2+} is the most stable chemical species, and the uranium dioxide is highly solubility. UO^{3+} in the U(V) state, found in the aqueous solution, easily causes the disproportionation of U(IV) and U(VI). U(IV) is stabilized in the reducing condition, and lowly solubility like UO_2, and exists as $U(OH)_4(aq)$ above pH 2. Also, dissolved U(III) is easily oxidized to U(VI) in most reducing conditions found in the natural environment. Accordingly, most uranium exists in the natural world as U(IV) and U(VI)[2].

2.3 Changes in the Uranium Chemical Species Depending on the Anion

In the weak neutral and alkaline region, U(VI) exists as a carbonate complex and complex ion like $UO_2CO_3^0(aq)$ and $UO_2(CO_3)_2^{2-}$, and as $UO_2(CO_3)_2^{2-}$ in the pH 7~8 region. Also, in the soil moisture of the pH 4.0~7.5, U(VI) exists in

the hydrolyzed state. Meanwhile, in the underground water in which phosphoric acid, sulfuric acid and carbonate ion exist, $[OH]^-$, $[H_2PO_4]^-$, $[HPO_4]^{2-}$ and $[HCO_3]^-$ and $[CO_3]^{2-}$ are key chemical species.

2.4 Changes in the Uranium Chemical Species Depending on Eh-pH

In the low Eh-pH condition, uranium exists in the solid phase of the U(IV) state with a low level of solubility, and in the high Eh-pH condition, uranium forms the uranium carbonate complex in the U(VI) state with a high solubility [3].

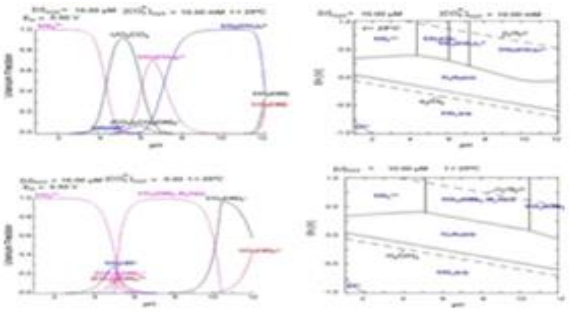

Fig. 1. Eh–pH and Uranium Species Distributions as a Function on pH for Oxidizing and Mildly Reducing Conditions [3].

In Fig. 1, uranium exists as UO_2^{2+} when Eh is 0.25V or higher, and pH is 7~8 and pH is 1~5. That is, when the soil has a condition of low pH and high Eh, solid compounds like uranite and schoepite, which do not dissolve, are not formed. Accordingly, in this condition, uranium in the soil can be easily decontaminated. Using this mechanism is electrokinetic separation. In this pH and Eh condition, uranium in the soil is found as UO_2^{2+}, and will move to the cathode, and be removed.

3. Conclusion

The retention and mobility of uranium in the soil vary depending on the physical and chemical properties of the soil, the stability of the uranium complex, pH, and oxidation/reduction potential. In the chemical environment which low pH and high Eh are maintained, solid compounds like uranite and schoepite with a very low level of solubility are not formed. If uranium chemical species are correctly understood and an appropriate technology is applied based on the analysis of the above properties, decontamination can be performed efficiently.

REFERENCES

[1] F. A. Cotton, G. Wilkinson, C. A. Murillo, M, Bochmann, 1999. Advanced Inorganic Chemistry. John Wiley & Sons, Inc., New York., P. Zhou, B. Gu, Extraction of oxidized and reduced forms of uranium from contaminated soils: effects of carbonate concentration and pH, Environ. Sci. Technol. 39, 4435–440 (2005).

[2] A. Sandino, J. Bruno, The solubility of $(UO_2)_3(PO_4)_2 \cdot 4H_2O(s)$ and the formation of U(VI) phosphate complexes: their influence in uranium speciation in natural waters, Geochim. Cosmochim. Acta 56 (1992).

[3] C. H. Lee, Uranium contaminated Soil Decontamination Technology Status, NDRI-TR002-2019.

Fenton-based Colorimetric Reaction for Sensitive Detection of Hydrazine Degradation

Jungsoon Park, Hee-Chul Eun, Seonbyeong Kim, Bumkyoung Seo, and Changhyun Roh*
Korea Atomic Energy Research Institute, 111, Daedeok-daero 989beon-gil, Yuseong-gu, Daejeon, Republic of Korea
*chroh@kaeri.re.kr

1. Introduction

Rapid, simple and convenient technologies for the identification of physical and analytical chemistry are of great significance in environmental monitoring, multidisciplinary science, technology and engineering field [1]. And, colorimetric assay is a technique used to determine the concentration of colored compounds in solution. Thus, detecting targeted species rapidly and simply with high sensitivity and specificity is challenging.

In this study, we demonstrated a colorimetric assay for sensitive detection of hydrazine degradation for chemical decontamination in the presence of hydrogen peroxide and metal ions. Furthermore, the colorimetric response is easy to monitor with the naked eye without any sophisticated instrumentation; this assay is thus suitable for on-site detection for adaptation of successfully chemical decontamination applicable to the internal loop of a nuclear power plant should have a good decontamination performance in nuclear facility.

2. Materials and Methods

2.1 Reagents and spectrometric assay

All reagents were of analytical grade and prepared using high pure water. UV-vis spectra were measured on a model UV-2600 spectrophotometer.

2.2 Characterization and colorimetric analysis

To analyze the samples prepared, it was imaged with a mobile phone camera in the high dynamic range mode with default settings. The mobile phone camera was fixed on a stand to stabilize the samples. Then each image of the samples prepared was saved in a JEPG format. Numerical color coordinate values of the colorimetric images were extracted from areas of each sample in the resulting image using ImageJ software [2]. The ΔR, ΔG, ΔB values were calculated from the RGB values before and after detecting images and were used for the histogram plot.

3. Results and Discussion

3.1 A colorimetric assay for hydrazine decomposition

The influence of different metal ions such as Fe^{2+}, Fe^{3+}, Mn^{2+}, Cr^{6+}, and Ni^{2+}, the degree of hydrazine decomposition in the presence of H_2O_2 were elucidated. As shown in Figure 1, the decomposition of hydrazine was relatively high at Fe^{2+} or Fe^{3+}, while Mn^{2+}, Cr^{6+}, and Ni^{2+} were not changed compared to the control. It is important that the selective color change from dark orange to brown induced by Fe^{2+} or Fe^{3+} sample solutions is easily discriminable by the naked eye. Thus, no significant color change was observed upon addition of other different cations except for Fe^{2+} or Fe^{3+}. The presence of

Fe^{2+} or Fe^{3+} could be readily distinguished by the naked eye (data not shown). These results indicated that the degree of hydrazine decomposition had a good relationship toward Fe^{2+} or Fe^{3+} over other different metal ions.

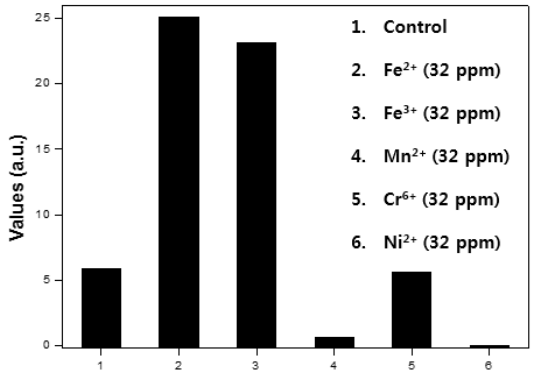

Fig. 1. Spectral responses for detection of hydrazine decomposition in the presence of H_2O_2 (0.2 M) and different metal ions (32ppm respectively).

3.2 A colorimetric assay for hydrazine decomposition

As shown in Figure 2, each RGB value was measured from specific areas of samples in the corresponding digital image, and then averaged to obtain the mean values in plot histograms. And, the colorimetric values of digital images were separated and converted into red (R), green (G), and blue (B). The RGB values mean a three-dimensional vector (ΔR, ΔG, and ΔB) were determined form the RGB values before and after response to different metal ions. Most importantly, the blue value (B) was meanly unchanged in the presence of Fe2+ or Fe3+ ion. However, the sample with Fe^{2+} or Fe^{3+} showed high responsibility in terms of decreased values in red (R) and green (G) compared to the control. This result suggests that on-site detection and monitoring using a colorimetric assay can be easily confirmed by a naked eye, even when the Fe^{2+} or Fe^{3+} like magnetite was existed in the unknown conditions.

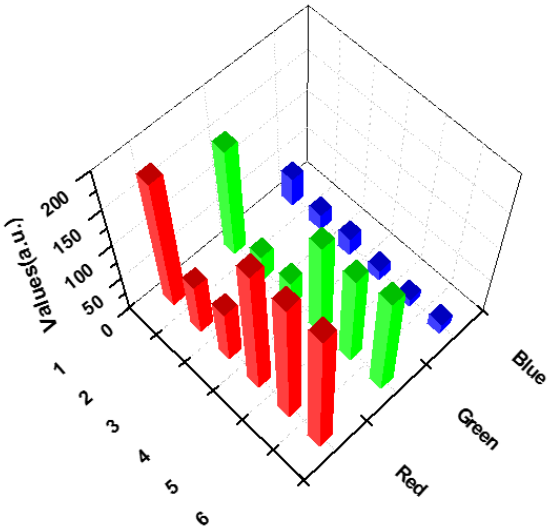

Fig. 2. RGB profiles of different metal ions.

4. Conclusion

In this study, we demonstrated a colorimetric assay for sensitive detection of hydrazine degradation for chemical decontamination. Furthermore, the colorimetric response is easy to monitor with the naked eye without any sophisticated instrumentation; this assay is thus suitable for on-site detection for adaptation of decontamination in nuclear facility. The proposed method is convenient, not invasive, low-cost and free of complex equipment, making it possible to successfully analyze hydrazine in industrial nuclear facilities.

REFERENCES

[1] H. Catherine, C. Edwin. “Chemistry: an introduction to organic, inorganic, and physical chemistry”. Pearson Education. pp. 349-353 (2006).

[2] S.M. Kang, S.C. Jang, Y.S. Huh, C.S. Lee, C. Roh. “A highly facile and selective Chemo-Paper-Sensor (CPS) for detection of strontium”, Chemosphere, 152, 39-46. (2016).

Solvent Extraction of Cobalt, Europium, and Calcium by Extractant D2EHPA in N-dodecane From the Hydrochloric Acid Solution

Iksoo Kim*, Maengkyo Oh, and Keunyoung Lee

Korea Atomic Energy Research Institute, 111, Daedeok-daero 989beon-gil, Yuseong-gu, Daejeon, Republic of Korea

*niskim@kaeri.re.kr

1. Introduction

As a part of the research to develop the technology to reduce the enormous amount of concrete waste generated from the decommissioning of nuclear facilities [1], this study is to develop a source technology for separating and removing radionuclides from the solution of radioactive concrete powder. In this context, a solvent extraction experiment was performed to separate nuclides from hydrochloric acid solution of concrete powder containing cobalt, europium, and calcium.

The present work discusses on the extraction behavior of Co, Eu, and Ca with extractant in diluent from chloride solutions. Various studies have been carried out on the extraction of Co, Eu, and Ca with different extraction systems. Di-2-ethylhexyl phosphoric acid (D2EHPA) was used as an extractant and n-dodecane (n-DD) was used as an organic phase solvent. The extraction behavior was investigated by changing the concentration of the extractant, pH of the aqueous solution, and the organic to aqueous phase ratio (O/A ratio) in order to efficiently separate and remove cobalt and europium from the hydrochloric acid media.

2. Experimental

2.1 Chemicals and equipment

All the chemicals and reagents used in the study were of analytical grade and used without further purification. D2EHPA, n-DD, and hydrochloric acid were procured from Sigma-Aldrich.

ICP-OES (Model No. PQ 9000 Elite) and Fisher Scientific accumet (XL 15 model) pH meter were used for the determination of metal concentrations in the aqueous phase and for measuring the pH values, respectively.

2.2 Experimental method

The stock solution of Co(II) and Eu(III) were prepared by digesting the corresponding Co and Eu oxide in hydrochloric acid and then made up to the mark with distilled water. The desired initial pH values of the Co and Eu solution were adjusted with NaOH. Equal volume (10 mL) of aqueous and organic solution were taken in a 50 mL conical tube for shaking up to 30 minutes. The aqueous and organic phases were allowed to separate, and the metal concentration in the aqueous phase was determined with ICP-OES after suitable dilutions and the concentration of metal in the organic phase was calculated from the mass balance. The distribution ratio (D) and extraction efficiency were calculated using Eq. (1) and (2).

$$D = \frac{[M]_{org}}{[M]_{aq}} \quad (1)$$

$$Extrn\ \% = \frac{[M]_{org}}{[M]_{org} + [M]_{aq}} \quad (2)$$

3. Results and discussion

The effect of equilibrium pH on the cobalt and europium extraction percentage in the initial pH range 1.0 - 6.0 are shown in Figure 1 and 2, where the D2EHPA concentration in the organic phase were 0.05 - 0.5 M, and the concentration of Co (II) and Eu (III) in aqueous phase was 10 ppm in HCl medium, respectively.

The data show that, the extraction of Co (II) in the pH range of 4.0 to 5.0 is quantitative, and the highest value of the cobalt extraction percentage was attained at initial pH 4.0. For the extraction of Eu (III), the highest value was attained at initial pH 1.0 - 2.0. Therefore, Cobalt and Europium can be removed from the concrete waste solution by a multi-step extraction process with different concentrations of pH.

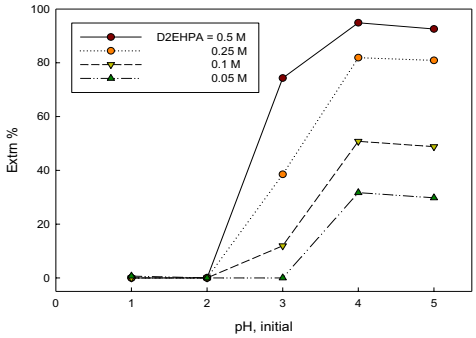

Fig. 1. Extraction percentage of cobalt vs. initial pH in solvent extraction. (O/A ratio = 1.0).

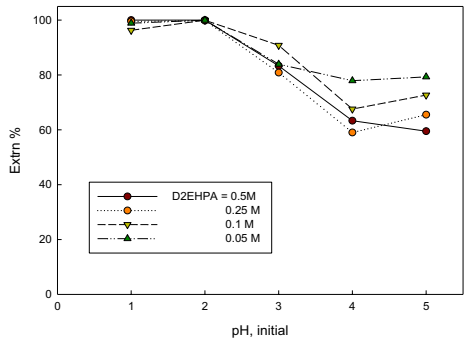

Fig. 2. Extraction percentage of europium vs. initial pH in solvent extraction. (O/A ratio = 1.0).

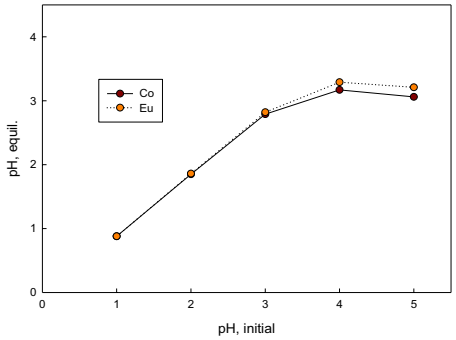

Fig. 3. Comparison of pHs before and after the solvent extraction of cobalt and europium.

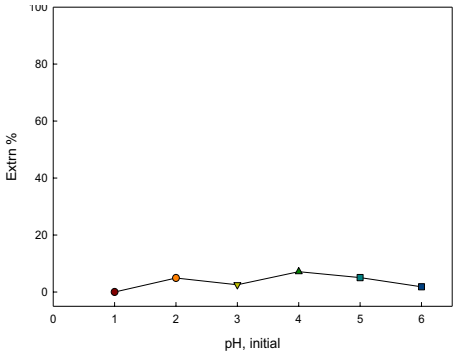

Fig. 4. Extraction percentage of calcium vs. initial pH in solvent extraction. ([Ca] = 20,000 ppm, O/A ratio = 1.0).

Figure 3 shows the variation of pH before and after solvent extraction of cobalt and europium. At the interval of low pH range, there is little change between initial and equilibrium pH. However, as the initial pH increases, the change in equilibrium pH decreases and equilibrium pH does not change in the pH range above 3. This may be due to the increase in hydrogen ions which increases the acid concentration of the aqueous phase.

Figure 4 shows the extraction percentage of calcium as a function of initial pH. The concentration of D2EHPA in the organic phase was 0.5 M, and the concentration of Ca in aqueous phase HCl was 20,000 ppm. As shown in figure, the extraction percentage of Ca is not very high in the whole range of pH. This is due to the high concentration of hydrogen ions produced from the reaction of extractant and very high concentrations of calcium. In order to reduce this effect, it is thought that saponification to substitute the hydrogen ions of the extractant and Na ions is necessary. Further research on this is under progress.

4. Conclusion

The higher the concentration of the extractant and the higher the O/A ratio, the higher the extraction rate. Europium was extracted up to 99% or more when the pH of the initial hydrochloric acid solutions was 2 or less, and cobalt was extracted up to 95% when the pH was 3 or more. It was confirmed that the europium and cobalt can be separated and removed from the concrete waste solution by a multi-step extraction process that adjusts the pH of the solution differently.

ACKNOWLEDGEMENT

This work was supported by the National Research Foundation of Korea (NRF) Grant funded by Korea government (MSIT) (no.NRF-2017M2A8A5015147.

REFERENCES

[1] K. Y. Lee et al., “Trends in Technology Development for the Treatment of Radioactive Concrete Waste”, JNFCWT, 16(1), 93-105 (2018).

The Influence of Work Activities During the Transition of a Permanently Shut-Down NPP on Worker

H.Y. Lee*, S.I. Kim, and J.S. Song

Chosun University, 309, Pilmun-daero, Dong-gu, Gwangju, Republic of Korea

*leehakyun1@naver.com

1. Introduction

The main objectives of the transition period are to reduce the exposure dose of decommissioning workers, and reduce the decommissioning cost and improving safety by removing elements that interfere with work, and the key activities include removal of spent fuel, system cleaning, decontamination or stabilization of radioactive pollutants, and partial removal of the system and equipment. Like this, as work is done close to the contaminated structure and radioactive matters, excessive exposure of workers is feared, but the measures again it and the relevant standards are relatively inadequate compared to full-scale decommissioning. Therefore, this study will analyze the characteristics of the transition period and work activities of a permanently shut-down NPP to prevent unnecessary exposure of workers during the transition period, and contribute to establishing safety and technical standards through evaluation of radiological characteristics.

2. Main Title

2.1 Transition Period Characteristics of Shut-Down NPP

For decommissioning permanently shut-down NPP have a lot of equipment that has been highly contaminated by neutrons and radioactive matters for several decades. Among them, the spent fuel in the permanently shut-down reactor accounts for more than 99% of the radioactive inventory in the NPP. So as Fig. 1 illustrates, after defueling from the reactor and moved to the storage pool and intermediate storage facility, the radioactive inventory inside the nuclear power plant will be greatly reduced.

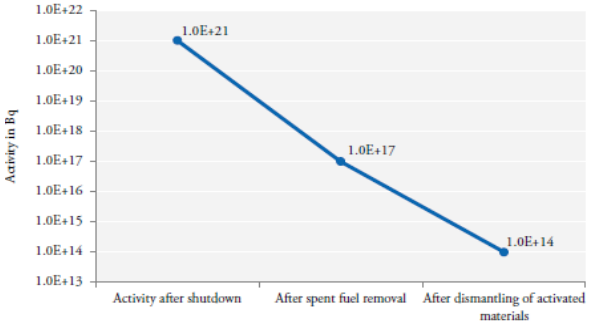

Fig. 1. Decrease of NPPs Activity Inventory over time.

Also, as for the key radioactive matters is ^{55}Fe, ^{60}Co, ^{94}Nb, ^{3}H, ^{14}C, ^{55}Fe and ^{154}Eu, etc. in the permanently shut-down nuclear reactor. Among them, ^{60}Co has more quantities than other radionuclides. Fig. 2 illustrates the changes in the key radioactive inventories after the final shutdown of PWR, the same type as domestic NPPs.

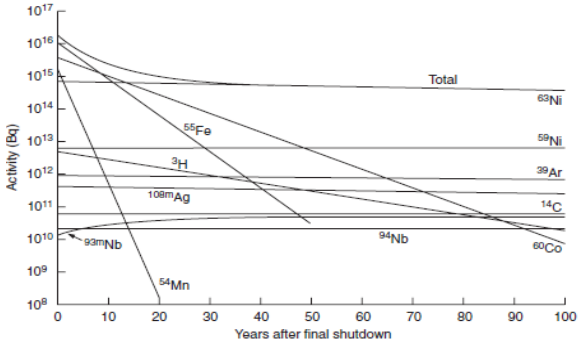

Fig. 2. Calculated Decay of Principal Radionuclides (PWR).

2.2. Activities during the Transition Period

The activities conducted during the transition period of NPP can be divided into 9 jobs: removal of spent fuel, system cleaning, decontamination or stabilization of radioactive pollutants, evaluating the characteristics of radioactive matters and hazardous materials and partial removal of the system and equipment, etc.

Among them, the direct handling of radioactive matters and the activities conducted near the contaminated equipment are likely to cause exposure of workers. Accordingly, to correctly assess the radiation risk during activities, the radiological characterization of permanently shut-down contaminated equipment and radioactive matters is required.

2.3 Exposure Evaluation Method & Factors

To assess worker exposure during the transition period of permanently shut-down NPP, it must be possible to predict the changes in doses due to the concentration of the radionuclides of contaminated equipment in the vicinities. VISIPLAN, MicroSheild, etc. are commercial software that meets this condition.

Among them, VISIPLAN is software that was developed to analyze worker dosage during the decommissioning of Belgium's BR-3 (Belgian Reactor-3). It uses the VRML (Virtual Reality Model Language) to implement 3D and calculate the external exposure of each work scenario. The input data necessary for calculating exposure includes the dimensions of equipment, the concentration of each radionuclide, and the distance from workers.

3. Conclusion

This paper analyzed the characteristics of a permanently shut-down NPP and the activities of workers during the transition period as a preliminary study of establishing safety and technical standards through evaluation of radiological characteristics. But to analyze the worker exposure effect of work scenarios, the radiological characteristics of individual contaminated equipment and structures, not overall characteristics, are required. So it will be necessary to study radiological characterization methodologies based on the representative samples of contaminated equipment.

REFERENCES

[1] OECD/NEA, "Preparing for Decommissioning During Operation and After Final Shutdown", 2018.

[2] IAEA, "Radiological Characterization of Shut Down Nuclear Reactors for Decommissioning Purposes", 1998.

Mock-up Test for the Decontamination Demonstration of a Contaminated RCP Shaft Using the Enhanced HyBRID Process Equipment

Jung-Hyun Lee, Jung-Yeop Cha, Dong-Yeon Kim, Ju-Hyeon Park, Dae-Kyun Kang,
Sung-Hyun Lee, Hye-Min Cho, and Ki-Chul Kim*
KEPCO KPS, 69-46, Munsan 2sandan 1-ro, Oedong-eup, Gyeongju-si, Gyeongsangbuk-do, Republic of Korea
*KICHKIM@kps.co.kr

1. Introduction

In the previous study, KEPCO KPS performed mock-up tests of the decontamination demonstration of a contaminated reactor coolant pump (RCP) shaft in Hanul#1 were conducted using loop test type of HyBRID decontamination equipment [1]. Through these tests, it was found that a filtering system for removing manganese oxides must be added to enhance the decontamination performance in the HyBRID decontamination equipment.

In this study, mock-up tests of the decontamination demonstration were conducted using the HyBRID decontamination equipment including the filtering system. Through these tests, the effects on removing manganese oxides were evaluated.

2. Experimental

2.1 Experimental equipment

Experimental equipment for the mock-up test was shown in Fig. 1. The equipment consists of RCP shaft surrogate, ultrasonic decontamination jacket (15L), and the loop test system, and a filtering system for removing manganese oxides.

2.2 Experimental method

The three STS304 specimens (10×10×2 mm) with simulated corrosion oxide film were mounted on the RCP shaft surrogate, and ultrasonic decontamination jacket was fastened. After 30L of DI water was charged into the decontamination part, the DI water was heated to 95°C, and then the oxidation and reduction processes were carried out for 1 hour, respectively. After an oxidation process, manganese oxides were removed with conducting a reaction between MnO_4^- and N_2H_4. The oxidation and reduction processes were carried out for 3 cycles. After these 3 cycles, the process water was cooled to 40°C, and then ultrasonic cleaning was conducted for 10 minutes. The process water transferred to the precipitation tank after completing the ultrasonic cleaning. The transferred water was purified using a wastewater treatment method.

Fig. 1. RCP shaft with specimen and loop test equipment.

2.3 Thickness reduction calculation of specimen

The thickness reduction before and after the HyBRID chemical decontamination process of STS304 specimen is expressed as Δd, and the formula is as follows:

$$\Delta d = \frac{Weight\ Loss\ (g)}{Oxide\ layer\ density\left(\frac{g}{cm^3}\right) \times surface\ area(cm^2)} \quad (1)$$

After the HyBRID chemical decontamination process, the weight loss for the three specimens in each cycle was averaged, and the weight of the measured metal was used to calculate the thickness reduction of the specimen.

2.4 Concentration of manganese ion

Concentration of manganese ion was measured to compare changes in the concentration between reduction and oxidation process using ICP-OES.

3. Experiments result

3.1 Decontamination result

The mock-up test results showed 20% of enhancement in the thickness reduction. The comparison between previous and present work is shown in Table 1.

Table 1. Comparison of Average Thickness Reduction results from previous and present work

Average Thickness Reduction [㎛]	
Previous work	5.012
Present work	6.189

3.2 Concentration variation result

It was confirmed that 38% of manganese ion was remained in the process water, and the rest was filtered after reduction process.

4. Conclusion

It was confirmed that 38% of manganese ion remained in the process water after the operation of the filtering system. In the mock-up test using the decontamination demonstration equipment including the filtering system, 6 ㎛ of oxide film was removed, and this means 20% off enhancement when comparing with the previous study. Thus, this equipment will be utilized successfully to demonstrate the HyBRID decontamination process using Hanul#1 RCP shaft.

ACKNOWLEDGEMENTS

This work was supported by the National Research Foundation of Korea (NRF) and the Ministry of Science and ICT (MSIT) of the Republic of Korea. (NRF-2017M2A8A5041776)

REFERENCES

[1] K. C. Kim, J. H. Park, J, H. Lee and D. Y. Kim, “Preliminary Study on HyBRID Chemical Decontamination Demonstration for the Reactor Coolant Pump Shaft”, Proc. of the KRS 2019 Spring Conference, 17(1), 05.08- 05.10, 2019, Busan.

Preliminary Study on Improving Wastewater Treatment for HyBRID Decontamination Demonstration of a Contaminated RCP Shaft

Jung-Hyun Lee, Dong-Yeon Kim, Sung-Hyun Lee, Hye-Min Cho, Ju-Hyeon Park, Sung-Sik Yoon, Seung-Ki Lee, Geun-Woo Kim, and Ki-Chul Kim*

KEPCO KPS, 69-46, Munsan 2sandan 1-ro, Oedong-eup, Gyeongju-si, Gyeongsangbuk-do, Republic of Korea

*KICHKIM@kps.co.kr

1. Introduction

In the previous study, KEPCO KPS performed mock-up tests of the decontamination demonstration on a contaminated reactor coolant pump (RCP) shaft in were conducted and then confirmed the decontamination performance and the amount of waste generation [1]. However, the concentration of impurities (sulfate, metal ions, and hydrazine) in wastewater generated after 3 consecutive HyBRID decontamination process is different from that of the normal process, Also, the normal process for solid-liquid separation during precipitation process takes long time which can increase radiation exposure. Thus, alternative method needs to be developed to derive optimal treatment conditions and decrease process time.

In this study, the wastewater treatment tests were conducted to effective treatment of wastewater generated after the continuous HyBRID process and the solid-liquid separation tests were conducted to shorten the process time using MF filter.

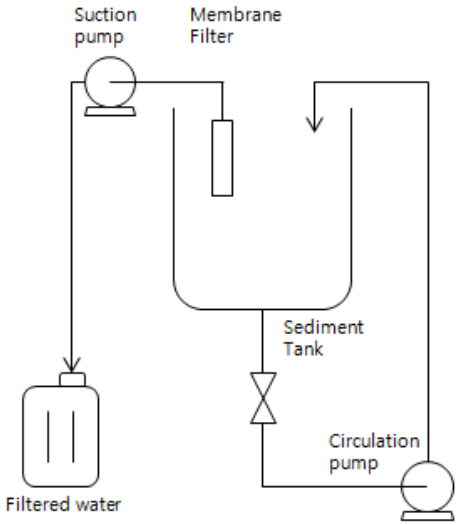

Fig. 1. Schematic diagram of the wastewater treatment equipment.

2. Experimental

2.1 Experimental equipment

Experimental equipment for the wastewater treatment was shown in Fig.1. The equipment is consisted of the loop test system, circulation pump, Sediment tank, suction pump and membrane filter (Hollow fiber, U type, pore size: 4㎛).

2.2 Experimental method

Impurity removal process was conducted into two processes: precipitation, and decomposition. Barium hydroxide ($Ba(OH)_2$) and Hydrogen peroxide (H_2O_2) were used for precipitation and

decomposition of hydrazine. Diaphragm pump was used to circulate process water. Filtration process using membrane filter was conducted after an hour of settling method.

2.3 Analysis

Filtered water was sampled and analyzed Total Suspended Solids (TSS) and Hydrazine (N_2H_4) using spectro-photometer (HACH DR3900, USA). The concentration of ions in process water and filtered water was measured using ICP-OES.

3. Experiments result

3.1 Precipitation and decomposition

The concentration of sulfate ions after 3 consecutive HyBRID process was significantly higher than that of normal process. For efficient N_2H_4 decomposition and maintaining pH level, less amount of $Ba(OH)_2$ was injected. With this condition, less than 1ppm of N_2H_4 was detected.

Table 1. TSS and N_2H_4 after the MF filtering

Time	TSS [mg/L]	N_2H_4 [mg/L]]
5 min	1	< 1
30 min	0	-
60 min	0	-
180 min	0	-

3.2 Solid-liquid separation

Solid-Liquid separation process was finished in 3 hours by using membrane filters. It was confirmed that concentration of ions in treated wastewater was decreased significantly after precipitation and filtration process.

Table 2. Ion concentration after the MF filtering

Ions	Concentration(ppm)	
	Before	After
Fe	85.9	< 1
Cr	11.6	1.85
Ni	20.05	< 1
S	3396	27.2

4. Conclusion

In this study, efficient process to treat wastewater after HyBRID decontamination process which decreases process time by 50% was derived.

From this result, this process is expected to decrease radiation exposure and utilized to demonstrate after HyBRID decontamination process at Hanul#1.

ACKNOWLEDGEMENTS

This work was supported by the National Research Foundation of Korea (NRF) and the Ministry of Science and ICT (MSIT) of the Republic of Korea. (NRF-2017M2A8A5041776)

REFERENCES

[1] K. C. Kim, J. H. Park, J, H. Lee and D. Y. Kim, “Preliminary Study on HyBRID Chemical Decontamination Demonstration for the Reactor Coolant Pump Shaft”, Proc. of the KRS 2019 Spring Conference, 17(1), 05.08- 05.10, 2019, Busan.

Decontamination of Radionuclides in Wastewater After Soil-washing Process

Jaeeun Kang*, Juhyeok Lee†, Seokju Hong, and Won-Seok Kim
Pohang University of Science and Technology, 77, Cheongam-ro, Nam-gu, Pohang-si, Gyeongsangbuk-do, Republic of Korea
*jenny94@posteh.ac.kr, †jhlee5489@postech.ac.kr

1. Introduction

Recently, due to long-term operation of nuclear power plants (NPP), the soil around the NPP site is contaminated with radioactive materials. There is a large amount of radioactive soil waste contaminated with radionuclide when the NPP is decommissioned. In particular, radioactive nuclides such as cobalt, cesium and strontium are highly adsorbed in particulate materials such as clay and silt, and these are also attached to surface of sand and gravel surfaces. In order to decontaminate the contaminated soil, the soil washing process was used in this study. The removed radionuclide from soil exist in wastewater. It is important to treat the secondary wastewater to reduce the volume of radioactive waste.

In this study, in order to decontaminate the radioactive soil waste and reduce the secondary wastewater, adsorption tests were conducted according to the behavior of radionuclides by soil particle size, and natural zeolite was used as adsorbent in groundwater to investigate the nuclide remove such as cesium.

2. Materials and Methods

2.1 Materials

To proceed with adsorption experiment, we used soils which sampled near Kori Unit 1 and classified into the various size (Table 1), with larger than very fine sand, very find sand, and smaller than very fine sand. In addition, nitrate-based aqueous solutions were prepared at a concentration of 15ppm and 30ppm for each nonradioactive nuclides (Co, Cs, and Sr). The ratio of soil to solution was 1:10, and adsorption experiments were performed on 0.1g and 0.5g soils.

Table 1. Particle size of soils

Large	0.15-2 mm
Medium	0.075-0.15 mm
Small	< 0.075 mm

In addition, Decontamination experiments were performed by 0.1g of natural zeolite (sampling in Guryongpo, Pohang, Gyeongsangbuk-do, and pre-treated in the laboratory) to adsorb Cs in groundwater conditions.

2.2 Methods

Nonradioactive nuclides adsorption experiments to soil proceeded to triplicate to ensure reproducibility. The equilibrium time for Co, Cs, and Sr to reach the adsorption equilibrium is 30, 90 and 120 minutes, respectively [1]. Adsorption time was based on 4 days to reach sufficient adsorption equilibrium. After 4 days, the soil and the solution were separated using a centrifuge and filtered using a Hydrophilic PVDF 0.45um filter. The supernatant was analyzed by ICP-MS

In addition, decontamination experiments proceeded to 7 days to ensure sufficient adsorption equilibrium.

3. Results

3.1 Adsorption experiment

We investigated that the adsorption of cobalt, cesium and strontium in soils. Small-sized soil has a higher adsorption rate than large-sized of soil (Fig. 1). In case of cesium, the adsorption rate is lower than cobalt. However, the adsorption rate according to particle size tend to be the correspond (Fig. 2). As a result of two different cases, strontium has the highest degree

of adsorption about 88~90% on medium-sized particles (Fig. 3).

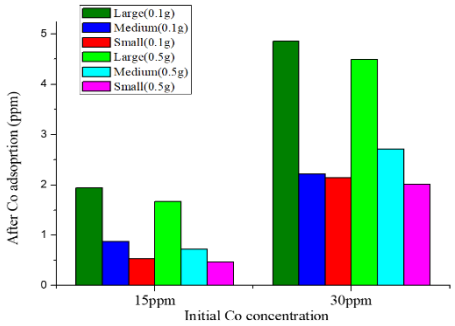

Fig. 1. Soil adsorption experiment using cobalt nitrate.

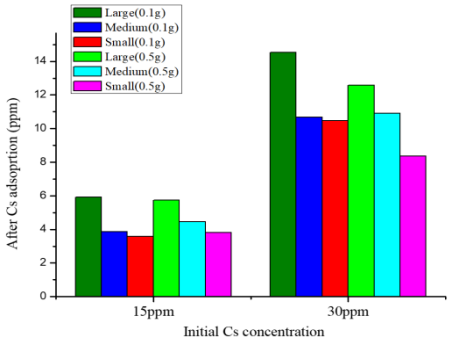

Fig. 2. Soil adsorption experiment using cesium nitrate.

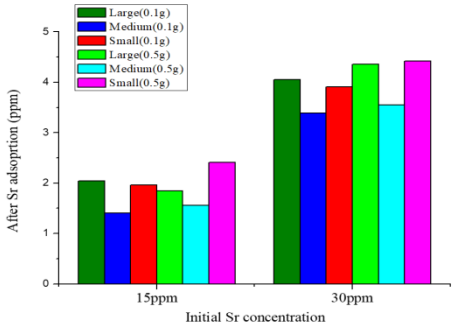

Fig. 3. Soil adsorption experiment using Strontium nitrate.

3.2 Decontamination experiment

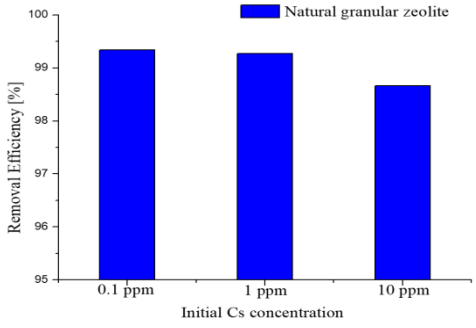

Fig. 4. Cesium sorption in groundwater condition.

In groundwater conditions, removal efficiency of cesium is about 97 to 99% at various initial concentrations (Fig. 4).

4. Conclusion

Nonradioactive nuclides such as Co, Cs, and Sr were adsorbed in the soil in significant quantities. In particular, radioactive materials tend to be highly adsorbed to small size of particles than large size.

Natural zeolite was indicated high removal efficiency of Cs in liquid waste under neutral conditions. Based on these results, an experiment will be conducted to develop adsorbent with a high removal efficiency for Co and Sr and to evaluate the zeolite adsorbent performance under various pH conditions in the secondary wastewater after soil washing process.

ACKNOWLEDGEMENT

This work was supported by the Korea Institute of Energy Technology Evaluation and Planning (KETEP) and the Ministry of Trade, Industry & Energy (MOTIE) of the Republic of Korea (No. 20181510300800).

REFERENCES

[1] K.M.A. El-Rahman, M.R. El-Sourougy, N.M. Abdel-Monem, I.M. Ismail, "Modeling the Sorption Kinetics of Cesium and Strontium Ions on Zeolite A", J. of Nuclear and Radiochemical Sciences, 7(2), 21-27 (2006).

Review of Groundwater Monitoring Program for the NPP Decommissioning

Chan-Geun Park and Hyung-Woo Seo*

KHNP Central Research Institute, 70, Yuseong-daero 1312beon-gil, Yuseong-gu, Daejeon, Republic of Korea

*sehywo1727@khnp.co.kr

1. Introduction

The final goal of decommissioning of nuclear facility is to remediate the contaminated site by decontaminating the site to a level below regulatory. To do this, decommissioning of nuclear facilities should provide information such as groundwater monitoring, the level of contaminations, and safety evaluation results.

One of the important factors in securing the safety assessment results for reliable deregulation is to establish a groundwater monitoring program.

Therefore, the purpose of this paper is to understand the difference groundwater monitoring program between the status of operation and decommissioning of nuclear power plants from overseas cases and EPRI guidelines.

2. Methods

2.1 Differences in groundwater monitoring between operation and decommissioning nuclear power plants [1]

The scope of the groundwater monitoring program carried out at the operating plant may differ from that of the decommissioning plant. This difference occurs as a result of the following factors.

- Operation period: groundwater monitoring program during operation of nuclear power plant is to identify, monitor and track the contamination.
- Decommissioning period: groundwater monitoring during the decommissioning of nuclear power plant is to identify the areas the need to be remediated and to monitor its effectiveness after remediation is complete.

Monitoring program in decommissioning is also to identify contamination areas and evaluate whether the remediation has been done properly. The contents of summary for groundwater monitoring program, as the EPRI guideline is presented, can be divided into operation, transition and decommissioning as shown in Fig. 1.

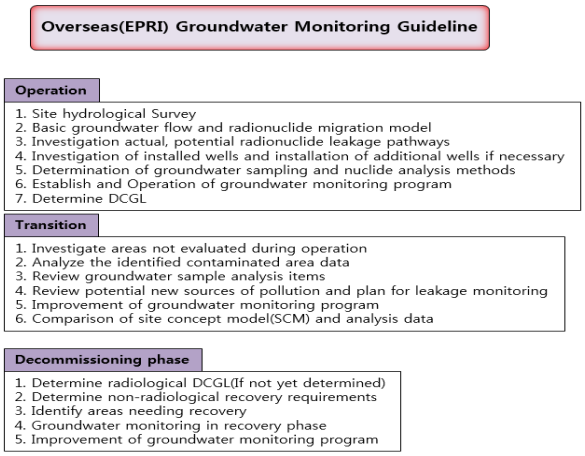

Fig. 1. Overseas (EPRI) Groundwater Monitoring Guideline.

2.2 Key elements of groundwater monitoring in decommissioning nuclear power plant [1]

Groundwater monitoring program should be established for the decommissioning plant by taking into account the view of transition and decommissioning phase. First, the licensee should conduct an investigation of areas which are not previously evaluated and an analysis of the data of the identified areas of contaminated groundwater. This may include historical site assessment (HSA) and investigation of some accidents that might affect any possible contaminations to the media (i.e. soil, groundwater). Based on this analysis, it is necessary to determine whether additional wells need to be installed and to improve the groundwater monitoring program from the operation nuclear power plant.

At this point, it is necessary to review the methodology of groundwater monitoring program established for operation phase, and to improve it by reflecting the main factors of groundwater monitoring of decommissioning nuclear power plant. It should be a procedure to investigate areas that have not been evaluated in the past, to analyze the data of contaminated groundwater, and to reflect them periodically in the Site Conceptual Model (SCM). From the EPRI guideline, the detailed activities to be considered during the transition period can be summarized as follows:

- ■ Survey areas not previously evaluated
- ■ Data collection : Areas of known groundwater contamination
- ■ Sampling for multiple radionuclides
- ■ Monitoring requirements for liquid systems that continue to exist during transition

The detailed activities to be considered during active decommissioning period can be summarized as follows:

- ■ Soils and groundwater monitoring
- ■ Determination of remediation
- ■ Confirmation of completion of remediation

3. Conclusion

This study reviewed groundwater monitoring of overseas experience, and provides information on guidelines and strategies by phase of operation, transition, and decommissioning. When the nuclear facilities are shutdown, appropriate groundwater monitoring should be carried out at each phase until the site is released through the phase of transition and active decommissioning. Especially, during the transition period, it is expected that monitoring of areas that have not been assessed in the past, wells in which contamination was found, systems that will be operated and existing liquid waste system should be considered while maintaining a groundwater monitoring program established during operation.

REFERENCES

[1] Groundwater Monitoring Guidance for Decommissioning Planning, EPRI 3002008167 (2016).

A Feasibility Study on Soil/Groundwater Remediation for Decommissioning NPP

Jong Sun Hwang*, Hyung-Woo Seo, and Jae Yong Oh
KHNP Central Research Institute, 70, Yuseong-daero 1312beon-gil, Yuseong-gu, Daejeon, Republic of Korea
*estwing1@khnp.co.kr

1. Introduction

The ultimate goal of decommissioning nuclear power plants is to release nuclear facilities and sites from regulations (the final status can be approved when the residual radioactivity is below the site release criteria). In addition, it is necessary to prove that residual radioactivity on the site is still not harmful through the exposure route of the site reuse scenario (usually calculated by ResRad code) even after a certain period of time after the site is released (over 1000 years, Nuclear Safety and Security Commission (NSSC) Notice, No. 2016-33). In the case of overseas nuclear power plants (US Connecticut Yankee, Yankee Rows, Jose Cabrera and etc.), soil and groundwater contamination – various radiation materials including tritium, cobalt 60, and etc. - was found during the site investigation in the process of decommissioning. Soil treatment using washing process were implemented and reduced the volume of waste, and it was directly connected to cost saving of decommissioning process.

According to a historical site assessment (HSA) on Kori Unit 1, no radiation related events that could affect soil or groundwater were found during the operation period.

There are two types of shallow fill are present at the Kori site. General fill is thin surface deposits in areas where no excavations and engineered backfill was required consisting of angular rock fragments in silt. Engineered Fill is predominately consisting of sand and gravel used to grade the constructed areas. Native Unconsolidated Sediments are found in the unexcavated areas of the site and are largely native marine and/or colluvium deposits consisting of well-rounded fine to coarse gravel with a sandy and silty matrix. Cobbles and boulders are common near the top of bedrock. This deposit is between 1 and 3 meters thick.

2. Methods & Current States

KHNP-CRI is carried-out an assessment/case study on restoration technology for soil/ groundwater contamination in the site where radiation leak/contamination can be found during decommissioning. Lab-scale and Pilot-scale equipment will be developed using several treatments technology.

Contaminated soil cannot be found in Kori unit-1 site, therefore, stable isotope will be mixed with soil and groundwater and test will be implemented with arbitrary samples.

Soil washing based on physical separation process is known as cost-effective when the

treated level of contamination is below the cite-specific clearance level. Preliminary assessment of soil treatment will be tested in lab-scale and representative soil samples will be selected. Most of activity is located in small sized particles (< 0.075mm) and decrease with the size. Therefore, soil size characteristics (gravel and sand content) will be examined.

The test parameters - include washing agent concentration, attrition treatment time, washing cycles and etc. - and automatic control will be verified from Lab-scale and Pilot-scale test (Fig. 1).

A groundwater treatment system will be combined with soil system and it make more compact and effective layout for Pilot-scale. In the process of washing cycle of Soil, secondary waste will be generated, and it also can be treated with groundwater system.

A hybrid system using pre-process, ceramic nano and reverse osmosis membrane filter will be applied to groundwater treatment, and condensed radioactive wasted will be absorbed to resin (Fig. 2).

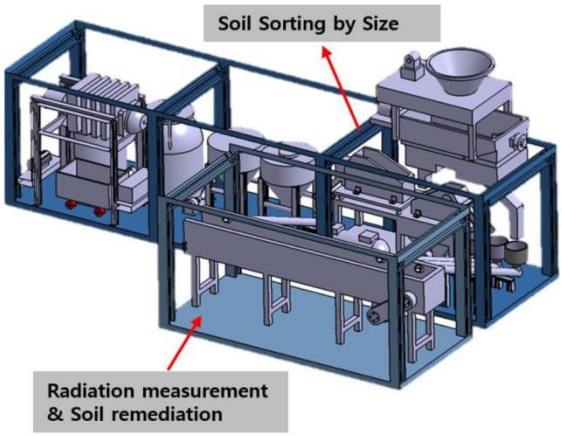

Fig. 1. Schematic Drawing of Soil Treatment System.

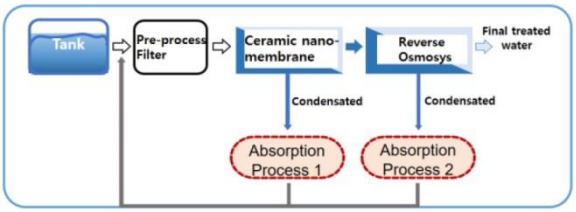

Fig. 2. Schematic map of GW Treatment System.

3. Conclusions

It is expected that research results on the site restoration will increase public acceptance, shorten the decommissioning period and reduce costs.

REFERENCES

[1] EPRI, “Characterization and Dose modeling if Soil, Sediment and Bedrock during Nuclear power Plant Decommissioning”, No. 1019228 (2009).

[2] EPRI, “Groundwater and Soil Remediation Guidelines”, No. 1021104 (2010).

[3] EPRI “Proceedings: 15th EPRI International Decommissioning Workshop, “Soil Washing Plant Jose Cabrera NPP” No. 3002013096 (2018).

[4] Dames & Moore consultant Report “Geologic and Seismologic Studies” (1971). & “Foundation Studies & Construction Inspection Service” (1974).

Study on Segmentation Process of the Bioshield Concrete

Ju-Young Yoon*, Young Hwan Hwang, and Sunghoon Hong
KHNP Central Research Institute, 70, Yuseong-daero 1312beon-gil, Yuseong-gu, Daejeon, Republic of Korea
*august63@khnp.co.kr

1. Introduction

The bioshield concrete in nuclear power plan (NPP) is continuously exposed to neutron and activated. In order to achieve the optimized concrete cutting plan, several principles should be carefully considered.

Since the bioshield concrete is relatively highly activated and surface contaminated, compared to other concrete, the careful control and implementation of the bioshield concrete segmentation is required. It is reported that in many cases, the cutting line design strongly affects the radiation exposure to workers and radioactive waste disposal plan.

In this paper, the development of optimal process for efficient segmentation of the bioshield concrete is reported.

2. Segmentation Line Design

2.1 Activation Evaluation

In order to perform the activation evaluation, the accurate modeling of the bioshield concrete structure and the source term are important.

MCNP and ORIGEN were performed by computational evaluation and radioactive waste was classified according to the results.

2.2 Structure Analysis

Considering the overall walls, floors, etc. in the CV, the impact on the bioshield concrete segmentation should be considered in terms of structural safety.

Since the bioshield concrete partially support the CV, the removal of the bioshield concrete before separation of other components might bring the negative effect in structural safety of the CV.

2.3 Segmentation line design

The segmentation line should be carefully designed, systematically considering the characteristics and stability of the structure. The diamond saw cutting is suggested as a primary cutting method.

The ex-core instrument structure is designed to reduce the number of coring.

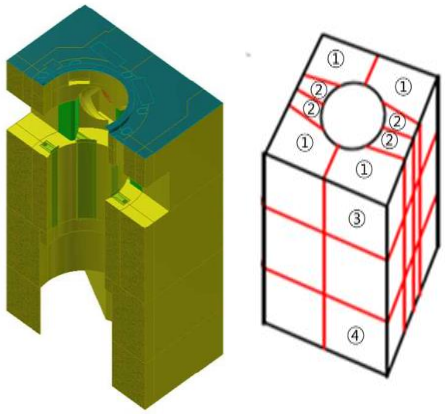

Fig. 1. Structure & Segmentation line of the Bioshield Concrete.

3. The Bioshield concrete segmentation Process

3.1 Decontamination

The inner and outer walls are mechanically removed for the sheath and decontamination before cutting. The ventilation line is installed to prevent the internal exposure of workers from the dust.

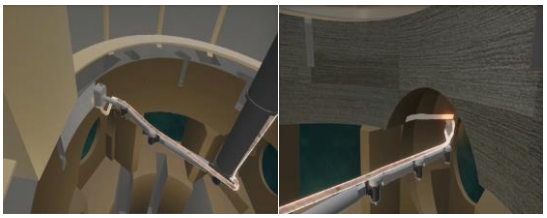

Fig. 2. Scrabbling and Decontamination.

3.2 Tent and Ventilation Installation

Due to the characteristics of radiation and concrete dust, the tents are installed throughout the bioshield concrete to prevent internal exposure and respiratory diseases caused by dust.

At this time, the high capacity ventilation is required. Because the cutting in the closed space, a HEPA filter or the like must be installed.

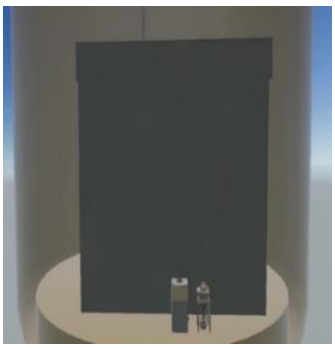

Fig. 3. Tent Installation.

3.3 Segmentation of the Bioshield Concrete

A diamond saw is used to perform the segmentation. This may not be performed by the segmentation method, but in some cases, the method of detailed segmentation after the segmentation is considered.

This has the advantage of reducing the operator's cover by dividing the space between the large segmentation and the detailed segmentation, and simultaneously performing the cutting and the detailed cutting.

A separate tent and ventilation are installed for the detailed segmentation work space.

In the case of detailed cutting, it is segmented and packaged according to the result of the activation evaluation. The bioshield concrete is divided into concrete blocks, powder, rebar and dust.

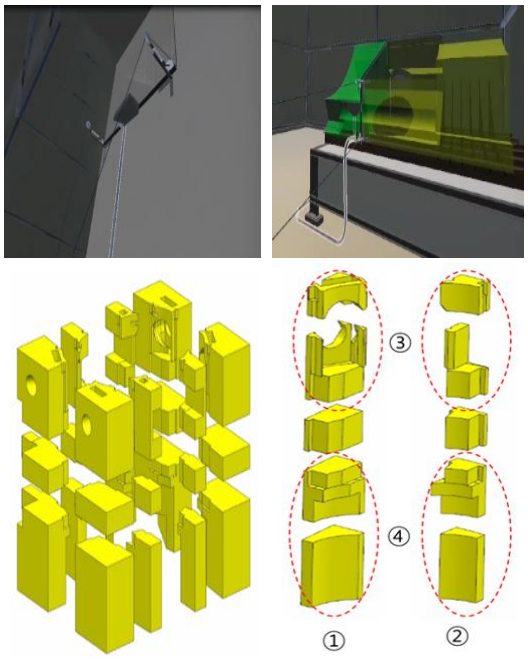

Fig. 4. Segmentation.

4. Conclusion

The bioshield concrete cutting plan is systematically developed, considering industrial safety and radiation protection. In order to be as safe as possible and minimize exposure, systematic segmentation processes should be established, such as characterization through activation evaluation results before segmentation, design of the segmentation lines, construction of segmentation methods and equipment, and packaging by radioactive waste classification.

ACKNOWLEDGEMENTS

This work was supported by the Korea Institute of Energy Technology Evaluation and Planning (KETEP) and the Ministry of Trade, Industry & Energy (MOTIE) of the Republic of Korea (20161510300430).

REFERENCES

[1] CPD, “Decontamination and dismantling of radioactive concrete structures”, NEA /RWM/R(2011)1, (2011).

A Study on Induction Melting of Radioactive Carbon Steel Waste for Decommissioning of NPPs

Ji-Hoon Lee

KHNP Central Research Institute, 70, Yuseong-daero 1312beon-gil, Yuseong-gu, Daejeon, Republic of Korea

leejihoon@khnp.co.kr

1. Introduction

The decommissioning of nuclear power plants results in large quantities of waste, such as concrete and metal which should take into account final disposal and recycling of resources. Melt processing technology is used for volume reduction or recycling of radioactive metal wastes. The largest volume reduction of radioactive metal wastes is mostly treated by melting using electric arc furnaces and induction heat furnaces.

Typical alloys used in structures and equipment in nuclear power plants are carbon steel, stainless steel and Inconel. In this study, induction melting method was applied for melting very low level radioactive metal wastes released by the decommissioning of nuclear power plants. The mostly generated radionuclides for decommissioning from nuclear power plants is corrosion products such as Co, Ni, Cr, Fe, Mn etc. Corrosion products such as Co need to reduce the viscosity of the slag to increase liquidity which is contributed the maximising contact with slag and securing it with stable oxide in slag. Therefore, a melting experiment was conducted through induction furnace for the assessing the melting characteristics and the distribution characteristics of Co with various additive in slag of radioactive metal waste.

2. Material and Methods

2.1 Lab. scale induction melter

The Lab. scale induction melter consists of a furnace, induction heaters, and coolers. Fig 1 shows the lab. scale induction melter. Induction melter adopted IGBT with high frequency waves from induction heat sources which use 3-phase 380 V with output of 30 kW. A crucible surrounded by induction coils was installed inside the container of furnace. The melting crucible uses a magnesia crucible suitable for melting the metal specimen, and is designed to be 100mm in diameter and 150mm in height. Temperature measurements inside crucible use an infrared thermometer (model GM-2200 of BENETECH). To measure the current and voltage, frequency, melting point, and time to reach the melting point, the device of FX1006 of Yokogawa was installed to record the data in real time.

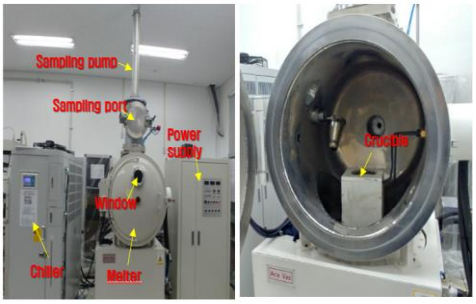

Fig. 1. Lab scale induction melter.

Table 1. Slag composition for Co partitioning

#	Slag Composition (wt%)
1-1	CaO(40%)-SiO_2(30%)-Al_2O_3(10%)-Fe_2O_3(20%)
1-2	CaO(40%)-SiO_2(30%)-Al_2O_3(10%)-CaF_2(20%)
1-3	CaO(40%)-SiO_2(30%)-Al_2O_3(10%)-MgO(20%)

2.2 Experimental Procedure

Temperature measurements were made using an infrared thermometer through the measuring ports installed in the induction chamber. When the target temperature is reached, the initial concentration measurement sampling was carried out for the determination of uniform melting between radionuclides and metal specimens and the concentration of initial nuclides. The Co simulant was used as 1.0g of Co_3O_4 and 2kg of carbon steel was used as

specimens. The tests were conducted to investigate the composition of slag with optimum distribution ratio of Cobalt by adding 20% of slag with Fe_2O_3, CaF_2, and MgO to the basic slag composition [CaO(40%), SiO_2(30%), and Al_2O_3(10%). (Table 1)

3. Results and discussion

After melting of carbon steel was confirmed, slag components were added and about 1,750°C was maintained. In the melting of carbon steel, the basic components of slag are kept at CaO-SiO_2-Al_2O_3, changing the components to Fe_2O_3, CaF_2, and MgO, and the distribution behavior of cobalt is observed. In general, Fe_2O_3 produces metal oxides with strong oxidation, reduces volatility by increasing the capture rate from dust to slag. CaF_2 increase liquidity by reducing the viscosity of slag. MgO is also increase slag liquidity and decontamination effect of Co. As shown in Fig. 2, the concentration of cobalt at the top, the middle, and the bottom of the ingot was not uniform in case of Fe_2O_3 addition to the slag. In addition, the amount of cobalt in ingot decreased over time. Assuming that the distribution of cobalt is stabilized through the boundary of slag and metal over time, the distribution ratio is calculated as the weight ratio of cobalt in the slag to the weight ratio of the cobalt in the top of the ingot.

The calculation result of distribution ratio according to slag compositions is shown in Fig. 4. When Fe_2O_3 was added to CaO-SiO_2-Al_2O_3, the base composition of the slag, the distribution ratio of Co is about 6%. The distribution ratio of Co is about 8% when CaF_2 was added, which was no significant difference compared to the previous one. But the distribution ratio of Co is about 48% when MgO was added, which was shown the significant effects of Co distribution ratio of slag.

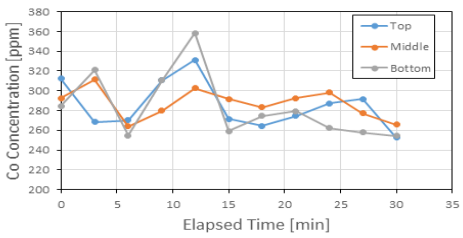

Fig. 2. Co concentration change in ingot according to elapsed time (Fe_2O_3 addition case).

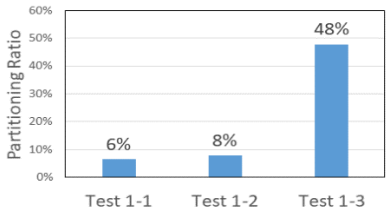

Fig. 3. Partitiong ratio for melting of carbon steel with slag components.

4. Conclusion

The lab scale induction melter was applied for melting very low level radioactive metal wastes for volume reduction or recycling of metal waste during the decommissioning of nuclear power plants. Through the melting test in induction melter, the conditions of melting parameter, Co in carbon steel and the composition effects of the additive in slag were evaluated. After melting of carbon steel was confirmed, slag components were added and about 1,750°C was maintained. The distribution ratio of Co showd about 48% when MgO was added which was shown the significant effects of Co distribution ratio in carbon steel. The results will be contributed for recycling and disposal strategies of radioactive metal waste during decommissioning of nuclear power plants.

REFERENCES

[1] J. Lorenzen, M. Lindberg, “20 years of experience on treatment of large contaminated components and on clearance of material for recycling”, Proc. of GLOBAL 2005, Tsukuba (Japan) (2005).

[2] U. Quade, T. Kluth, “Recycling by melting – 20 years operation of the melting plant CARLA by Siempelkamp Nukleartechnik GmBH”, International Journal for Nuclear Power (2009).

Verification of Integrated Human Error Model Related to Decommissioning of Nuclear Power Plants

Chang-Su Nam*, Byung-Sik Lee, and Sung-Mi Park

Dankook University, 119, Dandae-ro, Dongnam-gu, Cheonan-si, Chungcheongnam-do, Republic of Korea

*72180291@dankook.ac.kr

1. Introduction

As Kori Unit 1 was shut down, much attention has been attracted to decommissioning nuclear power plants. The decommissioning of nuclear power plants has many considerations, unlike other plants. Factors to consider may be mechanical or procedural, but also human factors because the work is performed by a person. Although much progress about technology has been made, accidents caused by human factors still exist. Therefore, task analysis and related performance shaping factors were derived in the previous study [1], in order to reduce the human error for the decommissioning activity, such as the reactor pressure vessel internal segmentation. Through the derived performance shaping factors, an integrated human error model was developed using the VENSIM Simulation Program.

2. Development of Integrated Human Error Model

Most people regard stability as the robustness or technical aspect of the facility. However, most nuclear power plant accidents are due to workers' mistakes. Accordingly, four kinds of human factors were selected to produce an integrated human error model. The four factors selected are as follows:

- Worker stress
- Worker fatigue
- Team efficiency
- Procedure efficiency

The integrated human error model developed by applying these factors is shown in Figure 1.

3. Integrated Human Error Model Verification

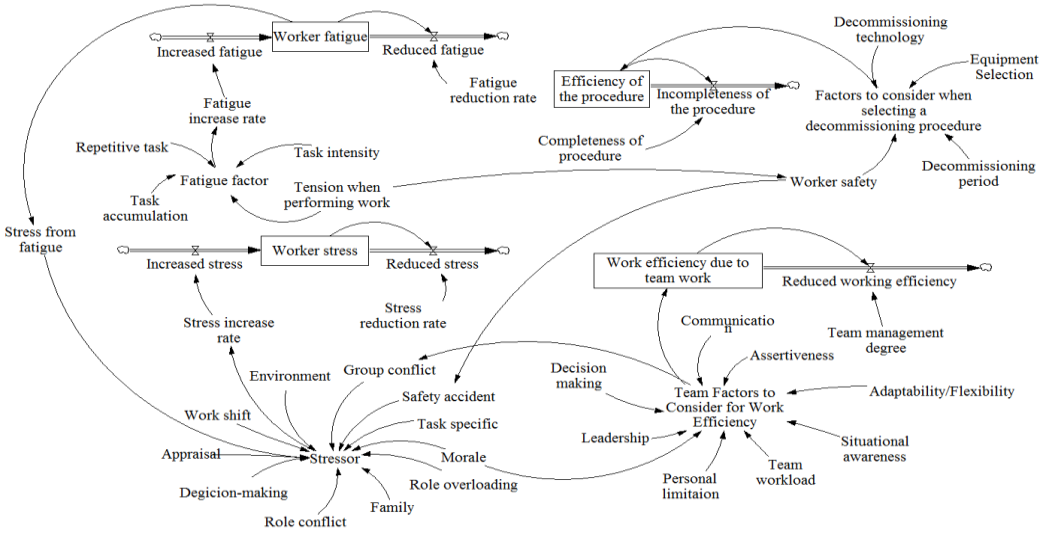

Fig. 1. Integrated Human error model about decommissioning of nuclear power plants.

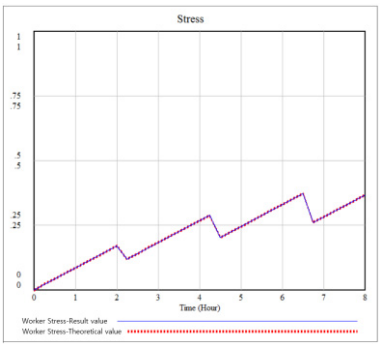

Fig. 2. Cumulative Stress Over Time.

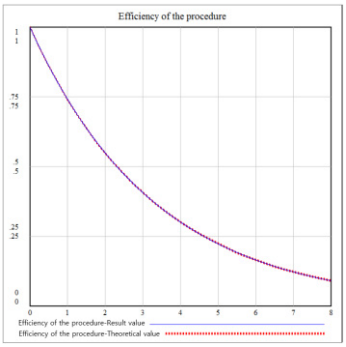

Fig. 4. Work efficiency according to the procedure over time.

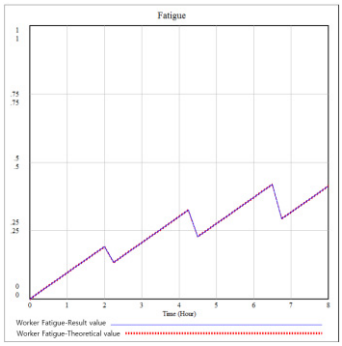

Fig. 3. Cumulative fatigue over time.

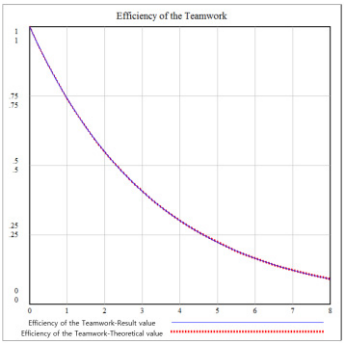

Fig. 5. Work efficiency according to the Teamwork.

Verification was performed by comparing the predicted theoretical values with the produced program values for the integrated human error model. In the task analysis for the reactor pressure vessel internal structure segmentation, the standard of working time was selected as two hours of work and 15 minutes rest. In the case of stress and fatigue, the stress or fatigue level increases during the two hours of work and then decreases during the break. Team factors or procedural factors decrease exponentially with management, based on eight hours of work per day. The mean error between the theoretical and the resultant values for each factor is shown in Table 1, and the result graph for each factor is shown in Figures 2, 3, 4, and 5.

Table 1. Average error between theoretical and resultant values for each factor

Factor	Mean error
Stress over time	0.233734545
Fatigue over time	0.000101964
Team work efficiency over time	0
Work efficiency according to the procedure over time	0

4. Conclusion

In this paper, an integrated human error model about reactor pressure vessel internal segmentation work was developed and verified. Through the integrated human error model developed, continuous management is required to prevent factors such as workers' stress and fatigue from affecting work. Afterward, further research will attempt to derive human error that may occur due to selected factors.

REFERENCES

[1] Chang-Su Nam, Byung-Sik Lee, “Event/accident simulation model of the reactor pressure vessel internal segmentation activity”, Korean Radioactive Waste Society Fall Meeting (2019).

[2] KAERI, Study on the state of the arts technologies and policy trends for the decommissioning of nuclear installations and facilities, RR-2608 (2005) .

Data Scientific Approach for the Data of KAERI's Decommissioning Experiences

Hyung Gon Jin [a,*] and Woori Kim[b]
[a]Korea Atomic Energy Research Institute, 111, Daedeok-daero 989beon-gil, Yuseong-gu, Daejeon, Republic of Korea
[b]Virtual Rx, 72-30, Gwandeul 2-gil, Yuseong-gu, Daejeon, Republic of Korea
[*]jhg@kaeri.re.kr

1. Introduction

Korea Atomic Energy Research Institute (KAERI) is the only research Institute in Korea that has experience in dismantling actual nuclear facilities, including the KRR 1 & 2. In this process, a large amount of decommissioning information has been accumulated, and it is expected that by applying machine learning to such data, the cost of decommissioning of nuclear facilities, such as Hanaro research reactor can be predicted. To do this, an analysis of existing accumulated experience data is required, and a judgment on whether it can be used for machine learning must be made beforehand.

2. Contents and scope

To apply existing data to machine learning, it is necessary to convert and organize it. In particular, the task of deriving hidden correlation between data by converting quantity information and unit productivity information of the dismantling facility into a graph form is required. If meaningful correlations are found in the data, they are classified using neural network theory, one of artificial intelligence (AI) technology, and used as basic machine learning data. However, the data collected during the decommissioning work was not intended for AI, so it could be difficult to correlating the data. If so, alternatives to what data should be collected more precisely in the future decommissioning process are provided in this paper.

3. Data Scope

It is divided into KRR (KRR-1 & 2), UCP, and WACID. KRR is a research reactor by KAERI (KRR-1, KRR-2 refers to Units 1 and 2), and UCP stands for Uranium Conversion Plant, which means uranium conversion facility. WACID is an abbreviation of WAste Comprehensive Infomation Database and is an integrated radioactive waste safety management information system developed to comprehensively manage safety management information on domestic radioactive waste and spent fuel [1]. Received the above experience data from KAERI and the details are as follows.

KRR data includes export packaging data, radioactive waste (for work), input data (radioactive, self-disposal), pre- and post-contamination contamination data, and UCP data for export packaging data, radioactive waste (for work), input data (radioactive, self-disposal, Container characteristics data), pre- and post-contamination inspection data, etc. WACID data is divided into the first and fourth quarters from 2002 to 2010.

4. Data Characterization Results

From the characteristics of data, it is difficult to find the correlation between unit cost factor (UCF) for cost evaluation due to unusual features and missing data. the basic method for estimating decommissioning costs is to subdivide all decommissioning activities into WBS, the total cost is calculated by multiplying the time for the equipment classify used for each WBS by the labor cost. The data used in this analysis, there are so many kinds of work connected to one WBS, as shown in the reference graph above. There are unusual cases where weight or volume has only one value, and even though the weight or volume varies depending on the work, it can be confirmed that the working time is the same. The initial expectation was that even if the same WBS had different weights, volumes, and working hours, it would be possible to infer unit productivity factors by weight. But such data could not be found in the actual data.

In the early 2000s, the decommissioning was

in progress, and the accurate recording and sorting of the dimensions of each waste would have been a cumbersome task. Types were divided into cubes, pipes, etc. in order to express them in size without photographs of wastes with different shapes. so, it seems that there was a limit in which the detailed characteristics such as the size and volume of the waste were difficult to reflect.

5. DB schema development

In order to derive meaningful data, it is required to record the shape of the waste as an image when dismantling the facility in the future, and to identify and store the shape and dimensions through the image identification technology.

KAERI is aware of these needs and plans to develop artificial intelligence-based waste sorting technology for future projects. the goal of this project to apply the 3D Vision system to the development of a system that can safely and accurately classify radioactive waste generated by KAERI is to develop a waste classification strategy algorithm, design a multi-joint robot and picking equipment, waste tracking management system and It is to establish an integrated management system and to introduce cooperative work procedures in which robots and workers coexist. As a result of analyzing the dismantling experience data, the following data should be obtained through this automated process.

As the shape of the waste may be suitable for diameter or longest length rather than width, length and height, the storage of size information linked to the waste photograph should be parallel and radiation dose measurement should be included in consideration of waste disposal.

As one of the technologies related to recording size information for estimating waste volume, it automatically records the size, weight and volume of dismantled waste using the 3D vision system capable of image analysis, and the time required for the dismantling operation. This can be used for cost evaluation

In the case of job time records, it is necessary to recognize workers' movements and record their history by action, since it is difficult to predict actual work times with the data that one person currently has if several types of decommissioning work were carried out per day.

COGNEX's 3D machine vision systems typically include multiple cameras or laser displacement sensors, and multi-camera 3D vision in robot guidance applications provides robots with part orientation information. This system includes multiple cameras mounted at different positions and triangulation of objective positions in 3D space. 3D laser displacement sensor applications typically generate 3D results, including surface inspection and volumetric measurements, where the height map is generated from the positional displacement of the laser reflected off the object. Moving objects or cameras to scan the entire product similar to line scans, and using a calibrated offset laser allows the displacement sensor to measure variables such as surface height and flatness within 20μm, making it more accurate to record decommissioning waste.

Table 1. Summary of DB schema

Data classification	Property	Purpose
Worker Information	Worker ID	To get working history
Working Time	Time (hour)	man/hour calculation
Working Video	Video	Work difficulty assessment
Waste Pictures	Ficture File	Estimated amount of waste (including size infomation)
Horizontal	Length(m)	Waste calculation
Vertical	Length(m)	Waste calculation
Height	Length(m)	Waste calculation
Weight	kg	Waste calculation
Volume	m^3	Waste calculation
Radiation dose	Radiation (Bq)	Waste classification

REFERENCES

[1] S. K. Park, S. B. Hong, et. al., “A Decommissioning Information Management System,” the Korean Nuclear Society Spring Meeting Vol.1 (2007).

Refinement of Performance Shaping Factors Through the Development of Integrated Human Error Model for Nuclear Power Plant Decommissioning Work

Chang-Su Nam*, Byung-Sik Lee, and Sung-Mi Park
Dankook University, 119, Dandae-ro, Dongnam-gu, Cheonan-si, Chungcheongnam-do, Republic of Korea
*72180291@dankook.ac.kr

1. Introduction

In the last study, Task analysis and performance shaping factors for the reactor pressure vessel internal cutting work were derived. The derived human error model for the dismantling of the nuclear power plant was developed through the derived performance shaping factors. In the process of developing an integrated Human error model, rather than applying the entire performance impact factor as an individual factor, the refinement of applying or removing the less important performance shaping factors into the factor, The process was carried out. The weights of performance shaping factors were derived using Fuzzy-AHP method.

2. Refinement of performance shaping factors by deriving the weighting factors of performance shaping factors

2.1 Deriving Performance Shaping Factors Weights

The Fuzzy AHP method was used to derive the weighting factors of the performance shaping factor. The Fuzzy – AHP method has been used as a mathematical model to analyze the uncertainty of factors for human subjective perception. The weighting factors of Level 3 of the representative performance shaping factors derived from Fuzzy – AHP through the previous studies are shown in Table 1.

Table 1. Typical Level 3 Performance shaping factors weighting factors

Level 3	Weighting factor
Stress	0.07
Emotional State	0.07
Fatigue	0.07
Physical Capability	0.06
Overall Planning	0.09
Team Factors	0.04
Work Process Design	0.04
Interaction Element	0.05
Familiarity of Equipment	0.05
Complexity of Equipment	0.03

2.2 Refinement of Performance Shaping Factor

Human error model was developed in the paper [1] through the weights of Table 1. In this process, the process of including or excluding low-weight PSF items in the high-weight PSF was conducted. Table 2 shows the PSFs that enhance the 32 existing PSFs at level 3.

Through refinement, as shown in Table 2, a total of 17 refined performance shaping factor sets were derived from the existing 32 performance shaping factor sets.

Table 2. Refinement of Performance shaping factors

Level 2	Level 3
Psychological State	Stress
	Emotional State Safety Awareness(Include in Stress)
Physical State	Fatigue
	Physical Capability Discomfort(Include in Fatigue)
Performance Capability	Task Knowledge and Memory
	Experience
Organizational Factors	Overall Planning
	Supervision of Management (Include in Team Factors)
	Team Factors
Task Management	Work Process Design(Include in Procedure and Information)
	Workload Management(Include in Team Factors)
	Problem Identification and Solution(Include in Team Factors)
	Communication Availability and Quality(Include in Team Factors)
Procedure and Information	Availability
	Complexity
	Accuracy and Completeness
	Feedback and Recency
HMI	Interaction Element Familiarity of Controller and Display Complexity of Controller and Display(Include in Maintenance)
	Maintenance
Workplace Design	Physical Access to Work Items Warning Sign Arrangement of Functional Areas Safety Device(Include in Maintenance)
Workplace Physical Environment	Noise
	Lighting
	Temperature
	Radiation Level

3. Conclusion

If the previously developed performance shaping factor set is a performance shaping factor for the overall dismantling of nuclear power plants, the PSF set refined through the development of Fuzzy-AHP and human error model is the PSF set for reactor pressure vessel internal cutting work. It is necessary to understand the mechanism of human error generation while developing human error models because it is necessary to lower the rate of increase of human error occurrence for cutting of the reactor pressure vessel internal structure. Since the PSF set in Table 2 is optimized for reactor pressure vessel internal cutting work, the work should be considered in the refinement of the factors affecting the refined PSF. Later, in deriving the probability of human error through the refined PSF set and human error model, the validity of the PSF will be increased through continuous PSF refinement. Accordingly, it is expected to be able to manage the cause factors before or after the occurrence of an event or accident or to quickly identify and resolve the cause after the occurrence of the event.

REFERENCES

[1] Chang-Su Nam, Byung-Sik Lee, “Event/ accident simulation model of the reactor pressure vessel internal segmentation activity”, Korean Radioactive Waste Society Fall Meeting (2019).

[2] Chang-Su Nam, Byung-Sik Lee, Hyun-Jae Yoo, Derived of the weighting factors of the performance shaping factors related the reactor pressure vessel internal structure cutting using Fuzzy AHP, Korean Radioactive Waste Society Fall Meeting (2018).

[3] KAERI, Study on the state of the arts technologies and policy trends for the decommissioning of nuclear installations and facilities, RR-2608 (2005).

Analysis of Design Characteristics of Radioactive Waste Treatment Facility in Accordance With NRC Regulatory Guide 4.21

San Chae[1,*], Seungkook Park[2], Jongjin Kim[1], Jeong-Guk Kim[1], and Dae-Seok Hong[1]

[1]Korea Atomic Energy Research Institute, 111, Daedeok-daero 989beon-gil, Yuseong-gu, Daejeon, Republic of Korea

[2]NUDECOMM, 3-Na-309, 530, Daedeok-daero, Yuseong-gu, Daejeon, Republic of Korea

[*]schae@kaeri.re.kr

1. Introduction

The Nuclear Safety and Security Commission (NSSC) legislates the submission of an initial decommissioning plan for all nuclear facilities. Section 5 facilitating decommissioning of initial decommissioning plan is a new concept to design the nuclear facility that there wasn't before. Design characteristics of nuclear facility should be managed due to minimization of contamination and waste generation during a whole period; from initial design to shut down. Therefore, it is important for analyzing of design characteristics of a nuclear facility. In this study, we analyze the design characteristics of RadWaste Treatment Facility (RWTF) in KAERI in accordance with Reg. Guide 4.21.

2. Design Characteristics of Radioactive Waste Treatment Facility

NRC Regulatory Guide 4.21 is a method acceptable to the U.S. Nuclear Regulatory Commission for use to minimize contamination and radioactive waste generation over the whole life cycle of a facility. The Guide was organized as follows: (1) Minimizing Facility Contamination, (2) Minimizing Contamination of the Environment, (3) Facilitating Decommissioning, (4) Minimizing the Generation of Waste. Before Reg. Guide 4.21 was provided, design criteria of nuclear facility followed the Reg. Guide 8.8 (ALARA) for safety of worker. This guide includes facility and equipment design features. U.S NRC improves Reg. Guide 8.8 into the 4.21 guidelines such as interface design and pipeline design for minimization of contamination and waste generation.

2.1 Design Characteristics in accordance with NRC Regulatory Guide 4.21

RWTF has been designed and operated in accordance with Reg. Guide 8.8 (ALARA), nevertheless, initial decommissioning plan of RWTF have to decide whether to satisfy the Reg. Guide 4.21 or not. Fig 1 shows the 4 radiological safety zones (red, amber, green, and white) due to control of cross-contamination between structure, systems, and components important to radiological safety and nonradioactive. It is designed in accordance with 2. Facility and Equipment Design Features in Reg. Guide 8.8, which coincides with Reg. Guide 4.21.

Fig. 1. Zoning for control of cross-contamination in Rad Waste Treatment Facility.

2.2 Waste Evaluation during decommissioning

Waste inventory influenced by Reg. Guide 4.21 requirements is shown in Table 1. The waste inventory (698.45 tons) in accordance with Reg. Guide 4.21 occupies about 45% of the total waste inventory (1,538 tons). This result has a meaning that reflection of the Regulatory requirements from initial facility layout and design is very important.

Table 1. Waste inventory in accordance with Reg. Guide 4.21 requirements during Decommissioning

	Bulk mat. (Tons)	Equipment		
		Waste Treat. (Tons)	RMS (Tons)	Tank, Pump etc. (Tons)
Metals (SS)	36.0			
Metals (FE)	108.9			
Metals (etc.)	0.0	296.4	1.07	256.1
Ceramic	0.0			
Wood	0.9			
Glass	0.4			
Total	146.2	296.4	1.07	256.1

3. Conclusion

Initial facility layout and design affect procedures for operation and concluding with final decontamination and dismantling at the time of decommissioning. Including facilitating decommissioning as one section of initial decommissioning plan, we analyze the design characteristics nuclear facility in accordance with Reg. Guide 4.21. Also, according to Reg. Guide 4.21, we analyzed how these requirements influence waste inventory at the time of decommissioning. About half of total waste generation at the decommissioning was influenced by the NRC Reg. Guide 4.21. Therefore, these requirements have to be considered from initial facility design plan.

REFERENCES

[1] U.S NRC Regulatory Guide 4.21, “Minimization of Contamination and Radioactive Waste Generation: Life-Cycle Planning”, U.S NRC, 2008.

[2] U.S NRC Regulatory Guide 8.8, “Information Relevant to Ensuring that Occupational Radiation Exposures at Nuclear Power Stations will be As Low As Is Reasonably Achievable”, U.S NRC,1978.

Analysis of Calculation Methodology on Gaseous Discharge During Decommissioning of NPPs

Hyun Min Kim* and Kwang Ho Jo

KHNP Central Research Institute, 70, Yuseong-daero 1312beon-gil, Yuseong-gu, Daejeon, Republic of Korea

*hyunmin.kim@khnp.co.kr

1. Introduction

Kori unit 1, the Korean oldest commercial NPP, was permanently shut down in 2017 and decommissioning activities are being conducted. KHNP should summit FDP (Final Decommissioning Plan) in accordance with regulations of Nuclear Facilities Decommissioning Plan, such as Nuclear Safety and Security Commission Notice 2018-10 "Which is the guideline for the FDP". As the Notice, the FDP consists of eleven chapters. Chapter 9 is about the radioactive waste management which includes solid, liquid, gaseous, mixed waste and operational radioactive waste.

In this paper, we have analyzed the method of calculating of the gaseous discharge and applicability of the Kori-1 FDP.

2. Amount of gaseous discharge

The amount of gaseous wastes depends on cutting technology, number of cutting pieces, cutting length, etc. Especially, each cutting methods such as plasma arc, thermal cutting, mechanical cutting has respectively different Kerf width and dispersion ratio during cutting activities. And the Kerf length depends on the type of the container in which the component will be stored. Shapes of components such as piping and ducts also affect the Kerf lengths. Therefore these factors need to be considered for the evaluating the amount of gaseous wastes. To calculate the quantity of generating aerosol, the following information is required and total amount of generating wastes (G_{ij}) is simply expressed in the below equation (1) [1].

$$G_{ij}(Bq) = \sum(C_i \times K_j \times D_{ij}) \quad (1)$$

Where,

- G_{ij} of radionuclide i and cutting tool j
- Concentration of radionuclide : C_i (Bq/cm^3 or Bq/cm^2)
- Kerf volume / surface : K_j (cm^3 or cm^2)
- Dispersion ratio of each cutting tool : D_{ij}

2.1 Radionuclide

The source term data were obtained from the Characterization Survey for Kori unit 1. The report categorized major components (RV, RVI, SG, PZR, and RCP) and others (Pipe, Valve, Pump, Scabbling Concrete, etc.) for decommissioning systems and structures. In case of Kori-1, the total number of components or devices is approximately 16,000 [2]. The components are classified into 6 shapes according to the type, and the example components by classification shape are shown in Table 1.

Table 1. Classification Shape

Shape	Example of components
Cuboid	Pump, concrete block
Circular piping	Piping
Large object with tube shape	Body of the RV, core shroud
Cylinder	Tank, motor
Plate	Liner
Hollow prismatic column	Rectangular duct

2.2 Kerf volume

The Kerf is defined as the width of material that is removed by a cutting process. The Kerf volume can be found as the product of the Kerf width and the total cutting length of each device. The Kerf width depends on cutting technology. This paper considers Arc saw, Oxygen torch, Acetylene-oxygen torch, High pressure water lance and Plasma torch for the cutting technique [3]. Table 2 show typical data in terms of the Kerf for some cutting technology.

Table 2. Cutting Parameters

Cutting technology	Kerf Width (cm)
Arc saw	0.95
Oxygen torch	0.965
Acetylene-oxygen torch	0.635
High pressure water lance	0.1143
Plasma torch	0.31 ~ 0.635

2.3 Dispersion ratio

In general, the dispersion ratio is comprehensively influenced by cutting technology, environment (in air or underwater), materials and etc. In case of Kori-1, detailed cutting technology for each component has not been determined yet, but it is assumed that a typical cutting technology is used. Also, the only component that can be cut underwater is RVI cutting.

2.4 Cutting length

The cutting length is determined by the number of cuts and the number of cuts is determined by the size of the cutting components and the waste container. Although the quantity information (volume, weight, thickness, width, height, length) for all components is retained, the details of the waste container are not determined and are calculated based on the 200L drum.

3. Conclusion

In this paper, we have analyzed the method of calculating of the gaseous discharge and applicability of the Kori-1 FDP. Then, we are using the results to calculate gaseous discharges and writing in chapter 9 of the FDP. As the detailed factors are decided, the accuracy of the result will be further improved.

REFERENCES

[1] Safety Assessment for Decommissioning, IAEA Safety Report Series No.77 Annex I (2013).

[2] KEPCO E&C, Characterization Survey for Kori unit 1 (2019).

[3] U. S. Nuclear Regulatory Commission, Technology, Safety and Costs of Decommissioning a Reference Pressurized Water Reactor Power Station, NUREG/CR-0130 (1978).

Study on Packaging Plan of Kori Unit 1 RV and RVI Segments

Young Hwan Hwang[1,*], Ju-Young Yoon[1], Mi-Hyun Lee[1], Seong-Hoon Hong[1], Ji-Hoon Lee[1], and Kwang-Soo Park[2]
[1]KHNP Central Research Institute, 70, Yuseong-daero 1312beon-gil, Yuseong-gu, Daejeon, Republic of Korea
[2]Doosan Heavy Industries & Construction, 22, Doosan volvo-ro, Seongsan-gu, Changwon-si, Gyeongsangnam-do, Republic of Korea
[*]yhhwang7@khnp.co.kr

1. Introduction

The decommissioning of nuclear power plan (NPP) consists of various critical paths. The segmentation of activated components, including reactor vessel (RV), reactor vessel internals (RVI), and bio-shield concrete, is one of the most important critical paths. It generates intermediate level waste (ILW), low level waste (LLW), very low level waste (VLLW), and clearance waste (CW) [1]. The ILW is only found in RVI segments. In many cases the reactor-related ILW are sent to independent spent fuel storage installation (ISFSI) [2]. Since the total activity of intermediate and low level waste disposal site is limited, it seems that the interim storage of ILW in ISFSI is reasonable and attribute to the efficient operation of disposal site, when considering expected operation and decommissioning waste.

The larger package for LLW and VLLW, generated from segmentation process, need to be developed for efficient packaging plan for RV segments. Although 200 L and 320 L drums are available in disposal site, it seems that the loading and packaging of metal segments with curvature and high thickness is not appropriate with currently available packages. The conceptual design of package for LLW and VLLW using IP-2 transportation package design basis was reported [3].

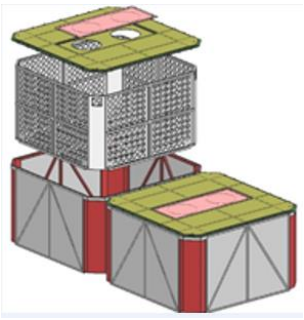

Fig. 1. Conceptual design of package (LLW/VLLW) [3].

In this study, the RV segments packaging plan considerations, scenario, and characterization are reported.

2. Packaging Plan Development

2.1 General Considerations

The waste acceptance criteria (WAC) of disposal facility regulates the radioactive waste strictly for safe and stable operation of the disposal facility [4]. The primary requirements, expected to be applied to RV and RVI segments LLW and VLLW, are listed below. It seems that the LLW and VLLW from RV and RVI segments will be packed and sent to the near surface disposal facility. The expected requirements are selected based on underground silo WAC. They can be changed after confirmation of near surface WAC.

- Specific activity limit for LLW
- Filling rate over 85%
- Free standing water less than 0.5wt%
- Surface contamination
- Surface dose rate less than 10mS/h
- Elimination of corrosive material
- Immobilization of segments

2.2 Packaging Plan of RV Segments

The critical feature of decommissioning waste is a massive waste generation in a short time. The absolute identification of waste during generation step is essential to avoid the confusion and mixing. The Fig. 2. shows the information which are collected during generation: segmentation tool, location, identification, physical properties, activity, etc.

Item	Equipment	Segment property							
		ID	Material	Density (g/cm^3)	Dimension (mm)	Mass (kg)	S.A. (Bq/g)	T.A. (Bq)	Class
Main Shell (Active Fuel)	Oxy-propane torch	LI-47	SA-508 Cl.3 Gr.2	7.83	877(H)×247(L)×1141(W)	1,251	3.3E+05	1.7E+09	LLW
Main Shell (Active Fuel)	Oxy-propane torch	LI-48	SA-508 Cl.3 Gr.2	7.83	877(H)×247(L)×1141(W)	1,251	3.3E+05	1.7E+09	LLW
Main Shell (Active Fuel)	Oxy-propane torch	LI-49	SA-508 Cl.3 Gr.2	7.83	877(H)×247(L)×1141(W)	1,251	3.3E+05	1.7E+09	LLW
Main Shell (Active Fuel)	Oxy-propane torch	LI-50	SA-508 Cl.3 Gr.2	7.83	877(H)×247(L)×1141(W)	1,251	3.3E+05	1.7E+09	LLW

Fig. 2. Determination of cutting tools and characterization of segments.

2.3 Characterization of RV Segments Package

The example of RV segments packaging plan is shown in Fig. 3. Various factors, including balance of segments, activity, shielding, etc., are considered in packaging plan. The Fig. 4., presents the characteristics of package (example), shows the primary characteristics of package, such as physical properties, activity, dose rate, etc.

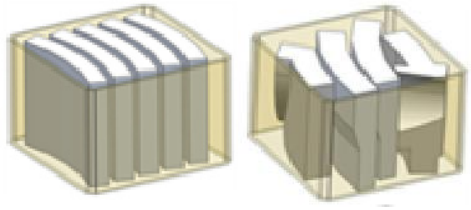

Fig. 3. Packaging plan of RV segments (example).

Category	Package	Loading item	Mass (kg)	Density (g/cm^3)	Filling rate (%)	S.A. (Bq/g)	T.A. (Bq)	Class
4	21	LI-47, LI-48, LI-49, LI-50	5,004	7.83	60%	3.3E+05	1.7E+12	LLW
4	22	LI-51, LI-52, LI-53, LI-54	5,004	7.83	60%	3.3E+05	1.7E+12	LLW
4	23	LI-55, LI-56, LI-57, LI-58	5,004	7.83	60%	3.3E+05	1.7E+12	LLW
4	24	LI-59, LI-60, LI-61, LI-62	5,004	7.83	60%	3.3E+05	1.7E+12	LLW

Fig. 4. Characteristics of package (example).

3. Conclusion

The waste packaging plan from RV segmentation process is studied. The absolute identification and preparation are prerequisite for efficient waste management. Since the segments are heavy and contain large amount of radiological inventory, various factors were systematically considered, such as balance, activity, shielding, etc.

ACKNOWLEDGEMENTS

This work was supported by the Korea Institute of Energy Technology Evaluation and Planning (KETEP) and the Ministry of Trade, Industry & Energy (MOTIE) of the Republic of Korea (20161510300430).

REFERENCES

[1] Y.H. Hwang, S.-J. Hwang, J.-Y. Yoon, "Study on Radiological Inventory Assessment of K1 Reactor Vessel", Proc. of the KRS 2019 Spring Conference, May 8-10, 2019, Busan.

[2] EPRI, Review of Waste Management Best Practices During Nuclear Plant, 300200525 (2015).

[3] D.-W. Jung, H. Kim, D.-G. Lee, K.-S. Choi, Y.H. Hwang, "Radiation Shielding Evaluation for IP-2 Transport Container including Activated Cutting Waste of KORI Unit 1 RV/RVI", Proc. of the KRS 2018 Spring Conference, May 8-10, 2018, Busan.

[4] B. Kim and C.-L. Kim, “Review of the Acceptance Criteria of Very Low Level Radioactive Waste for the Disposal of Decommissioning Waste”, Journal of Nuclear Fuel Cycle and Waste Technology, 12(2), 165-169 (2014).

Safety Assessment Approach for Deriving Potential Accident Scenarios During Decommissioning of Nuclear Power Plant

Kwangho Jo* and Hyun Min Kim
KHNP Central Research Institute, 70, Yuseong-daero 1312beon-gil, Yuseong-gu, Daejeon, Republic of Korea
*kwangho.jo@khnp.co.kr

1. Introduction

For nuclear power plants (NPPs) that already have a safety assessment methodology for the operational phase, parts of that safety assessment may be relevant to aspects of the decommissioning safety assessment. However, it is important to recognize that the main target of decommissioning safety assessment is fundamentally different from that of operating the NPPs. As all nuclear fuels are removed or stored in a passively safe form, the existing probabilistic safety assessment (PSA) is not necessarily appropriate method for identifying accident scenarios during decommissioning [1]. Instead, a deterministic approach to safety assessment is most commonly applied approach to derive accident scenario during safety assessment [2].

For this sake, we have carried out a review of IAEA safety assessment methodology and adopted a detailed method that be applicable to the decommissioning safety assessment from the according to the Korean Occupational Safety and Health Agency (KOSHA) guideline. Finally, this detailed approach is compared with the IAEA methodology in 7 steps and examples applied KOSHA methods are shown in Table 1 to help decommissioning safety assessment staff.

2. Applied KOSHA methods

KOSHA guidelines recommend that the hazards and accidents can be identified by brainstorming approach (HAZOP, What if method) and checklist approach (Checklist method). In addition, it is need to be used both approaches together complementarily [3]. Also, the risk matrix techniques can be adopted to evaluate the risk by considering both consequences and likelihood.

2.1 HAZOP

The HAZOP process is to identify and evaluate problems (hazards and accidents) that may endanger personnel or equipment. It should be carried out by suitably qualified and experienced persons including plant operator and engineers, radiological protection specialists, safety engineers.

The experts can determine the level of potential accident scenarios and eliminate low risk scenarios using the checklist, what if, and risk matrix methods.

2.2 Checklist

The use of checklist can be a useful approach for identifying hazards and initiating events for both experienced and less experienced safety assessment staffs. This list can be used as a starting point for hazard identification, but care needs to be taken to add hazards that may be relevant for the particular facility. For example, some hazards list can be initially excluded for facilities where natural disasters such as floods and typhoons are less likely to occur.

2.3 What if

The ‘What if’ is a method to discuss unexpected events and identify potential accident scenarios by a group of experts familiar with the equipment and the facility to be

decommissioned. Any questions may be asked regardless of category, such as “What if power loss happens? “What if fired? Then ~?”

2.4 risk matrix

A risk matrix is a matrix that is used during risk assessment to define the level of risk by considering the category of probability or likelihood against the category of consequence severity. Base on the expert judgment, the level for probability and likelihood can be determined.

3. Conclusion

The applicable safety assessment methodologies for deriving potential accident scenarios were reviewed and the detailed approaches are compared with IAEA safety assessment steps giving actual examples in Table 1. It may be helpful to understand the actual methodology of safety assessment at the early phases of planning decommissioning.

REFERENCES

[1] Safety Assessment for Decommissioning, IAEA Safety Report Series No.77 Annex I (2013).

[2] HEALTH AND SAFETY EXECUTIVE, Safety Assessment Principles for Nuclear Plants, UK HSE, London (1998).

[3] KOSHA Guide X-42, Guidance on information and approach to risk identification (2011).

Table 1. Actual methodology examples

I. IAEA Process	II. Applied KOSHA methods	Examples
1. framework	HAZOP	• Determine a regulatory criteria & requirements (Accident Criteria: 8) • Determine a risk matrix consequence & likelihood criteria (4×4, 5×5)
2. Description of facility / Activities	HAZOP	• Understand the decommissioning activities and facility • Use a facility drawings and
3. Hazard identification / Screening	Checklist	• External hazards such as aircraft, flood, seismic etc. events can be excluded from initial checklist • Radiological, Fire/explosion, Electrical, Chemical, Human etc. hazards are evaluated by experts using the final checklist • Evaluate the potential accident scenarios by checking the checklist for all decommissioning activities. • Derive and list all potential accident scenario
4. Hazard Analysis	HAZOP What if	• Assume the potential accidents from HAZOP with experts • What if fire break out in the radioactive waste storage area? • What if drop the radioactive waste drum during transfer to truck? • What if decontamination waste tank is broken and spilled?
5. Engineering Analysis	HAZOP Risk matrix	• Grouped by the similar derived potential accident list • Determine the consequence & likelihood by accident scenario • Ex) Radiological hazard: cutting the pipe (Consequence: 2, Likelihood: 3, Risk: 2×3 =6) • Ex) Radiological hazard: drop the drum (Consequence: 3, Likelihood: 3, Risk: 3×3 =9) • Select the accident scenarios above 8 score • Assess the “Drop the drum scenario”
6. Identification of measurements	HAZOP	• When cutting the pipe activity, put on the mask, protective clothing. • Take a measurements and lower the score (Consequence: 2, Likelihood: 3→2, Risk: 2×2 =4)
7. Compliance with Criteria	HAZOP	• If the accident scenario score is above 8, then evaluate the scenario.

Pilot Scale Synthesis of the PB-Coated Carbonyl Iron Particles for Removal of Radioactive Cesium

Hwa Min Kim, Hyo-Sun Bae, and Chul Am Kim*
Nspectra Co., Ltd., 11-319, 218, Gajeong-ro, Yuseong-gu, Daejeon, Republic of Korea
*cakim@nspectra.co.kr

1. Introduction

Magnetic nanoparticles (MNP), such as Fe_3O_4, have been introduced as the treatment material of contaminated water with heavy metals. Because they can be magnetically separated from a solution simply by application of an external magnet. Among the candidate of heavy metals including radioactive nuclides, radioactive Cesium (^{137}Cs) is the most problematic component of nuclear liquid waste due to its long half-life. So, MNP coated with Prussian blue (PB) were used to separate ^{137}Cs from the contaminated water [1, 2].

However, the synthesis processes of the MNPs have been known as the expensive processes to be commercialized due to low yield value. In addition, because of the lower magnetization property of the MNP than that of others (ex. carbonyl iron (CI) particles in here), it has high obstacle to adopt the commercial scale treatment.

To overcome these problems, we used the CI particles which have twice higher magnetization than that of Fe_3O_4, to adsorb Cs^+ in the radioactive wastewater. Our experiment is based on the pilot scale to verify the commercial scale treatment of PB coated CI (CI@PB).

2. Experimental

2.1 Materials

CI particles were purchased from BASF (HQ Grade) and were used as received. HCl (1 N), 3-Aminopropyltriethoxysilane, $FeCl_3 \cdot 6H_2O$, $K_4[Fe(CN)_6] \cdot 3H_2O$, CsCl and sodium tetraphenylborate (Na·TPB) were obtained from Sigma-Aldrich and were used without any purification.

2.2 Synthesis of prussian blue coated magnetic carbonyl iron clusters (CI@PB)

To obtain the prussian blue coated magnetic CI clusters, the raw CI particles were treated by HCl to introduce the -OH and -COOH functional groups on the particle surface.

After acid treatment step, we have proceeded the synthesis procedure to obtain the Cs^+ adsorbent particles using 1 kg of the oxidized CI particle according to the previous reports [1, 2].

3. Results and Discussion

Fig. 1 shows SEM images of the raw CI and the CI@PB particles. Firstly, from these results, we observed that the CI particles were well covered by PB.

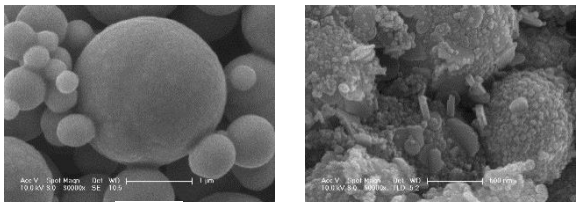

(a) (b)

Fig. 1. SEM images of (a) the raw CI particles and (b) PB coated CI particles.

To examine the Cs^+ adsorption capability of the PB coated CI particles qualitatively, we have dropped TPB^- solution (100 ppm) into the Cs^+ standard solution (100 ppm) and the CI@PB particles treated solution, respectively. Fig. 2 shows the results of the Cs^+ standard and the Cs^+ removed aqueous solution with the TPB^- solution.

The Cs^+ dissolved aqueous solution turns to turbid state when TPB^- molecular come in the Cs^+ solution [Fig.2(a)]. While, the CI@PB treated solution shows transparent state [Fig.2(b)]. It reveals that the CI@PB particles have good adsorption capability for the Cs ions in the water.

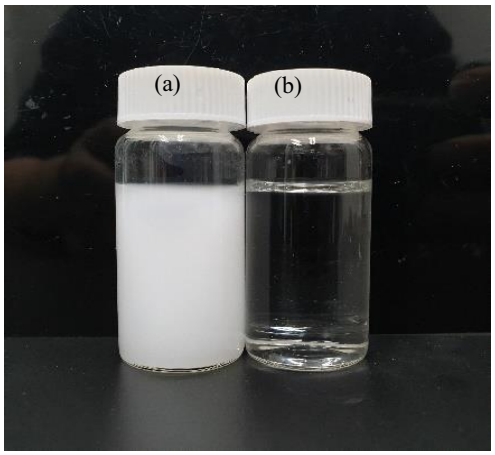

Fig. 2. (a) Turbid state of Cs standard solution with TPB, (b) the transparent state of Cs standard solution after CI@PB treatment.

4. Conclusion

We elucidated the ability of prussian blue coated CI particles (CI@PB) to eliminate radioactive cesium, as in radioactive contaminated water. The CI particles which we used in this study are commercial grade. The CI@PB particles showed high removal efficiency with respect the cesium.

ACKNOWLEDGEMENT

This work was supported by Technology development Program (S2679581) by the Ministry of SMEs and Startups (MSS, Korea).

REFERENCES

[1] H-M. Yang, S-C Jang, S-B Hong, K-W Lee, C Roh, Y-S Huh and B-K Seo, “Prussian blue-functionalized magnetic nanoclusters for the removal of radioactive cesium form water.” Journal of Alloys and Compounds, 675, 387-393 (2016).

[2] S-C Jang, H-M Yang, S-B Hong and J-K Moon, “Removal of radioactive Cesium using Prussian Blue Magnetic Nanoparticles.” Nanomaterials, 4, 894-901 (2014).

Contaminated Characteristic and Treatment Technology of Fine Particles (Silt/Clay) With Radionuclide

In-Ho Yoon*, Sung-Man Kim, Ilgook Kim, Chan-Woo Park, Hee-Man Yang, and Bum-Kyoung Seo
Korea Atomic Energy Research Institute, 111, Daedeok-daero 989beon-gil, Yuseong-gu, Daejeon, Republic of Korea
*ihyoon@kaeri.re.kr

1. Introduction

Serious environmental contamination with radionuclides resulted from the Fukushima Daiichi nuclear accident in Japan, and a very large amount of soil in a wide area became contaminated [1]. In addition to this critical accident, unintended leakages of radioactive substances from various nuclear facilities have also contaminated the environment, and most of the radio-contaminated soils are subject to low-level wastes [2]. Remediation of radio-contaminated soil has been attempted with various techniques, such as soil washing, phytoremediation, thermal treatment and electroremediation. Although considerable progress has been made in the development of soil remediation techniques for some radionuclides such as U and Co, the removal of radioactive cesium(Cs) from soil has been relatively inefficient or has required high energy consumption owing to the strong and irreversible interaction of Cs with 2:1 clay minerals in the soil [3]. Therefore, this study was investigated for the contaminated characteristic and treatment technology of fine particles (Silt/clay) with radionuclide.

2. Contaminated characteristic fine particles (Silt/clay) in radionuclide-contaminated soil

As a X-ray Absorption Fine Structure (XAFS) analysis, the first shell of the montmorillolite, vermiculite and illite was analyzed and compared with XAFS data in the previous literature. The first shell is oxygen and Cs bond, which is the outer sphere bond with hydrated Cs. The second shell is oxygen and Cs bond, which is the inner sphere bond with non-hydrated Cs bond. After all the single clay was adsorbed by the Cs, the outer and inner sphere bond was significantly shown by XAFS analysis.

In Cs-hydrobatite and Cs-montmorillonite was adsorbed by the Cs, the outer and inner sphere bond was significantly shown by XAFS analysis. In Cs-illite, Cs was mainly adsorbed on the planar site (outer-sphere bonding). In literature review, Cs was irreversibly adsorbed frayed edge site [3]. In Cs-montmorillonite and Cs-hydrobatite, Cs was adsorbed on the planar site (outer-sphere bonding) and interlayer (inner-sphere bonding).

3. Treatment technology of fine particles (Silt/clay) in radionuclide-contaminated soil

3.1 Radionuclide desorption of fine particles (Silt/clay)

Recently, the Korea Atomic Energy Research Institute (KAERI) has been conducting studies on the desorption characteristics of radionuclides from silts and clays that are concentrated in contaminated soil. A new approach has been reported to increase the removal of Cs from contaminated clay by inserting a cationic polymer electrolyte into the clay interlayer. The cationic polyelectrolyte, polyethyleneimine (PEI), is intercalated into an anionic clay interlayer and serves to easily replace Cs ions adsorbed in the montmorillonite interlayer. Low Cs concentrations are very difficult to remove by simple cation exchange methods because of the increased binding stability of Cs to clays. The synergistic effect of PEI and NH_4^+ is more than 95% Cs [3].

3.2 Separation technology of fine particles (Silt/clay) in contaminated soil

The simplest soil washing processes are generally based on the separation of the fine fractions (silt/ clay) from the soil (which in many cases contain the majority of the contamination). With this separation process, differences between particle grain size, settling velocity, specific gravity, surface chemical behavior and rarely magnetic properties are used to separate those particles which “host” the majority of the contamination from the bulk which are contaminant-depleted.

4. Conclusion

In this review, we investigate the Contaminated characteristic and treatment technology of fine particles (silt/clay) with radionuclide. Cs was adsorbed in outer-sphere bonding for planner site and inner-sphere bonding for interlayer. It is very difficult to remove the Cs in FES site due to the irreversible bonding. KAERI are developing the radionuclide desorption in fine particles and separation technology of fine particles in radio-contaminated soils. Firstly, fine particles are separated from the gravel, sand in contaminated soils to reduce the radioactive wastes. The desorption and stabilization/solidification are considered for the treatment of fine particles. The treatment method should be determined by evaluating the benefit/cost.

REFERENCES

[1] Yamamoto, T. J. Nucl. Sci. Technol., 49, 1116-1133, 2012.

[2] Zhu, Y., Shaw, G. Chemosphere, 41, 121-128, 2000.

[3] Park, C.W. Kim, B.H. Yang, H.M. Seo, B.K, Lee, K.W. J. Hazar. Mater. 327, pp 127-134. 2017.

High Resolution Measurement of Aerosols From Plasma Arc Torch Cuts on Various Metals for D&D Worker Internal Dose Calculation

Wonseok Yang*, Min-ho Lee, Nakkyu Chae, and Sungyeol Choi**

Korea Advanced Institute of Science and Technology, 291, Daehak-ro, Yuseong-gu, Daejeon, Republic of Korea

*abw94@kaist.ac.kr, **sungyeolchoi@kaist.ac.kr

1. Introduction

A plasma arc torch is a common method to cut metal while dismantling a nuclear power plant, because of fast cutting speed. However, plasma arc cutting has a drawback that generates a large amount of fume. When the activated metal in nuclear power plant cut with the plasma arc torch, a huge amount of radioactive aerosols are generated. Radioactive aerosols are a major source of worker internal dose. To estimate committed effective dose by radioactive aerosols, it is necessary to find out the properties of aerosols such as intakes of radionuclide, the chemical form, and the aerodynamic diameter [1].

Previous studies [2, 3] using low resolution measuring devices under inconsistent cutting conditions had a limitation; it was not possible to directly compare the physical and chemical properties of aerosol data.

To overcome the challenge, this study set out to investigate the aerodynamic distribution of the aerosols from plasma arc cuts on various metal in a controlled cutting condition by using a high-resolution measurement device.

2. Methods

2.1 The aerosol measurement system in K&FC

Fig. 1. The aerosol measurement system in K&FC.

The aerosol measurement system in KAIST Nuclear Fuel Cycle laboratory (Figure 1) is composed of an aerosol chamber (ca. 0.86 m^3), an x-stage automatic cutting system with a plasma arc torch (powermax125, Hypertherm), an isokinetic sampling system and a high-resolution electrical low-pressure impactor (HR-ELPI+, Dekati). The system can control cutting speed, plasma arc torch current, and cutting length. The constant cutting speed was achieved by using a servo motor. The isokinetic sampling condition was meet by using proper sampling diameter at the sampling point.

With our system, the physical properties of aerosols can be measured in real-time. After the cutting, chemical element distribution can be analyzed by using ICP-OES with collected and size classified aerosols.

2.2 High resolution electrical low pressure impactor

The HR-ELPI+ is a real-time instrument capable of measuring 6 nm to 10 μm particle aerodynamic diameter in resolution up to 500 size classes [4]. The HR-ELPI+ are composed of a unipolar corona charger, a cascade impactor, and 14 electrometers. The aerosols are charged by the corona charger and then pass through the cascade impactor with electrically isolated 14 collection stages. The charged aerosols are detected with sensitive electrometers. These measured current signals are converted to the number concentration using an advanced iterative inversion calculation method.

2.3 Samples and generation of the aerosols

Aluminum, mild steel, SS304, and SS316 were chosen as sample materials in this experiment. These materials are commonly used in nuclear facilities.

Metal plates (550*100*10 mm) were cut in the aerosol chamber. The plate was placed on the dross box and the distance between the plate and the plasma arc torch is adjusted to 5mm. The material was cut by moving the dross box

under a stationary torch which is fixed at the ceiling. All the materials are cut in the same cutting conditions. Cutting speed was set as 10 mm/s, cutting length was set as 3 cm, and the plasma arc torch current was set as 75 A.

3. Results and discussion

The purpose of the experiment was to compare the difference in aerodynamic distribution between aerosols from cut various materials. The number distribution and number concentration of aerosols changed with the type of metal being cut.

Figure 2 shows the number distribution data on cutting experiment. Both the aerosol distributions from aluminum and mild steel showed tri-modal distribution; on the other hands, the aerosol from SS304 and SS316 had bi-modals distribution. The around 10 nm-sized aerosols produced very small amounts in stainless cutting aerosols compared to other metal cutting aerosols.

The concentration of aerosols also varied depending on the type of metal. Table 1 present number concentrations of each experiment. The mild steel had the highest concentration of fine and ultrafine particles, followed by aluminum, SS316, and SS304.

In the same cutting condition, the size distributions and concentrations were different as the metal was changed. Therefore, even under the same cutting conditions, the internal dose by inhalation of identical radionuclide might vary depending on the metal type. Further research should be undertaken to investigate the aerosols characteristic by change cutting speed and plasma arc current and to analysis chemical composition in different cutting condition.

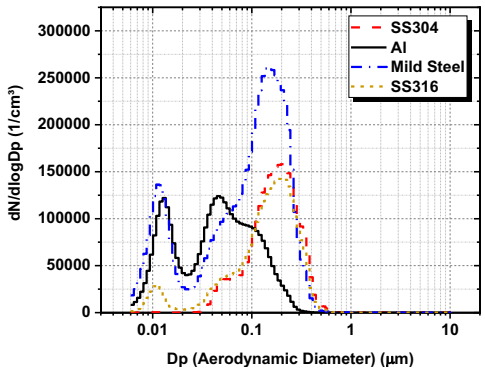

Fig. 2. Number distribution of aerosols from plasma arc cuts on aluminum, mild steel, SS304, and SS316 (cutting speed: 1 cm/s; cutting length 3cm; plasma arc current: 75A).

Table 1. Averaged concentration and count median aerodynamic diameter (CMAD) of aerosols from plasma arc cuts on aluminum, mild steel, SS304, and SS316 (cutting speed: 1 cm/s; cutting length 3cm; plasma arc current: 75A, collection time: 210 sec)

Metal	Concentration [1/cm^3]	CMAD [μm]
Aluminum	1.168×10^5	0.043
Mild steel	2.045×10^5	0.103
SS304	9.065×10^4	0.167
SS316	9.337×10^4	0.147

4. Conclusion

In this study, we compared the difference in aerodynamic distribution between aerosols from cut various materials. This study has identified the number distribution depend on and number concentration of different aerosols from plasma arc cut on four different metals. The number concentration from cutting the mild steel was about twice as high as when other metals were cut.

The study contributes to our understanding of the physical characteristic of aerosols from plasma arc cut on metal. This understanding could be used to accurately calculate an internal dose of workers by combining chemical analysis of aerosols. Furthermore, it could be used to suggest the best cutting methods to reduce the radiation risk to workers.

REFERENCES

[1] T.E. Johnson, “Introduction to Health Physics”, 5th Edition, McGraw-Hill education (2018).

[2] Novick, et al. "Aerosol measurements from plasma torch cuts on stainless steel, carbon steel, and aluminum" Proc the Topical Meeting on the Best of D&D. (1996).

[3] Bernard, J, et al. "Evaluation of Various Cutting Techniques Suitable for the Dismantling of Nuclear Components" EUR(Luxembourg) (1998).

[4] Saari, S., et al. "Performance Evaluation of the Hr-Elpi Plus Inversion", Aerosol Science and Technology 52, no. 9 (2018).

Simultaneous Removal of Both Cesium and Iodine Using Prussian Blue Functionalized Layered Double Hydroxides (PB-LDH)

Jueun Kim*, Jaehyuk Kang, and Wooyong Um

Pohang University of Science and Technology, 77, Cheongam-ro, Nam-gu, Pohang-si, Gyeongsangbuk-do, Republic of Korea

*jueun@postech.ac.kr

1. Introduction

Since the Fukushima Daiichi nuclear power plant accident occurred in 2011, radioactive cesium (Cs) and iodine (I) have become an emerging issue, because these elements have high radiotoxicity and high solubility, and volatilized into air. To protect the environment from the severe nuclear power plant accidents, various studies for developing the effective sorbent have been conducted to remove these radioactive Cs and I.

Prussian blue (PB) known as ferric hexacyanoferrate has a high removal efficiency for Cs^+, because its channel size is similar to Cs^+ ionic size [1]. In addition, layered double hydroxides (LDHs) show high I removal performance using ion-exchange, redox reaction, and reconstruction effects [2].

However, studies have rarely done for removing both Cs and I radionuclides at the same time. Based on the advantages of both PB and LDHs, in this study, we synthesized the LDHs and then functionalized the PB onto the LDHs to enhance the removal efficiencies and understand the removal mechanism of both Cs and I radionuclides.

2. Experimental section

2.1 Synthesis of PB-LDH

CoCr LDHs were prepared according to our previous study [2]. PB-LDH was synthesized by co-precipitation method. Both CoCr LDH (2.714 g) and $FeCl_3$ (0.648 g) were simultaneously dissolved in 15 mL of deionized water (DIW), and these mixed solution was vigorously stirred for 1h. Subsequently $K_4[Fe(CN)_6]$ (1.267 g) was dispersed in 5 mL of DIW and slowly added into the mixed solution. After that, all mixtures were centrifuged, washed with DIW for several times, and dried at 100 ˚C.

2.2 Characterizations

The powder X-ray diffraction (XRD) analysis using Miniflex 600 operating at 40 kV and 15 mA with Cu-Kα was conducted to obtain crystalline patterns of PB-LDH. Fourier transform infrared (FT-IR) spectrum analysis using NICOLET IS10 FT-IR was performed to determine molecular vibrational structures of PB-LDH.

2.3 Cs and I sorption experiments

The equilibrium sorption experiments were conducted to estimate sorption capacity of PB-LDH. PB-LDH (0.01 g) was dissolved in 10 mL of 5 ppm solutions (CsI, CsCl, NaI, and $NaIO_3$, respectively), and the samples were reacted on the shaker at 130 rpm for 3 d. After reaction, the supernatants were filtered with 0.45-μm syringe filter and analyzed by inductively coupled plasma-mass spectrometer (ICP-MS, NexION 300D) to determine the concentration of Cs and I ions. All sorption experiments were prepared in triplicate.

3. Result and Discussion

3.1 XRD analysis

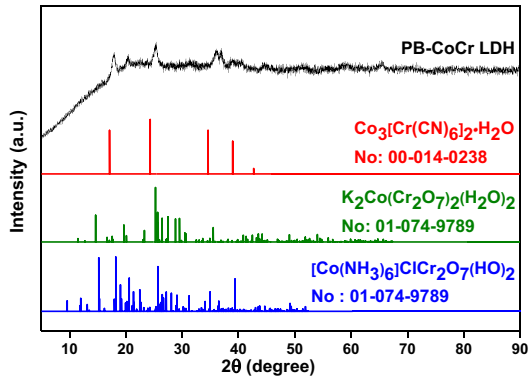

Fig. 1. XRD patterns of PB-LDH.

In the results of the XRD patterns, both peak positions and relative intensities of PB-LDH indicate that the main component is $Co_3[Cr(CN)_6]_2 \cdot H_2O$ (Fig. 1).

3.2 FR-IR analysis

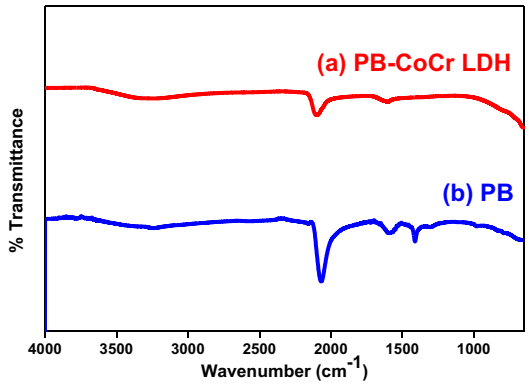

Fig. 2. FT-IR spectra.

In the FT-IR spectra results, the peaks around 2,080 cm^{-1} show that PB are well functionalized onto the LDHs (Fig. 2).

3.3 Sorption results

Table 1. Removal efficiencies for Cs^+, I^-, and/or IO_3^- using PB-LDH

Removal efficiency [%]	CsI		CsCl	NaI	$NaIO_3$
	Cs^+	I^-	Cs^+	I^-	IO_3^-
PB-LDH	99.4	15.6	98.5	9.0	94.4

In the sorption experiment results, the PB-LDH showed a high removal efficiencies for Cs^+ and IO_3^- (Table 1). It is assumed that channeling effect affected the removal of Cs^+ by the PB, and ion exchange/redox reaction influence on the removal of IO_3^- by LDH, as mentioned in Jiayi Liu et al. [1] and Jaehyuk kang et al. [2].

4. Conclusion

The PB-functionalized LDHs were synthesized and used to investigate the Cs and I removal efficiencies at the same time. As a result, the PB-LDH was identified using the XRD and FT-IR, and the independent Cs^+, I^-, and IO_3^- removal efficiencies were 98.5, 9.0, and 94.4 %, respectively. This PB-LDH could become a promising solution for simultaneous removal of both Cs^+ and IO_3^-, indicating inexpensive operation. In addition, PB-LDH would be deeply studied for the removal mechanism of both Cs and I radionuclides.

ACKNOWLEDGEMENT

This work was supported by the National Research Foundation of Korea (NRF) grant funded by the Korean government (MSIP: Ministry of Science, ICT and Future Planning) (No. NRF-2016R1D1A1B02013310).

REFERENCES

[1] Jiayi Liu et al., "Zinc-modulated Fe-Co Prussian blue analogues with well-controlled morphologies for the efficient sorption of cesium". Journal of Material Chemistry A, 5, 3284-3292 (2017).

[2] Jaehyuk Kang et al., "Nanostructured MgFe and CoCr Layered Double Hydroxides for Removal and Sequestration of Iodine Anions", Chemical Engineering Journal, 380, 122408 (2020).

Utilization on Industry of NPP Decommissioning of Large-Area Compton Imaging System for Concrete Internal Activation

Sanggeol Jeong[1], Sooyeun Park[1], Heekyung Kim[1], Hyeongmin Park[1], Taekyu Lee[1], Suri Park[1], Chan Hyeong Kim[2], Jae Hyeon Kim[2], Junyoung Lee[2], Hyun Su Lee[2], and Yong-Ho Hong[1,*]
[1]ACT, 1434, Yuseong-daero, Yuseong-gu, Daejeon, Republic of Korea
[2]Hanyang University, 222, Wangsimni-ro, Seongdong-gu, Seoul, Republic of Korea
[*]hyh@actbest.com

1. Introduction

The decommission of the nuclear power plant (NPP) will result in about 2,600 drums of concrete waste per plant, which is equivalent to about 70~80 % of the total waste [1].

Most of the concrete waste is classified as low or applicable to clearance level radioactive wastes, and it is very important to ensure economic feasibility through effective treatment. To this end, it is also urgent to have equipment that can quantitatively detect the radiative characteristics of concrete structures and the location and depth of the radioactive materials.

In this paper, the concept of a large-area Compton imaging system that provides spatial distribution information on radioactive contamination through three-dimensional high-speed measurements and the site utilization of NPP decommissioning.

2. Detecting System

2.1 General Information

Compton cameras are imaging equipment that can image the distribution of radioactive isotopes emitting gamma rays using position-sensitive radiation detectors and Compton kinematics. The Fig. 1 shows the principle of Compton camera and the equation (1) express to estimate the location of the radiation source using Compton scattering.

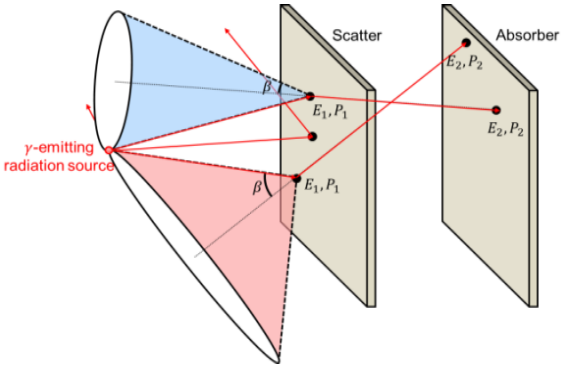

Fig. 1. The principle of Compton Imaging System.

$$\cos\beta = 1 + m_e c^2\left(\frac{1}{E_1+E_2} - \frac{1}{E_2}\right) \qquad (1)$$

2.2 Detector Module

The photomultiplier tube (PMT) array is coupled for NaI(Tl) scintillator to use Compton imaging. A total of four NaI(Tl) scintillators are coupled with 36 PMTs producing 144 channel PMT input signals. This Compton camera is under development by the HUREL (Hanyang University Radiation Engineering Laboratory) of Hanyang University [2]. Fig. 2 is a conceptual diagram of a large-area Compton

camera that measures the three-dimensional coordinates of a hot spot inside a concrete structure.

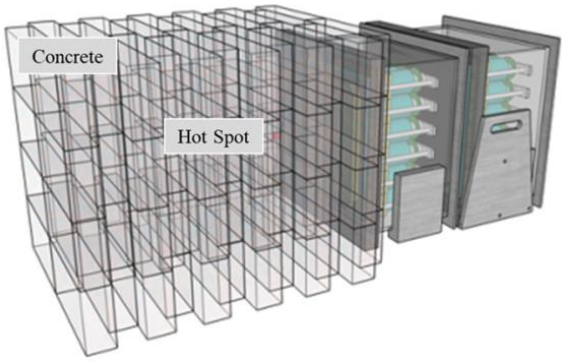

Fig. 2. Conceptual Diagram of Imaging Device.

3. Utilization on NPP Decommissioning

The large-area Compton camera is available for three-dimensional fast imaging with its unique Compton kinematics-based electronic collimation method. By providing source location information in layers of concrete or stacks of radioactive waste drums, it can be involved with operations such as dismantling and decontamination of NPP, and demolition of radioactive structures or facilities. As those projects must take into account the safety issues of not only the operating personnel, public general but any implications for the environment, the large-area Compton camera can be utilized to minimize the generation and spread of radioactive wastes.

In addition, it also helps effective management of the resulting materials which eventually leads to minimization of their impact on the environment and reduction in overall decontamination and decommissioning costs.

4. Conclusion

This study demonstrates the various advantages of newly developing large-area Compton camera and its great potential in industrial utilization.

With increased attention to strategies of the management and disposal of radioactive waste, the large-area Compton camera is expected to be widely utilized for decontamination and decommissioning operations of nuclear facilities.

ACKNOWLEDGEMENT

This study is the result of technology transfer by Hanyang University to carry out "Development of 3D Imaging System for NPP Concrete Internal Activation" project of the Korea Energy Technology Evaluation and Planning.

REFERENCES

[1] International Atomic Energy Agency, “Managing Low Radioactivity Material from the Decommissioning of Nuclear Facilities”, IAEA Technical Report Series No. 462 (2008).

[2] Y. S. Kim, J. H. Kim, J. Y. Lee and C. H. Kim*, “Large-Area Compton Camera for High-speed and Three-dimensional Imaging,” IEEE Trans. Nucl. Sci., 65(11): 2817-2822 (2018).

Plasma Assisted Cutting of Metals for Dismantling of Nuclear Reactor

Min-Gyu Choi, Junseok Nam, Sang-Min Jeong, In-Mok Yang, Shi-Young Yang, and Jun-Ho Seo*
Chonbuk National University, 567 Baekje-daero, Deokjin-gu, Jeonju, Jeollabuk-do, Republic of Korea
*jhseo@jbnu.ac.kr

1. Introduction

During the dismantling process of nuclear reactor, the technologies applicable to cutting the metal structures can be divided into mechanical cutting and thermal cutting. For example, most of metals used in nuclear reactor can be cut by using the mechanical cutting tools, such as milling cutters, drills, disk saws, reciprocating saws, shears, grinders, diamond wire cutting, water jet and pipe cutters. Compared with the thermal cutting tools such as plasma arc, laser and oxy-propane flame, these mechanical cutting tools can cut the metal structure without not only aerosol generation in air but also performance deterioration in water. However, due to the relatively large tensile strength of the metal material, the cutting load can be increased rapidly with the thickness of metal structures, which limits the cutting speed of mechanical tools depending on the thickness of metal structures. In addition, mechanical cutting technologies can also cause a serious problem, such as the generation of secondary pollutants due to the use of cutting oil and coolant, together with the high rate of tool wear.

On the other hand, thermal cutting tools feel hardly the cutting load because they are not contact with the metal structure. As a result, thermal cutting tools can provide a higher cutting speed compared with the mechanical cutting tools. However, thermal cutting technology generates a large amount of hum and dust during the cutting process, which may increase the risk of the radiation exposure to the workers.

Normally, most of the metallic materials show a drastic reduction of strength and hardness when the temperature is increased [1-2]. Accordingly, if the temperature of the metal surface is locally elevated by using an external heat source, such as plasma torch, the softened metal surface can be machined easily by the conventional mechanical tools without generation of hazardous hum.

Based on this idea, we proposed a plasma assisted milling cutter in this work as a new cutting way to overcome the disadvantages of the mechanical and thermal cutting technologies.

2. Experimental Set-up

Figure 1 shows a picture of a plasma assisted milling cutter used in this work. As shown in this picture, the plasma assisted milling cutter consists of conventional mechanical cutting tools combined with the plasma source. For the cutting test, the mechanical cutting tools were installed on a conventional three-axis milling machine as presented in Fig. 2 illustrating a schematic representation of the test bed.

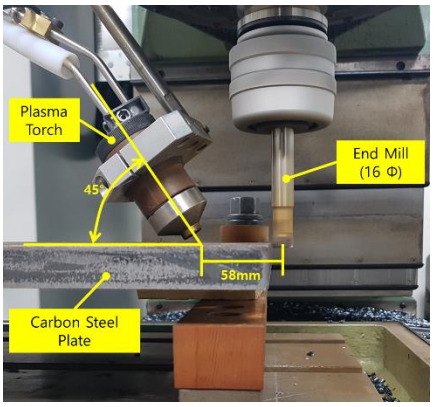

Fig. 1. A picture of a plasma assisted milling cutter.

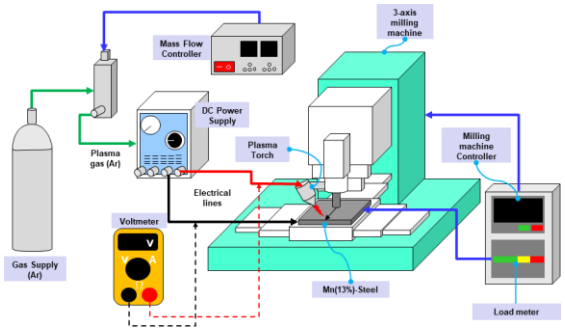

Fig. 2. A schematic of plasma assisted cutter system.

Carbon steel plates with a width, length and thickness of 400 × 300 × 25 mm were prepared as the test samples. For the prepared samples, plasma assisted cutting experiments were carried out at the test conditions listed in Table 1.

Table 1. Operation conditions of plasma assisted cutting system for carbon steel

	Parameters	Value
Plasma torch	Plasma power[kW]	3.9
	Plasma gas[slpm]	12(Air)
	Sheath gas[slpm]	40(Air)
Milling machine	Feeding speed[mm/min]	200
	Milling depth[mm]	3
	Spindle rotate speed[rpm]	1000
	Length of path[mm]	330

During the test, first, we measured the load of the spindle motor by using an electrical load meter [Manufacturer: KEM, Model: KEM-65]. Since the load of spindle motor is proportional to the cutting load of load meter, we estimated the reduction of the cutting load by comparing between the measured values obtained with and without plasma. In addition, the effect of plasma on the tool-life was also checked by comparing between the lengths of cutting paths obtained with and without plasma.

REFERENCES

[1] H.E.Boyer and T.L.Gal, Metals handbook: Dest Edition, ASM international, (1985), 610-620.

[2] S. Sun, M. Brandt and M. S. Dargusch, “Thermally enhanced machining of hard-to-machine materials—A review”, International Journal of Machine Tools & Manufacture, 50, 663-680 (2010).

6분과

방사선환경 및 안전 (Oral)

A Development Strategy for Fully On-line Monitoring of ^{14}C From Releasing Stack in Nuclear Facility

Sang-woo Noh, Joon-seok Lee, Seung-il Kim, Dam-hyang Kim, and Duk-won Kang*
Elim-Global Co. Inc., 767, Sinsu-ro, Suji-gu, Yongin-si, Gyeonggi-do, Republic of Korea
*dukwon.kang@elim-global.com

1. Introduction

The radioactive carbon having a long-term half-life of 5730 years, ^{14}C is a very important nuclide at the disposal site and one of the release monitoring list of nuclear power plants (NPPs). ^{14}C is generated naturally, but ^{14}C as artificial nuclide is mainly caused by the use of nuclear power, such as nuclear tests and the operation of NPPs. ^{14}C is defined and managed by gas or liquid emission standards concerning radiation protection. It is known that the ^{14}C is mainly generated as organic ($^{14}C_nH_m$) and inorganic ($^{14}CO_2$) types depending on the operation and reactor type at nuclear power plants. A relatively large amount of ^{14}C has been emitted from heavy water reactor rather than light water reactor [1].

Table 1. Average amount of radioactive carbon emission by reactor type for the past 3 years

	PHWR [Bq]	PWR [Bq]
2015	0.201	0.095
2016	0.207	0.088
2017	0.200	0.083

The amounts of ^{14}C emissions for reactor types were reviewed by the Korea Hydro & Nuclear Power Co., which was presented in the "Environmental Radiological Survey and Evaluation Report around NPPs", as Table 1 shows.

1.1 Problems

As shown in Fig. 1, most domestic NPPs install and operate the ^{14}C collection equipment in their exhaust stacks, and sampling cycles have been analyzed 1~2 a month during normal operation.

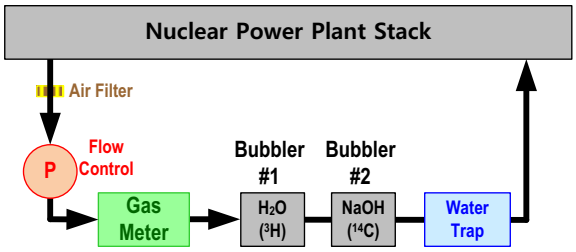

Fig. 1. Conceptual Diagram of Gas Emission Monitoring System from Heavy Water Reactors.

Since the entire process of collection, pre-treatment and analysis for ^{14}C is performed manually by the analyst, the analysis error factors can exist in the replacement of the collected solution, transfer of samples and pre-treatment process. Furthermore, it is difficult to quickly respond to emergency situations in the plant or leakage of local radioactive materials due to the long analysis time and cycle. In addition to $^{14}CO_2$, ^{14}C with $^{14}C_nH_m$ needs

periodic monitoring, but currently only $^{14}CO_2$ types are collected and monitored by operational conditions.

1.2 Objectives

To develop an automated on-line integral processing system to analyze and monitor the chemical type of ^{14}C released from the stacks of NPPs.

2. Monitoring System Strategy

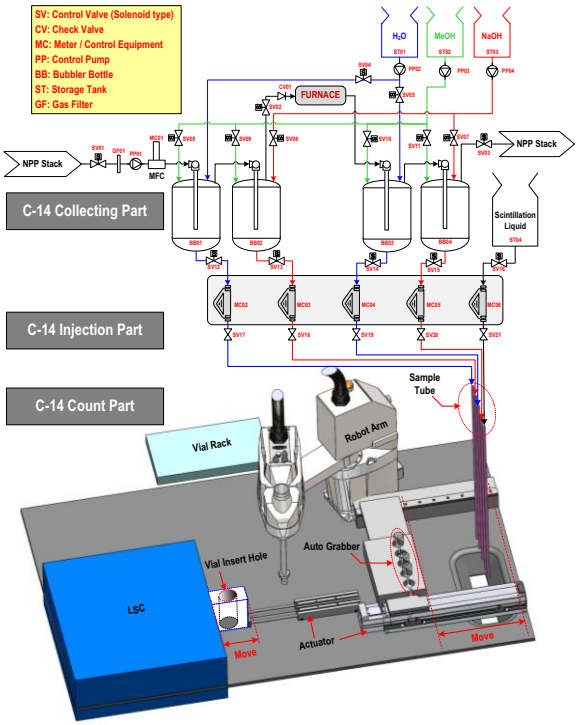

Fig. 2. Schematic Diagram for Automatic On-line Monitoring System for released ^{14}C.

Figure 2 shows the schematic diagram of the fully automated on-line monitor system to be developed in this study. The ^{14}C on-line monitoring system to be developed consists of 4 component technical units. The released gas sample collector will collect directly in a bubbler bottle containing a NaOH solution over a given period, and the organic $^{14}C_nH_m$ is oxidized to $^{14}CO_2$ in the catalytic reactor and collected. The second one is an automatic mixture unit to manufactures cells for analysis by mixing the sample and fluorescence solution. The third is an analysis unit to analyze ^{14}C with liquid scintillation counter (LSC) automatically, and last one is the on-line integral control unit.

3. Conclusion

The radioactive carbon is a very important nuclide at the disposal site and NPPs. However, the inorganic $^{14}CO_2$ types have only been analyzed and monitored. Since monitoring of organic $^{14}C_nH_m$ is important from a disposal perspective, therefore, this study is developing an automated on-line system that can analyze and monitor the organic as well as the inorganic type of ^{14}C simultaneously.

ACKNOWLEDGEMENT

This work was supported by the Korea Institute of Energy Technology Evaluation and Planning (KETEP) granted financial resource from the Ministry of Trade, Industry and Energy, Republic of Korea (No.20181520302310).

REFERENCES

[1] EPRI, “Estimation of Carbon-14 in Nuclear Power Plant Gaseous Effluents”, Technical Report (2010).

Introduction to Boron Removal Technology for LRS of NPP

Seungil Kim*, Woohyeon Lee, Duckwon Kang, Sangwoo Noh, Seongjoo Kang, and Damhyang Kim
Elim-Global Co. Inc., 767, Sinsu-ro, Suji-gu, Yongin-si, Gyeonggi-do, Republic of Korea
*seungil.kim@elim-global.com

1. Introduction

In the pressurized light-water nuclear power plant, boric acid is injected to control the power of the reactor and the boron concentration in RCS is about 2,000 ppm at the beginning of operation and about 10 ppm at the end of life.

The excess reactor coolant generated during operation is collected in the Hold Up Tank and most of boron in the Hold Up Tank were recovered using the Boric Acid Evaporator. But if the water quality does not meet the standard quality, the water transferred to the liquid radwaste treatment system (LRS). In NPP with waste evaporator, the boron (B) injected into the LRS is evaporated and concentrated using a Waste Evaporator and stabilized it with polymer and sent it to the disposal site.

However, at OPR 1000 and APR 1400, which are not equipped with Waste Evaporator, the ion-exchange resin and RO are used to treat the waste water in LRS. But the boron cannot be removed in RO system because boron exists on a molecular form such as boric acid. Currently, there is no release limit for boron concentration in discharge water, but worldwide, the standard for boron concentration in wastewater is strictly limited and managed. Regulations on boron concentration in industrial waste water are expected to be implemented in the future as Japan regulates the concentration of boron to less than 8 ppm and the U.S. regulates the concentration of boron to less than 1 ppm in wastewater.

Therefore, it is necessary to develop facilities that can effectively remove boron before it is discharged into the environment in preparation for the regulation of boron concentration in future discharge water.

In this study, the present situation of domestic light-water nuclear power plants and the boron removal technology applied in overseas nuclear power plants were reviewed to develop technologies for removing boron from LRS and a plan for developing LRS boron removal facilities suitable for domestic conditions was presented.

2. Design Requirement and Overseas Technology for Boron Removing

2.1 Design requirements

The development of boron removal technology from wastewater of nuclear power plant must take into account various conditions such as characteristics of boron to be removed, operation characteristics of nuclear power plant, install-ation space, etc.

Since boron is present as boric acid or borate ion according to pH, pH regulation is essential and the maximum concentration of boron is also considered because of self-polymerization problem. Because nuclear power plants are already design-optimized, additional equipment to be installed for boron removal must be installed and operated independently of existing

facilities, as well as smaller units because of the smaller available space.

Since two monitor tanks of 100 m^3 are currently operated for each unit and are released from each monitor tank for 5 hr (about 20 m^3/hr), sufficient capacity should be available for each to remove boron from LRS effectively.

Because concentrated boric acid water cannot be treated by connecting it to an existing Concentrate Treating System (CTS), separate equipment such as coagulation or sedimentation facilities must be configured to treat concentrated boric acid water generated by the boron removal system.

Boron removal system should be configured to avoid using chemicals or minimize the amount of use, because additional facilities may be required if additional chemicals are used for pH control.

2.2 Boron removal technology in Sweden

Necessity for removing boron (B) from discharged water has been recognized as common in overseas nuclear power plants, and in Sweden, boron contained in the reactor coolant system (RCS) and liquid radwaste treatment system (LRS) is recovered using ELIX (Electrochemical Ion Exchange) to minimize the occurrence of boron waste water. Sweden's ELIX technology is similar to the existing EDI technology, but it uses two ionizing membranes, which are different from the EDI technology that uses more than 50 separate membranes. This technology can selectively remove only boron even during system operation, and it can be applied in a relatively small and modular way to enrich boron up to 80% using electrodes.

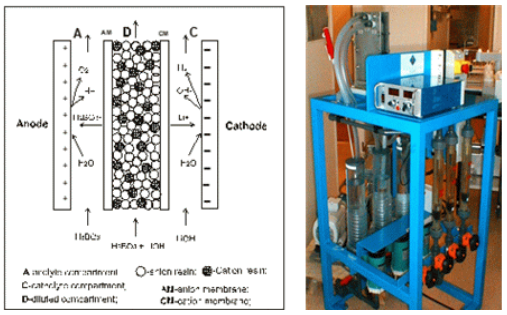

Fig. 1. Schematic diagram of ELIX and lab apparatus.

3. Conclusion

To satisfy the above design requirements and develop boron removal facilities applicable to the actual site, this study aims to develop a "MCDI-ELIX hybrid module" that applies MCDI (Membrane Capacitive Deionization) to the removal of interference ions and ionizing radionuclides and selective removal of boron by applying electrochemical technology.

ACKNOWLEDGEMENT

This work was supported by the Korea Institute of Energy Technology Evaluation and Planning (KETEP) granted financial resource from the Ministry of Trade, Industry and Energy, Republic of Korea (No.20191510301070).

REFERENCES

[1] B. K. Seo, “Decommissioning Experience of Nuclear Research Facilities and Current Status of Decommissioning Core Technology Development”, 2018 NPP Decommissioning Business Forum.

The Determination of Trace U and Th Concentrations in Large Volume Groundwater Sample Using Actinide Resin and Alpha Spectrometry

Yoo Gyum Kang[1,2], Ji-Young Park[1], Hyuncheol Kim[1], Jong-Myoung Lim[1,*], Won Young Kim[1], and Jin-Hong Lee[2]
[1]Korea Atomic Energy Research Institute, 111, Daedeok-daero 989beon-gil, Yuseong-gu, Daejeon, Republic of Korea
[2]Chungnam National University, 99, Daehak-ro, Yuseong-gu, Daejeon, Republic of Korea
*jimlim@kaeri.re.kr

1. Introduction

In this study, the rapid and automatically pre-treatments procedures were developed for large volume ground water sample, which have trace level U and Th- concentrations. Since U and Th are present in very low concentrations in the groundwater, a large amount of samples must be used to satisfy the minimum detectable activity.

The main purpose of this study is to reduce the time spending of pretreatment of large volume water samples and to make the sample a suitable matrix for chemical separation. For those purposes, extraction chromatography(e.g., Actinide resin was used for concentration of target nuclides in large volume ground water sample was used and UTEVA and TEVA resin were used for the sequential purification of U and Th) and automatic nuclide separator were used. Finally, the analytical time and chemical recovery for the ground water samples near the Korea Atomic Energy Research Institute site were presented.

2. Experimental

2.1 Instruments

During the method development and evaluation of performance of the chemical separation and experiment, ICP-MS(ICAP RQ, Thermo Scientific Inc.) was used to measure the chemical recovery and separation and purification capacity of the resin. The activity of U and Th in ground water samples were determined by Alpha spectrometer (Alpha Analyst, CANBERRA).

2.2 Automatic nuclide separator

The nuclide separator(KXT-H, KAERI) was used for automatic sample loading, rinsing, and elution of U and Th of the large volume of ground water samples.

3. Results and discussion

3.1 Performance test of Actinide resin

Actinide resin, which was offered by Eichrom®, have excellent binding ability for the actinide elements such as U, Th, Np, Pu, Am, etc. It is well known that Actinide resin shows uptake capability more than 90% for all actinide elements of bulk water sample [2]. Thus, the separation capacities of U and Th in case of using 10L ground water samples were tested with small amount of resin and KXT-H. The result of performance test reveals that the resin showed uptake capability over than 99% for U and Th for large volume samples. And the effect

of the flow rate in the step of sample loading for the uptake capacity also checked. When 1mL of Actinide resin was used with a 1L sample, breakthrough was not observed for the flow rate of 5, 20, 35, and 50 mL/min.

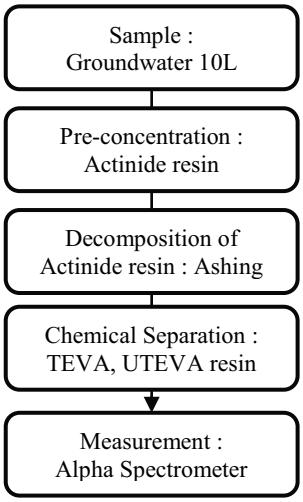

Fig. 1. Analytical procedure for uranium and thorium analysis by using Actinide resin in groundwater.

3.2 Analytical Procedure

The developed analytical procedure of U and Th in large volume of groundwater sample was shown in Figure 1. The groundwater sample was prepared with 2mL of concentrated HCl and filtered to eliminate suspended particulates. Prepared 10L sample was loaded using KXT-H with a flow rate of 50 mL/min. After the 10L sample was passed through the Actinide resin of 5mL, the resin was decomposed in the dry muffle furnace at 600 °C. 4 Hrs was spent in this dry ashing step. After ashing, a black residue was left, and the residue was digested for one hour with refluxed aqua regia. Finally, the samples were prepared with 3M HNO_3 Then, U and Th was separated and purified by UTEVA and TEVA resin, respectively. After chemical separation, the final eluates were electro-deposited and measured by Alpha spectrometer.

4. Conclusion

The traditionally used method of analyzing uranium in large volume of groundwater takes two or three days for pretreatment. However, using the method developed and evaluated from this study could be reduce the time to less than a day. Finally, analytical results used with the methods developed in this study showed the good agreement with those analyzed by conventional methods.

It will be expanded to simultaneously analyze the artificial radionuclides of Np, Pu and Am and to measure the gross alpha activity for monitoring nuclear accidents and nuclear tests.

REFERENCES

[1] J. Lehto and X. Hou, Chemistry and Analysis of Radionuclides, 1-3, WILEY-VCH (2012).

[2] KINS, The Annual Report on the Environmental Radiological Surveillance and Assessment around the Nuclear Facilities, 25, KINS/AR-140 (2018).

Study on the Influence of ^{232}Th Daughter Nuclide in ^{222}Rn Measurement

Giho Kwon, Seungjae Baek, and Hoon Lee*
Korea Institute of Nuclear Safety, 62, Gwahak-ro, Yuseong-gu, Daejeon, Republic of Korea
*lh@kins.re.kr

1. Introduction

Of the annual average natural radiation dose (3.08 mSv / y) in Korea, internal exposure from inhalation of radon gas accounts for about 46% (1.40 mSv / y) [1]. Accordingly, the International Committee on Radiation Protection studied the risk of lung cancer caused by radon and progeny nuclides (ICRP 115) for risk management and optimization of radon risk[2]. Recently, the "Radon bed" using monazite has increased the interest in the internal exposure by radon, which has strengthened the management of radiation exposure of products using natural radionuclide (NORM)[3].

The isotopes of radon are ^{222}Rn (half-life 3.82 d) and ^{220}Rn (half-life 55.6 sec). Radon radioactivity is measured using an "indirect method" of measuring ^{218}Po and ^{216}Po. At this time, interference or summation of energy peaks occurs due to a difference in collapse energy of the nucleus.

Therefore, this study evaluated the effect of ^{232}Th on ^{222}Rn using samples with a radioactivity concentration ratio of about 1 : 10 of ^{238}U and ^{232}Th.

2. Experiment

2.1 Analysis of ^{238}U, ^{232}Th

The sample was melted at 1100 °C. using an automatic melting apparatus (K2PRIME, KATANAX) and then dissolved in 3% HNO_3. After iron precipitation, U and Th precipitated, the supernatant was removed, and the precipitate was dissolved in 3 M HNO_3. [4]. The final dissolved sample is diluted approximately 1,000,000 times, The mass concentration ($\mu g \cdot kg^{-1}$) of ^{238}U and ^{232}Th, measured by ICP-MS (New Agilent ICP-MS 7900, Agilent Technologies), was converted into radiation concentration ($Bq \cdot g^{-1}$).

2.2 Measurement of ^{222}Rn, ^{220}Rn

The sample was placed in the bottom of a 150 mL glass beaker about 5 mm thick and the mouth opening was spaced about 5 mm vertically. Inflowing gas was maintained at a temperature of (21.2 ± 0.3) °C. and a humidity of (4 ± 1) % at a flow rate of 0.5 $L \cdot min^{-1}$.

RAD7 (RAD7-716, DURRIDGE) was used to measure radioactivity once per hour, for a total of 100 times (100 hours). In order to minimize the amount of radon gas released to the outside, the top of the beaker was sealed with a funnel as much as possible, and a dust filter was connected to the gas inlet to prevent direct inflow of solid phase samples.

3. Result and discussion

The samples used in this study were analyzed with ^{238}U (29.4 ± 0.6) $Bq \cdot g^{-1}$ and ^{232}Th (287 ± 5) $Bq \cdot g^{-1}$. Since ^{232}Th is about 10 times higher than ^{238}U, it was judged as a sample capable of confirming the effect of ^{232}Th on ^{222}Rn.

The resolution of RAD-7 used for ^{222}Rn radioactivity measurement is about 0.5 MeV, and the energy in the (5.4 ~ 6.4) MeV region is summed and counted as shown in Fig. 1. Thus, the ^{222}Rn nuclide, ^{222}Po(6.00 MeV, 3.05 min), is affected by ^{212}Bi(6.05 MeV, 60.6 min) and ^{216}Po(6.78 MeV, 0.15 sec), ^{232}Th with similar energy.

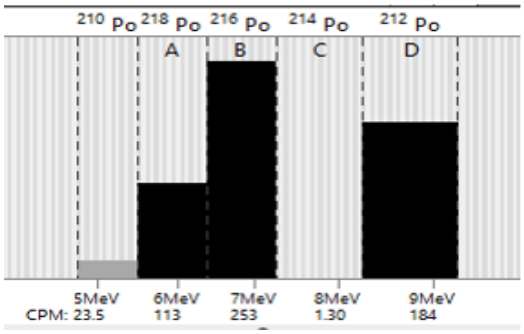

Fig. 1. Energy spectrum of RAD-7.

The effect that ^{218}Po and ^{212}Bi add up is called the branch effect. ^{212}Bi produces ^{212}Po(8.78 MeV, 0.3 μsec) with β-decay(64.1 %) and ^{208}T1(6.05 MeV, 3 min) with α-decay(35.9 %). Therefore, the measured ^{212}Po radioactivity can be used to calculate the effect of ^{212}Bi.

For high ^{232}Th samples, tailing of the ^{218}Po peak occurs and is added to ^{216}Po. This is called the tailing effect. The effect is presented at about 2.5% [5]. Therefore, the net coefficient value of ^{218}Po considering the branch effect and tailing effect can be expressed by the following equation.

$$[Count_{Po-218}] = Count_A - B_{Bi} \cdot Count_D - Count_B \cdot f_{tail} = Count_A - \frac{36}{64} \cdot Count_D - Count_B \cdot 0.025 \quad (1)$$

Figure 2 is a graph showing the concentration of 222Rn in the sample, 1) no correction values, 2) the branch factor correction concentration, and 3) the simultaneous correction of the branch factor and tailing factor.

Branching effects are similar to log graphs. This was judged by the radioactive equilibrium of the decay series from ^{232}Th to ^{212}Bi. The tailing effect is calibrated approximately 2.5% of the ^{218}Po count, regardless of time.

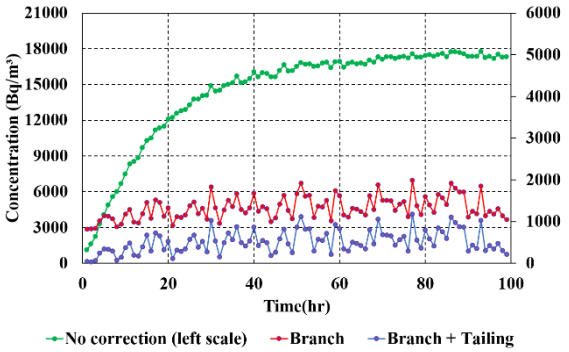

Fig. 2. Change in ^{222}Rn concentration due to correction.

The ratio of counts in the (5.4 ~ 6.4) MeV region over time is shown in Figure 3.

By the 2nd (2hr) measurement, the tailing effect was greater than the branch effect. After 10nd (10hr) measurements, tailing effect was 2.5% and the branch effect was about 90%.

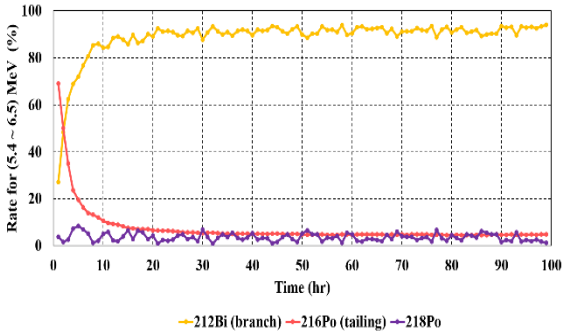

Fig. 3. Fraction of ^{212}Bi and ^{216}Po.

4. Conclusion

In this study, we measured ^{218}Po of the ^{238}U (29.4 ± 0.6) Bq·g^{-1}, ^{232}Th (287 ± 5) Bq·g^{-1} sample to evaluate the effect of ^{232}Th on ^{222}Rn. For samples with ^{232}Th approximately 10 times higher than ^{238}U, it was estimated that the branch effect by ^{212}Bi was about 90% and the tailing effect by ^{216}Po was about 2.5% for the measurement of ^{218}Po.

REFERENCES

[1] Korea Institute of Nuclear Safety, “Radiation Environment of Korea”, KINS/GR-365 (2009).

[2] M. Tirmarch, J.K. Harrison, at al., ICRP, “Lung Cancer Risk from Radon and Prgeny”, ICRP-115 (2011).

[3] Korea Nuclear Safety and Security Commission, “Strengthen the safety for using NORM product” (2018).

[4] Korea Institute of Nuclear Safety, “Development of Analytical Procedures and Method Validation for the Quantification of Nactural Radionuclides in Raw Materials or By-products”, KINS/HR-1382 (2015). KINS/GR-365 (2009).

[5] “RAD7 Manual”, DURRIDGE (2019).

Development and Performance of Environmental Radiation Monitoring System Based on Diverse Survey Platforms

Young-Yong Ji[1,*], Mee Jang[1], Taehyung Lim[2], Kun Ho Chung[1], and Mun Ja Kang[1]
[1]Korea Atomic Energy Research Institute, 111, Daedeok-daero 989beon-gil, Yuseong-gu, Daejeon, Republic of Korea
[2]SI Detection Co. Ltd., 21, Yuseong-daero 1628beon-gil, Yuseong-gu, Daejeon, Republic of Korea
[*]yyji@kaeri.re.kr

1. Introduction

With respect to the nuclear accident response, the purpose of environmental radiation survey technology is to develop the reliable procedure and method in the comprehensive radiation survey. The development of survey technology and its field applications are very important things to build the accurate data for decision making. The mapping project [1-3] of JAEA has been conducting to make contamination maps around the Fukushima Daiichi nuclear power plants (FDNPP) using diverse survey platforms, such as a tripod, backpack, carborne, and airborne unit.

The ground-based gamma-ray spectrometry using a tripod is widely used to estimate the radioactive deposition in the emergency response. In addition, the mobile gamma-ray spectrometry using a backpack or carborne unit is a useful survey platform to rapidly identify the radionuclide distribution in the wide area. The airborne gamma-ray spectrometry using manned or unmanned aerial vehicle can be an important option in the early phase of the nuclear accident and at the difficult area to be accessed.

In the research project about the comprehensive radiation survey in the environment, the MARK (Monitoring of Ambient Radiation of KAERI) system has been developing for the purpose of rapid and accurate assessment of radioactive deposition. Since this system consists of diverse survey platforms, the method development was conducted to support the data consistency in all survey results, which means results at 1 m above the ground in the air. Finally, the developed MARK system was experimentally verified in the field measurement.

2. Method and Results

2.1 Backpack survey platform

Figure 1 shows the developed MARK-B series representing backpack survey, which are divided into two kinds of detectors, such as 3”x3”NaI(Tl) and 2”x2”$LaBr_3$(Ce) detector. This system can be applied to the ground-based gamma-ray spectrometry using a tripod and mobile survey using a backpack platform. In the case of mobile gamma-ray spectrometry, measured energy spectra with a short acquisition time are linked with GPS (global positioning system) data and transferred to a PC using the Bluetooth interface. Figure 2 shows the application of MARK-B series to the contaminated area around the Fukushima Daiichi nuclear power plants (FDNPP). The dose rate of ^{134}Cs and ^{137}Cs was estimated around the survey site and the dose rate map was successfully built according to the Kriging interpolation method.

Fig. 1. MARK-B series using backpack survey platform.

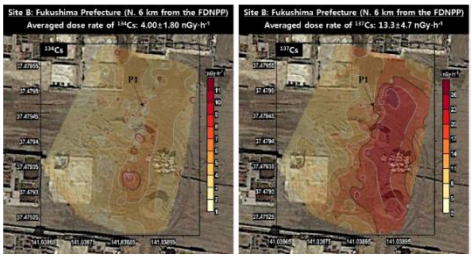

Fig. 2. The application of MARK-B series to the contaminated area around the FDNPP.

2.2 Carborne survey platform

The MARK-C is of carborne survey based on a large NaI(Tl) detector, as shown in Fig. 3. To assess the dose rate at 1 m above the ground in the air, the attenuation factor due to loading in a car was applied to all carborne survey results. This system was applied to make a baseline of dose rate around the construction site of a research reactor in Busan, before its operation.

Fig. 3. MARK-C using carborne survey platform.

2.3 Multipurpose survey platform

A multipurpose survey platform, which is called as MARK-M, was developed to apply to diverse survey platforms with one survey system, such as a tripod, backpack, carborne, and airborne unit. The purpose of MARK-M is to efficiently collect a number of survey results with the data consistency in the nuclear emergency response. This system is based on two 2"x2"$LaBr_3$(Ce) detectors to enhance the counting efficiency in the field measurement. The performance was successfully conducted by using four kinds of survey platforms in the same site.

Fig. 4. MARK-M for multipurpose applications.

3. Conclusion

The MARK system for the environmental radiation survey has been continuously developed in the diverse platforms. In addition to the hardware development, the algorithm was achieved to accurately and simultaneously assess the radioactivity and dose rate due to the radioactive deposition using MARK system. The experimental verification was conducted by comparing survey results of natural radionuclides with different platforms in the same site. Finally, for its availability in contaminated areas, the MARK system has been applied to the assessment of radioactive cesium deposition with high dose rate level around the FDNPP.

ACKNOWLEDGMENTS

This work was performed under the auspices of the Ministry of Science and ICT of Korea, NRF contract No. NRF-2017M2A8A4015256.

REFERENCES

[1] S. Mikami et al., "The air dose rate around the Fukushima Dai-ici Nuclear Power Plant: its spatial characteristics and temporal changes until December 2012", J. Environ. Radioact. 139: 250-259 (2012).

[2] S. Mikami et al., "In situ gamma spectrometry intercomparison in Fukushima, Japan", Jpn. J. Health Phys. 50(3): 182-188 (2015).

[3] S. Tsuda et al., "Characteristics and verification of a car-borne survey system for dose rate in air: KURAMA-II", J. Environ. Radioact. 139: 260-265 (2015).

Worker Dose Assessment of Continuous Radioactive Waste Treatment System

Hyun Sik Kang*, Kyoungyong Noh, Misuk Jang, and Seoung Rae Kim
Nuclear Engineering Services & Solutions, 756-27, Daedeok-daero, Yuseong-gu, Daejeon, Republic of Korea
*nessrnd@ness.re.kr

1. Introduction

The exposure dose of system operator is one of the key factors to be considered in designing the radioactive waste treatment system. In shielding analysis, the self-shielding effects of equipment and storage box in the workspace are generally ignored and evaluated for conservative evaluation.

The NESS is under developing the unmanned continuous treatment system that makes spent resin solidification and treats it safely. A conceptual drawing of the continuous radioactive waste treatment system is shown in Figure 1. As shown Figure 1, the operator works and manages the system in the operating room next to the treatment system room, and between the two rooms are shielded. To determine the shielding wall thickness, the operator dose in the operating room was evaluated using MCNP5.0 code in this paper.

2. Method and Results

2.1 Dose criteria

The International Commission on Radiological Protection (ICRP) recommends the maximum allowable annual doses for radiation workers and the public as follows[1]:

- Radiation Worker: 100 mSv for 5 years without exceeding 50 mSv per year
- Public: 1 mSv per year

2.2 Evaluation code

MCNP is well-known Monte Carlo codes for criticality analysis and a general-purpose Monte Carlo N-Particle code that can be used for neutron, photon, electron or coupled neutron / photon / electron transport, including the capability to calculate eigenvalues for critical systems[2].

2.3 Assumptions

The dimension of the continuous radioactive waste treatment system assumes 6.5m (w) * 1.8m (l) * 3m (h) and one treatment capacity is 10 kg. But the system capacity is conservatively assumed 100 kg. Fig. 1 shows the modelling schematic diagram of the system.

The accident is assumed that all 100 kg spent resins had been spilled and spread across the container floor. The actual spent resins are mostly consists of water, but is conservatively treated as air. The spent resins are assumed and loaded on the system with 5% Co-60, 10% Cs-137 and 85% air.

The specific radioactivity of Co-60 and Cs-137 are to be evaluated by changing from the self-disposable allowance to the low level waste limit (see Table 1). The self-disposable concentration of the two elements (Co-60 and Cs-137) is 0.1 Bq/g. In low-level wastes, the specific radioactivity of Co-60 is 3.70E+07 Bq/g and the specific radioactivity of Cs-137 is 1.11E+06 Bq/g. The total radioactivity of spent resins, 100kg is estimated as the maximum 1.96E+05 MBq.

The working time is assumed as 2,704 hours per year. The worker dose is assessed by arbitrarily increasing the shielding wall thickness. The selected shielding material is lead to compact and minimize the size of system.

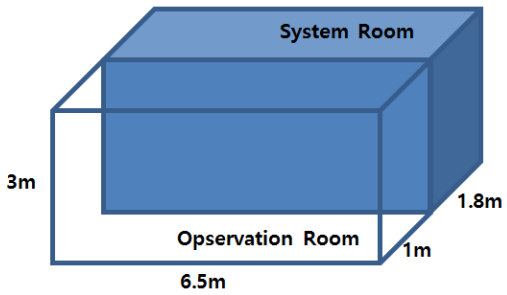

Fig. 1. Modeling schematic diagram.

Table 1. Specific radioactivity of Co-60 and Cs-137

Classification		Specific radioactivity (Bq/g)
The self-disposable concentration		1.00E-01
Maximum level of ultra low level waste		1.00E+01
Maximum level of low level waste	Co-60	3.70E+07
	Cs-137	1.11E+06

2.4 Result

The evaluation results without considering shielding shown in Table 2. The evaluation results showed that the worker's exposure dose was 1.98E-03 mSv/yr at the highest concentration level of the ultra low level waste, which satisfies the maximum allowable annual dose. However, at the highest concentrations of low-level wastes, the maximum allowable annual dose is 2.58E+03 mSv/yr, which does not satisfy the criterion.

The evaluation results with considering Pb shielding are shown in Table 3 and Fig. 2, respectively. To meet the criteria, the shielding thickness should be at least 5 cm. The worker dose was calculated 30.6 mSv/yr for 5 cm thickness. If the shielding wall thickness is 6 cm or more, the worker dose is 15.8 mSv/yr and it meets the maximum allowable annual doses for radiation workers of 20 mSv/yr, which is the average of 100 mSv for 5 years.

Table 2. Evaluation results without shielding material

Classification	Annual dose (mSv/yr)
The self-disposable concentration	1.99E-05
Maximum level of ultra low level waste	1.98E-03
Maximum level of low level waste	2.58E+03

Table 3. Evaluation results with shielding material (Pb)

Distance (cm)	Annual dose (mSv/yr)
1	7.22E+02
2	2.93E+02
3	1.36E+02
4	6.28E+01
5	3.06E+01
6	1.58E+01
7	7.53E+00
8	3.71E+00
9	2.14E+00
10	1.17E+00

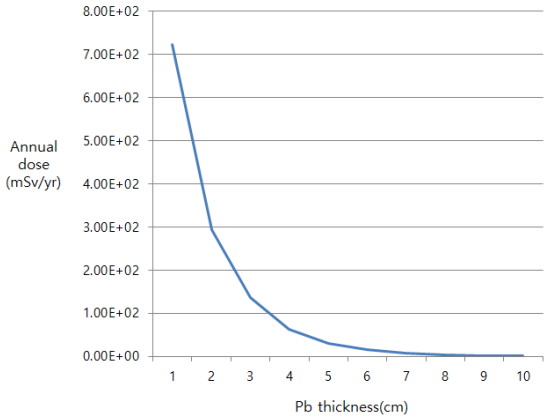

Fig. 2. Evaluation results with considering shielding.

3. Conclusions

In this paper, we presented that the work doses are evaluated in the continuous radioactive waste treatment system of various types and concentrations. The thickness of shielding wall thickness was estimated to be more t 6 cm.

In the future, we will determine the shielding wall thickness of system based on the exact characteristics of the spent resins.

ACKNOWLEDGEMENTS

This work was supported by the Korea Institute of Energy Technology Evaluation and Planning (KETEP) and the Ministry of Trade, Industry & Energy (MOTIE) of the Republic of Korea (No. 20171520000410).

REFERENCES

[1] IAEA, "1990 Recommendations of the International Commission on Radiological Protection" ICRP Publication 60.1991.

[2] X-5 Monte Carlo Team, LA-UR-03-1987/ LA-CP-03-0245, A general Monte Carlo N-Particle Transport Code, Version 5, Los Alamos National Laboratory, 2008.

6분과

방사선환경 및 안전 (Poster)

Measuring the Position of Gamma Emitting Radioactive Isotopes Using One-Dimensional Inorganic Scintillator Array Sensor

Si Won Song, JinHong Kim, Hyun Young Shin, and Bongsoo Lee*

Chung-Ang University, 84, Heukseok-ro, Dongjak-gu, Seoul, Republic of Korea

*bslee@cau.ac.kr

1. Introduction

Estimation of radionuclide inventory in radwaste drums by radiochemical analysis needs high cost and time consuming. In addition, due to the exposure risk of operators, it is difficult to measure the radionuclide concentration in all drums using a radiochemical analysis. Most of the radionuclides in the drum emit radiations that cannot be measured by non-destructive assay due to the penetration lengths of alpha and beta particles. In order to solve this problem, the scaling factor method is generally used [1].

In this study, we fabricated a one-dimensional scintillator array sensor system for position estimation of a gamma ray source.

2. Material and Methods

One dimensional scintillator array sensor system consists of inorganic scintillators, plastic optical fibers, and photon counting heads (H11890-210, Hamamatsu Photonics). LYSO:Ce (cerium doped lutetium yttrium silicate) inorganic scintillators are arranged in a linear array which is used as a sensing part. Each inorganic scintillator is in the shape of a rectangular parallelepiped whose size is 1.5 × 1.5 × 15 mm^3. They are covered by the aluminum tape to block the outside lights, and each scintillator is separated using a 0.5 mm thick lead plate [2]. To evaluate the performance of a one-dimensional scintillator array sensor system, a Co- 60 is used as a gamma-ray source.

Table 1. Physical properties of LYSO:Ce inorganic scintillator

	LYSO:Ce
Density [g/cm^3]	7.1
Wavelength of emission max [nm]	420
Light yield [photons/keV]	30
Decay time [ns]	41
Hygroscopic	No

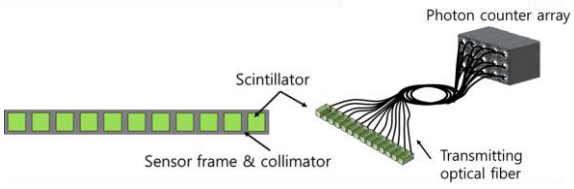

Fig. 1. Schematic diagram of one-dimensional scintillator array sensor.

Figure 1 shows a schematic diagram of one-dimensional scintillator array sensor. The scintillation signals generated from the inorganic scintillators are guided through the 1 m step index plastic optical fibers and are measured using photon counting heads. The Peak sensitivity wavelength of photon counting head is about, 400 nm and measurable wavelengths are from 230 nm to 700 nm.

3. Results

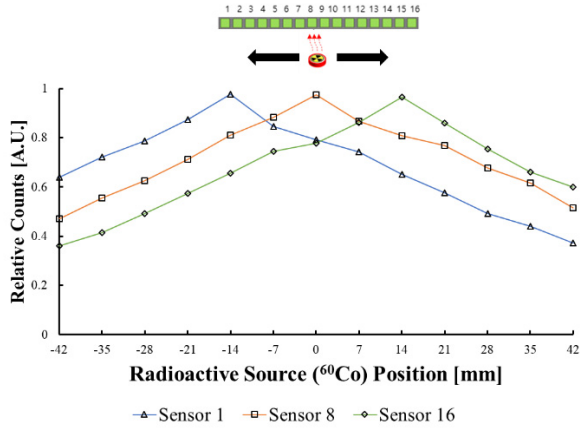

Fig. 2. Measurements of one-dimensional gamma ray distributions according to the position of radioactive source.

Figure 2 shows the measurements of one-dimensional gamma ray distributions using an inorganic scintillator array sensor according to the position of radioactive source. Co-60 source was moved horizontally by 7.0 mm from the center to the both ends of the array sensor. The measured values are reasonably acceptable without cross-talk for each sensor 1, 8 and 16 as shown in Figure 2.

This sensor system provides the highest counting value for each scintillator when the gamma ray source is aligned with the position of each scintillator.

4. Conclusion

In this study, one-dimensional fiber-optic radiation array sensor was fabricated using LYSO:Ce inorganic scintillators, plastic optical fibers, and a photon counting heads for real-time monitoring of low and intermediate level waste (LILW). We measured one-dimensional gamma-ray distributions with a Co-60 radioactive source according to its position, which is representative key nuclei contained in the LILW. It is expected that a one-dimensional scintillator array sensor system fabricated in this study can be used to find the positions of nuclear species in the LILW in real-time.

Acknowledgement

This research has supported by the National Research Foundation of Korea (NRF) grant funded by the Korea government (MSIT) (No. 2017R1A2B2009480, 2016M2B2B1945255).

REFERENCES

[1] K.W. Ji, et al., “A Strategy on the Disposal of Below Intermediate Level Radwaste”, KAERI Research Report, KAERI/RR-4041/2015 (2015).

[2] C. Domingo-Pardo, et al., “A Position Sensitive Gamma-Ray Scintillator Detector With Enhanced Spatial Resolution, Linearity, and Field of View”, IEEE Transactions on Medical Imaging, 28(12), 2007-2017 (2009).

Transfer Factors of ^{99}Tc Measured for Korean Staple Food Crops and Proposal on Their Usage

Yong-Ho Choi*, Kwang-Muk Lim, In-Jun, Dong-Kwon Keum, and Hyo-Joon Jeong
Korea Atomic Energy Research Institute, 111, Daedeok-daero 989beon-gil, Yuseong-gu, Daejeon, Republic of Korea
*yhchoi1@kaeri.re.kr

1. Introduction

The transfer factor (TF), which is defined as the ratio of the activity concentration in plant to that in associated soil, is a widely used model parameter for food-chain dose assessment.

Long-lived radionuclides such as ^{99}Tc may reach arable land following their release from an underground repository a long time after its closure. Arable land is usually plowed before planting. TFs are to be applied to a uniform soil concentration assumed to be created by plowing.

TF values of ^{99}Tc were measured for four major Korean food crops in different soils collected around a nuclear site in Gyeongju. The results, having been published elsewhere [1-3], are collated and combined with relevant IAEA data [4] in such a manner as to produce more generic TF values.

2. Domestic Data on ^{99}Tc TF

2.1 Methods of TF measurements

Amounts of the soils necessary to form the whole or upper about 20 cm soil layers in pots or lysimeters were thoroughly mixed with ^{99}Tc solutions using a mixing machine. Around 25 d after the labelling, rice seedlings were transplanted to the lysimeters and seeds of soybean, radish and Chinese cabbage were sown in the pots. The lysimeters and pots were placed in a greenhouse and plants were harvested at edible maturity. The plant ^{99}Tc concentrations were measured using a betta-counting method.

TF values were calculated as follows;

$$TF=\frac{\text{Plant concentration (Bq kg}^{-1}\text{-dry)}}{\text{Soil concentration (Bq kg}^{-1}\text{-dry)}} \quad (1)$$

In Equation (1), ‘soil concentration’ was the concentration at the start of plant growth estimated from the source activity (Type 1 TF), or the average of two concentrations – the above-mentioned concentration and the concentration measured at harvest (Type 2 TF).

2.2 Type 1 TF data

Table 1 shows Type 1 ^{99}Tc TF data for dried edible parts of the harvested plants – brown rice, soybean seed, radish root, and Chinese cabbage leaf. TF values are often based on at-harvest soil concentrations. Most radionuclides in soil are very low in mobility and phyto-availability. Therefore, it usually makes no significant difference whether a starting or at-harvest soil concentration is used. However, this is not the case with ^{99}Tc TF values for upland crops [3,4].

The mobility of ^{99}Tc in upland soil, where ^{99}Tc mostly exists in an oxidized form of $^{99}TcO_4^-$, is generally so high that the at-harvest soil concentration is usually much lower than the starting one [3]. This difference can lead to a

serious overestimation if a ^{99}Tc TF value derived from an at-harvest soil concentration is applied to an estimate of the starting soil concentration [4].

Table 1. Type 1 TF data for staple food crops

Crop plant	No of soils	Transfer factor (dimensionless)			
		Min.	Max.	GM	GSD
Rice	4	5.4E-04	2.5E-03	1.1E-03	1.92
Soybean	2	1.6E-01	2.0E-01	1.8E-01	1.20
Radish	2	1.1E+01	1.3E+01	1.2E+01	1.17
Ch.cabb.	2	1.2E+02	1.4E+02	1.3E+02	1.07

GM : Geometric mean, GSD: Geometric standard deviation.

2.3 Type 2 TF data

Being concerned about the possibility of the above-mentioned overestimation, the IAEA [4] chose to use Type 2 TF values for ^{99}Tc. Table 2 summarizes the Type 2 TF values measured for soybean in the same pots as for Table 1 [3].

The Type 2 TF values are about 30% higher than the corresponding values given in Table 1. Even in radish and Chinese cabbage, Type 2 TF values, if measured, would be somewhat higher than the Type 1 TF values.

Table 2. Type 2 TF data for soybean

No of soil	Transfer factor (dimensionless)				
	Min.	Max.	AM	GM	GSD
2	2.2E-01	2.7E-01	2.5E-01	2.4E-01	1.16

3. Usage of the ^{99}Tc TF Data

The most appropriate way of using TF data might be to apply Type 1 values to estimates of the starting soil concentrations. This usage is particularly important for a highly mobile radionuclide such as ^{99}Tc. During the growing period, significant changes can occur in both the soil concentration and activity distribution of ^{99}Tc. Therefore, the assumption of the uniformity in the activity distribution within a plowing depth is good only for a short time after plowing. In addition, the average concentration is more difficult to estimate than the starting one.

Proposed generic TF values of ^{99}Tc for a temporary domestic use are presented in Table 3. The radish and Chinese cabbage values are combinations of the TF values in Table 1 and the IAEA-based values, which were acquired by dividing the relevant TRS-472 values [4] by 1.3. For fresh vegetables, some conversions should be made using fresh-to-dry weight ratios.

Table 3. Proposed TF values of ^{99}Tc for major plant groups

Value	Rice	Legume	Root v.	Leafy v.
GM	1.1E-03	1.8E-01	2.0E+01	1.6E+02
GSD	1.92	3.20	2.52	7.29

4. Conclusion

^{99}Tc TF values for a temporary domestic use have been proposed for four major groups of food crops.

REFERENCES

[1] Y.H. Choi, K.M. Lim, I. Jun, D.K. Keum, et al., J. of the Korean Radioactive Waste Society, 8(4), 329-337 (2010).

[2] Y.H. Choi, K.M. Lim, et al., J. of Radiation Protection, 36(4), 209-215 (2011).

[3] Y.H. Choi, et al., J. of Environmental Radioactivity, 132(2014), 57-64 (2014).

[4] IAEA, TRS-472, IAEA, Vienna (2010).

Radiation Protection System in PRIDE Facility

Seonho Noh*, Youngwoo Kwon, Youngkuk Jang, Hee-seok Kang, and Il je Cho
Korea Atomic Energy Research Institute, 111, Daedeok-daero 989beon-gil, Yuseong-gu, Daejeon, Republic of Korea
*nohsh@kaeri.re.kr

1. Introduction

There is a facility named PRIDE in KAERI for developing Pyroprocessing technology. In PRIDE depleted Uranium feed material and a depleted Uranium mixed with some surrogate material are used for performing engineering scale Pyroprocessing.

Therefore the facility is using uranium, users should be careful of radiation in order to conduct an experiment in PRIDE. This paper will explain the radiation protection of the PRIDE facility.

2. Methods and Results

2.1 RMS Detector Model

The RMS(Radiation Monitoring System) detectors are made by CANBERRA and the model names are ICAM and G64. ICAM RMS is the detector which can detect alpha Radiation by absorbing the air in the facility. G64 RMS is the detector which can detect gamma radiation by the gamma probe. These RMS detectors are installed in several spots to detect radiation leakage and radiation background for the safety of users. Fig 1 is the ICAM RMS and G64 RMS appearance. ICAM RMS has one pump and a filter to test the contamination. G64 RMS has just one probe to detect the gamma radiation.

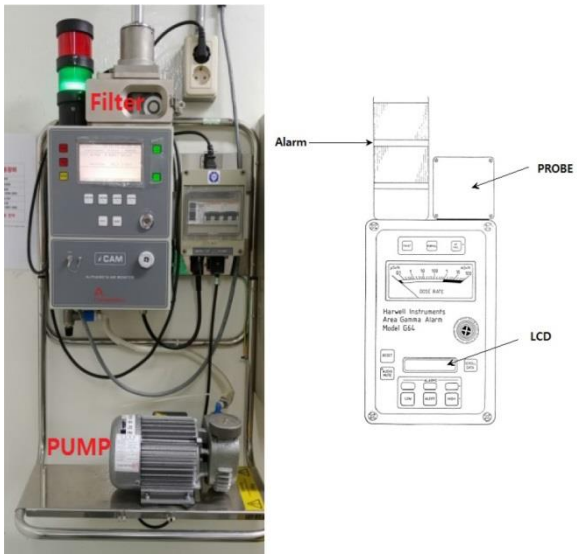

Fig. 1. ICAM (left), G64 (right) RMS.

2.2 Installation location

The RMS(Radiation Monitoring System) detectors are installed in several places for the safety of the users. Two ICAM RMSs and four G64 RMS had been installed in the facility. One G64 RMS on the first floor, three G64 and one ICAM on the Second floor. There is one ICAM RMS on the Third floor for detecting gamma radiation in the air conditioning pipe. Fig 2 is the installation schematic of RMS in PRIDE.

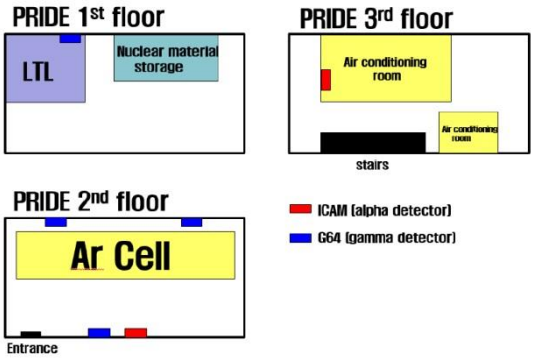

Fig. 2. Installation schematic of RMS.

2.3 Radiation Monitoring

All of the RMSs are connected to the main server to notify the manager about the radiation dose rate. The RMS server room is on the second floor and outside of the radiation zone in PRIDE. Fig 3 is the location of the RMS server room. The yellow place is the radiation zone in PRIDE.

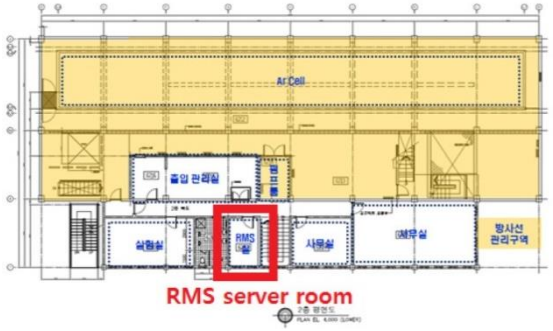

Fig. 3. Location of the RMS server room.

In the RMS server room, the manager of the facility can always check the dose rate of the facility. Also if the dose rate goes higher than the normal range, alarm goes off so the staff who is working at the side office can be notified. Fig 4 is the RMS server program screen.

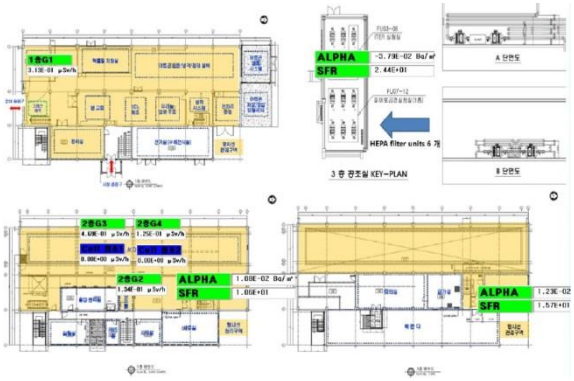

Fig. 4. RMS server program screen.

3. Conclusions

Every place that uses nuclear material directly or areas of concern for radiation exposure are always monitored by the RMS. Where RMS is not installed we use the portable radiation detector when the nuclear material is moved or used. As you can see in this paper, PRIDE is a well-monitored facility for radiation protection.

REFERENCES

[1] ANL-7959 Hot Fuel Examination Facility /North Facility Safety Report, February 1975, Argonne National Laboratory pp. 42-53.

[2] The EBR-II Fuel Cycle Story, Charles E. Stevenson, American Nuclear Society pp. 16-25.

Construction of Pretreatment and Detection System for Tritium and Gross Beta in Water Sample Around the Nuclear Facility

UkJae Lee* and Hee Reyoung Kim
Ulsan National Institute of Science and Technology, 50, UNIST-gil, Eonyang-eup, Ulju-gun, Ulsan, Republic of Korea
*dldnrwp@unist.ac.kr

1. Introduction

It is essential to secure radiation safety around nuclear facilities. In particular, water samples contain various radionuclides, including tritium. Groundwater around nuclear facilities contains various components such as debris, suspended solids, organic matter, heavy metals, microorganisms and ionic substances. In order to monitor the radionuclides in the water sample, a pretreatment method and a monitoring system are established. The tritium is separated through physical pretreatment using various filters and the detection system is adjusted to increase the detection efficiency.

2. Methods

2.1 Detection system

In order to increase the detection efficiency of the system and to reduce the background, the coincidence circuit is used [1]. The coincidence circuit defines the detection value as only pulses that have entered two input terminals within a given time as count values. This method sets the range of pulse magnitudes to screen out the specific nuclide, and excludes anything else by the recoupling counting technique, and then obtains the final count. The schematic diagram of the constructed coincidence circuit is shown in figure 1.

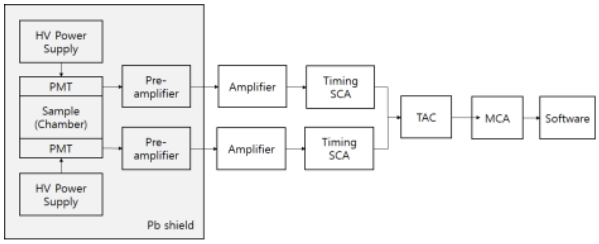

Fig. 1. The schematic diagram of the constructed coincidence circuit.

2.2 Main principle

In consideration of the extremely low energy tritium, the amplification of the amplifier is increased to secure a stable detection. For detection of gross beta, an appropriate amplification level is applied because of background increasement. In order to separate tritium from other nuclides, a pretreatment apparatus for producing pure water was applied.

2.3 Pretreatment system

A pretreatment system was designed to remove various substances such as organic matters, metal ion and floating things in the water sample. For gross beta measurement, a pretreatment procedure was applied to remove only suspended matter by applying a membrane filter which has pore size as 0.45 μm (Hydrophilic Polytetrafluoroethylene, LK LAB

Korea Inc.) [2]. In order to remove all materials and prepare pure water for tritium measurement, a pretreatment apparatus using a membrane and an ion-exchange resin was applied. The schematic diagram of the constructed pure water generating system are shown in the figure 2. The ^{90}Sr and ^{3}H sources were used for the actual measurements. The radioactivity concentration of ^{90}Sr and ^{3}H is 12.58 and 1.193E+06 Bq/L respectively.

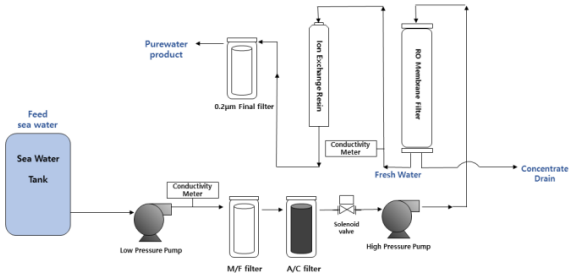

Fig. 2. The schematic diagram of the constructed pure water generating system.

3. Results and Discussions

3.1 Detection result

Table 1 shows detection results for ^{90}Sr and ^{3}H with carious amplification of coarse gain. The gain 40 was chosen for ^{90}Sr. This is because the measured value increased as the gain reached 100, but the background value also increased significantly. In case of tritium, a gain of 100 was chosen because as the gain increased, the measured value by the source increased significantly compared to the increased amount of background. The absolute detection efficiency of ^{90}Sr for coarse gain 40 and ^{3}H for coarse gain 100 is 38.73 % and 7.137E-03 % respectively.

Table 1. Detection results for ^{90}Sr and ^{3}H with carious amplification of coarse gain.

Coarse	10.00	20.00	40.00	100.00
BKG (cps)				
AVG	20.22	20.79	21.86	31.13
^{3}H (cps)				
AVG	19.87	21.02	30.56	67.22
^{90}Sr (cps)				
AVG	21.27	22.08	23.93	46.19

4. Conclusions

Pretreatment and measurement systems have been established to detect beta-nuclides including tritium in water samples. A simple physical pretreatment method was used to analyze tritium separation and adjustment of the setting of a measurement system to detect low energy beta rays. This system can be applied to radiation monitoring for water sample around nuclear facilities.

REFERENCES

[1] Lee, UkJae, et al. "In situ beta radiation monitoring system with enhanced efficiency for water samples from decommissioned nuclear environment." Review of Scientific Instruments 90.2 (2019): 025103.

[2] Korea Institute of Nuclear Safety, The Annual Report on the Environmental Radiological Surveillance and Assessment around the Nuclear Facilities, 2014.

3D Modeling of Hot Cell and Associated Utility Facility for Advanced Safety Analysis

Seungnam Yu* and Seokjun Seo
Korea Atomic Energy Research Institute, 111, Daedeok-daero 989beon-gil, Yuseong-gu, Daejeon, Republic of Korea
*snyu@kaeri.re.kr

1. Introduction

Hot cells located in KAERI are experimental facilities for the study of various kinds of radioactive materials. These facilities have confined area for experiment and operation area for the remote handling of experimental materials by workers and service area for maintenance as well. Generally, this kind of facility had been designed and managed by 2D-based CAD drawings. However, performance-based hazard analysis such as FDS (Fire Dynamics Simulation) for the building has recently become important issue for the safety of the facility and 3D modeling of the target building beyond the 2D drawing is considered as important process. Moreover, 3D modeling work has become easier by using up-to-date simulation software. This study introduces the recent activity for the 3D modeling of hot cell facility in KAERI and tried to propose the various application using it.

2. 3D modeling of Hot Cell Facility

2.1 ACPF (Advanced spent fuel Conditioning Process Facility)

Fig. 1 shows the progress of 3D modeling works for the target facility, 'ACPF' in KAERI. Most challenging issue in this work was the construction of 3D model of duct lines because the quality of the 3D modeling of duct line could make difference for the quality of the model of target facility while performing the various kinds of simulations to analyze the fire control and smoke dissipation in the target facility. Using this 3D model, investigations of pedestrian egress and congestion in emergency are also available for fire protection and safety planning [1].

2.2 DFDF (DUPIC Fuel Development Facility)

Fig. 2 show the 3D modeling of DFDF located in IMEF in KAERI. The modeling works had performed by SketchUp SW [2] based on the drawings of original planning of IMEF. This 3D model can be utilized for the various simulations, such as VR touring and fire hazard simulations and so on.

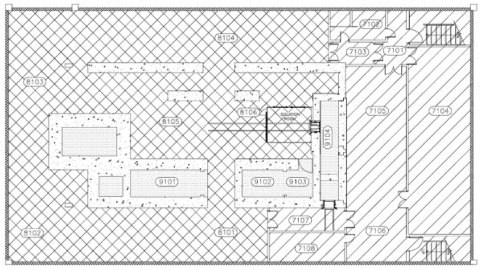

(a) Original planning of the basement of IMEF

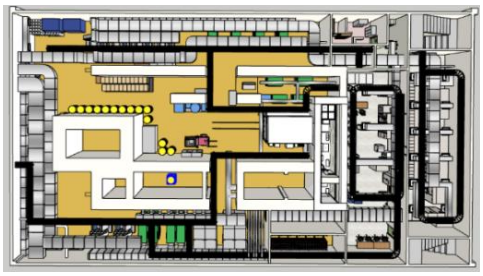

(b) 3D modeling based on the original 2D planning

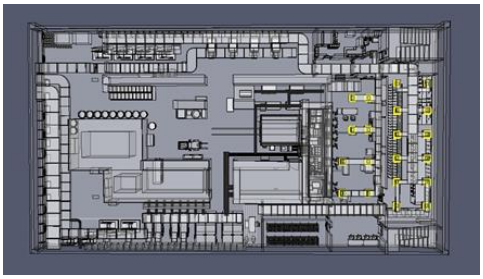

(c) Detail works for air circulation system

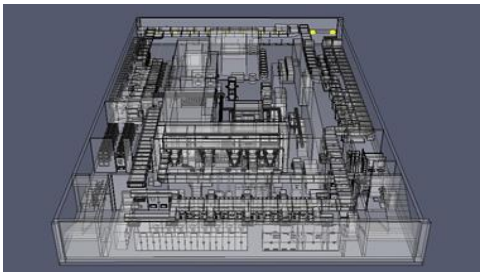

(d) Final 3D model of ACPF and the basement of IMEF

Fig. 1. 3D modeling of ACPF (Developed by SketchUp [2]).

3. Application of 3D model of Hot Cell Facilities

3.1 Virtual Reality (VR)

Recently, designers (or SW users) who utilize VR system are able to work alone, in small groups, or collaborate with distant colleagues in a virtual world created from extensive 3D object

Fig. 2. 3D modeling of DFDF located in IMEF (Developed by SketchUp [2]).

libraries and CAD/PLM datasets, providing realism and immersion without sacrificing performance [3]. Along with standard libraries of 3D objects, this study considered the application of Visionary Render for WITNESS which can import various kinds of CAD models of the target facility and the equipment and production lines within, using Virtalis's original library and adapters [4-5]. These can then be enhanced with textures and shadows, whilst the high-performance rendering ensures smooth, fast navigation within the 3D environment. For the first time, users can review their models at 1:1 scale and become immersed in the simulation, interacting with them to try out "what if" scenarios virtually. The SW platform for visualization that allows users to create dynamic and interactive virtual environments. It uses structured and unstructured data to connect engineering quality CAD to real time and contextual data to deliver standard models that are used across the life-cycle of the facility. Furthermore, user can test designs, plan manufacturing layouts and visualize 'Digital Twins' in the field. The same models can be used to improve safety and compliance by training operators, engineers and users with immersive, experiential training that links to learning management systems.

3.2 Advanced fire hazard analysis

As abovementioned, FDS is required to perform the fire hazard analysis of the target facility. In order to operate the FDS correctly, it had been necessary to acquire basic knowledge for fire hazard analysis such as, computational fluid dynamics, combustion engineering and fire mechanics. However, GUI-based fire hazard analysis software products have introduced since 2000 and fire hazard modeling becomes easier. In this study, PyroSim is selected for the simulation, and this SW has intuitive graphical user interfaces for FDS and it imports IFC, DXF, DWG, FBX, STL, and FDS files and Importing any of these files will greatly reduce the amount of time spent recreating the architectural geometry [1]. Moreover, a drawing in GIF, JPG, or PNG format can be imported and then used as a background to help you rapidly draw the target model directly over the image with familiar 3D CAD tools. A major feature recently introduced and applied to this study is the integration of HVAC (Heating, Ventilation, and Air Conditioning) systems into the CFD simulation because this kind system can transport contaminants and heat through the building. This HVAC system can be defined using ducts, nodes, fans, heat exchangers (Aircoils), and dampers and all of components can be edited and visualized in PyroSim. Associated simulation results for the considered facilities will be introduced on the next report.

4. Conclusions

This paper introduced 3D models of hot cell facilities and those perspective applications. As a future work, these models will be utilized to the computational fire hazard analysis or VR simulation, and those analysis reports will inspire to acquire the higher level of safety for the target facilities. The value of 3D visualization in the virtual space is not only for the design review in advance before the real construction but also for the better understanding and management of the target facility in operation.

REFERENCES

[1] Website: Thunderhead Eng., https://www.thunderheadeng.com/pyrosim/

[2] Website: Trimble Inc., http://www.sketchup.com

[3] Website: Lanner group, http://www.lanner.com

[4] Website: https://www.virtalis.com/products/visionary-render

[5] Yu, S.N., "Development of simulation systems for tele-manipulators in confined cell facilities", Nuclear Engineering and Technology, DOI: 10.1016/j.net.2019.07.020, 2019.

Application of Laser Marking Technology for Irradiated Material

Y.M. Jung*, S.J. Baik, G.S. Kim, B.O. Yoo, and Y.G. Jin
Korea Atomic Energy Research Institute, 111, Daedeok-daero 989beon-gil, Yuseong-gu, Daejeon, Republic of Korea
*jym@kaeri.re.kr

1. Introduction

The irradiated materials are treated only by manipulator in hot cell due to radioactivity of specimens. Mechanical test of irradiated materials is often performed under varying conditions on specimens have a same geometry. but it was difficult to distinguish specimens when mixed because they had a similar shape. One way to prevent this traceability loss is to mark the specimen with identification on it. Eventually, even if a number of specimens are handled in a hot cell, they will be able to be distinguished from each other by their unique identification number. Therefore, the purpose of this study is to develop laser marking technique for irradiated materials which has various shapes and to make sure that the ID is kept intact under severe conditions.

2. Methods and Results

2.1 Design

Initially, the design was divided into three parts. Laser oscillator acts as a laser source, controller system can operate the laser and scanning head system marks the ID on irradiated specimens. Since the space where the actual equipment will be installed (hot cell) and the space to operate were different, all connecting cables and laser fibers were installed more than 5 meters. Next, the following works were carried out to remote control.

First, a height control system was established. Because the height of the specimens to be marked was different, it was essential to control height. The focal length between the lens and the object is fixed at 167.2 mm, so it was useless if the height was not controlled. We set up a system that can automatically control the height of scanning head and LVDT(Linear Variable Differential Transformer), electric motor and controller were designed. LVDT can be controlled in 100 μm in real time. Working range is 330 x 2,800 x 50 mm and all parts are manufactured in a modular type that can be assembled and disassembled with bolts.

Second a monitoring system was constructed to view the irradiated specimen and the ID marking process in real time. The cam which can a view of the working area was mounted on the scanning head. And we installed modular type for maintenance and replacement. Laser marking machine was designed to be able to simulate with red guide beam before marking on specimen, it was made to minimize the failure in actual marking (Figure 1.).

Fig. 1. Simulation on specimen before actual marking.

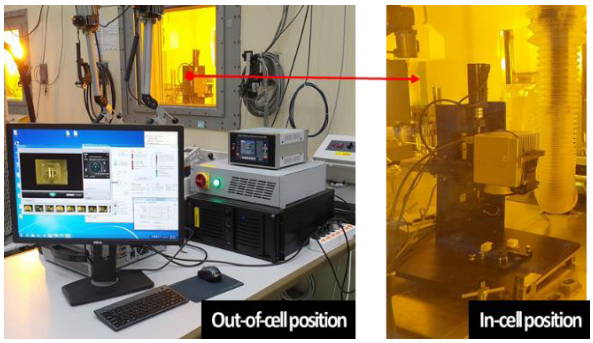

Fig. 2. Laser marking system in hot cell.

2.2 Application

The ID marked on the irradiated specimens was checked to be maintained under severe test condition. We tested the ID was maintained even when the oxide was generated at high temperature and the ID was maintained even after chemical treatment (pickling and etching).

First, after marking ID on the irradiated specimen, the specimen was oxidized at 350°C for 24hours in an oven. The ID of the specimen remained unchanged (Figure 3.).

Second, we tested pickling after marking the ID on Zr-Nb pressure tube. The remaining oxide layer on the OD surface of the tube section should be removed on a lathe using 36/120 grit paper prior to pickling. Pickling solution is 47 % water, 47 % nitric acid, and 6 % hydrofluoric acid by volume. The total reaction time was 15 minutes. The results were slightly blurred but there was no problem identifying the ID. If the laser power is increased, it is expected to be ineffective of these blur.

Fig. 3. Comparison of marked ID before and after oxidation.

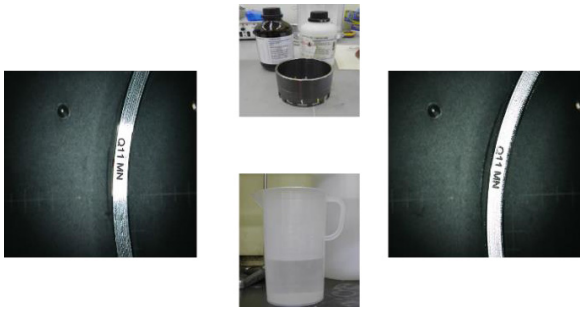

Fig. 4. Comparison of marked ID before and after pickling.

3. Conclusion

Laser marking technology which is widely used in the industry has been successfully applied to hot cell (Figure 2.). ID marking was possible for various shapes of irradiated materials and implement most functions of word processor including font size, style, rotation and alignment. The ID marking technology development in the hot cell was completed successfully by test that the marked ID is maintained under various severe conditions.

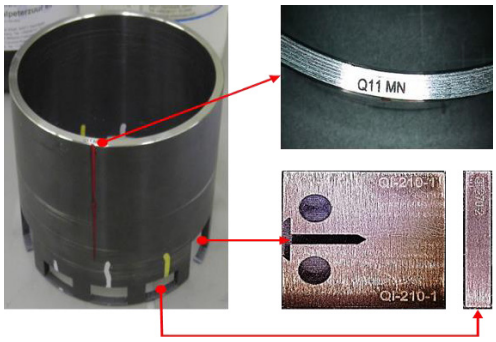

Fig. 5. Laser marking results for various types of specimens.

REFERENCES

[1] Peter Sachnik, Sheikh Enamul Hoque, Wolfram Volk, Burr-free cutting edges by notch-shear cutting, Journal of Materials Processing Tech. 249, p.229-245 (2017).

[2] Y. M. Jung, S. J. Baik, G. S. Kim, Y. G. Jin “Development of Specimen Traceability Technology in Hot Celll”, KNS spring meeting, 2019.

The Evaluation of Absorbed Dose for Robot Transportation Device in Spent Fuel Storage Cask

Kyoungyong Noh*, Hyun Sik Kang, Misuk Jang, and Seoung Rae Kim
Nuclear Engineering Services & Solutions, 756-27, Daedeok-daero, Yuseong-gu, Daejeon, Republic of Korea
*nessrnd@ness.re.kr

1. Introduction

Since domestic spent fuel storage facilities are expected to saturate the storage capacity after 2024, a separate intermediate storage facility would be considered and needed to store a large amount of spent fuel.

The operating period of the intermediate storage facility is generally known for 50 years [1], Therefore, internal defects in the spent fuel storage cask may occur during operation, and monitoring is required. Currently, research is underway to develop robot transportation equipment to monitor and detect internal integrity of spent fuel storage cask.

A schematic diagram is shown in Figure 1. There is a canister containing the spent fuels, and a robot for detecting the defect of the canister can enter through an air flow path between canister and concrete or stainless steel structure. The inner space of the concrete storage cask or metal cask is a high radiation area and is expected to have a big impact on the robot, so the radiation exposed into the robot must be evaluated.

This paper presents the intensity of source term of cask storing spent fuels to reflect the design of robot.

2. Methods and Results

2.1 Methods and Model

The internal dose rate was evaluated based on the external dose rate of the storage cask by applying an arbitrary source term to the spent fuel storage cask.

Most casks are manufactured based on the effective dose rate that a person receives outside the cask. The casks vary according to the type and the storage method, and the limit of the external radiation dose rate varies according to the conditions.

Therefore, we calculated the source term of the effective dose rate of 2 mSv/h on the outer surface of the cask and evaluated the dose rate in the cask [2].

The source term in the storage cask was assumed to be a WH17×17 spent fuel assembly with an initial concentration of 4.5 wt%, a burnup of 45,000 MWd/MTU, and a cooling period of 10 years. ORIGEN-ARP[3] module was used to calculate the gamma spectrum to apply the gamma source term released from spent fuel to MCNP6[4] code.

The major specifications of cask and canister are shown in Table 1, and the geometry is shown in Fig. 1. The overall specifications of the cask are based on the containers developed in Korea. Spectra calculated using ORIGEN-ARP were used to calculate the external radiation dose of the cask.

The spent fuel was cooled for 10 years and mostly in the energy region below 1 MeV. The spectrum is shown in Fig. 2.

MCNP6 [4] computer code was used to calculate the effective dose rate on the outer surface of the cask and MCPLIB04 was used for nuclear cross-sectional data. The concrete material information used in this calculation comes from Standard Composition Library [5].

Table 1. Specification of cask and canister

canister (stainless steel)	radius	82 cm
	height	484 cm
	thickness	2 cm
cask	radius	164 cm
	height	584 cm
	shielding thickness (carbon steel)	2 cm
	shielding thickness (concrete)	70 cm

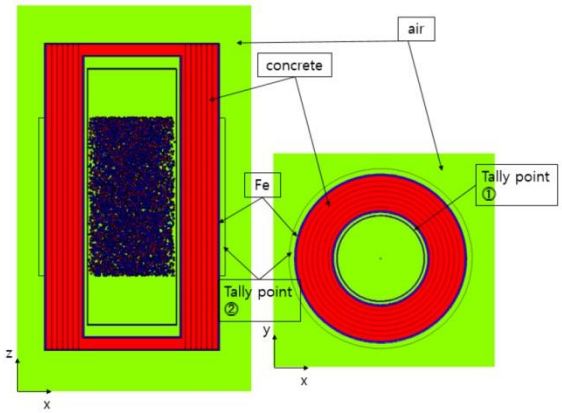

Fig. 1. Geometry of cask and canister.

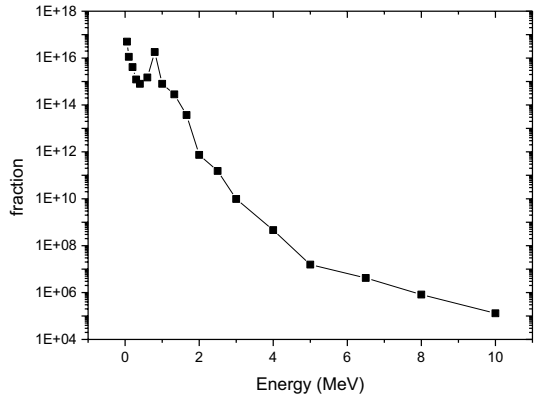

Fig. 2. Spectrum of source term.

2.2 Results

Intensity of source term is 3.786E+18 #/s as the result of calculating intensity so that cask outer surface dose rate is 2 mSv/h. Table 2 shows the results of calculating the absorbed dose inside and outside the cask using the corresponding intensity. The radiation dose rate inside cask was about 2.00E+07 mSv/h higher than outside.

Table 2. Result of dose rate in ventilation of cask

	T.P.①	R.E.	T.P.②	R.E.
Effective dose rate (mSv/hr)	4.09E+07	0.33%	2.00E+00	6.61%
Absorption dose rate (Gy/h)	3.90.E+04	0.33%	1.86.E-03	6.83%

cf) T.P. = Tally Point

R.E. = Relative Error

3. Conclusions

The absorbed dose rate for the robot entering the air channel was evaluated. As a result of dose assessment, the absorbed dose exposed to the robot in internal air channel of cask was predicted as 3.90E+04 Gy/h. Therefore, the integrated dose rate based on the result should be considered in the design of the robot structure. In addition, there may be difference results depending on the type and amount of spent fuels, so the error should be considered for the conservatism.

ACKNOWLEDGEMENTS

This work was supported by the Korea Institute of Energy Technology Evaluation and Planning (KETEP) and the Ministry of Trade, Industry & Energy (MOTIE) of the Republic of Korea (No.20171520101780).

REFERENCES

[1] IAEA Safety Standard, “storage of spent nuclear fuel,” No. SSG-15.

[2] “Rules on technical standards such as radiation safety management”[NSSC rules No. 23, 2019.5.10.]

[3] I. C. Gauld, S. M. Bowman, J. E. Horwedel, et al., "ORIGEN-ARP: AUTOMATIC RAPID PROCESSING FOR SPENT FUEL DEPLETION, DECAY, AND SOURCE TERM ANALYSIS," Version 6, Vol. I, Sect. D1, Oak Ridge, USA, 2009.

[4] Denise B. Pelowitz, ed., “MCNP6 User’s manual Version 1.0,” LA-CP-13-00634, Los Alamos National Laboratory, May 2013.

[5] L. M Petrie, P. B. Fox, and K. Lucius, "Standard Composition Library”, ORNL/TM-2005/39, Oak Ridge National Laboratory, 2009.

Effect of Exhaustion on the Indoor Thermal Environment

Heeseok Kang*, Youngwoo Kwon, Seonho Noh, Youngkuk Jang, and Ilje Cho
Korea Atomic Energy Research Institute, 111, Daedeok-daero 989beon-gil, Yuseong-gu, Daejeon, Republic of Korea
*hskang1@kaeri.re.kr

1. Introduction

Although the operation of the test facility is organically connected in various fields, the thermal environment of the laboratory is a major factor affecting the health and efficiency of the workers in the laboratory, and it is recognized as an important item for both the operator and the operator of the facility. The thermal environment of the laboratory has the effect of raising the room temperature by combining the radiant heat of the facility with the sunlight and the heat generated by the indoor laboratory. In the laboratory, room ventilation is controlled by ventilation through air supply and exhaust and air conditioning and heating in various ways. Laboratory ventilation aims to provide a more pleasant working environment for workers in the laboratory by discharging heat and moisture from the supply of fresh air and the replacement of air. In this study, the influence of the exhaust environment on the indoor temperature was investigated by measuring the temperature change at several points in the room according to the operation of the laboratory exhaust system.

2. Exhaust System in Facility

2.1 Increased ventilation by additional exhaust fan

The Nuclear Cycle Experimental Research Facility of The Korea Atomic Energy Research Institute (KAERI) operates six exhaust systems for exhaust gas and laboratory ventilation during process experiments. Figure 1 shows a conceptual diagram of the exhaust and ventilation method of the nuclear cycle laboratory. The exhaust gas from the various experimental devices on the first floor is discharged to the outside through the filter bank after passing through the third floor exhaust device connected to the exhaust duct. Laboratory ventilation is designed to open the end of the exhaust duct so that the indoor air also passes through the exhaust system and then passes through the filter bank to the outside for laboratory ventilation. As shown in Fig. 2, an additional exhaust system was operated considering only the laboratory ventilation.

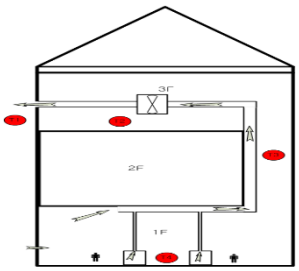

Fig. 1. Conceptual exhaust diagram in the laboratory.

Fig. 2. Exhaust duct for ventilation.

2.2 Room temperature effect by additional exhaust fan

The outside temperature of the laboratory during the day should be shown to change with time so that the temperature change at each point of the room can be accurately compared with the operation of the exhaust fan. The temperature change during the daytime without all exhaust fans running is shown in Fig. 3(a) for each preset point. It is shown to maintain the temperature of about 30°C steadily without being significantly affected by the gradual rise change of the external

temperature(T1). The temperature change at each measurement point when only six exhaust fans, which are in charge of the exhaust gas and indoor ventilation is operated is shown in Fig. 3(b). The room temperature due to the operation of the exhaust fan is initially started at a slightly lower temperature, but the room temperature is slightly increased due to the operation of the exhaust fan. In addition, when one exhaust fan is operated for ventilation purposes only, it is shown in Fig. 3(c). The increase in room temperature is slightly higher than that in Fig. 3(b).

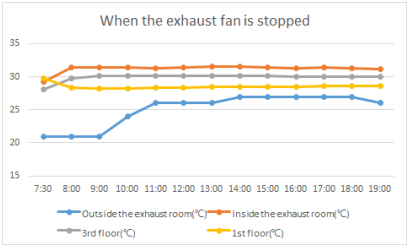

(a) When the exhaust fan is stopped

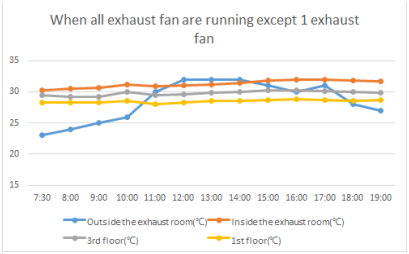

(b) When all exhaust fan are running except 1 exhaust Fan

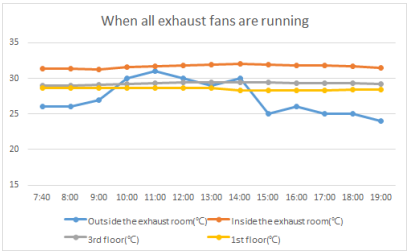

(C) When all exhaust fans are running

Fig. 3. Effect of extended ventilation exhaust fan on the indoor thermal environment.

Due to the rain, the outside temperature tends to change more significantly than the previous measurement, making it difficult to estimate the change in room temperature caused by the exhaust fan. As shown in (a), (b), and (c) of Fig. 3, the change in the temperature of the outside temperature of the laboratory shows a very different pattern with time. A consistent trend is a prerequisite to more accurately correlate the laboratory's internal and external temperatures with exhaust fan operation. Fig. 4 shows the results of the difference between the outside and the inside temperature according to the time during the day according to the operation of the exhaust fan. As more exhaust fans are operated, the temperature difference between the outside and the inside is decreased, but the effect of operating the exhaust fan is that the weather is severely changed and does not follow the trend.

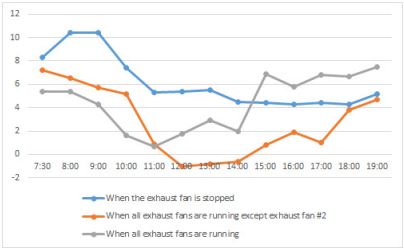

Fig. 4. Effect of exhaust fan operation on indoor and outdoor temperature difference with time.

3. Conclusions

When all the exhaust fans were not operated, they tended to maintain a temperature of about 30°C without being affected by the gradual increase in the external temperature. When the six exhaust fans, which are both the exhaust gas from the experimental device and the room ventilation, were operated, there was a slight increase in the room temperature. When an additional exhaust fan was operated only for the purpose of ventilation, it showed a slightly higher indoor temperature increase effect, but it was difficult to identify the tendency of the indoor temperature change due to the drastic change of the external air temperature due to the rain. In the future, it was necessary to obtain more temperature observation data for a wider range of weather conditions.

Evaluation of Radiocesium Wash-off by Soil Erosion Using USLE Model

Kyung-Suk Suh*, Byung-Il Min, Jiyoon Kim, and Kihyun Park
Korea Atomic Energy Research Institute, 111, Daedeok-daero 989beon-gil, Yuseong-gu, Daejeon, Republic of Korea
*kssuh@kaeri.re.kr

1. Introduction

A numerical model based on universal soil loss equation (USLE) has been developed for simulating the long-term migration and distribution of radiocesium after the Fukushima accident. The present work aims to improve USLE model by implementing new processes for radiocesium wash-off which transports in the vertical direction. The vertical migration of radiocesium in soil can be parameterized as equation by observed soil depth profile data [1], and it can be well described by an empirical model. It is important to clarify some assumptions. The vertical migration and long-term fixation are slow processes in timescales of ranging from months to years, and it assumes that the radiocesium depth profile and the fraction of radiocesium in fixed states are constants for individual typhoon or heavy rain.

2. Method

The annual soil erosion potential is defined by USLE: A = R × K × LS × C × P, where, R is the rainfall and runoff factor, K is the soil erodibility factor, LS is the topographic factor or landform factor, C is the cover and management factor or land-use factor, and P is the support practice factor. The rainfall and runoff factor were extracted in the Fukushima regions from the GloREDa (Global Rainfall Erosivity Database, [2]), and other factors were also calculated based on the soil database of the ISRIC Project [3] which used variables such as land use, soil type, organic content and soil size with spatial resolution of 250m. More detailed calculation methods are described in reference [4].

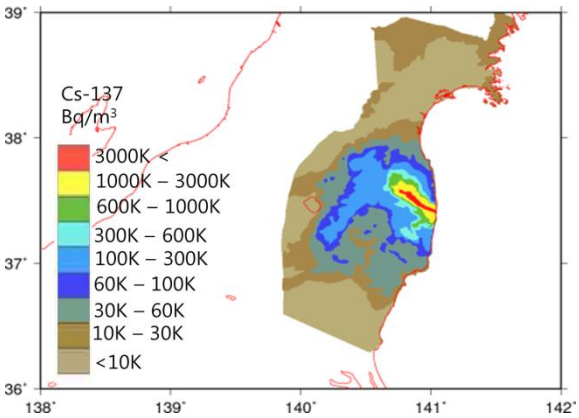

Fig. 1. Concentrations of Cs-137 were obtained from the Forth Airborne Monitoring Survey by MEXT [5].

The initial distribution of radioactive cesium deposited in surface soil and redistribution after deposition are influenced by various physical, physicochemical, and biological processes. To approximate the depth distribution, some fitting functions such as the Gaussian, double exponential, Lorentz, polynomial functions and Sech function have been proposed and developed [1, 2, 3]. These functions are not satisfied in all cases, however the empirical equation of Matsuda [1] and parameters in this study were used for calculating vertical distribution of radionuclide in soil, because they are fitted the equation using soil profile data from Fukushima site.

The initial concentration distribution of Cs-

137 (Fig. 1) was obtained from the Forth Airborne Monitoring Survey by MEXT [5].

3. Discussion

In the USLE model, annual soil erosion in the Fukushima region is estimated within the several centimeters, and the downward migration speed of Cs-137 in the soil was estimated to be 0.5 ~ 2cm/year [1]. Therefore, the results are very sensitive to the vertical movement speed in the soil.

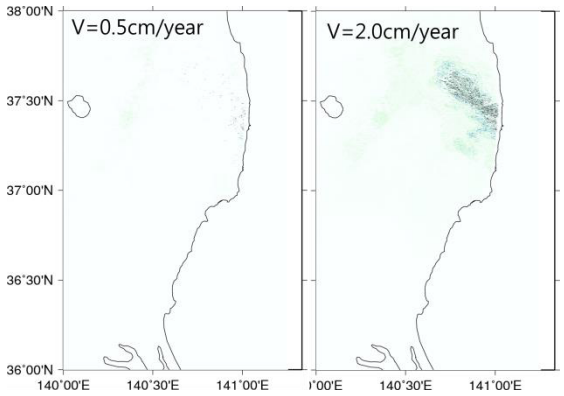

Fig. 2. The Wash-off rates of Cs-137.

Figure 2 shows the total wash-off rates of Cs-137 after 9 years from the Fukushima accident which assumed the downward migration speed(DMS) with 0.5 and 2.0 cm/year, respectively. Spatial wash-off of Cs-137 is highly dependent on soil characteristics, type and cover, but is estimated to be approximately 0.5-3.5% of the total deposited inventory. This study has the limitations of assumption that the vertical movement velocity is spatially the same. In the future, these limitations are expected to be improved by referring to the various data and other studies.

Acknowledgement

This work was supported by the National Research Foundation of Korea (NRF) and funded by the Korea government (MSIP) (MSIP: NRF-2017M2A8A4015253, NRF-2015M2A2B2 034282).

REFERENCES

[1] N. Matsuda, S. Mikami, S. Shimoura, J. Takahashi, M. Nakano, K. Shimada, K. Uno, and K. Hagiwara, “Depth profiles of radioactive cesium in soil using a scraper plate over a wide area surrounding the Fukushima Dai-ichi Nuclear Power Plant, Japan”, Journal of Environmental Radioactivity 139, 427-434 (2015).

[2] P. Panagos, P. Borrelli, K. Meusburger, B. Yu, A. Klik, K.J. Lim, J.E. Yang, J. Ni, C., et. al., “Global rainfall erosivity assessment based on high-temporal resolution rainfall records”, Scientific Reports 7, 4175 (2017).

[3] T. Hengl, DJ. Mendes, G. Heuvelink, M. Gonzalez, M. Kilibarda, et al., “SoilGrids250m: global gridded soil information based on Machine Learning”, PLos One 12(2), 169748 (2017).

[4] W.H. Wischmeier, and D.D. Smith, “Predicting Rainfall Erosion Losses: a Guide to Conservation Planning”, U.S. Department of Agriculture Washington, D.C. Agriculture Handbook No. 537 (1978).

[5] MEXT (Ministry of Education, Culture, Sports, Science and Technology), “Results of the Third Airborne Monitoring Survey by MEXT”, https://radioactivity.nsr.go.jp/en/contents/4000/3179/24/1270_1216.pdf (2011).

Optimum Sample to Detector Distance in Alpha Spectrometry

JeongHyeon Ryu[1,2], JiYoung Park[1], Young Gun Ko[1,*], Dong June Ahn[2], Jong-Myoung Lim[1], and Wanno Lee[1]
[1]Korea Atomic Energy Research Institute, 111, Daedeok-daero 989beon-gil, Yuseong-gu, Daejeon, Republic of Korea
[2]Korea University, 145, Anam-ro, Seongbuk-gu, Seoul, Republic of Korea
[*]ygko@kaeri.re.kr

1. Introduction

Alpha spectrometry with passivated implanted planar silicon(PIPS) detectors has been applied to various investigations in nuclear science and technology [1]. The advantage of PIPS detector is it exhibits such low background and high efficiency, which allows us to reach low detection limits on the basis of a few counts.

For accurate and precise measurement using PIPS detector, one of the most important factor is to choose sample-to-detector distance (SDD). The aim of this study is to help the user of PIPS detector in selecting SDD by giving useful information which is about correlation of level with efficiency and resolution.

2. Materials and method

The alpha analyst 7200-12, CANBERRA, was used for activity measurements. Inside each chamber, there is a sample holder that allows the measurement of the samples at different SDD in the range of 1-45mm, divided into 12 equal levels by the chamber wall slots. The measurements for determining efficiency and resolution depending on SDD were performed using alpha standard electro-deposited disc source of ^{238}U, ^{234}U, ^{239}Pu, and ^{241}Am which was certified by Eckert & Ziegler Analytics.

The source was placed on each level of the chamber and measured four times. The measurement time was set to when the approximate amount of detected ^{241}Am count becomes about 2000. By making the peak area constant, the variation in peak shape depending on SDD can be seen, which is informative data for understanding correlation of SDD with resolution. The reason that we roughly set is it is difficult to control measurement time based on the count due to limitation of the equipment.

3. Results and discussions

The variations in efficiency and FWHM against SDD were shown in Fig. 1 and Fig. 2. Fig.1 shows that the closer SDD demonstrates the better efficiency. On the contrary, it can be seen that the closer SDD displays, the worse the resolution gets according to the results in Fig. 2. Similar results were reported in other studies [1, 2].

Fig. 3 presents the variation in peak shape of measured alpha energy spectrum of ^{241}Am depending on SDD by making the peak areas constant. It can be seen that the longer SDD gets, the smaller tailing, which is informative data

that indicate cause of variation in FWHM.

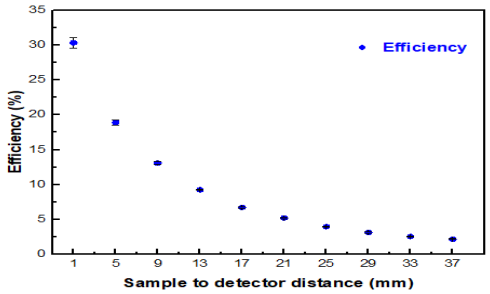

Fig. 1. Experimental efficiency as a function of SDD.

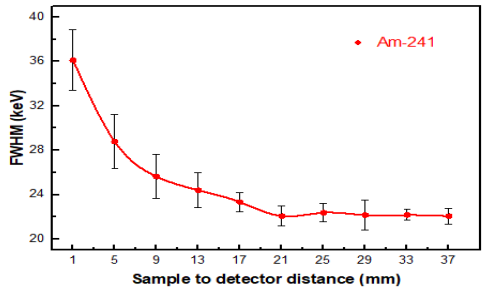

Fig. 2. Variation in detector resolution of ^{241}Am against SDD.

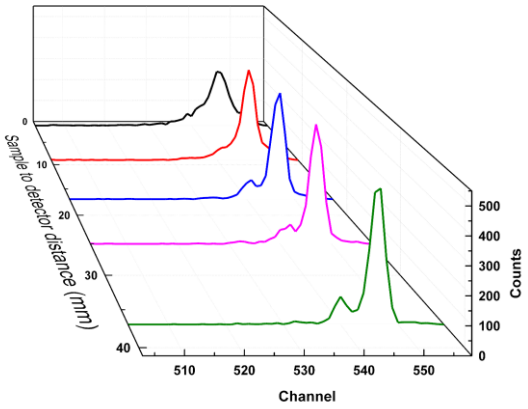

Fig. 3. Variation in peak shape of ^{241}Am against SDD.

In the radiometer chamber, while alpha particles emitted by the alpha nuclide source pass through the entrance window consisting of SiO_2, the particles lose their kinetic energy depending on the angle of incidence before the particles come into contact with the detector [1]. In case of large angle of incidence of the particle, more energy is lost than when the angle of incidence is small. The more energy is lost, the more tailing occurs, which is called energy straggling. The closer SDD shows the larger solid angle which gives rise to increasing the FWHM. However, if SDD is longer than a certain distance, variation in the solid angle according to SDD becomes insignificant. Thus, the meaningful high resolution cannot be obtained.

4. Conclusion

The variation in the efficiency rapidly decreases with the change of the measurement geometry, toward higher values of the SDD.

In case of the resolution, the FWHM decreases with increasing SDD. However, if SDD is longer than a certain distance, the high resolution cannot be obtained.

REFERENCES

[1] Hynh Nguyen Phong Thu et al., “Efficiency response of an aged PIPS detector used in high-resolution alpha-particle spectrometry” Nuclear Inst. and Methods in Physics Research, Vol. A908, 128–135 (2018).

[2] M. R. Calin et al., “Experimental characterization of a multi-chamber alpha spectrometry system using standard actinide sources” Nuclear Inst. and Methods in Physics Research Vol. A705, 13–16 (2013).

Strengthen the Gas Safety Management in PRIDE

Youngkuk Jang*, Seonho Noh, Youngwoo Kwon, Hee-seok Kang, and Ilje Cho
Korea Atomic Energy Research Institute, 111, Daedeok-daero 989beon-gil, Yuseong-gu, Daejeon, Republic of Korea
*jangyk@kaeri.re.kr

1. Introduction

Korea Atomic Energy Research Institute (KAERI) has a Pyro-processing Integrated Inactive Demonstration facility (PRIDE) for the development of pyro-technology. In essence, the PRIDE enable integrated pyro-systems testing at engineering scales using depleted uranium or surrogates for depleted nuclear fuels.

The PRIDE must maintain an inactive (argon) atmosphere due to the characteristics of processes that take place in it, such as electrochemical reduction, electrochemical refining, and electrochemical smelting. In concentrating impurities at the facility, oxygen and moisture must be lower than 100 ppm.

This paper describes the contents of strengthening safety of argon gas management for emergency supply used in PRIDE facilities.

2. Main

2.1 Consist of emergency Ar gas system

Outside the PRIDE facility, a 2,500 liter liquid argon tank with a charge capacity to maintain the atmosphere of argon cells and an emergency argon bottle in the event of a shortage of argon are installed outdoors next to the argon tank. (see figure 1)

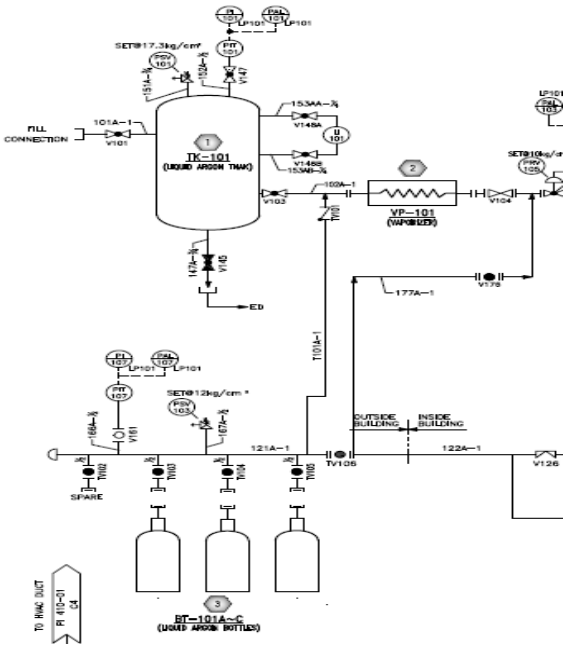

Fig. 1. Schematic of emergency Ar gas system.

2.2 Problem

The Pride facility uses a 170-liter liquid argon bottle as an emergency. In the event of a shortage of argon due to overuse, safe management of emergency argon gas bottle is required.

2.3 Handling and storage of gas bottles

The method of handling and storage of gas containers were referred to the listed below.

(a) Flammable gas containers shall be stored and stored in locations such as built ventilation and well ventilated buildings using non-flammable materials.

(b) Do not place electrical equipment, wiring, etc. near the ground line.

(c) Do not receive direct sunlight, so that the temperature of the container does not exceed 40°C.

(d) Take measures to prevent falling or rolling down.

(e) Shall not be placed with flammable gas containers, oxygen or chlorine gas containers.

(f) A molten acetylene container and a flammable gas container shall be erected and stored.

(g) The gas cabinet must be storable a two Ar bottle.

(h) Complete the connection work with the existing piping for immediate use after the argon cabinet is drawn in.

(i) The empty container is marked and clearly distinguished from the filling container.

2.4 Contents of inprovement

The cabinet for storing gas bottle was manufactured and installed in consideration of the handling and storage method of the gas container.

(a) Material : STS – 304

(b) Size : 1800(L) * 800(D) * 2000(H) * 1.5(T)

(c) Schematic diagram

3. Conclusion

Safety related to Argon gas bottle storage was ensured by making and installing cabinet for storing gas bottles in emergency situations. This ensured stability and crisis response to emergency situations in managing the atmosphere of the argon cell located in the facility.

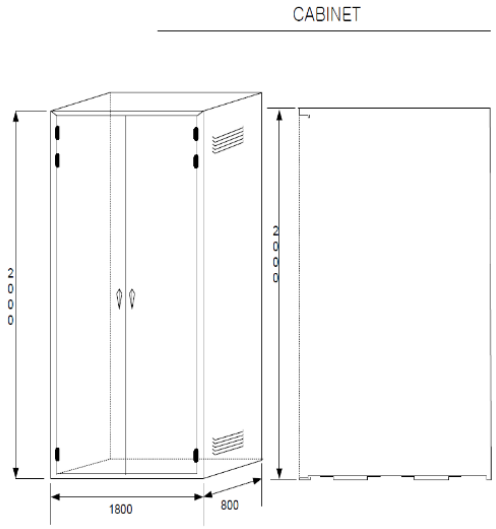

Fig. 2. Schematic of gas cabinet.

REFERENCES

[1] ANL-7959 Hot Fuel Examination Facility/North Facility Safety Report, February 1975, Argonne National Laboratory pp.42-53.

[2] The EBR-II Fuel Cycle Story, Charles E. Stevenson, American Nuclear Society pp.16-25.

Radioactivity of Silicon and Silicon Carbide After Neutron Irradiation

Ki-Man Lee* and Byung-Gun Park
Korea Atomic Energy Research Institute, 111, Daedeok-daero 989beon-gil, Yuseong-gu, Daejeon, Republic of Korea
*lkm@kaeri.re.kr

1. Introduction

Silicon carbide has been a substrate material for high power electronic devices because of its excellent thermal and electrical properties compared with silicon [1]. Silicon and silicon carbide (SiC) have been usually doped by NTD (neutron transmutation doping). But the research is insufficient to compare the activation problem of NTD-SiC with that of NTD-Si. In present study, the residual radioactivity and the ambient dose equivalent of NTD-SiC and NTD-Si were calculated to compare the activation problem.

2. Methods and Results

2.1 Monte Carlo simulation

The activity and the ambient dose equivalent of NTD-Si and NTD-SiC after neutron irradiation was calculated using the DCHAIN program linked to PHITS [2]. The energy spectrum of neutrons in the NTD2 irradiation hole of HANARO calculated by MCNP6.1 were considered as a neutron source. The neutron sources were assumed to be uniformly distributed on the surface of a vertical channel with a radius of 9 cm as the NTD2 irradiation hole. The samples for neutron irradiation were modeled as a 6-inch cylindrical structure. Impurities in the Si and SiC were not considered. For the t-dchain tally, the current of neutron beam was set to correspond to the neutron flux of 4.8×10^{13} n/cm^2·sec in the target ingot volume. Irradiation time was set to 24 hours. The residual radioactivity and the ambient dose equivalent were calculated until 10 days after irradiation.

2.2 Results of simulation

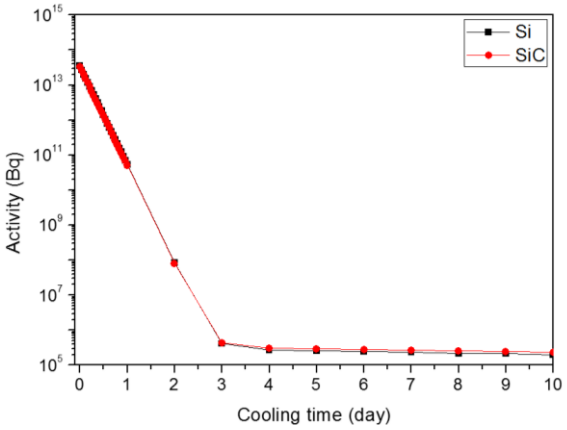

Fig. 1. Time variations of the residual radioactivity of the NTD-Si and the NTD-SiC after neutron irradiation.

The time variations of the radioactivity of the NTD-Si and the NTD-SiC after irradiation are showed in Fig. 1. The radioactivity continues to decrease rapidly from 3×10^{13} Bq to 8×10^{7} Bq for 3 days. After that, it decreases very slowly. The ambient dose equivalent of the NTD-Si and the NTD-SiC after irradiation are showed in Fig. 2. The ambient dose equivalent is recommended by the ICRP as the operational quantity for assessing effective dose in area monitoring. The ambient dose equivalent continues to decrease

since the end of neutron irradiation.

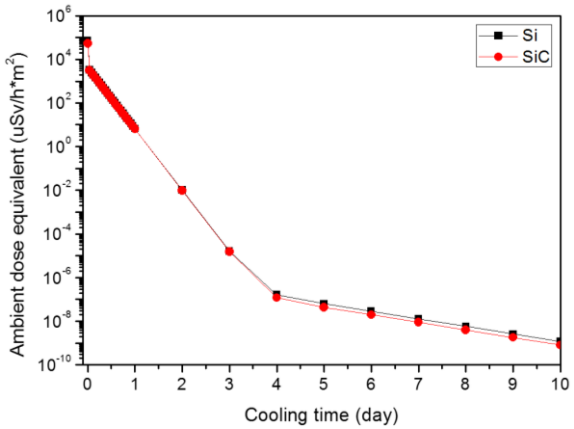

Fig. 2. Time variations of the ambient dose equivalent of the NTD-Si and the NTD-SiC after neutron irradiation.

The comparison results of the radioactivity and the ambient dose equivalent of the NTD-SiC with those of the NTD-Si are represented as SiC/Si ratio in Fig. 3. The SiC ingot has fewer silicon atoms than Si ingot in the same volume. And most of the induced radioactivity is come from the $^{30}Si(n,\gamma)^{31}Si$ reaction. Half-life of the ^{31}Si is relatively short (2.62 hours), and thus cooling time of 3 days is enough for sufficient decay of the ^{31}S. Thus the radioactivity of NTD-SiC is smaller than that of NTD-Si until 3 days. After the sufficient decay of the ^{31}S, the radioactivity of NTD-SiC becomes bigger than that of NTD-Si, because the ^{14}C of the NTD-SiC becomes one of main radionuclides. But the ambient dose equivalent of the NTD-SiC is always smaller than that of NTD-Si. Because the maximum energy of electrons emitted from ^{14}C of the NTD-SiC is 0.156 MeV, it is not enough to be released from the NTD-SiC ingot.

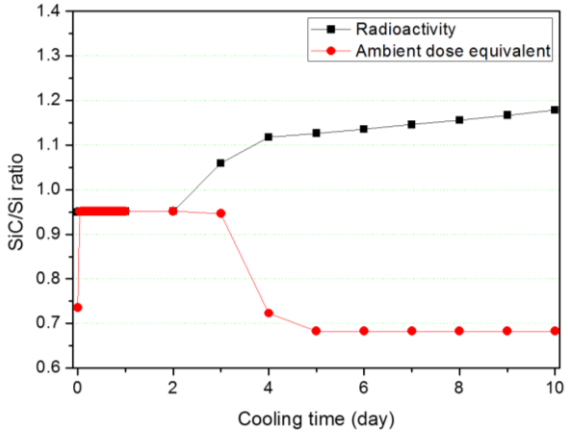

Fig. 3. Ratio of the radioactivity and the ambient dose equivalent of the NTD-SiC to those of the NTD-Si.

3. Conclusion

We conclude that the radioactivity of NTD-SiC becomes bigger than that of NTD-Si after 3 days of cooling, but the ambient dose equivalent of the NTD-SiC is always smaller than that of NTD-Si. In the near future, the effect of impurities on radioactivity will be studied.

Acknowledgement

This work was supported by the National Research Foundation of Korea (NRF) Grant funded by the Korea government (MSIP) (NRF-2017M2A2A6A05018527).

REFERENCES

[1] IAEA, “Neutron Transmutation Doping of Silicon at Research Reactors”, Report IAEA-TECDOC series, 1681 (2012).

[2] PHITS collaboration. “PHITS user’s manual (version 3.02) edition” (2017).

Development of a Dynamic Integrated Safety Analysis for Fuel Cycle Facilities

Seok-Jun Seo[1,*], Jong Yol Park[2], and Seung Nam Yu[1]

[1]Korea Atomic Energy Research Institute, 111, Daedeok-daero 989beon-gil, Yuseong-gu, Daejeon, Republic of Korea

[2]RIA Institute Inc., 9, Nongdae-ro 2beon-gil, Yuseong-gu, Daejeon, Republic of Korea

[*]sjseo@kaeri.re.kr

1. Introduction

There have been increased demands for safety in nuclear related facilities since 2011. An integrated safety analysis (ISA) has been also widely studied and conducted for license applications of fuel cycle facilities in U.S. Nuclear Regulatory Commission (NRC) [1]. In an ISA, potential hazards and their likelihood of occurrence are investigated based on various systematic methodologies [2]. Therefore, a semi-quantitative risk assessment from the ISA has some advantages in terms of a lower cost and short period of time compared to probabilistic safety analysis (PSA).

In this study, a concept of dynamic ISA (D-ISA) based on internet of things (IoT) technologies [3] is more specifically established with its basic operational logics as shown in Fig 1. Firstly, the hazard analysis is performed to verify characteristics of a nuclear related facility and to identify its potential hazards with categories of a likelihood of occurrence and consequence. And then, some selected events (i.e., hazard basis events) with a specific event tree are connected to IoT sensors. These IoT sensors could determine whether an event occurs or not. In this step, initial data from the hazard analyses are saved in a central data server computer in a form of the event tree, probable incident list, and their categories. Then, a real-time data from all the IoT sensors are collected and analyzed to obtain meaningful input to change the individual likelihood and consequence values. Finally, a risk index category with a multiply of the likelihood and consequence is calculated and priority of the incident list are changed, resulting in appropriate stepwise alarming measures [4].

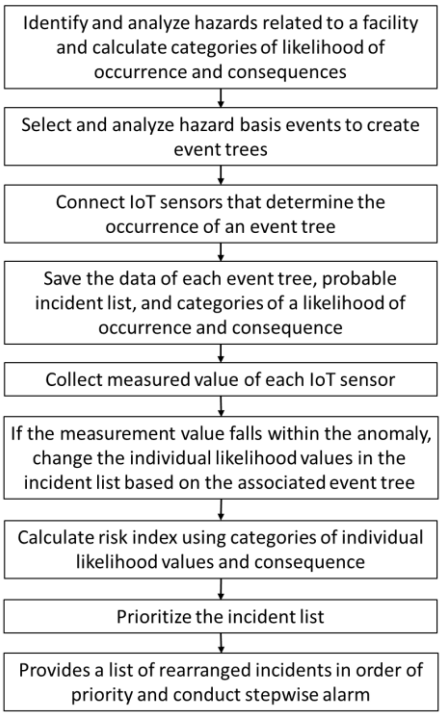

Fig. 1. Basic operational logics for dynamic integrated safety analysis (D-ISA) based on internet of things (IoT) technologies.

REFERENCES

[1] NUREG-1520, Standard Review Plan for Fuel Cycle Facilities License Applications, U.S. Nuclear Regulatory Commission (2015).

[2] NUREG-1513, Integrated Safety Analysis Guidance Document, U.S. Nuclear Regulatory Commission (2001).

[3] S-J Seo, J.Y Park, S.N. Yu, Development of a Concept of Dynamic Integrated Safety Analysis for Accident Predictions, Proc. of the KRS 2018 Fall Conference, Oct. 31 – Nov. 2, 2018, Jeju.

[4] Patent pending, 10-2019-0027048, Real-time accident prediction system using hazard assessment and method thereof.

An Estimation of Carbon-14 Production Rate at KIJANG Research Reactor

Ji Sung Park*, Gyuhong Roh, and Byungchul Lee
Korea Atomic Energy Research Institute, 111, Daedeok-daero 989beon-gil, Yuseong-gu, Daejeon, Republic of Korea
*jspark13@kaeri.re.kr

1. Introduction

C-14 is a radionuclide of considerable interest in nuclear reactor because of its long half-life (5730 years) and high biological risk (dose conversion factor = 5.8E-10 Sv / Bq [1]). The natural C-14 is produced by reaction of neutrons of cosmic ray origin with nitrogen in the upper atmosphere. Then, the naturally occurred C-14 is being balanced by accumulation in air, soil, water and plants.

Most biological effects by the natural C-14 is due to ingestion of the food in which C-14 is accumulated. However, C-14 produced in nuclear facility can directly affect radiation workers and neighboring residents by inhalation. Therefore, the continuous monitoring of C-14 emissions is necessary.

KIJANG Research Reactor (hereafter, KJRR) of 15MW is loaded with MTR (Material Testing Reactor)) type fuel assemblies surrounded by beryllium reflectors. KJRR is an open-tank-in-pool type, and thus it is not difficult to release C-14 to the environment due to evaporation of coolant. This paper presents the C-14 production rate of KJRR.

2. Methods and Results

2.1 Production Reaction for C-14

C-14 is formed from five reactions of neutrons with isotopes of elements that are normal or impurity components of fuel, structural materials, and the cooling water. The neutron-induced reactions are as follows:

(1) $^{15}N(n,d)^{14}C$;
(2) $^{16}O(n,^{3}He)^{14}C$;
(3) $^{17}O(n,\alpha)^{14}C$;
(4) $^{14}N(n,p)^{14}C$;
(5) $^{13}C(n,\gamma)^{14}C$.

In these reactions, reaction (1) and (2) are excepted in this study because the two reactions are the fast neutron reaction. In the case of KJRR with no heavy water reflectors, O-17 is present in the coolant water at 0.038% of natural existence. Therefore, the production of C-14 by (n,α) reaction of O-17 is evaluated only for the contribution by coolant in and out of the reactor core.

In the case of ^{14}N (n, p)^{14}C reaction, it is evaluated based on the amount of dissolved nitrogen gas (N_2) in the pool water. The solubility of N_2 gas is about 0.002 g in 100 g of 20°C water [2].

^{13}C (n, γ)^{14}C reaction occurs in B_4C, which is a neutron absorber in the epi-thermal PTS (pneumatic transportation system) and FNIF (Fast Neutron Irradiation Facility). Compared with the previous two reactions, however, the number density of atoms target and the reaction cross-section are very small. Therefore, the ^{13}C (n, γ)^{14}C reaction is excluded from this evaluation.

2.2 Calculation of C-14 Production Rate

The C-14 production rate can be evaluated using the following calculation formula;

$$R = \sigma_{th}\bar{\phi}_{th}N \quad (1)$$

Where, σ_{th} = thermal neutron cross section,
$\bar{\phi}_{th}$ = thermal neutron flux,
N = number density of target atom.

The thermal neutron flux and cross section are evaluated by obtaining the reaction rate at 16 fuel assemblies except 6 follower fuel assemblies as shown in Fig. 1. MCNP6 code [3] is employed in the reaction rate calculation.

Number density of target atom and total atom number are evaluated. O-17 can be produced through the ^{16}O (n, γ) ^{17}O reaction, but since the cross section of the reaction is very small. In addition, the amount of O-17 contained in the structural material of the reactor is relatively small compared to the amount in the coolant. Therefore, O-17 in the coolant is only considered.

N-14 is present as an impurity in fuel and structural materials, but an accurate assessment of the amount of C-14 released into the coolant has not been made for KJRR. In this pater, therefore, only the nitrogen gas dissolved in coolant are taken into account.

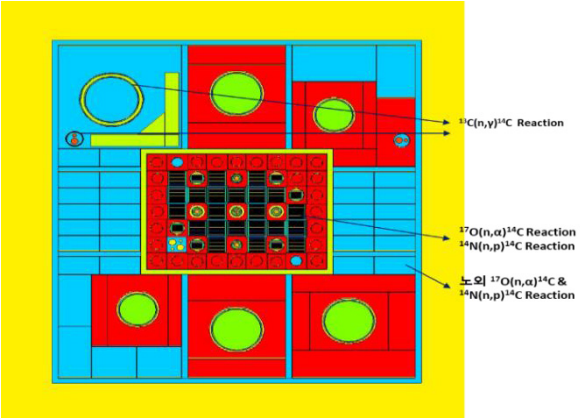

Fig. 1. C-14 Production Reaction and Position.

2.3 Results and Discussion

For the $^{17}O(n,\alpha)^{14}C$, the reaction rate at inner region of core (IR) and outer region of core (OR) are 2.1E+13 #-barn/cm^2-sec, 1.9E+10 #-barn/cm^2-sec, respectively. For the $^{14}N(n,p)^{14}C$ reaction, the reaction rate at IR and OR are calculated as 8.6E+13 #-barn/cm^2-sec, 1.4E+11 #-barn/cm^2-sec, respectively. Total number of atom of ^{17}O at IR and OR are 7.623E+23, 1.423E+27, and total number of atom of ^{14}N at IR and OR are 5.143E+22 and 9.601E+25, respectively.

Finally, the production rate of C-14 is evaluated as in Table 1. The calculations results include the uncertainty of 15%. The calculated production rate of C-14 is 7.037E-03 TBq/year, or 0.190 Ci/year. In the calculation results, $^{17}O(n, \alpha)\ ^{14}C$ reaction accounts for about 70%, and about 44% is due to the $^{17}O(n, \alpha)\ ^{14}C$ reaction at the outer region of core.

Table 1. C-14 Production Rate

Reaction	$^{17}O(n,\alpha)^{14}C$		$^{14}N\ (n,p)\ ^{14}C$	
	IR	OR	IR	OR
Production Rate (10^{13} #/sec)	1.85	3.10	0.51	1.62
(10^{-10}Ci/sec)*	19.2	32.1	5.25	16.8
(10^{-2}Ci/year)**	4.98	8.33	1.36	4.35
(10^{-3}TBq/year)	1.84	3.08	0.50	1.61

* Decay constant of C-14 = 3.83E-12 s^{-1}
** Effective full power day = 300 day

For a comparison, C-14 production rate in CANDU and PWR (OPR-1000 NPP) is known to be about 16 TBq/year [2] and 0.099 TBq/year [4], respectively. As shown in Table 2, the production rate of C-14 in KJRR is about 7.108% compared to PWR.

Table 2. Comparison of C-14 Production Rate

	KJRR	CANDU	PWR
Production Rate (TBq/year)	7.04E-03	~16	0.099
Compared to KJRR Result(%)	-	0.044	7.108

3. Conclusion

In the present study, C-14 production rate at KJRR is evaluated. The production rate of C-14 in KJRR is small compared to the value of commercial power plant which is controlled by regulation authority. Therefore, it is expected that the effect of C-14 in KJRR is not significant considering the comparison of production rate even if all C-14 produced in the reactor is released to the environment. As a future work, it is planned to analyze the behavior of C-14 in the reactor and coolant, and then the assessment of its release into the environment will be conducted.

REFERENCES

[1] "Annals of the ICRP: Compendium of Dose Coefficients based on ICRP Publication 60," ICRP 119, 2012.
[2] Oh, Soo-Youl et al, HAN-RR-CR-801-04-09, 2004.
[3] MCNP - A General Monte Carlo N-Particle Transport Code, Version 6.1.0, MCNP6 User's Manual, LA-CP-13-00634, Los Alamos National Laboratory, May 2013.
[4] Sung Il Kim, "The Status of Monitoring of Cabon-14 Emissions from LWRs in Korea," Proc. of KNS, 2014 Spring Conference, Jeju, May 29-30, 2014.

On-site Transport Risk Assessment in Hanul NPPs Using INTERTRAN Code

Minchul Kim
KHNP Central Research Institute, 70, Yuseong-daero 1312beon-gil, Yuseong-gu, Daejeon, Republic of Korea
kim.minchul@khnp.co.kr

1. Introduction

PWR spent fuels loading campaigns are conducted periodically to the neighboring nuclear power plants' pool. This paper describes the radiological risks of workers and the public on the on-site transport in the Hanul plants using INTERTRAN2 code.

2. Description of background information

2.1 INTERTRAN2 code

INTERTRAN2 was developed through the coordinated research program on probabilistic safety techniques related to the safe transport of radioactive materials by IAEA.

2.2 On-site spent fuels transport information

On-site spent nuclear fuel transports were implemented 6 times from Hanul unit 1 to unit 5 using KN-12 package carrying 12 WH type fuel assemblies each time and showed 1.09 man-mSv as 4 vehicle crew workers' whole exposure dose. The distance and vehicle velocity between Hanul unit 1 and unit 2 is approximately 1km, 8km/h respectively.

2.3 Assumptions for risk assessment

This paper was designed to assess the radiological transport risk due to transport distance, population density and fraction of effective dose that is gamma ratio respectively. 6 link modes of INTERTRAN2 code with different population density and transport distance were used as shown in Table 1. For the purpose of accident risk assessment as well as normal risk assessment, the accident rate and severity of the code default were used due to the fact that there were lack of data in domestic transport record. In addition, the shielding index was used as urban region, and the vehicle mode was exclusive use.

Table 1. Risk assessment scenario

Link mode	Population Density	Distance
Link 1	1,000 /km^2	1 km
Link 2	2,000/km^2	1 km
Link 3	3,000/km^2	1 km
Link 4	1,000/km^2	2 km
Link 5	2,000/km^2	2 km
Link 6	3,000/km^2	2 km

3. Transport risk assessment

Spent fuel on-site transport risk assessment was conducted for the normal and accident transport.

3.1 Normal transport risk

During the spent fuel transport, the exposure doses of interest are the 4 vehicle crew and the public being in the transport route as on-link and the public in the vicinity of transport route as off-link. As shown in Table 2, as growing the population density, the off-link doses were linearly increased, but the vehicle crew doses and on-link doses were constant. Table 2 also shows when the transport distance is longer, both on-link and off-link doses were linearly increasing.

As shown in Table 3, as the gamma ratio was decreased, off-link and on-link doses were slightly increased.

Table 2. Normal transport risk due to scenarios (man-Sv)

Link	Crew	Off-link	On-link	Totals
Link 1	1.01E-05	3.14E-06	9.74E-08	1.33E-05
Link 2	1.01E-05	6.29E-06	9.74E-08	1.65E-05
Link 3	1.01E-05	9.43E-06	9.74E-08	1.96E-05
Link 4	2.02E-05	6.29E-06	1.95E-07	2.66E-05
Link 5	2.02E-05	1.26E-05	1.95E-07	3.29E-05
Link 6	2.02E-05	1.89E-05	1.95E-07	3.92E-05

Table 3. Normal transport risk of gamma ratio (man-Sv)

γ ratio	Crew	Off-link	On-link	Totals
1.00	9.07E-05	5.66E-05	8.76E-07	1.48E-04
0.75	9.07E-05	5.86E-05	8.96E-07	1.50E-04
0.50	9.07E-05	6.07E-05	9.16E-07	1.52E-04
0.25	9.07E-05	6.27E-05	9.36E-07	1.54E-04
0.00	9.07E-05	6.48E-05	9.55E-07	1.56E-04

3.2 Accident transport risk

As shown in Table 4, various exposure pathways such as ground, inhaled, resuspended, cloudshine were linearly increased as the population density were increased.

Table 4. Accident transport risk due to population density

Link	Ground	Inhaled	Resuspd	cloudsh	Totals
Link 1	1.06E-11	4.19E-15	1.71E-14	1.91E-16	1.06E-11
Link 2	2.12E-11	8.37E-15	3.42E-14	3.81E-16	2.12E-11
Link 3	3.18E-11	1.26E-15	5.12E-14	5.72E-16	3.19E-11

4. Conclusion

On-site spent fuel transport risk assessment based on Hanul transport data and KN-12 package was performed using INTERTRAN2. Also sensitivity analysis on major variables such as population density, transport distance, gamma ratio affecting crew, on-link and off-link was conducted. Although the crew doses between the INTERTRAN2 and transport experience in Hanul plants were a lot different, both results were far below the regulatory dose limit related to the transport. In addition, the difference could be the reasons that the default data of the code was not representative of domestic conditions and the code was originally for the off-site transport risk tool.

REFERENCES

[1] A-M Ericsson, AMC Consult AB, INTERTRAN2 Transportation Risk Assessment Package User's Guide (2000).

[2] KHNP, Hanul unit 1, Spent fuel transport investigation report (2018).

Comparison of Atmospheric Dispersion Factors According to the Collection Period of Meteorological Data for Decommissioning of Nuclear Power Plants

Seung-Hee Lee[1], Won-Tae Hwang[2], and Chang-Lak Kim[1,*]

[1] KEPCO International Nuclear Graduate School, 658-91, Haemaji-ro, Seosaeng-myeon, Ulju-gun, Ulsan, Republic of Korea

[2] Korea Atomic Energy Research Institute, 111, Daedeok-daero 989beon-gil, Yuseong-gu, Daejeon, Republic of Korea

[*] clkim@kings.ac.kr

1. Introduction

During the decommissioning process, the management of radioactive effluents is very important task. It is necessary to protect the resident and environment from the radiation hazards.

The radioactive effluents released to the environment are dispersed depending on the surrounding meteorological conditions. For the accurate evaluation of off-site radiological dose, it is the first step to predict the atmospheric dispersion factor.

IAEA recommends at least three to five years of meteorological data collection for the assessment for the safety of decommissioning site [1]. It is necessary to evaluate how different the atmospheric dispersion factors are over the collection period of meteorological data.

In this study, comparison of atmospheric dispersion factors according to the collection period of meteorological data is performed.

2. Atmospheric Dispersion

2.1 Methods for Calculation of Atmospheric Dispersion Factors

A computer code XOQDOQ [2] has been developed to evaluate atmospheric dispersion in a routine release of radioactive effluents according to methodology recommended in the U.S. NRC's Regulatory Guide 1.111 [3].

A straight-line Gaussian plume model has been adopted to calculate annual averaged atmospheric dispersion factor (χ/Q, sec/m^3), which represents a dispersion capability of radioactive effluents released to the environment.

2.2 Meteorological Data

Joint frequency distribution (JFD) is a statistical data representing occurrence probability as function of wind speed and wind direction according to atmospheric stability.

We used two different period of meteorological data measured at a 10 meter height of a meteorological tower in Kori nuclear power plant site. One is the 3 years period from 2008 to 2010. The collection rate of meteorological data during this period is 97.35%. The other is the 5 years period from 2006 to 2010. The collection rate of meteorological data during this period is 94.91%. The occurrence probability of stability class for each period is shown in Table 1.

Table 1. Occurrence Probability of Stability Class (Unit: %)

Stability Class	A	B	C	D	E	F	G
3 years	20.64	3.18	3.44	22.57	34.28	12.97	2.93
5 years	18.59	2.86	3.03	20.67	37.61	14.04	3.20

And the occurrence probability of wind direction for each period is shown in Table 2. The greatest occurrence probability of wind

direction was the same in the NNW direction.

Table 2. Occurrence Probability of Wind Direction (Unit: %)

Wind Direction	N	NNE	NE	ENE	E	ESE	SE	SSE
3 years	9.85	4.99	4.91	4.61	4.02	3.67	2.69	2.72
5 years	7.43	4.21	3.74	3.78	3.76	4.47	4.07	4.54
Wind Direction	S	SSW	SW	WSW	W	WNW	NW	NNW
3 years	3.81	5.35	7.89	7.37	6.71	6.57	6.56	12.05
5 years	4.61	5.48	7.74	9.16	8.70	6.33	6.25	10.09

2.3 Comparison of Atmospheric Dispersion Factors

The evaluation areas are Exclusion Area Boundary (EAB) of 16 directions, a 700 meter radius. The maximum atmospheric dispersion factor was 4.56×10^{-5} (sec/m^3) during 3 years period and 4.74×10^{-5} (sec/m^3) during 5 years period. They were both in the ENE direction, as shown in Table 3. As a result of comparing the atmospheric dispersion factors, the difference was about 4%.

Table 3. Results of Atmospheric Dispersion Factors

Downwind Direction	3 years (A) (χ/Q, sec/m^3)	5 years (B) (χ/Q, sec/m^3)	Ratio (A / B)
ENE	4.56×10^{-5}	4.74×10^{-5}	0.96

3. Conclusions

According to the collection period of meteorological data, we compared the results of the atmospheric dispersion factors for decommissioning of nuclear power plants using XOQDOQ computer code.

The direction of maximum atmospheric dispersion factor is the same and the results were almost the same at 4% difference.

Considering the time and effort of collecting and analyzing meteorological data, an appropriate evaluation period need to be established. These results were based on the meteorological data in Kori nuclear power plant site. It should be kept in mind that the results might be different according to the site.

Acknowledgement

This research was supported by the Nuclear Safety Research Program through the Korea Foundation of Nuclear Safety (KOFONS), granted financial resources from the Nuclear Safety and Security Commission (NSSC), Republic of Korea (No. 1605008).

REFERENCES

[1] International Atomic Energy Agency, Prospective Radiological Environmental Impact Assessment for Facilities and Activities, IAEA Safety Standards, General Safety Guide No. GSG-10 (2018).

[2] U. S. Nuclear Regulatory Commission, XOQDOQ: Computer Program for the Meteorological Evaluation of Routine Release at Nuclear Power Stations, NUREG/CR-2919 (1982).

[3] U. S. Nuclear Regulatory Commission, Methods for Estimating Atmospheric Transport and Dispersion of Gaseous Effluents in Routine Releases from Light Water Cooled Reactors, Regulatory Guide 1.111 (1977).

Geochemical Factors Influencing the Radon Content in Groundwater

Jaeeun Kang*, Jinmo Ahn, and Wooyong Um
Pohang University of Science and Technology, 77, Cheongam-ro, Nam-gu, Pohang-si, Gyeongsangbuk-do, Republic of Korea
*jenny94@postech.ac.kr

1. Introduction

Radon is a naturally occurring and odorless gas, classified as a Class 1 carcinogen radionuclide [1]. It penetrates homes from the crushed rocks and minerals containing ^{238}U and ^{232}Th. Besides, radon released from uranium and thorium-containing minerals through the fractured rocks or cracks can be easily dissolved in groundwater. Its decay products are gaseous radionuclides such as ^{222}Rn, ^{219}Rn, and ^{220}Rn. Among them, ^{222}Rn, which has the longest half-life (3.82 days), is commonly known to radon. The actual risk of radon is mostly due to the radon's daughter species rather than the radon. Because radon exists as an inert gas, it can deposit in the lungs when inhaled into the body, causing lung cancer.

Although the radon transport in the air has been discussed a lot [2], the fundamental study on the radon species in groundwater is barley conducted. Therefore, it is a prerequisite to know which geochemical factors are involved in radon concentration or content in groundwater. In this paper, we analyzed the behavior of radon by the redundancy analysis with major components in groundwater to investigate of correlation between radon content and other geochemical factors in groundwater.

2. Materials and Methods

2.1 Analyzed data

The Icheon area is composed of granite in geology. For 63 groundwater samples [3], radon was analyzed using liquid scintillation counter (LSC) and major components of groundwater, including uranium, were analyzed by Korea Institute of Geoscience and Mineral Resources (KIGAM) using ICP-AES.

2.2 Statistical analysis

Nonmetric multi-dimensional scaling (NMDS) and redundancy analysis (RDA) performed by the Canoco 5 program predicts the variance that maximizes redundancy between a series of variables given two or more groups of variables. In particular, it is used to quantify the changes in responses for predictors (radon radioactivity, Eh, and EC). The direction of the graph is indicated by the arrow, and the longer the arrow is, the stronger the influence on the dispersion of the predictors is. In addition, the smaller is the angle of the two arrows, the greater is the positive correlation.

3. Results and Discussion

3.1 NMDS Analysis

NMDS analysis shows a similar cluster of data based on a series of variables. In Fig. 1, the distribution is represented by considering 17 variables based on wells collected for 63

groundwater samples. In particular, the data of 24 shows that the concentration of radon is very low, 40pCi/L, while 45 data shows the highest radon concentration, 23,400pCi/L.

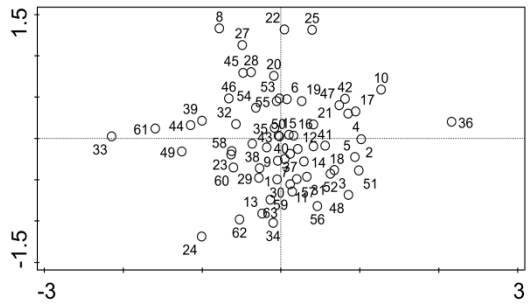

Fig. 1. NMDS distribution of 63 groundwater samples in Icheon area.

3.2 Correlation with radon

There was a positive correlation between radon and fluorine concentrations [4] whereas other main components of groundwater did not influence the radon content in groundwater (Fig. 2). Besides, Eh, nitrate, and silica are weakly correlated with radon concentration in groundwater. Although Radon is known to form solid compound (RnF_2) with fluoride, such compound can be easily decomposed. Therefore, aqueous fluorine species (or high F^- concentration) may have influenced the hold up of radon in groundwater, which makes more (or longer) radon can exist in aqueous phase.

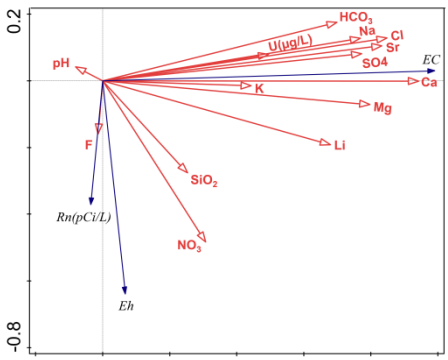

Fig. 2. RDA of radon and major components of groundwater.

4. Conclusion

The correlation between the presence of ^{222}Rn in groundwater and other groundwater components was investigated using 63 groundwater samples. Redundancy analysis showed that fluorine and radon showed a relatively strong correlation than other components including uranium. Because radon forms a strong complexation with fluorine, the higher fluorine concentration is the more radon concentration found in groundwater. The results of this analysis can be used as basic data to increase our understanding of the Henry's law constant for radon (K_H) in various groundwater conditions.

REFERENCES

[1] IARC, Monographs on the Evaluation of Carcinogenic Risks to Humans, vol. 100D, Radiation, ISBN 978 92 832 1321 5 (2012).

[2] Williams A, Chambers S, Conen F et al, "Radon as a tracer of atmospheric influences on traffic-related air pollution in a small inland city", Chemical and Physical Meterology, 68(1) (2016).

[3] Cho B, Choo C, Kim M et al, "Uranium and Radon Concentrations in Groundwater near the Icheon Granite", The Journal of Engineering Geology, 21(3), 259-269 (2011).

[4] Salih I, Bäckström M, Karlsson S et al, "Impact of fluoride and other aquatic parameters on radon concentration in natural waters", Applied Radiation and Isotopes, 60(1), 904 (2004).

$DCGL_{EMC}$ According to the Variation of Baseline Area in Kori Unit 1

Jihyang Byon, Sangjune Park, and Seokyoung Ahn*

Pusan National University, 2, Busandaehak-ro 63beon-gil, Geumjeong-gu, Busan, Republic of Korea

*sahn@pusan.ac.kr

1. Introduction

According to the Multi-Agency Radiation Site Survey and Investigation Manual (MARSSIM), Derived Concentration Guideline Level (DCGL) can be a criterion for confirming and determining decontamination activity according to the degree of pollution. For elevated residual radioactivity, an assessment is required to monitor decontamination levels, particularly in remedial action support survey for final status survey, which may limit activities. Therefore, $DCGL_{EMC}$, which were derived to evaluate the class 1, a small local area exceeding $DCGL_W$. As $DCGL_W$ was newly derived by realistic preliminary baseline area to derive $DCGL_{EMC}$. Additionally, it was compared to value which derived based on the default contaminated area.

2. Area factor and $DCGL_{EMC}$

The area affected by the residual radioactivity concentration that exceeds $DCGL_W$ is classified as Class 1, the area expected not to exceed $DCGL_W$ as Class 2, and the area expected to be much lower than $DCGL_W$ as Class 3 [1]. $DCGL_{EMC}$ is a guideline value that applies to an area where there is a locally elevated residual radioactivity in a small area to be measured. In other words, it is a site release standard concentration applicable to hot spot area, Class 1. The use of EMC is a conservative approach in that all measurements must be below the action level and the level of investigation for this comparison is $DCGL_{EMC}$.

As the DCGLEMC is derived by applying an area factor to DCGLW, RESRAD (RESidual RADioactivity)-ONSITE code was executed using site-specific radionuclides and parameters previously applied to the DCGL study. Potential radionuclides of the Kori Unit 1 were selected by combining the methodologies used in Rancho Seco and Zion NPP. Firstly, a suite of theoretical radionuclides with a half-life of more than two years is determined through the related documents, then site-specific radionuclides for soil are selected through the preceding characterization surveys. Since the characterization survey of Kori Unit 1 has just started, there is not enough information about radionuclides that can be directly applied to soil of the site. Therefore, concerned radionuclides for soil at Kori Unit 1 were preliminary selected as ^{14}C, ^{60}Co, ^{134}Cs, ^{137}Cs, ^{63}Ni, ^{90}Sr in the same manner as Rancho Seco NPP, which was confirmed as the same radionuclides as Zion NPP except ^{14}C. The preliminary security protected area of the Kori Unit 1 was designated as the full source term area of Kori Unit 1 was designated as 39,000 m^2 including Unit 2 referering to the case of SONGS (San Onofre Nuclear Generating Station) and Zion NPP in which neighboring unit exists.

3. $DCGL_{EMC}$ difference with baseline area variation

In general, the calculation using the maximum area of Class 2 proposed by MARSSIM, 10,000 m^2, is used to derive the initial basic DCGL [1]. Referring to SONGS and Zion NPP cases, Kori-site has been designated as a preliminary security protected area, the baseline area of 39,000 m^2 including adjacent unit. This is an area containing two units, Kori Unit 1 and Unit 2, but a fairly reduced area value, which can be changed by considering the reuse purpose of the Kori-site and the operation schedule of the remainder units and consideration of the common facilities. Figure 1 and Figure 2 show the $DCGL_W$ and $DCGL_{EMC}$ values applied with area factors as a result of changes in the baseline contamination area based on the regulatory guide provided by Korean regulatory body of 0.1 mSv/yr. The first vertical line of the both pictures is the newly derived $DCGL_W$ for 39,000 m^2 of the site-specific area of Kori Site and the second line is the $DCGL_W$ value derived from the preliminary 10,000 m^2 area, which assumed as single area of Kori Unit 1 in the previous study [2]. From the third line, it is $DCGL_{EMC}$ values obtained by applying the area factor of industrial worker scenario in Table 1 to the $DCGL_W$ value based

on these two baseline areas, that is, by adjusting the contamination area to be small.

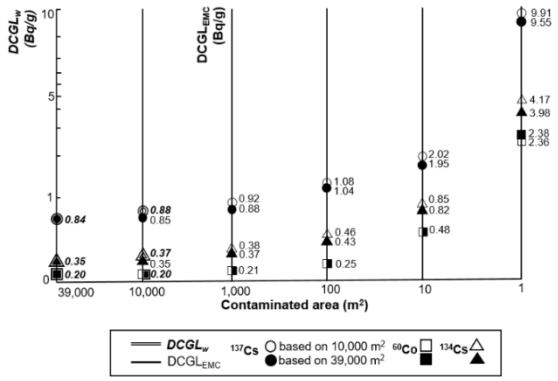

Fig. 1. $DCGL_{EMC}$ of gamma emitters.

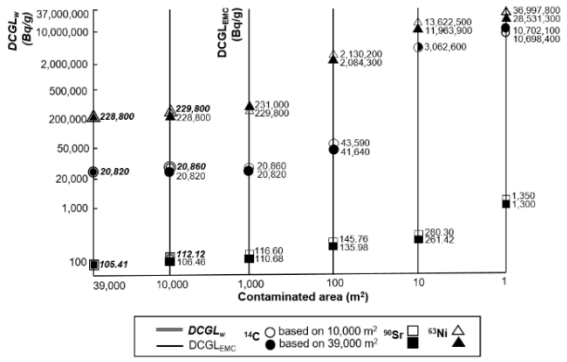

Fig. 2. $DCGL_{EMC}$ of beta emitters.

As the baseline area changed from default 10,000 m^2 to 39,000 m^2 in Figure 1, the $DCGL_W$ of ^{134}Cs showed the maximum difference and decreased by about 5%, showing a conservative value. $DCGL_{EMC}$ at 1 m^2 in the minimum contaminated area also showed the same maximum difference of about 5% at ^{134}Cs. For the beta emitters in Figure 2, the maximum difference of $DCGL_W$ when the baseline area was changed from 10,000 m^2 to 39,000 m^2 was ^{90}Sr, which reduced about 6%. The $DCGL_W$ of ^{14}C and ^{63}Ni decreased to less than 1% and showed a smaller change rate than the gamma emitters. Radionuclides that are relatively affected by baseline area setting in $DCGL_W$ derivation were found to be ^{134}Cs, ^{137}Cs in the gamma emitters and ^{90}Sr in the beta emitters. However, with the baseline area set to 39,000 m^2, the $DCGL_W$ of all radionuclides shows a slight change rate of within 6%, it is judged that the change in baseline area of the difference between 10,000 m^2 and 39,000 m^2 in the industrial worker scenario has little effect on $DCGL_W$. Gamma emitters showed the same rate of change of $DCGL_{EMC}$ with baseline area setting for almost all contaminated areas, but beta emitters showed different tendencies of $DCGL_{EMC}$ depending on their radionuclides as the contaminated area decreased. Based on 1 m^2 of contaminated area, ^{63}Ni showed about 23% decrease and showed the maximum difference among all radionuclides. When changing the baseline area from 10,000 m^2 to 39,000 m^2, $DCGL_{EMC}$ of ^{63}Ni showed a maximum reduction rate of 2.2% in the increased contaminated area including 100 m^2 and 28% in the contaminated area less than 10 m^2. The tendency is different from ^{90}Sr, where the change rate of $DCGL_{EMC}$ in all contaminated areas along the baseline area is similar.

4. Conclusion

Based on the most realistic scenario, the industrial worker scenario, the baseline areas reflecting the default area which was applied in the previous study for Kori Unit 1 and the site-specific area were considered and the $DCGL_{EMC}$ was derived respectively. With reference to the case of NPP with adjacent units, the site of Kori Unit 1 was set as a protected area including Unit 2. In industrial worker scenario, baseline area changes between 10,000 m^2 and 39,000 m^2 have had little impact on the $DCGL_W$ of all considered radionuclides. However, for beta emitters, different trends in small contaminated areas were identified for each radionuclide. Compared to gamma emitters, which feature highly conservative area factors and DCGLs, beta emitters are thought to be DCGL tunable by modifying area and scenario pathways.

ACKNOWLEDGEMENT

This work was was supported by the National Research Foundation of Korea grant funded by the Korea government [No. NRF-2018M2B2B1065637]; and was supported by the nuclear research and development program through the National Research Foundation of Korea funded by the Ministry of Science and ICT (MSIT, Korea). [NRF-2019M2C9A1057807].

REFERENCES

[1] NRC, EPA, DOD, DOE, “Multi-Agency Radiation Survey and Site Investigation Manual (MARSSIM)”, 2000.

[2] J. Byon, S. Park, S. Ahn, “Preliminary Surface Soil Derived Concentration Guideline Levels Derivation for Kori Unit 1 by RESRAD probabilistic analysis”, Nuclear Engineering and Technology (2018).

Study on Radiological Dose Assessment With Surface & Subsurface Layers Using RESRAD-ONSITE

Kun-Su Lim*, Sun-Kee Lee, and Chang-Lak Kim**
KEPCO International Nuclear Graduate School, 658-91, Haemaji-ro, Seosaeng-myeon, Ulju-gun, Ulsan, Republic of Korea
*etetet2005@naver.com, **clkim@kings.ac.kr

1. Introduction and Background

For the decommissioning of domestic nuclear power plants, nuclear operators and regulators should consider radiological safety through preliminary evaluation and simulation before decommissioning.

RESRAD-ONSITE code presents a methodology for deriving and calculating average values for inhomogeneous contamination when considering site contamination [1]. This paper is to check the possibility of this code for wider applications for inhomogeneous contaminations.

2. Evaluation According to Contamination Depth of RESRAD-ONSITE

2.1 Evaluation Methodology

By applying the same internal values for the other conditions of the contaminated site, we focused on comparing the difference between the sum of the calculations according to the depth and the value of the whole depth. The evaluation period used 0, 1, 5, 10, 25, 50, 75 and 100 years. The radionuclides to be evaluated were selected as ^{60}Co, which has little diffusion by water, and ^{3}H, which is easy to diffuse into deep soils and water. The depth of the site was evaluated using MARSSIM methodology [2] that surface layer and subsurface layer. And we made schematics as figure 1.

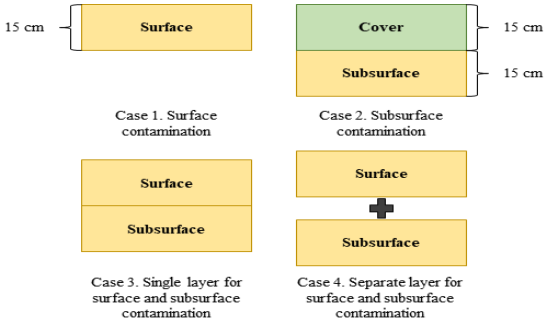

Fig. 1. Schematics of Evaluation Methods.

2.2 Evaluation Results

The sum of separated layer calculation for surface and subsurface contamination is similar to the calculation result of single layer calculation, as shown in Fig. 2. For ^{60}Co and in Fig. 3. for ^{3}H.

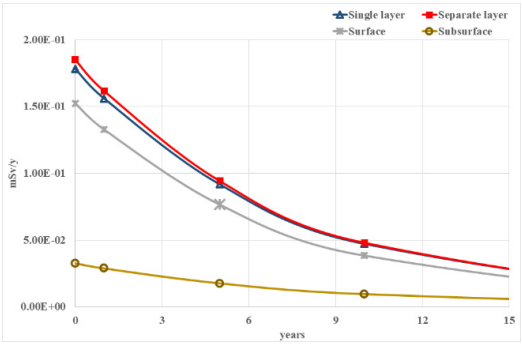

Fig. 2. Results of Each Case Calculation for ^{60}Co.

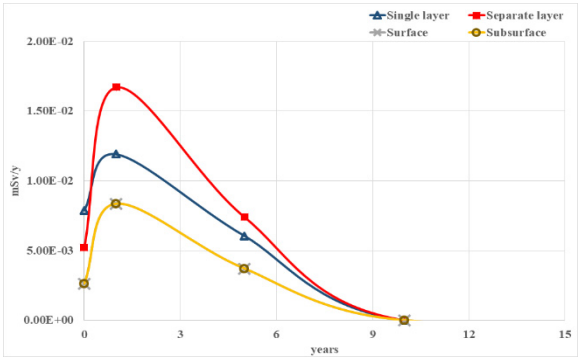

Fig. 3. Results of Each Case Calculation for ^{3}H.

2.3 Sensitivity Analysis

We checked the difference between calculating single layer and summing both separated layers from the previous calculations, we found that this difference is large in nuclide ^{3}H moving by water. We calculated for the inhomogeneous contamination using sensitivity analysis. So, we calculated different concentration situation for ^{60}Co as shown in Fig. 4, Fig. 5.

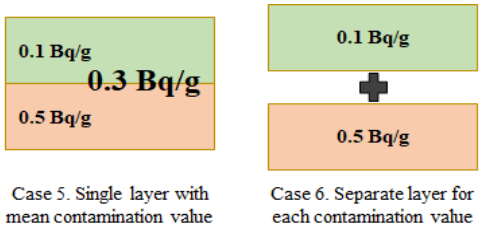

Fig. 4. Schematics.

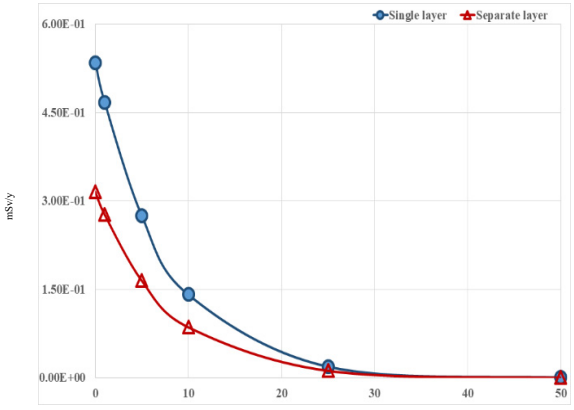

Fig. 5. Results of Sensitivity Analysis.

3. Conclusion

The difference shown in Fig. 5. can be due to the effect of shielding on the subsurface calculation.

If the lower layer contaminated greater than upper layer for nuclide without mobility such as ^{60}Co, it is considered that the sum of separate layers considering the shielding effect may be appropriate than the arithmetic mean concentration in single layer.

Acknowledgements

This research was supported by the Nuclear Safety Research Program through the Korea Foundation of Nuclear Safety (KOFONS), granted financial resource from the Nuclear Safety and Security Commission (NSSC), Republic of Korea (No.1605008).

REFERENCES

[1] C. Yu et al, “User’s Guide for RESRAD Code Version 7.2”, ANL/EVS/ TM-18/1 (2018).

[2] U.S. Nuclear Regulatory Commission, “Multi-Agency Radiation Survey and Site Investigation Manual”, NUREG-1575, Rev.1 (2000).

[3] Nuclear Safety and Security Commission, “Regulation on Classification of Radioactive Waste and Clearance Standards”, NSSC Notice No. 2017-65 (December 26, 2017), Republic of Korea.

Radiation Measurement Uncertainty for Radiological Evaluation of Simulated Radwaste

Ke Chon Choi*, Chang Heon Lee, Se Chul Sohn, Seung Su Shin, Pu reun Kim, and Seung Min You
Nuclear Decommissioning Research Institute, 20-13, Yulliyeonghae 2-gil, Cheongnyang-eup,
Ulju-gun, Ulsan, Republic of Korea
*c4016ck@naver.com

1. Introduction

The reliability of the chemical measurement results should be included in the measurement results as a quantitative expression of uncertainty existing in the stage of chemical measurement, but the chemical related fields are not realized as difficulties in application, and the importance is newly highlighted. Recently, reliable data for radionuclides among nuclear decommissioning wastes are required as a process of evaluating radiological characteristics for safe decommissioning of permanent shutdown nuclear plants.

The separation and quantitative analysis of spent nuclear fuel and radioactive nuclides contained in waste water, including the decommissioning wastes of permanent shutdown nuclear plants, are very difficult and complicated, and sometimes different analysis results are derived depending on the analysts. It is necessary to secure the reliability of the results by setting the suspicious section as a numerical value in these different analysis results. The reason why the calculation of measurement uncertainty is important is not only the confirmation of the confidence interval of the measurement value for the true value, but also the calculation of measurement uncertainty is necessary for determining whether to pass or not in the performance test of the product or for determining the allowable range.

2. Experimental

2.1 Calculation

$$A = \frac{CPM(S) - CPM(b)}{60 \times \varepsilon \times W \times F} = \frac{CPM'(S)}{60 \times \varepsilon \times W \times F}$$

A; Radiation dose of I-129 in radioactive waste, dpm / g

CPM (s); ^{129}I measured value in nuclear waste balance, cpm

CPM (b); ^{129}I measured value in blank sample, cpm

CPM '(s); Ipm minus background value, cpm

ε; Radiation measurement efficiency

W; Weight of sample g

F; Recovery Rate in AgI / KI

3. Discussion

3.1 Sample pretreatment step relative uncertainty, U(w)

$$u(W) = \sqrt{2 \times u(S(A))^2 + u(S(B))^2}$$
$$= \sqrt{2 \times (2.33 \times 10^{-5})^2 + (5.1 \times 10^{-5})^2} = 6.07 \times 10^{-5}$$

W = 2.017 g,

$$U(W) = \frac{u(W)}{W}(\%), = \frac{6.07 \times 10^{-5}}{2.017} \times 100 = 0.030\%$$

3.2 Standard sample recovery rate measurement step relative uncertainty, U(F)

$$F = \frac{WI(AgI)}{WI(KI)}, \quad = \quad \frac{0.009508}{0.004956} = 1.918$$

$$U(F) = \frac{u(F)}{F} \times 100 = \frac{0.0101}{1.918} \times 100 = 0.53\%$$

$$u(F) = F \times \sqrt{\left(\frac{u(WI(AgI)}{WI(AgI)}\right)^2 + \left(\frac{u(WI(KI)}{WI(KI)}\right)^2}$$

$$= 1.918 \times \sqrt{\left(\frac{0.0328)}{0.00950}\right)^2 + \left(\frac{0.0198}{0.004956}\right)^2} = 0.0101$$

3.3 Radiation dose rate measurement step relative uncertainty, U(ε)

$$\varepsilon = -0.00104 \times W(AgI) + 0.05397$$
$$= -0.00104 \times 17.59 + 0.05397$$
$$= 0.03567$$

$$CPM'(s) = CPM - CPM = 1.99 - 1.01 = 0.97$$

3.4 Extended uncertainty, U(A)

$$A = \frac{CPM'(s)}{60 \times W \times \varepsilon \times F}, = \frac{0.976}{60 \times 2.017 \times 0.03567 \times 1.918}$$

$$= 0.118 \text{ Bq/g}$$

$$\left(\frac{u(A)}{A}\right)^2 = \left[\frac{u(W)}{W}\right]^2 + \left[\frac{u(\varepsilon(}{\varepsilon}\right]^2 + \left[\frac{u(CPM')}{CPM'}\right]^2 + \left[\frac{u(F)}{F}\right]^2$$

$$= \left[\frac{6.0 \times 10^{-5}}{2.017}\right]^2 + \left[\frac{0.150}{0.976}\right]^2 + \left[\frac{0.00277}{0.03567}\right]^2 + \left[\frac{0.0010}{1.918}\right]^2$$

$$= 0.02967 \text{ Bq/g}$$

$$u(A) = A \times \sqrt{0.02967} = 0.118 \times \sqrt{0.02967} = 0.0203 \text{ Bq/g}$$

$$U(A)(\sigma) \equiv \frac{u(A)}{A}(\%), = \frac{0.0203}{0.118} \times 100 = 17.27\%$$

$$U(A) = 2 \times \frac{u(A)}{A}(\%) = 2 \times 0.1727 \times 100$$

$$= 34.4\%$$

4. Conclusion

To calculate the uncertainty of the separation and quantitative analysis of I-129 for radioactive waste, the relative uncertainty of each step was measured by dividing it into pre-treatment stage, radioactivity measurement stage, and recovery stage of standard additives. In the measurement stage, type A and type B uncertainty were calculated and the standard composite relative uncertainty and the extended standard relative uncertainty were evaluated using the error wave formula. The relative uncertainty of the extended standard of I-129 in radwaste was 34.40 % from 0.118 Bq/g detection and the relative uncertainty of measurement efficiency was the most influential factor on the relative uncertainty of standard synthesis.

REFERENCE

[1] Multi-Agency Radiological Laboratory Analytical Protocols Manual (MARLAP), V1, 3-29, NUREG-1576 EPA 402-B-04-001A NTIS PB 2004-105421.

[2] Multi-Agency Radiation Survey and Site Investigation Manual (MARSSIM), 6-49, NUREG-1575, Rev. 1 EPA 402-R-97-016, v. 1 DOE/EH-0624, Rev. 1.

[3] INTERNATIONAL ATOMIC ENERGY AGENCY, Treatment of Low- and Intermediate-Level Solid Radioactive Wastes, Technical Reports Series No. 223, IAEA, Vienna (1983).

7분과

방사화학 (Oral)

Applicable Chemical/Biological Technologies to the Removal and Isolation of Radionuclides From the Nuclear Decommissioning Wastewaters and Soils

Seung Yeop Lee*, Hyo Jin Seo, Hee Jae Ju, and Jae Kwang Lee
Korea Atomic Energy Research Institute, 111, Daedeok-daero 989beon-gil, Yuseong-gu, Daejeon, Republic of Korea
*seungylee@kaeri.re.kr

1. Introduction

Many environmental technologies to remove and isolate the radionuclides occurring from the decommissioning of nuclear power plant are largely developed by many scientists. Among them, we are particularly interested in the ones to treat radio-toxic and long half-live radionuclides such as iodine, cesium, and uranium.

Iodine generally exists as anionic (e.g., I^-) molecular (I_2), and organic (e.g., CH_3I) forms according to specific conditions. Their forms are affected by redox conditions. For example, the anionic form of I^- would be a dominant specie in a solution, if it is dissolved under anaerobic condition. Iodide (I^-) is soluble and mobile in water, so it is very difficult to capture and precipitate it with common adsorbents.

Until now, various exchanger and getter materials have been developed to capture radioactive iodine in wastewater. The materials developed generally showed a good performance under acidic conditions. However, the adsorption amounts were not relatively large in neutral and high pH conditions. Furthermore, the capacity to capture iodine is limited by their properties, such as the specific surface area and adsorbing affinity.

For radioactive Cs-137, various exchanger and getter materials have been also developed to uptake radioactive cesium from wastewaters. The adsorbent materials that have been developed usually showed a nice performance under fresh water conditions. However, the adsorption amounts were not large in seawater conditions. Furthermore, the cost to synthesize the adsorbents was high and their final waste volumes were not small.

Our new method that is proposed here offer great cost cutting by using bacteria or cheaper chemical reagents. This method is to crystallize soluble radionuclides into specific solid matters through chemical or biochemical processes. Their selectivity for target radionuclides are relatively high and thus radioactive waste could decrease to a very small volume.

2. Methods & results

2.1 Methods

To study the selective uptake of iodide from anion-rich water, some common anions such as Cl^-, HCO_3^-, and SO_4^{2-} were previously dissolved in distilled water in serum bottles. The anions are common in natural waters, and their concentrations injected were mM levels as chemicals of NaCl, $NaHCO_3$, and Na_2SO_4. Iodide was injected as NaI from a stock solution (100 mM). To study a potential binder for mobile iodide, copper was injected as $Cu(NO_3)$. The overall solution pH was around 7.3.

The SRB (sulfate reducing bacteria) isolated from natural bentonite or groundwater [1] were used in our experiment. To study the selective cesium removal and biomineralization from some cation-rich fresh or seawaters, we anaerobically prepared various solutions in serum bottles. From the cesium stock solution, 0.01-10 ppm of cesium were aseptically injected into the serum bottles containing other components, such as SO_4^{2-}, which was used as a basic chemical to biologically form "pautovite ($CsFe_2S_3$)", a cesium-mineral.

2.2 Removal of Aqueous Radionuclides

Copper was precipitated as copper carbonate, malachite ($Cu_2CO_3(OH)_2$), in the early stage. Most copper that was injected in water was initially combined with carbonate species forming low-crystalline malachite with spherical forms (Fig. 1). The malachite was very interactive with iodide. In particular, when sulfate was present in the media, the malachite

was gradually transformed into a cuprous form that incorporates iodide ions. The cuprous iodide (CuI) was crystallized as a halide mineral that is nearly insoluble. Iodide was removed along with copper in the experiment (Fig. 2). Most iodide was removed within a day and then slowly decreased from the anion-rich solution. Other anions such as Cl^- did not interfere with the iodide removal. Iodide was selective among anions by freely combining with copper. The merit of our system is to strongly restrict the mobilization of volatile iodide by transforming the mobile phase into an immobile phase of crystal. The crystal phase of iodide may be insoluble in nature, further ensuring its long-term stability.

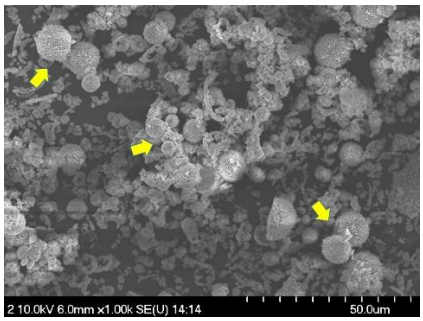

Fig. 1. SEM image of malachite particles (arrows) with a microscale spherical form.

In our biological experiment in a freshwater, about 95% of cesium was removed from the solution in a condition of Cs 0.1 ppm (Fig. 3). In 0.01 ppm concentration, most of cesium (nearly 100%) was removed from the solution after 1 day of the reaction. This result shows that our method is very effective to remove cesium compared with other previous technologies. This way has an additional advantage to produce a very small waste volume that is less than 0.1 g/l.

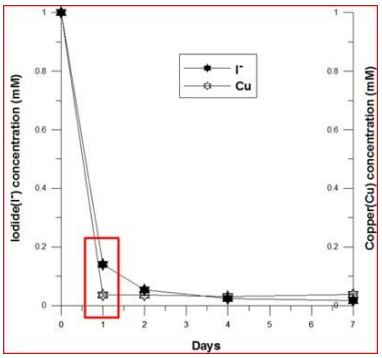

Fig. 2. Decline of aqueous iodide concentration along with copper (Cu^{2+}) in the presence of malachite precursor that was initially generated in the media.

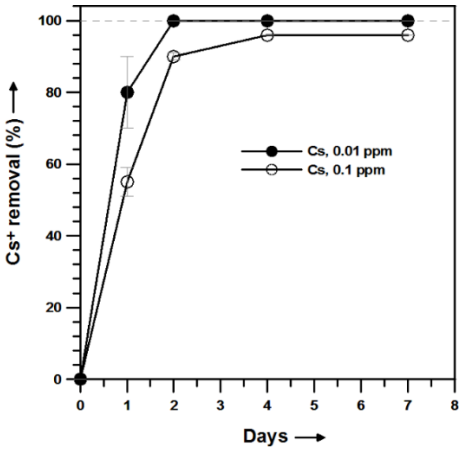

Fig. 3. Characteristic cesium removal patterns for Cs-containing freshwaters by microbial cesium biomineralization.

3. Conclusion

Radioactive isotopes such as iodide can be characterized as volatile and mobile species that are difficult to capture by adsorbents. In our study, we developed a new way to uptake and crystallize the mobile iodide as cuprous iodide (CuI). In addition, with our biotechnology, we overcame the problems of previous adsorption technology by using natural bacteria, by which soluble cesium can be easily transformed into a stable and solid matter with a compact volume even in seawater conditions.

Acknowledgement

This research was supported by National Research Foundation of Korea (NRF) funded by the Ministry of Science, ICT and Future Planning (The nuclear research and development program No. 2017M2A8A5014859).

REFERENCES

[1] J.M. Oh, S.Y. Lee, M.H. Baik, and Y. Roh, “Characterization of uranium removal and mineralization by bacteria in deep underground, Korea Atomic Energy Research Institute (KAERI)”, Journal of Mineralogical Society of Korea, 23(2), 107-115 (2010).

Chemisorption of Organic Iodides in a Metal-Organic Framework

Jinhee Park* and Byeongchan Lee
Daegu Gyeongbuk Institute of Science and Technology, 333, Techno jungang-daero, Hyeonpung-eup, Dalseong-gun, Daegu, Republic of Korea
*jinhee@dgist.ac.kr

1. Introduction

Because global demand for energy is rapidly rising, the operation of nuclear power plants is now indispensable. After the nuclear accident of Fukushima-Daiichi in 2011, however, the secure sequestration of radioactive wastes has been a critical issue. Among various forms of nuclear wastes, capturing radioactive organic iodide (ROIs) as the one of the important species in a gas phase waste has been challenged owing to the lack of proper sorbent materials. Especially compared to an iodine molecule (I_2), the ROIs exhibit low affinity for the conventional sorbents such as Ag@MOR and triethylenediamine (TED)@AC, resulting in low sorption rates and capacities. The release of the ROIs causes harmful effect into the environment owing to their high volatility; for example, the accumulation of the ROIs in thyroids can induce hypothyroidism or more seriously thyroid cancers.

2. Methods and Results

2.1 Metal-Organic Frameworks

Recently, metal-organic frameworks (MOFs) have been intensively studied as an effective alternative sorbent owing to their high porosities, surface areas, structural designability, and tailorability. Moreover, the well-defined crystalline structures of the MOFs allow in-depth study on the structure-properties relationship. Diverse structural MOFs have been applied for I_2 adsorption, and even the interaction between I_2 and the frameworks have been investigated by analyzing crystalline structures of MOFs. However, a very limited number of MOFs has been studied for ROIs adsorption, and most of them are based on highly reversible physisorption. For the secure sequestration of the volatile ROIs, the development of sorbents capable for chemisorption is highly desirable. However, as mentioned above owing to the relatively low affinity and reactivity of the ROIs, their chemisorption has been rarely reported.

2.2 Iodine Sorption Analysis

Previously, our group demonstrated that I_2 can be chemisorbed in Co_2(*m*-DOBDC) at 70 °C through electrophilic aromatic substitution of *m*-$DOBDC^{4-}$.[1] Consequently, the proton on the electron-rich C5 of m-$DOBDC^{-4}$ is substituted with I and remaining I^- is coordinated on an unsaturated Co^{2+} site. Based on this finding we speculate that ROIs can be adsorbed in Co_2(m-DOBDC) via a similar mechanism at the elevated temperature.

Firstly, the chemisorption of CH_3I, the most reactive ROI, was examined. Co_2(*m*-DOBDC) was synthesized according to the previously reported method and fully activated before the adsorption test. The vial containing the activated MOFs was inserted into the vial charged with CH_3I. The weight change of the MOFs was recorded, and the sorption capacity of CH_3I was calculated as a function of exposure time. Under

the same experimental conditions (e.g., 3 h exposure at 100 °C), Co_2(*m*-DOBDC) exhibited the higher sorption capacity, 120 wt% than Ag@MOR and TED@AC (Figure 1(a)). In fact, this capacity was 1.5 times larger than MIL-101-Cr-TED which has the record high CH_3I capacity among MOFs.[2] In order to prove the chemisorption of CH_3I, CH_3I@Co_2(*m*-DOBDC) was decomposed with HCl and the resulting ligand was analyzed by NMR spectroscopy.

The efficient adsorption of CH_3I prompts us to assess the chemisorption of other ROIs such as C_2H_5I and C_3H_7I. As like CH_3I, the sorption capacities were saturated within 3 h exposure time. However, the substitution of *m*-DOBDC^{4-} with ethyl and propyl groups was retarded due to the relatively low reactivity of C_2H_5I and C_3H_7I. While the conversion ratios for CH_3I and C_2H_5I reached 80% after 30 h and 40 h, respectively, the high steric hinderance of the propyl group significantly lowered the conversion rate as well as the conversion ratio just to 70%.

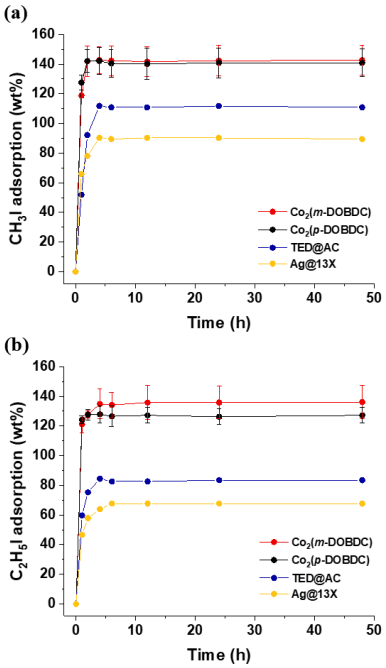

Fig. 1. Adsorption of CH_3I (a) and CH_2H_5I (b) as a function of exposure time.

3. Conclusion

The electron-rich aromatic ring of Co_2(m-DOBDC) along with the unsaturated Co^{2+} sites plays a pivotal role in the chemisorption of the ROI. This approach will pave the way for the application of the MOFs in capturing radioactive nuclides.

REFERENCES

[1] B. Lee, Y.-P. Chen, J. Park.; J. Park, "Visualization of Iodine Chemisorption Facilitated by Aryl C-H Bond Activation" ACS Appl. Mater. Interfaces, 11(29), 25817-25823 (2019).

[2] B. Li, X. Dong, H. Wang, D. Ma, K. Tan, S. Jensen, B. J. Deibert, J. Butler, J. Cure, Z. Shi, T. Thonhauser, Y. J. Chabal, Y. Han, J. Li, “Capture of organic iodides from nuclear waste by metal-organic framework-based molecular traps” Nat. Commun., 8, 485 (2017).

Treatment Technology for Contaminated Water Containing Iodine

Jei-Won Yeon*, TaeJun Kim, and Minsik Kim

Korea Atomic Energy Research Institute, 111, Daedeok-daero 989beon-gil, Yuseong-gu, Daejeon, Republic of Korea

*yeonysy@kaeri.re.kr

1. Introduction

Because iodine can exist as gaseous species I_2, suppressing the volatilization of iodine is an important area in the water treatment field. The most basic method of suppressing volatilization of iodine is to raise the pH of contaminated water over 10 [1]. Above pH 10, iodine (I_2) decomposes into ionic I^- and IO_3^- and loses its volatility. However, in this high pH range, most radioactive metal ions are hydrolyzed and deposited on the surface of the structural material of the water treatment system, thereby reducing mobility of radioactivity. Therefore, a technique is required to reduce the volatility of radioiodine in the appropriate pH range.

In this study, coprecipitation experiments of Cs and Sr with Fe ions were performed based on the properties of H_2O_2 acting a reducing agent for I_2 in a specific pH range. From the results, it was confirmed that volatilization of iodine can be mitigated by pH adjustment, while the coprecipitates of Cs and Sr also minimizes. The technology is expected to be useful for treating contaminated water containing iodine.

2. Experimental

All chemicals, NaI (99.5%), CsCl (99.9%), $SrCl_2$ (99.99%), $FeCl_36H_2O$ (97%), NaOH (97%), HI (57%), and HCl (36.5%) were purchased from Sigma-Aldrich, and all solutions were prepared using deionized water in glass vials with Teflon-lined caps (Milli-Q; resistivity: 18.2 M ohm cm). Before pH measurement, pH meters (827 pH lab, Metrohm; Orion Star A211 pH benchtop meter, Thermo Fisher Scientific) were calibrated with three different buffer solutions.

The three elements Fe, Cs, and Sr were quantitatively analyzed for precipitates formed at each unit pH from 7 to 13 in solutions of $FeCl_3$+CsCl, $FeCl_3$+$SrCl_2$, $FeCl_3$+CsCl +$SrCl_2$, and $FeCl_3$+CsCl+$SrCl_2$+NaI. The pH of each solution was adjusted using a 1 M NaOH solution. The concentrations of $FeCl_3$, CsCl, $SrCl_2$, and NaI were 36, 18, 9, and 9 mM, respectively. Using filter paper (Whatman Grade 541), precipitates were separated from samples that had been maintained as stationary for 1 week (or 2 months on a longer time scale). The samples were dried for 3 h at a temperature of 103°C, and portions of them were dissolved in 1 M HCl to prepare liquid samples for analyses. The drying time and temperature were selected to evaporate water but not Cs(I) and Sr(II). An inductively coupled plasma mass spectrometer (ELAN DRC II, PerkinElmer) was used to quantify the amount of Cs, and an inductively coupled plasma optical emission spectrometer (OPTIMA 7300 DV, PerkinElmer) was used to quantify the amounts of Fe and Sr. In the current study, Cs and Sr were assumed to be absent when their masses were measured below 1 ng and 1 μg, respectively.

3. Results and Discussion

Iodine loses its volatility over pH 10 but can lose volatility over pH 7 in the presence of H_2O_2 [1,2]. Therefore, by adding H_2O_2 to the contaminated water and maintaining over pH 7, it is possible to suppress the volatilization of iodine. Considering this property of iodine, the behavior of radioactive elements such as Cs and Sr were investigated.

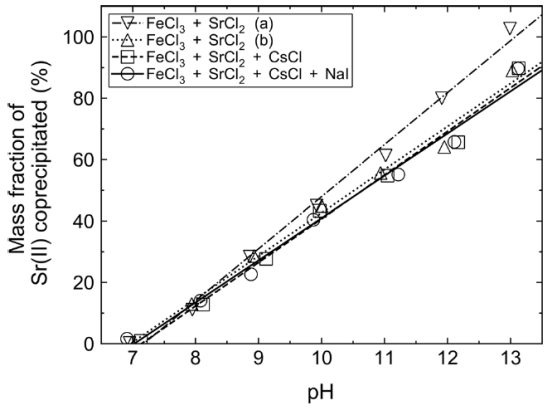

Fig. 1. Mass fraction of Sr(II) coprecipitated with $Fe(OH)_3$ for solutions containing Fe(III) and Sr(II) in common, plotted against initial solution pH. Straight lines: linear fits. Downward triangles: data from experiment conducted over a longer time scale [2].

Hydrolysis deposition was induced by pH control of the solutions in which Fe, Sr, and Cs ions coexist. The content of Sr in iron oxide deposits is shown in Fig. 1. The mass fractions of Sr were measured and found to be below the minimum of 2% at pH 7; they increased linearly to nearly 100% with increasing pH. The Sr mass fraction is not affected by Cs and I^- ions but only by pH. This result shows that Fe ions precipitate with hydrolysis occurring above pH 7, and Sr is also coprecipitated with iron oxides due to the ion-exchange process [3].

Figure 2 shows the mass fraction of Cs in iron oxide deposits under the same conditions.

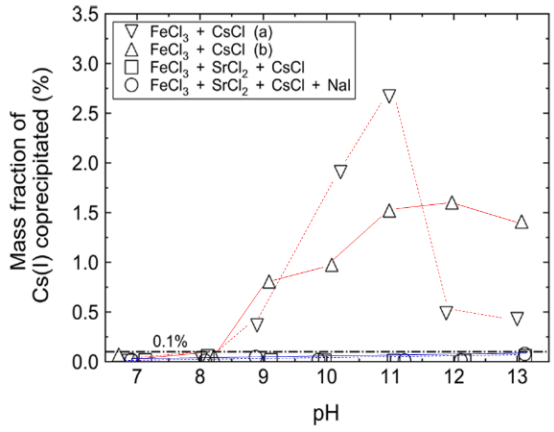

Fig. 2. Mass fraction of Cs(I) coprecipitated with $Fe(OH)_3$ for solutions containing Fe(III) and Cs(I) in common, plotted against initial solution pH. Downward triangles: data from experiment conducted over a longer time scale [2].

Below pH 8, no coprecipitation of Cs was observed under any of the experimental conditions. However, in the presence of Cs ions and Fe ions, the co-precipitation of Cs was observed above pH 8. However, in the presence of Sr ions, Cs coprecipitation was not observed in the pH range 7-13. This result shows that Cs can be coprecipitated when Fe ion is hydrolyzed and precipitated. However, if Sr is present in the solution, ion-exchange process occurs between Cs and Sr ions [3], and it was evaluated that Cs coprecipitation does not occur.

4. Conclusion

Iodine loses its volatility above pH 7 in the presence of H_2O_2. Sr ions are coprecipitated from pH 7 and Cs from pH 8. Therefore, by adding H_2O_2 and adjusting the pH between 7.5 and 8.0, we can obtain the optimal condition to minimize the coprecipitation of radioactive Cs and Sr species while suppressing iodine volatility.

REFERENCES

[1] S.-H. Jung, J.-W. Yeon, et al., “The Oxidation Behavior of Iodide Ion Under Gamma Irradiation Conditions”, Nuclear Science and Engineering, 181, 191 (2015).

[2] T.J. Kim, M. Kim, S.-H. Jung, J.-W. Yeon, “Mitigation of radionuclide deposition in contaminated water: effects of pH on coprecipitation of Cs(I) and Sr(II) with Fe(III) in aqueous solutions”, Journal of Radioanalytical and Nuclear Chemistry, 316, 1261-1266 (2018).

[3] P.S. Bull, J.V. Evans, R.J. Knight, “Removal of radioactive strontium from water by coagulation–flocculation with ferric hydroxide”, Journal of Applied Chemistry and Biotechnology, 25, 801-807 (2007).

Review on Chemical Characterization of Spent Nuclear Fuel at KAERI

Jong-Goo Kim*, Jong-Yun Kim, Jeong mook Lee, Tae-Hyeong Kim, Junghwan Park, and SangHo Lim
Korea Atomic Energy Research Institute, 111, Daedeok-daero 989beon-gil, Yuseong-gu, Daejeon, Republic of Korea
*njgkim@kaeri.re.kr

1. Introduction

Since commercial nuclear power generation began in 1978, finding a way how effectively and safely we dispose the spent fuels accumulating has been a national issue. On the other hand, R&Ds for increasing economic efficiency of nuclear fuel of NPP, that is development of high burnup fuel, have been carried out as national projects. From these perspectives, data of physicochemical characteristics of spent fuel for accurate estimate of source terms and experimental data of burnup behaviors to evaluate their safety and integrity of advanced nuclear fuels were needed. And, for the purpose, from the mid of the 1990s R & D on chemical characterization of spent fuel was begun at KAERI and being continued so far. This study reviews some works performed in the period.

2. Works with simulated nuclear fuel (SIMFUEL)

To examine the effect of fission products (FPs) on nuclear fuel behaviors, physicochemical properties were measured for a number of SIMFUELs that have different compositions of fission products. The effects of composition, oxidation state and size of FP metal ions on the structural change of UO_2, lattice parameters, stoichiometry were discussed with the experimental results.

When exposed to an oxidizing atmosphere, UO_2 oxidizes readily to U_3O_8 accompanied by phase transformation from cubic fluorite to orthorhombic and by a 36% volume expansion, which has been considered to be a reason of spent fuel rupture during dry storage condition. The effect of trivalent dopants, Ln^{3+}, on the oxidation behavior of doped UO_2 was investigated using thermogravimetry and X-ray diffraction analysis[1].

3. Measurement of insoluble residues of spent nuclear fuel

The insoluble residues were recovered from the dissolved solution of spent nuclear fuels (16 – 40 GWd/MtU). The distribution of its constituents, surface morphology and composition structure and chemical states were measured by SEM, EPMA, XRD and XPS[2]. Information on the insoluble residues containing Mo, Ru, Rh, Pd and Tc in dissolved solution of spent nuclear fuel was expected to play an important role in a process control, especially dealing with the homogeneity of spent fuel powder.

4. Development of technology for chemical characterization of spent nuclear fuel

Shielded micro analysis systems were

developed for the measurement of narrow local region of irradiated fuel.

4.1 Micro X-ray diffractometer (XRD)

Radiation shielded micro XRD system (beam size, 4 x 0.02 mm) was developed to identify the structural change in a very narrow region such as interaction region between pellet and cladding of irradiated nuclear fuel. The structural changes were investigated concerning a spent fuel pellet (57.6 GWd/MtU). The lattice parameters of the irradiated fuel revealed the larger values than that of non-irradiated UO_2 due to the radiation damage during the operation in reactor.

4.2 Laser ablation ICP-mass spectrometer

Radiation shielded laser ablation ICP mass spectrometer system (spatial resolution, < 50 μm) was developed to determine the radial isotopic distribution from the core to rim region of irradiated nuclear fuel. Radial isotopic distributions of U-236, Pu-239, Pu-240, Pu-241, Np-237, Am-243, Cm-244, Nd-144, Cs-137 and Mo-100 with respect to U-235 were measured.

4.3 Retained gas analysis system

Shielded measurement system for a retained gas in irradiated fuel was established.

5. Study on Fuel Cladding Chemical Interaction (FCCI)

During the operation of nuclear power reactor the volatile fission products including Cs are known to accumulate at the fuel cladding gap and these could react with UO_2 and/or cladding to give rise to the formation of secondary phases (Cs-U-O or Cs-Zr-O) or chemical bonding. Regarding on the high burnup and longer operation, the amount of these compounds should increase at the gap and could give unexpected effect on burnup behavior. The possible chemical interaction in the gap between fuel and cladding were simulated[3]. In order to simulate the secondary phase, U-Cs-O compound which was known to be found easily at the periphery of highly burnt PWR fuel was synthesized. To investigate the chemical interaction at the contact surface, the diffusion couple consisting of U-Cs-O/Zircaloy were assembled and then annealed. The morphology and elemental distributions on both sides of the annealed couple were measured by SEM and EPMA.

REFERENCE

[1] Jong-Goo Kim et al., “Effect of a trivalent dopant, Gd^{3+}, on the oxidation of Uranium dioxide”, Journal of Nuclear Materials 297, 327 (2001).

[2] Jong-Goo Kim et al., “Characterization of insoluble residues in nitric acid (1:1) solution of PWR spent nuclear fuel”, 14th Radiochemical Conference 14-19 April 2002, Marianske Lazne, Czech Republic.

[3] Jong-Goo Kim et al., “Study on the reaction between Cs_2O and Uranium oxide” 1st Asian Nuclear Fuel Conference, ANFC 2012 March 22-23, 2012, Osaka University, Osaka, Japan.

Study on the Interaction of Uranium(VI) With Aqueous Silicic Acid Using Time-resolved Laser Fluorescence Spectroscopy

Tae-Hyeong Kim[1,*], Euo Chang Jung[1], Yongheum Jo[2], Jong-Il Yun[2], Wansik Cha[1], and Sang Ho Lim[1]
[1]Korea Atomic Energy Research Institute, 111, Daedeok-daero 989beon-gil, Yuseong-gu, Daejeon, Republic of Korea
[2]Korea Advanced Institute of Science and Technology, 291, Daehak-ro, Yuseong-gu, Daejeon, Republic of Korea
[*]thkim@kaeri.re.kr

1. Introduction

For the long-term safety assessment regarding deep geological repository of nuclear waste, understanding of actinide migration is essential. The migration behavior of actinide is highly dependent on its aqueous speciation. Various studies were performed on aqueous speciation of uranium through time-resolved laser fluorescence spectroscopy (TRLFS) since it is a powerful speciation tool through analysis of luminescence characteristics. Silicic acid can be present in natural groundwater and surface water by dissolution of silica and other silicate minerals. Despite of its importance, only few studies on the interaction of uranium with silicic acid at low pH values (≤4.0) were reported [1, 2].

In the present study, the interaction between uranium with silicic acid was investigated by using TRLFS for the better understanding of its interaction in natural system.

2. Experimental

Orthosilicic acid stock solution was prepared by acid hydrolysis of tetramethylorthosilicate (TMOS) according to the procedure described by Jensen and Choppin [3]. The ionic strength of the solutions was kept constant at 0.1 M by using $NaClO_4$. The pH values of solutions were adjusted by adding $HClO_4$ or NaOH. All samples were prepared in the glove box under an argon atmosphere.

For TRLFS measurements, the excitation wavelength at 355 nm with a laser pulse energy of 1.0 mJ was used. The luminescence spectra were recorded from 450 nm to 650 nm with a gate width (t_w) of 1000 μs. The gate delay time (t_d) range and the gate step (t_s) were chosen selectively according as the pH of the samples. The lifetime of luminescence spectrum was determined by an exponential decay function with Levenberg Marquardt iteration algorithm by using Origin 2019.

3. Results and Discussion

Figure 1 shows a luminescence spectra and its decay behaviors measured at pH 4.0 and pH 7.5. The sample solutions contain the same uranyl ion and orthosilicic acid concentrations. At pH 4.0, the peak positions of the luminescence spectrum located around 499, 518, 542, and 569 nm and its lifetime was determined as 17.7 ± 0.2 μs with gate delay times ranging from 0.1 μs to 60.1 μs, with gate step of 1 μs. It is apparent that the luminescence characteristics measured at pH 7.5 are clearly different from those measured at pH 4.0. First, the luminescence intensity increased more than 80 folds. The spectrum was red-shifted with peak positions of 504, 525, 548, and 573 nm. Although the spectral shapes were almost identical, two different luminescence lifetimes were observed at pH 7.5. It means that two different components exist in the solution. In addition, the lifetime increased as the solution aged over time at pH 7.5. After 5 days, equilibrium was reached and the lifetimes were determined as 279.2 ± 19.8 μs and 633.7 ± 7.3 μs with gate delay times ranging from 0.1 μs to 1200.1 μs, with the gate step of 20 μs.

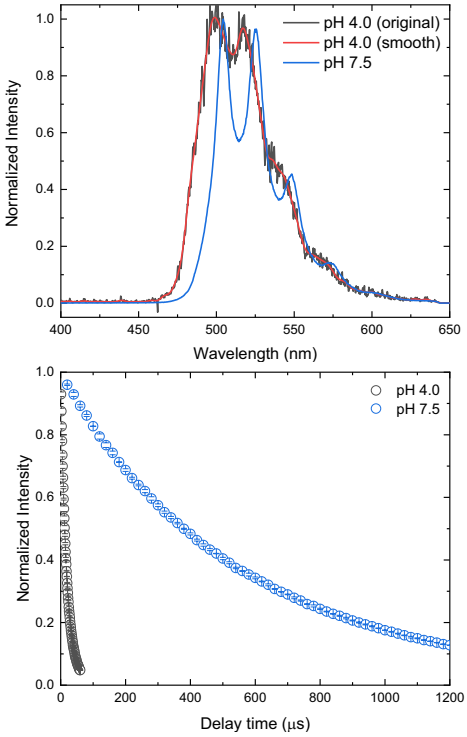

Fig. 1. Normalized luminescence spectrum at pH 4.0 (t_d = 2.1 μs) and pH 7.5 (t_d = 20.1 μs) and its decay for a solution containing 20 μM UO_2^{2+} and 5 mM $Si(OH)_4$.

The luminescence characteristics measured at pH 4.0 are comparable to previously reported values (the peak positions of 500, 521, 544, 570 nm and lifetime of 19 ± 4 μs) [1]. At this pH, hydrolyzed uranyl species was minimized and almost all of silicic acid were presented in a monomeric manner, where uranyl species can be postulated as $UO_2OSi(OH_3)^+$ [1, 2].

On the other hand, at pH 7.5, the orthosilicic acid is unstable, which results in formation of oligomer easily [4]. Thus, the uranyl species at pH 7.5 is thought to be a complex with oligomeric silicic acid, not a monomeric orthosilcic acid.

4. Conclusion

The luminescence characteristics of U(VI) complexes interacting with the oligomeric silicic acid are reported for the first time. The luminescence characteristics observed in the present study are quite different from those observed for U(VI)-monomeric orthosilicic acid complex, $UO_2OSi(OH_3)^+$. Interestingly, the luminescence characteristics measured at pH 7.5 are very similar to those of uranyl hydrolysis species adsorbed on silica surface. Further research on the interaction of aqueous uranyl species with silicic acid is necessary for a better understanding of its chemical speciation.

Acknowledgement

This work was supported by a grant from the Nuclear Research and Development Program of the National Research Foundation of Korea funded by the Korean Ministry of Science and ICT (Grant code: 2017M2A8A5014719).

REFERENCES

[1] H. Moll, G. Geipel, V. Brendler, G. Bernhard and H. Nitsche, “Interaction of uranium(VI) with silicic acid in aqueous solutions studied by time-resolved laser-induced fluorescence spectroscopy (TRLFS)”, Journal of Alloys and Compounds 271-273, 765-768 (1998).

[2] Takumi Saito, Noboru Aoyagi, and Takaumi Kimura, “Time-resolved laser-induced fluorescence spectroscopy combined with parallel factor analysis: a robust speciation technique for UO_2^{2+}”, Journal of Radioanlaytical Nuclear Chemistry, 303, 1129-1132 (2015).

[3] Mark P. Jensen and Gregory R. Choppin, “Complexation of europium(III) by aqueous orthosilicic acid”, Radiochimica Acta, 72, 143-150 (1996).

[4] Gregory R. Choppin, Priyanath Pathak, and Punam Thakur, “Polymerization and complexation behavior of silicic acid: A review”, Main Group Metal Chemistry, 31(1-2), 53-71 (2008).

Characterization of Colloidal U(IV) Particles Complexed With Organic Molecules Using Spectroscopic Techniques

Hyejin Cho*, Inhak Yoon, and Wansik Cha
Korea Atomic Energy Research Institute, 111, Daedeok-daero 989beon-gil, Yuseong-gu, Daejeon, Republic of Korea
*hcho921@kaeri.re.kr

1. Introduction

Tetravalent uranium (U(IV)) is considered an immobile species under reducing repository conditions due to its low solubility and strong tendency to be retained at mineral surfaces [1]. When colloidal nanoparticles dominate U(IV) speciation in groundwater, the apparent solubility can become higher due to the increase of the amount of mobile U. Consequently, the formation of colloidal nanoparticles and their interactions with natural organic matters (NOMs) in groundwater affect the migration of U in contaminated sites [2]. Thus, the precise understanding of the colloid-facilitated reaction mechanism with NOMs and the immobilization strategy of such colloids are of interest for the safety assessment of radioactive waste repository.

2. Results and Discussions

In this study, we developed a hydrothermally-induced U(IV) nanoparticle ($U(IV)_{NPs}$) preparation method using acidic U(IV) aqueous solutions (pH ~2) to investigate the complexation of organic molecules on the surfaces of $U(IV)_{NPs}$ employing various spectroscopic techniques. The characterization of $U(IV)_{NPs}$ itself was performed in advance studying the interaction with organic ligands. As demonstrated in Figure 1, $U(OH)^{3+}$ species is transformed to the $U(IV)_{NPs}$-intermediate which shows the peak increasing at 669 nm during the synthetic process of $U(IV)_{NPs}$ at pH 2-3 and raising temperature to 60 °C. The formation of intermediate is irreversible even the temperature is back to room temperature. However, the transformation of $U(OH)^{3+}$ from U^{4+} species is reversible depending on the pH and

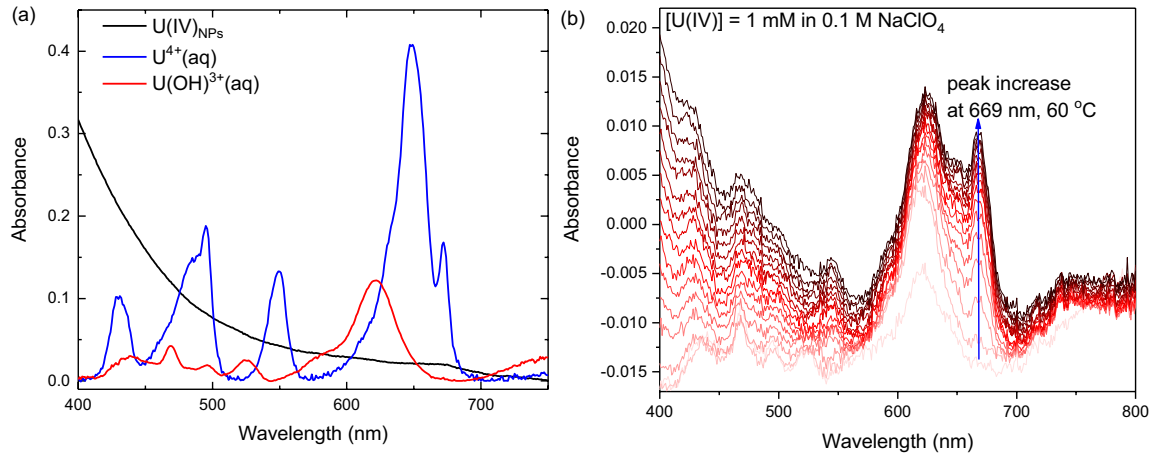

Fig. 1. UV-Vis absorption spectra; (a) a comparison of $U(IV)_{NPs}$ (1 mM, pH 2.3) spectra with ionic U(IV) species (U^{4+}(aq) at pH ~0 and $U(OH)^{3+}$(aq) at pH ~2, [U(IV)] = 6.3 mM); (b) synthetic process of $U(IV)_{NPs}$ from 1 mM U(IV) solution at pH 2.3.

temperature of the solution. In addition, the properties of the synthesized $U(IV)_{NPs}$, including particle size, stability, and crystallinity were analyzed using transmission electron microscopy (TEM), dynamic light scattering (DLS) and X-ray diffraction (XRD). Particularly, the results indicate that the produced nanoparticles have colloidal stabilities and crystallinity. Further characteristic analysis was carried out to investigate the physicochemical properties of $U(IV)_{NPs}$ complexed with organic ligands. Notably, the $U(IV)_{NPs}$-ligand complexes display unique colloidal properties, as measured by DLS (Fig. 2). As shown in Fig. 2, the colloidal stabilities (highly positive or negative zeta-potential values) can be maintained in the presence of excess amount ligands or nanoparticles. Conversely, the values of

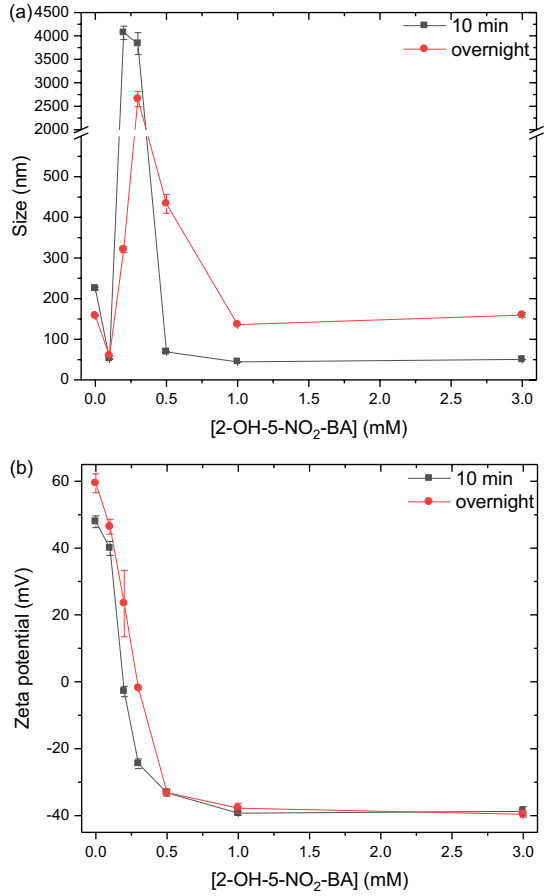

Fig. 2. Size and zeta potential measurements of $U(IV)_{NPs}$-organic ligand complexes as increasing [ligand] in 1 mM $U(IV)_{NPs}$ solution at pH 3 by DLS.

particle size and zeta-potential were significantly changed producing the ligand-bound $U(IV)_{NPs}$ aggregates or the fully saturated surfaces of $U(IV)_{NPs}$ with the ligands when the ligand concentration is between 0.2 and 0.5 mM in 1 mM $U(IV)_{NPs}$ solution. This phenomenon was also confirmed by the data obtained from ATR-FTIR and UV-Vis spectrometer analysis. Finally, it is found that the crystallinity of $U(IV)_{NPs}$ before and after adsorption of organic ligands was maintained using XRD analysis.

3. Conclusion

We conclude that the colloidal properties of such synthesized particles, highly positive values of zeta-potential values and large surface areas owing to their unique structures, are the major factors facilitating the surface adsorption of organic molecules on $U(IV)_{NPs}$. Further spectroscopic data will be analyzed to identify the structure of ligands-$U(IV)_{NPs}$ complexes.

Acknowledgement

This study is supported by the Nuclear Research and Development program of the National Research Foundation of Korea (Grant code: 2017M2A8A5014719).

REFERENCES

[1] J. –I. Kim, “Significance of actinide chemistry for the long-term safety of waste disposal”, Nuclear Engineering and Technology, 38(6), 459-482 (2006).

[2] H. Geckeis, T. Rabung, T. Schäfer, “Actinide-nanoparticle interaction: Generation, stability and mobility. In Actinide Nanoparticle Research”, Springer: Berlin, Heidelberg, pp 1-30 (2011).

Boron Isotope Analysis Using Double-pulse Laser Ablation Molecular Isotopic Spectrometry

Sung-Uk Choi, Sol-Chan Han, and Jong-Il Yun*
Korea Advanced Institute of Science and Technology, 291, Daehak-ro, Yuseong-gu, Daejeon, Republic of Korea
*jiyun@kaist.ac.kr

1. Introduction

In pressurized water reactors (PWRs), boric acid is employed to adjust the reactivity of fission reaction, which refers to as a chemical shim. At the beginning of cycle (BOC), the elemental concentration of boron is about 900 to 1800 ppm [1]. The difference between thermal neutron absorption cross-sections of two naturally occurring boron isotopes, i.e. 3840 barns for ^{10}B and 0.005 barns for ^{11}B, results in biased consumption of ^{10}B by (n,)-reaction. Therefore, for controlling the proper concentration of ^{10}B, the amount of boron isotopes in reactor coolant should be monitored in real time.

In this study, the applicability of laser ablation molecular isotopic spectrometry (LAMIS), which analyzes the molecular spectra from a laser-induced plasma, has been investigated for the boron isotope detection. In addition, a double-pulse laser configuration was adopted to enhance the sensitivity of boron isotope analysis.

2. Experimental

Fig. 1 shows the experimental set-up. The sequential dual laser pulses were produced by two Q-switched Nd:YAG laser (Continuum Co., Surelite-20), and focused on the laminar jet stream in a closed circulation chamber.

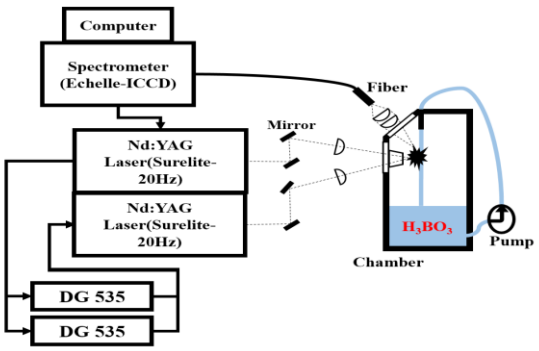

Fig. 1. Schematic diagram of experimental set-up.

An echelle spectrometer (LLA, ESA3000, $\lambda/\Delta\lambda$ = 40,000) was utilized for the measurement of emission from laser-induced plasma.

Aqueous solutions with various boron isotopic ratios were prepared by mixing 99% enriched $H_3{}^{11}BO_3$ and 99% enriched $H_3{}^{10}BO_3$ (both Sigma Aldrich Co.) with deionized water (Millipore, Milli-Q Synthesis).

3. Result and discussion

3.1 BO_2 emission spectra and detection limit

Fig. 2 shows the BO_2 spectrum obtained from the single-pulse (SP) and the double-pulse (DP) configuration. The emission intensity was enhanced in DP configuration in comparison to SP system. Particularly, the combination of 355 nm and 1064 nm lasers shows 10 times enhancement than SP. The UV laser has the advantage for plasma ablation in the aqueous medium, and NIR laser is suitable for reheating the plasma. Therefore, the 355/1064 nm (UV-NIR) combination showed a higher signal enhancement.

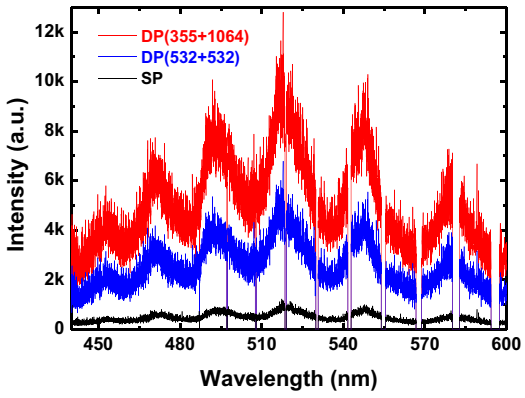

Fig. 2. BO_2 spectrum from SP and DP configuration.

The detection limit can be determined from the linear relationship between the emission intensity and the boron concentration. The limit of detection (LOD) was calculated as below.

$$C_L\,(LOD) = 3\sigma/S \qquad (1)$$

where S is the slope of the concentration-intensity linear fitting and σ is the standard deviation of noise signal. The LODs for boron in aqueous medium, which were obtained from the BO_2 molecular emission intensity at 517 nm, are summarized in Table 1. The lowest LOD (71 ppm) was achieved in a combination of sequential laser pulses with wavelengths of 355 nm and 1064 nm. This LOD is higher than that calculated from the atomic line in the previous study [2]. However, the molecular emission is more suitable for the isotope detection, and the obtained LOD (72 ppm) is sufficient for boron detection in PWR reactor coolant.

Table 1. Limit of detection (LOD) of boron

	SP	DP (532+532)	DP (355 + 1064)
LOD (ppm)	687	149	72

3.2 Quantitative analysis of boron isotopes

Isotopes have slightly different energy states depending on their electronic configuration. Therefore, the peak position of the emission spectrum is shifted, which is referred to as an isotopic shift. The isotopic shift is more pronounced in molecular species compared to atomic species. In practice, the BO_2 emission has a larger isotopic shift than atomic emission. The isotopic shift of BO_2 is greater than 0.1 nm compared to the B atom of less than 0.002 nm. Fig. 3 shows $^{10}BO_2$ and $^{11}BO_2$ emission spectra. The isotopic shift between these molecular emission bands was observed at individual rotational branches.

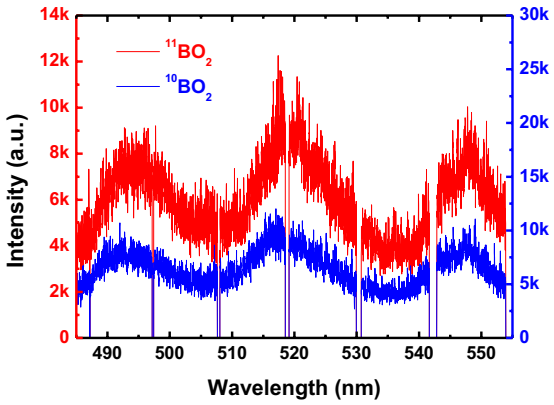

Fig. 3. $^{10}BO_2$ and $^{11}BO_2$ molecular emission bands (For comparison, the y-axis scale is differently adjusted for $^{10}BO_2$ and $^{11}BO_2$).

The boron isotope analysis was conducted using the distinct spectral difference of molecular emissions. Since the molecular emission has numerous rotational branches, the multivariate calibration method is powerful for quantitative analysis. In this study, we employed the partial least squares regression (PLSR). Based on a number of BO_2 spectra obtained from the samples with varying ratios of $^{10}B/^{11}B$, the PLSR structure was constructed. In addition, several validation samples were used for cross validation of PLSR. Fig. 4 shows the root mean squares error of prediction (RMSEP) of PLSR. The DP configuration with 355 nm and 1064 nm lasers has the lowest RMSEP, indicating the highest accuracy.

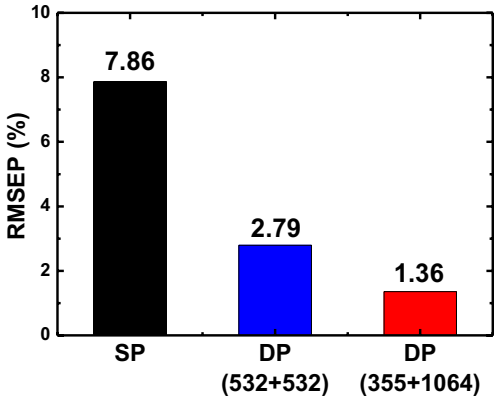

Fig. 4. RMSEP of predicted values for each PLSR spectrum.

4. Conclusion

We investigated boron isotopes in aqueous medium using the DP-LAMIS system. The limit of detection for boron in aqueous medium was obtained as 72 ppm using the molecular emission of BO_2. The PLSR result shows the RMSEP of 1.4 % for boron isotope analysis in the DP-LAMIS configuration. The results demonstrate the applicability of DP-LAMIS for the detection of boron isotopes in PWR reactor coolant.

REFERENCES

[1] Lundgren K., Riess R., Strasser A., Sandklef S., LCC-1 Annual Report, ANT International, Sweden (2005).

[2] D. H. Lee, S. C. Han, T. H. Kim, J.-I. Yun, Highly sensitive analysis of boron and lithium in aqueous solution using dual-pulse laser-induced breakdown spectroscopy. Analytical Chemistry, 83, 9456-9461 (2011).

7분과

방사화학 (Poster)

PUREX Solvent Extraction Experiments Using ^{238}U, ^{152}Eu and ^{85}Sr Solution

Il-Kwon Jung[a] and Jaeyeong Park[b,*]
[a]Korea Advanced Institute of Science and Technology, 291, Daehak-ro, Yuseong-gu, Daejeon, Republic of Korea
[b]Ulsan National Institute of Science and Technology, 50, UNIST-gil, Eonyang-eup, Ulju-gun, Ulsan, Republic of Korea
[*]jypark@unist.ac.kr

1. Introduction

Recently, uranium can be extracted from spent nuclear fuel by several separation processes such as solid-liquid extraction, solvent extraction, and ion exchange are widely used methods for uranium extraction. Among them, PUREX, which uses the solvent extraction method, is the most versatile and efficient technique for separating uranium from ionic solution.

In the present study, we conducted experiments to simulate it on a laboratory scale to understand the PUREX process and its mechanism. The distribution coefficient of U(VI) is confirmed by the Liquid Scintillation Counting (LSC) in the presence of Sr(II) and Eu(III). Likewise, the distribution coefficients of Sr(II) and Eu(III) were determined by using Ge semiconductor detector with high sensitivity.

2. Methods

2.1 Preparation of samples

In order to conduct a solvent extraction experiment, the stock solutions were prepared before pre-equilibrium experiment. To verify effect of nitric acid concentration for uranium extraction, three samples (S1, S2, and S3) with different nitric acid concentration were prepared. The ^{85}Sr and ^{152}Eu stock solutions were added to confirm competing ion effect in solvent extraction.

Table 1. Prepared samples (S1, S2, and S3)

Sample no.	S1	S2	S3
$[HNO_3]$	0.096 M	0.96 M	4.8 M
$[UO_2^{2+}]$		48 mM	
$[Sr^{2+}]$		0.96 mM	
$[Eu^{3+}]$		0.2 μM	

2.2 Pre-equilibrium and Uranium extraction

Before the solvent extraction, Pre-equilibrium experiment was conducted by contacting 15 mL of organic solution (30 % TBP + 70 % dodecane) with 10 mL 0.1 M HNO_3 solution to prevent volume change of organic phases and competing reaction between HNO_3 and $UO_2(NO_3)_2$. After mixing with aqueous solution, the organic solution was collected for further experiments.

3 mL of S1, S2, and S3 were pipetted and contacted with a collected organic solution. After adding uranium stock solution, mixed samples were shaken by shaker for 5 min at an angle of 45º to give a wider contact area. The final products were collected and analyzed by LSC and Ge detector.

2.3 Radiation measurement and determining distribution coefficients (D) of elements

To evaluate the separation of elements, radiation measurements by Liquid Scintillation Counting (LSC) and Ge semiconductor detector were conducted. For U-235 and U-238, since their major decay modes are α-decay, the LSC was used for measurement. On the other hand, the Ge semiconductor detector was used for Sr-85 and Eu-152 detection, because the γ-rays of Sr-85 and Eu-152 can be easily distinguished from other γ-rays sources.

The measurements were conducted until they reach a reliable time for calculation. α-ray measurements were conducted until it reaches 10000 counts, and γ-ray measurements were done for 800 sec.

Distribution coefficients (D) of the elements were determined by Eq. (1)

$$D_{element} = \frac{[element]_{org}}{[element]_{aqueous}} = \frac{cps_{org}}{cps_{aqueous}} \quad (1)$$

3. Results and Discussions

3.1 Chemical reaction of U(VI), Eu(III), and Sr(II)

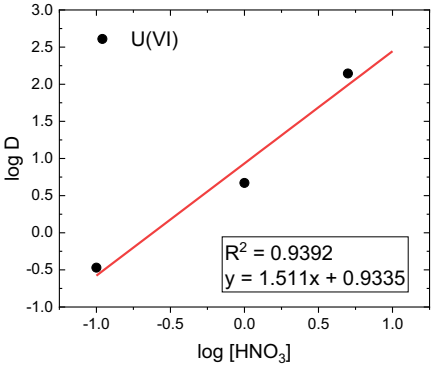

Fig. 1. Linear fitting result (log [HNO_3] vs log D) from experimental result of Uranium.

As can be seen from Fig. 1, the experimental result showed a slope value of 1.511, while the ideal slope value is 2. The possible reasons from the result are the reaction of Eu^{3+} and Sr^{2+} with nitrate, which can interrupt to form uranium nitrate. Besides, the decomposition of nitrate from nitric acid was not sufficient under experimental pH condition, which can result in different concentration of nitrate from ideal nitrate concentration.

3.2 Distribution coefficients of U(VI), Eu(III), and Sr(II) depends on nitric acid concentration

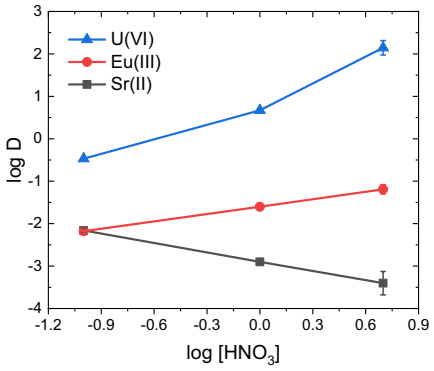

Fig. 2. Distribution coefficients (D) of Sr(II), Eu(III), and U(VI) depending on Nitric acid concentration ([HNO_3]).

From Fig. 2, the distribution coefficients of Eu(III) and U(VI) increased with increasing nitric acid concentration, suggesting that the concentration of nitrate can enhance the efficiency of solvent extraction. This trends also can be observed in the previous study [1]. On the other hand, the distribution coefficient of Sr(II) decreased due to its poor selectivity, indicating that the equilibrium constant of Sr(II) is less than that of hydrogen. Therefore, the expected equilibrium constant value should follow in order of ($K_U > K_{Eu} > K_H > K_{Sr}$).

Selection of proper nitric acid concentration was also done from the experiment results. Generally, the distribution coefficient (D) of uranium can be improved with increasing nitric acid concentration. The maximum distribution coefficient of uranium was observed when using 5 M of nitric acid sample in our experiment. However, the decrement of distribution coefficient of uranium was observed above 5 M of nitric acid condition in Stas et al's study [1] due to the competition of nitric acid complexing with TBP. To sum up, 5 M of nitric acid condition is a proper condition for U and Eu purification, whereas Sr purification could be efficient in a lower nitric acid condition.

4. Conclusion

The U(VI) solvent extraction experiment using TBP and dodecane mixed solution was successfully conducted. The distribution coefficient of U(VI), Eu(III), and Sr(II) was confirmed by Liquid Scintillation Counting (LSC) and Ge semiconductor detector. The distribution coefficients of elements according to nitric acid concentration showed the general trend as the previous study. The results indicate that the increased separation efficiency and high selectivity for U(VI) with increasing nitric acid concentration, suggesting the higher concentration of nitric acid is a proper condition for U(VI) separation process.

REFERENCES

[1] J. Stas., A. Dahdouh., H. Shlewit "Extraction of uranium(VI) from nitric acid and nitrate solutions by tributylphosphate/kerosene", Periodica Polytechnica Chemical Engineering, 49(1), 3-18 (2005).

Performance of a Virtual Frisch-grid CdZnTe Detector for Prompt γ-ray Induced by 14-MeV Neutrons

TaeWoong Lee[1,*], NakJeom Kim[1], SeongMin Jo[1], YoungHak Kim[2], AJin Jo[2], and WonHo Lee[2,**]
[1]KEPCO KPS, 211, Munhwa-ro, Naju-si, Jeollanam-do, Republic of Korea
[2]Korea University, 145, Anam-ro, Seongbuk-gu, Seoul, Republic of Korea
[*]superdapo@kps.co.kr, [**]wonhol@korea.ac.kr

1. Introduction

Prompt γ-ray neutron activation analysis (PGNAA) can be used for the online detection of a contraband material. The virtual Frisch-grid Cadmium zinc telluride (VFG CZT) detectors are suitable for use at room temperature without cooling. The electrode structure of the VFG CZT detectors that use small number of read-out channels per detector element is more attractive than the multi-pixel CZT detectors. In this work, the MCNPX code was used to simulate the PGNAA using a VFG CZT detector. The minimum detectable concentration (MDC) for the elements was estimated by using the concentration of carbon and oxygen in the target material. The carbon-to-oxygen (C/O) ratio was calculated using the effective counts of the characteristic γ-ray peak in the energy spectrum for material identification. Finally, the results of the simulation were compared to the performance of the HPGe detector.

2. Methods and Results

The schematic diagram of the Monte Carlo simulation study is shown in Figure 1. The actual model of the VFG CZT single crystal that was developed at the Brookhaven National Laboratory (BNL) [1]. The detector has a volume of 6 × 6 × 15 mm^3. For a more realistic simulation of the VFG CZT detector (density = 5.6 g/cm^3), a Gaussian energy broadening (GEB) was applied using a fitting function in MCNPX code.

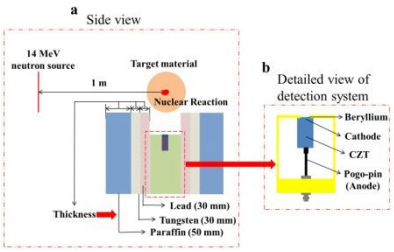

Fig. 1. Schematic diagram of simulation setup of prompt γ-ray neutron activation analysis (PGNAA). (a) The side view of geometry, and (b) detailed view of detection system.

Contraband materials can be distinguished by their characteristic C/O element ratio. TNT and cocaine were chosen for our study. Table 1 shows their elemental compositions.

Table 1. Elemental compositions of TNT and cocaine

Material	Density (g/cm^3)	H%	C%	N%	O%	Elemental ratio (C/O)
TNT $C_3H_5O_6N_3$	1.63	2.2	37	18.5	42.3	0.9
Cocaine $C_{17}H_{21}NO_4$	0.84	6.9	67.3	4.6	21.1	3.2

A sensitive nonlinear iterative peak (SNIP) clipping algorithm, including the subtraction of the background counts, was applied to obtain the energy spectrum rapidly and accurately, and the results of the energy spectrum were compared to those of the original energy spectrum. Figure 2 shows the comparison

between the experimental and simulated energy spectra using the MCNPX code.

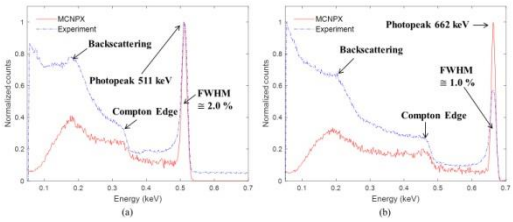

Fig. 2. Comparison between experimental and simulated pulse height distributions: (a) 511 keV, (b) and 662 keV.

Figure 3 shows the γ-ray yields as the function of carbon and oxygen concentrations in an artificial sample with CZT and HPGe detector. The solid line (blue) and dotted line (red) in the Figure represent the γ-ray yields in the original energy spectrum and energy spectrum, respectively, with the rejection of the background noise using the SNIP algorithm. The results of the MDC demonstrate that a VFG CZT detector is appropriate to measure main elements such as C and O in TNT and cocaine in the prompt γ-ray activation analysis.

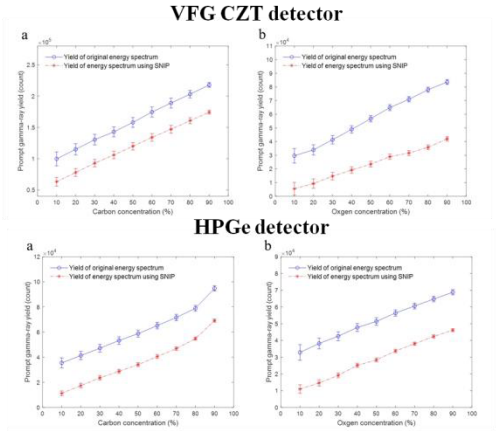

Fig. 3. Prompt γ-ray yield for each element calculated by virtual Frisch-gird CZT detector and HPGe. (a) Carbon, and (b) oxygen.

Figure 4 shows the prompt γ-ray spectra of the TNT and cocaine samples. All elements observed in the analyzed TNT and cocaine were clearly identified using the data obtained by the VFG CZT and the HPGe detector.

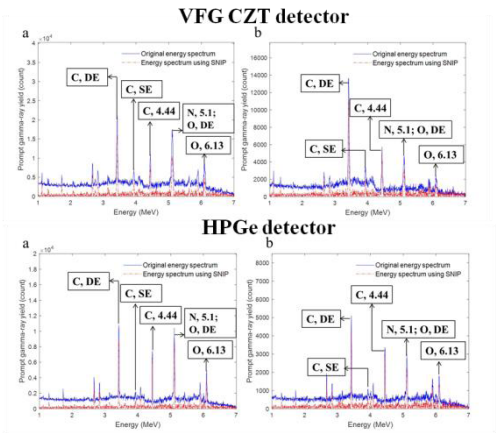

Fig. 4. Estimated prompt γ-ray energy spectrum after neutron inelastic scattering using the virtual-Frisch gird CZT detector and HPGe. (a) TNT, and (b) cocaine. SE and DE refer to the single escape peak and the double escape peak, respectively.

3. Conclusion

It is shown, using Monte Carlo simulations, that a virtual Frisch-grid (VFG) CZT detector can be used to detect the prompt γ-rays induced by 14-MeV neutron to detect the carbon and oxygen of the contraband materials. The performance of the simulation results demonstrated that the VFG CZT detector was suitable for the PGNAA application.

REFERENCES

[1] Bolotnikov, A.E., et al, “CdZnTe position-sensitive drift detectors with thickness up to 5 cm,” Appl. Phys. Lett, 108, 093504, 2016.

Bias Correction of Density Data Obtained Using Dynamic Bubbler for High-Temperature Molten Salts

Jong-Yun Kim*, Sang-Eun Bae, and Tae-Hong Park
Korea Atomic Energy Research Institute, 111, Daedeok-daero 989beon-gil, Yuseong-gu, Daejeon, Republic of Korea
*kjy@kaeri.re.kr

1. Introduction

Over the last decade we have developed several in-house designed measurement systems of physical properties and thermodynamic behavior of high-temperature corrosive molten salts. Among them, density data, together with liquid level data, is an important basic and fundamental physical property providing the useful information for custody transfer and inventory management as well as nuclear material accountancy. However, accurate density measurement are very challenging for molten salts. Plenty of bias sources are present in the density measurement because of the high-temperature corrosive molten salts. Thus, appropriate bias corrections are required for the accurate measurement of density.

2. Methodology

2.1 Density measurement

Patented single-probe dynamic bubbler was used to determine the density of molten salts. In our previous Potassium nitrate (KNO_3) was used as purchased without further purification. KNO_3 A cylindrical vessel containing the powder was placed inside an electrical furnace. The temperatures of the furnace were varied from 873 K to 1123 K. The bubbler probe was moved toward the liquid surface, and submerged at preset depths to measure pressures by means of a computer-controlled linear stepper motor. Measured pressures at each immersion depth were used to determine the liquid density based on Eq. (1)

$$\rho = \frac{P_2 - P_1}{g(d_2 - d_1)} \quad (1)$$

where ρ is a measured density ($g \cdot cm^{-3}$), and g is the gravity constant (9.8 $m \cdot s^{-2}$). P_1 and P_2 are the pressures measured at different d_1 and d_2, which are the distances from the surface, respectively.

2.2 Bias Correction

Our dynamic bubbler system has been optimized to achieve the target precision of the level and density measurements. The previous study showed that the precision was dependent on the probe traveling speed, pressure and temperature variations, bubbling frequency, tube size, etc. The dynamic bubbler with single probe has various sources of measurement bias such as liquid displacement, etc. The liquid displacement is caused by submerging the bubbler probe into the melt, which induce the level change and consequently affect the P_2

value as shown in Fig. 1. Since such bias of density is caused by the level change (Δ), the effect of Δ should be added to the denominator of Eq. (1).

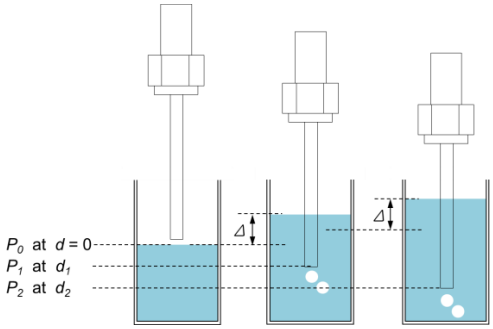

Fig. 1. Bias caused by the immersion of the bubbler probe.

3. Results and Discussion

Determination of the accuracy is far more difficult because currently there is no reference materials for high-temperature molten salts. Comparison of the measured values with the most reliable literature values known so far is an alternative to the evaluation of the accuracy. Without correction, between the measured density and literature values was *ca.* 6 % at P_0 (base pressure) = 70 Pa, T (set temperature) = 823 K, and 5-mm depth interval. After bias correction, average % difference decreased down to *ca.* 3 %

4. Conclusion

Bias correction caused by liquid displacement was effective in the density determination of molten salt. Under the experimental condition in the present study, liquid displacement bias correction improved the accuracy of the dynamic bubbler by 50 %. However, more careful examination of the accuracy improvement under various experiment conditions for robustness test is required in a future study.

Acknowledgement

This work was supported by the Nuclear R&D Program, through the National Research Foundation of Korea (NRF-2017M2A8A5014710), funded by the Korean Ministry of Science and ICT, Republic of Korea.

REFERENCES

[1] J.-Y. Kim, S.-E. Bae, J.W. Yeon, T.H. Park, and K. Song, “Measurement Device and Measurement Method for Liquid Surface Height”, Korean Patent KR10154097B1 (2015).

[2] J.-H. Lee, J.-Y. Kim, T.-H. Park, S.-E. Bae, “Liquid Level Measurement by the Detection of Abrupt Pressure Changes in a Tube in Contact with a Liquid Surface”, Journal of Nuclear Fuel Cycle Waste Technology, 13, 39-44 (2015).

[3] J.-Y. Kim, J.-H. Lee, S.-E. Baea, S. Paek, S. H. Kim, T-.J. Kim, and T-.H. Park, “Automated High-Temperature Liquid Level Measurement System Using a Dynamic Tube Pressure Technique”, Journal of Industrial and Engineering Chemistry, 49, 30-35 (2017).

In Situ High Temperature X-ray Diffraction Study of Dopant Doped Uranium Oxide

Dong Woo Lee[a], Jeongmook Lee[a], Jong-Yun Kim[a,b], and Sang Ho Lim[a,b,*]
[a]Korea Atomic Energy Research Institute, 111, Daedeok-daero 989beon-gil, Yuseong-gu, Daejeon, Republic of Korea
[b]University of Science & Technology, 217 Gajeong-ro, Yuseong-gu, Daejeon, Republic of Korea
[*]slim@kaeri.re.kr

1. Introduction

Uranium oxide, i.e., oxide materials containing U^{4+}, U^{5+}, and U^{6+} cations, have been of particular interest in broad nuclear fuels field. As one of them, rare-earth metal doped uranium oxides are widely studied as semiconductor. Therefore, research of the structural character of rare-earth metal doped uranium oxide is important to understand their properties such as electricity, and magneticity. [1, 2]

For the observation of structure of rare earth metal doped uranium oxide has been measured using neutron diffraction and x-ray diffraction after sintering experiments. In-situ x-ray diffraction provides the needed crystal structure information. In addition, x-ray diffraction with controlled temperature, which is analyzed and synthesized at the same time. Abril et el. [3] have researched the UO_2 nanoparticles with in situ XRD at 30°C -1200°C. The results showed the evolution of the lattice parameter, the crystallite size, and the strain up to 1200 °C.

In this work, we report the in situ high temperature XRD study of Gd doped uranium oxide. We measure the effect of temperature on the size of crystalline, which is a cell parameter in the sintering process. And then, the variation of lattice parameter are calculated using Rietveld refinement method.

2. Experimental

Gd doped uranium oxide powders were ground thoroughly with agate mortars and pestles and pressed into pellet. The pellet on the tungsten strip was evacuated and gradually heated to 1400 °C.

The X-ray powder diffraction data were collected on a Bruker D8-Advance diffractometer using Cu Kα radiation with 40 kV and 40 mA and an Anton Parr HTK 2000 heating chamber. The scan ranges were 20-110° with a step size of 0.02°, and a step time of 0.1s. The temperature ranges were 25 °C - 1400 °C. The diffraction patterns were analyzed using Rietveld method with the TOPAS program. The Structural refinement of the materials was carried out in the space group *Fm-3m* (no.225) with a starting model based on the reported data of UO_2 [PDF#: 00-041-1422].

3. Results and discussion

The results of the Gd doped uranium oxide pellet at various temperatures x-ray diffraction patterns are shown in Fig. 1. At room temperature, the powders were confirmed as UO_2 and Gd_2O_3 peaks showed in the XRD pattern. And the Gd doped UO_2 crystal structure was retained after heating at 1300°C because the XRD patterns did not show any obvious differences compared with that corresponding

from the R.T. However, the crystal structure changes of the powders were revealed from the XRD patterns corresponding to 1400°C. As shown in Fig. 1, the XRD patterns corresponding to the synthetic Gd-doped uranium oxide pellet at 1400°C are in agreement with that of $U_{1-y}GdyO_{2-x}$. [4]

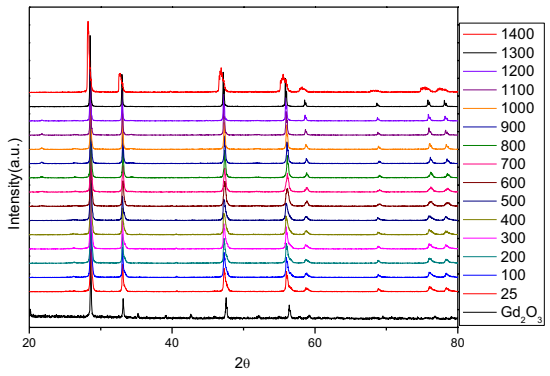

Fig. 1. In-situ high temperature powder X-ray diffraction patterns of the powder heated at different temperatures. The results showed that the UO_2, and Gd_2O_3 crystal structures formed by heating Gd doped uranium oxide pellet at 1400°C.

As seen in Fig. 2, the diffraction peaks move to the left with increasing temperatures. The peak positions slightly shift toward the left side as temperature increase.

4. Conclusions

The Gd doped uranium oxide phases have been studied in situ x-ray diffraction with temperature equipment. We measured the effect of the temperature on the cell parameter using calculation method. In situ high temperature x-ray diffraction observed that structural change in material. In further works, to follow various effects on the properties of UO_2 depending on the doped content in the matrix with in situ high temperature x-ray diffraction.

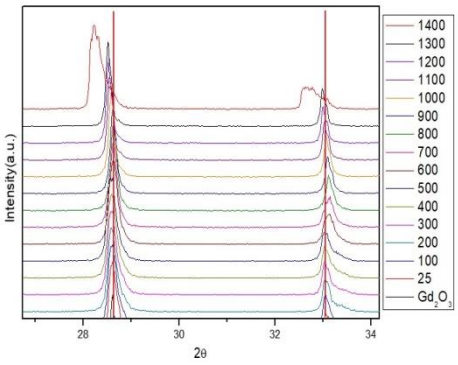

Fig. 2. Powder X-ray diffraction data for uranium oxide. The peak positons shift toward the left side.

ACKNOWLEDGEMENT

This work was supported by the National Research Foundation of Korea (NRF) grant funded by the Korean government (MSIP; No.2012M2A8A5025925).

REFERENCES

[1] M. Usman, J. B. Felder, G. Morrison, H-C. Loye, A family of rare earth uranium oxides, $RE_6UO_{12-\delta}$, (RE=Rare Earth). Synthesis, structure and magnetic behavior, 266, 210-216 (2018).

[2] Z. A. Munir, The electrical conductivity of doped and undoped uranium oxide, 2(2), 177-186 (1981).

[3] R. J. Abril, R. Eloirdi, D. Bouexiere, R Malmbeck, J. Spino, In situ high temperature X-ray diffraction study of UO_2 nanoparticles, Journal of Materials Science, 46, 7247-7252 (2011).

[4] J. Lee, J. Kim, Y-S. Youn, N. Liu, J-G. Kim, Y-K. Ha, D. W. Shoesmith, J-Y. Kim, Raman study on structure of $U_{1-y}Gd_yO_{2-x}$(Y=0.005, 0.01, 0.03, 0.05 and 0.1) solid solutions, 486, 216-221 (2017).

Algorithm for the Determination of Tafel Slope in the Electrochemical Analysis of Uranium Dioxide Oxidation

Junghwan Park[a,*], Jong-Yun Kim[a,b], Tae-Hyeong Kim[a], Jeongmook Lee[a], Sang-Eun Bae[a,b], and Sang Ho Lim[a,b]
[a]Korea Atomic Energy Research Institute, 111, Daedeok-daero 989beon-gil, Yuseong-gu, Daejeon, Republic of Korea
[b]University of Science & Technology, 217 Gajeong-ro, Yuseong-gu, Daejeon, Republic of Korea
[*]jpark7@kaeri.re.kr

1. Introduction

Tafel slope is a part of electrochemical kinetics which describes that the electrochemical reaction rate is on overpotential and it assumes the forward reaction is dominant than the reverse reaction [1].

To determine Tafel slope, it is common to rely on visual intuition. Since there was no such a numerical method on experimental data, we try to conceptualize a reliable determination method of Tafel slope on the linear region of electrochemical data.

Tafel slope is important and useful way to characterize the behavior of uranium dissolution with Cyclic Voltammetry (CV), Linear Sweep Voltammetry (LSV), and so on. In this study, we focus on the LSV of gadolinium doped - uranium dioxide Dissolution.

2. Experimental Method

Fresh uranium dioxide (UO_2) and gadolinium oxide (Gd_2O_3) powder are mixed and ground to fine powder in a mechanical device. Then, it is pressed at 300MPa to be ready for sintering. Within reducing atmosphere of hydrogen gas, uranium dioxide pellets are sintered in 1700°C furnace. The oxygen content can be determined by weight changes.

In uranium dioxide dissolution, a commercial electrode of saturated calomel electrode (SCE) is usually used as the counter electrode and a platinum electrode is used as the reference electrode. 3000 grit- Silicon Carbide paper is used to polish the electrodes and they are cleaned cathodically before the experiment. In our lab, electrochemical analysis, LSV, is performed with a potentiostat (CHI-600D, USA) controlling applied potentials and acquire current changes [2].

3. Algorithm for the Determination of Linear Tafel region

Since Tafel slope can be obtained on a linear region, the first derivative on the region should be constant. This is the simple principle to determine Tafel region. Since the data usually has fluctuation as a natural result of the experiment, it is necessary to be smoothed and differentiated using a numerical method such as Savitzky-Golay differentiation filter. Finite difference method can also be applied to obtain the first derivative value, but it still has fluctuation.

In an ideal condition of data, there should be a constant region on the first derivative graph. Then the region is decided as a Tafel region. If it is not, there should be a local extremum, a local minimum point or local maximum point, which can be considered as a center of Tafel region. It can be rarely reconfirmed by the second derivative as zero value as the mathematical character of the local extremum.

After obtaining the Tafel interval or central point, its width should be expanded to determine more accurate Tafel region. Starting from the local extremum of the first derivative, either side point of the region is expanded by each point on the original curve while R^2 is maintained as 0.999. There should be also a decision criterion of the interval of Tafel region as 100mV.

4. Conclusion

Tafel slope is easily determined for the simple experimental data, but it is difficult to decide the Tafel region in the complicated chemical behavior such as uranium dioxide dissolution, which is consisted of many chemical reactions. This method can be applied to determine Tafel region on various electrochemical analysis.

REFERENCES

[1] Allen J. Bard and Larry R. Faulkner, Electrochemical Methods: Fundamentals and Applications 2nd ed., John Wiley & Sons Inc., New York (2001).

[2] Jandee Kim, Jeongmook Lee, Young-Sang Youn, Nazhen Liu, Jong-Goo Kim, Yeong-Keong Ha, Sang-Eun Bae, David W. Shoesmith and Jong-Yun Kim, The Combined Influence of Gadolinium Doping and Non-stoichiometry on the Structural and Electrochemical Properties of Uranium Dioxide, Electrochimica Acta, 282, 1-31 (2017).

A Strategy for Desorption of Krypton Adsorbed on Porous Carbon Based on Vacuum Desorption for Krypton Enrichment

Ju Ho Lee*, Seok-Min Hong, Young-Soon Lee, and Yung-Zun Cho
Korea Atomic Energy Research Institute, 111, Daedeok-daero 989beon-gil, Yuseong-gu, Daejeon, Republic of Korea
*jhlee835@kaeri.re.kr

1. Introduction

In pyro-processing of spent-fuel, volatile fission products such as Krypton-85 and Xenon are released during high-temperature treatment in head-end processes. As Krypton-85 exhibits a half-life of 11 years, it should be trapped and stored until it reduces to non-radioactive species. Several trapping strategies [1] were developed and in KAERI, the process based on solid adsorption has been considered and tested [2,3]. The strategy for disposal of trapped Krypton is not clearly determined and the usage of high-pressure storage chamber is considered. The conventional desorption strategy for trapped Krypton are based on heating of adsorbed Krypton and purging with inert gas such as Argon. However, such strategy requires considerable amount of purging gas leading to the increased size of Krypton storage chamber, related to operating and equipment construction cost. In this study, for the reduction of size of storage chamber, a simple stragey for krypton desorption is proposed.

2. Proposed Krpton Desorption Strategy

Fig. 1. illustrates the proposed Krypton adsorption-desorption apparatus. The adsorption process is composed of gas supplying unit, adsorption column and concentration analyzer and desorption process of C1, the temporary gas storage chamber, C2, the final gas storage chamber, S, sampling pump for gas circulation and P, the manually-driven piston-cylinder assembly. This assembly is capable of generating pressure or vacuum since the volume can be reduced for compression and expanded for vacuum generation.

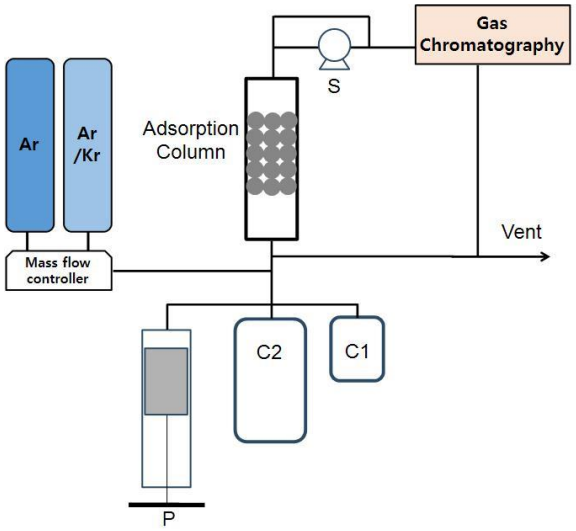

Fig. 1. schematic diagram of Kr adsorption-desorption process.

Adsorption process is closed when the concentration of outlet gas stream amounts to 35% of inlet Kr-Ar mixture. The trapped gas in adsorption column is recovered in two steps. The half of trapped gas is delivered to C1 using piston-cylinder assembly. Since mostly Krypton is adsorbed in porous carbon at low temperature,

the temporarily stored gas is considered to relatively krpton-lean gas mixture. Then adsorption column is heated to ambient temperature or 150 ^{o}C. Since the pressure in adsorption column is reduced due to the recovered gas mixture, the part of the recovered gas stored in C1 is re-introduced to adsorption column until the pressure becomes ambient pressure for prevention of leak. The remaining gas in adsorption column is circulated using sampling pump to eliminate composition localization in adsorption column. Finally, the remaining gas is mostly recovered using piston-cylinder assembly and stored into C2. The remaining Kr-lean gas in C1 and pure Argon is introduced into adsorption column until the pressure is increased to atmospheric pressure and re-circulated until the temperature is reduced to the trapping temperature and adsorption process begins. An experimental apparatus is being constructed to evaluate the performance of the proposed desorption process.

Acknowledgement

This work was supported by the National Research Foundation of Korea (NRF) grant funded by the Korea government (No. 2017M2A8A5015075).

REFERENCES

[1] W.R. A. Goossens, G.G. Eichholz and D.W. Tedder, "Treatment of Gaseous Effluents at Nuclear Facilities", Harwood academic publishers (1991).

[2] S.M.Hong, G.Lim, S.H.Kim, J.H.Kim, K.B.Lee, and H.C.Ham "Preparation of porous carbons based on polyvinylidene fluoride for CO2 adsorption: A combined experimental and computational study", Micropor. Mesopor. Mat, 15, 59-65 (2016).

[3] J.H. Lee, S.M. Hong, J-W. Lee and Y.J. Cho, “Adsorption of krypton on porous carbon at low tempeature”, Proc. of the KRS 2019 Spring Conference, 17(1), May 8-10, Busan.

24-hour Report on the 5th Collaborative Materials Exercise (CMX-5) for Nuclear Forensic Analysis

Na-Ri Lee*, Jinkyu Park, Ranhee Park, Sun-Ho Han, Sang Ho Lim, and Chi-Gyu Lee
Korea Atomic Energy Research Institute, 111, Daedeok-daero 989beon-gil, Yuseong-gu, Daejeon, Republic of Korea
*nari92@kaeri.re.kr

1. Introduction

Since the collapse of the Soviet Union in the early 1990s, illicit trafficking of nuclear or radioactive materials or undeclared nuclear activity was revealed in Europe[1]. Illicitly possessed nuclear or radioactive materials can be abused in some cases, such as nuclear terrorism, illegal weapons production, etc., and international cooperation is required to sanction it. Thus, laboratories involved in nuclear forensics cooperated to organize the Nuclear Forensics International Technical Working Group (ITWG) in 1996. Nuclear Forensics is a methodology that analyze physical/chemical properties of seized nuclear materials and provide the origin, history, transport route and purpose of these.

Collaborative Materials Exercise (CMX) organized by ITWG has the purpose of evaluation and comparison of nuclear forensics technique. Participants for CMX should analyze and report within 24-hour, 1-week, and 2-months on a hypothetical scenario that assumes illicit trafficking of unknown samples.

We participated in the 5th CMX (CMX-5) and carried out nuclear forensic analysis upon unknown nuclear materials. Here we present the analytical results that can be performed quickly within 24-hour to characterize the nuclear materials.

2. Experimental

2.1 Sample of CMX-5

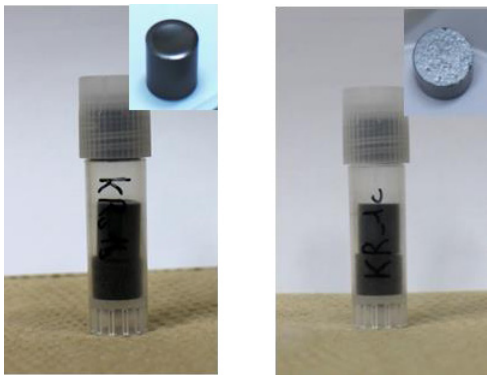

Fig. 1. Pictures of CMX-5 samples. Left is sample A(KR-1B) and right is sample B(KR-1C).

The delivered samples of CMX-5 were two types of pellet as shown in Fig. 1. Based on the exercise scenario, sample A was seized from a courier vehicle in country Alpha, and sample B was found in a scrap yard in country Beta. Sample A(KR-1B) has visually smooth surface, while sample B(KR-1C) has rough surface.

2.2 Analysis for 24hour report

In the analysis at 24-hour report, dose rate (β/γ) measured by AT6130D Geiger meter, and

surface contamination by smear method on β/γ and α was monitored using LBCS(S5-XLB). Weight and dimensional determination were measured by an analytical balance (Mettler Toredo, XP105) and a digital caliper, respectively. Measurement using high resolution Multi Collector-Inductively Coupled Plasma-Mass Spectrometry (MC-ICP-MS, Neptune plus) was carried out to determine mass of ^{235}U.

3. Results and Discussion

Results of the surface contamination measurement such as dose rate (β/γ), smear on β/γ and α for radioactivity determination were below the environmental level for both sample A and B.

Weights of sample A and B were 5.68996 g ± 0.0001 and 6.0068 g ± 0.0001, respectively. Densities of sample A and B were 10.13 g/cm^3 ± 0.038 and 10.39 g/cm^3 ± 0.0059, respectively.

Quantitative analysis of uranium in the sample was performed by using high resolution MC-ICP-MS. As a result, uranium is present in both sample A and B, with amounts of 4.811 g ± 0.026 and 5.272 g ± 0.033, respectively. MC-ICP-MS was also used to determine the quantity of ^{235}U.

According to scenario, country Alpha's law criminalize more than 4 g of greater than 1% enriched uranium relative to isotope ^{235}U. Total U content in sample A is more than 4 g, but ^{235}U mass % in it is 0.999 ± 0.0028 %, which is ambiguous. Considering the uncertainty, we concluded that sample A is suggestively illegal possession. Also, country Beta's law criminalize more than 5 g of greater than 1 % enriched uranium relative to isotope ^{235}U. Total U content in sample B is more than 5 g and ^{235}U mass % in it is 1.101 ± 0.0028 %. Consequently, sample B is obviously illegal possession.

4. Conclusions

In this study, we participated in the ITWG's CMX-5 and conducted 24-hour analysis to determine radioactivity, physical properties, and ^{235}U content in sample. Uranium content analysis was performed using high resolution MC-ICP-MS without chemical separation process. As a result, uranium with about 1 % enrichment relative to ^{235}U was confirmed in sample A and B. According to the laws defined in the scenario we concluded that both of the samples were illegally possessed, and our conclusions were consistent with the consensus of other participants.

REFERENCES

[1] K. Mayer, M. Wallenius, and T. Fanghanel, "Nuclear forensic science – From cradle to maturity", Journal of Alloys and Compounds, 444(445), 50-56 (2007).

2-month Report on the 5th Collaborative Materials Exercise (CMX-5) for Nuclear Forensic Analysis : Uranium Age Dating

Ranhee Park*, Sun-Ho Han, Sang Ho Lim, Jinkyu Park, Na-Ri Lee, and Chi-Gyu Lee
Korea Atomic Energy Research Institute, 111, Daedeok-daero 989beon-gil, Yuseong-gu, Daejeon, Republic of Korea
*ranhee@kaeri.re.kr

1. Introduction

The currently accepted definition of nuclear forensics is the examination of nuclear or other radioactive materials or of evidence contaminated with radionuclides in the context of international or national law or nuclear security. The analysis of nuclear or other radioactive material seeks to identify what the materials are, how, when, and where the materials were made, and what were their intended uses. The development of radiochronometry, or age dating, and its application to nuclear materials is one area of intense research for nuclear forensics. Radiometric model ages are determined from measurements of parent and progeny isotopes (typically daughter, but also granddaughter) that accumulate in a material due to decay of the radioactive parent isotope. The age of nuclear material is an important forensic signature because it can be used to constrain the time of purification or production (a predictive signature) and establish or eliminate potential genetic links among different samples of nuclear materials (a comparative signature).

Various analytical methods for age-determination of uranium samples have been being developed in many laboratories. These methods are based on the accurate determination of a daughter-mother radionuclide pair such as $^{230}Th/^{234}U$, $^{231}Pa/^{235}U$, $^{214}Bi/^{234}U$. Because the half-life of ^{234}U is relatively short (2.45×10^5 years) compared to the other naturally occurring uranium(U) isotopes, ^{235}U and ^{238}U, the ^{234}U–^{230}Th chronometer is one of the most straightforward chronometers to measure, and certainly the most widely applied. [1,2]

Our laboratory participated in 5th collaborative materials exercise (CMX-5) for nuclear forensic analysis. Age dating was performed to estimate an association between two samples and origin of the two samples (sample A and B).

2. Experimental

2.1 Chemical separation

Thorium(Th) isotopes were separated twice by TEVA resin (Eichrom, 100-150 mesh). 0.8 mL of 0.02 M HF/0.02 M HNO_3 solution was used as an eluting solution for Th isotopes and 0.2 mL of 5% nitric acid added to be 1 mL of final volume for mass spectrometry analysis. For the IDMS of Th isotopes, portion of sample A and B solution was taken and spiked with ^{232}Th. For the IDMS of U isotopes, no chemical separation was applied. Sample A and B

solution was diluted with 3% HNO_3 to make 100~150 ppt of sample solution and spiked with ^{233}U.

2.2 Isotopic analysis

Isotopic measurements of $^{230}Th/^{234}U$ within exercise samples were performed using highly sensitive MC-ICP-MS equipped with desolvation system (Aridus Ⅱ). MC-ICP-MS is capable of a simultaneous measurement using multi-detectors. Th and U isotopes were determined based on the simultaneous measurements using SEM and Faraday cup.

3. Results and Discussion

The amounts of U and Th contained in each sample were determined using isotope dilution mass spectrometry (IDMS). The age of the sample is calculated as follows,

$$\frac{N_{Th230}}{N_{U234}} = \frac{\lambda_{U234}}{\lambda_{Th230} - \lambda_{U234}}(1 - e^{(\lambda_{U234} - \lambda_{Th230})t}) \quad (1)$$

$$t = \frac{1}{\lambda_{U234} - \lambda_{Th230}} \ln(1 - \frac{N_{Th230}}{N_{U234}} \frac{\lambda_{Th230} - \lambda_{U234}}{\lambda_{U234}}) \quad (2)$$

where,

N_{Th230}/N_{U234} : the atomic ratio in the sample,

λ_{U234} *and* λ_{Th230} : the decay constants of ^{234}U and ^{230}Th,

t : the elapsed time after the separation of the radionuclides.

The age dating results of sample A and B for CMX-5 were 4.7 ± 0.1, 4.5 ± 0.1 years, respectively. The results showed no significant differences between sample A and B. Average for both samples was 4.2 ± 0.7 year. Uncertainties are expanded combined standard uncertainties (U_c) with k = 2.

4. Conclusion

In the CMX-5 exercise, our laboratories successfully performed radiochronometry on the two CMX-5 samples (sample A and B) by $^{234}U/^{230}Th$ chronometer. Ages of two samples (sample A and B) were estimated with decent precision. And the results were consistent with the consensus data from 20 participating laboratories.

REFERENCES

[1] SP. LaMont, G. Hall, “Uranium age determination by measuring the $^{230}Th/^{234}U$ ratio”, J Rodioanal Nucl Chem, 264(2), 423-427 (2005).

[2] AM. Gaffiney, A. Hubert, WS. Kinman, M. Magara, A. Okubo, “Round-robin ^{230}Th–^{234}U age dating of bulk uranium for nuclear forensics”, J Rodioanal Nucl Chem, 307(3), 2055-2060 (2016).

1-Week Report on the 5th Collaborative Materials Exercise for Nuclear Forensic Analysis

Jinkyu Park*, Ranhee Park, Sang Ho Lim, Sun Ho Han, and Chi-Gyu Lee
Korea Atomic Energy Research Institute, 111, Daedeok-daero 989beon-gil, Yuseong-gu, Daejeon, Republic of Korea
*Jinku1004@kaeri.re.kr

1. Introduction

Nuclear forensics is to investigate the origin and the trafficking of unidentified nuclear materials by physical and chemical analyses on the materials in combination with law enforcement and intelligence information. Materials analysis plays an essential role in the nuclear forensics by providing decisive information for estimating history of unknown materials. Typically, the materials analysis is performed in a timeframe of 24 hours, a week or two months after the seizure of unknown nuclear materials, according to the urgency of an information and the time taken to obtain the information [1].

The Nuclear Forensics International Technical Working Group, an informal, multinational association of nuclear forensic practitioners, organizes a practical exercise program for nuclear forensic analysis, called Collaborative Materials eXercise (CMX), every other years. KAERI, with 19 other institutes, participated in the 5th CMX program in 2016-2017. Here, we reported a part of the program, which describes analytical procedures, results and tentative conclusions based on the analysis during a week after the seizure of the materials.

2. Materials and Procedure

2.1 Materials

Fig. 1. Seized nuclear materials.

Based on the CMX-5 scenario, a dense radioactive object was seized from a courier van without a certificate of a radiation inspection (Sample A). Before this event, another dense radioactive object was discovered in a scrap yard (Sample B). 24 hours-analysis revealed that two samples are uranium fuel pellets with 1.00 and 1.10% of ^{235}U, respectively, which were turned out to be illegal possessions. The next step is to investigate the relationship between two samples by a week-analysis.

2.2 Procedure

Physical assessment for the samples were conducted by visual inspection and scanning electron microscopy-energy dispersive X-ray spectroscopy (SEM-EDS). Inductively coupled plasma mass spectrometry (ICP-MS) and isotope dilution mass spectrometry (IDMS) were used for elemental and isotopic analyses. Finally, chemical composition of the samples was analyzed by X-ray diffraction spectroscopy (XRD).

3. Results and Discussions

SEM images from Sample A and B clearly show that they have different grain sizes. Grain sizes of Sample B were larger than them of Sample A. The lager grain size might be related to weaker mechanical strength. Indeed, Sample B was more easily crushed compared to Sample A. This indicates that two samples might be processed in different ways such as in different sintering methods. Visual inspection also strengthened this conclusion. Sample A has smooth surface, while Sample B has rough surface, implying that Sample A might be processed by surface smoothing. In addition, top and bottom of Sample A were dented whereas those of Sample B were flat. This indicates that two pellets were shaped in different compaction methods.

Elemental and isotopic analysis data prove that the source materials used for the preparation of two samples were different. Mass % of uranium in Sample B was ~ 88% close to that of pure UO_2, whereas mass % of uranium in Sample A was ~ 84% which indicates the presence of U_3O_8 or other components. XRD data demonstrated that both samples were pure UO_2 (no U_3O_8), and thus Sample A can be estimated to be made of UO_2 and another materials.

4. Conclusion

The different grain sizes of two samples indicate that the samples were sintered under different conditions such as temperature and pressure. Elemental and isotopic analysis data indicate the different source materials. Collectively, we can conclude that two samples were prepared with different materials and manufacturing conditions.

REFERENCES

[1] J.M. Schwantes, O. Marsden, and D. Reilly, “Fourth Collaborative Materials Exercise of the Nuclear Forensics International Technical Working Group”, J. Radioanal. Nucl. Chem., 315(2), 347-352 (2018).

Complementary Raman Spectroscopy and Simulation Approach to Verify the Structure of Metal-doped UO_2

Jeongmook Lee[1,*], Choah Kwon[2], Jandee Kim[1], Young-Sang Youn[3], Jong-Yun Kim[1], Byungchan Han[2], and Sang Ho Lim[1]

[1]Korea Atomic Energy Research Institute, 111, Daedeok-daero 989beon-gil, Yuseong-gu, Daejeon, Republic of Korea

[2]Yonsei University, 50, Yonsei-ro, Seodaemun-gu, Seoul, Republic of Korea

[3]Yeungnam University, 280, Daehak-ro, Gyeongsan-si, Gyeongsangbuk-do, Republic of Korea

[*]leejm@kaeri.re.kr

1. Introduction

The physical and chemical properties of spent nuclear fuels are totally different from initial fresh UO_2 fuel. For example, some actinide and lanthanide elements produced during irradiation of UO_2 can form a solid solution with UO_2 lattice and make non-stoichiometry depending on their oxidation state and specific conditions. These alterations of UO_2 lattice could strongly be related to chemical reactivity such as corrosion and oxidation of UO_2 [1-2]. Thus, it is critical to characterize the physical and chemical properties of spent nuclear fuels affected by specific elements doping. Those characterizations should be useful to plan the final disposal or interim storage of spent nuclear fuels.

Herein, the influence of metal-doping on the surface structure of UO_2 has been investigated by X-ray diffraction (XRD) and Raman spectroscopy. The simulation using metal-doped UO_2 matrix model was successfully performed to compare with the experimental results.

2. Experimental sections

UO_2 and Nd_2O_3 (or Gd_2O_3, ZrO_2, ThO_2) powders for $U_{1-y}Nd_yO_2$ (or $U_{1-y}Gd_yO_2$, $U_{1-y}Zr_yO_2$, $U_{1-y}Th_yO_2$) with various components (y) were mixed and pelletized. The sample pellets were sintered in the tube furnace at 1700 °C for 18 h with hydrogen atmosphere. XRD data was collected by Bruker D8 Advance using CuKα line source (beam current 40mA at 40kV). The lattice parameters of the samples were calculated from XRD spectra with refinement process. Raman spectra were measured using ANDOR Shamrock SR500i spectrometer with a wavelength of 632.8 nm from He-Ne laser and analyzed by peak deconvolution method. Using first-principles we optimized model structures and calculated vibration frequencies in the frame of DFT implemented in the Vienna *Ab-initio* Simulation Package (VASP) [3]. Vibrational frequencies and Raman-active modes were calculated using the finite difference method as implemented in the phono3py code [4].

3. Results

The lattice parameters for $(U,Nd)O_2$, $(U,Gd)O_2$, $(U,Zr)O_2$, and $(U,Th)O_2$ were linearly changed as the doping level increased. These linear relationships indicate that sample pellets were made as solid solutions with remaining UO_2 fluorite structure. For $(U,Zr)O_2$, it was

confirmed that the simulated linear relationship was consistent with the experimental results.

The distinct defect peaks around 530 cm^{-1} was observed in the Raman spectra of Nd-, Gd-doped UO_2. This peak has been ascribed to the defect structure due to oxygen vacancy to compensate the charge imbalance, caused by substitution of U^{4+} by Nd^{3+} or Gd^{3+}. No peaks are expected in this region of the Raman spectra of the $(U,Zr)O_2$ pellets since the dopant is a tetravalent element. For instance, Th^{4+}-doped UO_2 pellets did not have the peak corresponding to the defect structure because the dopants do not generate oxygen vacancies.

In the Raman spectra of all $(U,Zr)O_2$ pellet, a peak about 598 cm^{-1}, could originate from the ZrO_8-type complex in the UO_2 matrix. First-principles DFT calculations revealed that this peak could be assigned ad vibration of O in the ZrO_8-type complex moving longer distance with respect to the equilibrium position, compared to O in other positions (Fig. 1).

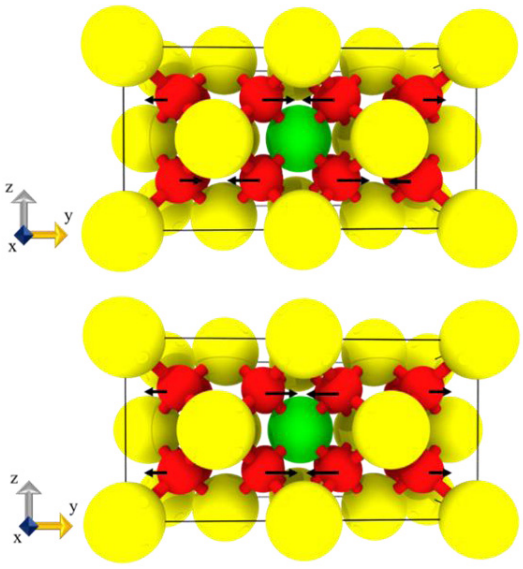

Fig. 1. Normal modes of the peaks at (up) 466.82 cm^{-1} and (down) 596.15 cm^{-1}. The yellow, green and red spheres represent U, Zr and O atoms, respectively.

4. Conclusion

We identified that the surface structure of metal-doped UO_2. XRD analysis and Raman spectroscopic observation was consistently supported by first-principles DFT calculations. Our study is systematic tool to understand and characterize fundamental structural properties of metal-doped UO_2.

Acknowledgement

This work was supported by the National Research Foundation of Korea (NRF) grant funded by the Korean government (MSIT) (2017M2A8A5014754).

REFERENCES

[1] M. Razdan, D.W. Shoesmith, “Influence of trivalent-dopants on the structural and electrochemical properties of uranium dioxide (UO_2)”, Journal of Electrochemical Society, 161, H105–H113 (2013).

[2] Jandee Kim, Jeongmook Lee, Young-Sang Youn, Nazhen Liu, Jong-Goo Kim, Yeong-Keong Ha, Sang-Eun Bae, David W. Shoesmith, Jong-Yun Kim, “The Combined Influence of Gadolinium Doping and Non-stoichiometry on the Structural and Electrochemical Properties of Uranium Dioxide”, Electrochimica Acta, 282, 1-31 (2017).

[3] G. Kresse, J. Hafner, “Ab initio molecular dynamics for liquid metals”, Phys. Rev. B, 47, 558–561 (1993).

[4] A. Togo, L. Chaput, I. Tanaka, “Distributions of phonon lifetimes in Brillouin zones” Phys. Rev. B, 91, 094306 (2015).

Determination of Chelating Agents by High Performance Liquid Chromatography-diode Array Detection (HPLC-DAD)

Jihye Kim[1,*], Kihwan Choi[2], Jai Il Park[1], and Tae-Hong Park[1]
[1]Korea Atomic Energy Research Institute, 111, Daedeok-daero 989beon-gil, Yuseong-gu, Daejeon, Republic of Korea
[2]Korea Research Institute of Standards and Science, 267, Gajeong-ro, Yuseong-gu, Daejeon, Republic of Korea
[*]jihyekim21@kaeri.re.kr

1. Introduction

Chelating agents are composed of complex mixtures such as anionic, cationic, and nonionic materials. They have the potential to perturb the metal speciation and may lead to the remobilization of metals from environment (sediment, soil, and water). As a result, it gives rise to posing a risk to groundwater, drinking water and even products from soil.

Traditional method for the determination of chelating agents has been widely used in a titration method by spectrophotometric detection which requires labor-intensitve pipetting, time consuming, and large sample volume.

In this study, to overcome the difficulties of previous method, the chromatographic separation has been developed for the determination of ethylendiaminetetraacetic acid (EDTA), nitrilotriacetic acid (NTA), and citric acid. The separation of complex chelating agents is very difficult in a single chromatographic run without chemical modifier for ion pairing. Here, reverse-phase chromatographic method was adopted to separate those three chelating agents (EDTA, NTA, and citric acid) in a single column. This chromatographic method provides fast analysis (40 min for one sample) and easy quantification, and requires low sample volume (tens microliters). Under the optimal conditions, the calibration curves obtained from 0 ~ 5000 mg/L standard samples (EDTA, NTA, and citric acid) showed good linearities with the square of the linear correlation coefficients in the range of 0.9998~0.9999. The LODs ranged from 41 to 99 mg/L.

2. Materials and methods

2.1 HPLC-DAD conditions

The column was an YMC-Pack ODS (4.6 × 250 mm) (AQ12S05-2546WT, Waters). Sample injection volume was 10 μL and flow rate was at 0.5 mL/min. Acetonitrile and water was HPLC grade (Fisher Scientific). All of the other solvents and chemicals were of analytical grade and purchased from Merck (St. Luis, MO). The gradient started with 100% A (0.01 M sulfuric acid in H_2O) and 0% B (acetonitrile) after 20 min, changed to 65% A over 10 min, and then 0% A over 1 min, followed by 100% A in 4 min. Finally, over 10 min, it was held to the original 100% A resulting in a total separation time of 45 min.

2.2 Instrument

HPLC was performed on an ACQUITY UPLC system from Waters (Milford, PA, USA) with preprogrammed Empower software (Fig. 1). Analytes were monitored using a UV detector at 210 nm.

Fig. 1. ACQUITY UPLC system from Waters.

3. Results and discussion

The chromatogram of three standard mixture are shown in Fig. 2, and their retention times are described in Table 1. NTA and EDTA are baseline separation in Fig. 2. Because the p*K*a values are 1.78, 2, and 2.92 for NTA, EDTA, and citric acid, respectively, those components can be partitioned with reverse-phase chromatography under acidic mobile phase.

Linearity was assessed by injecting 3 consecutive times 6 standards (0, 50, 100, 500, 1000, 2000, 5000 mg/L of NTA, EDTA, and citric acid, respectively), using peak area (y) as a calibration parameter plotted against concentrations (x): a linear graphs were obtained with an $y = 448.38x + 3827.62$, $y = 2615.42x - 12237.47$, and $y = 1111.02\,x + 3827.62$ for NTA, EDTA, and citric acid, respectively.

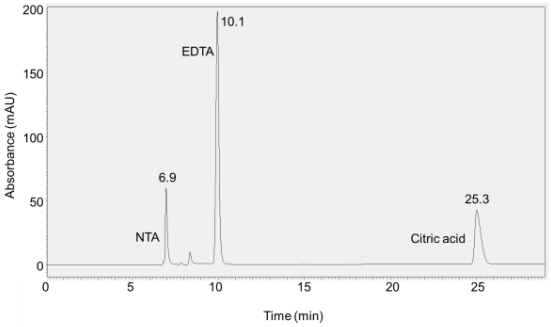

Fig. 2. HPLC Chromatogram of the standard samples (NTA, EDTA, and citric acid).

Table 1. Retention time of HPLC for chelating agents

No.	Analyte	Retention time (min)
1	NTA	6.9
2	EDTA	10.1
3	Citric acid	25.3

4. Conclusions

This method has been developed that three chelating agents, NTA, EDTA, and citric acid for analyzing radioactive wastes in a single chromatographic run with a 45 min total analysis time which is much easier and faster than the conventional titration method.

REFERENCES

[1] P. Laine and R. Matilainen, “Simultaneous determination of DTPA, EDTA, and NTA by UV-visible spectrometry and HPLC” Anal Bioanal Chem 382, 1601-1609 (2005).

Determination of O/U Ratio of UO_{2+x} by Chemical Method

Jong-Goo Kim*, Jong-Yun Kim, Jeong mook Lee, Tae-Hyeong Kim, Junghwan Park,
Hye-Ryun Cho, and SangHo Lim
Korea Atomic Energy Research Institute, 111, Daedeok-daero 989beon-gil, Yuseong-gu, Daejeon, Republic of Korea
*njgkim@kaeri.re.kr

1. Introduction

Although uranium dioxide is provided as stoichiometric state ($UO_{2.+x}$, x=0) from vendor, O/U ratio can be easily changed to hyper-stoichiometric state ($UO_{2.+x}$, x>0) even in ambient atmosphere. And so, when we use uranium dioxide stored in laboratory, we often need to determine O/U ratio of it to identify.

This study investigated several analytical methods for the determination of O/U ratio, especially by measuring U(IV) and U(VI) concentrations of dissolved solution of the sample and compared the simplicity and accuracy of each methods.

A method selected using 2M H_2SO_4-HF for dissolving Uranium dioxide sample and spectrophotometry for measuring U(IV) and U(VI) was examined.

2. Chemical methods for the determination of O/U ratio

O/U ratio determination by chemical method is based on the assumption, that is, x is equal to y in $U_{1-y}{}^{4+}U_y{}^{6+}O^{2-}{}_{2+x}$ and the ratio U(VI)/U(IV) in the dissolved solution is the same as that of the solid sample.

2.1 Non- oxidizing dissolving acids

Two Acids, SPA (Strong Phosphoric Acid)[1] and 2M H_2SO_4-HF[2] are known to be used as non- oxidizing dissolving acid, which make U(IV) stable in dissolved solution and so, retain the U(VI)/U(IV) ratio same with the solid sample.

2.2 Measuring of U(IV) and U(VI)

The concentration of U(IV) and U(VI) in dissolved solution can be measured by electro-analytical methods (polarography, coulometry) or spectrophotometry.

3. Determination of O/U ratio of UO_2 pellet sample by spectrophotometry

3.1 Dissolution

UO_2 pellet (10mm dia., 2mm thick) was dissolved using 10 ml of 2M H_2SO_4-HF in pressure vessel (~200 °C) equipped in argon atmosphere glove box [Fig. 1].

Fig. 1. Pressure vessel for dissolving sample.

3.2 Measurement of standards for preparation of calibration curves

UV-Vis spectra of U(IV) standard solutions (0.204, 0.509, 1.02, 2.04, 4.08 mM) and of U(VI)

standard solutions (0.0546, 0.109, 0.218, 0.546, 1.09 mM) were measured [Fig. 2, 3] . Calibration curves for U(IV) and U(VI) were obtained from absorbance values of standard solutions [Fig. 4, 5].

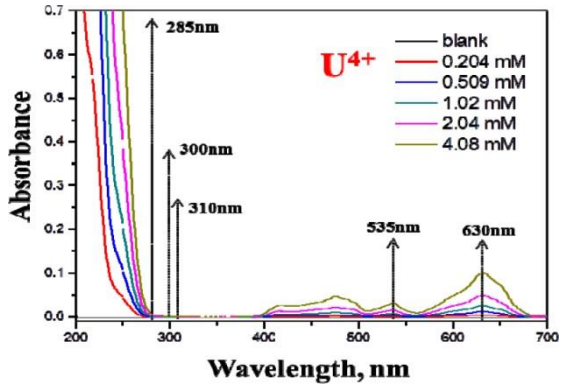

Fig. 2. Spectra of standard solutions of U(IV).

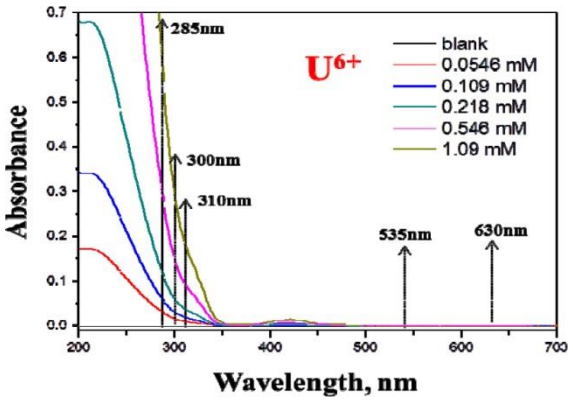

Fig. 3. Spectra of standard solutions of U(VI).

3.3 Measurement of U(IV) and U(VI) concentrations of dissolved UO_2 pellet sample and calculation of O/U ratio of sample

The concentration of U(IV) and U(VI) can be obtained using calibration curves and absorbance values of U(IV) and U(VI) in the spectra of dissolved solution.

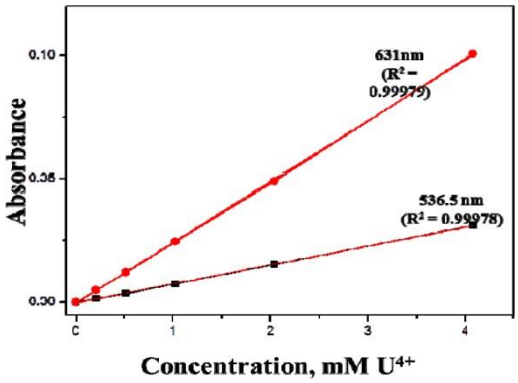

Fig. 4. Calibration curves for (IV).

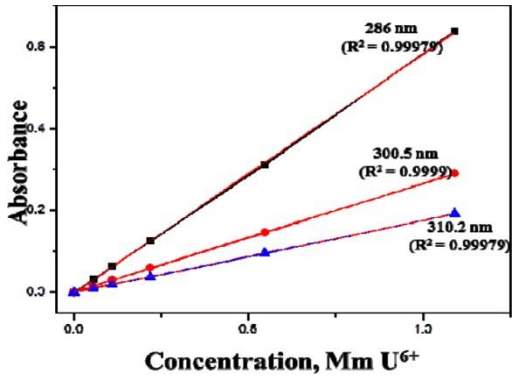

Fig. 5. Calibration curves for U(VI).

And so, O/U ratio = $2 + [U^{6+}] / [U^{4+} + U^{6+}]$

= 2.05

4. Conclusion

It was confirmed that spectrophotometric method using 2M H_2SO_4-HF is effective in the simplicity to determine O/U ratio of uranium dioxides.

REFERENCE

[1] S. R. Sarkar et al., Journal of Radio analytical and Nuclear Chemistry, 220(No 2), 155 (1997).

[2] B. Narasimaha Murty et al, Talanta 38 (11), 1335 (1991).

Study of 4-Nitrocatechol Adsorption on the Surface of U(IV) Nanoparticles Using Various Spectroscopic Methods

I. H. Yoon[1,2], H. Cho[2], H.-R. Cho[1,2], and W. Cha[2,*]
[1]University of Science & Technology, 217 Gajeong-ro, Yuseong-gu, Daejeon, Republic of Korea
[2]Korea Atomic Energy Research Institute, 111, Daedeok-daero 989beon-gil, Yuseong-gu, Daejeon, Republic of Korea
*wscha@kaeri.re.kr

1. Introduction

Lately, disposal of high-level radioactive waste in deep underground repository is major issue. Thus, the behaviors of actinides species under anaerobic and reducing conditions of repository environment are needed to be studied in detail. In this study, tetravalent uranium (U(IV)) was adopted since it represents a dominant oxidation state of U in deep aqueous environments. Complexation of organic molecules may affect mobility of U species including their colloidal particle. The main work of this study is to characterize the interaction of U(IV) nanoparticles ($U(IV)_{NPs}$) with organic molecules under reducing conditions by using various spectroscopic techniques such as ATR-FTIR and UV-Vis spectroscopic methods.

2. Results and Discussions

In this study, 4-nitrocatechol was selected as model organic ligands. Before studying the interaction of this ligand with $U(IV)_{NPs}$, the characteristics of synthetic $U(IV)_{NPs}$, was first exmained. To prepare $U(IV)_{NPs}$, an aqueous U(IV) solution of 3 mM was prepared, and subsequently heated 90 °C for 5 hours by using heating block. Thereafter, size distribution and zeta potential values of $U(IV)_{NPs}$ were measured by dynamic light scattering analysis (DLS). The measured size of nanoparticles was 23 ± 2 nm and the zeta potential levels were +38 ± 2 mV. Such high positive zeta potential values indicate a fair colloidal stability under acidic conditions (pH 2.3). Also, the colloidal stability of $U(IV)_{NPs}$ was maintained up to 2 months.

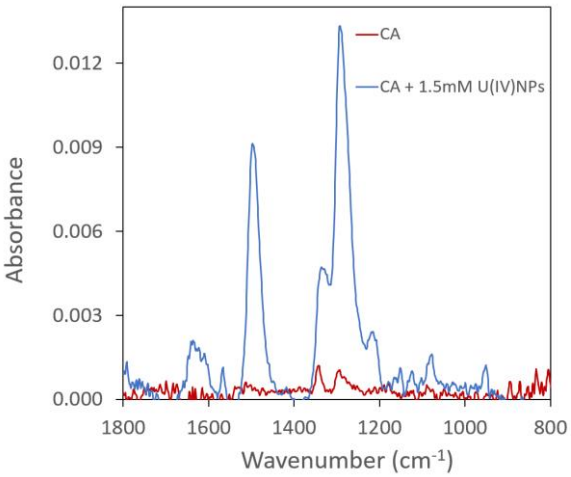

Fig. 1. ATR-FTIR spectra of 1 mM 4-nitrocatechol in the presence and absence of $U(IV)_{NPs}$ at pH 3.

By using the synthetic $U(IV)_{NPs}$ prepared as shown above we have monitored spectroscopic changes upon complexation of organic molecules with $U(IV)_{NPs}$ in aqueous solutions. Figure 1 shows ATR-FTIR spectra of 5mM 4-

nitrocatechol without $U(IV)_{NPs}$ and with 0.5mM $U(IV)_{NPs}$. IR absorption of 4-nitrocatechol was significantly enhanced in the presence of $U(IV)_{NPs}$ with the strong band at 1300 cm^{-1} and 1500 cm^{-1}. These SEIRA effects indicate chemisorption of organic molecules on the surface of $U(IV)_{NPs}$. SEIRA is a near-field phenomenon where IR absorption of molecules adsorbed on or in the vicinity of small metal-/metal oxide-clusters is enhanced by a factor of 10 to 1000 due to the electromagnetic fields produced by the surface plasmon of clusters [1].

Adsorption capacity of $U(IV)_{NPs}$ was measured by using UV-Vis spectrophotometry. After the addition of 4-nitrocatechol into $U(IV)_{NPs}$ solution, the mixture was stored overnight. Then, it was centrifuged to 38,000 rpm at 25 °C for 2 hours and the obtained supernatant was analized by using UV-Vis absorption spectroscopy. Figure 2 shows UV-Vis spectra of 0.2 mM 4-nitrocatechol in the presence and absence of $U(IV)_{NPs}$ at pH 3. UV absorption of 4-nitrocatechol was significantly decreased in the increase of $U(IV)_{NPs}$ concentration at 340 nm. These indicate 4-nitrocatechol adsorption on the surface of $U(IV)_{NPs}$.

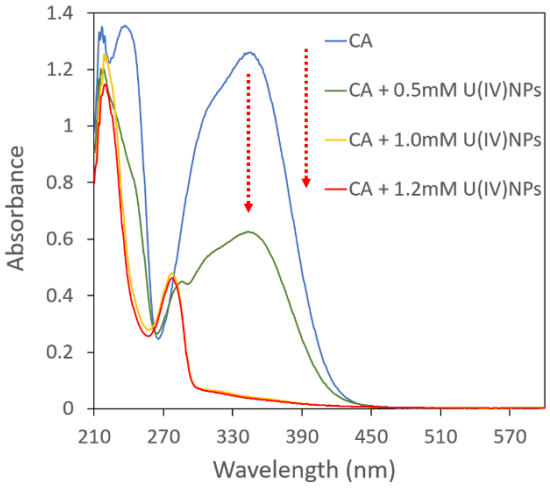

Fig. 2. UV-Vis spectra of 0.2 mM 4-nitrocatechol in the presence and absence of $U(IV)_{NPs}$ at pH 3.

3. Conclusion

By using ATR-FTIR and UV-Vis spectroscopy, it is shown that 4-nitrocatechol is in fact chemisorbed on the surfaces of $U(IV)_{NPs}$. Based on UV-Vis adsorption measurement we also demonstrate that adsorption equilibria between $U(IV)_{NPs}$ and 4-nitrocatechol can be obtained. SEIRA effects are expected to be useful to examine the interaction of $U(IV)_{NPs}$ with organic molecules under anaerobic groundwater systems.

REFERENCES

[1] P. R. Griffiths, “Surface-enhanced infrared absorption spectroscopy: principles and applications” Spectroscopic Properties of Inorganic and Organometallic Compounds, 44, 95-122 (2013).

Trivalent Plutonium Hydrolysis Thermodynamics in Aqueous Solution

S. K. Cho[1,2], H.-R Cho[1,2,*], H.-K. Kim[1], and W. Cha[1]
[1]Korea Atomic Energy Research Institute, 111, Daedeok-daero 989beon-gil, Yuseong-gu, Daejeon, Republic of Korea
[2]University of Science & Technology, 217 Gajeong-ro, Yuseong-gu, Daejeon, Republic of Korea
*hrcho@kaeri.re.kr

1. Introduction

For the safety assessments of the deep underground repository for high-level radioactive wastes, thermodynamic data of long-lived actinide are essential. Chemical behaviors of actinides in the underground environment are affected by temperature, pH, redox potential, dissolved molecules in groundwater, and so on. The underground disposal environment would be a reducing and high-temperature condition. However, up to now, aqueous trivalent plutonium researches performed at various temperature have been scarce. The purpose of this work is to obtain formation constant of trivalent plutonium hydrolysis species and solubility of plutonium hydroxide for determining thermodynamic constant. These experiments were conducted at a temperature of 10 °C and 40 °C. With the previous results obtained at 25 °C [1], we look forward to obtaining thermodynamic constants.

2. Methodology

2.1 Sample preparations

A Pu(Ⅲ) stock solution in 0.1 M $HClO_4$ was prepared by electrolysis with a chemically purified Pu(Ⅵ) solution in 0.1 $HClO_4$. Pu(Ⅲ) samples with different concentrations at various pHs were prepared by electrolysis at 10 and 40 °C in ionic strength 0.1M $NaClO_4$ medium. pH value of plutonium solution in a reactor was increased by three-electrode system. The hydrogen concentration in the solution was decreased by hydrogen evolution reaction as a supplying negative voltage. Fig.1 shows the scheme of device setup for electrolysis. The working and counter electrodes were made of platinum gauzes for bulk electrolysis. Teflon vessel and quartz tubes were used for minimizing the adsorption of colloidal particles. Vycor frits were used for the reference and counter electrodes to conserve the condition of plutonium solutions during the electrolysis. The temperature of the solution was kept constant using a water bath.

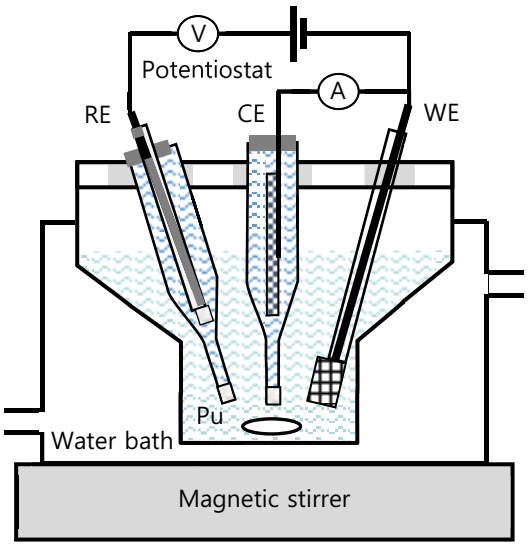

Fig. 1. Electrolysis setup with three-electrode system.

2.2 Measurement setup

Plutonium hydroxide complexes are generated by increasing pH value in the solution. Absorption spectra of trivalent plutonium were measured with a spectrophotometer (Cary5000, Agilent Tech) to determine the concentration of plutonium in solutions. Laser-induced breakdown detection (LIBD) was used to detect the formation of colloidal particles of $Pu(OH)_3$ (am) dispersed in the solution.

3. Results & Discussion

3.1 Thermodynamics calculation of Pu(Ⅲ) Hydrolysis

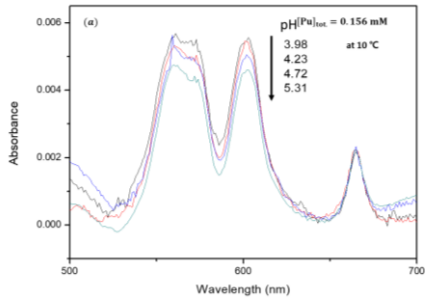

(a)

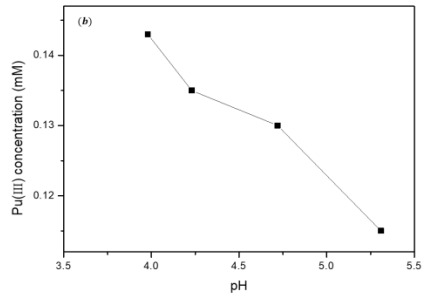

(b)

Fig. 2. Absorption spectra of Pu(Ⅲ) solution at 10 °C and 0.1M $NaClO_4$ were obtained within pH 3.98 to 5.31. (a) Absorbance decreases with pH increasing. (b) Pu^{3+} ion concentration changes by the varied pHs on the constant total plutonium concentration.

Fig. 2(a) shows absorption spectra of plutonium samples measured from 500 to 700 nm in wavelength. These spectra were consistent with the reference spectrum Pu^{3+} ions in 0.1 M $HClO_4$. The plutonium concentration measured by LSC (Liquid Scintillation Counter) was 0.156 mM which maintained constant with the increase of pH. As the solution pH increases, the absorbance of Pu^{3+} ions decreased due to the formation of Pu(Ⅲ) hydroxide complexes. Fig. 2(b) shows Pu^{3+} ion concentrations determined by analysis of the measured spectra. During the increase of pH from 3.98 to 5.31, Pu^{3+} ion concentrations decrease from 0.156 to 0.115 mM due to hydrolysis. Formation constant and solubility product constant were calculated by the following equations, respectively.

$$[Pu]_{tot.} = [Pu^{3+}](1 + \sum^{*} \beta'_n /[H^+]^n) \quad (1)$$

, and

$$^{*}K'_{s,0} = \{[Pu]_{tot.}/(1 + \sum^{*} \beta'_n /[H^+]^n)\}/[H^+]^3 \quad (2)$$

3.2 Thermodynamic constants

$$\ln K_{eq} = - \Delta H^{\Theta}/RT + \Delta S^{\Theta}/R \quad (3)$$

Van't Hoff expression is the simplest equation for approximating enthalpy and entropy. This equation is recommended to be used in a temperature range equal to or less than ±10 K for a less error [2]. Even though the temperature variation is as large as 15 K, the estimation value of thermodynamic parameters was conducted for quantitative analysis for now.

4. Conclusion

Formation constants of plutonium hydroxide species and solubility products of Pu(Ⅲ) hydroxide were determined at different temperature of 10 and 40 °C. Approximation of thermodynamic constants is carried out. Owing to the large difference of temperature, results have some uncertainty. To obtain precise thermodynamic constants, additional experiments at different temperature should be conducted.

REFERENCES

[1] H.-R. Cho, Y-S. Youn, E. C. Jung, W. Cha, Dalton Trans. 45, 19449-19457 (2016).

[2] TDB-4: Temperature corrections to thermodynamic data and enthalpy calculations, 2.2.1. Constant enthalpy of reaction (1999).

Experimental Study on Electrolytic Reduction and Oxidative Extraction of Ce in LiCl-KCl/Bi System

Jae Hong Yim, Beom Kyu Kim, Hwajeong Han, and Byung Gi Park*
Soonchunhyang University, 22, Soonchunhyang-ro, Sinchang-myeon, Asan-si, Chungcheongnam-do, Republic of Korea
*byunggi@sch.ac.kr

1. Introduction

A sequential process of electrolytic reduction and oxidative extraction can be proposed to decontaminate the high-level salt waste released from the pyroprocess. Major composition of the salt waste is lanthanides and residual actinides. In the process, all ions dissolved in molten LiCl-KCl eutectic are electrolytically reduced to liquid Bi metal and then exist in the form of intermetallic compounds depending on the concentration of the reduced lanthanide. After that, selectively oxidative extraction process is applied to remove lanthanide from liquid Bi metal into molten salt. A series of the processes to decontaminate the salt waste need to demonstrate to find parameters affecting on the processes. In the experiment, Ce, which is known to have a very fast reaction rate, was used among the lanthanide elements.

2. Experimental

Experiments were carried out in a glovebox maintained in an inert atmosphere, keeping oxygen and moisture below 0.1 ppm. In order to maintain the proper experimental temperature of molten LiCL-KCl eutectic and liquid Bi metal at 500 ° C, an electric furnace attached to the bottom of the glove box was used. Figure 1 shows a schematic of the experimental apparatus for making a mixture of Ce and Bi metals by electrolytic reduction. In the experimental apparatus, the liquid metal electrode is mounted in an alumina crucible and the cathode and the anode are electrically insulated by putting a small crucible in a large crucible. Solartron 1470E was operated in the galvanostatic mode. After electrolytic reduction was performed for a prescribed time, the Bi metal of the alumina crucible was collected and cut to an appropriate size. Samples were taken from the cleaved Bi metal and the concentration of Ce was measured using ICP-AES.

For oxidative extraction of Ce from Bi metal, molten salt was prepared by adding about 4 wt% of $BiCl_3$, which may serve as an oxidizer, to molten salt LiCl-KCl. Experiment was conducted with a static test apparatus which could collect samples at prescribed time intervals. The static test apparatus was made of copper to hold eight quartz cells with 14 mm diameter. Bi metals containing Ce obtained in the electrolytic reduction experiment were cut into appropriate sizes, placed in a quartz cell, and placed in a static test apparatus by adding LiCl-KCl molten salt and $BiCl_3$. After the temperature reached 500 °C, the cells were taken out at intervals of 5 minutes and naturally cooled to room temperature, and then a sample analyzed with ICP-AES to measure concentration variation.

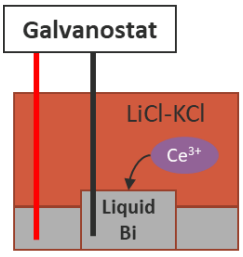

Fig. 1. Experimental setup for electrolytic reduction.

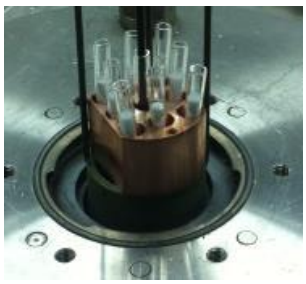

Fig. 2. Experimental set up for oxidative extraction.

3. Results and Discussion

Ce was placed in 5 wt% of molten salt LiCl-KCl to prepare an electrolytic reduction experiment. 0.5 A set by deriving the amount of charge was applied between the two electrodes At the beginning of constant current application, the potential dropped gradually to -2 V over time at about -1.9 V. This increase in potential is a phenomenon in which the concentration of Ce ions decreases at the interface between the molten salt and the electrode due to a reduction reaction, but the concentration difference polarization is increased due to delayed transfer of Ce ions from the molten salt body to the interface.

After electrolytic reduction experiment, three specimens were taken from molten salt, anode Bi metal and cathode Bi metal and analyzed for Ce using ICP-AES. In the experiment, almost all Ce ions were reduced to the Bi metal electrode at the initial 5 wt% to 0.047 wt%. The concentration of Ce in the Bi metal of the inner crucible that acted as the cathode was 4.6 wt% and the Bi metal of the outer crucible that served as the anode showed a small amount of Ce. The microstructures of Ce-reduced Bi metals were observed by SEM-EDS. A needle-shaped crystal structure showing region boundaries was formed the EDS results for this crystal shows that the concentration of Ce in Bi metal is approximately 5.6 wt%.

The samples were brought into contact with the molten salt containing the oxidizing agent to analyze the oxidation reaction. Eight test tubes containing molten salt and liquid metal were installed in a high-temperature electric furnace. After confirming that the molten salt and liquid metal were completely molten, test tube samples were collected one by one at intervals of five minutes, and the concentrations of Ce and Bi in each phase were analyzed. The ICP-AES analysis of solidified molten salt and liquid metal in the test tubes shows the concentration variation of Ce and Bi. Bi ion added to LiCl-KCl at 5 wt% gradually decreased over time, indicating that it was almost consumed to oxidize Ce in liquid Bi metal at about 0.67 wt% in 40 minutes. The concentration of oxidized Ce ions gradually increased to reach 3.63 wt% after 40 minutes, whereas the concentration of Ce in Bi liquid metal decreased to 0.23 wt%. The trend of concentration change over time is normalized from the initial state to the concentration in Fig. 3. As shown in Fig. 6, the oxidation reaction changed drastically after 15 minutes. Before 15 minutes, the concentration of Ce in the Bi metal was slowly decreased, and after 15 minutes, the concentration of Ce remained about 0.24. In molten salt, the concentration of Ce stayed at about 0.12 wt% 15 minutes before and increased after 15 minutes to 3.63. wt% was reached. This phenomenon can be deduced that Ce moves from the liquid metal and molten salt interface to the interface of the liquid metal, oxidizes, stays as Ce ions at the molten salt interface, and then moves to the entire molten salt by diffusion with increasing concentration. However, Bi ions, which act as oxidants in molten salts, tend to decrease in concentrations in molten salts due to the continual movement to the interface as consumed by the oxidation reaction.

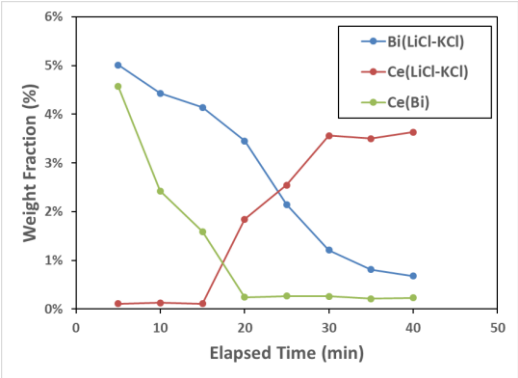

Fig. 3. Concentration variation during oxidative extraction process of Ce from liquid Bi metal.

4. Conclusion

The electrolytic reduction and oxidative extraction process in LiCl-KCl/Bi system was preliminary conducted with Ce. Each experiment was separately performed. The product of electrolytic reduction was used to oxidative extraction process. Electrolytic reduction of Ce into liquid Bi metal showed that almost Ce was removed from the molten salt. Oxidative extraction of Ce from liquid Bi metal also showed that almost Ce was extracted from liquid Bi metal. But time delay of Ce and Bi was observed. The results indicate that oxidative extraction process need to be improved through auxiliary functions such as stirring.

2019 추계학술논문요약집

발행인 김창락

발행처 한국방사성폐기물학회

주 소 대전광역시 유성구 대덕대로 989번길 111
한국원자력연구원 원자력성과확산관(E7) 202호

연락처 **Tel** +82-42-861-5851, +82-42-866-4205
Fax +82-42-861-5852 **E-mail** krs@krs.or.kr

인쇄처 신진기획인쇄사 **Tel** +82-42-638-7887

Abstracts of Proceedings of the
Korean Radioactive Waste Society AUTUMN 2019

www.krs.or.kr

KOREAN RADIOACTIVE WASTE SOCIETY

사단 한국방사성폐기물학회
법인 Korean Radioactive Waste Society